

ICONST EST 2024

International Conferences on Science and Technology

Engineering Science and Technology

September 4-6, 2024 in Durres, ALBANIA

ABSTRACTS & PROCEEDINGS BOOK

ICONST EST 2024

International Conferences on Science and Technology

Engineering Science and Technology

September 4-6, 2024 in Durres, ALBANIA

Editors

Dr. Mustafa Karaboyacı
Dr. Abdullah Beram
Dr. Hamza Kandemir
Dr. Serkan Özdemir

Technical Editors

Dr. Tunahan Çınar
MSc. Şerafettin Atmaca
Ma. Fıratcan Çınar

Cover design & Layout

Dr. Okan Koç

Copyright © 2024

All rights reserved. The papers can be cited with appropriate references to the publication. Authors are responsible for the contents of their papers.

Published by

Association of Kutbilge Academicians, Isparta, Türkiye
E-Mail: info@kutbilge.org

Publication Date: 20/10/2024
ISBN: 978-625-98911-4-9

ICONST EST 2024

International Conferences on Science and Technology

Engineering Science and Technology

September 4-6, 2024 in Durres, ALBANIA

Scientific Honorary Committee

Prof. Dr. Shkëlqim Fortuzi, University of Durres, ALBANIA
Prof. Dr. İlker Hüseyin ÇARIKÇI, Member of Council of Higher Education, TÜRKİYE
Prof. Dr. Mehmet SALTAN, Suleyman Demirel University, TÜRKİYE
Prof. Dr. Yılmaz ÇATAL, Isparta University of Applied Sciences, TÜRKİYE
Prof. Dr. Rade RATKOVIC, Fakultet za biznis i turizam Budva University, MONTENEGRO
Prof. Dr. Vujadin VEŠOVIĆ, Faculty of Transport Communications and Logistics, MONTENEGRO
Prof. Dr. Mentor ALİSHANİ, University of Prizren, KOSOVO
Prof. Dr. Edmond HAJRIZI, University for Business and Technology, KOSOVO
Prof. Dr. Naime BRAJSHORI, Kolegji Heimerer, KOSOVO
Prof. Dr. Nermina HADŽIGRAHIĆ, University of Tuzla, BOSNIA AND HERZEGOVINA
Prof. Dr. Kürşad ÖZKAN, Isparta University of Applied Sciences, TÜRKİYE

Organizing Committee

Dr. Mustafa Karaboyacı, Suleyman Demirel University, TÜRKİYE
Dr. Hamza Kandemir, Isparta University of Applied Science, TÜRKİYE
Dr. Serkan Özdemir, Isparta University of Applied Science, TÜRKİYE
Dr. Abdullah Beram, Pamukkale University, TÜRKİYE
Dr. Ergin Kala, University of Prizren, KOSOVO
Dr. Joanna Machnik-Slomka, Silesian University of Technology, POLAND
Dr. Elzbieta Pawlowska, Silesian University of Technology, POLAND
Dr. Izabela Zimoch, Silesian University of Technology, POLAND
Dr. Adelina Rakaj, University of Prizren, KOSOVO
Dr. Serdan Kervan, University of Prizren, KOSOVO
Dr. Indrit Bimi, Durres University, ALBANIA
Dr. Viliem Kurtulaj, Qiriazi University, ALBANIA
Ma. Dragana Zecevic, Fakultet za biznis i turizam Budva University, MONTENEGRO

Technical Committee

MSc. Şerafettin Atmaca, Suleyman Demirel University, TÜRKİYE
Dr. Tunahan Çınar, Düzce University, TÜRKİYE
Ma. Fıratcan Çınar, Isparta University of Applied Sciences, TÜRKİYE

ICONST EST 2024

International Conferences on Science and Technology

Engineering Science and Technology

September 4-6, 2024 in Durres, ALBANIA

Scientific Committee

- Dr. Alev Akpınar Borazan, Bilecik Seyh Edebali University, Türkiye
Dr. Amer Kanan, Al-Quds University, Palestine
Dr. Andrea G. Capodaglio, University of Pavia, Italy
Dr. Aybeyan Selim, International Vision University, North Macedonia
Dr. Apostolos Kiritsakis, Alexander Tech. Educational Ins. of Thessaloniki, Greece
Dr. Ayodeji Olalekan Salau, Obafemi Awolowo University, Nigeria
Dr. Bülent Derviş, International Vision University, North Macedonia
Dr. Cristian Fosalau, Technical University of Iasi, Romania
Dr. Driton Vela, University of Business and Technology, Kosovo
Dr. Eda Mehmeti, University of Business and Technology, Kosovo
Dr. Elvida Pallaska, University of Business and Technology, Kosovo
Dr. Ernek A. Aubakirov, Al – Farabi Kazakh National University, Kazakhstan
Dr. Fecir Duran, Gazi University, Türkiye
Dr. Gauss M. Cordeiro, Federal University of Pernambuco, Brazil
Dr. Gholamhossein Hamedani, Marquette University, USA
Dr. Gülcan Özkan, Süleyman Demirel University, Türkiye
Dr. Hamid Doost Mohammadian, FHM University of Applied Sciences, Germany
Dr. Ines Bula, University of Business and Technology, Kosovo
Dr. Izabela Zimoch, Silesian University of Technology, Poland
Dr. Joanna Boguniewicz-Zabłocka, Opole University of Technology, Poland
Dr. Kari Heliövaara, University of Helsinki, Finland
Dr. Kłosok-Bazan Iwona, Opole University of Technology, Poland
Dr. Kubilay Akçaözöglü, Niğde Ömer Halisdemir University, Türkiye
Dr. Leyla Tavacıoğlu, Istanbul Technical University, Türkiye
Dr. Lulzim Beqiri, University for Business and Technology, Kosovo
Dr. Mathew Ademola Jayeola, Obafemi Awolowo University, Nigeria
Dr. Mehmet Kitiş, Suleyman Demirel University, Türkiye
Dr. Merita Barani, University for Business and Technology, Kosovo
Dr. Mirosław Kwiatkowski, AGH- University of Science And Technology, Poland
Dr. Mohd Aswadi Bin Alias, University Kuala Lumpur- Bm1, Malaysia
Dr. Muhamet Ahmeti, University of Business and Technology, Kosovo
Dr. Naushad Ali Mamode Khan, University of Mauritius, Mauritius
Dr. Nicholas Baldacchino, Malta College of Arts, Science & Technology, Malta
Dr. Nuray Benli Yıldız, Duzce University, Türkiye
Dr. Rahmon Ariyo Badru, Obafemi Awolowo University, Nigeria
Dr. Ramazan Şenol, Suleyman Demirel University, Türkiye
Dr. Salina Muhamad, Universiti Selangor, Malaysia
Dr. Sami Makolli, University of Business and Technology, Kosovo
Dr. Serhat Oğuzhan Kıvrak, Hitit University, Türkiye
Dr. Shpend Dragusha, University of Business and Technology, Kosovo
Dr. Şule Sultan Uğur, Suleyman Demirel University, Türkiye
Dr. Valmir Hoxha, University of Business and Technology, Kosovo
Dr. Vehebi Sofiu, University of Business and Technology, Kosovo
Dr. Vincenzo Naddeo, University of Salerno, Italy
Dr. Zhandos T. Mukayev, Shakarim State University of Semey, Kazakhstan

ICONST 2024

International Conferences on Science and Technology Engineering Science and Technology

September 4-6, 2024 in Durres, ALBANIA

Dear Readers;

The seventh of ICONST organizations was held in Durres/Albania between September 4-6, 2024 with the theme of '*science for sustainable technology*' again. In recent years, weather changes due to climate change have reached a perceptible level for everyone and have become a major concern. For this reason, scientific studies that transform technological progress into a sustainable one is seen as the only solution for humanity's salvation. Here we ask ourselves "which branch of science is responsible for sustainability?". Sustainability science is an interdisciplinary field of study that covers all basic sciences with social, economic, ecological dimensions. If we consider technology as the practical application of scientific knowledge, the task of scientists under these conditions is to design products that consume less energy, require less raw materials, and last longer.

ICONST organizations organize congresses on sustainability issues of three main fields of study at the same time in order to present different perspectives to scientists. This year, 194 papers from 21 different countries presented by scientists in **ICONST Organizations**.

68 papers from 14 countries (Afghanistan, Albania, Algeria, Bangladesh, Croatia, Hungary, Iran, Italy, Kosovo, Montenegro, North Macedonia, Pakistan, Poland, and Türkiye) presented in our **International Conference on Engineering Science and Technology** organized under ICONST organizations. Turkey is the country with the highest participation with 48%, followed by Kosovo with 13%, Albania with 9%, Algeria and Poland with 6%, Iran and Azerbaijan 3%, Afghanistan, Bangladesh, Croatia, Hungary, Italy, Montenegro, North Macedonia, Pakistan with 1.4%. Outside of Türkiye participant rate is totally 52%.

As ICONST organizations, we will continue to organize organizations with the value you deserve in order to exchange ideas against the greatest threat facing humanity, to inspire each other and to contribute to science. See you at your future events.

ICONST Organizing Committee

ICONST EST 2024

International Conferences on Science and Technology

Engineering Science and Technology

September 4-6, 2024 in Durres, ALBANIA

Contents

Paper	Presentation Type	Country	Page
Value-based Adoption of UAVs in Agriculture: A Systematic Literature Review Murat Tahir Çaldağ	Oral	Türkiye	1
Applications of Artificial Intelligence in Railway Traffic Control Gökçe Aydın	Oral	Türkiye	2
Low Power Consumption Data Security Implementation for Artificial Intelligence Based Smart Systems Muhammet Cihat Mumcu, Beray İkinci, Elif Öztürk, Kubilay Ataş, Abdullah Güngör	Oral	Türkiye	3
The Development and Applications of Unmanned Surface Vehicles for The Monitoring of Water Quality Eray Şahin, Aynur Yücel, İbrahim Murat Ozulu	Oral	Türkiye	4
Numerical study on the thermal performance of Nano-PCM heat sink with different configurations of pin fins Burcu Çiçek	Oral	Türkiye	5
Visible Light Photocatalytic Degradation of Malachite Green Using Ti3C2Tx MXene Film Halime Ak, Ayşenur Özler, Bircan Haspulat Taymaz, Volkan Eskizeybek, Handan Kamış	Oral	Türkiye	6
Predicting Customer Behavior and Developing Personalized Marketing Strategies with Machine Learning Ergin Kala, Şerafettin Atmaca	Oral	Kosovo	7
Treatment Techniques for Anionic Surfactants in Wastewater Iwona Kłosok-Bazan, Joanna Boguniewicz-Zablocka, Mustafa Karaboyacı	Oral	Poland	8
The Effect of Different UV Wavelengths on Wastewater Treatment Joanna Boguniewicz-Zablocka, Iwona Kłosok-Bazan, Mustafa Karaboyacı	Oral	Poland	9
Structural Stability and Biochemical Modifications of Food Proteins from a Chemical Engineering Perspective Cengiz Cesko	Oral	Kosovo	10
Artificial Intelligence-Supported Adaptive Learning Systems and Their Impact on Student Achievement Samedin Krrabaj	Oral	Kosovo	11
Performance Analysis of Deep Learning Algorithms for Classification of EEG Signals Muhammet Cihat Mumcu, Beray İkinci, Elif Öztürk, Kubilay Ataş, Abdullah Güngör	Oral	Türkiye	12

<u>SMART Energy transition of traditional generation to RES</u>			
<u>Vehebi Sofiu, Nafije Shabani, Sami Gashi, Nexhat Balaj, Muhaxherin Sofiu, Besa Veseli</u>	Oral	Kosovo	13
<u>The Impact of Ultrasounds on Convective Drying Kinetics and Properties of Fermented, Frozen/Thawed and Osmotically Dehydrated Beetroot Chips</u>			
<u>Magdalena Zielinska, Konrad W. Nowak, Izabela Staniszewska, Bartosz Pszczółkowski, Wojciech Rejmer</u>	Oral	Poland	14
<u>Developing a Graph Visualization Mechanism for Transport Route Optimization Algorithms and Creating An Efficient Visualization Method on A Dynamically Changing Situational Map</u>			
<u>Adam Galuszka, Tomasz Grzejszczak, Jarosław Smieja</u>	Online	Poland	15
<u>Design and Implementation of a Web Based Event Management System Using Django and CSS</u>			
<u>Kazi Rafiqul Islam, Bilkis Akter Dalia</u>	Online	Bangladesh	16
<u>A Decision Support System for Medicinal Plants</u>			
<u>Fatih Sakar, Selin Su Demirkıran, Yiğit Kuru, Çağla Yurter, Melis Almula Karadayı</u>	Online	Türkiye	17
<u>Drinking Water Quality Assessment Before and After Using the Eco-Soft Cross 90 filter: Case Study</u>			
<u>Stela Sefa, Elma Kodra, Eli Vyshka, Blerta Gërmënji, Drita Hima</u>	Oral	Albania	18
<u>Drinking Water Quality Assurance: Consumer protection for a healthy future</u>			
<u>Elma Kodra, Stela Sefa, Erion Mali, Justin Mihani, Luiza Lluri</u>	Oral	Albania	19
<u>The Dynamics of Pollution in the Lumbardh River from Industrial Wastewater Discharges in Prizren</u>			
<u>Sami Gashi, Vehebi Sofiu, Besa Veseli, Shkelzim Ukaj</u>	Oral	Kosovo	20
<u>Neural Network Visualization for The Study of Parallel Algorithm Building Skills</u>			
<u>Zoltan Attila Godo</u>	Online	Hungary	21
<u>Effect of Acidic Electrolyte on Energy Storage of Supercapacitor with Pure Ti3C2Tx MXene Film Electrodes</u>			
<u>Aleyna Akıllı, Ayşenur Özler, Bircan Haspulat Taymaz, Volkan Eskizeybek, Handan Kamış</u>	Poster	Türkiye	22
<u>Energy Efficiency for The Network Power Supply in Kosovo. Challenges and Opportunities for The Grid Infrastructure Integration of RES</u>			
<u>Fuat Pallaska</u>	Oral	Kosovo	23
<u>Optimal Controller Design for Load-Frequency Control in a Two-Area Power System</u>			
<u>Kenan Yanmaz</u>	Oral	Türkiye	24
<u>Evaluation of Photovoltaic System Capacity For Self-Sustaining Irrigation System in Kosovo</u>			
<u>Nexhmi Krasniqi, Armend Ymeri, Kadri Kadriu, Banush Dragusha</u>	Oral	Kosovo	25
<u>Evaluation of Antibacterial Activity of ZnO-NP Synthesized by Different Methods on <i>Staphylococcus aureus</i></u>			
<u>Ummahan Temel, Caner Vural</u>	Online	Türkiye	26
<u>Performance indicators of the general cargo terminal. The case of Durres Port</u>			
<u>Osman Metalla, Shpetim Pupa, Indrit Bimi, Eduart Ndokaj, Keidi Metalla</u>	Oral	Albania	27

Hydrogen and Power Generation with PVT-Assisted ORC Using LNG Cold Energy for Low Temperature Applications	Online	Türkiye	33
<u>Gamze Soyuturk, Onder Kizilkan</u>			
Single Flash Geothermal Power Plant with Bottoming Helium Brayton Cycle: A Comprehensive Evaluation	Online	Türkiye	42
<u>Gamze Soyuturk, Onder Kizilkan</u>			
Analysis of Glass Fiber Utilization Rates in G-7 and Türkiye and The Role of Şişecam in The Türkiye Glass Fiber Sector	Oral	Türkiye	52
<u>Tugay Üstün, Sinan Can Altuntaş</u>			
Combining Multi-Source Bearing Fault Datasets and Analyzing the Impact of Welch Method Parameters on Classification	Oral	Türkiye	63
<u>Yunus Emre Acar</u>			
Enhancing Obesity Level Prediction with Feature Selection Methods and LSTM Network	Oral	Türkiye	72
<u>Züleyha Yılmaz Acar</u>			
Optimizing Thermal Comfort: Comparing Shading Elements and Aerogel Glazing	Oral	Türkiye	80
<u>Damla Yağmur Sağ Bayram, Tugce Pekdogan</u>			
Flexural Behavior of 3D Printed PLA Fiber Reinforced Cement-Based Composites	Oral	Türkiye	86
<u>Eren Gödek, Serhat Oğuzhan Kıvrak, Julide Kıvrak</u>			
The Importance Of Using Durable Concrete In Underground Floors	Oral	Albania	93
<u>Boriana Vrusho, Alma Golgota, Indrit Bimi</u>			
The reliability of inner bottom plating of fuel tanks on aging bulk carriers	Oral	Montenegro	100
<u>Špiro Ivošević, Joanna Soszyńska-Budny</u>			
Modeling of Thermoelectric Generator and Photovoltaic Panel Hybrid System	Oral	Türkiye	109
<u>Mehmet Ali Ustuner, Onur Emre Golen, Abidin Sahinoglu, Hayati Mamur</u>			
Characterization of Aromatic Water Obtained from Dried and Fresh Passiflora Edulis Sims Peels	Oral	Türkiye	114
<u>Özlem Karaboyacı</u>			
Maximum Entropy (MaxEnt) Method Using Wind Farm Site Selection Modeling for Aegean Region (Türkiye)	Online	Türkiye	120
<u>Senem Tekin, Müge Ünal, Ahmet Çilek</u>			
Seismic Risk and Damage Assessment of Adıyaman Province during February 6, 2023 Earthquakes	Online	Türkiye	126
<u>Seyhan Okuyan Akcan, Senem Tekin, Ali Yeşilyurt</u>			
Evaluation of the Alternative Locations for Solar Power Plant in Turkey	Online	Türkiye	136
<u>Mehmet Salih Değirmenci, Mehtap Dursun, Nazli Goker</u>			
Effects of the Influencer Marketing on e-commerce	Online	Türkiye	141
<u>Feyza Cokak, Mehtap Dursun, Nazli Goker</u>			
Eco-Friendly Wool Dyeing Using Pistachio Soft Shell Extract	Online	Türkiye	145
<u>Enfal Kayahan</u>			
Real-Time Detection of Improperly Parked Vehicles with Unmanned Aerial Vehicles and Acceleration of Emergency Response Processes	Online	Türkiye	153
<u>Mustafa Melikşah Özmen, Muzaffer Eylence, Bekir Aksoy</u>			

Basic Principles And Methods Of Cryptography	Online	Azerbaijan	160
<u>Aytac Rüstəmli</u>			
Comparative Analysis of Communication Standards in Industrial and Sensor Technologies: Evaluating Protocols for Performance, Reliability, and Efficiency	Oral	Kosovo	163
<u>Sertaç Şalçini</u>			
Optimal power flow of a power system including wind energy sources using nutcracker optimization algorithm	Online	Türkiye	174
<u>Burçin Özkaya</u>			
FEM Model and Frequency Response Analysis of PCB Coils for Wireless Power Transfer	Online	Croatia	184
<u>Žarko Martinović</u>			
Examination of Chemical Elements in Animal Feed	Online	North Macedonia	189
<u>Julijana Tomovska, Ilmije Vllasaku, Vezir Januzi</u>			
Extending, Integrating and Recovering: Tools for The Architectural and Social Rehabilitation of The Augusta Slaughterhouse	Online	Italy	199
<u>Fernanda Cantone, Francesca Castagneto</u>			
Applications of Artificial Intelligence (AI) in Plastic Recycling	Oral	Albania	208
<u>Luiza Lluri, Faldi Lluri, Dalip Qorri, Ramadan Dollani</u>			
The Analytical Study Of Passive And ActiveFiltering In A Low Voltage Electrical NetworkFrom The Point Of View Of Energy Quality	Online	Algeria	216
<u>Ben Haoua Larbi Daouli, Hassan Mana</u>			
The method of obtaining Electrical Energy Quality (EEQ) according to the remedies required by EMC: Reduction and Elimination of Electromagnetic harmonics	Online	Algeria	222
<u>Boudjelal Dounia, Mana Hassan</u>			
Potential Strategies to Improve Air Quality in Tirana for Current and Future Generations	Oral	Albania	229
<u>Luiza Lluri, Fald Lluri, Stela Sefa</u>			
Design And Comparative Analysis Of A Geothermal-Driven Flash Organic Rankine Cycle For Power And Heat Generation	Online	Türkiye	237
<u>Fatih Yılmaz</u>			
A Comprehensive Examination Of The Solar Energy-Based A Novel Combined Plant For Producing Power, Hydrogen, And Heating	Online	Türkiye	244
<u>Fatih Yılmaz</u>			
The Relationship Between Usability and Aesthetic in Interaction Design (for Islamic Arts)	Online	Iran	251
<u>Mir Alireza Daryabeygi, Ayin Fazlollahi, Sara Mohamadzadeh Moghadam</u>			
Carnival: Holding the first workshop on the creation of an “Ecosystem of Innovation and Soft Artistic Technology” at the Islamic Azad University, Central Tehran branch	Online	Iran	257
<u>Mir Alireza Daryabeygi</u>			
Intuitionistic Fuzzy Cognitive Map Approach for Determining the Effectiveness of Digital Marketing Tools Evaluation Factors	Online	Türkiye	260
<u>Nazli Goker, Mehtap Dursun</u>			

A Decision Making Framework for Assessing Photovoltaic Potential In Turkey: Determining Suitable Cities For Optimal Solar Energy Production	Online	Türkiye	264
<hr/>			
Mustafa Berk Basakin, Nazli Goker, Mehtap Dursun			
Development of a Financial Web Application For Budget and Expense Management For Individual and Company	Oral	Kosovo	273
<hr/>			
Genit Sopa, Faton Kabashi, Vehebi Sofiu, Lamir Shkurti, Sami Gashi			
Comparison of Phosphorus Removal Performance and Characteristics of Dried and Undried MgFe Layered Double Hydroxides	Oral	Türkiye	291
<hr/>			
Hüseyin Yazıcı, Mustafa Karaboyacı			
Application Of GIS And Remote Sensing for Solid Waste Management	Online	Pakistan	302
<hr/>			
Muhammad Ishaq Iqbal			
Improving Power Quality By Using Active Power Filter Based On DQ Frame Of Reference Theory	Online	Algeria	305
<hr/>			
Hassan Mana, Ben Haoua Larbi Daouli			
Simulation of Fuzzy Logic Control System of Autonomous Mobile Robot in Matlab Environment	Online	Azerbaijan	311
<hr/>			
Mammadova K.A., Alieva A.A			
Automatic Detection and Control of Weeds in Agricultural Fields with Artificial Intelligence Image Processing	Online	Türkiye	317
<hr/>			
Mustafa Melikşah Özmen, Muzaffer Eylence, Bekir Aksoy			
Production of Thermoregulating and Reversibly Colour Changing Polyester Fabric Treated with Thermochromic Nanocapsules and ZnO Particles	Oral	Türkiye	327
<hr/>			
Sennur Alay Aksoy, Cemil Alkan, Simge Özkayalar, Demet Yılmaz			
Asphalt Binder Modification in Flexible Pavement Using Different Amounts of Crumb Rubber	Online	Afghanistan	336
<hr/>			
Saber Shah -Saber, Raidy Gul-Hamdard, Waliullah Qasimi			
Simulation of a Series Active Filter Using Hysteresis Control from an Electromagnetic Compatibility Perspective: Solution against Unwanted Harmonics	Online	Algeria	358
<hr/>			
Mana Hassan, Boudjelal Dounia			

Value-based Adoption of UAVs in Agriculture: A Systematic Literature Review

Murat Tahir Çaldağ*¹

Abstract: The emergence of Industry 4.0 technologies has revolutionized the way workers, businesses, and governments operate to compete on national and global scales. With change, new approaches are required to address existing challenges which can be seen in sustainable development goals of the United Nations. Industry 4.0 technologies such as artificial intelligence, big data, internet of things, unmanned aerial vehicles (UAV), robotics, and automation technologies have the potential to improve various industries in different ways. As the emergence of agriculture transformed human civilization, UAV-based agriculture can revolutionize farmers' operations. UAVs present opportunities such as significant increases in productivity, safer ways of agriculture, environmental advantages, and real-time data for tracking, analysis, and decision-making. However, there can be some drawbacks of UAVs in agricultural contexts as privacy, lack of awareness, and security issues. The aim of this study is to identify the determinants of UAVs in agriculture and provide a framework for further analysis. A systematic literature review (SLR) is conducted to determine the factors affecting UAV acceptance by farmers in agriculture. The review results presented 124 factors that are reduced to 25 significant determinants of UAV acceptance. Innovativeness, perceived usefulness, complexity, skill expertise, social influence, task variability, self-efficacy, infrastructure, investment costs, and efficiency are some of the identified factors affecting the farmers' acceptance of UAVs in agriculture. The identified determinants of farmers' acceptance of UAVs are proposed as a research model according to the value-based adoption (VAM) model. Even though there are several well-established and accepted models for acceptance, the reasoning behind the selection of VAM is that it provides a value-based perspective consisting of perceived benefits and sacrifices that individuals need to consider. This study provides significant insights and a comprehensive value-based framework for farmers' acceptance of UAVs in agriculture. The results of this study can be used as a guideline in agriculture for individuals and businesses for UAV adoption decisions.

Keywords: UAV, Drone, Agriculture, Smart Farming, Acceptance.

¹**Address:** Başkent University, Department of Technology and Knowledge Management, Ankara/Turkey

***Corresponding author:** mtcaldag@baskent.edu.tr

Applications of Artificial Intelligence in Railway Traffic Control

Gökçe Aydın

Abstract: Artificial Intelligence (AI) is increasingly becoming a part of everyday life. It revolutionizes the majority of industries, and engineering disciplines, where it enhances efficiency and bring in innovation, is no exception. In railway traffic control, which is a too high workload task for human brain to effectively manage, AI's role is becoming ever more critical as it offers sophisticated tools to manage complex systems. This study provides an introductory overview of the applications of AI in railway traffic control. We discuss basic AI technologies such as simple algorithms, machine learning, data analytics tools etc. that can assist in improving the scheduling and management of train operations. The primary focus is on how these AI tools can help railway operators better analyze the conflicts due to train movements and make informed decisions to enhance the efficiency and reliability of train services. Our discussion includes examples of AI being used to analyze and predict train traffic data, leading to more effective train scheduling that reduces waiting times, knock-on delays and improves timetable adherence. We also explore the potential of these technologies to provide real-time insights that help manage daily operations more smoothly. The findings presented are based on general knowledge and common applications of AI in similar industries, providing a starting point for railway infrastructure managers considering the adoption of these technologies. The study also aims to introduce AI applications in railway traffic control for a non-specialist audience, emphasizing potential benefits of the potential implementations. The presentation will conclude with a brief outline of the next steps for integrating basic AI tools into existing traffic management systems, highlighting the ease of adoption and the immediate improvements they can bring to railway operations.

Keywords: Railway operation, Railway traffic control, artificial intelligence, delay management.

¹**Address:** Aksaray University, Faculty of Engineering, Aksaray/Turkiye

***Corresponding author:** gokceaydin@aksaray.edu.tr

Low Power Consumption Data Security Implementation for Artificial Intelligence Based Smart Systems

Muhammet Cihat Mumcu*¹, Beray İkinci², Elif Öztürk², Kubilay Ataş², Abdullah Güngör²

Abstract: Power consumption optimisation is becoming more crucial in the design of artificial intelligence (AI)-powered smart systems. Data security is becoming a major issue in an era where the use of these systems is growing, particularly in applications that demand low power consumption. Due to their high sensitivity and complexity, artificial intelligence applications typically handle massive volumes of data, making data security crucial. Nonetheless, it seems that low-power AI systems are pushing the boundaries of conventional security techniques and algorithms. In this context, researchers are working on realistic approaches for ensuring data security and privacy in artificial intelligence-based systems that require less power. One strategy for improving energy efficiency and ensuring data security is to employ lightweight cryptography (LWC) algorithms, which are suitable for microprocessors with limited memory and power in various architectures used in smart system design. Lightweight cryptography techniques on the Internet of Things (IoT) platform allow a wide range of low-resource and resource-constrained devices to compute, make decisions, and communicate securely across networks. Numerous advantages have been achieved through the design and optimization of various structured algorithms. This study investigated the integration and optimization of lightweight cryptography algorithms with a focus on data security in the application field, as well as the wide application field of artificial intelligence-based systems that require low power consumption. Furthermore, a RISC microprocessor was used to model image processing, and data security and confidentiality were evaluated by integrating an algorithm chosen from a list of lightweight cryptography algorithms that complied with the model. Performance metrics such as memory usage area and power consumption were identified, and the analysis's results are presented.

Keywords: Artificial Intelligence (AI), RISC Processor, Low Power Consumption, Lightweight Cryptography (LWC).

¹**Address:** Istanbul Gelisim University, Gelisim Vocational School, İstanbul/Türkiye

²**Address:** Istanbul Gelisim University, Faculty of Engineering and Architecture, İstanbul/Türkiye

***Corresponding author:** mcmumcu@gelisim.edu.tr

The Development and Applications of Unmanned Surface Vehicles for The Monitoring of Water Quality

Eray Şahin¹, Aynur Yücel¹, İbrahim Murat Ozulu*¹

Abstract: All living organisms are dependent on water in order to sustain their existence. The assessment of surface water quality is of the most significant importance for the protection of human health, the maintenance of ecological balance and the preservation of other living organisms. In the case of large surface water bodies, such as natural lakes and dam ponds, irregular samples are typically collected from the shore or by boat. The collection of samples from multiple locations is both costly and time-consuming. In recent years, unmanned surface water vehicles have been developed for a variety of purposes. The objective of this study is twofold: firstly, to ascertain whether unmanned surface water vehicles can be utilized for the automated collection of water samples from specified points and depths for the purposes of water quality monitoring; and secondly, to develop an autonomous vehicle capable of undertaking the procedure of taking water samples. In order to achieve the primary objective of the project, which is to sample the water, two water pumps and sample containers are integrated on the carrier platform. The water is obtained from different depths (50 cm and 2 m) using tubing of varying lengths connected to the pumps. The sampling process was conducted using the installed system via remote control, resulting in the acquisition of two distinct samples from two disparate depths.

Keywords: Unmanned sea surface vehicles, Water quality, Water sampling, Autopilot.

Acknowledgements: This research was supported by The Scientific and Technological Research Council of Türkiye (TÜBİTAK) under the 2209-A University Students Research Projects Support Program with the project number 1919B012304750.

¹**Address:** Hitit University, Department of Architecture and Urban Planning, Çorum/ Türkiye

***Corresponding author:** imuratozulu@hitit.edu.tr

Numerical study on the thermal performance of Nano-PCM heat sink with different configurations of pin fins

Burcu Çiçek*¹,

Abstract: In this study, a finned heat sink model with Nano-PCM materials in different configurations of fins, for cooling electronic devices, was numerically investigated. Three different configurations of fins, such as regular pentagon, rhombus and square, were used in analyses at a constant heat flux of 5000 W/m². To observe the melting process of the Nano-PCM and the heat transfer rate of finned heat sink, the governing equations and the enthalpy-porosity techniques were applied by means of ANSYS Fluent software. First, empty heat sink, PCM-heat sink and Nano-PCM heat sink models with square fins were designed and analyzed, for comparison with each other. RT-35HC was selected as the PCM and Fe₃O₄ was added into PCM as the nanoparticle to form a Nano-PCM. Second, the Nano-PCM heat sinks with differently shaped pin fins were investigated for revealing thermal behaviors of the heat sinks. Furthermore, effects of nanoparticle concentrations (2%, 4% and 6%) were investigated for determining the optimum amount to be added to PCM. The results show that, best heat transfer rate was attained by using Nano-PCM heat sink. When using rhombus fin configuration in heat sink, a 3.17 and 2.22 K lower heat sink base temperature was achieved compared to the pentagon and square fin configurations, respectively, for a 0.6% Fe₃O₄ concentration of Nano-PCM. Therefore it can be said that the best fin configuration is the rhombus one. In addition, it was observed that, as Fe₃O₄ concentration in the nano-PCM increased, the conductivity and therefore the heat transfer rate of Nano-PCM increased slightly.

Keywords: Nano-PCMs, thermal management, pin fins, melting, CFD.

¹**Address:** Aksaray University, Faculty of Engineering, Aksaray/Turkiye

***Corresponding author:** cicekb@aksaray.edu.tr

Visible Light Photocatalytic Degradation of Malachite Green Using $Ti_3C_2T_x$ MXene Film

Halime Ak¹, Ayşenur Özler¹, Bircan Haspulat Taymaz^{1*}, Volkan Eskizeybek², Handan Kamsı¹

Abstract: Heterogeneous photocatalysis method shows great promise in breaking down harmful organic pollutants and rendering them harmless. In photocatalytic processes where light is used actively, photocatalysts that are active in visible light should be developed in order to benefit from the sun, which is the most powerful and inexpensive energy source. Two-dimensional (2D) nanomaterials are among the most important functional materials used in photocatalysis and energy storage applications due to their high surface area. The general formula of MXene, a 2D nanomaterial, is $M_{n+1}X_nT_x$, where M is the transition metal, X is carbon or nitrogen, and T is the surface terminator group (-OH, -F, -O). In this study, the MILD method, in which both etching and delamination processes can be carried out simultaneously by selectively etching A in $M_{n+1}AX_n$ (MAX), was preferred for the synthesis of MXene $Ti_3C_2T_x$. The synthesized MXene suspension was filtered using a vacuum filtration system in which a porous filter was placed, and $Ti_3C_2T_x$ films were formed. After the drying process was completed, the film was separated from the filter paper and independent $Ti_3C_2T_x$ films were obtained. Malachite Green (MY) dye, which is used as a model compound in many studies in the literature, has been used in optimization studies in the production of materials. The photocatalytic performance of the synthesized MXene film was examined by monitoring the decolorization of MY dye under visible light. Photocatalytic performance of MXene film; effects of dye pH, photocatalyst surface area, and dye concentration were examined. The pH value at which the maximum photocatalytic activity occurred was found to be 7 and the photocatalyst surface area for 10 μ m dye concentration was 0.0083 m²/L. Additionally, the photocatalytic reaction kinetics were examined and it was determined that the photocatalytic degradation reaction of MY dye in the presence of Mxene film was first order. In addition, the photocatalytic performance of the MXene film almost did not change during the five-time use of the photocatalytic study under these conditions.

Keywords: $Ti_3C_2T_x$ MXene film, photocatalysis, malachite green

¹**Address:** Chemical Engineering/Faculty of Engineering and Natural Sciences, Konya Technical University, Turkey,

²**Address:** Materials Science and Engineering/ Faculty of Engineering, Çanakkale 18 Mart University, Turkey

***Corresponding author:** hkamis@ktun.edu.tr

Predicting Customer Behavior and Developing Personalized Marketing Strategies with Machine Learning

Ergin Kala¹, Şerafettin Atmaca²

Abstract: In the contemporary digital era, businesses have come to place considerable emphasis on data analysis as a means of gaining deeper insights into customer behaviour and developing more efficacious marketing strategies. In particular, machine learning algorithms provide a robust tool for identifying customer trends within vast data sets, thereby facilitating the development of personalized marketing strategies. This study examines the role of machine learning techniques in predicting customer behavior and developing tailored marketing approaches. The application of machine learning algorithms enables the prediction of crucial parameters, including purchasing tendencies, product preferences, and loyalty levels, through the modelling of customer data. For example, classification algorithms can assist in identifying customers' product preferences, whereas regression analyses can predict purchase frequencies. In light of these insights, businesses are able to provide product recommendations that are tailored to the individual customer, thus enhancing customer loyalty. In this study, customer data was analyzed from a variety of sources, including past purchase records, online behavior tracking, and social media interactions. A variety of machine learning algorithms, including decision trees, support vector machines, and neural networks, were employed to assess the extent to which customer behavior can be predicted. The results demonstrate that personalized marketing strategies can markedly improve customer engagement and satisfaction. In conclusion, the application of machine learning technologies affords businesses the opportunity to develop strategies that are tailored to the specific needs of their customers, thereby conferring a competitive advantage. Such personalized approaches have been demonstrated to enhance customer satisfaction and long-term loyalty, which in turn has been shown to increase profitability. The findings of our study underscore the significance of employing machine learning-based analytical techniques for the formulation of customer-centric marketing strategies.

Keywords: Machine Learning, Customer Behavior Prediction, Personalized Marketing, Big Data, Customer Engagement

¹**Address:** Ukshin Hoti Str. No.13, Prishtina 10000, Kosovo-Ziraat Bank, Kosovo.

²**Address:** Isparta University of Applied Sciences, Isparta/Türkiye.

***Corresponding author:** erginkala@gmail.com

Treatment Techniques for Anionic Surfactants in Wastewater

Iwona Klosok-Bazan ^{*1}, Joanna Boguniewicz-Zablocka², Mustafa Karaboyaci³

Abstract: Anionic surfactants, which are commonly found in a variety of consumer and industrial products, have been identified as a significant contributor to wastewater pollution. Their persistence in the environment poses significant risks to aquatic ecosystems and human health. These risks include toxicity to aquatic organisms, interference with oxygen levels, and impact on water quality. This study examines a range of treatment techniques for the effective removal of anionic surfactants from wastewater, encompassing both established and emerging methods. The principal techniques for the treatment of wastewater containing anionic surfactants can be classified into three main categories: physical, chemical, and biological. Adsorption is a prevalent physical method that involves the binding of surfactants to adsorbent materials, such as activated carbon. Although effective in reducing surfactant concentration, the regeneration of adsorbents represents a significant cost consideration. Chemical treatments, including coagulation and flocculation, employ the use of coagulants to neutralize and aggregate surfactant particles, which are subsequently removed through sedimentation. Advanced oxidation processes (AOPs), including ozonation and Fenton reactions, have also been demonstrated to be effective in breaking down surfactants into non-toxic components with strong oxidants. Biological treatments employ the use of microorganisms that are capable of naturally degrading surfactants, thereby converting them into less harmful byproducts. Notably, activated sludge systems and aerobic treatments have demonstrated efficacy in this regard, as microbes are capable of metabolizing surfactants for energy. Biological methods are environmentally compatible, though they may necessitate longer treatment times and specific conditions to be effective. The application of emerging methods, such as membrane filtration and electrocoagulation, has demonstrated potential due to their capacity for selective removal, particularly in the presence of low concentrations of surfactants. The combination of multiple methods often produces the most effective results, particularly in the context of complex wastewater matrices. For example, a combined approach that employs adsorption followed by biological treatment has the potential to enhance the efficacy of the process.

Keywords: Anionic Surfactants, Wastewater Treatment, Adsorption, Coagulation, Advanced Oxidation Processes.

¹**Address:** Opole University of Technology, Opole, Poland.

²**Address:** Opole University of Technology, Faculty of Mechanical Engineering, Opole, Poland.

³**Address:** Suleyman Demirel University, Engineering Faculty, Isparta, Türkiye.

***Corresponding author:** i.klosok-bazan@po.edu.pl

The Effect of Different UV Wavelengths on Wastewater Treatment

Joanna Boguniewicz-Zablocka*¹, Iwona Kłosok-Bazan², , Mustafa Karaboyacı³

Abstract: Anionic surfactants, which are commonly found in a variety of consumer and industrial products, have been identified as a significant contributor to wastewater pollution. Their persistence in the environment poses significant risks to aquatic ecosystems and human health. These risks include toxicity to aquatic organisms, interference with oxygen levels, and impact on water quality. This study examines a range of treatment techniques for the effective removal of anionic surfactants from wastewater, encompassing both established and emerging methods. The principal techniques for the treatment of wastewater containing anionic surfactants can be classified into three main categories: physical, chemical, and biological. Adsorption is a prevalent physical method that involves the binding of surfactants to adsorbent materials, such as activated carbon. Although effective in reducing surfactant concentration, the regeneration of adsorbents represents a significant cost consideration. Chemical treatments, including coagulation and flocculation, employ the use of coagulants to neutralize and aggregate surfactant particles, which are subsequently removed through sedimentation. Advanced oxidation processes (AOPs), including ozonation and Fenton reactions, have also been demonstrated to be effective in breaking down surfactants into non-toxic components with strong oxidants. Biological treatments employ the use of microorganisms that are capable of naturally degrading surfactants, thereby converting them into less harmful byproducts. Notably, activated sludge systems and aerobic treatments have demonstrated efficacy in this regard, as microbes are capable of metabolizing surfactants for energy. Biological methods are environmentally compatible, though they may necessitate longer treatment times and specific conditions to be effective. The application of emerging methods, such as membrane filtration and electrocoagulation, has demonstrated potential due to their capacity for selective removal, particularly in the presence of low concentrations of surfactants. The combination of multiple methods often produces the most effective results, particularly in the context of complex wastewater matrices. For example, a combined approach that employs adsorption followed by biological treatment has the potential to enhance the efficacy of the process.

Keywords: Anionic Surfactants, Wastewater Treatment, Adsorption, Coagulation, Advanced Oxidation Processes.

¹**Address:** Opole University of Technology, Faculty of Mechanical Engineering, Opole, Poland.

²**Address:** Opole University of Technology, Opole, Poland.

³**Address:** Suleyman Demirel University, Engineering Faculty, Isparta, Türkiye.

***Corresponding author:** J.Boguniewicz-Zablocka@po.edu.pl

Structural Stability and Biochemical Modifications of Food Proteins from a Chemical Engineering Perspective

Cengiz Cesko*¹

Abstract: The structural stability and biochemical modifications of food proteins are of critical importance with regard to the quality, nutritional value, and digestibility of foodstuffs. During the processing of food proteins, the proteins are subjected to a variety of conditions, including temperature, pH, and the activity of enzymes. These conditions can lead to structural changes in the proteins, which in turn can directly impact their functionality. This study examines the techniques and optimization methods employed in chemical engineering to maintain the structural stability of food proteins and achieve the desired biochemical modifications. Chemical engineering techniques are of great importance in the preservation of food proteins, the prevention of quality loss, and the maintenance of nutritional value. For instance, the denaturation of proteins during thermal processing is frequently an unavoidable consequence. Nevertheless, the optimization of temperature and duration can serve to minimize the occurrence of undesired structural degradation while simultaneously preserving the functionality of the protein. Similarly, the storage of foodstuffs within a specific pH range serves to maintain the structural stability of proteins. Furthermore, biochemical modifications are commonly utilized to enhance the functional properties of proteins. For example, enzymatic hydrolysis can enhance protein digestibility or facilitate the release of specific amino acids. Additionally, the use of chemical cross-linkers can enhance the gelation capacity of proteins, thereby positively impacting texture. In conclusion, the optimization of processes that preserve the structural stability and enhance the functional properties of food proteins represents a primary objective in the application of chemical engineering to food technology. This study highlights the positive effects of advanced techniques for biochemical modifications and structural stability of proteins on food quality and nutritional value.

Keywords: Food Proteins, Structural Stability, Biochemical Modifications.

¹**Address:** Food Science and Biotechnology, University for Business and Technology, Higher Education Institution, Kosovo.

***Corresponding author:** cengiz.cesko@ubt-uni.net

Artificial Intelligence-Supported Adaptive Learning Systems and Their Impact on Student Achievement

Samedin Krrabaj *¹

Abstract: The objective of individualized approaches in education is to facilitate a more effective learning experience by providing content that is tailored to the specific pace and needs of each student. In this context, artificial intelligence (AI)-supported adaptive learning systems represent a highly effective tool for offering students a customized, dynamic learning process. This study assesses the influence of AI-supported adaptive learning systems on student outcomes. AI-supported adaptive learning systems are capable of monitoring students' real-time performance and progress, suggesting pertinent content and providing targeted assistance for areas requiring improvement. These systems analyze student data, learning patterns, and error trends in order to identify the optimal learning path for each student. For instance, students who are experiencing difficulties with a particular subject are provided with supplementary exercises, while those who have demonstrated proficiency are presented with more advanced content, thereby optimizing the learning process to align with the specific requirements of each individual. The present study assesses the impact of AI-supported adaptive learning systems on student achievement through a series of pilot studies. The findings indicate that these systems enhance students' success rates, promote greater engagement in the classroom, and foster enhanced motivation in the learning process. In conclusion, AI-supported adaptive learning systems provide an innovative solution by adopting a student-centered approach to education, thereby enhancing both learning quality and student achievement. The extensive implementation of this technology can facilitate the development of an education system that is responsive to individual learning needs, thereby providing a valuable reference point for future educational models.

Keywords: Artificial Intelligence, Adaptive Learning, Educational Technology.

¹**Address:** Faculty of Computer Science, "Ukshin Hoti" University of Prizren, Kosovo.

***Corresponding author:** samedin.krrabaj@uni-prizren.com

Performance Analysis of Deep Learning Algorithms for Classification of EEG Signals

Muhammet Cihat Mumcu*¹, Beray İkinci², Elif Öztürk², Kubilay Ataş², Abdullah Güngör²

Abstract: Recording and analysing brain activity is an important field of study in neuroscience and medicine. Electroencephalography (EEG) is a popular non-invasive technology for recording brain activity with high time resolution. Electroencephalography (EEG) has many uses in medicine, neurology, and brain engineering. Classification of EEG signals is an important step for extracting meaningful information from these signals. Many applications rely heavily on classification, such as recognising specific brain functions or illness states, discriminating between cognitive processes, or monitoring the user's mental state. Traditional EEG classification approaches rely on statistical and machine learning algorithms to analyse retrieved information. However, these approaches may have limits in classification performance since they do not capture all of the signal's intricacy and linkages. Many methods have been developed to automatically classify EEG signals. These approaches identify non-redundant salient features from EEG time series data and feed them into a machine learning classification model. The majority of these methods extract characteristics from EEG time series utilising temporal components. The brain is a highly interconnected complex system with connections at numerous levels, including individual neurons, neuronal populations, and brain regions. These interactions, known as brain networks, are assumed to be the origin of the EEG signals collected on the scalp. As a result, a classification model that can use this network structure in the learning process may perform better.

In recent years, the tremendous success of deep learning algorithms has sparked a great deal of interest in the field of EEG signal classification. Deep learning employs artificial neural networks' multilayer structure to automatically extract features from data. Deep learning algorithms use several structures, including Convolutional Neural Networks (CNN), Recurrent Neural Networks (RNN), and Long Short-Term Memory (LSTM). These algorithms perform better on complicated and high-dimensional data, and they have the potential to improve EEG signal classification accuracy. In this study, EEG waves were classified using various deep learning methods in MATLAB. The deep learning techniques employed are Convolutional Neural Networks (CNN), Recurrent Neural Networks (RNN), and Long Short-Term Memory (LSTM). The data collection comprised EEG recordings of various brain activity.

Keywords: Electroencephalography, Signal Classification, Deep Learning Algorithms, Artificial Intelligence.

¹**Address:** Istanbul Gelisim University, Gelisim Vocational School, İstanbul/Turkiye

²**Address:** Istanbul Gelisim University, Faculty of Engineering and Architecture, İstanbul/Turkiye

***Corresponding author:** mcmumcu@gelisim.edu.tr

SMART Energy transition of traditional generation to RES

**Vehebi Sofiu¹, Nafije Shabani², Sami Gashi¹, Nexhat Balaj¹, Muhaxherin Sofiu¹,
Besa Veseli⁺¹**

Abstract: Kosovo promotes the traditional energy strategy represented by the RES related to the decarbonization of energy sustainability. The national objective of the EU has visibly increased in recent years and requires alignment with an advanced European energy strategy that eliminates energy generation from fossil fuel combustion with a transition of the RES. This research presents an algorithmic alternative to increase the investment actions needed to structure Kosovo's electro-energy mixed system to 100% with zero emissions. The objective of this work is to include all types of generation and transportation of electric vehicles to carry them into the transition of artificial intelligence in the vessel planning energy software, to evaluate SMART systems in the transition of energy storage according to the digital smart EMS system. Artificial intelligence offers a version of sustainable development in efficiency and energy effectiveness. The concept of this work supports the actors of integrated services across all sectors to facilitate the implementation of communications aimed at achieving a digital agent for the development of controls and the services. When it comes to the energy transition, it turns out that there are many new elements in the context of the future generation system, as a challenging factor to unite all types of generations with electric grid connections according to the regulatory matrix framework. The scenarios indicate that gradually the products based on CO₂ will be replaced with renewable energy sources using innovative systems.

Keywords: traditional energy, transition, storage, efficiency, clean energy, sustainable development.

¹Unievrsity for Business and Technology - Higher Education Institution, Faculty Engineer of Energy, Lagja Kalabria-street Rexhep Krasniqi, Nr.56 Prishtine, Kosovo.

²Cyril and Methodius University in Skopje, Faculty of Engineer, blvd. Goce Delcev 9, 1000 Skopje, Republic of North Macedonia

***Corresponding author:** besa.veseli@ubt-uni.net

The Impact of Ultrasounds on Convective Drying Kinetics and Properties of Fermented, Frozen/Thawed and Osmotically Dehydrated Beetroot Chips

Magdalena Zielinska*¹, Konrad W. Nowak¹, Izabela Staniszevska²,
Bartosz Pszczółkowski¹, Wojciech Rejmer¹

Abstract: The study aimed to investigate the effects of ultrasound-assisted drying on raw, fermented, frozen, and osmotically dehydrated beetroots, focusing on drying kinetics and selected nutritional and functional properties. The mechanisms of ultrasound, fermentation, freezing/thawing, and osmotic dehydration on cellular structure were also examined. Ultrasounds enhanced drying rates and reduced drying times for raw (RCUS) and osmotically dehydrated (FOCUS) beetroots due to cavitation effects, which created micro-channels and increased porosity. Fermentation increased drying rates and reduced drying times (FC) due to enzymatic breakdown of cell walls, creating a porous structure. Freezing/thawing increased porosity and water migration efficiency, leading to higher drying rates for fermented and frozen/thawed beets (FFC). Osmotic dehydration showed synergistic improvement with ultrasounds (FOCUS), increasing drying efficiency. Ultrasounds slightly reduced red color intensity. Fermentation shifted color towards green and brown-orange hues, which were further reduced by ultrasounds (FCUS). Freezing/thawing shifted color towards ruby hues, which were partially restored by ultrasounds (FFCUS). Osmotic dehydration created a shiny sugar layer, and ultrasounds even improved color stability. The results show that the highest TPC and FRAP values were found in raw samples dried with ultrasounds (RCUS). Fermentation and freezing/thawing reduced TPC and FRAP values, and they were further decreased by ultrasound-assisted drying (FFCUS). Osmotic dehydration reduced TPC and FRAP due to phenol leaching, while ultrasounds (FOCUS) improved retention compared to FOC samples. Additionally, ultrasounds increased hydroxyl group band intensity, indicating higher carbohydrate content and pigment changes. Fermentation reduced hydroxyl group bands due to sugar degradation. Freezing/thawing increased hydroxyl group bands due to higher water content, indicating pigment loss. Osmotic dehydration showed high hydroxyl group band intensity due to increased sugar content, with ultrasounds causing additional changes. These methods enhanced drying efficiency, improved microstructure, stabilized color, retained bioactive compounds, and showed distinct FTIR spectral changes. However, the complex interactions between these processes require further research to better understand the mechanisms influencing the drying kinetics of different types of beets and material properties. In order to optimize the ultrasound-assisted drying of beetroots, further studies should be carried out in terms of other processing parameters like ultrasounds power level, time and frequency of application, concentration of osmotic solution, etc. The findings can be essential for optimizing beetroot drying processes to improve quality of dried chips and energy efficiency.

Keywords: beetroots; pretreatment; drying kinetics; bioactive compounds; color, microstructure.

¹**Address:** University of Warmia and Mazury in Olsztyn, Faculty of Technical Sciences, Olsztyn, Poland

²**Address:** University of Warmia and Mazury in Olsztyn, Faculty of Food Sciences, Olsztyn, Poland

***Corresponding author:** m.zielinska@uwm.edu.pl

Developing a Graph Visualization Mechanism for Transport Route Optimization Algorithms and Creating An Efficient Visualization Method on A Dynamically Changing Situational Map

Adam Galuszka^{1*}, Tomasz Grzejszczak¹, Jaroslaw Smieja¹

Abstract: There are many components involved in LTL (Less Than Truckload) and FTL (Full Truck Load) transport planning for specific destinations in a transportation company. In this work we are focused on two key milestones of the project POIR.01.01.01-00-0142/21, titled "Development of the Polish Digital Logistics Operator – PCOL". This phase focuses on: developing a graph visualization mechanism for transport route optimization algorithms (KM1) and creating an efficient visualization method on a dynamically changing situational map (KM2). For KM1, the objective was to develop a mechanism capable of visualizing 100,000 transport routes simultaneously on graphs. This capability was successfully implemented and validated. For KM2, the goal was to create a method to visualize at least 10,000 loads/routes on a dynamic situational map, with data model updates occurring at least once every five minutes, and to support multiple levels of data aggregation. This milestone was also achieved, with the system able to visualize 10,000 loads, update data every minute, and provide dynamic aggregation with four spatial resolutions. Key tasks completed included the integration of modules within the PCOL infrastructure, ensuring compatibility and cooperation between modules, and establishing a robust infrastructure with high availability and regular backups. This infrastructure comprises two physical hosts forming a cluster through Ovirt KVM virtualization, with four virtualized environments: DEV, RC, PROD, and SRV. Services are deployed in isolated Docker containers with gateway Haproxy for HTTP and TCP traffic, and high availability is ensured by Docker Swarm orchestration and floating IPs managed by keepalived. Critical data backups are performed nightly to private AWS S3 buckets, encrypted and compressed. The development and implementation of the visualization mechanisms involved creating algorithms for Big Data clustering and feature identification for geographic area impact visualization. End-users are enabled to view maps with identified characteristic features and variable spatial resolutions. In summary, both milestones KM1 and KM2 were successfully met, with all specified parameters achieved. The project established a scalable, efficient, and dynamic visualization system that integrates well within the existing infrastructure. This document provides a detailed account of the tasks, methodologies, and technical specifics involved in achieving these milestones, along with diagrams and tables to illustrate the processes and outcomes.

Keywords: Logistics, Discrete Optimization, Machine learning-supported simulation, Real-data example

Acknowledgement: The work has been developed within grant No. POIR.01.01.01-00-0142/21 "Development of the Polish Digital Logistics Operator - PCOL" in 2024. The work of Adam Galuszka was partially supported by the SUT under BK grant - the subsidy for maintaining and developing the research potential in 2024.

¹**Address:** Silesian University of Technology, ul. Akademicka 2A, 44-100 Gliwice, Poland

***Corresponding author:** adam.galuszka@polsl.pl

Design and Implementation of a Web Based Event Management System Using Django and CSS

Kazi Rafiqul Islam*¹, Bilkis Akter Dalia¹

Abstract: Event management system (EMS) have become increasingly critical in recent years, converting how conferences are organized and attended. Traditional occasion control techniques of paper-based systems are rapidly replaced by intelligent answers that improve efficiency and decorate the user. VibeVento is event control complete programming designed to facilitate the advent, business enterprise, and participation of occasions, Whether online or offline. This overview paper offers an in-depth evaluation of VibeVento and highlights its packages, event introduction, attendance management, and user acceptance as accurate. It attracts interest and emphasizes the critical role of the admin in dealing with the general gadget. It additionally permits adaptive interfaces. VibeVento's intuitive design and sturdy functions make it a green and sensible solution for today's event management needs.

Keywords: Event Management, Django, CSS, Event Tracking

¹**Address:** International Islamic University Chittagong, Department of Computer and Communication Engineering, Chittagong/Bangladesh

***Corresponding author:** kr.rafiqul@gmail.com

A Decision Support System for Medicinal Plants

Fatih Sakar¹, Selin Su Demirkıran¹, Yiğit Kuru¹, Çağla Yurter¹, Melis Almula Karadayı*¹

Abstract: Plants that have therapeutic properties or beneficial pharmacological effects on the human or animal body are called medicinal plants. Consequently, they are processed as high-demand raw materials in the pharmaceutical industry. Due to its geographical location and agricultural potential, Türkiye has significant opportunities for the production and commercialization of medicinal plants. This study aims to utilize the diversity and agricultural potential of medicinal plants in Türkiye more efficiently. The study's primary goal is to optimize the selection of medicinal plants suitable for the Mediterranean climate and their matching with suitable soils, ensuring the maximum number of crops. Within the scope of the study, "sage", "anise", "thyme", "black cumin", and "mint"—medicinal plants with high export potential and suitable for cultivation in the Mediterranean climate are selected as decision alternatives. Soil features such as pH, organic matter content, humidity and salinity are determined as evaluation criteria. The proposed Decision Support System (DSS) is interfaced with the Python programming language and utilizes the TKinter GUI programming tool. This interface allows the user to input appropriate values and obtain results using a hybrid MCDM approach, integrating the SWARA and EDAS methods. Firstly, selected criteria are weighted using the SWARA method which is purely based on expert opinions. The user can incorporate as many expert opinions as desired. After applying the SWARA method, the DSS can apply the EDAS method and matches the optimal plant for the user's soil. While aiming to efficiently utilize the diversity and commercial potential of medicinal plants, the DSS offers a tool with a user-friendly interface to meet the increasing demand for medicinal plants in Türkiye and worldwide. Selecting medicinal plants for suitable soils optimizes costs and resources in medicinal plant cultivation. Therefore, the proposed DSS can reduce unnecessary resource usage, lower costs, and promote sustainable agricultural practices.

Keywords: Medicinal Plant, Decision Support System, MCDM, SWARA, EDAS

¹**Address:** Istanbul Medipol University, Faculty of Engineering and Natural Sciences, Istanbul/Türkiye

***Corresponding author:** makaradayi@medipol.edu.tr

Drinking Water Quality Assessment Before and After Using the Eco-Soft Cross 90 filter: Case Study

Stela Sefa¹, Elma Kodra, Eli Vyshka, Blerta Gërmënji, Drita Hima

Abstract: The quality of drinking water is a permanent concern for public health in Albania, as it is a major risk factor for high incidence of diarrhea. This has led to a decrease in people's confidence using of tap water and an increase in purchases of bottled water. The study is focused on the city of Durres which is the second largest city of Albania. During the investigation, physicochemical and bacterial parameters were analysed in order to determine the water quality from different reservoirs and collection taps at area A in city centre in Durres during the year of 2024. The objective of the study was to evaluate the quality of the drinking water prior to and following use of the Eco Soft Cross 90 Filter.

For this purpose, 5 water samples were taken from the tap and water reservoirs between January and March 2024, before the filters were installed. After installing eco soft filters, the experiment was repeated from April to June. Analyses were performed for 7 physiological chemical parameters (colour, smell, taste, turbidity, ammonia, nitrite, residual free chlorine) and 3 microbiological parameters (total coliforms, Escherichia coli, and faecal Streptococcus).

The analysis of drinking water before using the filters revealed a significant amount of free chlorine. The high levels of free chlorine in tap water make it unfit for drinking due to its unpleasant taste and odour. The EU drinking water directive stipulates that free chlorine should not exceed 0.5-2 mg/l. Any result above this level is an excess for free chlorine. After the filters were installed, the analyses showed that the tap water was in accordance with the reference values of Directive 98/83/EC.

Key words: drinking water, quality, physicochemical parameters, microbiological parameters, consumer health

¹**Address:** "Aleksander Moisiu" University, Professional Studies Faculty, Marine and Engineering Sciences Department, Durres, Albania

***Corresponding author:** stelasefa@gmail.com

Drinking Water Quality Assurance: Consumer protection for a healthy future

Elma Kodra, Stela Sefa, Erion Mali, Justin Mihani, Luiza Lluri

Abstract: Albania is one of the countries with the largest sources of drinking water in Europe, but yet today it still suffers from the problem of drinking water. Due to the amortized network of water pipes, the lack of investments as well as the demographic movements of its inhabitants, the supply of drinking water and its quality are today one of the basic problems of consumer protection.

This study aimed to assess Albanian consumers' perceptions on the quality of drinking water. The National Water Agency, Waterworks in Albania and the related Ministry's and Institute of Public Health's policies are the main subjects of this study, which aims to enhance the drinking water quality services provided to customers.

All of the recent investments made to upgrade the water supply network have been reviewed and considered for this study, along with a comparison of the results of the physicochemical and bacteriological analyses of tap water from the data of Albania's waterworks companies with published scientific studies on drinking water quality.

200 residents of various Albanian cities were surveyed, and the results showed that in order to improve the quality of drinking water for a healthy future, the following needs needed to be met: better drinking water that satisfies EU and state standards; lower tariff costs; better infrastructure for the drinking water distribution network; better wastewater management systems; and a 24-hour supply of water.

Key words: drinking water, quality assurance, consumer health

¹Address: "Aleksander Moisiu" University, Professional Studies Faculty, Marine and Engineering Sciences Department, Durres, Albania

***Corresponding author:** stelasefa@gmail.com

The Dynamics of Pollution in the Lumbardh River from Industrial Wastewater Discharges in Prizren

Sami Gashi¹, Vehebi Sofiu¹, Besa Veseli¹, Shkelzim Ukaj¹

Abstract: The effluents from wastewater and water discharges resulting from the use of water both as a raw material in production and for maintaining the cleanliness of industrial plants are among the main contributors to surface water pollution. In this study, we analyzed several physico-chemical parameters in the discharge pipelines of wastewater in the industrial zone of Prizren and their discharge into the Lumbardh River. In total, eight water samples were taken: two at the source, four in the pipelines, and two during discharge into the river. The evaluation of physico-chemical parameters was conducted on all samples in the industrial zone, which includes various mixed industries, the production of liquid detergents, and several food industries and service businesses, over the time period of May and June 2024. The study analyzed the concentrations of physico-chemical parameters such as temperature, pH, suspended solids, biochemical oxygen demand (BOD₅), chemical oxygen demand (COD), and dissolved oxygen. These parameters were analyzed to reflect the current state of pollution. It was assessed that the source water in the industrial zone was clean during the analyzed period, while the chemical parameters analyzed showed pollution in both May and June, with the most significant pollution observed at locations two and three for both time periods. In this research, the pollution concentrations ranged from 130-36 mg/l MTSS (Total Suspended Solids) in May and 122-27 mg/l MTSS in June; 244-50 mg/l BOD₅ in May, 154-34 mg/l in June; 233-111 mg/l COD in May and 133-67 mg/l in June 2024. According to the classification of polluted waters, surface water at locations two and three falls into categories II and III, while at location four, pollution decreased due to the mixing of discharge water with the flow of the Lumbardh River, which is believed to be a result of the higher surface water inflow of the river during this period. Comparing the results of the two-time intervals, higher pollution was observed in May, while at location four, the river's flow improved water quality. In other locations, the values were similar, with some parameters exceeding the allowed limits.

Keywords: Suspended Solids (TSS), Biochemical Oxygen Demand (BOD₅), Chemical Oxygen Demand (COD), Dissolved Oxygen (DO), Temperature (t).

¹**Address:** UBT, Higher Education Institution, Kosova

***Corresponding author:** vehebi.sofiu@ubt-uni.net

Neural Network Visualization for The Study of Parallel Algorithm Building Skills

Zoltan Attila Godo*¹

Abstract: In our previous studies, we have shown that algorithm building skills provide the most important foundation for later programming ability. To measure this, we developed a one-dimensional light programming system on a web interface that allows for age-independent evaluation. However, the system only tested single-threaded algorithm creation. In modern programming paradigms, multithreaded program units are coded. This requires much more complex thinking. The underlying parallel algorithm building skill can only be tested in 4D visualization. The visualizer we developed for our multiprocessor neural network, which maps each processor to a node, is precisely suited to visualize a spatial, time-varying light program. The movement of the spatial bodies, meeting and stopping each other's cascade-like starts, emulates the running of parallel programs. The subject is able to simultaneously move the spatial bodies and their interdependent behaviour. The subject tries to replicate as closely as possible the light program of the test sample. The test program measures the correctness of the solution to the task, the mathematical distance to the correct solution, the number of incorrect clicks and several time parameters such as the time between clicks. A total of 36 parameters are recorded during a single measurement, from which further calculated data series can be generated. The evaluation of the test results was compared with measures of programming ability, such as students' grades in programming or the results of solving specific programming problems. The evaluations show a strong correlation between test scores and programming ability. The visualization of the neural network is thus suitable for a valid measure of parallel algorithm building skills. The system can help in the early identification of programming talent and in advising on a career in programming. Which may even help to alleviate the shortage of programmers in the computer science profession.

Keywords: light programming , algorithm building skill , neural network , visualization

¹**Address:** University of Debrecen, Faculty of Information Technology, Debrecen/Hungary

***Corresponding author:** zoltan.godo@inf.unideb.hu

Effect of Acidic Electrolyte on Energy Storage of Supercapacitor with Pure $Ti_3C_2T_x$ MXene Film Electrodes

Aleyna Akıllı*¹, Ayşenur Özler¹, Bircan Haspulat Taymaz¹, Volkan Eskizeybek², Handan Kamaş¹

Abstract: Supercapacitors can be divided into two categories based on their charge storage mechanisms: electrical double layer capacitors (EDLCs) and pseudocapacitors. EDLCs, in which the electrode/electrolyte interface facilitates the reversible electrochemical adsorption/desorption of electrolyte ions, which is the primary method of charge storage. Meanwhile, fast ion intercalation and/or redox processes in the vicinity of a fast surface enable the faradaic process of charge storage in pseudocapacitors. Supercapacitors have emerged as one of the most widely used energy storage technologies in recent years due to its high-power density, extended life, rapid charging, and affordable price. The formula $E = \frac{1}{2} CU^2$ indicates that the electrode capacitance, C, and the operating potential window, U, impose the primary limitations on the possible energy density. The energy density of supercapacitors can be enhanced by the development of materials with higher specific capacitance and the expansion of the working potential window, which are made possible by either new electrode materials with a wider capacitive potential window or novel electrolytes with a wider stable potential window. Recently, 2D transition metal carbides, carbonitrides and nitrides (MXenes) have attracted great attention due to their high intrinsic electronic and ionic conductivity, highly accessible surface area and the presence of redox active sites. MXenes (of the formula $M_{n+1}X_nT_x$, where M is a transition metal, X is C and/or N, and T_x denotes surface functionalization) are created by selectively etching the A-group (usually group IIIA and IVA elements) layers from the MAX phases.

In this study, pure $Ti_3C_2T_x$ MXene films was synthesized by the in-situ HF method using $LiF+HCl$. MXene films are produced by vacuum filtration method. Electrochemical performance of the MXene film was investigated in a 3-electrode Swagelok cell using 3 M H_2SO_4 electrolyte to achieve high-performance supercapacitor configuration with CV, GCD, and EIS methods. The highest specific capacitance value for pure MXene was obtained as 663 F/g at a scan rate of 1 mV s⁻¹ in a expanded potential window of 2V. Additionally, excellent cycle stability performance was achieved, with only a 3% drop even after 5000 cycles.

Keywords: $Ti_3C_2T_x$ MXene, supercapacitor, operating voltage, energy density

¹**Address:** Chemical Engineering/Faculty of Engineering and Natural Sciences, Konya Technical University, Turkey,

²**Address:** Materials Science and Engineering/ Faculty of Engineering, Çanakkale 18 Mart University, Turkey

*Corresponding author: aakilli@ktun.edu.tr

Energy Efficiency for The Network Power Supply in Kosovo. Challenges and Opportunities for The Grid Infrastructure Integration of RES

Fuat Pallaska¹

Abstract: For the sustainable economic and social development based on the contemporary demand for energy networks and the uninterrupted supply of sufficient quantity and quality of power energy is one of the necessary requirements, especially for countries that are still developing, such as Kosovo. Some of the main requirements for the energy efficiency must be met in order to have quality and uninterrupted supply are: the right voltage, the availability of energy according to demand and high reliability of power supply infrastructure. Considering these requirements, the demands for qualitative and efficient energy from the Energy users have to increased recently. However, in recent times the use of energy from other forms has started to increase. RES (Renewable energy sources) now represents infrastructure grid from which the clean energy can be produced and integrated in the power supply systems. Every day there is an attempt to integrate renewable sources as much as possible into the energy network. Therefore, this paper will try to address the challenges and integration technologies for renewable energies in the grid. The problems of grid stability with renewable energy sources and their solution will be addressed in this paper. The second part of paper then continues with the integration of RES in the Energy network of Kosovo, with challenges from the changes that must be made in the current network of Kosovo after the integration of these sources for raising Energy efficiency demand from power supply systems.

Keywords: Energy efficiency, Renewable sources, Stability, Challenges, grid infrastructure, RES

¹**Address:** UBT -college -Prishtina , Kosovo.

***Corresponding author:** fuat.pallaska@ubt-uni.net

Optimal Controller Design for Load-Frequency Control in a Two-Area Power System

Kenan Yanmaz*

Abstract: The rapid increase in the world's population, the development of technology day by day, and the increase in industrialization mean that the need for electrical energy is constantly increasing. In power systems, which are defined for the process from energy production to consumption, the importance of electrical energy quality emerges at the point of generating electrical energy with high efficiency and transmitting it to the user. A two-area power system can be defined as an interconnected electric power system with two separate areas or control areas and aims to manage and balance the energy production and consumption of different areas, mostly in large-scale power grids. In two-area power systems, energy is transferred between areas to maintain system stability. In interconnected power systems, the different connected power generation regions must operate synchronously in a balanced manner. Considering that the loads in the system have a dynamic structure, the frequency and voltage values of the system are affected. Changes in the amount of power produced by the generation units in the system or changes in the demanded load will disrupt the active power balance of the system and deviations or fluctuations in the value of the system frequency will occur. For power quality, the system frequency and voltage values must be within certain limits and it is desirable that these quantities, especially the frequency, be constant to ensure power balance. In interconnected power systems with two or more areas, both generation and frequency quantities must be controlled to maintain the specified power variations of the load flowing over the tie lines. This is because, in such power systems, changes in the operating state change the frequency and the load flow over the lines. The process of keeping these quantities at their nominal values is called load frequency control (LFC). LFC is an important control mechanism, especially for large and multi-area power systems, and is of critical importance. Because a possible frequency fluctuation can cause serious problems in the system and serious damage to equipment. The task of LFC is to set the frequency to a certain nominal value and keep it constant, to exchange power between control areas by varying the active power of generators, and to share the variation in generation between units to minimize operating costs. In this study, classical PI controllers and fractional order PID controllers are used in both areas for a two-area power system. Similar studies in the literature have been reviewed and the parameters of these controllers have been calculated by running the system repeatedly with the Coati Optimization Algorithm (COA) their optimum values have been calculated and it is observed that the performance is better.

Keywords: Two-area power system, Load frequency control, Coati Optimization Algorithm.

¹**Address:** Giresun University, Bulancak Vocational School, Giresun/Turkiye

***Corresponding author:** kenan.yanmaz@giresun.edu.tr

Evaluation of Photovoltaic System Capacity For Self-Sustaining Irrigation System in Kosovo

Nexhmi Krasniqi¹, Armend Ymeri^{2*}, Kadri Kadriu³, Banush Dragusha⁴

Abstract: This paper presents an assessment of photovoltaic (PV) system capacity for autonomous irrigation systems in Kosovo, evaluating the feasibility and effectiveness of solar power in meeting the energy demands of agricultural water management. The study focuses on quantifying the PV system's capacity to sustainably power autonomous irrigation technologies, considering Kosovo's specific geographical and climatic conditions. Key aspects such as PV system efficiency, reliability under varying weather conditions, and economic viability compared to conventional power sources are analysed. In practice, average daily solar radiation, often expressed as "peak sun hours" (kWh/m²/day), is crucial for estimating PV system energy generation. Geographic Information System (GIS) tools highlight peak solar radiation periods, notably in June, July, and August, coinciding with peak irrigation needs. Findings from this research provide insights into the potential integration of renewable energy solutions for enhancing agricultural productivity and sustainability in Kosovo.

Keywords: Photovoltaic System, Solar Modules, Water Pump, Drip Irrigation, PV GIS, Power.

¹**Address:** Energy Engineering, University for Business and Technology, Pristina, 10000, Kosovo.

***Corresponding author:** armend.ymeri@ubt-uni.net

Evaluation of Antibacterial Activity of ZnO-NP Synthesized by Different Methods on *Staphylococcus aureus*

Ummahan Temel¹, Caner Vural*¹

Abstract: Nanotechnology is a multidisciplinary field with a wide range of applications based on fabrication, design, and special properties of nanoscale materials (1-100 nm). These nanoparticles (NP) offer unique physicochemical properties due to their high surface area, thermal conductivity, and quantum effects. Chemical precipitation, gas condensation, sonochemical, and sol-gel methods are used in synthesizing the NPs. These different methods can influence the properties of NPs and their application potential. Antibiotic-resistant bacteria pose a significant problem, particularly in hospital settings, by limiting the effectiveness of traditional antibiotics. Pathogenic bacteria such as *Staphylococcus aureus* are among these resistant bacteria and represent a major threat to healthcare systems. The high surface area and nanoscale size of ZnO-NP allow them to effectively penetrate the bacterial cell membranes. These properties enable ZnO-NP to create an effective antibacterial mechanism and make it difficult for bacteria to develop resistance. Due to these characteristics, ZnO-NPs are attracting attention, particularly for their potential for antibacterial activities. The antibacterial activity of chemically synthesized (dried and calcined) ZnO-NP forms was investigated in this study. In addition, the minimum inhibitory concentration (MIC) and minimum bactericidal concentration (MBC) values were determined. Agar diffusion tests confirmed the strong antibacterial activity of ZnO-NP against *S. aureus*. The results indicate that the prepared ZnO-NPs provide an effective alternative treatment option against pathogenic bacteria and may be a potential solution to antibiotic resistance.

Keywords: Biofilm, nanoparticles, *S.aureus*, antibacterial activity

¹**Address:** Pamukkale University, Faculty of Science, Department of Biology, Denizli/Türkiye

***Corresponding author:** canervural@gmail.com

Performance indicators of the general cargo terminal. The case of Durres Port

¹Osman Metalla, ²Shpetim Pupa, ³Indrit Bimi, ⁴Eduart Ndokaj, ⁵Keidi Metalla

Abstract: Durres Port is the largest seaport in Albania. It comprises four terminals: A general cargo terminal (GCT) or west Terminal, a Container terminal, a Ferry terminal, and a bulk cargo terminal or an east Terminal. The performance measurement of general cargo terminals is critical for enhancing operational efficiency, ensuring competitiveness, and supporting economic growth. This paper evaluates the performance of the general cargo terminal at the Port of Durrës, Albania's largest seaport. The study identifies key performance indicators (KPIs) influencing terminal efficiency, including cargo handling rate, berth utilization, turnaround time, and traffic congestion for the Terminal. Through a comprehensive analysis, the paper highlights the challenges faced by the Terminal, such as infrastructure limitations, technological gaps, and regulatory constraints. It also explores improvement opportunities, including adopting modern technologies, capacity expansion, and operations optimization. The findings provide valuable insights for Durre's port authority and operators, offering recommendations to enhance the Terminal's performance and positioning the Port of Durrës as a more competitive player in the regional maritime industry.

Keywords: Durres port, Performance, Congestion Factor, Berth Utilization,

^{1,2,4} Department of Engineering and Maritime Sciences, Faculty of Professional Studies, "Aleksander Moisiu" University, Durres, Albania

³Department of Technical Medical Sciences, Faculty of Professional Studies, "Aleksander Moisiu" University, Durres, Albania

⁵Bachelor ⁵Diploma in Global Economics and Management, Jacobs University, Bremen, Germany

*Corresponding author: osmanmetalla@uamd.edu.al

1. INTRODUCTION

The Port of Durrës stands as Albania's main and largest port, handling a significant portion of the nation's imports. In fact, it manages 63.3% of national imports and 44.7% of exports (INSTAT, 2023). When it comes to seaborne cargo, Durrës is responsible for over 95% of all seaborne cargo handled in Albanian seaports. This port is home to four terminals: the west Terminal, or the Terminal of general cargo; the containers terminal, the ferry terminal; and the east Terminal, or the bulk cargo terminal. Out of these, the west Terminal, or the general cargo terminal (GCT), is the only Terminal that Durrës Port Authority operates; the rest are concessions out. Figure 1 below shows the layout of the Terminal.

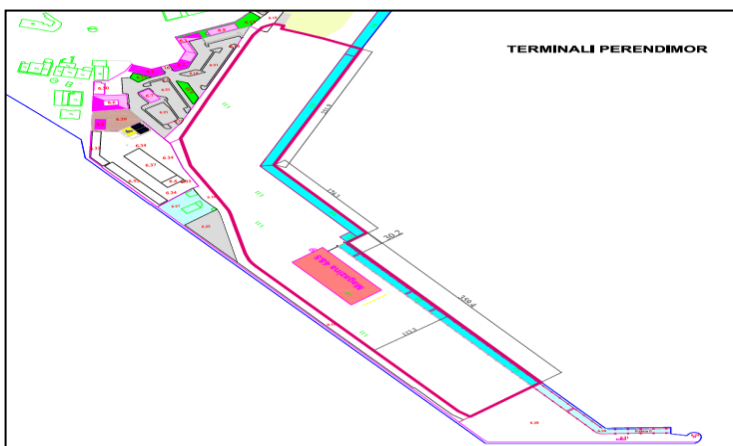


Fig. 1. The layout of West Terminal

Source: Google Earth Picture

The Terminal is in the western part of Durres Port and comprises berths 1-1, 1-2, 1-3, 1-4, and 1-5. Berth 1-3 has only a small offset of some 30m and can, therefore, be ignored as a commercially functional berth.

Table 1. Wets terminal composition

Berth	Length
1 and 2	359.4
3	30.2
4	174.3
5	251.9
Total length	785,6

Source: DPA

Considerable volumes of cargo are handled in direct load mode. This leads to a comparably low demand for storage capacities and slow quayside operations, as truck availability can only sometimes be maintained to meet the cranes' potential productivity rate. In addition to direct load, the bunker hoppers at berths 1-5 are also used to store grain and other cereals for mid-term periods. These bunker hoppers have capacities of max. 300 tones each. Four bunker hoppers are available; the maximum storage capacity is 1,200 tons. However, the cargo must be removed from the hoppers before the next discharging operations commence. DPA manages only quayside equipment; the stevedoring companies own almost all the stacking, transport, and handling equipment. The following quantities and types of quayside equipment are currently allocated to WTD by DPA and available for takeover by the concessionaire (HPC, 2017).

Table 2. Quayside equipment, west Terminal

No.	Quantity	Type	Capacity	Age (years)
1	1	Quay Crane	45t	22
2	2	Quay Crane	10t	28
3	2	Grabs	8cbm	15
4	2	Grabs	3cbm	20

Table 3 below shows the types and lot sizes of the cargo handled at the West Terminal.

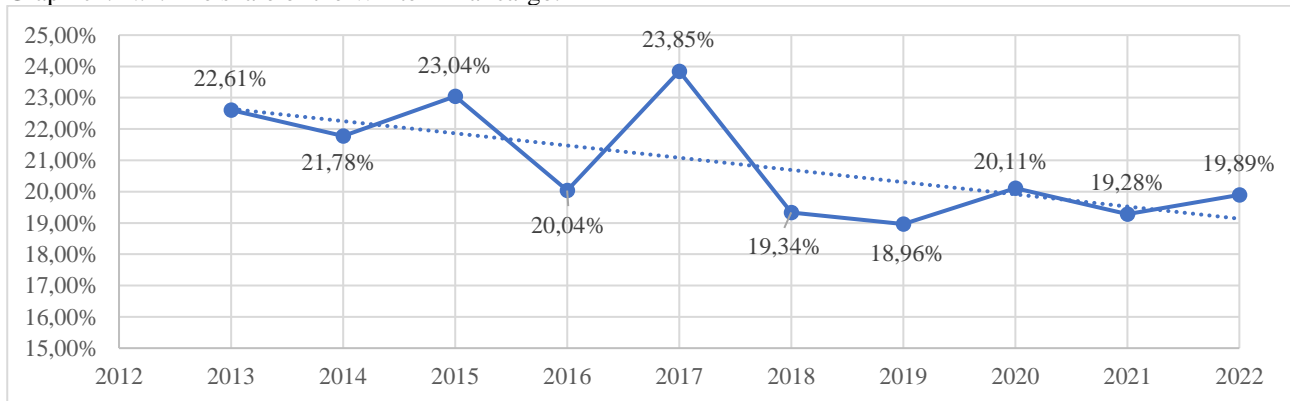
Table 3. Indicators of the West Terminal

Commodity	Calls	Av. Time Berthed	TTL Time Berthed	Av. Tonnes / Vessel W-Hour	Av. Lot Size	Max Lot Size
<i>Bulk</i>						
Grain, Corn, Oil Cake, etc.	116	44	5,113	112	2,714	6,600
Fertilizers	35	49	1,714	59	2,131	3,560
Cement	57	63	3,588	84	1,745	12,900
<i>Break Bulk</i>						
Steel, Metal Products	73	38	2,779	173	1,633	9,420
Wood Panels	12	33	396	99	2,652	3,276
Edibles	24	45	1,118	22	840	1,703
Stones	4	27	105	69	1,607	2,003
Glass	8	73	580	33	2,058	2,457
Salt	1	27	36	139	3,200	3,200
Ferrosilite	1	19	25	106	1,596	1,596
Lime	2	65	152	21	1,274	1,313
Machinery	10	36	355	24	631	2,252
Water	1	30	30	36	947	947
Detergents	1	81	81	16	1,208	1,208
Other	9	42	387	24	912	2,835

Source: DPA

Due to the continuous increase of (Osman Metalla, 2020) containerized cargoes, the volumes of cargoes transported by general cargo ships have been reduced, and the total share of the cargo handled at the west Terminal has dropped from 23,85% in 2017, which was the peak of the total cargo share, to 19,89% of the total cargo (Osman Metalla, 2020). The graphic below shows the share of the west Terminal versus the total cargo handled in Durres Port.

Graphic1. N.1. The share of the WT terminal cargo.

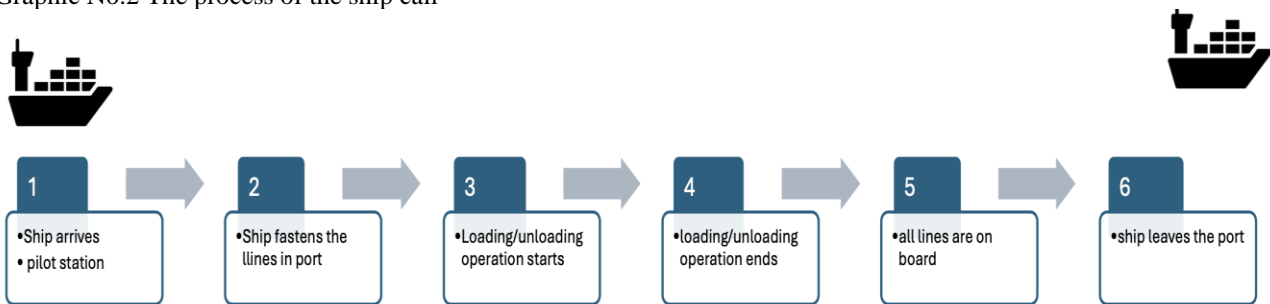


Source: adapted by author

2. METHODOLOGY

To analyze the performance of the West Terminal, the following indicators (UN, 1976) were considered: the average time of ships in port, the average berthing time, the average working time of a ship, the average idle time, the average cargo quantity handled daily in this Terminal, the average ton/meter of quay length, and the average tonnage of the ships (GT and DWT) that have called the West Terminal. To calculate the average time the ship spends in port, it is important to note the time the ship arrives at the pilot station when she enters the port, fastens all lines, and is ready for the loading/unloading operation, when the first lift starts, and the last lift ends, when the lines are up and when the ship leaves the port. All these elements are shown graphically in the following graph No. 2 below:

Graphic No.2 The process of the ship call



Source: adopted by authors

After collecting the data for the west Terminal, we calculated the congestion factor for the Terminal. The congestion factor was computed considering the time the ship stayed at the pilot station waiting for instructions to enter the port and the time the ship spent at berth. Then, the berth occupancy rate was computed. To do that, we have divided the working hours of the ship at berth with the total number of hours the ship stayed at berth.

3. RESULTS

The data we analyzed in this paper refer to the first five months of 2022. The following table shows the main data for the five individual quays of the west Terminal.

Table 4. Main data for each quay, West Terminal

Quay	No. of calls	Main cargo types handled	Total quantity tons (Jan – May)	Average time at berth (hrs)	Daily handling rate	Tons/linear meter of quay
1	16	Cement, wood panels, soya beans, iron, edibles	42 820,58	104,16	704,84	228,987
2	17	Cement, grain, fertilizer, soya beans	51 996,60	74,40	1 235,34	178,68
3	-	-	-	-	-	-
4	24	Grain, wooden panels, fertilizer, cement, urea, etc.	72 970,70	70,56	1 063,43	419,37
5	53	Glass, iron, marble stones, etc.	145 674,96	51,84	1 676,22	617,27

Source: adopted by authors

To calculate the berth occupancy rate (BOR), we computed the time the ship stayed at the berth and the time the berth was available for the ships to be berthed. Table 5 presents the data regarding the ship's time at berth and the available time of the berth.

Table 5. Berth occupancy rate

Quay	Time of ship at berth (hrs)	Available time (hrs)	Berth occupancy rate
1	1667	3624	45,99%
2	1268	3624	34,98%
3	-	-	-
4	1694	3624	46,74%
5	2742	3624	75,66%
West Terminal	7372	14496	50,85%

Terminal congestion happens when a vessel arrives at the pilot station but cannot enter the port because the berth where it is to operate is occupied by another vessel. Terminal congestion issues can happen due to various factors, such as supply chain delays, low terminal handling rates, failure of equipment, or other external factors. The West Terminal congestion factor is another important performance indicator we have computed to evaluate the Terminal's overall performance. We compute each berth's congestion factor and then calculate the overall Terminal congestion factor (BEACON, n.d.).

Table 6. Congestion factor of West Terminal

Quay	Number of calls	Tons handled	Waiting time at pilot station	Time at berth	Congestion factor
1	16	42 821	259	1 667	0,16
2	17	51 997	446	1268	0,35
3	-	-	-	-	-
4	24	72 971	585	1 694	0,35
5	53	145 675	627	2 742	0,23
West Terminal	110	313 463	1 918	7 372	0,26

Effective working hours (the time the ship is being handled) were computed by dividing the ship's working time by the time spent at the berth. We have calculated each berth's working hours and the terminal effective time (Mokhatar, 2013). Table 7 below shows the results of the berth and terminal usage rate.

Table No. 7 West terminal productivity

Quay number	Hours at berth	Hours available	Berth productivity
1	1 491	1 676	89,44%
2	1 023	1 268	80,67%
3	-	-	-
4	1 474	1 694	87,01%
5	2 198	2 742	80,16%
West Terminal	6 186	7 372	83,91%

4. DISCUSSION

Even though the volume of general cargo in Durres Port is likely to be reduced due to the continuous increase of containerized cargoes, the West Terminal remains an important terminal for Durres Port. Such materials as iron, pieces of machinery, wooden panels, fertilizers, urea, edibles, etc., will continue to be transported by general cargo vessels. Grain remains another commodity that will continue to be handled in this Terminal. Considering the enlargement of the container terminal and the need for more yard spaces (Osman et al., 2015), parts of the West Terminal area, particularly at quay 4 and 5, are being used by this Terminal. This results in less terminal yard area for the West Terminal.

Consequently, terminal performance is very important. The higher the performance, the lower the congestion factor, the lower the berth occupancy rate, and the higher the terminal productivity rate. The results of section 4 show that the Terminal's berth occupancy rate is 50,85%, which reveals that the Terminal can handle more ships and increase the annual cargo throughput. Due to the different nature of cargoes in different quays, the average time at berth varies from 104,16 hrs. at quay 1 to 51,84 hrs. at quay 5.

The congestion factor for the West Terminal was 0.26, which shows that the time the ship waits to enter the port and the Terminal is relatively short. This is another positive indicator for the Terminal, which indicates that there is still unused potential.

Based on the results above, the berth usage rate is relatively high, with an average of 83,91% for the West terminal. Quay 4 is where the idle time is reduced compared to other quays.

5. CONCLUSIONS

The paper highlights a shift in cargo types at the port with a decrease in general cargo due to the rise of containerized cargo. Despite this, the West Terminal remains crucial for handling specific types of general cargo such as iron, machinery, wooden panels, fertilizers, and grain.

Developments in other terminals of Durres port are reducing the terminal space of the West terminal, which is an appeal for higher terminal productivity. Based on the results of the observations done, with a berth occupation rate of 50.85%, the West Terminal has significant capacity to accommodate more ships, suggesting it can handle increased cargo throughput.

There is a notable variation in average berth time across different quays, ranging from 51.84 hours at quay 5 to 104.16 hours at quay 1. This variation may reflect differing operational efficiencies or cargo handling processes at each quay.

A congestion factor of 0.26 indicates that ships experience relatively short waiting times to enter the port and Terminal, suggesting efficient management and operational flow.

The relatively low congestion factor and high berth occupancy rate suggest that the West Terminal has additional capacity and the potential to handle more ships and cargo.

Overall, the West Terminal at Durres Port is performing well but faces challenges due to the reduction in available space caused by the container terminal's expansion. Effective management and optimization of berth and yard space are crucial to maintaining and enhancing the Terminal's performance.

Author Contributions

All authors have read and agreed to the published version of the manuscript.

Conflict of Interest

The authors have no conflicts of interest to declare.

Funding

The authors declared that this study has received no financial support.

REFERENCES

INSTAT. (2023). Albania in figures 2022. Tirana: INSTAT.

Osman Metalla, E. K. (2020, December). Durres's container terminal cargo demand analyses and reallocation of Terminal. *International Journal of advanced research in engineering and technology (IJARET)*, 11(12), 2215-2223.

HPC, H. P. (2017). Feasibility Study Durres West Terminal. Hamburg Germany: HPC.

UN. (1976). Port performance Indicators. United Nations Conference on Trade And Development.

BEACON. (n.d.). Beacon port congestion report. Retrieved from https://26871664.fs1.hubspotusercontent-eu1.net/hubfs/26871664/Reports/Beacon-port-congestion-report.pdf?utm_campaign=Port%20congestion&utm_medium=email&_hsenc=p2ANqtz-_vZcOCy515e9r-jpwYzjKbkj9G0Zl6sBmaSrED24cIMo7WWZKkk-9-A1RseF2hbd-B3RteP0hsWCf1O5ULQ8CZA

Mokhatar, K. &. (2013). Efficiency of operations in Container terminal method. *European Journal of Business and Management*, 5, 91-106.

Osman Metalla, E. V. (2015, October). Defining the most important port performance indicators: A case of Albanian Ports. *International Journal of Economics, Commerce and Management*, III(10), pp. 808–819.

Hydrogen and Power Generation with PVT-Assisted ORC Using LNG Cold Energy for Low Temperature Applications

Gamze Soy Turk, Onder Kizilkan*

Abstract: This study investigates the performance of a novel hybrid system for power generation, integrating hydrogen production and a photovoltaic-thermal (PVT) assisted Organic Rankine Cycle (ORC) utilizing liquefied natural gas (LNG) cold energy. The proposed system addresses the challenges of low-temperature applications by synergistically utilizing LNG cold energy to enhance the efficiency of power generation processes. By harnessing solar energy through PVT panels and utilizing LNG cold energy, the system aims to optimize energy utilization and increase overall efficiency. The aim is to evaluate the performance and efficiency of the system by considering the effect of various working fluids in the ORC. Commonly studied working fluids such as R1234yf, R134a, R245fa, and R141b are evaluated according to their thermodynamic properties, environmental properties, power generation, energy, and exergy efficiency. The results show that the highest ORC power generation rate of 26.6 kW was calculated for the cycle using R141b, followed by R245fa. In addition, parametric studies are also carried out to determine the effect of system parameters on cycle performances.

Keywords: PVT, ORC, LNG, Hydrogen Production, Energy, Exergy

Address: Isparta University of Applied Sciences, Faculty of Technology, Department of Mechanical Engineering, Isparta, Türkiye

*Corresponding author: onderkizilkan@isparta.edu.tr

1. INTRODUCTION

For the last decades, different measures have been implemented globally to address climate change, including the promotion of renewable energy sources, particularly solar energy, which holds promise for meeting future energy needs. Solar energy is mostly utilized for two different objectives: generating thermal energy and producing electrical energy. Photovoltaic (PV) panels are utilized to transform solar energy into electric energy. Converting solar energy into electricity through PV is the most advantageous means of utilizing solar power (Kumar et al., 2015), and because of its environmental and economic benefits as a clean energy source for power generation, PV technology has gained substantial attention from scientists, manufacturers, and policymakers. Presently, the efficiency range for converting solar radiation into electricity using PV panels falls between 12% and 18%, with up to 80% of solar irradiation being either converted to heat energy or reflected (Al-Waeli et al., 2017; Sathe and Dhoble, 2017). The operational temperature of PV panels is widely acknowledged to significantly impact their performance, with efficiency decreasing as solar cell temperature rises (Ji et al., 2009; Al-Nimr and Al-Ammari, 2019). Studies have indicated that a one-degree Celsius increase in solar cell temperature can lead to an efficiency reduction of 0.25% to 0.45% for various solar cell types (Kasaeian et al., 2018). While thermal energy generated by PV cells typically goes unused, there exists potential to harness and utilize this energy for solar thermal applications such as tap water heating, space heating, and solar cooling, showcasing high cost-effectiveness under specific economic conditions (Mittelman et al., 2009). To address the limitations posed by reduced electricity generation efficiency in PV technology due to increased operating temperatures, the integration of photovoltaic-thermal (PVT) collectors has been proposed. PVT collectors merge photovoltaic and thermal components into a unified system, enabling simultaneous power and thermal energy production. The concept and design of PVT panels aim to improve the electrical efficiency of photovoltaic modules when operating at elevated temperatures (Hussain et al., 2013). In recent years, there has been a surge in global interest in PVT (photovoltaic-thermal) technology. Reported PVT systems commonly utilize water and air for the thermal aspect of the process. Additionally, significant progress has been made in developing highly efficient PV cells capable of effectively capturing and converting light into electrical current. Numerous design principles have emerged in this domain (Moradi et al., 2013). Scientific literature indicates a substantial body of research focusing on integrating PVTs with various thermal applications to utilize waste heat effectively, such as integrating PVT with thermoelectric generator modules (Salari et al., 2020), heat pumps (Zhao et al., 2011), hot water production (Dubey and Tiwari, 2008), air heating (Guiavarch and Peuportier, 2006), among others.

Integrating PVT collectors with Organic Rankine Cycle (ORC) and refrigeration cycles presents an emerging alternative in integrated solar systems. However, PVT modules typically achieve limited temperatures within the 40–

60°C range with acceptable efficiency. Some applications may necessitate inlet temperatures higher than what PVT collectors can provide for satisfactory performance (Mittelman et al., 2009). To enhance the effectiveness of solar modules, concentrated photovoltaic thermal (CPVT) systems have been developed, concentrating solar radiation onto PV modules (Hosseini and Butler, 2021). With concentration, collector temperatures can surpass 100°C, enabling the utilization of heat energy for moderate-temperature processes like absorption refrigeration (Mittelman et al., 2007), desalination (Mittelman et al., 2009), and steam generation, particularly for ORC. Kosmadakis et al. (2011) conducted an evaluation of an ORC driven by CPVT, a study parallel to research by Golonis et al. (2021), where CPVT supplied heat temperatures for the ORC ranging between 70 and 90°C, alongside an economic analysis. Kurs and Okten (2019) conducted analyses investigating the impact of preheating the ORC with CPVT collectors, incorporating a hydrogen generation unit, and analyzing different operating parameters. Another study proposed by Hosseini and Butler (Hosseini and Butler, 2021) explored a CPVT-based ORC system for hydrogen production, with energy demand for hydrogen production and storage supplied by the CPVT-ORC system.

This study examined the system, which consists of PVT-supported LNG and ORC cycles designed to produce hydrogen and energy, from a thermodynamic perspective. Additionally, the effects of using four different working fluids, namely R1234yf, R134a, R245fa, and R141b, on the system performance were examined. Parametric studies were conducted to determine the effect of solar radiation on system performance.

2. SYSTEM DESCRIPTION

Figure 1 shows the schematic representation of the system consisting of PVT-supported ORC and LNG cycles. LNG is commonly used as a fuel for various applications, and during its storage and transportation, a significant amount of cold energy is wasted. The system incorporates a heat exchanger to capture this cold energy and transfer it to the ORC system for power generation. The ORC is a thermodynamic cycle that uses an organic working fluid instead of water to generate power from heat sources at lower temperatures. In this system, the LNG cold energy is used as the heat source for the ORC. The ORC operates by vaporizing the organic fluid at low temperatures, expanding it through a turbine to generate mechanical power, and then condensing it back into a liquid using the cold energy from LNG. The mechanical power generated by the ORC turbine can be converted into electricity using a generator. PVT panels combine photovoltaic (PV) and solar thermal technologies to generate both electricity and heat simultaneously. The PV cells convert sunlight into electricity, while the thermal component absorbs excess heat and transfers it to a fluid for various applications. In this system, PVT panels are utilized to supplement the energy generation process by providing additional electricity and thermal energy. The excess electricity generated by the ORC and PVT panels can be used to electrolyze water, separating it into hydrogen and oxygen. Hydrogen is a versatile energy carrier that can be used in various applications, including fuel cells for electricity generation or as a clean fuel for transportation.

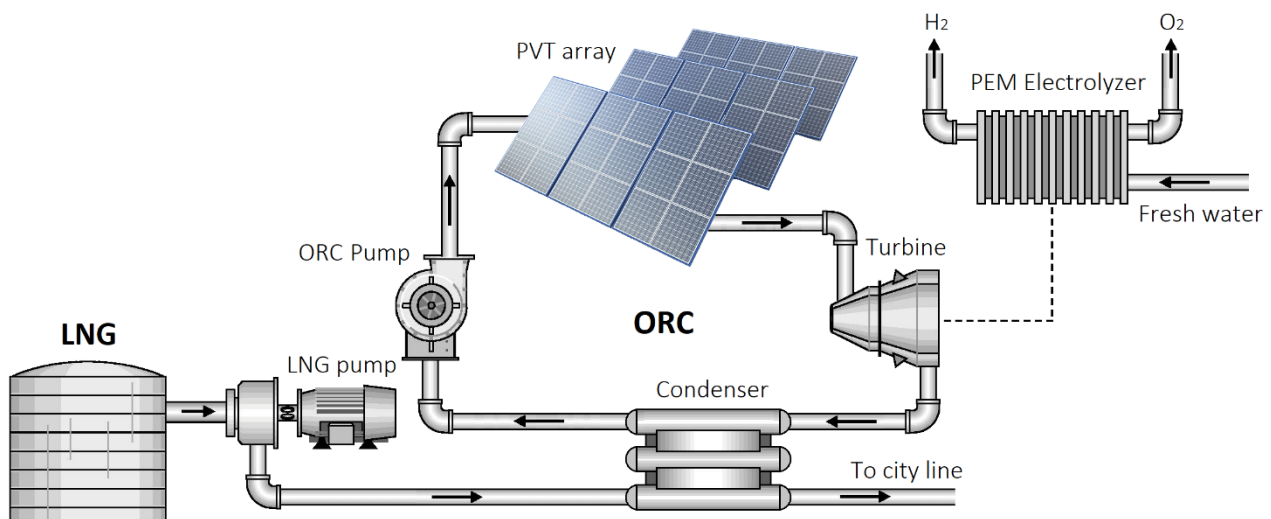


Figure 1. Schematic representation of the system consisting of PVT-assisted ORC with LNG

3. THERMODYNAMIC ANALYSIS

In this subchapter, a detailed definition of the thermodynamic methodology utilized in this paper is introduced. Energy and exergy analyses are performed using the EES (Engineering Equation Software) program for the system's performance evaluation. In this paper, the thermodynamic analysis is made under the following assumptions:

- The system operates at steady-state conditions.
- Kinetic and potential energies and exergy changes are ignored.
- Pressure is constant in the heat exchangers.
- There are no heat losses in the heat exchangers.
- The turbine and pump operations are assumed to be adiabatic.
- The reference state properties are 22°C and 100 kPa.

The mass balance equation for steady-state and steady-flow processes can be written as (Cengel and Boles, 2006):

$$\sum \dot{m}_{in} = \sum \dot{m}_{out} \quad (1)$$

In the above equation, \dot{m} is the mass flow rate, and the subscripts *in* and *out* stand for inlet and outlet, respectively. The energy balance equation can be written as:

$$\dot{Q} + \sum \dot{m}_{in} h_{in} = \dot{W} + \sum \dot{m}_{out} h_{out} \quad (2)$$

Here, \dot{Q} is the rate of heat, \dot{W} is the rate of work, and h is the specific enthalpy. For the exergy analysis, the balance equation is defined as (Dincer and Rosen, 2007):

$$\dot{E}x_Q - \dot{E}x_W = \sum \dot{E}x_{in} - \sum \dot{E}x_{out} + \dot{E}x_{dest} \quad (3)$$

where the first and the second terms are exergy of heat and work respectively, $\dot{E}x$ is the rate of flow exergy, $\dot{E}x_{dest}$ is exergy destruction. In the above equation, each term is defined as follows:

$$\dot{E}x_Q = \dot{Q} \left(\frac{T - T_0}{T} \right) \quad (4)$$

$$\dot{E}x_W = \dot{W} \quad (5)$$

$$\dot{E}x = \dot{m} ex \quad (6)$$

$$\dot{E}x_{dest} = T_0 \dot{S}_{gen} \quad (7)$$

In equation (8), ex is the specific flow exergy and can be calculated using the equation below:

$$e = (h - h_0) - T_0(s - s_0) \quad (8)$$

4. RESULTS

In this study, an intricately integrated system comprising PVT, PEM electrolyzer, LNG, and an ORC systems is meticulously designed. A comprehensive comparative analysis of energy and exergy is conducted, evaluating various working fluids within the designed system. The design parameters of this integrated system, essential for understanding its operational dynamics, are meticulously outlined in Table 1.

Figure 2 presents a pivotal aspect of the study, showcasing the net power output and hydrogen production of the ORC system across different working fluids. The findings reveal intriguing insights: the utilization of R141b yields the highest net power output, reaching a substantial 26.6 kW, surpassing other working fluids such as R245fa, R134a, and R1234yf. Furthermore, the study unveils that when R141b is employed, the ORC system exhibits a remarkable hydrogen production rate, peaking at 478.4 g/hour. These revelations underscore the critical role of working fluid selection in dictating system performance and underscore the potential of R141b for maximizing both power generation and hydrogen production within the integrated system framework.

Table 1. Design parameters for the proposed multi-generation system

Design Parameters	Values
PV/T length, [m]	1.649
PV/T width [m]	0.992
Number of PV/T [-]	200
Number of pipes [-]	10
PVT packing factor	0.9
Mass flow rate for one pipe [kg/s]	0.007
Reference temperature [°C]	20
Reference pressure [kPa]	101.325
Solar radiation [W/m ²]	800
Wind speed [m/s]	2
Temperature of the sun [K]	5770

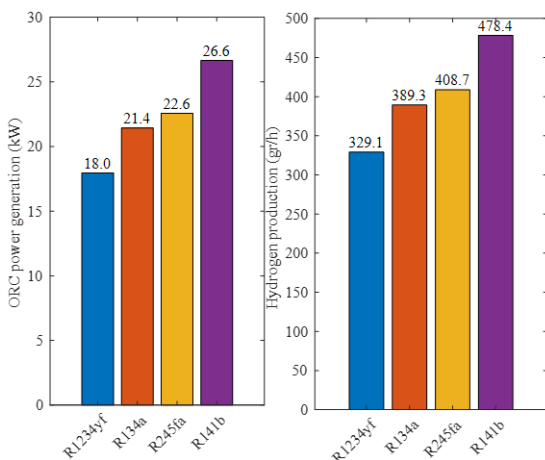


Figure 2. ORC power generation and hydrogen production for different working fluids

Figure 3-a provides a detailed analysis of the net power production and total exergy destruction within the PVT system across various working fluids. The findings reveal intriguing trends: the utilization of R134a yields the highest PVT power production, reaching an impressive 19.4 kW, followed closely by R1234yf, R134a, and R245fa. Furthermore, the study identifies a substantial exergy destruction peak of 217.2 kW when R1234yf is employed, contrasting with the least exergy destruction observed with R141b, calculated at 213.9 kW. In Figure 3-b, the focus shifts to the overall energy efficiency and exergy efficiency of the system across diverse working fluids. The data showcases notable variations in efficiency metrics: the utilization of R141b demonstrates the highest energy efficiency at 21.4%, outperforming other fluids such as R245fa, R134a, and R1234yf. Similarly, when considering exergy efficiency, R1234yf emerges as the optimal choice, mirroring its performance in energy efficiency. These findings underscore the significance of selecting the most suitable working fluid to achieve optimal system performance, balancing energy and exergy efficiency considerations to enhance the overall effectiveness and sustainability of the integrated system.

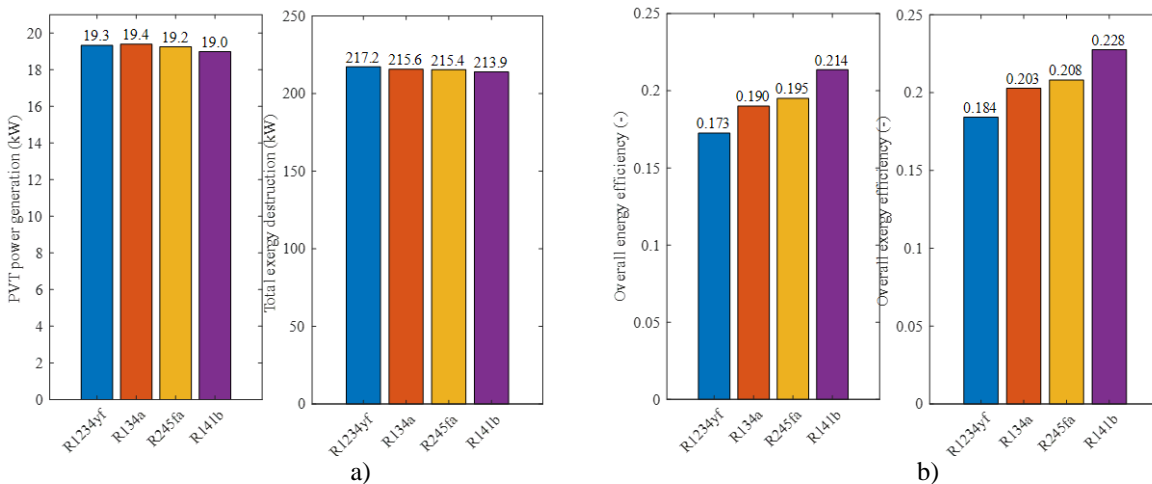


Figure 3. a) PVT power generation and total exergy b) Overall energy efficiency and overall exergy efficiency

In the second phase of the study, parametric studies were conducted to investigate the influence of solar radiation on the overall performance of the system. Figure 4 provides a comprehensive analysis of the effect of solar radiation on ORC power production. The findings reveal a consistent trend: as solar radiation levels increase from 500 W/m² to 950 W/m², there is a corresponding rise in ORC power production across all working fluids. This observation underscores the direct correlation between solar radiation intensity and the system's power output, highlighting the significance of solar energy as a primary driver of ORC performance. In Figure 5, the focus shifts to the effect of solar radiation on the refrigerant temperature at the outlet of the photovoltaic-thermal (PVT) system. The data illustrates a clear relationship: as solar radiation levels escalate from 500 W/m² to 950 W/m², the refrigerant temperature at the PVT outlet exhibits a noticeable increase. This phenomenon can be attributed to the enhanced heat transfer mechanisms facilitated by higher solar radiation levels. With increased solar energy absorption by the PVT collectors, more heat is transferred to the working fluid (refrigerant), elevating its temperature as it traverses through the system.

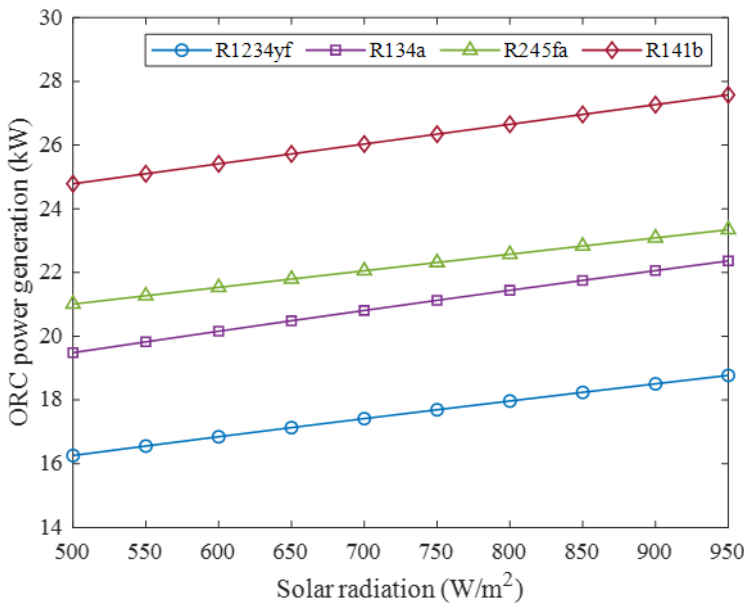


Figure 4. Effect of solar radiation on ORC power generation for different working fluid

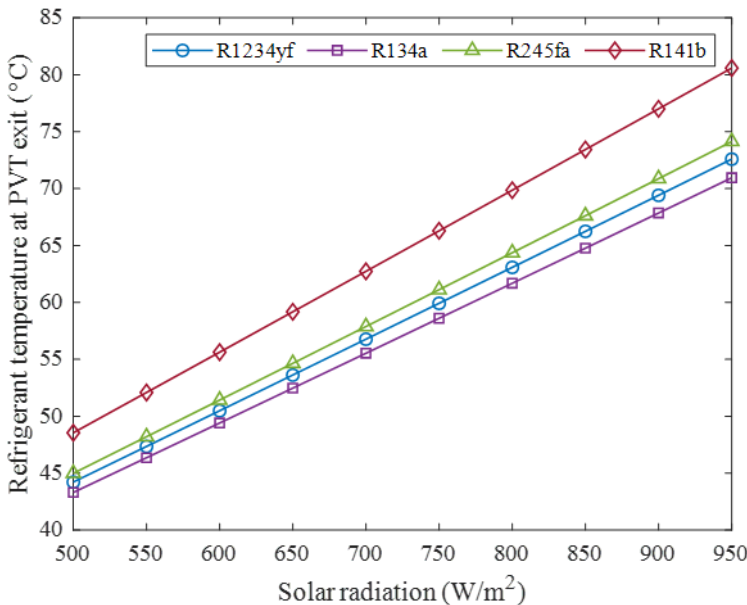


Figure 5. Effect of solar radiation on the refrigerant temperature at PVT exit for different working fluid

Figure 6 provides insight into the impact of solar radiation on total exergy destruction within the system. The data depicted in the figure reveals a consistent trend: as solar radiation levels escalate from 500 W/m² to 950 W/m², there is a

corresponding increase in exergy destruction across all working fluids. This phenomenon can be attributed to the elevated solar radiation levels, which lead to higher refrigerant temperatures within the system. As the refrigerant temperature rises, the system may encounter greater thermodynamic inefficiencies. These inefficiencies, represented as exergy destruction, signify the portion of energy within the system that cannot be converted into useful work due to irreversibilities. Thus, the observed increase in exergy destruction underscores the importance of managing system temperatures and optimizing operational parameters to mitigate thermodynamic losses and enhance overall system efficiency. In Figure 7, the focus shifts to the effect of solar radiation on photovoltaic-thermal (PVT) power generation. The data presented in the figure demonstrates a clear correlation: as solar radiation levels rise, PVT power production increases across all working fluids. This relationship is rooted in the fundamental operation of the PVT system, wherein the photovoltaic component directly converts incident solar radiation into electrical energy.

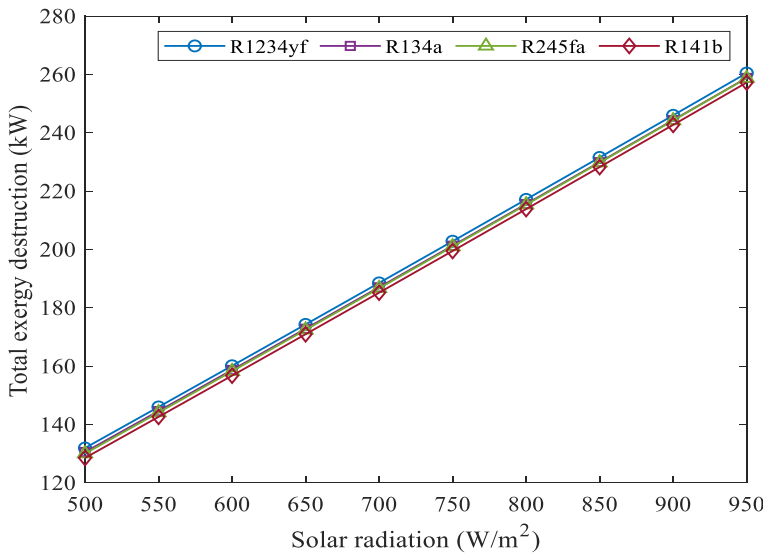


Figure 6. Effect of solar radiation on total exergy destruction for different working fluid

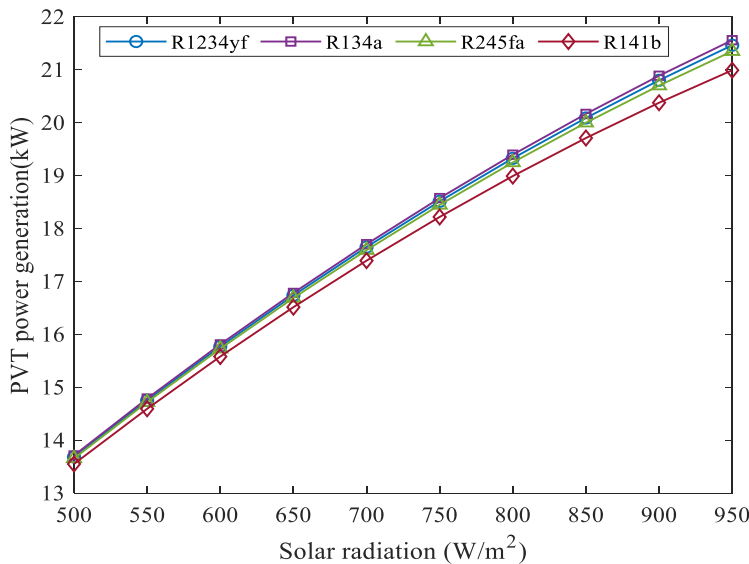


Figure 7. Effect of solar radiation on PVT power generation for different working fluid

Figure 8 provides a comprehensive illustration of the impact of solar radiation on energy efficiency within the system. The data depicted in the figure elucidates a significant trend: as solar radiation levels escalate, there is a corresponding decrease in energy efficiency across all working fluids. This phenomenon can be attributed to the escalating temperature difference between the primary heat source (solar radiation) and the working fluid (refrigerant) within the system. As solar radiation intensifies, so does the temperature gradient, amplifying the potential for thermodynamic irreversibilities in the heat transfer processes. These irreversibilities, which manifest as entropy generation, contribute to a decline in the overall thermal efficiency of the system. The larger temperature gradient exacerbates heat transfer inefficiencies, resulting in diminished energy conversion efficiency.

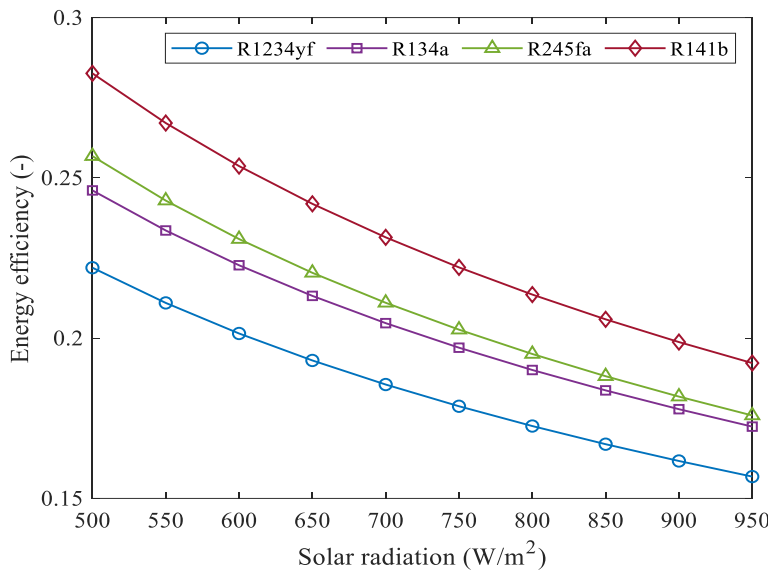


Figure 8. Effect of solar radiation on energy efficiency for different working fluid

In Figure 9, the focus shifts to the effect of solar radiation on exergy efficiency. The data presented in the figure reveals a noteworthy trend: as solar radiation levels increase, exergy efficiency diminishes across all working fluids. This relationship is intricately linked to the heightened energy absorption by the system as solar radiation intensifies, leading to elevated temperatures within the photovoltaic-thermal (PVT) components. Higher temperatures inherently foster greater irreversibilities in the heat transfer processes, culminating in increased exergy destruction. Exergy destruction signifies the lost potential to perform useful work due to inefficiencies and entropy generation within the system. Therefore, as irreversibility escalates with rising solar radiation levels, the exergy efficiency of the system experiences a concomitant decline.

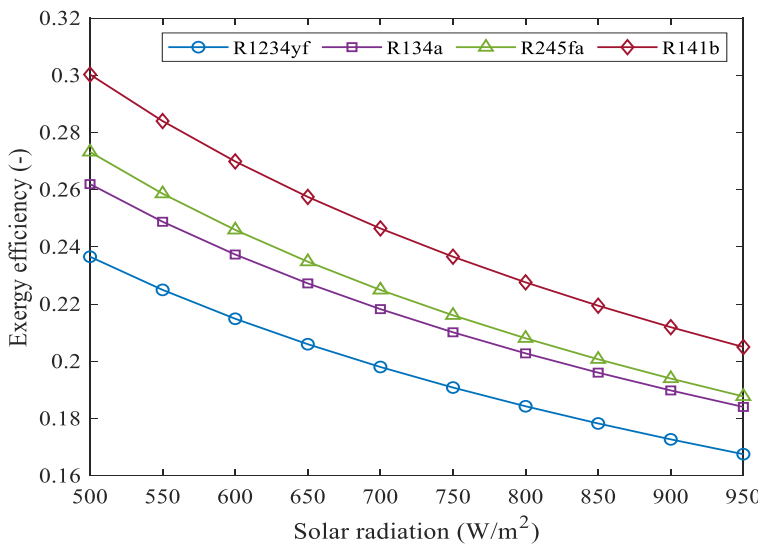


Figure 9. Effect of turbine outlet pressure on net power generation and energy efficiency

Figure 10 provides a comprehensive overview of the impact of solar radiation on hydrogen production within the system. The data depicted in the figure unveils a notable trend: as solar radiation levels rise, there is a corresponding increase in hydrogen production across all working fluids. This phenomenon is intricately linked to the operation of the photovoltaic component within the photovoltaic-thermal (PVT) system. As solar radiation intensifies, the photovoltaic cells generate a greater amount of electrical power through the conversion of incident sunlight. This surplus electrical energy can then be effectively utilized to drive the electrolysis processes more intensively. During electrolysis, electrical energy is employed to split water molecules into hydrogen and oxygen gases. With increased electrical power available from the heightened solar radiation levels, the electrolysis processes can operate more efficiently and at higher rates, resulting in an augmented production of hydrogen. Consequently, the observed increase in solar radiation directly translates to enhanced hydrogen production, underscoring the pivotal role of solar energy in driving sustainable hydrogen generation processes within the integrated system framework.

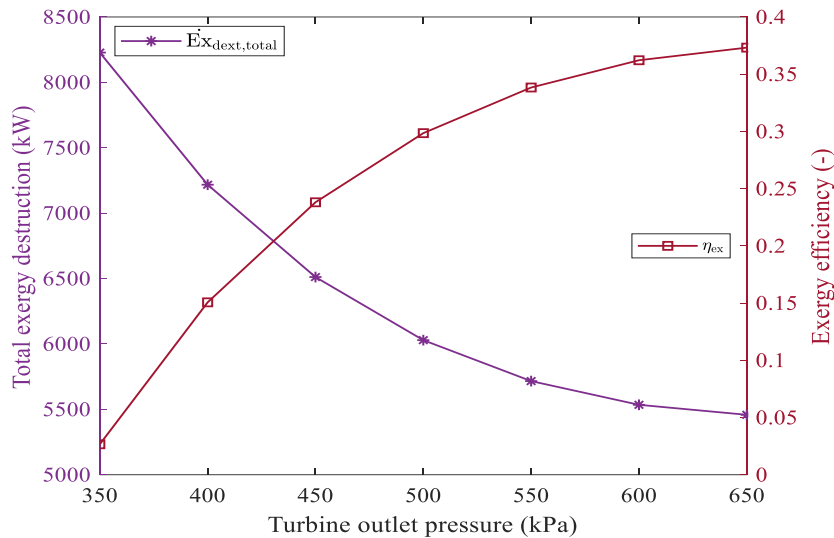


Figure 11. Effect of solar radiation on hydrogen production for different working fluid

5. CONCLUSIONS

The investigation into hydrogen and energy production utilizing a PVT-supported ORC system, complemented by LNG cold energy for low-temperature applications, presents a pioneering and highly efficient strategy for harnessing renewable and unconventional energy sources to drive integrated power and hydrogen generation. The following key conclusions emerge from the comprehensive research:

- The integration of PVT systems with ORC and LNG cold energy represents a robust approach to maximizing the utilization of diverse energy sources. By synergistically combining solar energy and LNG cold energy, the system achieves heightened levels of overall power generation and hydrogen production efficiency, demonstrating the potential for sustainable energy solutions.
- Enhanced solar radiation levels significantly augment both the electrical and thermal outputs from the PVT system, leading to increased energy capture and utilization. However, the escalating solar radiation also introduces challenges related to thermal management and efficiency optimization, underscoring the need for meticulous system design and operational strategies.
- Notably, the study identifies distinct performance trends among different working fluids within the system. For instance, R134a emerges as the optimal choice for PVT power production, generating a peak output of 19.4 kW, followed closely by R1234yf, R134a, and R245fa. Additionally, the analysis reveals varying levels of exergy destruction, with R1234yf exhibiting the highest exergy destruction at 217.2 kW, while R141b demonstrates the lowest at 213.9 kW.
- Furthermore, the evaluation of energy efficiency highlights notable variations across different working fluids. The utilization of R141b yields the highest energy efficiency of 21.4%, outperforming other fluids such as R245fa, R134a, and R1234yf. Similarly, in terms of exergy efficiency, R1234yf emerges as the optimal choice, mirroring its performance in energy efficiency.

These conclusions underscore the multifaceted nature of integrated energy systems and emphasize the importance of optimizing system components and operational parameters to maximize performance, efficiency, and sustainability in renewable energy applications.

REFERENCES

- Al-Nimr, M.A., Al-Ammari, W.A., 2019. A novel PVT/PTC/ORC solar power system with PV totally immersed in transparent organic fluid. *Int J. Energy Res* 43, 4766–4782. <https://doi.org/10.1002/er.4615>.
- Al-Waeli, A.H.A., Sopian, K., Kazem, H.A., Chaichan, M.T., 2017. Photovoltaic/Thermal (PV/T) systems: Status and future prospects. *Renew. Sustain. Energy Rev.* 77, 109–130. <https://doi.org/10.1016/J.RSER.2017.03.126>.
- Dubey, S., Tiwari, G.N., 2008. Thermal modeling of a combined system of photovoltaic thermal (PV/T) solar water heater. *Sol. Energy* 82, 602–612. <https://doi.org/10.1016/J.SOLENER.2008.02.005>.

- Guiavarch, A., Peupartier, B., 2006. Photovoltaic collectors efficiency according to their integration in buildings. *Sol. Energy* 80, 65–77. <https://doi.org/10.1016/J.SOLENER.2005.07.004>.
- Golonis, C., Skiadopoulos, A., Manolakos, D., Kosmadakis, G., 2021. Assessment of the performance of a low-temperature Organic Rankine Cycle engine coupled with a concentrating PV-Thermal system. *Renew. Energy* 179, 1085–1097. <https://doi.org/10.1016/j.renene.2021.07.103>.
- Hussain, F., Othman, M.Y.H., Sopian, K., Yatim, B., Ruslan, H., Othman, H., 2013. Design development and performance evaluation of photovoltaic/thermal (PV/T) air base solar collector. *Renew. Sustain Energy Rev.* 25, 431–441. <https://doi.org/10.1016/J.RSER.2013.04.014>.
- Hosseini, E.S., Butler, B., 2021. Design and analysis of a hybrid concentrated photovoltaic thermal system integrated with an organic Rankine cycle for hydrogen production. *J. Therm. Anal. Calor.* 144, 763–778. <https://doi.org/10.1007/s10973-020-09556-4>.
- Ji, J., He, H., Chow, T., Pei, G., He, W., Liu, K., 2009. Distributed dynamic modeling and experimental study of PV evaporator in a PV/T solar-assisted heat pump. *Int. J. Heat. Mass Transf.* 52, 1365–1373. <https://doi.org/10.1016/j.ijheatmasstransfer.2008.08.017>.
- Kasaeian, A., Nouri, G., Ranjbaran, P., Wen, D., 2018. Solar collectors and photovoltaics as combined heat and power systems: a critical review. *Energy Convers. Manag* 156, 688–705. <https://doi.org/10.1016/j.enconman.2017.11.064>.
- Kosmadakis, G., Manolakos, D., Papadakis, G., 2011. Simulation and economic analysis of a CPV / thermal system coupled with an organic Rankine cycle for increased power generation. *Sol. Energy* 85, 308–324. <https://doi.org/10.1016/j.solener.2010.11.019>.
- Kumar, A., Baredar, P., Qureshi, U., 2015. Historical and recent development of photovoltaic thermal (PVT) technologies. *Renew. Sustain Energy Rev.* 42, 1428–1436. <https://doi.org/10.1016/J.RSER.2014.11.044>.
- Kurs B., Okten K. Thermodynamic analysis of a Rankine cycle coupled with a concentrated photovoltaic thermal system for hydrogen production by a proton exchange membrane electrolyzer plant 2019;4. <https://doi.org/10.1016/j.ijhydene.2019.07.003>
- Mittelman, G., Kribus, A., Dayan, A., 2007. Solar cooling with concentrating photovoltaic/thermal (CPVT) systems. *Energy Convers. Manag* 48, 2481–2490. <https://doi.org/10.1016/J.ENCONMAN.2007.04.004>.
- Mittelman, G., Kribus, A., Mouchtar, O., Dayan, A., 2009. Water desalination with concentrating photovoltaic/thermal (CPVT) systems. *Sol. Energy* 83, 1322–1334. <https://doi.org/10.1016/J.SOLENER.2009.04.003>.
- Moradi, K., Ali Ebadian, M., Lin, C.X., 2013. A review of PV/T technologies: effects of control parameters. *Int. J. Heat. Mass Transf.* 64, 483–500. <https://doi.org/10.1016/J.IJHEATMASSTRANSFER.2013.04.044>.
- Salari, A., Parcheforosh, A., Hakkaki-Fard, A., Amadeh, A., 2020. A numerical study on a photovoltaic thermal system integrated with a thermoelectric generator module. *Renew. Energy* 153, 1261–1271. <https://doi.org/10.1016/J.RENENE.2020.02.018>.
- Sathe, T.M., Dhoble, A.S., 2017. A review on recent advancements in photovoltaic thermal techniques. *Renew. Sustain. Energy Rev.* 76, 645–672. <https://doi.org/10.1016/j.rser.2017.03.075>.
- Zhao, X., Zhang, X., Riffat, S.B., Su, Y., 2011. Theoretical study of the performance of a novel PV/e roof module for heat pump operation. *Energy Convers. Manag.* 52, 603–614. <https://doi.org/10.1016/j.enconman.2010.07.036>

Single Flash Geothermal Power Plant with Bottoming Helium Brayton Cycle: A Comprehensive Evaluation

Gamze Soy Turk, Onder Kizilkan*

Abstract: This study comprehensively assesses the thermodynamic performance of integrating a geothermal energy-based helium turbine into a closed Brayton cycle. The primary objectives are to evaluate the proposed system's thermodynamic efficiency and performance parameters under diverse operating conditions. Additionally, the study aims to calculate the exergy destruction occurring in different system elements and analyze the impact of key parameters such as geothermal source temperature, flash chamber pressure, and turbine inlet/outlet pressure on the overall system performance. According to the results of the analysis, a total of 2591.324 kW of power is produced: 603.7 kW from the gas turbine and 1987.62 kW from the steam turbine. The total exergy destruction occurring in the system was calculated as 6029.048 kW. In the second stage of the study, parametric studies were carried out to examine the effects of geothermal source temperature, flash chamber pressure, and turbine inlet/outlet pressure on system performance. According to the parametric analysis results, net electricity production and overall energy efficiency increase when the geothermal source temperature increases from 200°C to 250 °C. It is also concluded that exergy efficiency and destruction decrease as the flash chamber pressure rises.

Keywords: Geothermal energy, Helium turbine, Brayton cycle, Energy, Exergy

Address: Isparta University of Applied Sciences, Faculty of Technology, Department of Mechanical Engineering, Isparta, Türkiye

***Corresponding author:** onderkizilkan@isparta.edu.tr

1. INTRODUCTION

The surge in global population, alongside the expansion of various industries, has propelled a significant uptick in fossil fuel consumption, consequently exacerbating the emission of diverse environmental pollutants (Rahbar et al., 2016). In response to this pressing challenge, researchers are actively exploring avenues to supplant fossil fuels while concurrently enhancing the efficacy of energy-utilizing systems. Broadly, there exist two pivotal strategies in this endeavor. Firstly, the adoption of renewable energies emerges as a prominent solution. Secondly, efforts are directed towards optimizing and bolstering the efficiency of existing systems, which has spurred the development of diverse methodologies (Delovato et al., 2019). Extensive research and empirical evidence underscore the transformative potential of multi-generation systems, such as combined cooling, heating, and power systems, in markedly augmenting efficiency while mitigating emissions (Kavvadias and Maroulis, 2010). Furthermore, harnessing waste heat from various industrial and refinery processes to drive multi-generation systems is a highly effective approach to enhancing operational efficiency (Deymi-Dashtebayaz et al., 2019; Huang et al., 2019). The recuperated waste heat, contingent upon the thermal energy dissipation quality and the system's energy requisites can be leveraged for power generation, cooling, potable water production, and other purposes (Ma et al., 2018; Amiri et al., 2020; Sharaf Eldean et al., 2017). A pivotal determinant in selecting the type of heat recovery system hinges on the quality of dissipated energy, which is intricately influenced by the gas flow rate and temperature. The Brayton cycle, adaptable to temperatures reaching up to 1000°C depending on the application, offers remarkable flexibility in heat source selection (Rovira et al., 2020). This cycle can manifest in open or closed configurations (Khalil et al., 2018). In an open cycle, atmospheric air serves as the working fluid, providing requisite energy to a turbine through combustion with fuel (Meas, 2017). In this case, other gases, such as helium, CO₂, etc., cannot be used as the working fluid. However, this configuration is unsuitable from an energy and environmental efficiency standpoint due to the discharge of combustion byproducts into the atmosphere, often necessitating its integration with other cycles (Kumar and Kaushik, 2013). Conversely, the closed Brayton cycle obviates the need for discharging the working fluid into the environment, thereby affording designers the latitude to explore diverse working fluids. Nonetheless, the fluid's high temperature at the turbine outlet mandates incorporating additional systems to enhance energy efficiency in this configuration.

Many studies have been on integrated systems, and researchers have investigated various hybrid systems. Naserian et al. (Naserian et al., 2017). They studied the cycle introduced by Alali and Al-Shaboul (Alali and Al-Shaboul, 2018) and

introduced a closed Brayton cycle using waste heat from a nuclear reactor. They also used the exhaust gases from the Brayton cycle to produce steam and heating. Four working fluids were studied: N_2 , He, CO_2 , and air. According to the results obtained, N_2 and air produced higher specific power while exhibiting the best performance in energy production. Additionally, CO_2 demonstrated superior performance in steam production (heating system). Xia et al. (Xia et al., 2016) attempted to combine an internal combustion engine, closed Brayton cycles, refrigeration, and organic Rankine cycle (ORC). Abbasi and Pourrahmani (Abbasi and Pourrahmani, 2020). Abbasi and Pourrahmani studied solar energy as a heat source and studied a hybrid system consisting of the Brayton cycle, ORC, and absorption cooler using multi-objective optimization and eco-exergy methods. They used a (phase change material) PCM tank to use the system at night. Thus, the system can operate 24 hours a day by storing solar energy in the ammonia storage source during the day and utilizing this energy at night. Additionally, the reverse osmosis (RO) desalination system was operated using the power generated by the ORC system. According to the results, the pressure ratio, turbine inlet pressure, exergy efficiency, and energy efficiency of the Brayton cycle compressor in the optimal case were 9.06, 3300 kPa, 14.40%, and 40.5%, respectively. In addition, the amounts of electricity, cooling, and water produced were 2.42 MW, 1.6 MW, and 5209.5 m³/day, respectively. In another study, Feng et al. (Feng et al., 2020) conducted a thermodynamics and optimization study on a hybrid Brayton-Kalina cycle. In this research, diesel generator exhaust was accepted as the heat source. According to the results, annual fuel costs decreased by 16.62%, and energy efficiency increased by 15.01%. Ahmadi et al. (Ahmadi et al., 2012) studied the combination of the open Brayton cycle with ORC and absorption refrigerant cycles. The system proposed in this research had the capacity of heating, cooling, and power cogeneration. The results showed that the highest irreversibility and exergy loss occurred in the combustion chamber and heat exchanger. Moreover, a study on emitted CO_2 showed that its emissions are reduced due to the simultaneous use of this gas.

The main aim of this study is to comprehensively evaluate the thermodynamic performance of integrating a geothermal energy-based helium turbine into a closed Brayton cycle. Additionally, the aims of this study can be listed as follows:

- Evaluating the proposed system's thermodynamic efficiency and performance parameters under various operating conditions.
- Calculation of exergy destruction in system elements.
- Analyzing the effect of key parameters such as geothermal source temperature, flash chamber pressure, turbine inlet/outlet pressure on system performance.

2. SYSTEM DESCRIPTION

Figure 1 shows a schematic representation of the integrated system consisting of a geothermal-based helium turbine integrated into a closed Brayton cycle. The system essentially uses the abundant and renewable energy reservoir of geothermal resources to power a helium turbine that drives the Brayton cycle for energy production. This innovative configuration capitalizes on helium's unique properties as a working fluid, known for its exceptional heat transfer characteristics and suitability for high-temperature applications. The geothermal component of the system taps into the natural heat emanating from beneath the Earth's surface, exploiting the temperature differentials to produce steam. This steam is then utilized to drive a turbine, generating mechanical energy. Subsequently, the mechanical energy is transmuted into electrical power through the Brayton cycle, a thermodynamic process renowned for its versatility and efficiency. The helium turbine is central to this system's efficacy, designed to operate optimally within the high-temperature environment facilitated by geothermal energy. Helium, which was chosen for its superior thermodynamic properties, serves as the primary working fluid within the turbine, efficiently transferring heat energy into mechanical work. In conjunction with the helium turbine, the Brayton cycle further enhances energy conversion efficiency, ensuring maximum utilization of the geothermal heat source. Moreover, integrating a geothermal-supported helium turbine with the Brayton cycle offers several advantages, including enhanced energy efficiency, reduced environmental impact, and greater operational flexibility. By leveraging geothermal energy and helium's exceptional properties, this system represents a promising avenue for sustainable energy generation, with potential applications in various industrial and power generation sectors.

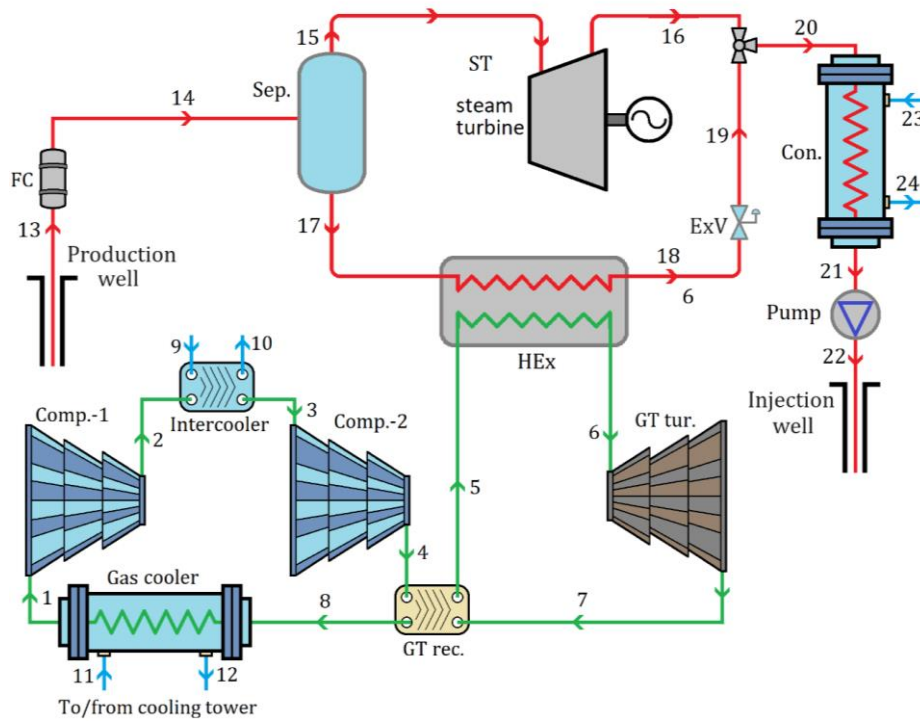


Figure 1. Schematic representation of the geothermal-based helium turbine integrated with closed Brayton cycle

3. THERMODYNAMIC ANALYSIS

A thermodynamic model is constructed using Engineering Equation Solver (EES) software (Klein, 2020) in order to evaluate the energetic and exergetic performance of a geothermal-based helium turbine integrated with a closed Brayton cycle. The main assumptions of the model are given as:

- The system operates at steady-state conditions.
- Kinetic and potential energies and exergy changes are ignored.
- Pressure is constant in the heat exchangers.
- There are no heat losses in the heat exchangers.
- The turbine and pump operations are assumed to be adiabatic.
- The reference state properties are 22°C and 100 kPa.

The mass balance equation for steady-state and steady-flow processes can be written as (Cengel and Boles, 2006):

$$\sum \dot{m}_{in} = \sum \dot{m}_{out} \quad (1)$$

In the above equation, \dot{m} is the mass flow rate, and the subscripts *in* and *out* stand for inlet and outlet, respectively. The energy balance equation can be written as:

$$\dot{Q} + \sum \dot{m}_{in}h_{in} = \dot{W} + \sum \dot{m}_{out}h_{out} \quad (2)$$

Here, \dot{Q} is the rate of heat, \dot{W} is the rate of work, and h is the specific enthalpy. For the exergy analysis, the balance equation is defined as (Dincer and Rosen, 2007):

$$\dot{E}x_Q - \dot{E}x_W = \sum \dot{E}x_{in} - \sum \dot{E}x_{out} + \dot{E}x_{dest} \quad (3)$$

where the first and the second terms are exergy of heat and work respectively, $\dot{E}x$ is the rate of flow exergy, $\dot{E}x_{dest}$ is exergy destruction. In the above equation, each term is defined as follows:

$$\dot{E}x_Q = \dot{Q} \left(\frac{T - T_0}{T} \right) \quad (4)$$

$$\dot{E}x_W = \dot{W} \quad (5)$$

$$\dot{E}x = \dot{m} ex \tag{6}$$

$$\dot{E}x_{dest} = T_0 \dot{S}_{gen} \tag{7}$$

In equation (8), ex is the specific flow exergy and can be calculated using the equation below:

$$e = (h - h_0) - T_0(s - s_0) \tag{8}$$

4. RESULTS

This study aims to conduct comprehensive thermodynamic analyses and parametric studies to evaluate the performance of the integrated system consisting of a geothermal-assisted closed Brayton cycle, including energy and exergy efficiency, power production, and exergy destruction. Using balance equations and under the assumptions given above, analyses are performed using EES software. The default operational parameters of the proposed system are tabulated in Table 1.

Table 1. The default initial parameters

<i>Parameter</i>	<i>Value</i>
Reference temperature	22 °C
Reference pressure	100 kPa
Gas turbine high pressure	1000 kPa
Gas turbine low pressure	500 kPa
Gas cycle compressor inlet temperature	30 °C
Gas cycle recuperator efficiency	0.75
Geothermal source temperature	235 °C
Flash chamber pressure	1400 kPa
Condenser pressure	35 kPa
Mass flow rate of geothermal water	40 kg/s
Pump efficiency	0.85
Turbine efficiency	0.90
Hex efficiency	0.85

Figure 2 provides a comprehensive illustration of the power production, total exergy destruction, and energy-exergy efficiencies of the individual components that constitute the geothermal power generation system. According to the detailed analysis presented, the system produces a total power output of 2591.324 kW. This total is composed of 603.7 kW generated by the gas turbine and 1987.62 kW generated by the steam turbine. These values indicate the distribution of power generation between the two primary turbines in the system. In addition to power production, the analysis also quantifies the total exergy destruction within the system, which amounts to 6029.048 kW. Exergy destruction is a critical parameter as it represents the inefficiencies and irreversibilities within the system, highlighting areas where improvements can be made to enhance overall performance. Figure 2 also presents the energy and exergy efficiencies on the right side of the figure. The overall energy efficiency of the system is calculated to be 10%, which reflects the ratio of useful power output to the total energy input. In contrast, the exergy efficiency, calculated at 30%, indicates the effectiveness of the system in converting available energy into useful work while accounting for irreversibilities.

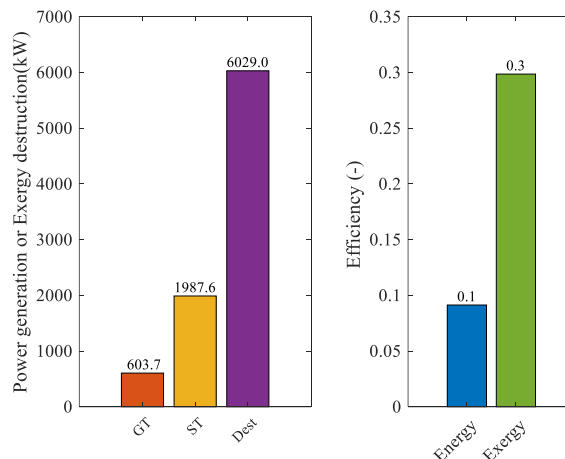


Figure 2. Power generation/exergy destruction and energy/exergy efficiencies of the system

Figure 3 delves deeper into the exergy destruction occurring in the various components of the system. It reveals that the highest exergy destruction takes place in the condenser, amounting to 1609.4 kW. This significant loss is likely due to the large temperature differences and phase changes occurring in the condenser. Following the condenser, the gas turbine experiences the second-highest exergy destruction at 997.1 kW, which can be attributed to the high-temperature gradients and combustion processes involved. The intercooler also contributes substantially to exergy destruction, with a value of 760.49 kW, indicating potential inefficiencies in the heat exchange process. Conversely, the separator and mixing chamber exhibit the lowest exergy destruction within the system, suggesting that these components operate relatively efficiently compared to others.

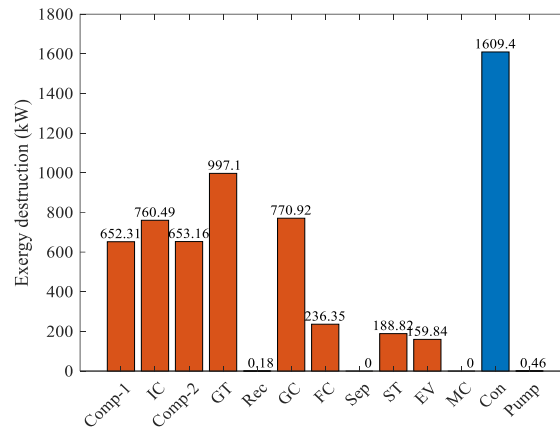


Figure 3. Total exergy destruction rates of system components

In the second stage of the study, extensive parametric studies were conducted to investigate the influence of key operational parameters on the performance of the geothermal power generation system. These studies focused on three critical variables: geothermal source temperature, flash chamber pressure, and turbine inlet/outlet pressure. By systematically varying these parameters, the study aimed to understand their individual and combined effects on the system's net power generation and overall energy efficiency. The impact of geothermal source temperature on net power generation and energy efficiency is illustrated in Figure 4. As observed, increasing the geothermal source temperature from 200 °C to 250 °C leads to a significant improvement in both net power generation and overall energy efficiency. This positive trend can be attributed to several thermodynamic principles. Higher geothermal source temperatures enhance the thermal energy available for conversion into mechanical work. This increase in thermal energy raises the enthalpy of the working fluid, which directly translates into higher power output from the turbine. Essentially, the higher the geothermal source temperature, the greater the potential for energy extraction and conversion into electricity. Furthermore, the increase in geothermal source temperature also improves the system's energy efficiency. Higher temperatures reduce the relative energy losses and improve the effectiveness of the heat exchange processes within the system. This means that a larger portion of the input thermal energy is converted into useful work, enhancing the overall efficiency of the power generation process.

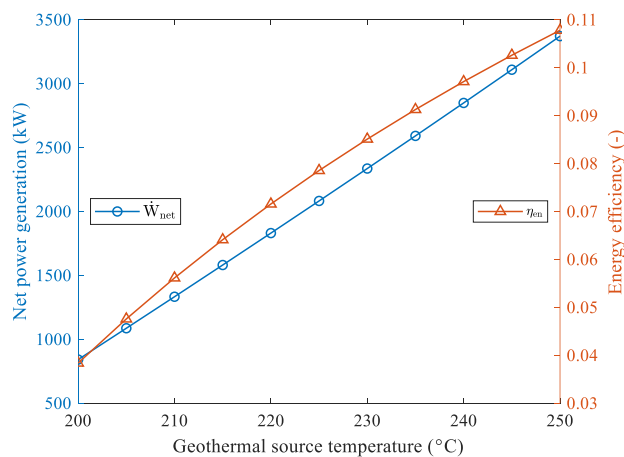


Figure 4. Effect of geothermal source temperature on net power generation and energy efficiency

Figure 5 shows the effect of geothermal source temperature on total exergy destruction and exergy efficiency. As seen in the figure, when the geothermal source temperature increases from 200 °C to 250 °C, total exergy destruction and efficiency increase. Higher geothermal water temperatures imply greater thermal energy available for conversion into mechanical work. This results in higher heat input into the system, contributing to increased exergy destruction, particularly in components such as heat exchangers and turbines where energy conversion takes place. The higher temperature of the geothermal water results in higher turbine inlet temperatures. This leads to increased turbine efficiency due to improved thermodynamic properties of the working fluid (helium) and higher energy extraction from the hot fluid stream. However, despite this improvement, there is still an increase in total exergy destruction, mainly due to the increased heat input and the irreversibilities associated with the conversion process.

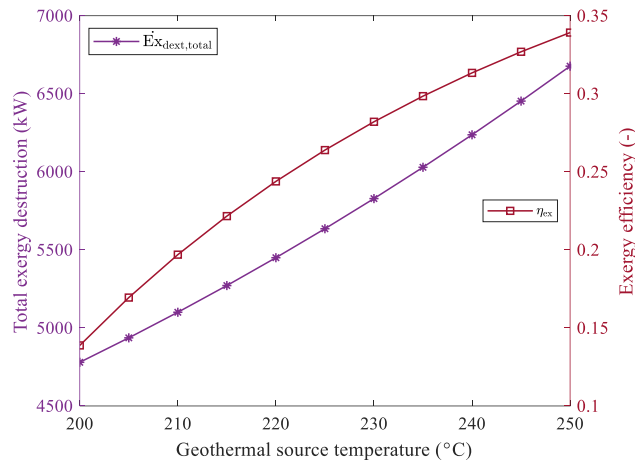


Figure 5. Effect of geothermal source temperature on total exergy destruction and exergy efficiency

Figure 6 demonstrates the effect of flash chamber pressure on net power generation and energy efficiency. The data presented in the figure reveals a positive correlation between increasing flash chamber pressure and enhancements in both net power generation and energy efficiency. Specifically, as the flash chamber pressure is elevated from 1300 kPa to 1500 kPa, there is a notable increase in the system's total net power output and overall energy efficiency. This improvement can be attributed to the thermodynamic behavior of the working fluid, which in this case is helium. At higher flash chamber pressures, the pressure of the helium entering the turbine is significantly increased. This higher inlet pressure enhances the turbine's performance by allowing for a more extensive expansion of the working fluid as it passes through the turbine. The increased expansion results in a more efficient conversion of thermal energy into mechanical work, thereby boosting the power generation capacity of the turbine. Moreover, the elevated inlet pressure also contributes to improved energy efficiency of the entire system. With higher pressure, the thermodynamic cycle operates closer to its ideal efficiency, reducing the relative losses and irreversibilities. This means a greater portion of the input thermal energy from the geothermal source is effectively converted into useful electrical power.

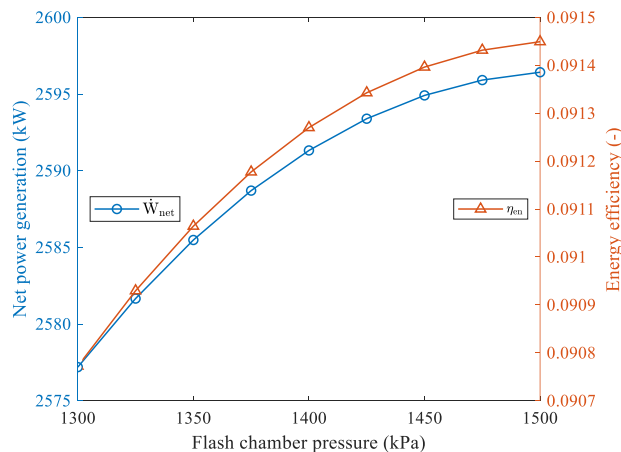


Figure 6. Effect of flash chamber pressure on net power generation and energy efficiency

Figure 7 depicts the effect of flash chamber pressure on total exergy destruction and exergy efficiency. As seen in the figure, as the flash chamber pressure increases, exergy efficiency increases and exergy destruction decreases. Increasing the flash chamber pressure results in a higher pressure differential between the geothermal fluid and the working fluid (helium) in the heat exchanger. This higher pressure difference facilitates more efficient heat transfer between the two fluids, reducing thermal irreversibilities and consequently lowering exergy destruction associated with heat transfer processes. Moreover, higher flash chamber pressure leads to higher turbine inlet pressure, enabling the turbine to operate more efficiently. With increasing pressure, the turbine can extract more work from the expanding working fluid, thus reducing the exergy destruction within the turbine itself and increasing the exergy efficiency.

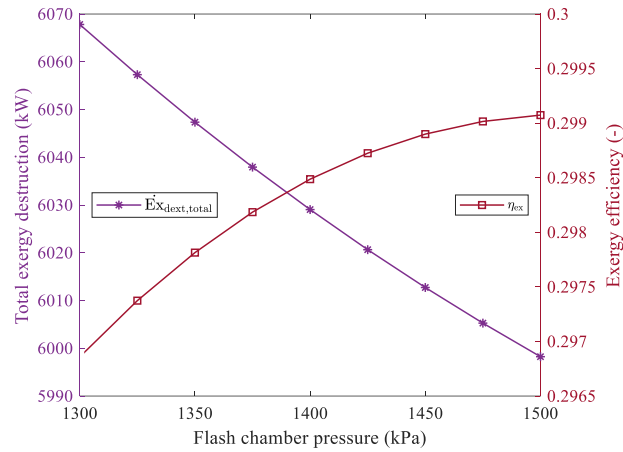


Figure 7. Effect of flash chamber pressure on total exergy destruction and exergy efficiency

Figure 8 illustrates the relationship between turbine inlet pressure and two critical performance metrics: net power production and energy efficiency. The data shows that increasing the turbine inlet pressure from 700 kPa to 1300 kPa leads to a decrease in both net power production and energy efficiency. This counterintuitive outcome arises due to the higher losses that occur within the turbine at elevated inlet pressures. Specifically, increased friction and leakage losses become more pronounced. Friction losses result from the greater resistance encountered by the turbine’s moving parts, dissipating energy as heat rather than converting it into useful work. Leakage losses occur when the working fluid escapes through small gaps and seals, further reducing the energy available for power generation. These inefficiencies cumulatively decrease the turbine’s efficiency and net power output by diverting energy away from productive use.

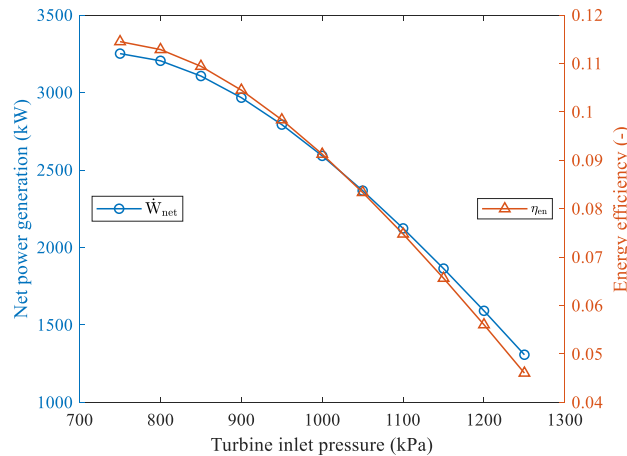


Figure 8. Effect of turbine inlet pressure on net power generation and energy efficiency

In a complementary analysis, Figure 9 highlights the impact of turbine inlet pressure on total exergy destruction and exergy efficiency. As turbine inlet pressure increases, the total exergy destruction also rises, while exergy efficiency declines. The higher pressure ratios across the turbine, though potentially increasing expansion work, introduce significant irreversible processes such as frictional losses, turbulence, and blade losses. These processes dissipate energy that could otherwise be converted into useful work. Frictional losses, caused by the interaction between the working fluid and turbine components, generate heat. Turbulence within the fluid flow path further dissipates energy,

and aerodynamic inefficiencies in the turbine blades contribute to blade losses. Together, these irreversibilities increase exergy destruction, reducing the overall efficiency of the energy conversion process.

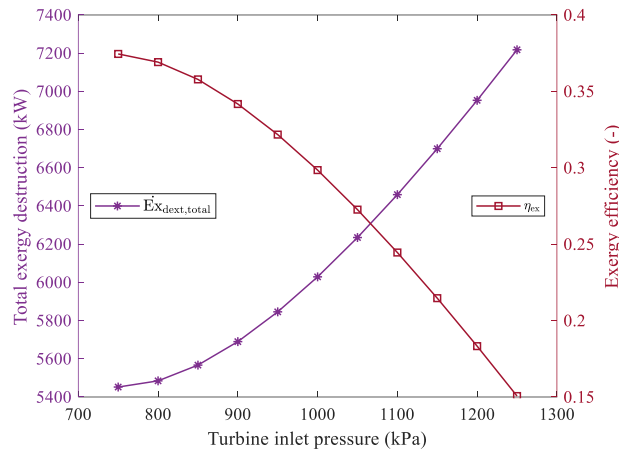


Figure 9. Effect of turbine inlet pressure on total exergy destruction and exergy efficiency

Figure 10 illustrates the impact of turbine outlet pressure on net power production and energy efficiency. The data demonstrates that increasing the turbine outlet pressure from 350 kPa to 650 kPa leads to significant improvements in both metrics. Higher turbine outlet pressure allows for an increased pressure ratio across the turbine, enhancing the expansion process of the working fluid, which in this case is helium. This more efficient expansion results in a greater amount of work being extracted from the turbine, thereby boosting net power production. The improved efficiency of energy conversion processes at higher outlet pressures translates into better overall system performance, highlighting the importance of optimizing turbine outlet pressure to maximize power generation and energy efficiency.

Figure 11 further explores the effect of turbine outlet pressure, focusing on total exergy destruction and exergy efficiency. The figure shows that as turbine outlet pressure increases, exergy destruction decreases and exergy efficiency improves. Higher outlet pressures help to minimize the irreversibilities associated with fluid flow and heat transfer processes within the system. By reducing the pressure differences across the system components, the fluid dynamics are improved, leading to fewer inefficiencies and losses. This reduction in irreversibilities translates into lower exergy destruction, which means that a greater portion of the available energy is converted into useful work. Consequently, optimizing turbine outlet pressure not only enhances power production and energy efficiency but also improves exergy efficiency, making the overall energy conversion process more effective and sustainable. These insights emphasize the critical role of turbine outlet pressure in enhancing the performance of geothermal power systems, suggesting that careful control and optimization of this parameter can lead to substantial improvements in both energy and exergy efficiencies.

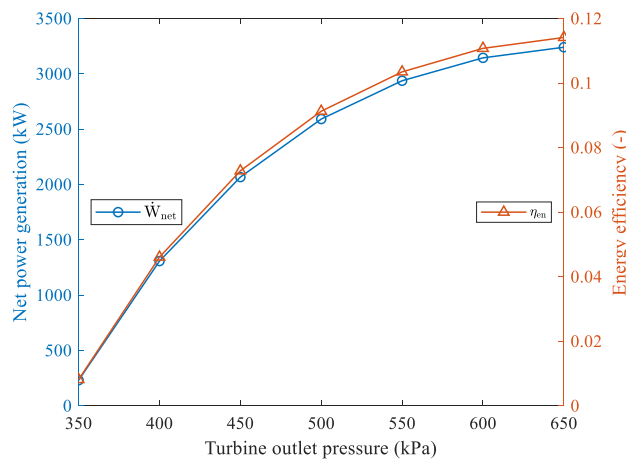


Figure 10. Effect of turbine outlet pressure on net power generation and energy efficiency

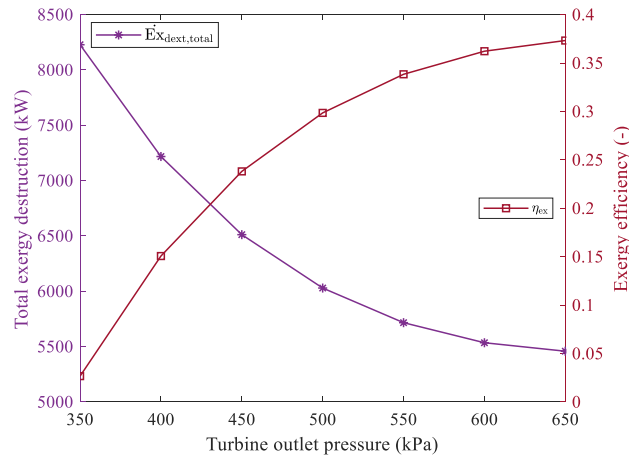


Figure 11. Effect of turbine outlet pressure on total exergy destruction

5. CONCLUSIONS

The comprehensive evaluation of integrating a geothermal energy-based helium turbine into a closed Brayton cycle yielded significant insights into the proposed system's thermodynamic performance and operational characteristics. The analysis revealed a total electricity production of 2591.324 kW, with 603.7 kW generated from the gas turbine and 1987.62 kW from the steam turbine. The total exergy destruction occurring in the system was calculated as 6029.048 kW. This assessment provides valuable information regarding the efficiency and effectiveness of different system elements, guiding efforts toward minimizing exergy losses and enhancing overall performance. Parametric studies were conducted to investigate the impact of key operating parameters on system performance. Increasing the geothermal source temperature from 200°C to 250°C resulted in a notable improvement in net electricity production and overall energy efficiency. This finding underscores the significance of optimizing geothermal resource utilization to maximize power generation output. The analysis indicated that as the flash chamber pressure increases, there is a corresponding increase in exergy efficiency and a decrease in exergy destruction. This suggests the importance of carefully selecting and controlling operational parameters to enhance system performance and efficiency. Further investigation into turbine inlet and outlet pressure effects revealed valuable insights into the optimal operating conditions for maximizing electricity production and overall system efficiency.

REFERENCES

- Abbasi R.H, Pourrahmani H. Multi-objective optimization and exergoeconomic analysis of a continuous solar-driven system with PCM for power, cooling and freshwater production. *Energy Convers Manag.* 2020;211:112761. <https://doi.org/10.1016/j.enconman.2020.112761>.
- Ahmadi P, Dincer I, Rosen MA. Exergo-environmental analysis of an integrated organic Rankine cycle for trigeneration. *Energy Convers Manag.* 2012;64:447–53. <https://doi.org/10.1016/j.enconman.2012.06.001>.
- Alali E, Al-shboul KF. Annals of nuclear energy performance analysis of the closed Brayton power cycle in a small-scale pebble bed gas cooled reactor using different working fluids. *Ann Nucl Energy.* 2018;121:316–23. <https://doi.org/10.1016/j.anucene.2018.07.040>.
- Amiri Rad E, Mohammadi S, Tayyeban E. Simultaneous optimization of working fluid and boiler pressure in an organic Rankine cycle for different heat source temperatures. *Energy.* 2020;194:116856. <https://doi.org/10.1016/j.energy.2019.116856>.
- Cengel, Y.A., Boles, M.A. (2006). *Thermodynamics: an engineering approach*. McGraw-Hill, New York.
- Delovato N, Sundarnath K, Cvijovic L, Kota K, Kuravi S. A review of heat recovery applications for solar and geothermal power plants. *Renew Sustain Energy Rev.* 2019;114:109329. <https://doi.org/10.1016/j.rser.2019.109329>.

- Deymi-Dashtebayaz M, Tayyeban E. Multi objective optimization of using the surplus low-pressure steam from natural gas refinery in the thermal desalination process. *J Clean Prod.* 2019;238:117945. <https://doi.org/10.1016/j.jclepro.2019.117945>.
- Dincer, I., Rosen, M.A. (2007). *Exergy: Energy, Environment and Sustainable Development*. Elsevier Science.
- Feng Y, Du Z, Shreka M, Zhu Y, Zhou S, Zhang W. Thermodynamic analysis and performance optimization of the supercritical carbon dioxide Brayton cycle combined with the Kalina cycle for waste heat recovery from a marine low-speed diesel engine. *Energy Convers Manag.* 2020;206:112483. <https://doi.org/10.1016/j.enconman.2020.112483>.
- Huang W, Wang J, Xia J, Zhao P, Dai Y. Performance analysis and optimization of a combined cooling and power system using low boiling point working fluid driven by engine waste heat. *Energy Convers Manag.* 2019;180:962–76. <https://doi.org/10.1016/j.enconman.2018.11.041>.
- Kavvadias KCĀ, Maroulis ZB. Multi-objective optimization of a trigeneration plant. *Energy Policy.* 2010;38(2):945–54. <https://doi.org/10.1016/j.enpol.2009.10.046>.
- Khalil KM, Mahmoud S, Al-dadah RK. Development of innovative non-repeated annular area dual stage small-scale nitrogen axial turbine for hybrid open-closed Rankine cycle. *Energy Convers Manag.* 2018;164(February):157–74. <https://doi.org/10.1016/j.enconman.2018.02.088>.
- Kumar O, Kaushik SC. Thermo-economic evaluation and optimization of a Brayton–Rankine–Kalina combined triple power cycle. *Energy Convers Manag.* 2013;71:32–42. <https://doi.org/10.1016/j.enconman.2013.03.017>.
- Ma Y, Zhang X, Liu M, Yan J, Liu J. Proposal and assessment of a novel supercritical CO₂ Brayton cycle integrated with LiBr absorption chiller for concentrated solar power applications. *Energy.* 2018. <https://doi.org/10.1016/j.energy.2018.01.155>.
- Mahmoudi A, Fazli M, Morad MR. A recent review of waste heat recovery by Organic Rankine Cycle. *Appl Therm Eng.* 2018. <https://doi.org/10.1016/j.applthermaleng.2018.07.136>.
- Meas MR. Thermodynamic design optimisation of an open air recuperative twin-shaft solar thermal Brayton cycle with combined or exclusive reheating and intercooling. *Energy Convers Manag.* 2017;148:770–84. <https://doi.org/10.1016/j.enconman.2017.06.043>.
- Naserian MM, Farahat S, Sarhaddi F. New exergy analysis of a regenerative closed Brayton cycle. *Energy Convers Manag.* 2017;134:116–24. <https://doi.org/10.1016/j.enconman.2016.12.020>.
- Rahbar K, Mahmoud S, Al-dadah RK, Moazami N, Mirhadizadeh SA. Review of organic Rankine cycle for small-scale applications. *Energy Convers Manag.* 2017;134:135–55. <https://doi.org/10.1016/j.enconman.2016.12.023>.
- Rovira A, Muñoz M, Sánchez C, Barbero R. Advanced thermodynamic cycles for finite heat sources: proposals for closed and open heat sources applications. *Appl Therm Eng.* 2020;167:114805. <https://doi.org/10.1016/j.applthermaleng.2019.114805>.
- Sharaf Eldean MA, Soliman AM. A novel study of using oil refinery plants waste gases for thermal desalination and electric power generation: energy, exergy and cost evaluations. *Appl Energy.* 2017;195:453–77. <https://doi.org/10.1016/j.apenergy.2017.03.052>.
- Xia J, Wang J, Lou J, Zhao P, Dai Y. Thermo-economic analysis and optimization of a combined cooling and power (CCP) system for engine waste heat recovery. *Energy Convers Manag.* 2016;128:303–16. <https://doi.org/10.1016/j.enconman.2016.09.086>.

Analysis of Glass Fiber Utilization Rates in G-7 and Türkiye and The Role of Şişecam in The Türkiye Glass Fiber Sector

Tugay Üstün*¹, Sinan Can Altuntaş¹

Abstract: In today's world, composite materials are widely preferred to give better mechanical properties to the products produced. Although there are composite materials that are easy to produce, there are also types of materials with complex structures that are defined as engineering materials. With the use of fibers as reinforcing elements in composite materials, lighter and more durable products are produced. When glass fibers are examined in terms of cost and production, they are the most preferred reinforcement. When examining the glass industry worldwide, glass fibers have a share of approximately 4%. Glass fibers are highly preferred in sectors such as defense, aviation, automotive and maritime. Due to its use in many sectors and the difficulties encountered in product production, glass fibers can be found in several types. In this study, foreign trade data were used to compare the glass fiber usage rates of G-7 countries and Türkiye. In order to find these data, Customs Tariff Statistics Position (GTIP) numbers were determined and foreign trade data for 2022 and 2023 were found from the GTIP numbers. The fact that there are several types of glass fibers (yarn, roving, ribbon, mat) causes the GTIP numbers to differ. In this direction, foreign trade data of G-7 countries and Türkiye were analyzed individually, and products and countries were compared. As a result of the analysis, it was revealed that G-7 countries and Türkiye are importers of glass fiber products. In addition, it has been determined that there are serious decreases in the export and import rates of glass fiber products in G-7 countries and Türkiye in 2023 compared to 2022 and that this market has shrunk. It was found from foreign trade data that the United Kingdom is an exporter of glass fiber roving, France is an exporter of chopped glass fiber and Italy is an exporter of glass fiber mat products. On the other hand, Türkiye is by far an importer of glass fiber roving compared to other glass fiber types. In addition, the impact of Şişecam, Türkiye's largest glass fiber producing company, on export rates was examined. Accordingly, Şişecam's financial reports for 2023 and 2022 were analyzed. As a result of the analysis, this company undertook almost all of Türkiye's exports of 28.5 million dollars in 2023..

Keywords: Glass fiber, import values, export values, G-7, Türkiye.

¹**Address:** Başkent University, Kahramankazan Vocational School, Ankara/Türkiye

***Corresponding author:** tugayustun@baskent.edu.tr

1. GİRİŞ

Sürekli gelişmeye devam etmekte olan teknolojiyle beraber mühendislik malzemeleri önem kazanmaktadır. Kompozit malzemeler verimliliği artıran, geleneksel malzemelere farklı özellikler kazandıran, sorunlara yenilikçi çözümler getiren malzemelerdir (Clyne & Hull, 2019). Bu sebeplerden dolayı günümüzde çokça tercih edilen bir malzeme türü olarak karşımıza çıkmaktadır. Kompozit malzemeleri tasarımı yapılırken uygun proses, malzeme seçimi ve kalite kontrol en önemli kriterler olarak karşımıza çıkmaktadır. Metal malzemeler ile kıyaslandığında birçok uygulama alanının olmasının temel sebebinde düşük yoğunlukları bundan dolayı ağırlık kazanımı, yüksek dayanım sergilemeleri olarak gösterilebilir (Mallick, 2007). Bu malzemelerle elektronik kartlar, robotik kollar gibi elektronik, rüzgâr tribünleri gibi enerji, dişliler, rulmanlar gibi makine, havacılık ve savunma gibi birçok sektöre ürün üretilmektedir (Sathishkumar et al., 2014).

Kompozit malzemeler farklı malzemelerden oluştuğundan birçok seçenek karşımıza çıkmakla beraber günümüzde en çok polimer matrisli elyaf takviyeli olanları tercih edilmektedir (Şişecam). Bu tercihin sebebi ise savunma, havacılık, otomotiv, altyapı ve rüzgâr enerjisi gibi sektörlerde yaygın olarak kullanılması gösterilebilir. Kompozit malzemelerde takviye elemanı olarak tercih edilen elyaflar ağaçtaki selüloz gibi, kendiliğinden doğada var olan doğal elyaflar ve sentetik olarak üretilen sentetik elyaflar olmak üzere ikiye ayrılırlar (Wang et al., 2011). Günümüzde en çok kullanılan sentetik elyaflar cam, karbon ve aramid olarak karşımıza çıkmaktadır. Tüketim ve satış miktarları açısından, en geniş ölçüde kullanılan takviye malzemesi ise cam elyafıdır (Güvenbaş). Elyaflar kendi içerisinde çok sayıda farklı türleri karşımıza çıkmaktadır. Son ürün gereksinimleri ve proses özellikleri açısından başlıca elyaf türleri fitil, kırılmış lifler, iplik, kumaş, şerit ve keçe gibi türleri bulunmaktadır. Cam elyaflar, güverteler, gövde panelleri, yük zeminleri, gösterge paneli tertibatları, tekerlek yuvası tertibatları, ön kaplama ve akü kutuları gibi otomobil parçalarının imalatında

da kullanılır (Birliđi, 2012). Otomotiv sektöründe artan satışlarının etkisiyle cam elyaf pazarını da yönlendirmesi beklenmektedir. Otomotiv sektörü, tüketim ürünleri ve elektronik ürünlerde cam elyaf kullanımı nedeniyle Çin, Hindistan gibi hızla büyüyen ekonomilerin varlığı bu pazarda en büyük cam elyaf üretici ve tüketici durumunda olmalarını sağlamaktadır. 2020 yılında dünya genelinde cam elyaf üretimine ait bilgiler Tablo 1’de verilmiştir (Şişecam, 2020).

Tablo 1. Dünya Cam Kurulu Üretim Kapasitesi Faaliyet Alanı (Şişecam, 2020)

	Kapasite (Milyon Ton)	Pay %
Düzcam	82	47
Cam Ambalaj	80	46
Cam Ev Eşyası	6	3
Cam Elyaf	6	4
Toplam	175	100

2020 yılında yıllık 6 milyon ton üretimi yapılmış olan cam elyafın, 2020’den 2027’ye kadar gelir açısından %4,5’luk büyüme oranında büyümesi beklenmektedir (Şişecam, 2020). Bu da cam elyaf üretimi ve tüketimi açısından incelendiğinde önemli bir pazar payına sahip olduğunu göstermektedir. Türkiye açısından incelendiğinde ise talebin düşük olduğu, ton başına fiyatlar ise stok seviyelerinin yüksek ve endüstriyel müşterilerin makroekonomik koşullar nedeniyle genellikle düşük seviyelerde seyretmektedir (Şişecam, 2023). 2023 yılında, fiyatlama ortamı özellikle Avrupa Birliğinde düşük maliyetli ithal ürün varlığı ile oluşan arz fazlası sebebiyle zayıf kalmıştır.

65 yıllık bir geçmişe sahip olan Türk Cam Sanayi, yıllar içerisinde gelişmesini ve büyümesini sürdürmüştür (Müdürlüğü, 2022). Bugün camın ana gruplarını oluşturan düz cam (işlenmiş camlar dahil), cam ev eşyası, cam ambalaj, cam elyafı, taş yünü ve cam yünü üretiminde en ileri teknolojilerle gerçekleştirilmektedir. Cam elyaf üretiminde Türkiye’de en büyük üreticisi firması olan Şişecam, sektöre yön verir konumundadır. Şişecam, 2023 yılında elyaf sektörde yaşanan olumsuzluklara rağmen mevcut pazarlama faaliyetlerine ek olarak alternatif pazarlara yönelerek ve katma değerli ürün geliştirme çalışmalarına odaklanarak pazardaki rekabet gücünü korumaya çalışmıştır (Şişecam, 2023). Kompozit malzemelerin takviye elemanı oluşturan cam elyafları (mat, çok uçlu fitil, tek uçlu fitil ve kırılmış elyaf) üreten Şişecam, rüzgâr türbini kanatları, otomotiv parçaları, mühendislik plastikleri, denizcilik ürünleri, endüstriyel uygulamalar ve inşaat gibi birçok sektöre girdi sağlamaktadır (Şişecam, 2020). Bu da cam elyaf sektörünün önemini artırmaktadır. Savunma, havacılık, otomotiv, altyapı ve rüzgâr enerjisi gibi sektörlerin ham madde özelliği taşıyan, stratejik bir öneme sahip cam elyaf sektörü geçen zaman içerisinde özellikle Çin ve Hindistan gibi Dünya genelinde en büyük üretici konumunda olan ülkelerden kaynaklı olarak fiyat rekabetine uğramıştır (Şişecam, 2023). Bu da cam elyaf satış hacminde önemli rol oynamaktadır.

Bu çalışmanın amacı kompozit malzemelerde takviye elemanı olarak kullanılan elyaf türlerinden biri olan cam elyafın ikincil verilerden elde edilerek değerlendirilmesi yapılmaktadır. Birçok sektörde kullanılan farklı türlerdeki cam elyaf ürünlerinin 2022 ve 2023 yıllarında G-7 ülkelerinin ve Türkiye’nin ithalat ve ihracat rakamları kıyaslanması yapılırken, Türkiye’de bu ürünlerin üretimini gerçekleştiren Şişecam firmasının ülke pazarı özelinde incelemesi yapılmıştır.

2. MATERYAL VE METOT

Dünya gümrük sisteminde emtiaların ihracat, ithalat ve gümrük rejimi uygulamalarındaki operasyonlarında gerekli olan rakamları gösteren kodlama uygulaması GTİP’tir. GTİP terimi; T.C. Ticaret Bakanlığı tarafından Türk Gümrük Tarife Cetvelinde kullanılan 12 rakamlı kod olarak belirtilmektedir. Bu kodun ilk altı hanesi Dünya Gümrük Örgütü’ne üye tüm ülkelerce kullanılan Armonize Sistem (HS: Harmonized System) Nomanklatürü kodunu, yedinci ve sekizinci haneleri Avrupa Birliği (AB) ülkeleri tarafından kullanılan Kombine Nomanklatür (Combined Nomenclature-CN) kodunu, dokuzuncu ve onuncu haneleri farklı vergi uygulamaları nedeniyle açılan pozisyonları gösteren kodlarını, on birinci ve on ikinci haneler ise ilgili ülkelerdeki istatistik kodlarını göstermek için kullanılmaktadır (Bakanlığı, 2024).

Uluslararası Ticaret Merkezi (UTM) tarafından oluşturulmuş ve koordine edilen Trademap.org internet sitesi, 200’den fazla ülkenin ve bölgenin harmonize sistemde kayıtlı bulunan 5.000’den fazla ürününü içerecek şekilde tasarlanmıştır. Trademap.org internet sitesi sisteme dâhil olan ülkelerin resmi istatistik kurumlarının veri tabanlarından ilgili ürünlerin ihracat ve ithalat rakamlarını çeşitli ölçütler (aylık, 3 aylık, 6 aylık, yıllık, kg/ton/lt, para birimi vb.) doğrultusunda kendi bünyesinde bulunan veri tabanına aktarmaktadır. Trademap.org isimli internet sitesini kullanan araştırmacılar, ülkelerin ilgili ürünlerdeki ticari verilerine, dünya payına, yeni pazarların ekonomik ve ticari yapısına, rekabetçi

pazarlara, ihracatçı-ithalatçı detaylarına sayısal veriler, tablolar, grafikler ve haritalar şeklinde ulaşabilmektedir. Kısaca; trademap.org isimli ticaret temelli internet sitesi, uluslararası ticaretin ve iş olanaklarının geliştirilebilmesi için kullanılan istatistiki bilgiler sağlayan veri tabanı niteliğinde bir ara yüz sağlayıcısı ve sistemidir.

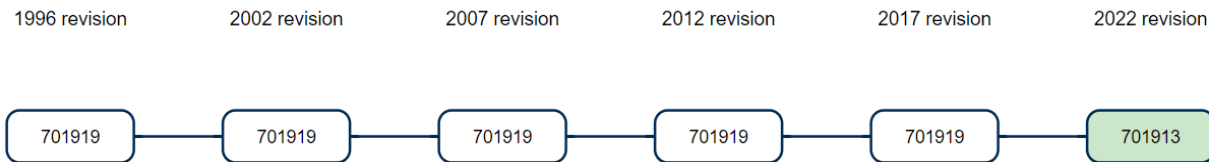
Dünyada ve Türkiye’de hem uluslararası hem de yurt içi ticarete konu ürünlerden olan cam elyaf iplikleri ve fitilleri ürünlerinin uluslararası arenadaki Gümrük Tarife İstatistik Pozisyon (GTİP) numaraları sırası ile Tablo 2’de sunulmuştur.

Tablo 2. Cam Elyaf İplikleri ve Fitilleri Ürünlerinin GTİP’i ve Ürün Tanımları

GTİP	Ürün Tanımı
701911000000 (701911)	Cam elyaf iplikler "kıyılmış şeritler", <= 50 mm uzunluklarda kesilmiş ürünler
701912000000 (701912)	Cam elyaf fitilleri ürünleri
701913000000 (701913)	Cam elyafından iplik ve şeritler (uzunluğu <= 50 mm olan doğranmış şeritler ve fitiller hariç) ürünleri
701914000000 (701914)	Cam elyafından mekanik olarak bağlanmış keçeler ürünü
701915000000 (701915)	Cam elyafından kimyasal olarak bağlanmış keçeler ürünü

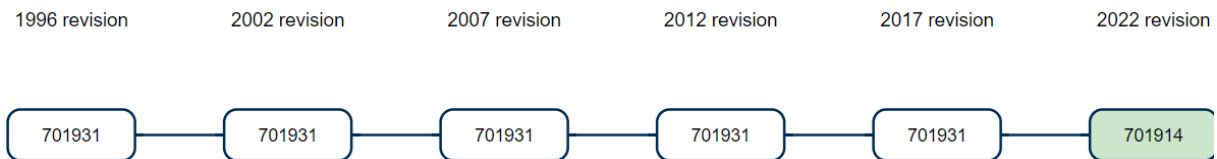
Çalışma kapsamında ele alınan 701911 ve 701912 GTİP kodlu ürünlerin son yirmi yıla ilişkin ticari verileri Trade Map ara yüzünde bulunmasına karşın; 701913, 701914 ve 701915 GTİP kodlu ürünler 2022 yılı başına kadar farklı ürün GTİP’lerinin altında hesaplanmış ve verileri farklı kodlar doğrultusunda paylaşılmıştır. 701913 GTİP kodlu ürün, 2022 yılı başına kadar 701919 (Cam elyaf kekleri "tekstil kekleri" ve uzunluğu >50 mm olan doğranmış cam elyaf şeritleri) GTİP kodlu ürünün içerisinde, 701914 ve 701915 GTİP kodlu ürünler, 2022 yılı başına kadar 701931 (Düzensiz lamine cam elyaflardan yapılmış paspaslar) GTİP kodlu ürünün içerisinde hesaplanmıştır. 2022 yılında yapılan HS revizyonu ile birlikte 701913, 701914 ve 701915 kodlu GTİP’lere sahip olan ürünler bireysel GTİP’leri üzerinden hesaplanmaya başlanmıştır. Belirtilen bu duruma istinaden 701913, 701914 ve 701915 GTİP kodlu ürünlerin 2022 yılına kadar ki ihracat ve ithalat rakamları tam anlamı ile hesaplanamamakta ancak bireysel hesaplamaya geçilen 2022 yılı itibari ile kesin rakamlara ulaşılmaktadır. 2022 yılında HS revizyonu olan GTİP’lere ilişkin görseller Şekil 1, Şekil 2 ve Şekil 3’te sunulmuştur.

Harmonized System revisions correspondences



Şekil 1. 701913 Kodlu GTİP’e Sahip Ürünüdeki 2022 Yılı HS Revizyonu (Trademap, Mayıs 2024)

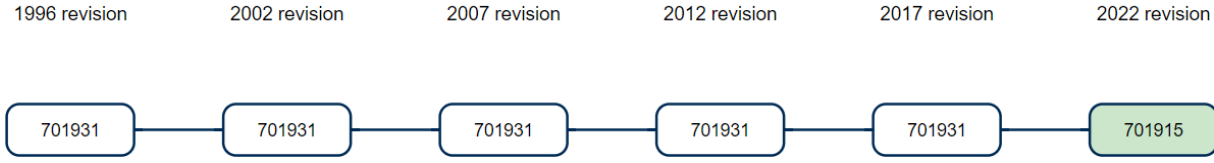
Harmonized System revisions correspondences



Şekil 2. 701914 Kodlu GTİP’e Sahip Ürünüdeki 2022 Yılı HS Revizyonu (Trademap, Mayıs 2024)

Harmonized System revisions correspondences

I



Şekil 3. 701915 Kodlu GTİP'e Sahip Ürünüdeki 2022 Yılı HS Revizyonu (Trademap, Mayıs 2024)

Günün değişen ekonomik koşullarına ve ticari şartlarına istinaden Dünya Gümrük Örgütü (DGO) GTİP'ler üzerinde değişikliğe giderek hesaplamaları ve verileri daha doğru şekilde sonuçlandırmaya gayret göstermektedir. Şekil 1, Şekil 2 ve Şekil 3'te belirtilen açıklamaya örnek bir durum bulunmaktadır.

Çalışmanın kapsamına; 701911, 701912, 701913, 701914 ve 701915 GTİP koduna sahip olan ürünlerin Türkiye'den Dünya ülkelerine ve G-7 ülkelerinden Dünya ülkelerine yapmış olduğu ihracat ve ithalat rakamlarını 2022 ve 2023 yıllarını milyon USD para birimi cinsinden içermektedir.

3. BULGULAR

Çalışmada cam elyaf iplikleri, fitilleri ve bu ürünlerin çeşitleri ilgili GTİP kodları doğrultusunda ele alınmıştır. Konu kapsamına giren ürünlerin ihracat ve ithalat rakamları Amerikan doları cinsinden sadece 2022 ve 2023 yıllarını kapsayacak şekilde ve öncelikle Türkiye açısından sonrasında ise dünyanın en gelişmiş 7 ülke ekonomisi (G-7) açısından araştırılmıştır (Trademap, Mayıs 2024). Tablo 3'te Türkiye'nin ilgili ürünlerdeki dış ticaret verileri paylaşılmıştır.

Tablo 3. 7019(11),(12),(13),(14),(15) GTİP Koduna Sahip Ürünlerin Türkiye'deki Dış Ticareti (Milyon USD, 2022 ve 2023 Yılları)

Ürün GTİP Kodu	Ürün Tanımı	Türkiye'den Dünyaya İhracat Verileri		Türkiye'nin Dünyadan İthalat Verileri	
		2022	2023	2022	2023
701911000000 (701911)	Cam elyaf iplikler "kıyılmış şeritler", <= 50 mm uzunluklarda kesilmiş ürünler	10,211	9,068	37,586	30,794
701912000000 (701912)	Cam elyaf fitilleri ürünleri	14,554	12,399	138,400	83,074
701913000000 (701913)	Cam elyafından iplik ve şeritler (uzunluğu <= 50 mm olan doğranmış şeritler ve fitiller hariç) ürünleri	0,81	0,664	4,454	4,586
701914000000 (701914)	Cam elyafından mekanik olarak bağlanmış keçeler ürünü	3,354	3,430	2,902	2,981
701915000000 (701915)	Cam elyafından kimyasal olarak bağlanmış keçeler ürünü	6,845	2,933	19,988	15,248

Tablo 3'ten de anlaşılacağı üzere; Türkiye 701911 GTİP kodlu üründen 2022 yılında yaklaşık 10 milyon, 2023 yılında ise yaklaşık olarak 9 milyon dolar ihracat gerçekleştirmiştir. Bu duruma karşın 2022 ve 2023 yılında Türkiye'nin 701911 GTİP kodlu üründe ithalatı yaklaşık olarak 37,5 milyon ve 30,8 milyon dolar düzeyindedir. Türkiye 701912 GTİP kodlu üründen 2022 yılında yaklaşık 14,5 milyon, 2023 yılında ise yaklaşık olarak 12,4 milyon dolar ihracat gerçekleştirmiştir. Bu duruma karşın 2022 ve 2023 yılında Türkiye'nin 701912 GTİP kodlu üründe ithalatı yaklaşık olarak 138,4 milyon ve 83 milyon dolar düzeyindedir. Türkiye 701913 GTİP kodlu üründen 2022 yılında yaklaşık 81 bin, 2023 yılında ise yaklaşık olarak 664 bin dolar ihracat gerçekleştirmiştir. Bu duruma karşın 2022 ve 2023 yılında Türkiye'nin 701913 GTİP kodlu üründe ithalatı yaklaşık olarak 4,5 milyon ve 4,6 milyon dolar düzeyindedir. Türkiye 701914 GTİP kodlu üründen 2022 yılında yaklaşık 3,3 milyon, 2023 yılında ise yaklaşık

olarak 3,4 milyon dolar ihracat gerçekleştirmiştir. Bu duruma karşın 2022 ve 2023 yılında Türkiye'nin 701914 GTİP kodlu üründe ithalatı yaklaşık olarak 2,9 milyon ve 2,9 milyon dolar düzeyindedir. Türkiye 701915 GTİP kodlu üründen 2022 yılında yaklaşık 6,8 milyon, 2023 yılında ise yaklaşık olarak 3 milyon dolar ihracat gerçekleştirmiştir. Bu duruma karşın 2022 ve 2023 yılında Türkiye'nin 701915 GTİP kodlu üründe ithalatı yaklaşık olarak 20 milyon ve 15,2 milyon dolar düzeyindedir. Bu durumlar göstermektedir ki; Türkiye'de 701911, 701912, 701913 ve 701915 GTİP kodlu ürünlerin dış ticaretinde açık bulunurken, 701914 GTİP kodlu üründe az da olsa dış ticaret fazlası bulunmaktadır. Türkiye 2022 ve 2023 yılında 701911 GTİP kodlu üründen en çok ihracatı İtalya'ya gerçekleştirmiştir. 701912 GTİP kodlu ürünü 2022 yılında en çok Macaristan'a, 2023 yılında ise Almanya'ya ihraç etmiştir. 701913 GTİP kodlu ürünü 2022 yılında İran'a ve ABD'ye eşit seviyede ihraç edebilmiş ve 2023 yılında da İtalya'ya en fazla ihracat gerçekleştirilmiştir. 701914 GTİP kodlu ürünü 2022 ve 2023 yılında Brezilya'ya, 701915 GTİP kodlu ürünü 2022 ve 2023 yıllarında İtalya'ya en yüksek şekilde ihraç etmiştir.

Çalışma kapsamında ele alınan ürünler hem özel hem de endüstriyel alanda kullanılan ürünlerdir. Dolayısı ile bu tarz ürünlerin üretiminin, ihracatının ve ithalatının gelişmiş ve gelişmekte olan ülkelerde daha çok döngüsünün olacağına kanaat getirilmesine istinaden bu ülkelerin de araştırılması çalışmaya dâhil edilmiştir. Araştırma kapsamında yapılan incelemeler Tablo 4, Tablo 5, Tablo 6 ve Tablo 7'de paylaşılmıştır (Trademap, Mayıs 2024).

Tablo 4. G-7 Ülkelerinin 701911 GTİP Kodlu Üründeki Dış Ticaret Verileri (Milyon USD, 2022 ve 2023 Yılları)

GTİP: 701911000000 - Cam elyaf iplikler "kıyılmış şeritler", <= 50 mm uzunluklarda kesilmiş ürünler				
G-7 Ülkeleri	İhracat (\$)		İthalat (\$)	
	2022	2023	2022	2023
Almanya	23,941	16,038	342,594	283,085
ABD	75,960	55,065	223,186	123,514
Birleşik Krallık	11,381	8,572	35,878	29,760
Fransa	128,454	144,154	53,539	44,788
İtalya	16,083	6,635	147,352	95,637
Japonya	66,477	39,376	69,170	73,449
Kanada	13,204	13,021	9,495	9,637
Dünya	1,694,587	*Veriler tam değildir	1,796,143	*Veriler tam değildir

(*) Trademap.org sitesinde bazı ülkelerin ilgili ürünlerde 2023 yılı ithalat ve ihracat verileri paylaşılmadığından dolayı veri bilgisine ulaşılamamış olup ticari verilere eklenmemiştir.

Tablo 4'ten anlaşılacağı üzere; 701911 GTİP kodlu üründe G-7 ülkelerinin 2022 ve 2023 yıllarını kapsayacak şekilde ihracat ve ithalat rakamları paylaşılmıştır. G-7 ülkeleri içinde 2022 ve 2023 yıllarında sırası ile en fazla ihracat 128 milyon dolar ve 144 milyon dolar ile Fransa tarafından gerçekleştirilmiştir. G-7 ülkeleri içinde 2022 ve 2023 yıllarında sırası ile en fazla ithalat 342,5 milyon dolar ve 283 milyon dolar ile Almanya tarafından gerçekleştirilmiştir.

Tablo 5. G-7 Ülkelerinin 701912 GTİP Kodlu Üründeki Dış Ticaret Verileri (Milyon USD, 2022 ve 2023 Yılları)

GTİP: 701912000000 - Cam elyaf fitilleri ürünleri				
G-7 Ülkeleri	İhracat (\$)		İthalat (\$)	
	2022	2023	2022	2023
Almanya	18,959	14,598	142,578	131,231
ABD	85,713	94,224	439,208	331,569
Birleşik Krallık	74,249	63,152	36,524	25,386
Fransa	78,599	69,363	61,826	50,725
İtalya	47,613	38,776	89,922	83,600
Japonya	23,965	20,305	34,264	29,549
Kanada	2,800	1,364	53,762	42,868
Dünya	1,739,582	*Veriler tam değildir	2,146,678	*Veriler tam değildir

(*) Trademap.org sitesinde bazı ülkelerin ilgili ürünlerde 2023 yılı ithalat ve ihracat verileri paylaşılmadığından dolayı veri bilgisine ulaşılamamış olup ticari verilere eklenmemiştir.

Tablo 5'ten anlaşılacağı üzere; 701912 GTİP kodlu üründe G-7 ülkelerinin 2022 ve 2023 yıllarını kapsayacak şekilde ihracat ve ithalat rakamları paylaşılmıştır. G-7 ülkeleri içinde 2022 ve 2023 yıllarında sırası ile en fazla ihracat 85 milyon dolar ve 94 milyon dolar ile ABD tarafından gerçekleştirilmiştir. G-7 ülkeleri içinde 2022 ve 2023 yıllarında sırası ile en fazla ithalat 439 milyon dolar ve 331 milyon dolar ile ABD tarafından gerçekleştirilmiştir.

Tablo 6. G-7 Ülkelerinin 701913 GTİP Kodlu Üründeki Dış Ticaret Verileri (Milyon USD, 2022 ve 2023 Yılları)

GTİP: 701913000000 - Cam elyafından iplik ve şeritler (uzunluğu <= 50 mm olan doğranmış şeritler ve fitiller hariç) ürünleri				
G-7 Ülkeleri	İhracat (\$)		İthalat (\$)	
	2022	2023	2022	2023
Almanya	18,528	16,226	66,771	53,553
ABD	72,161	37,837	158,552	130,820
Birleşik Krallık	23,870	27,745	23,457	19,187
Fransa	6,962	3,709	40,398	28,341
İtalya	0,374	0,595	36,763	33,450
Japonya	38,343	34,630	65,581	43,245
Kanada	3,534	5,444	1,584	2,15
Dünya	381,207	*Veriler tam değildir	561,599	*Veriler tam değildir

(*) Trademap.org sitesinde bazı ülkelerin ilgili ürünlerde 2023 yılı ithalat ve ihracat verileri paylaşılmadığından dolayı veri bilgisine ulaşılamamış olup ticari verilere eklenmemiştir.

Tablo 6'dan anlaşılacağı üzere; 701913 GTİP kodlu üründe G-7 ülkelerinin 2022 ve 2023 yıllarını kapsayacak şekilde ihracat ve ithalat rakamları paylaşılmıştır. G-7 ülkeleri içinde 2022 ve 2023 yıllarında sırası ile en fazla ihracat 72 milyon dolar ve 37 milyon dolar ile ABD tarafından gerçekleştirilmiştir. G-7 ülkeleri içinde 2022 ve 2023 yıllarında sırası ile en fazla ithalat 158 milyon dolar ve 130 milyon dolar ile ABD tarafından gerçekleştirilmiştir.

Tablo 7. G-7 Ülkelerinin 701914 GTİP Kodlu Üründeki Dış Ticaret Verileri (Milyon USD, 2022 ve 2023 Yılları)

(*) Trademap.org sitesinde bazı ülkelerin ilgili ürünlerde 2023 yılı ithalat ve ihracat verileri paylaşılmadığından dolayı

GTİP: 701914000000 - Cam elyafından mekanik olarak bağlanmış keçeler ürünü				
G-7 Ülkeleri	İhracat (\$)		İthalat (\$)	
	2022	2023	2022	2023
Almanya	24,954	19,440	8,131	9,709
ABD	10,510	9,828	31,677	17,343
Birleşik Krallık	5,793	3,905	8,982	9,822
Fransa	25,419	25,056	9,085	11,540
İtalya	9,325	11,612	10,797	12,071
Japonya	9,968	12,631	7,536	7,590
Kanada	0,404	0,289	10,273	5,865
Dünya	175,007	*Veriler tam değildir	165,430	*Veriler tam değildir

veri bilgisine ulaşamamış olup ticari verilere eklenmemiştir.

Tablo 7'den anlaşılacağı üzere; 701914 GTİP kodlu üründe G-7 ülkelerinin 2022 ve 2023 yıllarını kapsayacak şekilde ihracat ve ithalat rakamları paylaşılmıştır. G-7 ülkeleri içinde 2022 ve 2023 yıllarında sırası ile en fazla ihracat 25 milyon dolar ve 25 milyon dolar ile Fransa tarafından gerçekleştirilmiştir. G-7 ülkeleri içinde 2022 ve 2023 yıllarında sırası ile en fazla ithalat 31,6 milyon dolar ve 17,3 milyon dolar ile ABD tarafından gerçekleştirilmiştir.

Tablo 8. G-7 Ülkelerinin 701915 GTİP Kodlu Üründeki Dış Ticaret Verileri (Milyon USD, 2022 ve 2023 Yılları)

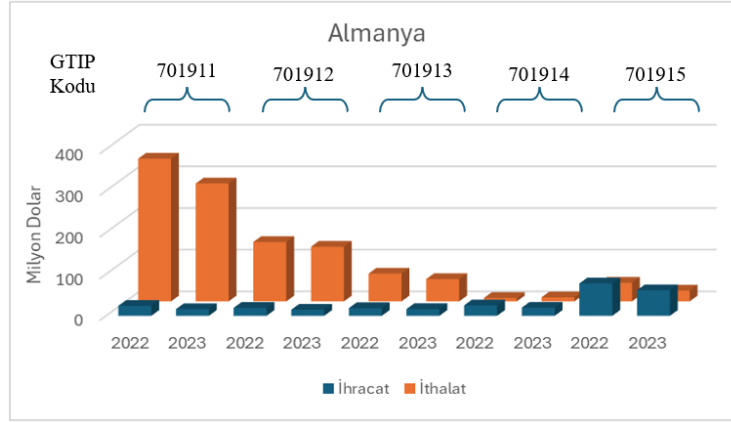
GTİP: 701915000000 - Cam elyafından kimyasal olarak bağlanmış keçeler ürünü				
G-7 Ülkeleri	İhracat (\$)		İthalat (\$)	
	2022	2023	2022	2023
Almanya	77,607	61,346	44,808	26,243
ABD	28,821	32,233	117,908	95,389
Birleşik Krallık	6,643	12,024	9,947	14,390
Fransa	3,012	2,185	20,568	12,231
İtalya	69,301	67,093	18,102	14,739
Japonya	3,201	3,181	17,250	15,673
Kanada	22,428	34,918	15,342	16,500
Dünya	571,016	*Veriler tam değildir	539,144	*Veriler tam değildir

(*) Trademap.org sitesinde bazı ülkelerin ilgili ürünlerde 2023 yılı ithalat ve ihracat verileri paylaşılmadığından dolayı veri bilgisine ulaşamamış olup ticari verilere eklenmemiştir.

Tablo 8'den anlaşılacağı üzere; 701915 GTİP kodlu üründe G-7 ülkelerinin 2022 ve 2023 yıllarını kapsayacak şekilde ihracat ve ithalat rakamları paylaşılmıştır. G-7 ülkeleri içinde 2022 ve 2023 yıllarında sırası ile en fazla ihracat 77 milyon dolar ile Almanya ve 67 milyon dolar ile İtalya tarafından gerçekleştirilmiştir. G-7 ülkeleri içinde 2022 ve 2023 yıllarında sırası ile en fazla ithalat 117,9 milyon dolar ve 95 milyon dolar ile ABD tarafından gerçekleştirilmiştir.

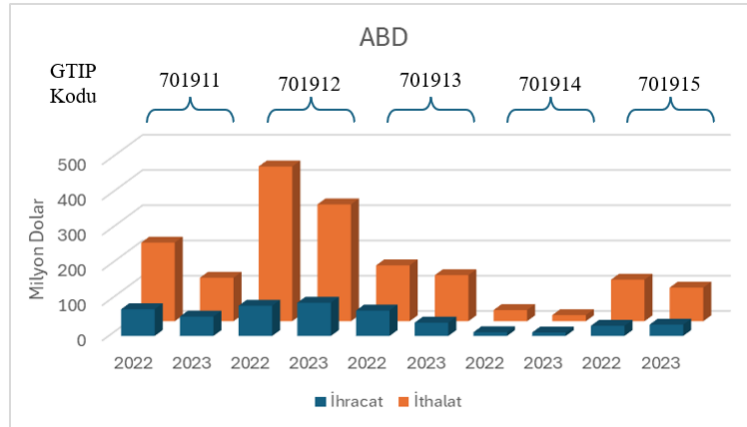
Tablolarda belirtilen ürünler için ülke bazlı incelenmesi de gerçekleştirilmiştir. Bu doğrultuda cam elyafların farklı GTIP kodlarındaki ürünler ülke bazında incelenmesi Şekil 4-11 arasında verilmiştir. Özellikle G-7 ve Türkiye açısından 2023 yılına bakıldığında cam elyaf ürünlerinin kullanılmasında 2022 yılına göre ciddi bir düşüş sergilemiştir. Bu da ithalat rakamlarına yansımakta ve cam elyaf pazarında bir daralmanın olduğunu göstermektedir. Şekil 4'te Almanya'nın bu belirtilen cam elyaf ürünlerinin tamamına yakında ithalatçı konumunda yer aldığı gözükürken, 701915 GTIP kodlu

kimyasal olarak bağlanmış cam elyaf keçenin ihracatçı konumunda yer aldığı belirlenmiştir. 701911 GTIP kodlu cam elyaf iplikler en çok kullanılan ürün olarak karşımıza çıkmaktadır.



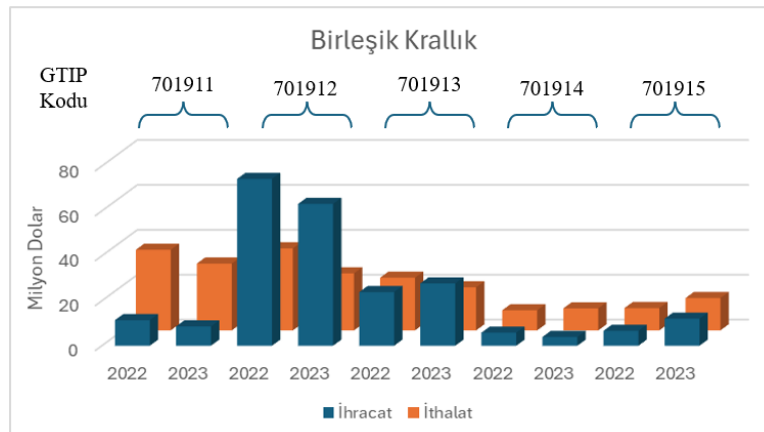
Şekil 4. Almanya'nın cam elyaf ürünlerinin 2022 ve 2023 yıllarındaki ihracat ve ithalat verileri

Şekil 5'te ABD'nin cam elyaf ürünlerindeki 2022 ve 2023 yıllarındaki ihracat ve ithalat verileri görülmektedir. GTIP kodları verilen bu beş cam elyaf ürününün tümünde ithalatçı konumunda olmakla beraber cam elyaf fitilleri en çok kullandığı ürün olarak karşımıza çıkmaktadır.



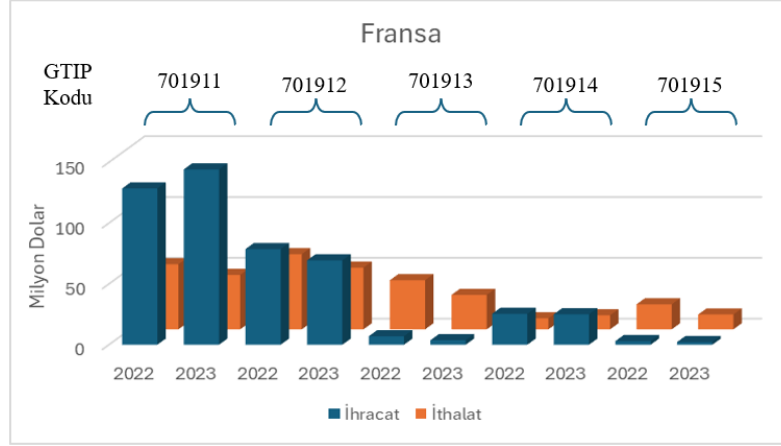
Şekil 5. ABD'nin cam elyaf ürünlerinin 2022 ve 2023 yıllarındaki ihracat ve ithalat verileri

Şekil 6'da Birleşik Krallık'a ait 2022 ve 2023 yıllarındaki ihracat ve ithalat verileri gösterilmektedir. Cam elyaf fitilleri ve iplik ve şeritlerinin ihracatçı konumunda olan Birleşik Krallık diğer cam elyaf ürünlerinde ise ithalatçı konumunda yer almaktadır. Fakat tüm cam elyaf ürünlerinin açısından bakıldığında Almanya ve ABD'nin ihracat ve ithalat oranlarının yanında düşük olduğu görülmektedir.



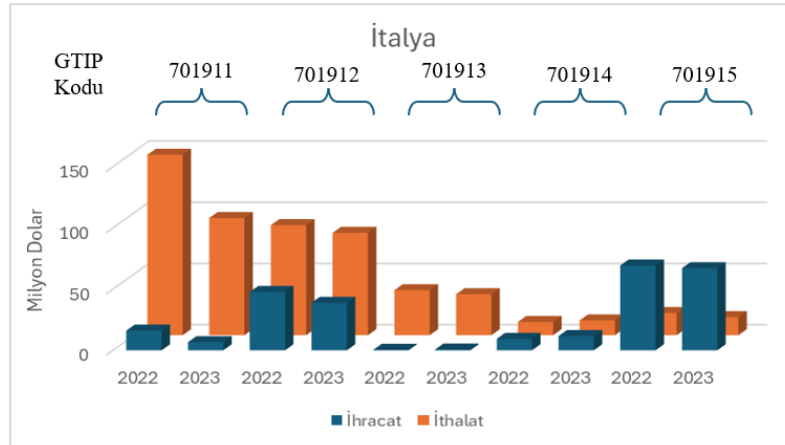
Şekil 6. Birleşik Krallık'ın cam elyaf ürünlerinin 2022 ve 2023 yıllarındaki ihracat ve ithalat verileri

Fransa'ya ait 2022 ve 2023 yıllarındaki ihracat ve ithalat verileri şekil 7'de gösterilmektedir. Cam elyafların ürün bazlı incelendiği takdirde 701911, 701912 ve 701914 GTIP kodlu ürünlerin ihracatçısı konumunda yer alırken diğer 701913 ve 701915 GTIP kodlu ürünlerde ithalatçı durumundadır. Fransa'da bu sektörün büyüklüğü açısından bakıldığı Almanya ve ABD'nin gerisinde kaldığı görülmektedir.



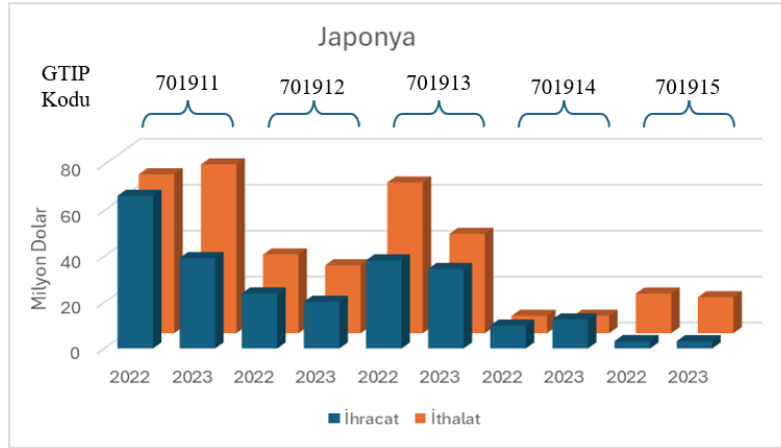
Şekil 7. Fransa'nın cam elyaf ürünlerinin 2022 ve 2023 yıllarındaki ihracat ve ithalat verileri

İtalya'ya ait 2022 ve 2023 yıllarındaki ihracat ve ithalat verileri şekil 8'de gösterilmektedir. İtalya yalnızca 701915 GTIP kodlu cam elyafından kimyasal olarak bağlanmış keçeler ürünlerinde ihracatçı konumunda yer alırken diğer cam elyaf ürünlerinin ithalatçısı durumundadır. 701911 GTIP kodlu cam elyaf iplik ürünlerinin kullanımında 2022 ve 2023 yılı incelendiğinde ihracat ve ithalat rakamlarında ciddi bir oranda düşüş kaydedildiği ortaya çıkmaktadır. Diğer ürünlerin açısından incelendiğinde 2022 ve 2023 yılında hemen hemen aynı değerlerde ihracat ve ithalat rakamları mevcuttur. Diğer ülkelerde bu pazar payının ciddi bir oranda daralma gözükürken İtalya'da tek bir ürün haricinde daralma gözükmemektedir.



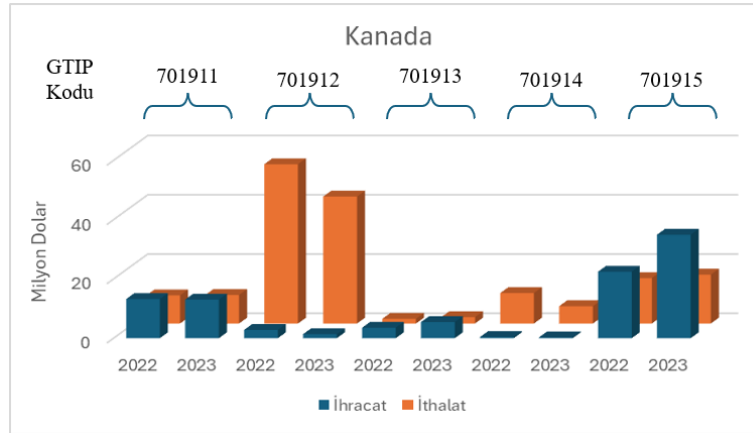
Şekil 8. İtalya'nın cam elyaf ürünlerinin 2022 ve 2023 yıllarındaki ihracat ve ithalat verileri

Şekil 9'da Japonya'ya ait 2022 ve 2023 yıllarındaki ihracat ve ithalat verileri gösterilmektedir. Bu rakamlar incelendiğinde Japonya ithalat ve ihracat oranlarının dengeli olduğu çok büyük farklar oluşmadığı tespit edilmiştir. Cam elyaf sektörünün 2023 yılında daralma yaşanmasına karşın 701911 GTIP kodlu cam elyaf iplikler ithalat rakamlarında artış kaydedilmiştir.



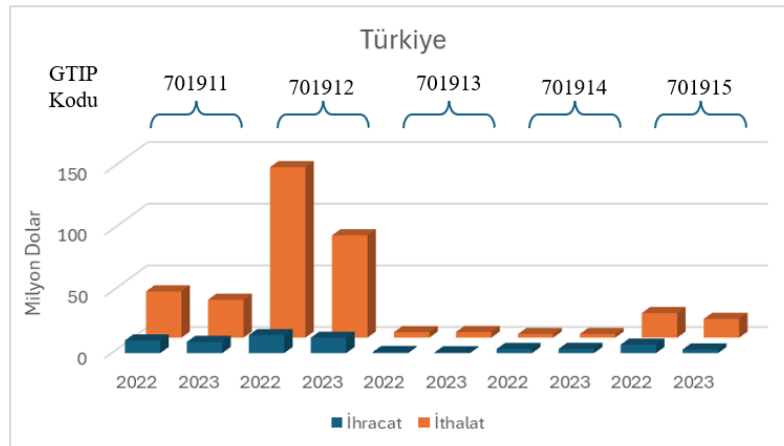
Şekil 9. Japonya'nın cam elyaf ürünlerinin 2022 ve 2023 yıllarındaki ihracat ve ithalat verileri

Şekil 10'da Kanada'ya ait 2022 ve 2023 yıllarındaki ihracat ve ithalat verileri gösterilmektedir. Kanada 701912 GTIP kodlu cam elyaf fitil ürünlerin ciddi oranda ithalatçısı durumunda yer almaktadır. Benzer şekilde cam elyaf sektörün 2023 yılında daraldığını bu ülkede de görmekteyiz. Fakat Fransa'da olduğu gibi 701915 GTIP kodlu cam elyafından kimyasal olarak bağlanmış keçeler ürünlerinin 2023 yılındaki ihracat oranını artırmış bulunmaktadır.



Şekil 10. Kanada'nın cam elyaf ürünlerinin 2022 ve 2023 yıllarındaki ihracat ve ithalat verileri

Türkiye'ye ait 2022 ve 2023 yıllarındaki ihracat ve ithalat verileri şekil 11'de gösterilmektedir. Öncelikle yıl bazlı incelendiği takdirde tüm cam elyaf ürünlerinin 2023 yılında ihracat ve ithalat rakamlarında düşüşler meydana geldiği belirlenmektedir. Ürün bazlı inceleme yapıldığında 701912 GTIP kodlu cam elyaf fitiller Türkiye'de en çok kullanılan cam elyaf ürünü olarak karşımıza çıkmaktadır. Bu ürünün ihracat ve ithalat rakamları arasında ciddi bir oranda fark bulunmaktadır. Türkiye, Almanya ve ABD gibi ithalatçı konumunda olan bir ülke olarak karşımıza çıkmaktadır.



Şekil 11. Türkiye'nin cam elyaf ürünlerinin 2022 ve 2023 yıllarındaki ihracat ve ithalat verileri

Cam elyaf ürünleri üretimi açısından en büyük üretici olarak bulunan Şişecam firması Türkiye'nin ihracat rakamlarına etkisinin belirlenebilmesi için 2023 ve 2022 yılına ait finansal tabloları incelenmiştir. GTIP kodlarında bahsi geçen bu 5 ürünün üretimini yapan Şişecam yıllık 70 bin ton üretim kapasitesine sahip olduğunu belirtmiştir (Şişecam, 2023). 2023 yılında gelir yıllık bazda %11 düşüşle 152 Milyar TL seviyesinde kaydedilirken, cam elyaf bu gelirin %1'ini oluşturarak yaklaşık olarak 1,5 milyar TL'lik (~64 milyon USD) kısmını oluşturmaktadır (Şişecam, 2023). Türkiye'nin 2023 yılında cam elyaf ürünlerinde 28 milyon USD değerinde ihracat rakamına ulaşmıştır (Trademap, Mayıs 2024). Bu rakamlar sonucunda Şişecam'ın iç pazarda önemli bir ihtiyacı karşıladığını ortaya çıkarmaktadır. Ayrıca Türkiye'nin ihracat rakamının tamamına yakını Şişecam tarafından karşılandığı belirlenebilmektedir. Firmanın finansal raporlarına da yansdığı gibi 2023 yılında önemli bir daralmanın gerçekleştiği görülmektedir. Bu durumu Çin'deki tüketiminin azalmasına bağlı olarak ortaya çıkan arz fazlası olduğu söylenebilmektedir.

4. TARTIŞMA VE SONUÇLAR

Kompozit malzemelerde yaygın olarak kullanılan cam elyaf ürünlerinin G-7 ve Türkiye açısından 2022 ve 2023 yılına ait ihracat ve ithalat rakamlarının incelenmesi yapılmıştır. Rakamlar incelendiğinde cam elyaf sektörünün 2023 yılında önemli bir ölçüde daraldığı görülmektedir. Bu daralmanın sebebi olarak Çin ve Hindistan gibi cam elyaf ürünlerinin en büyük üreticisi ve tüketicisi konumunda yer alan bu iki ülkede 2023 yılında tüketimin azalmasına bağlı olarak arz fazlası olarak gösterilebilir. Cam elyaf ürünlerinin ihracat ve ithalat rakamlarının belirlenebilmesi için geçerli olan GTIP kodlarından faydalanılmış ve 5 farklı cam elyaf türü bulunmuştur. Fransa 701911, Birleşik Krallık 701912, İtalya, Kanada ve Almanya 701915 GTIP kodlu ürünlerde ihracatçı konumunda yer alırken diğer ürünlerde ithalatçı durumundadır. ABD ve Türkiye tüm cam elyaf ürünlerde ithalatçı durumunda iken, Japonya ise ihracat ve ithalat rakamları birbirine yakın bir biçimdedir. Savunma, havacılık, otomotiv, altyapı ve rüzgâr enerjisi gibi sektörlerde kullanılan cam elyaflar özellikle elektrikli araçların satış miktarının artması ile birlikte otomotiv sektörün büyümesine bağlı olarak 2024 yılında cam elyaf pazarının da büyüyeceği düşünülmektedir.

KAYNAKLAR

Ticaret Bakanlığı, (2024). <https://ticaret.gov.tr/gumruk-islemleri/sikca-sorulan-sorular/ticari/tarife>.

Türkiye Odalar ve Borsalar Birliği, (2012). *Cam ve Cam Ürünleri Sanayi Meclisi Raporu*.

Clyne, T. W., & Hull, D. (2019). *An introduction to composite materials*. Cambridge university press.

Güvenbaş, Ö. Dünya ve Türkiye Cam Sanayi Sektörüne Genel Bakış.

Mallick, P. K. (2007). *Fiber-reinforced composites: materials, manufacturing, and design*. CRC press.

Sanayi Genel Müdürlüğü, (2022). *Cam Sektör Raporu 2021*.

Sathishkumar, T., Satheeshkumar, S., & Naveen, J. (2014). Glass fiber-reinforced polymer composites—a review. *Journal of Reinforced Plastics and Composites*, 33(13), 1258-1275.

Şişecam. *CTP Atölye Bilgileri*.

Şişecam. (2020). *Cam Sektörü Raporu "Dünya&Türkiye"*.

Şişecam. (2023). *Faaliyet Raporu*

Trademap. (Mayıs 2024). www.trademap.org.

Wang, J., Geng, C., Luo, F., Liu, Y., Wang, K., Fu, Q., & He, B. (2011). Shear induced fiber orientation, fiber breakage and matrix molecular orientation in long glass fiber reinforced polypropylene composites. *Materials Science and Engineering: A*, 528(7-8), 3169-3176.

Combining Multi-Source Bearing Fault Datasets and Analyzing the Impact of Welch Method Parameters on Classification

Yunus Emre Acar^{1*}

Abstract: This study integrates four distinct bearing fault datasets to create a comprehensive dataset for enhanced fault classification. The combined dataset encompasses vibration data recorded with different sampling frequencies for bearing types under distinct operational conditions like fixed or variable rotational speeds. Utilizing the Welch method on these vibration signals derives power spectral density (PSD) signals of uniform length suitable for classifier input. This approach unifies the datasets into a common domain through PSD signals. The PSD signals are the input of the classifier without any preprocessing. The performance of the Welch approach to create a domain for bearing fault data is investigated by analyzing the impact of Welch method parameters. After directly supplying the PSD as the input, the Chi2 algorithm is employed for feature selection to increase the classification accuracy further. The findings demonstrate the effectiveness of this approach, achieving an accuracy of 98.2%, and underscore the significance of parameter adjusting and feature selection in the Welch method for accurate fault classification in heterogeneous bearing datasets.

Keywords: bearing, fault detection, machine learning, PSD, Welch approach.

¹**Address:** Selcuk University, Faculty of Technology, Department of Electrical and Electronics Engineering Konya/Turkiye

***Corresponding author:** yacar@selcuk.edu.tr

1. INTRODUCTION

Rolling bearing is a vital component of rotating machinery widely employed in various industrial applications. Shen Zhang et al. emphasize the results of some IEEE Industry Application Society (IEEE-IAS) surveys revealing that 30% to %40 of all machinery failures are caused by bearing faults (Zhang et al., 2020). Since bearings often work in extremely harsh working conditions, such as elevated temperature, overload, and high moisture they face many localized failures such as spalling, cracking, and pitting. Once these bearing malfunctions occur, they directly affect the operation and safety of the machinery (Hou et al., 2021) and bring high maintenance costs and financial losses. As reported in (Saha et al., 2023), the maintenance expenses account for nearly 15-20%, and %30 of this budget is cast away with improper maintenance strategies. To monitor the progression of bearing health and create a proper plan, one must be aware of the prognostics and diagnose the failures accurately.

Traditionally, bearing fault research is employed model-based (Bianchini et al., 2010; Rahman et al., 2022) and data-based (Giantomassi et al., 2015; Wang et al., 2021). Model-based approaches extract knowledge from the measured signals and relate them to the bearing faults using the previously developed physical bearing fault models. Since establishing the physical model is difficult, data-based approaches have flourished widely. The prognostics are searched on the data captured via various sensors. Unlike model-based methods, specifically, data-based techniques require no expertise on the bearing failure data. The captured data collected by miscellaneous means, including vibration (Mitra & Koley, 2023; Xia et al., 2020), stator current (Nath et al., 2020), acoustic (Kang et al., 2014), and fusion of the severe sensors (Esfahani et al., 2013) is processed. Rather than analyzing the data manually intelligence-based systems are created to use the processed data. Researchers are actively developing signal processing algorithms, using various time-frequency transform techniques, exploring optimal features to differentiate faults, and focusing on various classification models. Mitra and Koley combined a technique that utilizes the time-frequency characteristics of vibration signals by leveraging a two-dimensional Convolutional Neural Network (CNN) and the super-resolution capability of wavelets (Mitra & Koley, 2023). Chêrrez et al. developed a custom bearing fault simulator and employed machine learning techniques to classify bearing faults using vibration and acoustic data (Pacheco-Chêrrez et al., 2022). In (Lei et al., 2024), a semi-supervised innovative methodology for intelligent fault diagnosis is introduced, employing deep transfer learning grounded on the Joint Generalized Sliced Wasserstein Distances (JGSWD) technique. In (Hu et al., 2021), the authors introduce a novel approach aimed at enhancing the labor-intensive and time-consuming process of analyzing substantial volumes of unlabeled data for diagnostic purposes. Termed as the deep adaptive fuzzy clustering algorithm (DAFC), this two-stage unsupervised fault recognition algorithm is devised specifically for the clustering of

faults without the need for labeled data. In addition to the previously mentioned studies, numerous investigations have focused on exploring time-frequency transforms known for their ability to provide appropriate features that facilitate the discrimination of various bearing failures. Commonly favored methodologies include the Short-Time Fourier transform, Gabor transform, Hilbert Huang transform, and wavelet transform, as emphasized in the scholarly literature (Wei et al., 2020).

In (Zheng et al., 2020), Zheng et al. shed light on an alternative perspective regarding the issue, noting that many existing studies primarily focus on developing end-to-end diagnostic schemes within limited datasets characterized by uniform distributions. They emphasize that datasets used to train diagnostic models are often sourced from diverse operational conditions, machines of various types, or laboratory-based simulation faults, potentially exhibiting dissimilar distributions from those encountered during testing. Consequently, in the past five years, numerous research efforts have emerged, introducing cross-domain diagnostic methods based on transfer learning or domain adaptation, leveraging data disparities originating from various sources (Oh et al., 2017; Yang et al., 2019; Zhang et al., 2017).

This study examines the performance of the Welch method in fault classification using vibration data recorded under various working conditions, on different machines, and with distinct equipment. A comprehensive dataset has been created by combining multiple state-of-the-art datasets through a PSD-based domain generalization approach and the performance of the model constructed on this extensive dataset has been assessed.

The organization of the rest of the article is as follows. The second section reviews the PSD approach and describes the datasets, while the results are evaluated in Section III. Finally, the conclusion section summarizes the study.

2. MATERIAL AND METHOD

This paper combines four widely used datasets in bearing fault classification research to generate a larger multi-source dataset. This comprehensive dataset contains vibration data for a total of five different fault conditions. Healthy cases and the failures on the four principal components of a bearing, which are shown in Figure 1, are subjected.

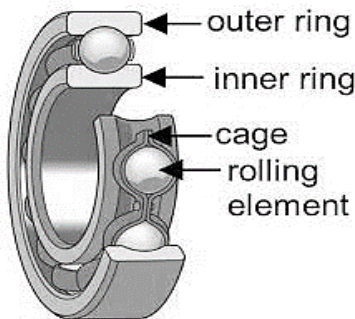


Figure 1. Principal components of a bearing (Nabhan et al., 2015)

2.1. Datasets

The MFPT dataset (Dataset, 2020), produced by the Society for Machinery Failure Prevention Technology, includes data from a bearing test rig. It contains three datasets for the baseline condition under a load of 270 lbs. It also provides ten outer race fault data with two different types. Three of these data were recorded under a constant load of 270 lbs with a sampling rate of 97,656 samples per second (sps) for 6 seconds. The remaining seven data were recorded under varying loads ranging from 25 to 300 lbs. The dataset includes seven inner race fault datasets recorded under various loads with a sampling rate of 48,828 sps for 3 seconds. Table 1 details the specifications of the dataset.

Table 1. The MFPT data content in the combined dataset

Classes	# of data	Explanation
Normal	3	270 lbs of loads, the sampling rate of 97656 sps, for 6 seconds
Outer	3	270 lbs of loads, the sampling rate of 97656 sps, for 6 seconds
Outer	7	25-300 lbs of various loads, the sampling rate of 48828 sps, for 3 seconds
Inner	7	25-300 lbs of various loads, the sampling rate of 48828 sps, for 3 seconds

Table 2. The MaFaulDa data content in the combined dataset

Classes	# of data	Explanation
Normal	49	No fault
Cage Fault	98	To induce a detectable effect imbalance fault is also created.
Outer	98	To induce a detectable effect imbalance fault is also created.
Ball Fault	99	To induce a detectable effect imbalance fault is also created.

The Ottawa (Huang & Baddour, 2018) dataset comprises vibration data collected from ER16K bearing operating under time-varying speeds. This dataset offers vibration records sampled at a frequency of 200 kHz for 10 seconds. Researchers conducted 36 experiments covering no-fault cases, inner-race faults, and outer-race faults. The varying speed scenarios include increasing speed (A), decreasing speed (B), increasing and then decreasing speed (C), and decreasing and then increasing speed (D). Table 3 provides a detailed overview of the dataset.

Table 3. The Ottawa data content in the combined dataset

Classes	# of data	Explanation
Normal	12	Three experiments for each scenario A, B, C, and D with various speed ranges.
Outer	12	Three experiments for each scenario A, B, C, and D with various speed ranges.
Inner	12	Three experiments for each scenario A, B, C, and D with various speed ranges.

The HIT-SM (Wang et al., 2022) dataset includes vibration data collected using two different test rigs: the Machinery Fault Simulator (MFS) and a custom-built rig at the Harbin Institute of Technology. Researchers conduct experiments at three fixed rotational speeds: 600, 900, and 1200 RPM. They use both test rigs to study scenarios involving no fault, inner race faults, and outer race faults. The inner and outer race faults contain slight, moderate, and severe fault levels. The data is acquired with a sampling frequency of 51.2 kHz for approximately 5 seconds. Table 4 provides a detailed summary of the dataset.

Table 4. The HIT-SM data content in the combined dataset

Classes	# of data	Explanation
Normal	6	3 experiments with each test rig with different speeds
Outer	18	3x3 experiments with each test rig with different speeds and fault levels
Inner	18	3x3 experiments with each test rig with different speeds and fault levels

The datasets above are combined to create a larger dataset to analyze the performance of PSD for the vibration data collected under various operation conditions and over several types of bearings. Table 5 summarizes the content of the expanded dataset.

Table 5. The content of the combined dataset

Class	MFPT	MaFaulDa	Ottawa	HIT-SM	Total
Normal	3	49	12	6	70
Outer	10	98	12	18	138
Inner	7	-	12	18	37
Cage	98	-	-	-	98
Ball	99	-	-	-	99

2.2. PSD with Welch approach

The most common method used to observe the frequency components of a signal is the Fourier transform. The Fourier transform $X[n]$ of a discrete sequence $x[k]$ with N elements is calculated as given in (1).

$$X[n] = \sum_{k=0}^{N-1} x[k] e^{-j\frac{2\pi}{N}nk} \quad (n = 0: N - 1) \tag{1}$$

By taking the square of the signal $X[n]$, the power spectrum $P[n]$ can be calculated using a basic approach, as given in (2).

$$P[n] = \frac{1}{N} |X[n]|^2 \quad (n = 0:N - 1) \tag{2}$$

This traditional approach performs calculations over the entire signal, providing high-frequency resolution, but is sensitive to noise. It is also possible to define the power distribution of frequency components by calculating the power spectral density using the Welch method. Unlike the traditional approach, this method does not perform calculations over the entire signal. The signal is first divided into K overlapping segments of length L with D overlapped samples. The segments are weighted by multiplying with a window function $w[n]$, aiming to reduce the spectral leakage that will occur after the Fourier transform. The weighted segments can be expressed as given in (3).

$$y_k[m] = x_k[m + kD]w[m] \quad (k = 0,1, \dots, K - 1; m = 0,1,2, \dots, L - 1) \tag{3}$$

After calculating the power spectrum $P_k[m]$ for each weighted segment, the power spectral density $\hat{P}[n]$ is obtained by averaging the power spectra of all segments, as given in Equation (4).

$$\hat{P}[n] = \frac{1}{K} \sum_{k=0}^{K-1} P_k[n] \tag{4}$$

3. RESULTS AND DISCUSSIONS

This section details the classification results for different PSD parameters. When the dataset has been classified by state-of-the-art machine learning methods such as Support Vector Machine (SVM), Decision Trees (DT), K-nearest Neighborhood (KNN), Naive-Bayes classifiers, and various ensemble methods, KNN has outperformed the others in most trials. Consequently, the presented results focus solely on KNN. Table 6 lists the hyperparameters for the KNN model used. The presented results in the following parts are the five-fold cross-validated results.

Table 6. Hyperparameters of the KNN model used

Number of neighbors	1
Distance metric	Euclidean
Distance weight	equal
Data standardize	yes

PSD, as introduced in the previous section, constitutes an N -length time series. When used directly as an input for a classifier, the number of inputs N significantly influences the classification performance. The length of a PSD calculated using only positive frequency components corresponds to half the number of FFT ($nfft$) points plus one. Table 7 presents the accuracies of KNN with an N -length PSD input and illustrates the impact of varying the $nfft$ value while keeping other parameters constant. The confusion matrix for the best results of Table 7 is presented in Figure 2.

Table 7. Effect of $nfft$ on classification accuracy

$nfft$	Other parameters	Acc. (%) (No feature selection)	Acc. (%) (50 % of features)
256	window: hamming	96.6	97.5
512	$L = 256$	95	97.3
1024	$D = 64$	94.3	96.6

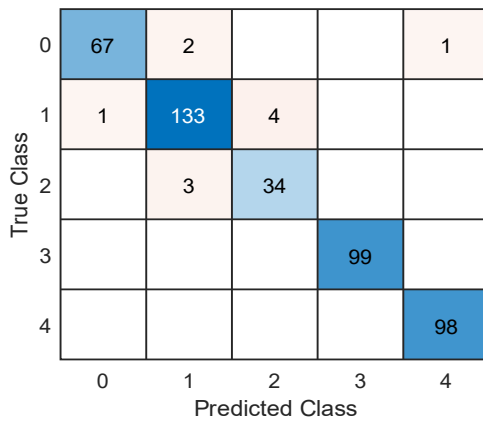


Figure 2. Confusion matrix for $nfft = 256, L = 256, D = 64$, and 50% of feature selection

Table 7 illustrates that increasing the $nfft$ length negatively impacts classifier performance. Although representing the $0 - fs/2$ range with more frequency points might seem beneficial, the increased number of features complicates the classifier's learning process. The enhancement in performance through feature selection supports this observation. This specific aspect falls beyond the scope of the current study and will be explored in future research.

Unlike the traditional periodogram approach, power spectral density is estimated by dividing the signal into equal-length windows and normalizing the power spectra calculated from these windows. Longer windows enhance frequency resolution, while shorter windows increase noise immunity. Due to the trade-off between high-frequency resolution and noise immunity, window size determination is crucial. Table 8 illustrates the effect of window size on classifier performance, keeping all other parameters constant. Figure 3 illustrates the confusion matrix of the best results among the parameter combinations given in Table 8.

Table 8. Effect Of L on Classification Accuracy

L	Other parameters	Accuracy (%) (No feature selection)	Acc. (%) (50% of features)
128	window: hamming $nfft = 256$ $D = L/2$	97.1	96.8
256		96.2	96.6
512		95.2	96.8

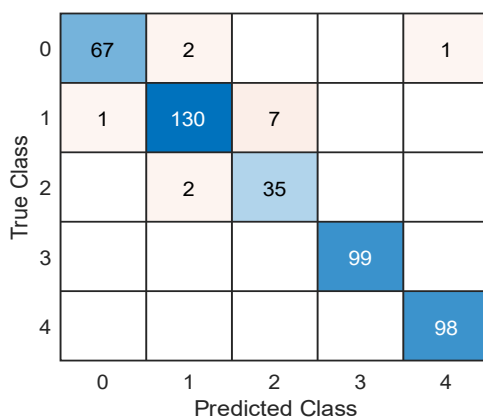


Figure 3. Confusion matrix for $nfft = 256, L = 128, D = 64$, without feature selection

Another crucial parameter for power spectral density estimation is the overlapping ratio. As the window function slides over the signal by a certain overlapping ratio, the number of evaluated power spectrums varies according to this ratio. A higher overlap ratio increases the signal length to which FFT will be applied, resulting in a cleaner spectrum. Conversely, a lower overlap ratio reduces computational complexity and processing time. Table 9 shows the effect of D , while Figure 4 gives the confusion matrix for the best accuracy case for Table 9.

Table 9. Effect of D on Classification Accuracy

D	Other parameters	Accuracy (%) (No feature selection)	Acc. (%) (50% of features)
128	window: hamming $nfft = 256$ $L = 256$	96.2	96.6
64		95.2	95.9
32		95.0	96.4

Last but not least, the windowing function used in the power spectral density calculation reduces spectral leakage. Windowing functions differ in their performance regarding spectral leakage reduction, side lobe magnitude, and frequency resolution. Table 10 compares the performance of the common window functions regarding classification accuracy.

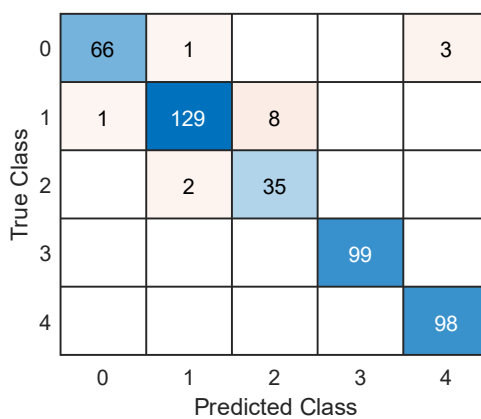


Figure 4. Confusion matrix for $nfft = 256$, $L = 256$, $D = 128$, and 50% of feature selection

Table 10. Effect of window function on classification accuracy

window	Other parameters	Acc. (%) (No feature selection)	Acc. (%) (50% of features)
Hamming	$nfft = 256$ $L = 256$ $D = L/2$	96.2	96.6
Blackman-Harris		95.9	95.9
Hann		95.7	96.4

The results discussed above provide insights into selecting parameters for the Welch method by adjusting only one variable at a time. Beyond the specified parameters, additional feature selection or extraction techniques can further enhance classification performance. Moreover, changes in classifier parameters can significantly affect outcomes. To improve the classification performances reported, commonly used feature selection approaches such as MRMR, Chi2, ReliefF, and ANOVA algorithms have been applied to the data. The best results from these manual experiments have been achieved with an accuracy of 98.2% using the parameters illustrated in Figure 5. Figure 6 gives the confusion matrix for the best result obtained by the adjustments given in Figure 5.

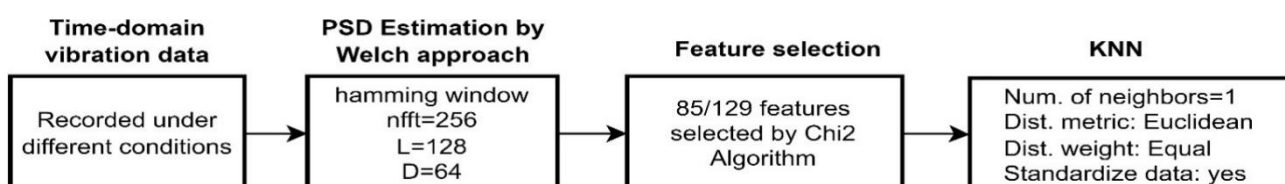


Figure 5. The block scheme of the classification process

0	67	2			1
1		135	3		
2		2	35		
3				99	
4					98
	0	1	2	3	4

Figure 6. Confusion matrix for the best result obtained with $nfft = 256$, $L = 128$, $D = 64$, and 85 of 129 feature selection with Chi2 Algorithm

4. CONCLUSIONS

This study addresses the critical task of bearing fault classification, underscoring the necessity for prompt fault detection and the processes of effective maintenance strategies due to the pivotal role of rolling bearings in mechanical systems. Bearing failures can result in significant system damage, highlighting the need for automated fault detection through sensor data. While numerous studies employ machine learning and deep learning techniques on vibration signals, these approaches are often tailored to specific datasets and may not perform well across varied datasets.

In this research, four different bearing fault data sets were integrated, each recorded under different conditions, including fixed or varying speeds, loads, hardware, and sampling frequencies, without any prior pre-processing. The Welch method was used to derive PSD signals from these vibration signals, thereby transforming the data into a common domain suitable for classification.

The key findings indicate that PSD signals provide a robust common domain for the combined datasets, achieving over 90% accuracy with multiple classifiers. The KNN classifier demonstrated the best performance. While increasing the $nfft$ value reduced performance, the optimal result was obtained at $nfft = 256$, corresponding to a 129-sample-length power spectrum. Shorter window lengths enhanced performance, and higher overlap ratios positively influenced results. The Hamming window function yielded the best outcome. Using $nfft = 256$, window length $L = 128$, and overlap $D = 64$, the most effective power spectral density was achieved. Feature selection with the Chi2 algorithm, reducing the feature set to 85, resulted in the highest accuracy of 98.2%.

These results confirm that PSD signals effectively create a common domain across different operating conditions, bearing types, test setups, and sampling frequencies. The determination of the method parameters and the selection of the number of features were performed manually by trial and error. Future research will aim to automate these steps using optimization approaches to further improve the methodology.

Acknowledgments

This paper is financially supported by Selcuk University Scientific Research Projects.

Ethics Committee Approval

N/A

Peer-review

Externally peer-reviewed.

Conflict of Interest

The authors have no conflicts of interest to declare.

Funding

This paper is financially supported by Selcuk University Scientific Research Projects.

REFERENCES

- Bianchini, C., Immovilli, F., Cocconcelli, M., Rubini, R., & Bellini, A. (2010). Fault detection of linear bearings in brushless AC linear motors by vibration analysis. *IEEE Transactions on Industrial Electronics*, 58(5), 1684-1694.
- Dataset, M. (2020). Society for machinery failure prevention technology. In: Accessed: Mar.
- Esfahani, E. T., Wang, S., & Sundararajan, V. (2013). Multisensor wireless system for eccentricity and bearing fault detection in induction motors. *IEEE/ASME transactions on Mechatronics*, 19(3), 818-826.
- Giantomassi, A., Ferracuti, F., Iarlori, S., Ippoliti, G., & Longhi, S. (2015). Signal based fault detection and diagnosis for rotating electrical machines: Issues and solutions. *Complex System Modelling and Control Through Intelligent Soft Computations*, 275-309.
- Hou, J., Wu, Y., Ahmad, A. S., Gong, H., & Liu, L. (2021). A novel rolling bearing fault diagnosis method based on adaptive feature selection and clustering. *Ieee Access*, 9, 99756-99767.
- Hu, X., Li, Y., Jia, L., & Qiu, M. (2021). A novel two-stage unsupervised fault recognition framework combining feature extraction and fuzzy clustering for collaborative AIoT. *IEEE transactions on industrial informatics*, 18(2), 1291-1300.
- Huang, H., & Baddour, N. (2018). Bearing vibration data collected under time-varying rotational speed conditions. *Data in brief*, 21, 1745-1749.
- Kang, M., Kim, J., & Kim, J.-M. (2014). An FPGA-based multicore system for real-time bearing fault diagnosis using ultrasampling rate AE signals. *IEEE Transactions on Industrial Electronics*, 62(4), 2319-2329.
- Lei, N., Cui, J., Han, J., Chen, X., & Tang, Y. (2024). Rolling Bearing Fault Diagnosis Using Deep Transfer Learning Based on Joint Generalized Sliced Wasserstein Distance. *Ieee Access*.
- Mitra, S., & Koley, C. (2023). Early and intelligent bearing fault detection using adaptive superlets. *IEEE Sensors Journal*, 23(7), 7992-8000.
- Nabhan, A., Ghazaly, N., Samy, A., & Mousa, M. (2015). Bearing fault detection techniques-a review. *Turkish Journal of Engineering, Sciences and Technology*, 3(2), 1-18.
- Nath, S., Wu, J., Zhao, Y., & Qiao, W. (2020). Low latency bearing fault detection of direct-drive wind turbines using stator current. *Ieee Access*, 8, 44163-44174.
- Oh, H., Jung, J. H., Jeon, B. C., & Youn, B. D. (2017). Scalable and unsupervised feature engineering using vibration-imaging and deep learning for rotor system diagnosis. *IEEE Transactions on Industrial Electronics*, 65(4), 3539-3549.
- Pacheco-Cherrez, J., Fortoul-Diaz, J. A., Cortes-Santacruz, F., Alosa-Valerdi, L. M., & Ibarra-Zarate, D. I. (2022). Bearing fault detection with vibration and acoustic signals: Comparison among different machine learning classification methods. *Engineering Failure Analysis*, 139, 106515.
- Rahman, A., Hoque, M. E., Rashid, F., Alam, F., & Ahmed, M. M. (2022). Health condition monitoring and control of vibrations of a rotating system through vibration analysis. *Journal of Sensors*, 2022.
- Saha, D., Hoque, M. E., & Chowdhury, M. E. (2023). Enhancing Bearing Fault Diagnosis Using Transfer Learning and Random Forest Classification: A Comparative Study on Variable Working Conditions. *Ieee Access*.
- Wang, Z., Huang, W., Chen, Y., Jiang, Y., & Peng, G. (2022). Multisource cross-domain fault diagnosis of rolling bearing based on subdomain adaptation network. *Measurement Science and Technology*, 33(10), 105109.
- Wang, Z., Zhao, W., Du, W., Li, N., & Wang, J. (2021). Data-driven fault diagnosis method based on the conversion of erosion operation signals into images and convolutional neural network. *Process Safety and Environmental Protection*, 149, 591-601.
- Wei, S., Wang, D., Wang, H., & Peng, Z. (2020). Time-varying envelope filtering for exhibiting space bearing cage fault features. *IEEE Transactions on Instrumentation and Measurement*, 70, 1-13.

Xia, P., Xu, H., Lei, M., & Zhang, S. (2020). An improved underdamped asymmetric bistable stochastic resonance method and its application for spindle bearing fault diagnosis. *Ieee Access*, 8, 46824-46836.

Yang, B., Lei, Y., Jia, F., & Xing, S. (2019). An intelligent fault diagnosis approach based on transfer learning from laboratory bearings to locomotive bearings. *Mechanical Systems and Signal Processing*, 122, 692-706.

Zhang, S., Zhang, S., Wang, B., & Habetler, T. G. (2020). Deep learning algorithms for bearing fault diagnostics—A comprehensive review. *Ieee Access*, 8, 29857-29881.

Zhang, W., Peng, G., Li, C., Chen, Y., & Zhang, Z. (2017). A new deep learning model for fault diagnosis with good anti-noise and domain adaptation ability on raw vibration signals. *Sensors*, 17(2), 425.

Zheng, H., Yang, Y., Yin, J., Li, Y., Wang, R., & Xu, M. (2020). Deep domain generalization combining a priori diagnosis knowledge toward cross-domain fault diagnosis of rolling bearing. *IEEE Transactions on Instrumentation and Measurement*, 70, 1-11.

Enhancing Obesity Level Prediction with Feature Selection Methods and LSTM Network

Züleyha Yılmaz Acar*¹

Abstract: Obesity is defined as having a body mass index above the limits set by the World Health Organization. Considered a public health problem, obesity often leads to a range of general health issues. The level of obesity can be influenced by various factors such as eating habits, physical conditions, or demographic characteristics. This study proposes a prediction process for determining seven levels of obesity. Two feature selection methods are employed to identify the effective factors. The aim is to select the most effective features and apply to a long short-term memory (LSTM) network. In this study, ordinary least squares (OLS) and least absolute shrinkage and selection operator (lasso) methods are utilized as feature selection methods. The LSTM network is performed on all features, OLS features, and lasso features, respectively. The results indicate that the model is achieved 93.60% accuracy by all features, 94.08% by OLS analysis, and 95.02% by the lasso method.

Keywords: lasso, LSTM, obesity level, ordinary least squares.

¹**Address:** Selçuk University, Faculty of Technology, Konya/Turkiye

***Corresponding author:** mail@mail.com

1. INTRODUCTION

According to the World Health Organization, body mass indices are categorized into seven different levels: Insufficient Weight, Normal Weight, Overweight Level I, Overweight Level II, Obesity Type I, Obesity Type II, and Obesity Type III. Obesity, which is generally associated with excessive weight gain, can be influenced by factors such as genetics, environmental factors, physical activity level, dietary habits, or demographic characteristics. Additionally, obesity can lead to serious health issues like type 2 diabetes, heart disease, joint problems, or psychological issues (Fruh, 2017). The early detection of obesity levels and identifying the factors influencing obesity are important.

Many approaches have been proposed so far for predicting obesity levels. These can be classified as traditional machine learning (ML) methods, deep learning methods, and various preprocessing steps for improvements. Eom and Byeon present a comparative analysis of recurrent neural network (RNN) and long short-term memory (LSTM) methods by examining the impact of the COVID-19 pandemic on obesity through a text-based analysis of the changing and new habits affecting obesity (Eom & Byeon, 2022). Gupta et al. perform a prediction study on childhood obesity using LSTM at both the timestamp level and feature level (Gupta, Phan, Bunnell, & Beheshti, 2022). Xue et al. with data from electronic medical records and wearable devices, attempt to determine obesity level. They present a study examining both traditional ML techniques and RNN-based LSTM methods (Xue et al., 2018). Solomon et al. present the results from eight different ML algorithms using a voting-based ensemble method (Solomon et al., 2023). Gozukara Bag et al. propose a feature selection method using the recursive feature elimination technique, which iteratively eliminates features (Gozukara Bag et al., 2023). Yagin et al. perform classification by combining trained neural network methods using both the full feature set and selecting five important features through chi-square, F-classify, and mutual information classification feature score methods (Yagin et al., 2023).

In this study, the feature selection process is performed using ordinary least squares (OLS) and least absolute shrinkage and selection operator (lasso) methods for obesity level determination and classification. The LSTM network is used as the classifier, and feature selection method performances are compared. LSTM, with its memory cells that store information, is capable of discovering patterns in the data (Hossain et al., 2023). This study aims to identify the most effective features for determining obesity levels by using OLS and lasso methods in conjunction with the pattern exploration capability of the LSTM network.

2. MATERIAL AND METHOD

2.1. Dataset

The dataset was collected to study the impact of eating habits and physical conditions on obesity levels (Palechor & Manotas, 2019). It includes 2111 records and 17 attributes. There are 7 class labels: Weight, Normal Weight, Overweight Level I, Overweight Level II, Obesity Type I, Obesity Type II, and Obesity Type III. These labels are determined based on individuals' body mass indices. The attributes in the dataset are frequent consumption of high caloric food (FAVC), frequency of consumption of vegetables (FCVC), number of main meals (NCP), consumption of food between meals (CAEC), consumption of water daily (CH20), consumption of alcohol (CALC), calories consumption monitoring (SCC), physical activity frequency (FAF), time using technology devices (TUE), transportation used (MTRANS), smoking habit (SMOKE), gender, age, height, weight, and family history with overweight. The last attribute is the class label, which is obesity level.

The dataset consists of both categorical and numeric data. Categorical data is transformed into numerical data to convert all data into the same format. However, attributes that are converted to numerical data and naturally numeric data may have different scales, which can lead to different effects in statistical analysis (for example, gender and weight). To reduce these effects, z-score normalization is applied to columns, which is expressed as (1):

$$z = \frac{x - \bar{X}}{S} \quad (1)$$

where z refers to z-score normalization value of x ; x refers to a sample data; \bar{X} refers to the mean and S refers to the standard deviation for the attribute. This process standardizes the dataset, setting its mean to zero and its standard deviation to one.

The dataset is also checked for missing data. Since no missing data is found, no further action is taken. Thus, the data manipulation steps are completed.

2.2. Feature selection methods

In the study, both all attributes and also feature selection methods are integrated into the models to analyze the most impactful attributes on obesity levels. In this way, the performance of the LSTM network is analyzed in this study. At the same time, the most important features are identified by feature selection methods which are OLS and lasso methods.

OLS analysis examines the effect of independent variables on the dependent variable by creating a linear relationship model. The goal is to form a regression equation that minimizes the sum of the residuals (Lim, Na, Hong, & Bae, 2023). An equation is obtained through OLS analysis as shown in (2):

$$Y = \beta_0 + \beta_1 X_1 + \beta_2 X_2 + \beta_3 X_3 + \dots + \beta_i X_i + v \quad (2)$$

where Y is the dependent variable (obesity level); β is the constant; X is the independent variable (determined among attributes); and v is the residual errors. OLS analysis determines a p-value for each variable. A p-value lower than 0.05 demonstrates a statistically significant correlation between the independent and dependent variables. Based on this result, the independent variables that affect the dependent variable are identified, and related features are selected.

Another feature selection method used is lasso. The lasso method is a state-of-the-art regression analysis technique used for model regularization and identifying redundant attributes (Czajkowski, Jurczuk, & Kretowski, 2023). On lasso, 5-fold cross-validation is used with the one standard error of the minimum mean squared error metric (Chen & Yang, 2021) to identify coefficients of independent variables. If the coefficient of an attribute is 0, it is identified as a redundant variable and removed from the feature set.

2.3. LSTM network

The LSTM network is a special type of RNN model. The RNN model contains recurrent connections that allow it to maintain previous information (Moein, Moizad, & Keramati, 2024). This enables the model to discover hidden features by relating previous data to subsequent data. However, RNN is insufficient in integrating long-term

information. LSTM, on the other hand, is a specialized network where this insufficient characteristic structure of the RNN model has been improved. Due to its ability to transmit long-term information throughout the network, LSTM can retain relationships between records. Thus, the LSTM network learns hidden patterns within the dataset.

In this study, the LSTM network is modeled as a classifier. The layers it contains are illustrated in Figure 1.

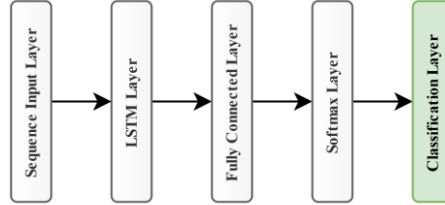


Figure 1. The model architecture of the LSTM network in the study

3. RESULTS

3.1. Performance metrics

In this study, obesity level prediction is carried out by assigning test data to one of seven different classes using the LSTM network. The results are stored in confusion matrices. Using these matrices, performance metrics such as Recall, Precision, F1-score, and Accuracy are calculated. Figure 2 shows a multi-class confusion matrix.

		Predicted Class		
		Class1	Class2	Class3
True Class	Class1	TP1	FN1	FN1
	Class2	FP1		
	Class3	FP1		

Figure 2. A multi-class confusion matrix

Figure 2 indicates a multi-class confusion matrix, where TP refers to true positive, FN refers to false negative and FP refers to false positive. The equations for the performance metrics are listed in (3)–(8):

$$Recall = \frac{TP}{TP + FN} \tag{3}$$

$$Precision = \frac{TP}{TP + FP} \tag{4}$$

$$Overall\ Recall = \frac{Recall}{mean(Recall)} \tag{5}$$

$$Overall\ Precision = \frac{Precision}{mean(Precision)} \tag{6}$$

$$F1 - score = \frac{2 \times Overall\ Recall \times Overall\ Precision}{Overall\ Recall + Overall\ Precision} \tag{7}$$

$$Accuracy = \frac{\sum_{c \in \{Classes\}} TP_c}{All\ observations} \tag{8}$$

Since it is a multi-class classification problem, recall and precision values are calculated after each class is determined as a positive class. Overall results are obtained by averaging the recall and precision values calculated separately for seven classes.

3.2. Hyperparameters

The hyperparameters for the LSTM network are set as follows: the number of hidden units is set to 150, the maximum number of epochs is set to 20, and the mini-batch size is set to 8.

3.3. Experimental Analysis

To test the performance of the methods, the dataset is randomly split into 80% training and 20% testing sets. Subsequently, the results are obtained using the holdout method with 10 independent runs, and the best accuracy values are retained. The number of training and testing samples used in the study is provided in Table 1.

Table 1. Number of samples

Total number of records (100%)	Train dataset (80%)	Test dataset (20%)
2111	1689	422

With OLS analysis, the p-value value is obtained for each feature in the obesity level identification dataset. These values are listed in Table 2.

Table 2. The p-values obtained by OLS analysis

Feature	p-value
Gender	0.3476
Age	0.0000
Height	0.0001
Weight	0
Family history with overweight	0.0000
FAVC	0.0000
FCVC	0.0099
NCP	0.0000
CAEC	0
SMOKE	0.0191
CH2O	0.1388
SCC	0.0047
FAF	0.0247
TUE	0.4726
CALC	0.0000
MTRANS	0.0171

The p-value obtained from the OLS analysis in Table 2 indicates that there is no meaningful relationship between the independent and dependent variables when the p-value is less than 0.05 value. Based on this information, the features Age, Height, Weight, Family history with overweight, FAVC, FCVC, NCP, CAEC, SMOKE, SCC, FAF, CALC, and MTRANS are identified as significant variables influencing the obesity level. Thus, the number of features is reduced from 16 to 13.

Besides, the lasso method calculates the regularization coefficient for the independent variables. The coefficients calculated by the method for all features in the obesity level dataset are listed in Table 3.

Table 3. The coefficients obtained by the lasso method

Feature	Coefficient
Gender	0
Age	0.1951
Height	-0.0950
Weight	0.4669
Family history with overweight	0.2530
FAVC	-0.0853
FCVC	0
NCP	-0.1066
CAEC	0.3726
SMOKE	0
CH2O	0
SCC	0.0052
FAF	-0.0605
TUE	0
CALC	-0.0976
MTRANS	0

With the lasso method, the redundant variables in Table 3 are identified by their coefficient value of zero. A coefficient value of zero indicates that the independent variable does not affect the dependent variable. As a result of the lasso method, the features Age, Height, Weight, Family history with overweight, FAVC, NCP, CAEC, SCC, FAF, and CALC, which have coefficients different from zero, are determined to have a significant relationship with the obesity level. Thus, the number of features is reduced from 16 to 10. Numbers of features obtained by OLS and lasso methods are illustrated in Figure 3 and Figure 4.

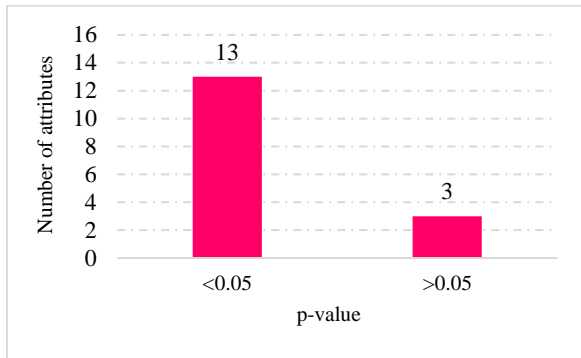


Figure 3. Number of attributes obtained by OLS

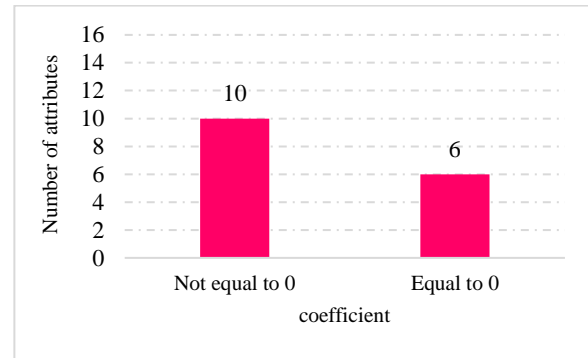


Figure 4. Number of attributes obtained by lasso

The LSTM network modeled as a classifier is run on obesity-level classification tasks on all features, on features selected by OLS analysis, and on features selected by the lasso method. The obtained results are presented in Table 4.

Table 4. Obtained results by LSTM network

Methods	Performance Metrics (%)			
	Overall Recall	Overall Precision	F1-score	Accuracy
LSTM with all features	93.31	93.51	93.41	93.60
LSTM with OLS features	93.77	94.02	93.89	94.08
LSTM with lasso features	94.56	95.15	94.85	95.02

According to Table 4, 93.60% accuracy is obtained with all features, 94.08% accuracy is achieved with features selected by OLS, and 95.02% accuracy is achieved with features selected by the lasso method. The LSTM with the lasso method, which has the highest accuracy of 95.02%, reaches an overall recall of 94.56%, an overall precision of 95.15%, and an F1-score of 94.85%. Additionally, even without using any feature selection, the LSTM network achieves 93.60% accuracy, 93.31% overall recall, 93.51% overall precision, and 93.41% F1-score.

A visual comparison of the results is illustrated in Figure 5.

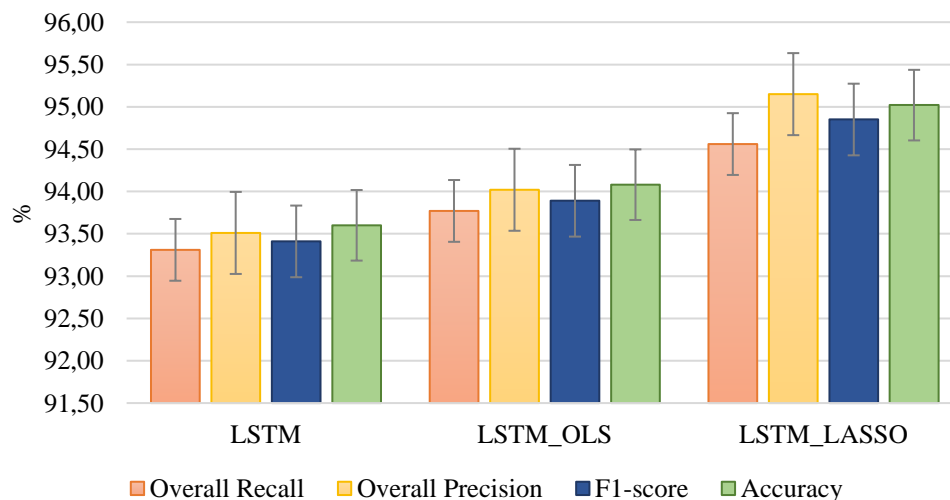


Figure 5. Visual comparison of performance metrics

The method with the highest performance metric values among the methods is the classification performed by the LSTM network using lasso features. The confusion matrix obtained by this method is indicated in Figure 6.

		Predicted Class						
		Weight	NWeight	OLevel1	OLevel2	OType1	OType2	OType3
True Class	Weight	56	2	0	0	0	0	0
	NWeight	1	46	0	0	0	7	1
	OLevel1	0	0	74	0	0	0	0
	OLevel2	0	5	3	53	0	0	1
	OType1	0	0	0	0	70	0	0
	OType2	0	1	0	0	0	54	0
	OType3	0	0	0	0	0	5	48

Figure 6. Confusion matrix by obtained LSTM Network with lasso features

Figure 6 shows the confusion matrix results of LSTM with lasso features on the test data according to Weight, Normal Weight (NWeight), Overweight Level I (OLevel1), Overweight Level II (OLevel2), Obesity Type I (OType1), Obesity Type II (OType2), and Obesity Type III (OType3) class labels.

Additionally, the Recall and Precision values of the results achieved by the LSTM network with lasso features for each class are listed in Table 5.

Table 5. The recall and precision results achieved by the LSTM network with lasso features for each class

Class	Recall (%)	Precision (%)
Weight	96.55	98.25
NWeight	83.64	93.88
OLevel1	100	96.10
OLevel2	92.98	100
OType1	100	100
OType2	98.18	81.82
OType3	90.57	96.00
Overall	94.56	95.15

4. DISCUSSION AND CONCLUSIONS

In this study, the goal is to predict obesity levels, categorized into seven classes: Weight, Normal Weight, Overweight Level I, Overweight Level II, Obesity Type I, Obesity Type II, and Obesity Type III. The prediction is based on features related to eating habits (frequent consumption of high caloric food, frequency of consumption of vegetables, number of main meals, consumption of food between meals, daily water consumption, alcohol consumption), physical conditions (calories consumption monitoring, physical activity frequency, time using technology devices, transportation used), smoking habit, gender, age, height, weight, and family history with overweight. The LSTM method aims to reveal hidden connections in the dataset through its long-term memory capability. To enhance the performance of the LSTM, OLS, and lasso feature selection methods are incorporated into the classification model.

The results indicate that the LSTM model demonstrates satisfactory performance using all features. Also, it presents that the method can retain information transfer between records and can be effectively used on datasets composed of numerical data. Furthermore, it is observed that feature selection methods improve performance. OLS and lasso methods allow classification based on the most impactful feature sets affecting obesity levels. The features identified as most significant by these methods are listed in Table 6.

Table 6. The features selected by OLS and lasso methods

All Features	OLS Features	Lasso Features
Gender		
Age	✓	✓
Height	✓	✓
Weight	✓	✓
Family history with overweight	✓	✓
FAVC	✓	✓
FCVC	✓	
NCP	✓	✓
CAEC	✓	✓
SMOKE	✓	
CH2O		
SCC	✓	✓
FAF	✓	✓
TUE		
CALC	✓	✓
MTRANS	✓	

According to the OLS analysis, the features that are not significantly related to predicting obesity levels are gender, consumption of water daily, and time using technology devices. The other features are important for determining obesity levels. On the other hand, according to the lasso method, all features except for gender, frequency of consumption of vegetables, smoking habit, consumption of water daily, time using technology devices, and transportation used are significant for predicting obesity levels.

When examining the LSTM results, it is observed that even without using any feature selection method, the LSTM network achieves an accuracy of 93.60%. Additionally, the high precision, recall, and F1-score results indicate that the method provides balanced performance across the 7 classes. With the integration of OLS analysis into the model, the accuracy increases to 94.08%. Also, the high and balanced classification is confirmed by the recall, precision, and F1-score metrics. With the integration of the lasso method, the highest accuracy among the methods, 95.02% accuracy, is achieved.

Further analysis of the lasso method using the confusion matrix and the recall and precision values for each class reveals that 100% precision is achieved for the Overweight Level 1 and Obesity Type 1 classes, and 100% recall is achieved for the Overweight Level 2 and Obesity Type 1 classes. All data belonging to the Obesity Type 1 class are correctly classified by the proposed model. Other classes also achieve high and remarkable results.

This study shows that with the high success of OLS and lasso feature selection methods, it is possible to identify both the most impactful features on obesity levels and the redundant features. Additionally, it shows that the LSTM network can be effectively applied to such datasets, and the performance can be improved with different feature selection methods or hyperparameter optimization.

Acknowledgements

This study is supported by Selçuk University Scientific Research Projects Commission.

Conflict of Interest

The authors have no conflicts of interest to declare.

Funding

The authors declared that this study has received no financial support.

REFERENCES

- Chen, Y., Yang, Y. (2021). The One Standard Error Rule for Model Selection: Does It Work? *Stats*, 4(4), 868-892. <https://doi.org/10.3390/stats4040051>
- Czajkowski, M., Jurczuk, K., Kretowski, M. (2023). Steering the interpretability of decision trees using lasso regression - an evolutionary perspective. *Information Sciences*, 638, 118944. <https://doi.org/10.1016/j.ins.2023.118944>
- Eom, G., Byeon, H. (2022). Development of Keyword Trend Prediction Models for Obesity Before and After the COVID-19 Pandemic Using RNN and LSTM: Analyzing the News Big Data of South Korea. *Frontiers in Public Health*, 10. <https://doi.org/10.3389/fpubh.2022.894266>

- Fruh, S. M. (2017). Obesity: Risk factors, complications, and strategies for sustainable long-term weight management. *J Am Assoc Nurse Pract*, 29(S1), S3-s14. <https://doi.org/10.1002/2327-6924.12510>
- Gozukara Bag, H. G., Yagin, F. H., Gormez, Y., González, P. P., Colak, C., Güllü, M., Ardigò, L. P. (2023). Estimation of Obesity Levels through the Proposed Predictive Approach Based on Physical Activity and Nutritional Habits. *Diagnostics*, 13(18), 2949. <https://doi.org/10.3390/diagnostics13182949>
- Gupta, M., Phan, T. T., Bunnell, H. T., Beheshti, R. (2022). Obesity Prediction with EHR Data: A deep learning approach with interpretable elements. *ACM Trans Comput Healthc*, 3(3). <https://doi.org/10.1145/3506719>
- Hossain, M. M., Ali, M. S., Ahmed, M. M., Rakib, M. R. H., Kona, M. A., Afrin, S., Rahman, M. H. (2023). Cardiovascular disease identification using a hybrid CNN-LSTM model with explainable AI. *Informatics in Medicine Unlocked*, 42, 101370. <https://doi.org/10.1016/j.imu.2023.101370>
- Lim, D.-H., Na, W.-J., Hong, W.-H., Bae, Y.-H. (2023). Development of a fire prediction model at the urban planning stage: Ordinary least squares regression analysis of the area of urban land use and fire damage data in South Korea. *Fire Safety Journal*, 136, 103761. <https://doi.org/10.1016/j.firesaf.2023.103761>
- Moein, T., Moinzad, H., Keramati, M. A. (2024). Designing a model to detect and separate data anomalies caused by sensors and medical wearables using LSTM neural network algorithm. *International Journal of Nonlinear Analysis and Applications*. <https://doi.org/10.22075/ijnaa.2023.30411.4391>
- Palechor, F. M., Manotas, A. d. I. H. (2019). Dataset for estimation of obesity levels based on eating habits and physical condition in individuals from Colombia, Peru and Mexico. *Data in Brief*, 25, 104344. <https://doi.org/10.1016/j.dib.2019.104344>
- Solomon, D. D., Khan, S., Garg, S., Gupta, G., Almjally, A., Alabdullah, B. I., Abdallah, A. M. A. (2023). Hybrid Majority Voting: Prediction and Classification Model for Obesity. *Diagnostics*, 13(15), 2610. <https://doi.org/10.3390/diagnostics13152610>
- Xue, Q., Wang, X., Meehan, S., Kuang, J., Gao, J. A., Chuah, M. C. (2018, 17-20 Dec. 2018). Recurrent Neural Networks Based Obesity Status Prediction Using Activity Data. Paper presented at the 2018 17th IEEE International Conference on Machine Learning and Applications (ICMLA). <https://doi.org/10.1109/ICMLA.2018.00139>
- Yagin, F. H., Güllü, M., Gormez, Y., Castañeda-Babarro, A., Colak, C., Greco, G., Cataldi, S. (2023). Estimation of Obesity Levels with a Trained Neural Network Approach optimized by the Bayesian Technique. *Applied Sciences*, 13(6), 3875. <https://doi.org/10.3390/app13063875>

Optimizing Thermal Comfort: Comparing Shading Elements and Aerogel Glazing

Damla Yağmur Sağ Bayram^{*1}, Tugce Pekdogan²

Abstract: Achieving optimal thermal performance in hot climates for buildings with large glazing areas presents a significant challenge. Various solutions, ranging from traditional shading elements to advanced nanomaterials, have been employed to mitigate the heating effect of solar radiation. Recently, aerogel granular glazing systems have gained attention for their ability to allow daylight penetration while maintaining a low heat transfer coefficient. This research investigates the impact of traditional shading elements and translucent aerogel granular glazing systems. It compares them with double glazing in an office building prototype of the Directorate buildings of the Ministry of Environment, Urbanization, and Climate Change. The study focuses on a T-shaped office building covering an area of 9,740m², comprising six stories, including a basement. By setting operative temperature set points to 20-24°C for winter and 23-26°C for summer, summer and winter design week simulations were conducted to determine the heating and cooling loads using DesignBuilder and EnergyPlus.

Keywords: Aerogel, glazing, insulation, simulation.

¹**Address:** Adana Alparslan Turkes Science and Technology University, Department of Architecture Adana, Turkiye

²**Address:** Adana Alparslan Turkes Science and Technology University, Department of Architecture Adana, Turkiye

***Corresponding author:** damlayagmursag@gmail.com

1. INTRODUCTION

With the growth of the global population, building energy consumption is now responsible for more than one-third of global energy consumption (Gupta & Deb, 2023). This highlights the importance of reducing energy consumption in buildings to protect the environment. However, achieving this reduction while maintaining indoor quality, providing thermal comfort, and achieving optimal illuminance levels presents a considerable obstacle. Windows account for 60% of the total energy consumption in buildings due to inadequate thermal insulation (Du et al., 2024) as well as providing a visual connection between interior and exterior by letting daylight penetrate the interior, which also affects heating and cooling loads (Mohammad & Ghosh, 2023). Aerogel is regarded as one of the most promising insulation materials thanks to its ultra-low thermal conductivity (0.01–0.02 W/mK) (Leung et al., 2020). High insulation properties and the transparency of the aerogel make it useful for window applications (Buratti et al., 2021).

Ihara et al. (2015) investigated aerogel granulated glazing facades from an energy-saving perspective by combining aerogel and triple glazing systems for cold climates. The results indicated that double-glazing facades are more suitable for cooling-dominated climates, achieving higher energy demand reductions. Additionally, the study stated that using aerogel glazing systems may provide further energy savings by allowing daylight to pass through translucent spandrels. This research highlights the potential of aerogel granulated glazing in enhancing energy efficiency in building facades, particularly in cold climate regions. Mohammed A. et al. (2023) assessed the performance of aerogel-glazed windows in classrooms with varying orientations by comparing them with conventional windows. The study used DesignBuilder software to simulate daylighting. The results indicated that aerogel glazing on the southern and northern façades reduces window-specific heat gain by 26.88 and 7.46%, respectively and concluded that Aerogel Glazing provides effective building insulation, balancing heat gain from windows with daylight in hot dry regions. Dongmei et al. (2023) conducted a comparative experimental study on discomfort glare assessment and daylighting performance of granular aerogel glazing and double-glazing systems on overcast and sunny days. Experiments indicated that the daylighting performance of the Aerogel Glazing System is lower than the double-glazing system, and the indoor daylight environment of the Aerogel Glazing System test room is always more uni-form than that of the double-glazing system test room.

Beatens et al. (2011) investigated Aerogels' thermal, optical and acoustic properties. A granular aerogel-based glazing was designed to conduct an experiment, including two glass panels with a Low-E coating between two air gaps and an

aerogel-filled PMMA double-skin-sheet. A visual directional-hemispherical transmittance of granulated aerogel was between 0.24 and 0.54, and a total solar transmittance was between 0.33 and 0.45.

Bektas et al. (2022) comprehensively evaluated the effects of outer window shading elements and different window-to-wall ratios on heating, cooling, and lighting loads. Using the DesignBuilder program, they modeled a building with dimensions of 10m x 10m and a height of 4m, varying the window-to-wall ratios and the angles of the shading elements. The study found that designing with only the concern of heating and cooling loads reduces internal illuminance levels due to the exterior shading elements, resulting in higher lighting expenditures. Elouadjeri et al. (2021) carried out a comprehensive study on the impact of the geometry of exterior fixed shading devices on heating and cooling loads, thermal comfort, and daylighting. The study involved modeling a building with 6m x 4m dimensions. Solar heat gains, heating and cooling loads were calculated using TRNSYS 17. For illuminance calculations, the DAYSIM software was utilized. The research indicates the significant role of shading device geometry in optimizing building energy performance and occupant comfort.

In this research, an office building, one of the prototype buildings of the Ministry of Environment, Urbanization, and Climate Change, is modeled using DesignBuilder. The heating and cooling loads for the summer and winter design weeks are investigated. Three building envelopes are compared: double-glazed, partly aerogel-glazed, and double-glazed with exterior shading elements. To better understand the differences between aerogel and traditional shading elements, the dimensions of the aerogel glazed windows are fixed to match those of the traditional shading elements.

2. MATERIAL AND METHOD

2.1. Study Site and Building Description

The research was conducted on a T-shaped (Figure 1) office building prototype from the Directorate buildings of the Ministry of Environment, Urbanization, and Climate Change. The building encompasses a total area of 9,740m² and comprises six stories, including a basement. In the ground level for office rooms the standard window size is 3m x 3.90m, and for typical levels is 1.25m x 2.75m. The building site is in Adana City, Turkiye, marked as Csa according to the Köppen climate classification. This indicates a Mediterranean climate characterized by mild, wet winters and hot, dry summers.

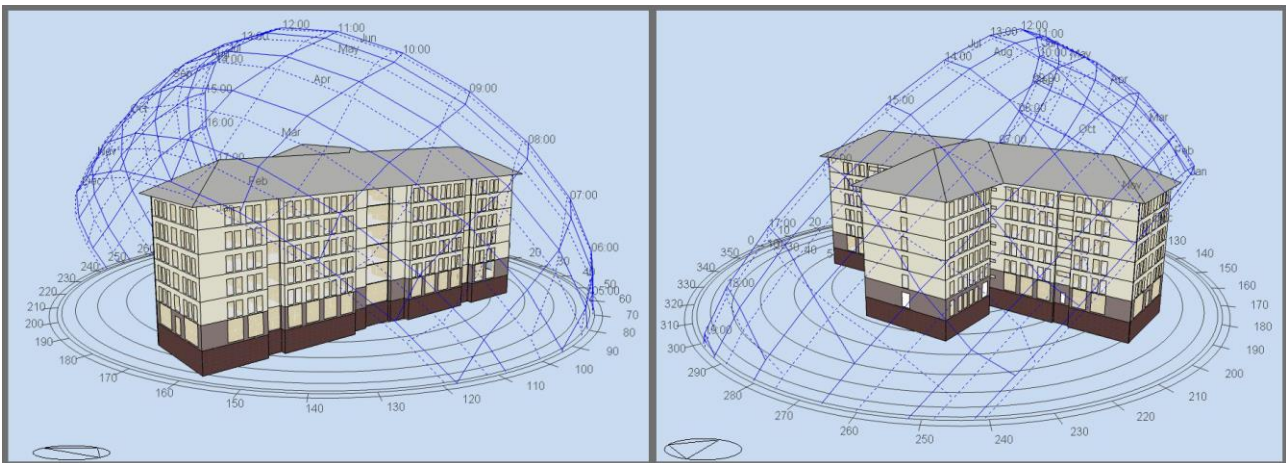


Figure 1. Geometry visualization for office building design

2.2. Glazing Systems and Shading Elements

Three window types were analyzed, each maintaining the same dimensions and placements but differing in pane types and exterior shading elements.

Table 1 reveals the properties of three window types. Operative temperatures, Exterior shading availability, Total solar transmission, Light transmission and U values for each type are given in the table. N/A denotes unavailable, and Dbl Clr and AGG denote double clear and aerogel glazing, respectively.

Table 1. Window properties

	Window Type					
	Type1		Type2		Type 3	
	Winter	Summer	Winter	Summer	Winter	Summer
Operative Temperature	20-24°C	23-26°C	20-24°C	23-26°C	20-24°C	23-26°C
Glazing	Double Clear Glazing		Double Clear Glazing		Double Clear Glazing+Aerogel Granulated Glazing	
Exterior shading	N/A		In Place/available		N/A	
Total solar transmission	0.697		0.697		Db1 Clr 0.697	AGG 0.488
Light transmission	0.781		0.781		0.781 0.307	
U value (W/m ² -K)	2.708		2.708		2.708 0.802	

Window Type 1 consists of a double-glazing panel with two clear glass panes, each 6mm wide, separated by an air gap of 13mm (**Fig.2a**). This type is considered the baseline combination for heating and cooling load calculations. The U-value and total solar transmission values for the double clear glazing are 2.708W/m²-K and 0.697, respectively (**Table 1**).

Window Type 2 features the same glazing system as Window Type 1, augmented with exterior local shading. At the ground level, the local shading measures 3.20m x 1.45m, and for the typical levels, it measures 1.45m x 1.20m (**Fig. 2b**).

Window Type 3 comprises two different glazing systems (**Fig. 2c**). One part uses the same glazing as Window Types 1 and 2. The other part incorporates an aerogel granular glazing system at the ground level, measuring 3.00m x 1.45m and 1.20m x 1.20m for the typical levels. The aerogel granular glazing's U-value and total solar transmission value are 0.831W/m²-K and 0.488, respectively (**Table 1**).

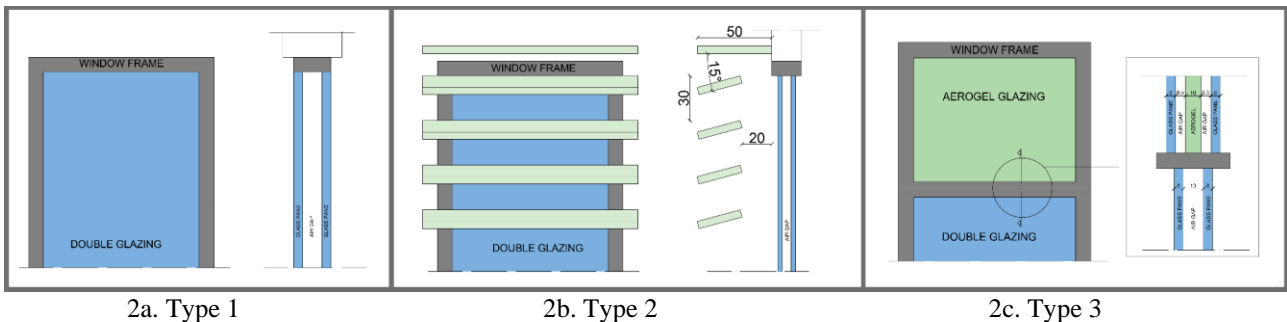


Figure 2. Simulated Windows: 2a. Double Glazing (Type 1), 2b. Shading (Type 2), and 2c. Aerogel Glazing (Type 3)

For each window type combination, in DesignBuilder, heating and cooling load simulations were conducted for winter and summer design weeks, automatically the hottest summer week and cooler winter week according to DesignBuilder climate data. Obeying the ASHRAE 55 thermal requirements for office buildings, the heating and cooling set points during the summer typical week were 23-26°C. The typical winter week's heating and cooling set points were set to 20-24°C.

3. RESULTS

The heating and cooling loads for each glazing type are presented for both the summer and winter design weeks in **Table 2**. The "Total" column represents the combined heating and cooling loads for the winter design week, and the "Grand Total" column provides the overall energy loads for each glazing type.

Table 2. The results of the simulations

Window Type	Summer Design Week		Winter Design Week			Grand Total (kWh)
	Heating Load(kWh)	Cooling Load(kWh)	Heating Load(kWh)	Cooling Load(kWh)	Total	
Type 1	-	69,041.28	8,148.15	392.61	8540.76	77582.04
Type 2	-	63,293.94	9,491.88	133.67	9625.55	72919.49
Type 3	-	65,898.81	8,939.34	280.41	9219.75	75118.5

Type 2 has the lowest cooling load (63,293.94kWh), indicating that adding exterior local shading effectively reduces the cooling demand compared to Types 1 and 3. Type 1 has the highest cooling load (69,041.28kWh), showing the highest demand for cooling without any additional shading or advanced glazing systems. Type 3 falls in between, with a cooling load of 65,898.81kWh, suggesting that the aerogel granular glazing provides some reduction in cooling demand but not as much as the exterior shading in Type 2.

Type 1 requires a heating load of 8,148.15kWh, serving as the baseline for comparison. Type 2 has the highest heating load (9,491.88kWh), which can be attributed to the reduction in passive solar gains due to the exterior shading. Type 3 has a slightly higher heating load (8,939.34 kWh) than Type 1, indicating that the aerogel glazing system also reduces passive solar gains, though not as significantly as the exterior shading.

The cooling loads during the winter design week are significantly lower for all types, with Type 1 having the highest at 392.61 kWh. Type 2 has the lowest cooling load (133.67kWh), demonstrating the effectiveness of shading even in winter. Type 3 has a cooling load of 280.41 kWh, again showing a moderate reduction compared to Type 1.

Type 2 has the lowest total load (72,919.49kWh), suggesting that the exterior shading provides the most significant energy savings overall. Type 1 has the highest total load (77,582.04kWh), making it the least efficient option in this study. Type 3 has a total load of 75,118.56kWh, showing that while the aerogel granular glazing offers some benefits, it is not as effective as exterior shading.

For summer Design Cooling Loads, Window Type 2 has the lowest cooling load (63,293.94kWh), indicating that adding exterior local shading effectively reduces the cooling demand compared to Types 1 and 3. This represents a decrease of approximately 8.32% compared to Window Type 1; Window Type 3 falls in between, with a cooling load of 65,898.81kWh, suggesting that the aerogel granular glazing provides some reduction in cooling demand but not as much as the exterior shading in Window Type 2. This represents a decrease of approximately 4.55% compared to Window Type 1.

During the winter design week, exterior shading (Window Type 2) increased heating loads (9,491.88kWh), likely due to the reduced passive solar gains that would otherwise help warm the building. Window Type 3 also showed an increase in heating loads (8,939.34kWh) compared to the baseline, but to a lesser extent than Window Type 2. This suggests that while aerogel granular glazing provides some thermal insulation benefits, it also reduces beneficial solar heat gain during the winter.

The simulations indicate that adding exterior shading elements (Type 2) results in the most substantial reduction in overall energy loads, particularly in cooling demand during the summer. The aerogel granular glazing (Type 3) also offers benefits over the baseline (Type 1) but is less effective than the exterior shading. These findings highlight the importance of selecting appropriate glazing and shading strategies to enhance the energy efficiency of buildings in hot climates like Adana/Turkiye.

4. DISCUSSION AND CONCLUSIONS

The results of this study highlight the significant impact that different glazing systems and shading elements can have on the thermal performance and energy consumption of buildings, especially summer cooling loads in hot climates such as Adana/Turkiye. Elauadjeri et al. (2021) found that external shading devices effectively reduced building cooling loads in summer, providing up to 19% energy savings. Simulations have shown that exterior shading elements (Window Type 2) are the method that reduces total energy loads the most in summer months by 8,32%. Mohammed et al. (2024) stated that aerogel glazing reduces heat gain by 7.46% to 26.88%, depending on the orientation. According to simulation results, the Aerogel granular glass system (Window Type 3) outperformed the double-glazed system (Window Type 1) but was less effective than exterior shading. The thermal insulation benefits of the Aerogel glass system reduce passive solar gains in winter months. In contrast, exterior shading elements were more effective in

reducing cooling loads in the summer months. Specifically, the data shows that integrating exterior shading elements and advanced glazing materials can substantially reduce cooling loads during the summer and influence heating and cooling requirements during the winter. (Mohammed & Ghosh 2023) stated that aerogel granulated glazing can increase window heat energy transfer by 32.69 %. In the simulation results, using a partly glazed aerogel system, winter design week energy loads decreased by 7,94%. The partial implementation of the aerogel glazed system causes a difference between the results.

These findings emphasize the importance of selecting appropriate glass and shading strategies to increase the energy efficiency of buildings in hot climates. Future studies will evaluate the validity of these findings by testing them across a wider range of building types and climatic conditions.

Acknowledgments

We thank everyone who contributed to the realization of this study. Additionally, we thank the organizers of ICONST-2024 for their support.

Ethics Committee Approval

N/A

Peer-review

Externally peer-reviewed.

Author Contributions

Conceptualization: T.P.; Investigation: D.Y.S.B.; Material and Methodology: T.P., D.Y.S.B.; Supervision: T.P.; Visualization: D.Y.S.B.; Writing-Original Draft: D.Y.S.B.; Writing-review & Editing: T.P.; Other: All authors have read and agreed to the published version of the manuscript.

Conflict of Interest

The authors have no conflicts of interest to declare.

Funding

The authors declared that this study has received no financial support.

REFERENCES

- Gupta, V., & Deb, C. (2023). Envelope design for low-energy buildings in the tropics: A review. In *Renewable and Sustainable Energy Reviews* (Vol. 186). Elsevier Ltd. <https://doi.org/10.1016/j.rser.2023.113650>
- Du, R., Wang, S., & Li, T. (2024). Energy-saving windows derived from transparent aerogels. *Nano Research Energy*, 3(1). <https://doi.org/10.26599/NRE.2023.9120090>
- Khaled Mohammad, A., & Ghosh, A. (2023). Exploring energy consumption for less energy-hungry building in UK using advanced aerogel window. *Solar Energy*, 253, 389–400. <https://doi.org/10.1016/j.solener.2023.02.049>
- Leung, C. K., Lu, L., Liu, Y., Cheng, H. S., & Tse, J. H. (2020). Optical and thermal performance analysis of aerogel glazing technology in a commercial building of Hong Kong. *Energy and Built Environment*, 1(2). <https://doi.org/10.1016/j.enbenv.2020.02.001>.
- Buratti, C., Belloni, E., Merli, F., & Zinzi, M. (2021). Aerogel glazing systems for building applications: A review. In *Energy and Buildings* (Vol. 231). Elsevier Ltd. <https://doi.org/10.1016/j.enbuild.2020.110587>.
- Ihara, T., Gao, T., Grynning, S., Jelle, B. P., & Gustavsen, A. (2015). Aerogel granulate glazing facades and their application potential from an energy saving perspective. *Applied Energy*, 142, 179–191. <https://doi.org/10.1016/j.apenergy.2014.12.053>
- Mohamed, A. F., Gomaa, M. M., Amir, A. A., & Ragab, A. (2023). Energy, Thermal, and Economic Benefits of Aerogel Glazing Systems for Educational Buildings in Hot Arid Climates. *Sustainability (Switzerland)*, 15(8). <https://doi.org/10.3390/su15086332>
- Zheng, D., Chen, Y., & Peng, J. (2023). Daylighting performance and discomfort glare assessment of granular aerogel glazing system: A full-scale comparative experiment. *Building and Environment*, 236.

<https://doi.org/10.1016/j.buildenv.2023.110297>

Baetens, R., Jelle, B. P., & Gustavsen, A. (2011). Aerogel insulation for building applications: A state-of-the-art review. In *Energy and Buildings* (Vol. 43, Issue 4, pp. 761–769). <https://doi.org/10.1016/j.enbuild.2010.12.012>

Bektas Ekici, B., Orhan, G., & Yuksel, E. N. (2022). Investigation of the Effect of Window and Shading Elements on Building Energy Needs. *PLANARCH - Design and Planning Research*, 6(2), 40–46. <https://doi.org/10.5152/Planarch.2022.221325>

Elouadjeri, S. M., Boussoualim, A., & Haddou, H. A. (2021). Evaluating the effect of external horizontal fixed shading devices' geometry on internal air temperature, daylighting and energy demand in hot dry climate. Case study of ghardaïa, algeria. *Buildings*, 11(8). <https://doi.org/10.3390/buildings11080348>

Mohamed, A. F., Amir, A. A., & Ragab, A. (2024). The effect of aerogel glazing on daylight and heat gain in school buildings in hot and dry climate. *Environment, Development and Sustainability*. <https://doi.org/10.1007/s10668-024-04963-1>.

Flexural Behavior of 3D Printed PLA Fiber Reinforced Cement-Based Composites

Eren Gödek*¹, Serhat Oğuzhan Kıvrak¹, Julide Kıvrak¹

Abstract: This study examined the impact of poly-lactic acid (PLA) based fibers produced via 3D printing technology on the mechanical performance of cementitious systems subjected to flexural loading. In this context, reinforcements that met the macro fiber criteria were produced using PLA filament, and the resulting fibers were utilized as reinforcement in a cement-based matrix. The flexural strength, deflection capacity, delayed deflection capacity, and toughness values of the specimens were 1.89 ± 0.04 MPa, 0.11 ± 0.004 mm, 0.72 ± 0.14 mm, and 2.86 ± 1.06 J, respectively. In comparing the results with those of the reference composite, it was observed that the PLA fibers exhibited controlled crack growth similar to that of the conventional macro polypropylene fibers used in the literature. Furthermore, the composite toughness could be increased without a significant loss in flexural strength.

Keywords: 3D printing, PLA, fiber, cement-based composites.

¹Address: Hitit University, Vocational School of Technical Sciences, Dept. of Construction Technology, Çorum/Türkiye

***Corresponding author:** erengodek@hitit.edu.tr

1. GİRİŞ

İnşaat alanında lif takviyesinin tarihi, 3500 yıldan uzun bir süre önce tuğlalara saman, at kılı vb. eklenmesiyle başlamış ve 19. yüzyıldan günümüze kadar betona çeşitli liflerin eklenmesiyle devam etmiştir (Naaman, 2018). Şu ana kadar betonda takviye olarak kullanılan lifler kökenine göre çelik, cam ve polimer, boyuta göre ise makro ve mikro boyutlu fiberler olarak sınıflandırılabilir (ACI 544.3R-08).

Polimer esaslı makro lifler, en yaygın kullanılan beton takviyelerinden biri olarak kabul edilebilir. Betona herhangi bir tür lifin eklenmesi, çatlak direncini ve mekanik özellikleri genellikle arttırmaktadır. Ancak polimerik lifler, hafiflikleri, kimyasal ve alkali ortamlardaki kararlılıkları ve maliyet etkinlikleri nedeniyle çelik liflere göre bazı avantajlara da sahiptir (Arafa vd., 2013; Gautam ve Awasthi, 2018; Nematzadeh vd., 2021; Narule ve Visapure, 2022). Günümüzde kullanılan makro lifler genellikle polipropilen kökenli olup gerek lüferatür gerekse uygulama alanında kendileri yer edinmişlerdir. Arafa vd. (2013) makro polipropilen lif kullanarak ürettikleri betonları 7, 14 ve 28 günlük mekanik özelliklerini incelemiş ve bu liflerin beton çekme dayanımını %20,6-%30,8 aralığında, eğilme dayanımını %16,6-%26,1 aralığında ve basınç dayanımını ise %1,0-%7,2 aralığında artırabileceğini rapor etmişlerdir. Narule ve Visapure (2022) tarafından yapılan bir çalışmada, betondaki polipropilen makro lif dozajlarının 3 ila 7 kg/m³ mertebelerinde kullanılmasıyla betonun basınç dayanımının %10-20 aralığında iyileştirilebileceği bildirilmiştir. Akın vd. (2023) tarafından yapılan bir diğer çalışmada ise makro liflerin kullanımının erken yaş basınç dayanımını (7 günde) %28,1'e kadar, 28 günde ise basınç dayanımını %14,4'e kadar artırabileceğini göstermiştir.

3D baskı, günümüzde birçok alanda geliştirilen ve kullanılan popüler bir üretim yöntemidir. 3D baskı teknolojisinde, belirleyici yüksekliğe sahip birden fazla katman üst üste bindirilir ve çeşitli CAD yazılımları tarafından tasarlanan çeşitli ürün tipleri kolayca üretilebilir (Kun, 2016). Kaynakların maliyet etkinliği, daha az kusurlu otomatik üretim, metaller veya polimerler gibi geri dönüştürülebilir hammaddelerin kullanımı, tasarımların kolay hazırlanması ve paylaşılması gibi durumlar 3D baskının başlıca avantajlarıdır (Berman, 2012). İnşaat sektöründe, son zamanlarda komple beton yapıların 3D baskısı büyük ilgi görmektedir (De Schutter vd., 2018; Asprone vd., 2018). Ek olarak, çimento esaslı malzemeler için 3D baskılı takviyeler üretme konusunda da birkaç çalışma mevcuttur. Bir çalışmada, araştırmacılar polimerik ve metalik liflerin tasarımı ve üretimi için 3D baskıyı kullanmaktadırlar (Farina vd., 2016). Yapılan bir çalışmada, akrilonitril bütadien stiren (ABS) esaslı 3D baskılı takviyeler üretilerek çimento esaslı kompozitlerde güçlendirme elemanı olarak kullanılmış ve hem eğilme hem de çekme performanslarında önemli iyileştirmeler elde edilmiştir (Xu ve Şavija, 2019). Salazar vd. (2020), çelik takviye yerine PLA ve ABS malzemelerinden yapılmış 3D oktet kafes yapıların kullanımını araştırmış ve 3D takviyeli çimento esaslı kompozitlerin tepe yüke kadar gerinim sertleşmesi sergilediğini göstermiştir. Ayrıca, numunelerde eğilme yüklemesi süresince tepe yüke kadar çoklu çatlama ve kontrollü çatlak genişlemesi gözlemlendiğini rapor etmişlerdir. Gödek vd. (2020)

tarafından yapılan bir diğer çalışmada düz ve çıkıntılı kombinasyona sahip iki farklı kalınlıkta (1 ve 2 mm) petek şeklindeki takviye elemanları PLA filamentini kullanılarak üretilmiş ve çimento esaslı kompozitlerde güçlendirme elemanı olarak kullanılmış ve eğilme yüklemesi altındaki mekanik performansları incelenmiştir. Sonuç olarak kompozitlerin eğilme performansının kalınlık ve çıkıntı kombinasyonlarına bağlı olarak değiştiği ve eğilme mukavemetlerinin, sehim kapasitelerinin ve tokluk değerlerinin sırasıyla 2,30-3,04 MPa, 0,045-0,588 mm ve 15,92-652,37 N.mm arasında değiştiği görülmüştür. 2 mm kalınlığında ve çıkıntılı yapıdaki 3D baskı takviyesi içeren kompozitlerde, performans iyileştirme için önemli bir kriter olarak kabul edilen yalnızca deformasyon sertleşmesi davranışında iyileşme olduğu rapor edilmiştir.

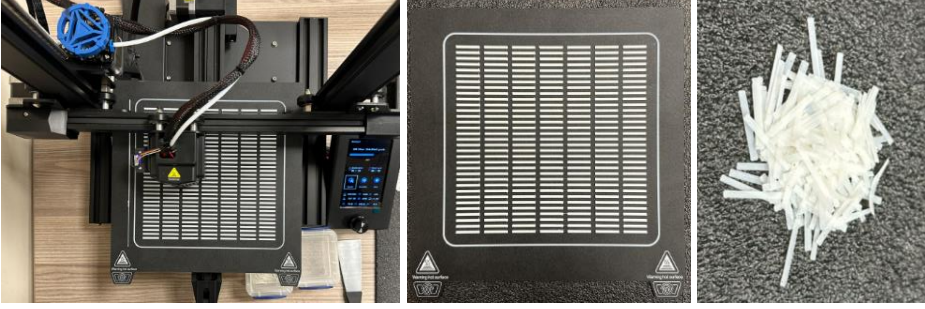
Bu çalışma kapsamında, literatürden farklı olarak PLA filamentini kullanılarak makro lif kriterlerini sağlayan beton donatıları üretilmiş ve üretilen lifler çimento esaslı bir matris içerisinde güçlendirme elemanı olarak kullanılmıştır. Üretilen numunelerin üç noktalı eğilme yüklemesi altında mekanik özellikleri incelenerek rapor edilmiştir.

2. MATERYAL VE METOT

Matris olarak 0,45 su/çimento oranına sahip çimento hamuru CEM I 42,5 R tipi çimento kullanılarak hazırlanmıştır. Çimentoya ait kimyasal, fiziksel ve mekanik özellikler Tablo 1'de sunulmuştur. 3D baskı ile makro lif üretimi sürecinde ise polilaktik asit (PLA) filamentini kullanılarak 200 mikron kalınlığa ve 20 mm uzunluğa sahip polimer lif üretimi Creality Ender 3 V2 Neo marka bir 3D yazıcı ile üretilmiştir. Üretim aşaması ve üretilen PLA makro lifler Şekil 1'de gösterilmiştir. Laboratuvar tipi bir mikserde ilk olarak çimento ve su karıştırılarak çimento hamuru hazırlanmıştır. Hazırlanan matris şahit numune üretimi amacıyla 40x40x160 mm çelik kalıplara doldurulmuştur. Ardından hazırlanan çimento hamuru içerisine toplam matris hacminin %1'i oranında PLA makro lif karışımına ilave edilerek 1 dk süre ile karıştırma işlemine devam edilmiştir. Hazırlanan lifli matris de yine 40x40x160 mm çelik kalıplara doldurularak numune alımı tamamlanmıştır. Numuneler 1 gün süre ile priz alması için laboratuvar ortamında bekletilmiş ardından kalıptan alınarak 28 gün süre ile suda kür işlemi uygulanmıştır.

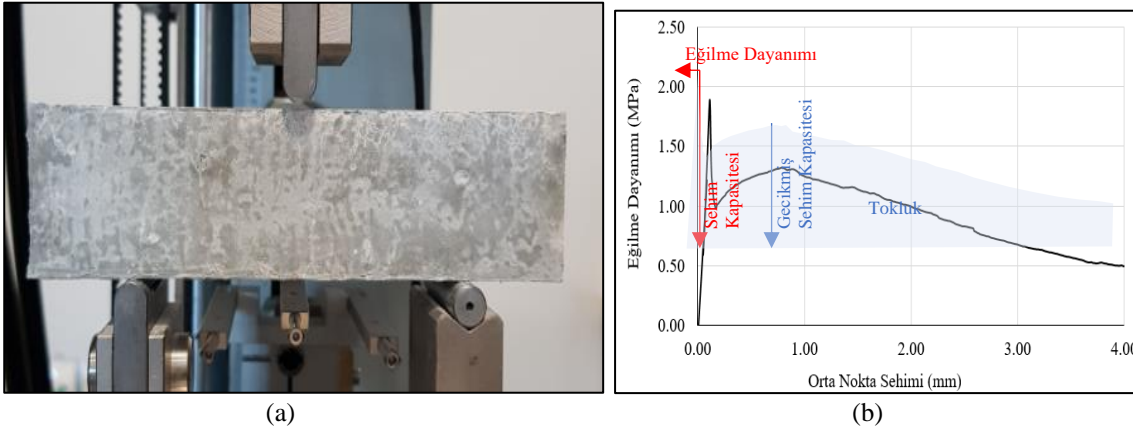
Tablo 1. Çimentoya ait kimyasal, fiziksel ve mekanik özellikler

Kimyasal Özellikler (%)	
SiO ₂	17.62
Al ₂ O ₃	5.01
Fe ₂ O ₃	3.17
CaO	63.78
MgO	0.97
Na ₂ O	0.39
K ₂ O	0.77
SO ₃	3.10
Kızdırma kaybı	2.48
Cl ⁻	0.006
Çözünmeyen kalıntı	0.19
Serbest CaO	1.09
Fiziksel Özellikler	
Özgül ağırlık	3.11
Blaine özgül yüzey alanı (cm ² /kg)	3485
90 µm eleküstü bakiye (%)	0.6
45 µm eleküstü bakiye (%)	17.4
Mekanik Özellikler (MPa)	
Basınç Dayanımı (2 günlük)	28.3
Basınç Dayanımı (7 günlük)	40.1
Basınç Dayanımı (28 günlük)	49.9



Şekil 1. 3D baskı ile makro lif üretim süreci

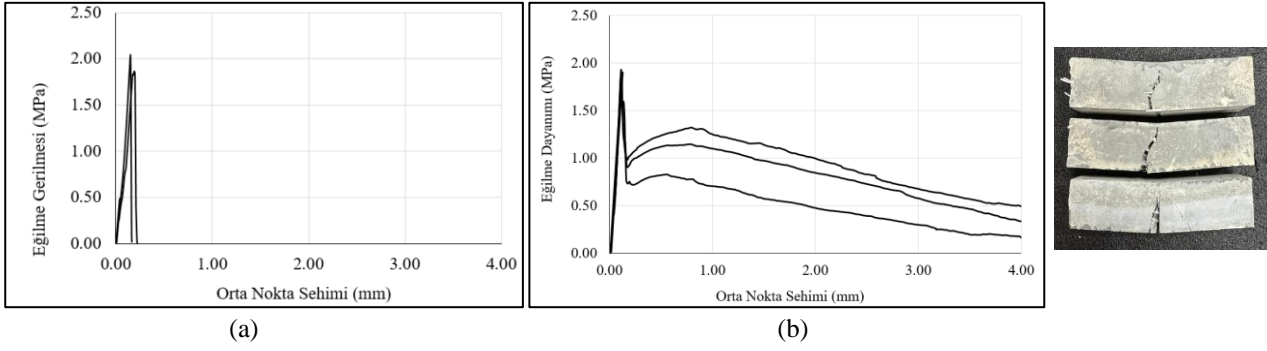
Numunelerin mekanik özelliklerini belirlemek amacıyla üç noktalı eğilme deneyleri gerçekleştirilmiştir. Deneylerde Zwick Roell marka bir hidrolik yükleme cihazı kullanılmıştır. Eğilme deneylerinde 0,5 mm/dakika olacak şekilde 4 mm orta nokta sehimine kadar yükleme yapılmış ve yükleme süresinde numune orta noktasından sehim değerleri cihaza entegre bir deformasyon ölçer yardımıyla kaydedilmiştir (Şekil 2a). Elde edilen veriler kullanılarak gerilme-orta nokta sehimi eğrileri çizdirilmiş ve mekanik parametreler bu eğri üzerinden hesaplanmıştır (Şekil 2b). Numunenin taşıyabildiği en büyük gerilme değeri eğilme dayanımı olarak nitelendirilmiştir. Deneysel çalışma kapsamında sehim kapasitesi ve gecikmiş sehim kapasitesi olmak üzere iki farklı terim kullanılmıştır. Sehim kapasitesi eğilme dayanımına karşılık gelen sehim değeri olarak alınmıştır (Şekil 2b). Gecikmiş sehim kapasitesi ise liflerin yükü köprülemeye başlayarak yeniden bir yük artışının gerçekleştiği ikinci tepe noktasına denk gelen sehim değeri olarak nitelendirilmiştir (Şekil 2b). Söz konusu gecikmiş sehim kapasitesi değeri, kompozitin halen yük taşımaya devam etmesi ve kırılmaya karşı gösterdiği direncin bir göstergesi olarak düşünülebilir. Numunelerin enerji yutma kapasiteleri her bir numune için yük-sehim eğrisi altında kalan alanın hesaplanmasıyla elde edilmiştir (Şekil 2b). Bu değer de tokluk olarak nitelendirilmiştir.



Şekil 2. a) Üç noktalı eğilme yüklemesi, b) Eğilme dayanımı – orta nokta sehimi eğrisi

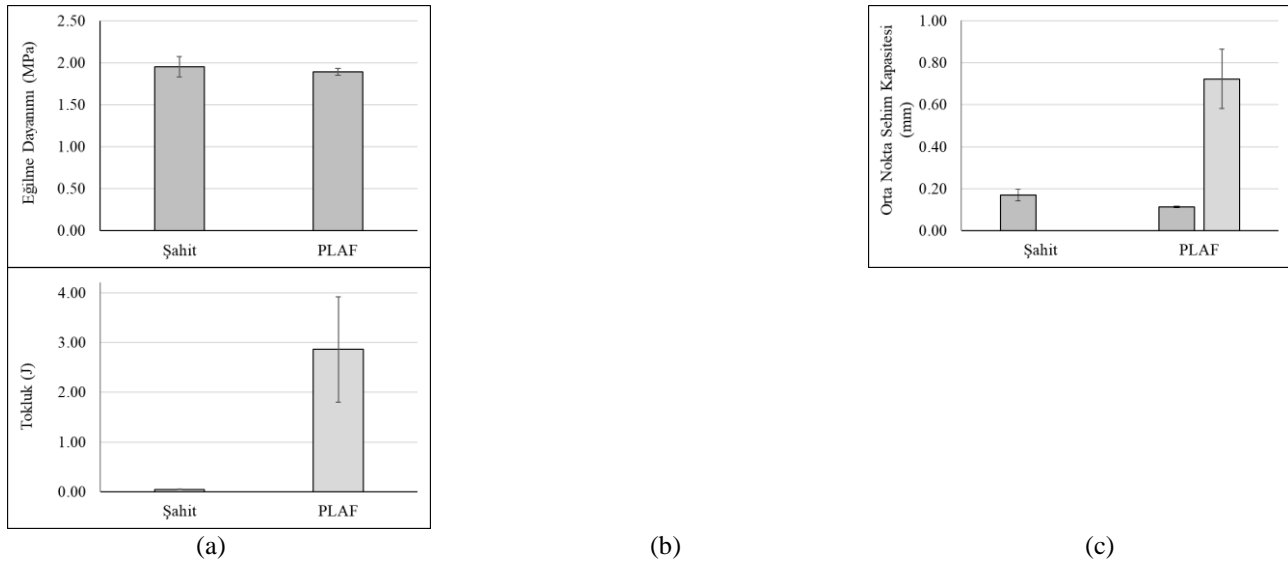
3. BULGULAR

Numunelere ait eğilme dayanımı-orta nokta sehimi eğrileri Şekil 3'te sunulmuştur. Eğriler incelendiğinde, 3D baskı ile üretilen PLA liflerin kullanımı ile tüm numunelerde eğilme yüklemesi altında ani bir yük kaybı yerine sehim yumuşaması davranışının gerçekleştiği görülmektedir. Bu kapsamda numunelerin orta nokta sehimi lifler sayesinde gerçekleşen kontrollü çatlak genişlemesine bağlı olarak 4 mm'ye kadar sürdürülebilir.



Şekil 3. Eğilme dayanımı – Orta nokta sehimi eğrileri a) Şahit numuneler, b) 3D baskı PLA lif içeren numuneler

Eğriler üzerinden elde edilen eğilme dayanımı, sehimi kapasitesi, gecikmiş sehimi kapasitesi ve tokluk verileri Şekil 4'te sunulmuştur. Eğilme dayanımları değerlendirildiğinde şahit numunelere kıyasla 3D baskı PLA içeren numunelerin eğilme dayanımlarının birbirine yakın olduğu görülmektedir. Eğilme dayanımları şahit ve PLAF serileri için sırasıyla 1.96 ± 0.12 MPa ve 1.89 ± 0.04 MPa olarak elde edilmiştir (Şekil 4a). Sehimi kapasiteleri ise yine şahit ve PLAF serileri için 0.17 ± 0.03 mm ve 0.11 ± 0.004 mm olarak elde edilmiştir (Şekil 4b). Sehimi kapasitesindeki bu az miktardaki düşüşün PLA lif takviyesine bağlı olarak matris içerisinde kusur oluşumunun tetiklenmesiyle göreceli olarak daha erken kırılan matrise ve bir miktar düşen eğilme dayanımına bağlı olarak elde edildiği söylenebilir. Ancak, kırılma gerçekleşikten sonra PLAF serisinde 3D baskı ile üretilen PLA liflerin kesitler arasında bir köprüleme gerilmesi oluşturmasıyla sehimi yumuşaması davranışının görülmesine bağlı olarak kontrollü bir çatlak genişlemesi elde edilmiş ve numunelerden elde edilen gecikmiş sehimi kapasitesi verisi 0.72 ± 0.14 mm seviyelerine kadar artırılabilmiştir (Şekil 4a). Bu durumun bir sonucu olarak PLAF numunelerinden elde edilen tokluk verileri şahit numuneye kıyasla artarak 0.05 ± 0.01 J seviyelerinden 2.86 ± 1.06 J seviyelerine yükselmiştir (Şekil 4c).



Şekil 4. a) Eğilme dayanımı, b) Sehimi kapasitesi ve gecikmiş sehimi kapasitesi, c) Tokluk

4. TARTIŞMA VE SONUÇLAR

Bu kısa kapsamlı çalışmada 3D baskı teknolojisi ile kullanılarak üretilen PLA esaslı liflerin çimentolu sitemlerin eğilme yüklemesi altındaki mekanik performansına etkisi araştırılmıştır. Şahit harçla yapılan kıyaslamalarda üretilen PLA liflerin literatürde yer alan geleneksel makro polipropilen liflerle benzer olarak kontrollü çatlak gelişimi sağladığı ve kompozit tokluğunun eğilme dayanımında belirgin bir kayıp yaşanmadan artırılabilirdiği görülmüştür. Bu kapsamda, sunulan bu çalışma sonuçlarının, farklı polimerler kullanılarak üretilebilecek farklı geometrik özellikteki 3D baskılı liflerin kullanımıyla yeni araştırmalarda çimento esaslı kompozitlerin mekanik özelliklerinin geliştirilmesinde fayda sağlayabileceği düşünülmektedir.

Teşekkür

Mekanik deneylerde test cihazlarının kullanımı süresince desteklerini esirgemeyen HÜBTUAM Yapı Malzemesi Birimine teşekkürlerimizi sunarız.

Etik Kurul Onayı

N/A

Akran Değerlendirmesi

Harici hakemli.

Yazar Katkıları

Kavramsallaştırma: E.G., S.O.K.; Araştırma: E.G., J.K.; Materyal ve Metodoloji: E.G., S.O.K, J.K.; Denetim: E.G., S.O.K.; Görselleştirme: J.K.; Orijinal Taslağın Yazımı: E.G., S.O.K.; İnceleme ve Düzenleme: E.G., S.O.K. Tüm yazarlar makalenin yayımlanmış versiyonunu okumuş ve kabul etmiştir.

Çıkar Çatışması

Yazarların beyan edecekleri bir çıkar çatışması yoktur.

Finansal Destek

Yazarlar bu çalışmanın finansal destek almadığını beyan etmişlerdir.

KAYNAKLAR

ACI 544.3R-08, Guide for specifying, proportioning, and production of fiber-reinforced concrete.

Akın, S. K., Kul, İ. & Sarıgüzel, M. Investigation of Bond between Polypropylene Fiber Reinforced Hybrid Concrete and Reinforcement by Hinged Beam Test Method. Available at SSRN: <https://ssrn.com/abstract=4369076> or <http://dx.doi.org/10.2139/ssrn.4369076>

Arafa, M. H., Alqedra, M. A., & Almassri, H. G. (2013). Effect of forta-ferro fibers on fresh and mechanical properties of ultra high performance self compacting concrete. *Int. J. Eng. Tech. Res*, 1(7), 43-47.

Asprone, D., Auricchio, F., Menna, C., & Mercuri, V. (2018). 3D printing of reinforced concrete elements: Technology and design approach. *Construction and Building Materials*, 165, 218-231. <https://doi.org/10.1016/j.conbuildmat.2018.01.018>

Berman, B. (2012). 3-D printing: The new industrial revolution. *Business horizons*, 55(2), 155-162. <https://doi.org/10.1016/j.bushor.2011.11.003>

De Schutter, G., Lesage, K., Mechtcherine, V., Nerella, V. N., Habert, G., & Agusti-Juan, I. (2018). Vision of 3D printing with concrete—technical, economic and environmental potentials. *Cement and Concrete Research*, 112, 25-36. <https://doi.org/10.1016/j.cemconres.2018.06.001>

Farina, I., Fabbrocino, F., Carpentieri, G., Modano, M., Amendola, A., Goodall, R., ... & Fraternali, F. (2016). On the reinforcement of cement mortars through 3D printed polymeric and metallic fibers. *Composites Part B: Engineering*, 90, 76-85. <https://doi.org/10.1016/j.compositesb.2015.12.006>

Gautam, A., & Awasthi, A. (2018). Use of FORTA-FERRO fiber in structural concrete mix: A review. *Int. Res. J. Eng. Technol*, 5(05).

Gödek, E., Şevik, S., Özdilli, Ö. (2020). A study on flexural behavior of cement paste reinforced by using 3D-printed polylactic acid-based reinforcement. In *Proc., 2nd International Icontech Symposium on Innovative Surveys in Positive Sciences*, pp. 270–277, Budapest, Hungary.

Kun, K. (2016). Reconstruction and development of a 3D printer using FDM technology. *Procedia Engineering*, 149, 203-211. <https://doi.org/10.1016/j.proeng.2016.06.657>

Naaman, A. E. (2018). Fiber reinforced concrete: Five decades of progress. In *Proceedings of the 4th Brazilian Conference on Composite Materials*, Rio de Janeiro, July, Brazil (pp. 22-25).

Narule, G. N., & Visapure, A. N. (2022). Experimental investigation on compressive and flexural performance of Forta-fiber reinforced concrete. *Materials Today: Proceedings*, 56, 406-411. <https://doi.org/10.1016/j.matpr.2022.01.244>

Nematzadeh, M., Maghferat, A., & Herozi, M. R. Z. (2021). Mechanical properties and durability of compressed nylon aggregate concrete reinforced with forta-ferro fiber: experiments and optimization. *Journal of Building Engineering*, 41, 102771. <https://doi.org/10.1016/j.jobbe.2021.102771>

Salazar, B., Aghdasi, P., Williams, I.D., Ostertag, CP., Taylor, HK. (2020). Polymer lattice-reinforcement for enhancing ductility of concrete. *Materials and Design*, 196, 109184. <https://doi.org/10.1016/j.matdes.2020.109184>

Xu, Y., Šavija, B. (2019). Development of strain hardening cementitious composite (SHCC) reinforced with 3D printed polymeric reinforcement: Mechanical properties. *Composites Part B: Engineering*, 174, 107011. <https://doi.org/10.1016/j.compositesb.2019.107011>

The Importance Of Using Durable Concrete In Underground Floors

Boriana Vrusho^{1*}, Alma Golgota², Indrit Bimi²

Abstract: Today in Durres, even wider, buildings constructed with durable concrete are very few in these days. Geological studies show that the soil in the foundation has low retaining capacity for this city due to high friction angle. This is also one of the other factors that Seismicity of the area is very high, up to level 9 ball of Richter. The purpose of this article is the production of durable concrete with low permeability of water. The project is constructed in our country and in particular in Durres where the groundwater level is higher and the use of space efficiently needs to build parking with underground floor. The study is a case study of an object in the city of Durrës, built in the "former Kenete" area, an area with a high level of underground water. The aim of the study is to monitor the phase of use of underground environments built with durable concrete, with a water/cement ratio of 0.4-0.42 and with penetron additives. The result is that the object, not isolated from the outside with waterproofing materials, has no problem with humidity or with the filtration of underground water. The study recommends for builders to use durable concrete and suitable additives that make the concrete waterproof.

Keywords: Concrete durability, foundation, permeability of foundation concrete, seismology of Durres city

¹**Address:** Polytechnic University of Tirana, UPT/ Faculty of Civil Engineering, Albania

²**Address:** Universiteti Alexander Moisu, Durres, Albania

***Corresponding author:** borianavrusho@gmail.com

1. INTRODUCTION

Durability of foundation concrete structures is a widespread and universal problem. We can build underground floors, in the presence of groundwater, without the need for additional isolation works. Repairing can be made even within the object, but in the case of this isolation is almost impossible to do it. The aim is that in any case should have limited penetration of the devastating effects of water that are present in the environment of exposure and hence reduce the number, intensity and importance of maintenance interventions. To obtain the durable concrete which meet our project specifications, the concrete should have a coefficient of permeability K , smaller or equal to 1.10^{-11} m/s or a resistance to water penetration under ISO 7031-1994 standard specifications, or otherwise rely on standard EN 206-1, permeability should be up to 20 to 50 mm.

1.1 Geotechnical study of the project

The maximum expected magnitude for Durres city is $M_{max}=6.5-7.0$. Durres City is included within the area of isoline of mean return period of $T_p=200-250$ years, for shakings with intensity $I_0=VIII$ (MSK-64) or $PGA=0.2g$. It means that shakings with intensity VIII or $PGA=0.2g$ is not going to be exceeded every 25 years with a probability of 90%. Concerning shakings with intensity IX degree mean return period will be about 1000 years.

1.2 Seismic risk of Durres city

Based on studies carried out for seismic hazard assessment at local it was observed: For a $PGA=0.2g$ value on bedrock, the highest 2-D response ($PGA=11m/s/s$ at $T_s=0.5s$) was observed on the deepest part of Durres graben, where the thickness of poor sediments is about 130m. Comparing these data with 1-D solutions it can be seen that S_a spectra for 1-D solution on this part of the graben are characterized by much smaller peak amplitudes ($PGA=1.5-2.0m/s/s$) but for a wider range of periods. The shape of 1-D S_a spectra is almost flat. This can be explained by the degradation of G moduli and increase of strains for thick models. On the basis of analysis results is discussed seismic risk calculation made for construction site (Frankel et al.1995). The calculations were carried out for PGA values and periods at 0.1 seconds, 0.2, 0.3, 0.5, 1 and 2, the four repetition periods 95, 475, 975, and 2475 years, which was corresponding probabilities of exceeding 10% in 10 years, 10%, 5% and 2% in 50 years, respectively.

Amplification with strong surface model for earthquakes reached DYRR EW type and $DAF A_{max} = 0.43g$ 1:48. At maximum acceleration 5.0M average depth is between $A_{max} = 0.31g$, $DAF = 1.069$. Average maximum acceleration on the surface of the soil is between $A_{max} = 0.38g$ and $DAF = 1.31$.

Table 1.2.1: Maximal values of spectral and horizontal accelerating

Period Sec	Spectral acceleration			
	RP = 95 Years	RP = 475 Years	RP = 975 Years	RP = 2475 Years
PGA	0.189	0.286	0.333	0.404
0.10	0.271	0.459	0.563	0.720
0.20	0.358	0.593	0.722	0.916
0.30	0.316	0.528	0.653	0.832
0.50	0.203	0.352	0.440	0.578
1.00	0.083	0.151	0.193	0.261
2.00	0.044	0.080	0.102	0.138

Table 1.2.2: PGA (Amax) values and DAF in construction site according TIR-NS, LSK EW, AL-NS DURR-EW and DURR-NS.

H (m)	DURR-EW		DURR-NS		AL-NS		LSK-EW		TIR-NS		Amax (mes)	DAF (mes)
	A max	DAF	A max	DAF	A max	DAF	A max	DAF	A max	DAF		
0	0.43	1.48	0.42	1.45	0.35	1.21	0.38	1.31	0.32	1.10	0.38	1.31
4.0	0.36	1.24	0.36	1.24	0.30	1.03	0.37	1.28	0.29	1.00	0.34	1.17
5.0	0.32	1.10	0.35	1.21	0.28	0.97	0.36	1.24	0.25	0.86	0.31	1.07
10.0	0.26	0.90	0.29	1.00	0.25	0.86	0.31	1.07	0.29	1.00	0.28	0.97
12.0	0.22	0.76	0.22	0.76	0.25	0.86	0.23	0.79	0.27	0.93	0.24	0.83
15.0	0.23	0.79	0.20	0.69	0.26	0.90	0.25	0.86	0.26	0.90	0.24	0.83
28.0	0.29	1.00	0.30	1.03	0.27	0.93	0.31	1.07	0.30	1.03	0.29	1.00
66.0	0.29	1.00	0.29	1.00	0.29	1.00	0.29	1.00	0.29	1.00	0.29	1.00

1.3 Hydrological study of construction site

Results of the study showed that hydro-geological groundwater level is up to 0.8-1.5m from the ground system. Also the content of groundwater is aggressive, containing ph = 7.3 (according to the attached analysis), the amount of chloride Cl is 26.1 g/ l; sulphates SO4 = 6.21g/ l; dry content 7.85 g/ l = 7850 mg / l measured by the standard EN 1008. Standard limits for aggressive environmental conditions, for soils and underground water within the temperatures 5-25°C. The highest value determines the class.

Table 1.3.1: Standard limits for aggressive environmental conditions

Chemical characteristics	Test method	XA1	Parameter of water in site
SO ₄ ²⁻ (mg/l)	EN 196-2	≥ 200 and ≤ 600	621
pH	ISO 4316	≤ 6.5 and ≥ 5.5	7.3
CO ₂ (mg/l)	prEN 13577	> 15 and ≤ 40	-
NH ₄ ⁺ (mg/l)	ISO 7150-1 ISO 7150-2	> 15 and ≤ 30	-
MG ²⁺ (mg/l)	ISO 7980	≥ 300 and ≤ 1000	-
Soil			
SO ₄ ²⁻ (mg/kg)	EN 196-2	≥ 2000 and ≤ 3000	-
Acidity (ml/kg)	DIN 4030-2	-	-

* (-) not measured

1.4 Engineering-geological conditions of construction

Based on field observations, lithological composition of the construction site, evidence INSITU and physic-mechanical characteristics of soils and rocks that our construction site meets studies shows that only layer 3 and 4 with the given limit standard specification are suitable to construct and maintain bearing loads for foundation constructions:

Layer No. 3 Represented by small grain sand and gray silt impregnated with water and moderately compressed. Geological composition is given in the table below:

Table 1.4.1: Soil characteristics for layer no.3 and 4

Properties	Specifications/Index	Analysis results for layer no.3	Analysis results for layer no.4
Clay content	<0.00 2mm	8.9%	18.60%
Sand content	>0.05 mm	19.60%	37.80%
Silt content	0.002-0.05 mm	71.50%	43.60%
Specific density	ρ	2.69T/m ³	2.71T/m ³
Bulk density	Δ	1.98 T/m ³	1.5 T/m ³
Porosity coefficient	ϵ	0.7	0.78
Compression modulus	E	110kg/cm ²	65kg/cm ²
Friction angle	ϕ	320	240
Compressive load allowed	σ	1.8kg/cm ²	0.10 kg/cm ²

2. MATERIALS AND METHODOLOGY

2.1 Materials

2.1.1 Cement

The details of the experimental program have been reported in this study. Concrete ingredients produced by the Albanian standard S SH EN 206-1:2003, with resistance class C25/30, were taken in Fushe Kruja from Vega concrete production site. The concrete is produced in SAG concrete plant. Composition of Portland cement, CEM I 42.5 R, from ANTEA, type cement conforming EN 197-1 was used in this study.

2.1.2 Aggregates

Coarse and fine aggregates obtained from Milot and Kruja quarry units have been used for this study. Maximum size of coarse aggregate used is 25 mm and specific gravity of ranging from 2.6 - 2.7 kg/m³ based on standard S SH 509:1987; bulk density 1484 kg/m³ and fine modulus 6.07. For fine aggregates maximum size used is 5 mm and specific gravity of ranging from 2.687 kg/m³ based on standard S SH 509:1987; and fine modulus 2.74.

2.1.3 Water

Potable tap water available production site was used for mixing and curing of concrete. The water is filtrate based on standard 2751:1987.

Table 2.1.3.1: Chemical analysis of water used in mix design

No.	Characteristics	Units	Test results	Standard limit EN 1008
1	Water resource		Well water	-
2	Colour		Transparent	-
3	Odour		None	-
4	Water density @ 190 C	kg/ l	1.0082	0.9982
5	Total hardness (CaCO3)	mg/l	2.91	-
6	Total dissolved solids at 180 °C	mg/l	3.82	≤4
7	pH value		7.61	≥4
8	Chloride content Cl-	mg/l	1241	≤ 1000
9	Sulphate content SO4-	mg/l	4996	≤ 2000
10	Salts content	mg/l	0.02	≤ 100

2.1.4 Concrete admixtures

Additives used in this project are; Chryso-Fluid Premia 180(superplasticizer) and Penetron Admix (uperplasticizer) and in quantities 3 l/m3 concrete. Additives were used to produce concrete class C25/30 MPa and the result was decreasing the amount of water. The effect of using the lowest amount of water is increasing the durability and resistance of concrete.

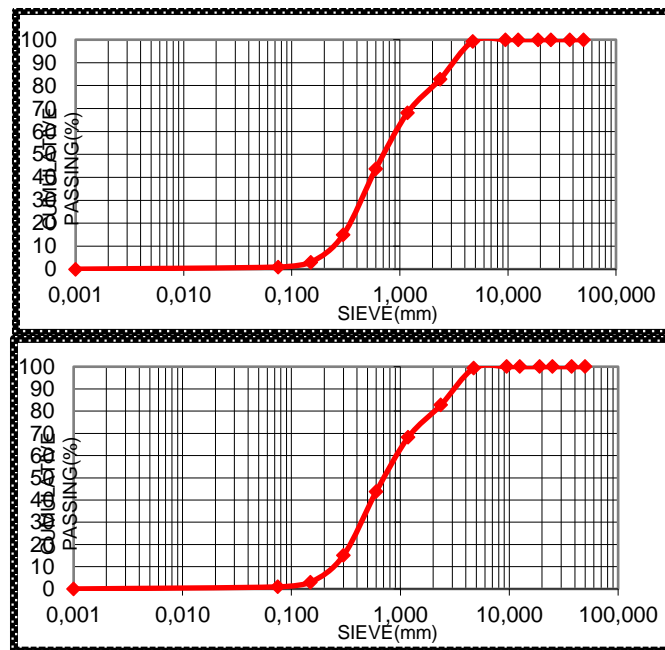


Figure 2.1.4.1: a) Coarse and b) fine aggregates PSD analysis.

2.2 Methodology

2.2.1. Durable concrete mix design

Mix design is a process of selecting suitable ingredients for concrete and determining their proportions which would produce, as economically as possible, a concrete that satisfies the Orion project requirements.

All mix designs data for durable concrete used in our project are represented in Table 2.2.1.1. In present study durable concrete class C30/45 was produced with river raw material. All mix designs are formulated based on specifications of EN 206-1 standard.

Table 2.2.1.1: Mix design of concrete

Class	C25/30	Slump	S4	Exposure class	XS ₃	D _{max}	20
		w/c ratio	0,40		19 ⁰ c		
Standard applied		S SH EN 206-1:2003			31.10.2013		
		Concrete for underground construction					
No.	Ingredients			Units/m ³	Quantity		
1	Natural river sand 0-04 mm			kg	850		
2	Crashed sand 0-04 mm			kg	152		
3	Crashed river gravel 5-10 mm			kg	285		
4	Crashed river gravel 10-25mm			kg	650		
5	Cement CEM I 45.2 R/A-LL			kg	350		
6	Additive Chryso-Fluid Premia 180 (superplasticizer) Reduction. 15%; Dosage 0.8 lit/100 kg cement)			lit/m ³	3		
	Additive PENETRON ADMIX (uperplasticizer) Reduction. 15%; Dosage 0.8 lit/100 kg cement)			lit/m ³	3		
7	Well water			lit	139		
8	w/c ratio			-	0.4		

The compressive strength of concrete is considered as the index of its quality. Therefore the mix designs are generally carried out for a particular compressive strength of concrete with adequate workability so that the fresh concrete can be properly mixed, placed and compacted.

After 28 days period of curing, the specimens were taken out of the curing tank and there were tested besides measuring the fresh properties (workability, air content and concrete temperature); following tests such as permeability of concrete cubes and chlorides contents are measured.



Figure 2.2.1.1: a); b);c);d) Concrete production site

3. RESULTS & TABLES

3.1 Compressive strength of concrete cubes in Orion construction site

Compressive strength, of mixes was determined at various ages as per EN 12390-3:1999 and EN 12390-5:1999 are given in table 3.1. Cube Compressive strength at the age 28 days. After casting the specimens were covered with sheets to minimize the moisture loss from them. Specimens were demoulded after 24-hours and then cured in water at approximately room temperature till testing. Compressive strength tests for cubes were carried out at 28 days. All the specimens were tested in an automated compressive strength machine shown in Figure 3.1:



Figure 3.1.1: Compressive strength machine

Table 3.1.1: Results for compressive strength test of concrete cubes taken from ORION object.

No.	Report number	Casting date [dd/mm/yy]	Testing date [dd/mm/yy]	Curing age [Days]	Density [kg/m3]	C.S [MPa]
1	5416/13	18.11.2013	16.12.2013	28	2430	32.78
2	5414/13	20.11.2013	18.12.2013	28	2444	33.66
3	5412/13	25.11.2013	24.12.2013	28	2490	34.69
4	5411/13	25.11.2013	24.12.2013	28	2467	37.90
5	4769/13	15.11.2013	13.12.2013	28	2405	30.47
6	4768/13	15.11.2013	13.12.2013	28	2415	33.34
7	4767/13	29.11.2013	06.12.2013	28	2455	33.19
8	4764/13	12.11.2013	10.12.2013	28	2449	32.93
9	4762/13	05.11.2013	03.12.2013	28	2402	38.85
10	4552/13	31.10.2013	28.11.2013	28	2443	35.91

3.2 Durability of concrete

The durability of concrete depends largely on the movement of water enters and moves through it. Permeability is a measure of flow of water under pressure in a saturated porous medium while Sorptivity is materials ability to absorb and transmit water through it by capillary suction. The porous structure of concrete is intimately related with its permeability. A low water/cement ratio results in concrete structures which are less permeable because they are characterized by having small pores which are not interconnected. The water penetration under pressure test is a standard test procedure (EN 12390-8).



Figure 3.2.1: Images of water penetration and chloride content test

Table 3.2.1: Water depth penetration and chloride content for concrete cubes tested.

No.	Concrete class	Depth of water penetration [mm] EN 12390-8	Concrete chloride content [%] EN 196-2
1	C 25/30	22.4	0.027
2	C 25/30	20.8	0.015
3	C 25/30	23.6	0.033
4	C 25/30	22.4	0.012
5	C 25/30	24.6	0.036
6	C 25/30	20.4	0.015
7	C 25/30	20.3	0.069
8	C 25/30	20.5	0.012
9	C 25/30	20.5	0.011
10	C 25/30	20.6	0.023

The depth of water penetration test made on concrete cubes revealed in creation of protective layer structures for reinforced concrete. Specifically in our project, this protective cover on plate will be carried out on 7cm and 3cm underground floor walls. Here are some views of realization of underground floor of this building.



Figure. 3.2.1: The foundation of the project

4. CONCLUSIONS

Seismologic project data showed that layer 3 and 4 are adaptable for making foundation of the project. Based on geological project information, durable concrete for deep underground basements is an important component of new urban building construction. This is often because parking in most large cities is generally inadequate and often serviced by aging, outdated, and deteriorated above-grade parking structures that do not fit the surrounding architecture and occupy valuable aboveground space.

So in this thesis, I wanted to say that it is very important to produce and to use the durable concrete, in our country, in the structure of the ground floors when we have a high level of underground water. This is reached by decreasing the permeability through the decreasing of water/cement ratio and increasing the protective cover of reinforcement concrete according to the level of the penetration of water and chloride test.

Using durable concrete we have some benefits such are:

1. Using durable concrete is economic and social benefit product
2. Increase the lifetime of the concrete structural
3. Better utilization of urban spaces
4. Increase the number of floors underground.
5. We have no maintenance costs or use for calculating the period of stability.
6. Degradation of deferred from the standard 50 years today, in 80-100 years.
7. Used in normal conditions and all underground facilities for any activity, since the presence of moisture is eliminated.
8. Albanian goes towards housing facilities Contemporary with European Standards. The corresponding entry in the EU.

ACKNOWLEDGMENTS

I would like to thank all those people who have been involved directly or indirectly with my research work. I appreciate the valuable support of my friends and colleagues, during the implementation of this research, including construction company, concrete production site company, the additives supply company, testing laboratories.

REFERENCES

- A.L.T.E.A report-Study of geological and engineering conditions of the building height 7-8-10 floors with one floor underground at the roadside "Deshmoret" in Durres. Pg 16-20.
- Arum, C., and Udoh, I., 2005." Effect of dust inclusion in aggregate on the compressive strength of concrete", Journal of Science, Engineering and Technology, Vol.12 No. 2, Chyke-Cee, Enugu. pp. 6170-6184.
- C. Arum and A.O. Olotuah, " Making of strong and durable concrete", Received February 2006 and accepted may 2006 in Emirates Journal for Engineering Research, 11(1),25-31(2006)
- Edited by John Newman & Ban Seng Choo, "Advanced Concrete Technology" Part 2, Concrete Properties, pp. 8/3-8/9.
- Edited by C.W.Yu and John W. Bull : " Durability of Materials and Structures in Building and Civil Engineering" book Michael S. Mamlouk and John P. Zaniwski : " Materials for Civil and Construction Engineers
- EN 206-1:2004 Concrete specification, performance, production and conformity. pg
- Eurocod 2: Cement structures design. Generally rules and houses rules.
- GeoSeis-IT Consulting report-Study of geological and engineering conditions of the building height 7-8-10 floors with one floor underground at the roadside "Deshmoret" in Durres. Pg 16-20.
- I.Struct.E/ICE Joint Committee, 1985. Manual for the Design of Reinforced Concrete Building Structures, Institution of Structural Engineers, London

Integral Capillary System Concrete Waterproofing- Foundation Structure- Foundation from Penetron

M. Collepardi, Admixtures used to enhance placing characteristics of concrete, Cement-Concrete Compose 20 (1998) 103-112.

M. Collepardi, L.Coppola, Cement Italian Industry 665(1992).

Raheem, A.A. and Aderounmu, O.M., 2002. "The effect of aggregate sizes on the strength of concrete", Journal of Science, Engineering and Technology, Vol.9 No. 2, Chyke-Cee, Enugu. pp. 4041-4051.

Richardson M., " Fundamentals of durable reinforced concrete" , Modern concrete technology 11, series editors, pp. 51-101

S SH EN 13139: 2002

Significance of Tests and Properties of Concrete and Concrete-Making Materials (STP169D) (LT205)

Traeger PA. Evaluation of the constructive use of foundry wastes in highway construction. MS thesis, The University of Wisconsin- Madison, Madison, Wisconsin, 1987.

UA_2008_22_additional for concrete , conform Standard SK EN 206-1, first part

The reliability of inner bottom plating of fuel tanks on aging bulk carriers

Špiro Ivošević*¹, Joanna Soszyńska-Budny²

Abstract: Cargo holds on general cargo ships are exposed to multiple environmental influences such as highly corrosive cargoes, environmental factors, different and destructive cargo-handling equipment, etc., which contribute to the accelerated deterioration of structural steel elements. The inner bottom plate, mainframes with brackets, and transfer bulkheads between cargo holds are prone to structural failures such as cracks, deformation, or corrosion. Corrosion significantly accelerates the aging of metal plates, especially at the bottom of the holds, whose steel plates are exposed to multiple impacts from both sides of the steel plate. From cargo holds they are under the influence of cargo, atmosphere, and contacts with manipulative equipment, while from the below side of the plate, they are exposed to the effects of ballast water, fuel, or dry spaces depending on the outgoing ship and location. In this paper, we analyze steel plates that are exposed from the upper side to the influences of cargo from the cargo holds, while from the lower side, they are exposed to the influences of the fuel oil from the fuel tanks. We consider a database of 25 bulk carrier ships aged from 5 to 25 years. Measurements were performed on a total of 110 fuel tanks and a total of 3070 measurement data. By measuring the thickness of the steel plate during regular special surveys, following a precisely defined methodology, the values of the reduction in the thickness of the steel plates due to corrosion over time were obtained. By introducing a unique criterion of an acceptable deviation of 20%, i.e. a reduction of the measured value concerning the built-in value of the thickness of the steel plate, excessive corrosion values were identified that required the replacement of corroded surfaces. Values of excessive corrosion defined in this way were considered as a failure. By applying the reliability theory, calculations of the reliability failure intensity and failure indicator determined the time when the condition of structural elements deteriorates due to corrosion up to the levels that require extensive maintenance services. The results showed that the usability dropped significantly after 15 years of exploitation.

Keywords: Corrosion, fuel oil tanks, reliability, damage, failure, inner bottom plating

¹**Address:** Put I Bokeljske brigade 44, 85330 Kotor, University of Montenegro, Faculty of Maritime Studies of Kotor

²**Address:** Morska 81-87, 81-225 Gdynia, Poland, Gdynia Maritime University, Faculty of Navigation, Department of Transport

*Corresponding author: spiroi@ucg.ac.me

1. INTRODUCTION

Although numerous actions have been taken by International Maritime Organization (IMO), Flag authorities, Classification Societies and other relevant bodies in maritime industry in order to improve maritime safety and environment protection, the number of accidents involving various ships still remains significant. Research in the maritime sector published by Knapp et al. (2011), Heij and Knapp (2019) has confirmed that general and dry cargo vessels exhibit the highest likelihood of casualties. That casualties were connected with various incidents as they are: collision, fire, explosion, flooding, loss of control, hull failure, contact, damage to ship equipment, grounding and etc. (EMSA, 2019).

A significant effort was conducted by different international bodies in order to reduce hull structure deterioration in the last two decades. In that sense, it can be conclude that number of hull defect was reduced significantly. Research between 1997. and 2001. was recorder more than 15 % hull failures, while between 2002. and 2006. was recorder around 4 % of hull defects (Wang, et al., 2009). Recent research by European Maritime Safety Agency (EMSA) announce that number of casualties that was connected with hull failure was around 1% (EMSA 2019).

Different influenced factors as well as predictable and unpredictable complex influences of the atmosphere, marine environment and ship-specific factors significantly influence on the deterioration of ship structures over time (Ivošević et al. 2019). The structural deterioration depending of many internal and external factors and can be appear in the forms as corrosion, crack, deformation, coating breakdown and biofouling which can significantly accelerate the deterioration of ship different structural areas (Bosen and Xinghui, 2023). Due to different environments, operation procedures,

ship's route etc., corrosion forms as general corrosion, pitting, intergranular, galvanic, stress-corrosion, corrosion fatigue, fretting, microbiological, crevice, erosion and cavitation can be found in different ship hull areas and at different times of exploitation of a vessel (Barbulescu and Dumitriu, 2023; Peric, 2022).

In order to identify surface defect, they location or internal defect in the hull structure different nondestructive testing methods were used. Visual inspection, acoustic based testing, electromagnetic testing and imagine based testing were used (Bosen and Xinghui, 2023.). Recent years unmanned vehicles and robots without a pilot onboard have been extensively used for the underwater inspection, in dock inspection or different type of inspection (Bosen and Xinghui, 2023.; Poggi, 2020.).

In order to have safe and secure vessel, different condition assessment methods were applied. Furthermore, different structural reliability approach were development as: Time-variant reliability formulation, Failure probability and reliability, Inspection and maintenance planning, Reliability Centered Maintenance and etc. (Wang, et al., 2009.).

So far, numerous studies calculated corrosion rates over time (Ivošević et al. 2019; Ivošević et al. 2017) assessed risks, reliability (Guedes 1996) and the probability of the damage to particular structural areas (transverse bulkheads and inner bottom plating) (Ivošević et al. 2020; Qin 2003), or to all structural elements and areas (Guedes et al. 1996; Paik et al. 1998; Paik et al. 2003). That research analyses type of failure, corrosion model, different environmental factor and etc.

Information about the condition of hull structural and the reliability of the ship is of critical importance for ship owners and operators, both from the design aspect and from the aspect of the economic viability and reliability of the ship. The condition of the structure over time may require extensive overhauls that cause significant ship delays and extensive work on the repair of the ship's systems. Overhaul often requires the replacement of significant amounts of steel in open spaces, ballast tanks and cargo areas, which may require partial or complete replacement of structural parts of the ship. Repairs of fuel tanks are particularly demanding, considering that the complexity of the repairs is due to the discharging of fuel, degassing of the tank and special safety measures for the manipulation of steel surfaces that are in contact with fuel, such as the replacement of steel surfaces.

Corrosion of metal materials takes place depending on the environmental conditions to which the materials are exposed. Ship's structural elements (plates, brackets, etc.) are exposed to multiple environmental conditions as water ballast tanks, cargo tanks, sea water or open spaces. In that sence, in design phase it is important to predict resonable corrosion margins. Namely, the Cammon Structure Rules provide a corrosion margin for each side of a structural element, depending on the environment to which that element is exposed (IACS, 2024).

In order to improve vessel safety, New Common Structural Rules (CSR) were introduced in 2006 in order to enhance the strength and safety of ships. The corrosion addition is based on the statistical analysis of thickness loss measurements, which is specific to the member location and corrosion environment taken as the 95% quantile of the predicted corrosion depth (and assuming the 25-year service life) (Woloszyk and Garbatov, 2022.). In that sense, at the ship design stage, to mitigate the corrosion degradation, corrosion addition and additional thickness are required by classification societies (IACS, 2024) and strength criteria are satisfied for the net thickness (neglecting the complete corrosion addition or half of it). Following proposed calculation, gross thickness according to the CSR is determined by corrosion addition which is added to the net thickness and special owners addition. Furthermore, each suggested corrosion addition depending of environment to which it is exposed.

One of significant regulation in order to decrease corrosion process are sacrificial anodes or impressed current cathodic protection (ICCP). However, the optimal approach to prevent corrosion is Performance Standards for Protective Coatings (PSPC), implemented in April 2006, which significantly enhance coating quality and efficiency (Zriouel et al. 2023.).

Regarding adopted a significant thickness measurement data of hull structure, this research is a continuation of prior research conducted by Ivosevic et al. (2019, 2021) that analyzed the corrosion process in fuel oil tanks (Ivošević and Kovač, 2022) and the influence of environmental factors on corrosion in different structural areas by Ivosevic et al. (2023a, 2023b). In this article, the authors focus on reliability analysis of inner bottom plating of aging bulk carriers which are the part of fuel oil tanks located in double bottom area.

This paper contains 4 chapters. The second chapter analyzes relevant database and used method. The third chapter presents the results of the research, while the fourth chapter contains the concluding remarks.

2. MATERIAL AND METHOD

Using an extensive database on structural damage to steel plates of ships in operation, and respecting the rules of classification societies on permissible damages due to corrosion, in this work we apply the theory of reliability. Namely, measurements are provided by ultrasonic thickness devices of the structural plates of ships in operation at different time intervals in accordance with the rules of the classification societies. Then, from the comprehensive measurements, systematization and data processing is carried out in such a way that objectively consider the state of the construction at the time of measurement. Applying the theory of reliability, in this work reliability, failure intensity function and failure indicator are determined based on defined acceptance criteria proposed by classification Societies.

2.1. Database of thickness damages

Research database consists of 25 bulk carriers from 5 to 25 years of explanation. In this research only thickness measurement records conducted during the Special Survey were considered, and all data which are connected to intermediate survey were included in special survey. In that way, 5 year cycles of vessels were considered.

All bulk carriers examined were built in the last century and investigated between 2005 and 2017. The research focuses to measure inner bottom plating as a cover of the fuel tanks located in double bottom area (one sample of double bottom arrangement were presented on Figure 1.a) (Ivošević et al. 2019). Each surveyed bulk carrier has between 2 and 4 fuel oil tanks and the total number of tanks is presented in Table 1. Totally 110 Fuel oil tanks were analyzed in a way that each tank is divided on five parallel sections, two sections at the end of tanks, one in the middle of tanks and two between ends of tank and middle of tank length (Figure 1.b). All gauging are done on the cross section of the inner bottom plating steel plates. On that way totally 3070 gauging are representing corrosion process of plates during the time of exposure. Main data information about vessels were presented on Table 1.

Table 1. The database used for the research on inner bottom plating

The age of ships (years)	The number of ship surveys	The number of tanks	The number of measured points	The number of sections	The mean values of plate thickness diminution caused by corrosion (%)
0-5	4	9	230	45	0,5 %
5-10	4	10	296	55	2,2 %
10-15	7	19	530	100	8,9 %
15-20	13	43	998	220	11,7 %
20-25	10	29	1016	150	18,2 %
Total:	38	110	3070	570	

The research database includes the age of the ships, the number of special surveys and fuel tanks, total measuring positions during the time of exposure and the arithmetic mean of the damages percentage of steel plates in relation to the original values (Table 1).

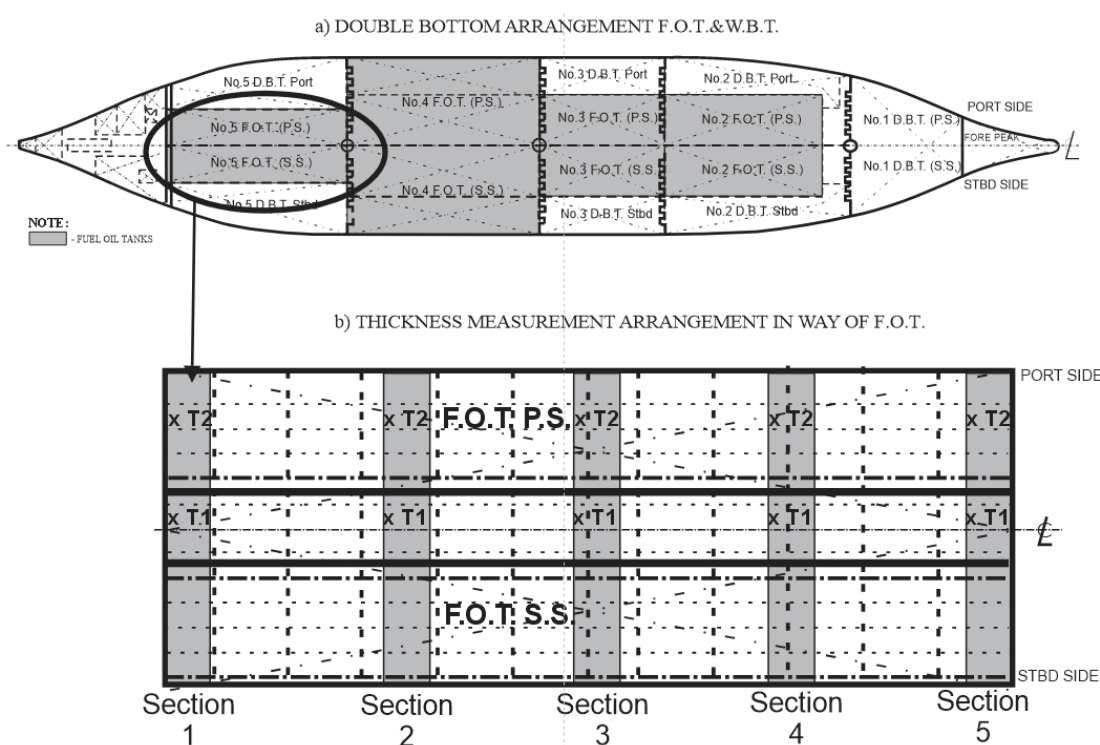


Figure 1. a) Tank arrangement, b) Data collection scheme of inner bottom plating in way of F.O.T

A detailed analysis of the systematization of data and measurements is given in the paper (Ivošević et al., 2017, Ivošević et al., 2019). Considering the data on the importance of the percentage of thickness diminution of steel plates (Ivošević et al. 2017), this paper examines the reliability of steel plates of the inner bottom plating between cargo holds and fuel oil tanks in accordance with the measurement locations in Figures 1.

The considered database enabled the analysis of the corrosion damages expressed in percentage of steel diminution due to time of exposure and reliability of the inner bottom plating as well as the further assessment of fuel tank exploitation.

2.2. Method

The paper analyzes the reliability of inner bottom plates between cargo holds and fuel tanks located in double bottom area of vessel. Reliability calculation were considered on based on the diminution percentage of the original thickness caused by corrosion. The research was motivated by previous studies which dealing with thickness diminution percentage of inner bottom plating (Ivošević et al. 2017, Ivošević et al. 2020) and numerous papers that analyzed the millimeters of the wear of structural steel plates (Paik et al 1998, Paik et al. 2003, Soareas and Garbatov, 1996.).

As the thickness of steel plates decrease over time, classification societies prescribed the scope and intensity of thickness measurements and acceptable reduction steel thickness in relation to the original values. The deviations of inner bottom plating can vary according to the rules of classification societies, and can be between 20% and 25% (DNV, RINA, ABS, LR) or 20%+1mm (ClassNK) (Hussein et al. 2007). Furthermore, classification societies allow the wear of 10% in particular structural areas i.e., accept the reliability level of 90% (Ivošević et al. 2017).

From another side, for instance, due to regulation issued by CSR, one side corrosion diminution corenspond to the CSR addition for inner bottom plating of cargo oil tank assume 0,3 mm addition while inner bottom plate of dry bulk cargo hold of bulk carrier assume 3,7 mm of corrosion addition (IACS, 2014; IACS, 2024).

The reliability calculations of the study are based on the allowable damage of 20% of the original thickness. Namely, the values that were below 80% of the original thickness were considered unacceptable i.e., interpreted as a failure. Although the remaining thickness ensures the impermeability of steel plates, classification societies still require the replacement of corroded surfaces in those cases. With a failure defined in this way, we are dealing with a two-state system (object) in the reliability sense (Kołowrocki and Soszyńska-Budny 2011; Kołowrocki et al. 2015). We define the

reliability of such system as the probability that the system is working at the moment t (the system performs its task at the moment t). Thus, the reliability of the system may be determined from the following formula

$$R(t) = \frac{n_i(t)}{n(t)}, \quad t \geq 0, \tag{1}$$

where

$n_i(t)$ – the number of acceptable measurement positions of steel plate thickness,

$n(t)$ – the total number of events.

Another important indicator of reliability is failure intensity function $\lambda(t)$. In our case we can define it as a probability of a system failure in the interval time $(t, t+\Delta t)$ to the duration of the interval Δt .

$$\lambda(t) = \frac{n'_i(t)}{n(t)\Delta t}, \tag{2}$$

where

$n'_i(t)$ – number of faults of steel plate in time interval $(t, t+\Delta t)$,

$n(t)$ – the total number of events.

We can also define a failure indicator $Z(t)$ and treat it as a synonym for risk.

$$Z(t) = \frac{n(t)-n_i(t)}{n(t)}, \tag{3}$$

where

$n_i(t)$ – the number of acceptable measurement positions of steel plate thickness,

$n(t)$ – the total number of events.

Using the formulas 1-3 in the follow paragraph will be presented results of this research which present the measured data and the determined reliability characteristics $R(t)$, $\lambda(t)$ and $Z(t)$ for the steel plates of the inner bottom plating.

3. RESULTS

Reliability characteristics $R(t)$, $\lambda(t)$ and $Z(t)$ are calculated based on the previously described empirical data (Paragraph 2.1.) on the damage of the steel plates of inner bottom plating and according to the equations (1) - (3) (Paragraph 2.2). Table 2 presents the obtained results of the calculations that have been performed.

Table 2. The reliability characteristics for the steel plates of the inner bottom plating

Number of measurements	Time (years)	Number of failures	$R(t)$	$\lambda(t)$	$Z(t)$
230	0-5	0	1	0	0
296	5-10	0	1	0	0
530	10-15	25	0,953	0,009	0,047
998	15-20	196	0,804	0,039	0,196
1016	20-25	452	0,555	0,089	0,445

The analysed results include times after 5,10,15,25 years of the ship's operation, as the sampled data correspond to measurements during a special survey carried out every five years. The relevant thickness measurement data collected during the specific time of explatation (every five years) and number of failure were presented in Table 2. Furthermore, from the results given in the Table 2 it can be seen that the reliability decreases with time (Figure 2), while the failure intensity function (Figure 3) and the failure indicator (Figure 4) increase with time.

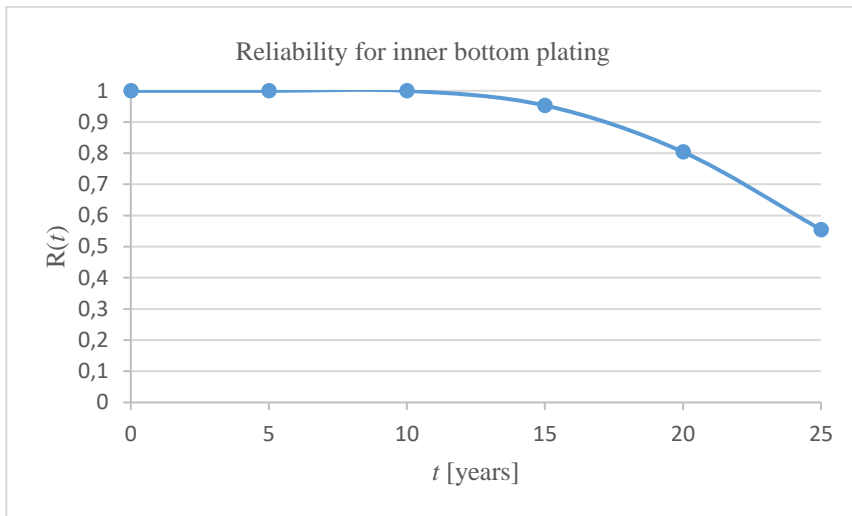


Figure 2. Graphical presentation of reliability

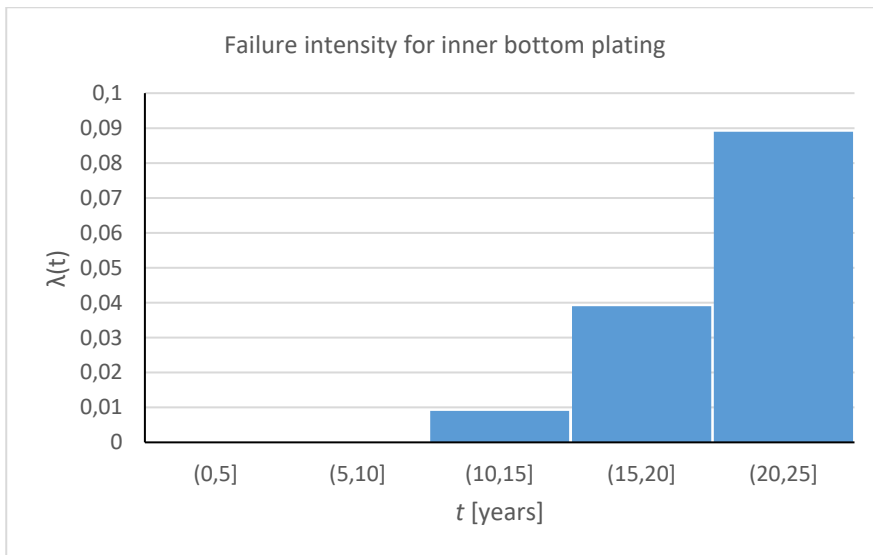


Figure 3. Graphical presentation of failure intensity

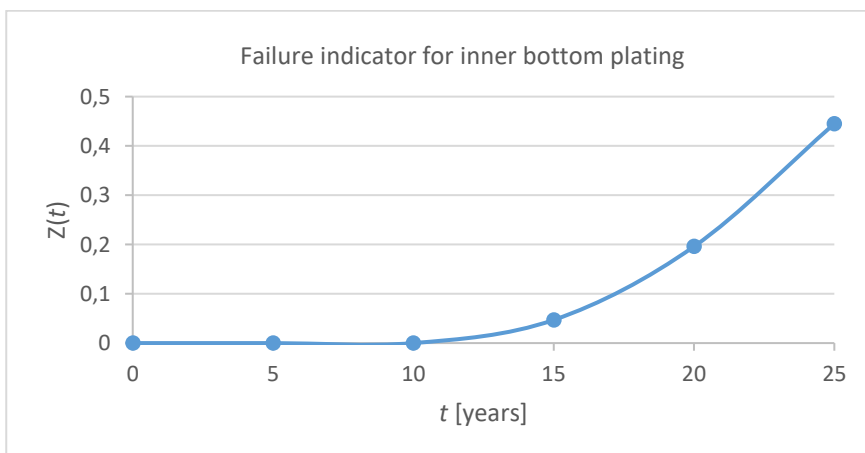


Figure 4. Graphical presentation of failure indicator

The data on the number of failures during the inspections carried out show an increase in the number of failures over time. After 20 years of operation, we observe more than 19% failures in the study sample. After 25 years the number of failures increases rapidly to 45%. An increase in the number of failures over time indicates that the failures are caused by ageing components.

Similarly, the failure intensity function $\lambda(t)$ and failure indicator $Z(t)$ become more significant after 20 years of operation. The risk of failure after 25 years is approximately 45%. Since the projected life expectancy of ship structures is 25 years, it is expected that all structural areas meet the technological requirements during the entire life expectancy.

Analyzing the reliability of steel plates of the inner bottom plating, we observe that after 15 years of operation the reliability remains at a high level of 95%. However, after 20 years, the reliability decreases by 20% compared with the initial time. If we assume, according to expert opinion, that acceptable level of reliability is 90%, then we suggest replacement of corroded inner bottom plating after 15 years of operation in order to prevent reliability dropping below 90%. The results show that after this time the reliability exceeded acceptable limit of 90%. If the necessary repairs are not performed on time, it may lead to environmental pollution or cargo contamination.

We have observed that the reliability of the system decreases significantly after 25 years and is 55,6%. That means that more than 44% of 25-year-old ships have damaged steel plates of the inner bottom.

4. DISCUSSION AND CONCLUSIONS

The paper presented a reliability analysis of steel plates thickness of inner bottom plating between cargo holds and fuel oil tanks. The analysis carried out confirmed that the reliability remains at a maximum level (100%) over a period of 10 years of operation. Between 10 and 15 years of operation, the reliability drops to 95%, so it is still at a very high level. However, after 20 years we observe a reliability level of 80%, which indicates that between 15 and 20 years it drops below the acceptable level of 90%. Based on the obtained results we suggest replacing corroded surfaces after 15 years of operation, i.e. after the third special survey. Such activity could reduce hazardous effects of corrosion such as the possibility of environmental pollution, structural damage or cargo contamination.

This research encourages ship management and maintenance companies to carefully examine steel plates of inner bottom plating after 15 years of exploitation. Monitoring and appropriate preventive maintenance which improves reliability could extend the life expectancy while the costs of potential subsequent major repairs would be greatly reduced.

Future research can be focused on the application of the reliability theory to other structural elements, ship areas or other types of ships, as well as by increasing the input data base of thickness damages.

Acknowledgements

This research is supported and approved by INVAR-Ivošević, a company specializing in thickness measurement. Further details regarding the company can be found at <http://www.invar.me/index.html>.

Author Contributions

Conceptualization: Š.I., J.S.B.; Investigation: Š.I.; Material and Methodology: Š.I., J.S.B.; Supervision: J.S.B.; Visualization: J.S.B.; Writing-Original Draft: Š.I., J.S.B.; Writing-review & Editing: Š.I., J.S.B.

Conflict of Interest / Çıkar Çatışması

The authors have no conflicts of interest to declare.

Funding / Finansal Destek

The authors declared that this study has received no financial support.

REFERENCES

Barbulescu, A., Dumitriu, C.S., (2023). Fractal Characterization of Brass Corrosion in Cavitation Field in Seawater. Sustainability 15, 3816.

Bosen, L., Xinghui, D. (2023). Ship hull inspection: A survey, Ocean Engineering, 289,1, 1-36, <https://doi.org/10.1016/j.oceaneng.2023.116281>.

EMSA, European Maritime Safety Agency. (2019). Annual overview of marine casualties and incidents 2019, Lisbon, Portugal. www.emsa.eu.

Guedes Soares, C., Garbatov, Y. (1996). Reliability of maintained ship hulls subjected to corrosion. *Journal of Ship Research*. 40, 235–243.

Heij, C., Knapp, S., (2019). Shipping inspections, detentions, and incidents: an empirical analysis of risk dimensions. *Maritime Policy & Management*. 46(7):866–883. doi:10.1080/03088839.2019.1647362.

Hussein, A. W., Teixeira, A. P., Soares, C.G. (2007). Impact of the new common structural rules on the reliability of a bulk carrier. In: *Advance in Marine Structures- Proceedings of MARSTRUCT 2007, The 1st International Conference on Marine Structures, Glasgow, United Kingdom, 2007*, pp. 529-538.

IACS, 2024. Common Structural Rules for Bulk Carriers and Oil Tankers.

IACS. (2014). TB Report; Corrosion Additions and Wastage Allowance, Report No., Pt 1, CH 3, Sec 3.

Ivošević, Š., Kovač, N. (2022). A probabilistic approach to the modelling of the corrosive wear percentage of bulkhead panels for bulk ships, *International Conferences on Science and Technology, Engineering Sciences and Technology, ICONST EST 2022. 7-9 September, 2022. Budva, Montenegro*, pp.162-171.

Ivošević, Š., Kovač, N. (2023a). Comparative analysis of environmental factors and the amount of replaced steel on the structural degradation of bulk carriers, *SMATECH 2023, 4th International Conference on 'Smart & Green Technology for Shipping including Offshore Decommissioning, Surrey, England, 6-13*.

Ivošević, Š., Kovač, N. (2023b). Assessment of Cargo Hold Wastage Due to Corrosion in General Cargo Ships: Nonlinear approach, *International Conferences on Science and Technology, Engineering Sciences and Technology, ICONST EST 2023. Budva, Montenegro*.

Ivošević, Š., Kovač, N., Momčilović, N., Vukelić, G. (2021). Analysis of corrosion depth percentage on the inner bottom plates of aging bulk carriers with an aim to optimize corrosion margin. *Brodogradnja*, 72(3), 81-95.

Ivošević, Š., Meštrović, R., Kovač, N. (2017). An approach to the probabilistic corrosion rate estimation model for inner bottom plates of bulk carriers. *Brodogradnja/Shipbuilding*. 68, 57–70.

Ivošević, Š., Meštrović, R., Kovač, N. (2019). Probabilistic estimates of corrosion rate of fuel tank structures of aging bulk carriers, *International Journal of Naval Architect and Ocean Engineering*, 11, 1, 165-177, <https://doi.org/10.1016/j.ijnaoe.2018.03.003>; ISSN: 2092-6782.

Ivošević, Š., Meštrović, R., Kovač, N., (2020). A Probabilistic Method for Estimating the Percentage of Corrosion Depth on the Inner Bottom Plates of Aging Bulk Carriers. *Journal of Marine Science and Engineering*. 8(6), 442. DOI: 10.3390/jmse8060442.

Knapp, S., Bijwaard, G., Heij, C. (2011). Estimated incident cost savings in shipping due to inspections. *Accident Analysis and Prevention*. 43:1532–1539.

Kołowrocki, K., Kuligowska, E., Soszyńska-Budny, J. (2015). Reliability of complex system under operation Process influence – Monte Carlo simulation approach. *Journal of Polish Safety and Reliability Association, Summer Safety and Reliability Seminars – SSARS 2015, Vol. 6 No. 1*,145-153.

Kołowrocki, K., Soszyńska-Budny, J. (2011). *Reliability and Safety of Complex Technical Systems and Processes: Modeling - Identification - Prediction – Optimization*. London, Dordrecht, Heildeberg, New York: Springer.

Paik, J.K., Kim, S.K., Lee, S.K. (1998). A probabilistic corrosion rate estimation model for longitudinal strength members of bulk carriers. *Ocean Engineering*. 25(10), 837–860.

Paik, J.K., Lee, J.M., Park, Y.I., Hwang J.S., Kim, C.W. (2003). Time-variant ultimate longitudinal strength of corroded bulk carriers. *Marine Structures*. Vol. 16, pp. 567–600.

Perić, M. (2022). Prediction of cavitation on ships. *Brodogradnja/Shipbuilding*, 73(3), 39-58.

Poggi, L., Gaggero, T., Gaiotti, M., Ravina, E., Rizzo, C. (2020). Recent developments in remote inspections of ship structures, *International Journal of Naval Architect and Ocean Engineering*, 12, 881–891. doi: <https://doi.org/10.1016/j.ijnaoe.2020.09.001>.

Qin, S., Cui, W. (2003). Effect of corrosion models on the time-dependent reliability of steel plated elements. *Marine Structures*. 16, 15–34.

Wang, G., Boon, B. et al., (2009). Committee V.6, Condition assessment of aged ships and offshore structures, 17th International ship and offshore structures congress, Seoul, Korea.

Woloszyk, K.; Garbatov, Y. (2022). Advances in Modelling and Analysis of Strength of Corroded Ship Structures. *Journal of Marine Sciences and Engineering*. 10, 807. <https://doi.org/10.3390/jmse10060807>.

Zriouel, W., Bentis, A., Majid, S., Hammouti, B., Gmouh, S., Umoren, P.S., Umoren, S.A. (2023). The Blue Tansy Essential Oil–Petra/Osiris/ Molinspiration (POM) Analyses and Prediction of Its Corrosion Inhibition Performance Based on Chemical Composition. *Sustain*. 15, 14274. <https://doi.org/10.3390/su151914274>.

Modeling of Thermoelectric Generator and Photovoltaic Panel Hybrid System

Mehmet Ali Ustuner¹, Onur Emre Golen¹, Abidin Sahinoglu², Hayati Mamur*¹

Abstract: Thermoelectric generators (TEGs) are semiconductor electrical energy generators used in waste heat recovery. TEGs convert the temperature difference between their surfaces into electrical energy. On the other hand, photovoltaic (PV) panels are semiconductor electrical energy generators that convert solar energy into electrical energy. In this study, a MATLAB/Simulink simulation of the system was performed to investigate the behavior of a hybrid electrical energy source with TEG and PV panel as electrical energy source. In this simulation, 50 W TEG system and 12 V 130 W PV panel were used. In total, approximately 150 W power was obtained from the system. Maximum power point tracking (MPPT) was performed using perturb and observation (P&O) algorithm and designed boost converters separately for TEG system and PV systems. In order to use the TEG-PV hybrid system established using TEG system, PV panel, and boost converters in battery charging, a two-way DC-DC converter and current control with proportional integral (PI) controller were performed and the battery management system (BMS) simulation was included in the system.

Keywords: Thermoelectric generator, Photovoltaic panel, Boost converter, MPPT.

¹Address: Manisa Celal Bayar University, Faculty of Engineering and Natural Sciences, Manisa/Türkiye

²Address: Manisa Celal Bayar University, Technical Sciences Vocational School, Manisa/Türkiye

*Corresponding author: hayati.mamur@cbu.edu.tr

1. INTRODUCTION

Today, it has become important to use existing energy in a sustainable and efficient way. In order to achieve this, many governments support such studies and researchers and engineers are working in this field. In addition, efforts are being made to use renewable energy sources in order to meet the goals of the United Nations' zero carbon emission policies in 2050.

Thermoelectric generators (TEGs) are semiconductor electrical energy converters that convert the temperature difference between their surfaces into electrical energy. They produce electrical energy linearly with the temperature difference between their surfaces. TEGs have no moving parts, which allows them to operate silently (Mamur et al., 2022). TEGs have a long life thanks to their construction of n- and p-type semiconductor elements. They also have zero carbon emissions. In addition, they increase energy efficiency by contributing to the conversion of waste heat into electrical energy. Along with these advantages, they also have a couple of disadvantages (Kanagaraj, 2021). These are the cost of their installation and their low conversion efficiency (Ustuner et al., 2024).

On the other hand, photovoltaic (PV) panels are semiconductor electrical energy direct current (DC) generators that convert solar energy, known as a renewable energy source (RES), into electrical energy. Since they use RES, electrical energy is produced as long as the sun is present. Since PV panels are produced with semiconductor technology, they do not have moving parts. They do not release any harmful gases into the environment (Yang et al., 2023). The efficiency of commercially used PV panels has approached 20%. Recently, there has been a significant decrease in installation costs and they have started to be used as the most preferred RES converters today (Riyadi et al., 2023). PV panels have started to contribute significantly to electrical energy production by establishing PV panel farms both on the roofs of houses and in large fields. Since the output DC voltage values of TEGs and PV panels vary depending on the temperature difference between the TEG surfaces and the illumination of the solar energy, they are used with DC-DC converters. These DC-DC converters provide regulated voltage to end-user devices by boost, buck and buck-boost the voltage value of the electrical energy source they are connected to (Pandit et al., 2024). They also contribute to increasing energy efficiency by performing load matching of TEGs and PV panels with MPPT algorithms (Mohammed and Qasim, 2023).

In this study, a hybrid operation of a TEG used for waste heat recovery and a PV panel that converts solar energy into electrical energy is modeled using MATLAB/Simulink. In order to maximize the electrical energy obtained from TEG and PV panels, a DC-DC boost converter with perturb and observation (P&O) MPPT algorithm is modeled.

2. MATERIAL AND METHOD

2.1. Thermoelectric generator

TEGs are made of p- and n-type semiconductor thermoelectric elements (TEs). These TEs are connected in series to increase the voltage values. In order to increase the thermal conductivity, they are connected in parallel between ceramic plates. The voltage value of a TEG cannot operate some systems. Therefore, TEGs are connected in series and parallel to increase the voltage, current and power values. The data of the TEG used in the modeling is shown in Table 1. TGM-199-1.4-0.8 model/brand TEG was used in the system.

Table 1. TEG properties

Properties	Value	Properties	Value
Number of TE	199	Open circuit voltage (V_{OC})	8.19 V
TEG	1	Short circuit voltage (I_{SC})	5.61 A
MPP output power (P_{MPP})	11.4 W	Internal resistance (R_{TEG})	1.46 Ω
MPP output voltage (V_{MPP})	4.1 V	Hot side temperature (T_{hot})	200°C
MPP output current (I_{MPP})	2.8 A	Cold side temperature (T_{cold})	30°C

2.2. PV panel

The voltage and current values of PV panels vary according to the solar radiation obtained. The power values obtained also vary with the connected load. The characteristics of the PV panel used in the system are shown in Figure 1.

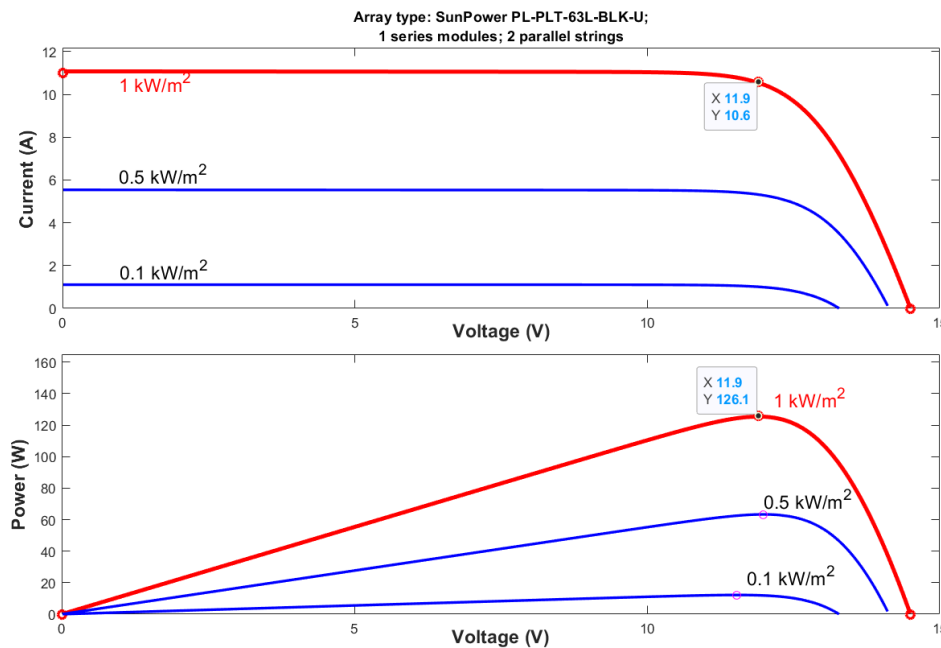


Figure 1. PV panel curves

2.3. DC-DC boost converter

A boost converter is a group of converters that increase the DC voltage level from low to high voltage while reducing the current. It typically consists of a coil, a switching element, and a diode. The conversion ratio of this converter is given by the following equations.

$$\frac{V_o}{V_{in}} = \frac{I_{in}}{I_o} = \frac{1}{1-D} \tag{1}$$

$$V_{in} = V_o(1 - D) \tag{2}$$

$$I_{in} = \frac{I_o}{1-D} \tag{3}$$

where V_o , V_{in} , I_o ve I_{in} output, input voltages, output and input currents of boost converters, respectively. Thus, the internal resistance of boost converter can be found by knowing the values of V_{in} and I_{in} as shown in the equation below.

$$R_{converter} = R_{PROG} = \frac{V_{in}}{V_o} = \frac{V_o(1-D)}{I_o/(1-D)} = \frac{V_o(1-D)^2}{I_o} = R_L(1 - D)^2 \tag{4}$$

(4) shows that the internal resistance of the converter can be varied by the duty cycle, D . Therefore, when D is varied in the range $[0, 1]$, $R_{converter}$ gives the range $[R_L, 0]$.

While designing the boost converter, a 100 W converter in Figure 2a was designed for the PV system and a 50 W converter in Figure 2b was designed for the TEG system. The following design parameters in Table 2 were used to calculate the coil and capacitor values.

Table 2. Boost convertor design parameters

Parameter	Definition	Value
ΔI_L	Loat voltage oscillation	30% of I_o
ΔV_o	Output voltage oscillation	0.1% of V_o
f_s	Switching frequency	20 kHz
V_o	Output voltage	110 V
R_L	Load resistance	20 Ω

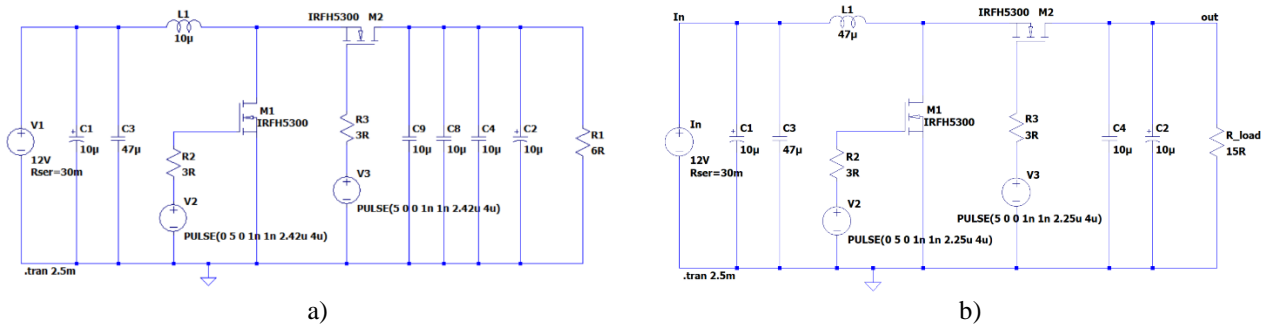


Figure 2. Boost converters for a) TEG system and b) PV system

2.4. MPPT principle

Converters regulate the output voltage and also provide the maximum power point (MPP) obtained from the TEG-PV system. The converter connected between the TEG-PV system and the load resistor creates the load value of the TEG-PV system. Now the current and voltage values received from the TEG-PV system depend on the resistance of the converter. The resistance value of this converter is changed by programming the switch on-off times of the current value passing through the coil. Thus, a programmable resistor is attached to the output of the TEG-PV system. In this way, the resistance value of the TEG-PV system and the converter is equalized and the MPP is achieved. The MATLAB/Simulink simulation of the 150 W PV-TEG hybrid system is shown in Figure 3.

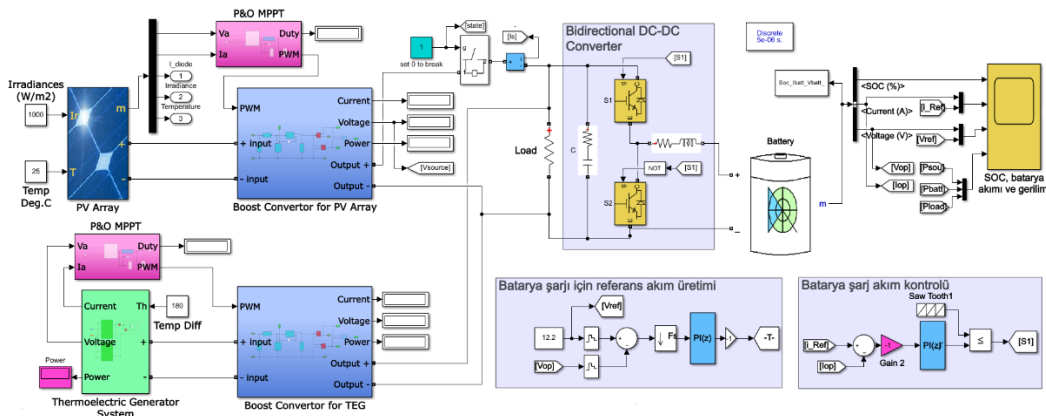


Figure 3. 150 W TEG-PV hybrid system

3. RESULTS AND DISCUSSION

In the simulation modeled, 50 W TEG system and 12 V 130 W PV panel were used. In total, approximately 150 W power can be obtained from the system. TEG system and PV system were separately made MPPT using P&O algorithm and designed boost converters. In order to use PV-TEG hybrid system established using PV panel, TEG system and boost converters in battery charging, BMS simulation was included by performing current control with bidirectional DC-DC converter and PI controller.

In this simulation, the reference voltage for battery charging was determined as 12.2 V, and the battery charge rate was simulated from 60% to 60.023% as the battery voltage reached the reference voltage. As the battery voltage reached the reference voltage, the current passing through the battery approached zero and the battery charging process was completed. The battery charge rate and current as a function of time are shown in Figure 4.

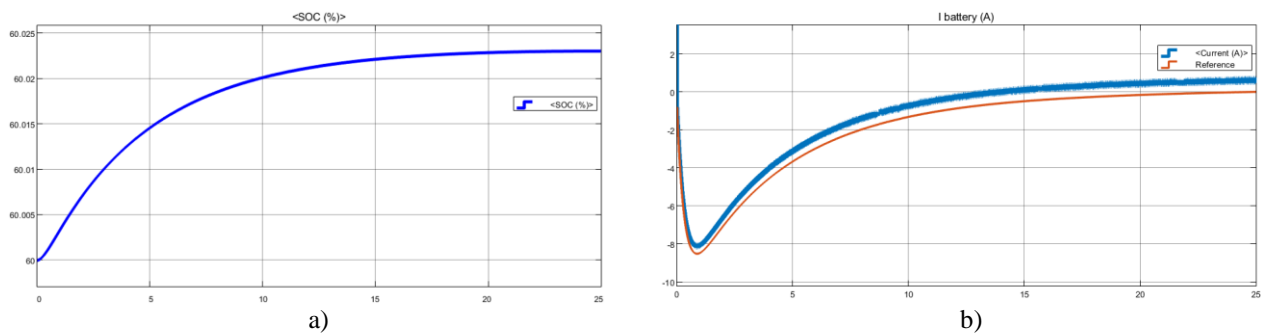


Figure 4. Battery a) charge rate and b) current as a function of time

In these simulations, the reference voltage can be adjusted to ensure that the battery reaches the desired charge level. In addition, the PI controller limits the current passing through the battery, i.e. current control, to prevent damage to the battery until the battery voltage reaches the reference voltage. The battery charge voltage and TEG-PV system – battery – load values as a function of time are shown in Figure 5.

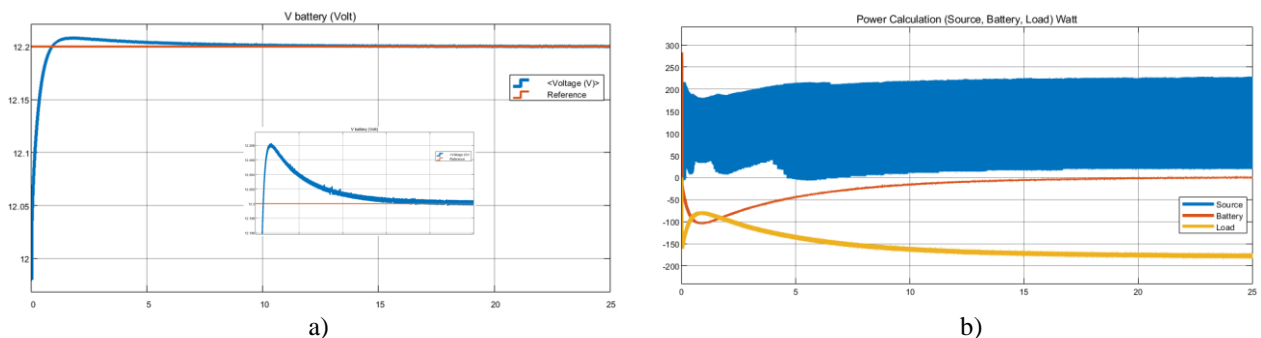


Figure 5. System battery a) charge voltage and b) powers of TEG-PV system – battery – load as a function of time

4. CONCLUSIONS

In this study, a 50 W TEG used in waste heat recovery and a 100 W PV used in RESs and a 150 W hybrid system were created to ensure energy sustainability and the system was modeled with MATLAB/Simulink software to examine the behavior of the system. In order to increase the efficiency of both the TEG system and the PV panels and to provide voltage regulation, separate P&O MPPT algorithm DC-DC converter designs were made for the TEG system and the PV panel. A BMS system was created to store the unused energy so that the obtained electrical energy could be used later.

Acknowledgements

This study was supported by the Manisa Celal Bayar University Scientific Research Coordination Unit (Project No. 2023-048).

Ethics Committee Approval

N/A

Peer-review

Externally peer-reviewed.

Author Contributions

Conceptualization: H.M.; Investigation: M.A.U., O.E.G.; Material and Methodology: M.A.U., O.E.G.; Supervision: H.M., A.S.; Visualization: A.S.; Writing-Original Draft: H.M., M.A.U; Writing-review & Editing: H.M., A.S.; Other: All authors have read and agreed to the published version of manuscript.

Conflict of Interest

The authors have no conflicts of interest to declare.

Funding

This study was supported by the Manisa Celal Bayar University Scientific Research Coordination Unit (Project No. 2023-048).

REFERENCES

- Kanagaraj, N. (2021). Photovoltaic and thermoelectric generator combined hybrid energy system with an enhanced maximum power point tracking technique for higher energy conversion efficiency. *Sustainability*, 13(6), 3144. <https://doi.org/10.3390/su13063144>
- Mamur, H., Üstüner, M. A., & Bhuiyan, M. R. A. (2022). Future perspective and current situation of maximum power point tracking methods in thermoelectric generators. *Sustainable Energy Technologies and Assessments*, 50, 101824. <https://doi.org/10.1016/j.seta.2021.101824>
- Mohammed, M. F., & Qasim, M. A. (2023). Design of a battery charging system fed by thermoelectric generator panels using MPPT techniques. *Journal of Electrical Engineering*, 74(5), 357-364. <https://doi.org/10.2478/jee-2023-0043>
- Pandit, S., Mal, R., Purwar, A., & Kumari, K. (2024). Waste heat regeneration from thermoelectric generator based improved biomass cookstove (TIBC): Modelling of TEG system utilizing DC-DC converter with fuzzy logic MPPT. *Energy Conversion and Management*, 300, 117977. <https://doi.org/10.1016/j.enconman.2023.117977>
- Riyadi, T. W. B., Effendy, M., Utomo, B. R., & Wijayanta, A. T. (2023). Performance of a photovoltaic-thermoelectric generator panel in combination with various solar tracking systems. *Applied Thermal Engineering*, 235, 121336. <https://doi.org/10.1016/j.applthermaleng.2023.121336>
- Üstüner, M. A., Mamur, H., Taşkın, S., Nil, M., Bhuiyan, M. R. A., Kherkhar, A., & Chiba, Y. (2024). Selection of Load Resistance for Boost Converters with Maximum Power Point Tracking Algorithm in Thermoelectric Generators. *Electric Power Components and Systems*, 1-22. <https://doi.org/10.1080/15325008.2024.2333975>
- Yang, B., Wu, S., Huang, J., Guo, Z., Wang, J., Zhang, Z., Xie, R., Shu, H. & Jiang, L. (2023). Salp swarm optimization algorithm based MPPT design for PV-TEG hybrid system under partial shading conditions. *Energy Conversion and Management*, 292, 117410. <https://doi.org/10.1016/j.enconman.2023.117410>

Characterization of Aromatic Water Obtained from Dried and Fresh *Passiflora Edulis* Sims Peels

Özlem Karaboyacı *

Abstract: The present study is concerned with the characterization of aromatic water obtained from both dried and fresh peels of *Passiflora edulis* Sims, commonly known as passion fruit. The reason for the study of *Passiflora Edulis* Sims bark is that the plant contains a high percentage of bark such as 50%. The objective of this research is to analyze the phenolic content, antioxidant activity, and volatile compounds in both forms, thereby providing insight into their nutritional and sensory profiles. Phenolic compounds are renowned for their antioxidant properties, which can contribute to the salutary effects associated with passion fruit peel extracts. The study employed high-performance liquid chromatography (HPLC) and gas chromatography-mass spectrometry (GC-MS) to quantify the bioactive compounds and characterize the aroma profile of the water derived from fresh and dried peels. The findings demonstrate that fresh *Passiflora edulis* peels exhibit a higher phenolic concentration (4.10 mg GAE/mL) and greater antioxidant activity (23% DPPH radical scavenging) in comparison to their dried counterparts (3.02 mg GAE/mL, 16.5% DPPH radical scavenging). It seems plausible to suggest that the drying process may result in a reduction of the moisture content of the material, which could potentially lead to the degradation of certain bioactive compounds and a subsequent decline in antioxidant activity. In terms of aroma, the fresh peels exhibited a more vibrant and complex volatile profile, containing a higher concentration of esters and alcohols, which contributed to a fruity and floral scent. In contrast, the dried peel juice displayed a more subdued aromatic profile. The findings underscore the superior nutritional and aromatic qualities of fresh *Passiflora edulis* peels in comparison to their dried counterparts. This research highlights the potential for utilizing fresh passion fruit peel extracts in the food and beverage industries due to their elevated antioxidant levels and rich aromatic profile. Furthermore, the study suggests further investigation into the optimization of drying techniques to preserve bioactive and aromatic compounds in.

Keywords: *Passiflora edulis* sims, passion fruit, *passiflora*, extraction, distillation

¹Address: Pamukkale University, Department of Acipayam Vocational High School, Denizli/Turkiye

*Corresponding author: okaraboyaci@pau.edu.tr

1. INTRODUCTION

Introduction to *Passiflora Edulis* Sims Peels

Passiflora edulis Sims, commonly referred to as passion fruit, is a tropical vine belonging to the Passifloraceae family. Passion fruit is widely cultivated for its edible fruit, which is known for its strong aromatic flavour and nutritional benefits. The peels of *Passiflora edulis*, which are often considered a by-product in the food industry, possess various bioactive compounds that have garnered scientific interest. These peels are rich in dietary fibre, polyphenols, and other phytochemicals, which may contribute to health benefits such as antioxidant, anti-inflammatory, and antimicrobial properties (Kishore et al, 2006 ; Biswas et al, 2021).

Passion fruit (*Passiflora edulis*) is a tropical fruit belonging to the Passifloraceae family. The passion fruit, which originated in South America, has been employed extensively in folk medicine in the region to treat a range of ailments, including anxiety, insomnia, asthma, bronchitis, and urinary tract infections. Presently, this fruit is cultivated globally and utilized as an edible fruit by the food industry. There are several cultivars of this fruit, including the purple passion fruit (*P. edulis* Sims), granadilla (*Passiflora ligularis*), gulupa (*P. edulis* Sims. fo *edulis*), and yellow passion fruit (*P. edulis* var. *flavicarpa* Degenerer). The fruit is composed of numerous bioactive compounds, including phenolic acids, flavonoids, alkaloids, cyanogenic compounds, glycosides, vitamins, minerals, and terpenoids. These compounds have been demonstrated to possess a range of functional properties, including anti-inflammatory, antidiabetic, and anti-anxiety activities, as well as the capacity to protect against cardiovascular disease. (Jaiswal, 2020).

Recent studies have explored the potential utilization of passion fruit peels in food formulations, dietary supplements, and functional foods due to their rich nutrient profile and bioactivity. For instance, the incorporation of passion fruit peel powder has been shown to enhance the functional and nutritional quality of various food products . Additionally,

the environmental aspect of utilizing these peels addresses sustainability concerns in waste management by transforming a discarded by-product into a health-promoting ingredient.

An aromatic water, or hydrosol, is a fragrant liquid obtained by distilling fresh flowers, leaves, bark, or roots. It is the water that remains below the essential oil after distillation. Unlike essential oils, which are very concentrated, aromatic waters are more subtle in scent. They capture the essence and subtle scent of the plants from which they are derived.

These aromatic waters can be used in a variety of applications, offering both the aromatic and therapeutic benefits of the plants.

Passiflora edulis Sims peels aromatic water is an adaptable product that encapsulates the essence of passion fruit peels. It is distinguished by its complex volatile compound profile, which contributes to its distinctive sensory properties and potential health benefits. Its applications span a diverse range of sectors, including the culinary arts and the cosmetics industry. As a result, it has emerged as a valuable by-product in both the food and fragrance industries (He et al, 2020).

2. MATERIAL AND METHOD

2.1. Distillation

The Clevenger apparatus is a laboratory apparatus utilized for the extraction of essential oils from plants through the process of water vapor distillation. The distillation flask is filled with a solution of *Paciflora* bark in water at a ratio of 1:10 (w/v). The quantity of water should be sufficient to ensure comprehensive wetting of the plant material. The mouth of the flask is then placed within the apparatus and hermetically sealed. The apparatus is heated with the assistance of a mantle heater. At this juncture, the water begins to boil and the steam rises, carrying the essential oils with it. At this juncture, the plant cells are disrupted, and the essential oils are carried with the water vapor. The condensed liquid mixture reaches the oil collection tube of the Clevenger apparatus, where the water and essential oils form two distinct phases due to their differing densities. The essential oil accumulates on the surface of the water, while the distillate is obtained as aromatic water underneath the oil.



Figure 1. Stages of obtaining aromatic water in Clevenger device. Yellow arrow points to aromatic water.

2.2. Determination of volatile compounds

GC-MS SPME technique was used in the analysis of volatile components of shell extracts. The SPME technique is a simple and precise sample preparation method that extracts the components in the sample to be analyzed by impregnating them on the fiber coated with a thin polymeric fixed phase on silica.

2.3. Determination of total phenolic substance by Folin Ciocalteu (FC) method

In the experiment, phenolic substances were determined according to the Folin-Ciocalteu method applied by Singleton and Rossi (1965). According to this method, 300 μ l of extract solution and 1.5 ml of 2 N Folin-Ciocalteu reagent diluted in appropriate proportions were mixed. After adding 1.2 mL of 7.5% (w/v) sodium carbonate solution, the tubes were

mixed in vortex and kept in the dark at 25 °C for 90 minutes and the absorbance was measured at 765 nm in the UV-Vis spectrophotometer. Total phenol content is given as gallic acid equivalent using the gallic acid calibration curve.

2.4. DPPH Radical Scavenging Test

The antiradical activity was measured by using the 2,2-diphenyl-1-picrylhydrazyl (DPPH•) radical scavenging method according to Dorman and co-workers (2003) and the results were given as % of inhibition.

2.5. Calculation of the Passiflora Edulis Sims peel ratio

The calculation of the peel ratio of Passiflora Edulis Sims fruits was made according to the formula below.

$$\text{Peel Ratio (\%)} = \frac{\text{Peel weight}}{\text{Total fruit weight}} \times 100$$

Sıra No	Tespit edilen bileşikler	% Miktar	Sıra No	Tespit edilen bileşikler	% Miktar
1	4,6-Dimethyl undecane	0.81	1	4,6-Dimethyl undecane	0.76
2	2,6-Dimethyl nonane	0.77	2	2,6-Dimethyl nonane	0.82
3	4,7-Dimethyl undecane	2.67	3	4,7-Dimethyl undecane	3.31
4	2,6-Dimethyl-7-octene	0.53	4	2,6-Dimethyl-7-octene	0.48
5	n-Undecane	1.01	5	n-Undecane	0.90
6	2-Methyl undecane	0.28	6	2-Methyl undecane	0.27
7	n-Dodecane	5.87	7	n-Dodecane	2.46
8	n-Tridecane	0.49	8	n-Tridecane	0.89
9	n-Pentadecane	1.05	9	n-Tetradecane	1.14
10	2,3,4-Trimethyldecane	0.73	10	2,3,4-Trimethyldecane	0.86
11	2,3,5,8-Tetramethyldecane	0.30	11	2,3,5,8-Tetramethyldecane	0.34
12	4,6-Dimethyl dodecane	1.01	12	4,6-Dimethyl dodecane	1.14
13	n-Pentadecane	2.43	13	n-Pentadecane	2.73
14	2,7,10-Trimethyl dodecane	4.98	14	2,7,10-Trimethyl dodecane	6.82
15	2-Methyl tetradecane	11.33	15	2-Methyl tetradecane	2.33
16	5-Methyl tetradecane	1.30	16	5-Methyl tetradecane	1.82
17	n-Hexadecane	1.38	17	n-Hexadecane	2.44
18	BHT-quinone methide	13.60	18	BHT-quinone methide	10.91
19	n-Heptadecane	6.48	19	n-Heptadecane	9.66
20	3-Methyl heptadecane	3.68	20	3-Methyl heptadecane	1.02
21	2,6,11,13-Tetramethyl tetradecane	7.69	21	2,6,11,13-Tetramethyl tetradecane	12.22
22	1-Nonadecene	2.19	22	1-Nonadecene	4.55
23	n-Nonadecane	4.94	23	n-Nonadecane	9.09
24	2,6,10,14-Tetramethyl hexadecane	2.27	24	2,6,10,14-Tetramethyl hexadecane	5.97
25	Palmitic acid	8.82	25	n-Eicosane	2.67
26	n-Eicosane	1.01	26	n-Heneicosane	8.75
27	n-Heneicosane	4.49	27	Diğer Bileşikler	5.68
28	Stearic acid	2.83			100.00
29	Diğer Bileşikler	5.06			
		100.00			

Table 1. GC-MS analysis of aromatic waters obtained from fresh (right) and dried (left) shells

3. RESULTS

Due to the high shell ratio, the shell ratio of Passiflora Edulis Sims fruit, which is the subject of our study, was calculated as 46.8% according to the above formula. In a study on the characterization of passion fruit peels in 2023, Ju et al. reported that passion fruit peel constitutes 50% of the fruit weight and contains high levels of bioactive compounds. The results obtained in this respect are consistent with the literature.

As a consequence of the comparison between the two tables shown in table 1, a considerable number of compounds have been identified in both. This finding suggests that the overall chemical structure of fresh and dried peels is largely similar.

Upon analysis of the differences, it was found that the concentration of BHT-quinone methide was 13.60% in the dried peel and 10.91% in the fresh peel. This suggests that the concentration of this compound increases during the drying process. n-Heptadecane: 9.66% in fresh shell and 6.48% in dried shell. The compound is present at a diminished concentration in the dried peels.

The concentration of 2,6,11,13-tetramethyltetradecane was found to be 12.22% in fresh peels and 7.69% in dried peels. This compound is present in higher concentrations in fresh peels. n-Pentadecane: 2.43% in dried shells and 2.73% in fresh shells. Despite the relatively small difference in concentration, there is a slight increase in this compound in fresh peels.

Palmitic acid and stearic acid: These two compounds are present in dried peels (8.82% and 2.83%) but not in fresh peels. This suggests that the drying process results in the release of these fatty acids.

Fresh and dried peels generally have the same basic compounds, but there were marked changes in the concentrations of some compounds with the drying process. In particular, compounds such as fatty acids were released during drying. Some compounds, such as BHT quinone methide, became more concentrated during drying, while the ratios of some other compounds were higher in fresh peels.

In order to facilitate a comparison of the tables by organic chemical classes, it is necessary to group the compounds into several categories. These include aliphatic hydrocarbons (aliphatic volatile compounds), alcohols, fatty acids, ketones and other volatile organic compounds (VOCs). A comparison of volatile aliphatic hydrocarbons reveals a higher concentration of these compounds in fresh peels (13.28% of n-Dodecane), whereas the amount of these compounds is reduced in dry peels. The drying process may have resulted in the loss of some aliphatic hydrocarbons.

In the context of alcohol comparison, fresh peels exhibit a higher concentration of compounds such as 1-tetradecanol. A reduction in alcohol ratios is evident with the progression of the drying process. To illustrate, the ratio of 1-tetradecanol decreased from 12.33% in the fresh shells to 4.95% in the dried shells.

With regard to fatty acids, while stearic acid (19.92%) was markedly more prevalent in fresh shells, this ratio underwent a notable decline in dry shells, with both fatty acids decreasing to more balanced levels. This may indicate that the fatty acids are partially broken down or converted into other compounds during the drying process.

Zhang et al. 2015 in their study on changes in volatile aldehydes formed during oil frying process and Tian et al. 2016 in their study on the effects of different drying methods on product quality and volatile compounds of whole shiitake mushrooms obtained similar results. In our findings, the drying process had some effect on the VOC content. The reduction in alcohol and volatile content may be due to the evaporation or thermal decomposition of these compounds during the drying process.

Benzyl alcohol is a compound that occurs spontaneously when plants are dried. Benzyl alcohol was the most abundant aroma compound in chestnuts dried by the other four drying methods, and the benzyl alcohol content obtained by the four drying methods was 36.622%, 36.117, 44.069, 27.029%, respectively (Zhang et al. 2018).

Sample	Total Phenolic (mg GAE/mL)	DPPH %
Dried	3,02	16.5
Fresh	4,10	23

Table 2. Total phenolic and DPPH % inhibition values of aromatic juices obtained from fresh and dry peels

Table 2 presents the analysis of dried passiflora peels, which exhibited a total phenolic content of 3.02 mg GAE/mL in their dried form. This suggests that dried passiflora peels contain a certain level of phenolic components, although the drying process may result in the loss of some nutrients.

Fresh Passiflora Peels (4.10 mg GAE/mL): Fresh peels exhibited a higher value in terms of total phenolic content (4.10 mg GAE/mL). This suggests that fresh passiflora peels may contain a greater concentration of phenolic compounds. Given that fresh plants typically possess a higher water content, the concentration of phenolic compounds is consequently elevated.

In terms of percentage of DPPH radical inhibition, dried passiflora peels exhibited an average of 16.5%. The percentage of DPPH radicals leached was determined to be 16.5%. This suggests that the antioxidant activity of the dried peels is

limited. The process of drying may result in the loss of certain antioxidant compounds, which could explain the observed reduction in this value. Fresh Passiflora Pods (23%): The fresh peels were found to leach 23% of DPPH radicals, indicating that the fresh form exhibits a higher antioxidant activity. Fresh passiflora peels typically contain a higher concentration of active phenolic compounds, which may contribute to the high success observed in the DPPH leaching test.

The data presented in the table demonstrate that fresh passiflora peels exhibited superior antioxidant activity compared to their dried counterparts, as evidenced by their higher total phenolic content and higher DPPH radical scavenging percentage. This indicates that fresh passiflora peels possess more potent antioxidant properties and may offer greater potential for health benefits.

These findings are in accordance with the existing literature, which underscores the significance of antioxidant activities associated with phenolic compounds (Guiné et al. 2015). In particular, fresh plants are typically regarded as being more nutritionally dense. In the field of health supplements and natural products, a logical strategy may be to favor fresh passiflora peels in order to gain more benefits from the high phenolic content and antioxidant activity.

4. DISCUSSION AND CONCLUSIONS

The present study revealed notable differences in the chemical composition and antioxidant activity of fresh and dried *Passiflora edulis* peels. An analysis of the chemical compounds present in both fresh and dried samples revealed that, while the profiles of the compounds are largely similar, the drying process results in alterations to the concentrations of key bioactive compounds. This consequently impacts the overall antioxidant potential and aromatic profile of the peels.

With regard to specific compounds, the drying process resulted in an increase in BHT-quinone methide concentration (13.60% in dried vs. 10.91% in fresh), indicating a potential concentration effect due to moisture loss. In contrast, the concentrations of n-heptadecane and 2,6,11,13-tetramethyltetradecane were significantly higher in the fresh peels. The reduction of these aliphatic hydrocarbons upon drying is consistent with findings in the literature, which indicate that compounds such as alcohols and aliphatic hydrocarbons typically decrease due to evaporation and potential thermal breakdown during drying (Zhang et al., 2015; Tian et al., 2016). Furthermore, palmitic and stearic acids were identified in the dried peels but not in the fresh samples, suggesting that the drying process may facilitate the release or formation of these fatty acids, potentially due to lipid breakdown or rearrangement.

Table 2 illustrates that fresh peels exhibited a higher total phenolic content (4.10 mg GAE/mL) and DPPH radical scavenging activity (23%) in comparison to dried peels (3.02 mg GAE/mL and 16.5%, respectively). These findings indicate that the fresh peels retain a higher antioxidant capacity, which may be due to the degradation or reduction of phenolic content that occurs during the drying process. This finding is consistent with existing research indicating that fresh plant materials frequently exhibit elevated antioxidant activities due to the presence of intact phenolic and volatile compounds (Guiné et al., 2015).

The data substantiate the hypothesis that fresh *Passiflora edulis* peels offer superior antioxidant and health benefits compared to dried peels, due to higher concentrations of phenolics and certain volatiles. In applications such as health supplements and natural flavoring, fresh peels may be preferable to maximize the health benefits associated with high phenolic content and antioxidant properties. Future research could explore optimized drying techniques to better retain these bioactive compounds, potentially broadening the applications of dried passion fruit peels while preserving their health-promoting qualities.

REFERENCES

- Biswas, S., Mishra, R., & Bist, A. S. (2021). Passion to profession: A review of passion fruit processing. *Aptisi Transactions on Technopreneurship (ATT)*, 3(1), 48-57.
- Deng Y, Luo Y, Wang Y, Zhao Y. Effect of different drying methods on the myosin structure, amino acid composition, protein digestibility and volatile profile of squid fillets. *Food Chem.* 171: 168–176 (2015)
- He, X., Luan, F., Yang, Y., Wang, Z., Zhao, Z., Fang, J., ... & Li, Y. (2020). *Passiflora edulis*: an insight into current researches on phytochemistry and pharmacology. *Frontiers in pharmacology*, 11, 617.
- Jaiswal, A. K. (Ed.). (2020). *Nutritional composition and antioxidant properties of fruits and vegetables*. Academic Press.

Ju, Y., Huang, L. L., Luo, H. L., Huang, Y. C., Huang, X. Y., Chen, G., ... & Liu, X. Z. (2023). Passion fruit peel and its zymolyte enhance gut function in Sanhuang broilers by improving antioxidation and short-chain fatty acids and decreasing inflammatory cytokines. *Poultry Science*, 102(6), 102672.

Kishore, K., Pathak, K. A., Yadav, D. S., Bujarbaruah, K. M., Bharali, R., & Shukla, R. (2006). Passion fruit. *Technical Bulletin*, ICAR Research Complex for NEH Region, Meghalaya, India.

Zhang Q, Qin W, Lin D, Shen Q, Saleh ASM. The changes in the volatile aldehydes formed during the deep-fat frying process. *J. Food Sci. Technol.* 52: 7683–7696 (2015)

Tian Y, Zhao Y, Huang J, Zeng H, Zheng B. Effects of different drying methods on the product quality and volatile compounds of whole shiitake mushrooms. *Food Chem.* 197: 714–722 (2016)

Dorman, H.J.D., Peltoketo, A., Hiltunen, R. & Tikkanen, M.J. (2003): Characterization of Antioxidant properties of de-odourized aqueous extracts from selected Lamiaceae herbs. *Fd Chem.*, 83, 255–262.

Singleton, V.L., Rossi, J.A., 1965. Colorimetry of total phenolics with phosphomolybdic-phosphotungstic acid reagents. *American journal of Enology and Viticulture*, 16(3), 144-158.

Guiné, R. P. F., Barroca, M. J., Gonçalves, F. J., Alves, M., Oliveira, S., & Correia, P. M. R. (2015). Effect of Drying on Total Phenolic Compounds, Antioxidant Activity, and Kinetics Decay in Pears. *International Journal of Fruit Science*, 15(2), 173–186. <https://doi.org/10.1080/15538362.2015.1017073>

Maximum Entropy (MaxEnt) Method Using Wind Farm Site Selection Modeling for Aegean Region (Türkiye)

Senem Tekin*¹, Müge Ünal², Ahmet Çilek³

Abstract: This study examines the use of the Maximum Entropy (MaxEnt) model for the selection of wind farm sites across all of Aegean Region (Türkiye). As a critical step in harnessing wind energy potential, site selection must account for various environmental, topographical, and socio-economic factors. MaxEnt, which is traditionally used in ecological niche modeling, is here adapted to assess and predict suitable locations for wind farm installations by integrating climate data, terrain characteristics, and other relevant parameters. The model is a powerful tool for renewable energy planning because it can handle incomplete datasets and predict spatial distribution in different climate change scenarios. The results of this study emphasize the most promising locations in the country for wind energy development, laying the groundwork for sustainable energy policy and infrastructure planning. The results emphasize the importance of incorporating advanced modeling techniques like MaxEnt in the strategic expansion of renewable energy resources to meet the growing energy demands while mitigating environmental impacts.

Keywords: Türkiye, Maximum Entropy (MaxEnt), wind energy potential, predict.

¹**Address:** Mining and Mineral Extraction Department, School of Technical Sciences, Adiyaman University, 02040, Adiyaman, Türkiye

²**Address:** Fırat University, Faculty of Architecture, Landscape Architecture Department, Elazığ 23000, Türkiye

³**Address:** Cukurova University, Landscape Architecture Department, Remote Sensing and GIS Lab, 01330, Adana, Turkey

*Corresponding author: senemtekin@adiyaman.edu.tr

1. INTRODUCTION

The growing demand for renewable energy has positioned wind power as a pivotal component of Türkiye's sustainable energy strategy. As one of the most promising sources of clean energy, wind energy offers significant potential for reducing greenhouse gas emissions and decreasing dependency on fossil fuels. However, the effectiveness and efficiency of wind energy production are highly dependent on the strategic selection of wind farm sites. Accurate site selection is crucial to maximizing energy output, minimizing environmental impacts, and ensuring the economic viability of wind energy projects.

In recent years, various modeling techniques have been employed to optimize wind farm site selection, with the Maximum Entropy (MaxEnt) model emerging as a particularly effective tool. Originally developed for ecological niche modeling, MaxEnt has proven to be adaptable across various domains due to its ability to work with incomplete datasets and its predictive accuracy in spatial analysis. This study explores the application of MaxEnt in modeling wind farm site selection across Türkiye, taking into account the unique geographical, climatic, and socio-economic factors that influence the suitability of different regions for wind energy development.

The selection of suitable sites for wind farms in Aegean Region (Türkiye) involves complex decision-making processes that require the integration of diverse data sources, including wind speed, topography, land use, and proximity to infrastructure. Traditional site selection methods often struggle to handle such complexity, particularly in the face of uncertainties posed by climate change. MaxEnt offers a robust alternative by providing a probabilistic framework that can accommodate these challenges and predict optimal locations under various scenarios.

The Aegean Region is a region located in the west of Türkiye (Figure 1), where the Mediterranean climate prevails, and stands out with its agricultural productivity and natural beauty. Due to its geographical location, this region, which is coastal to the sea, is rich in agricultural activities such as olive groves, vineyards and cotton fields. The wide coastline opening to the Aegean Sea has enabled the development of the tourism sector and has become an attractive destination

for local and foreign tourists with its historical ancient cities and natural beaches. One of the most important cities of the region, Izmir, stands out as the economic center of the Aegean with its port and industry. In addition, the Aegean

Region, which has a high wind energy potential, makes significant contributions to Turkey's renewable energy targets by offering suitable areas for wind farms, especially in coastal areas.

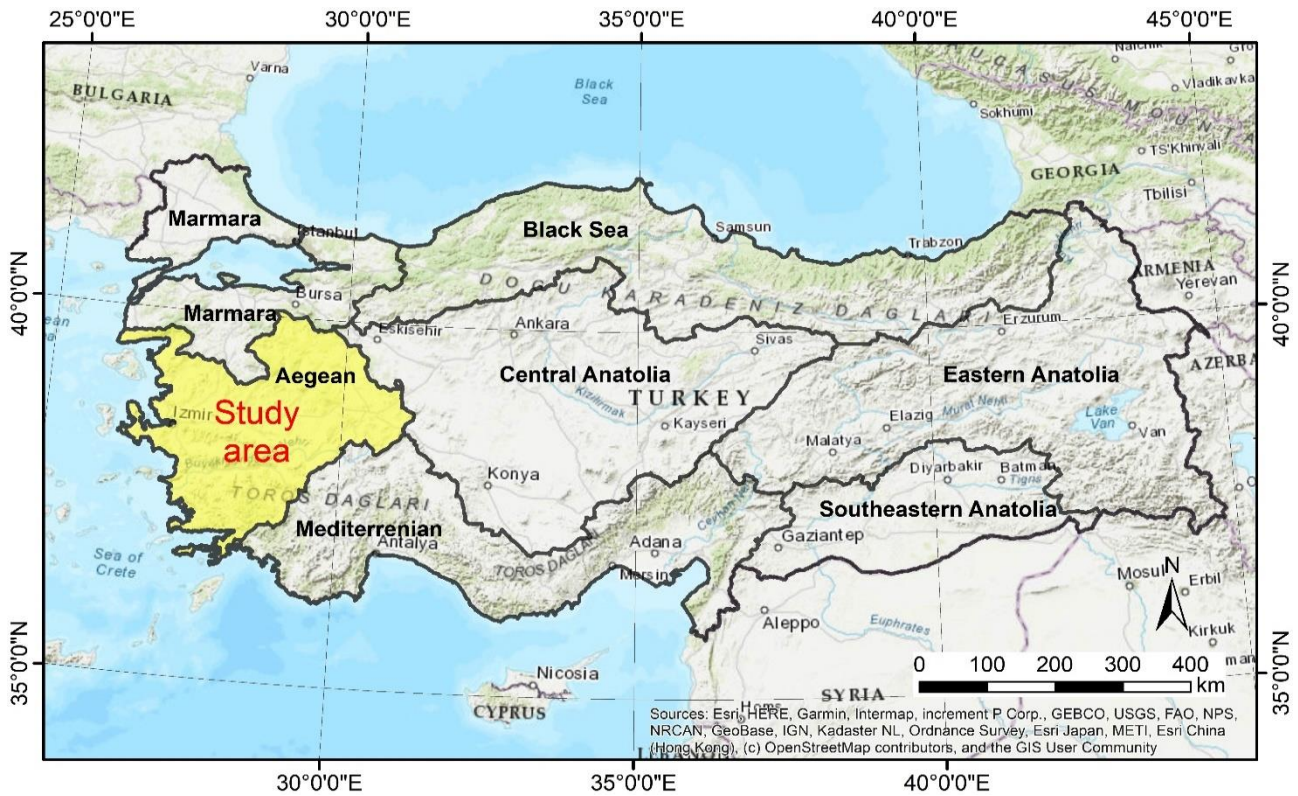


Figure 1. Study area.

This study aims to leverage the capabilities of the MaxEnt model to identify the most suitable locations for wind farm development in Türkiye. By doing so, it contributes to the strategic planning and expansion of the country's renewable energy infrastructure, aligning with global efforts to combat climate change and promote sustainable development. The results of this research are expected to guide policymakers, planners, and investors in making informed decisions that will enhance the efficiency and sustainability of wind energy projects in Aegean Region.

2. MATERIAL AND METHOD

When it comes to effectively harnessing wind energy, the selection of suitable wind farm sites is a complicated process that takes into account social, economic, climatic, and geological factors (Xu et al., 2020). Environmental and socio-economic assessment systems, minimize environmental risks, stimulate economic development, and address local community concerns. Nowadays, due to increasing environmental and ecological problems, the selection of suitable locations for power plants is very important because it is very important from both economic and sustainability perspectives in the renewable energy revolution. Finding reliable, environmentally and topographically suitable locations requires difficult decisions, especially because climate change affects wind patterns and other climate variables, which in turn affect the performance and profit of wind energy projects (Rekik and Alimi, 2023). In the study, firstly the wind power plant inventory was prepared and 681 wind power plants were mapped (Figure 2). Later, the factors effective in wind power plant location selection were prepared in GIS environment to be used in the study.

30 Arc-Second Digital Elevation Data taken from Advanced Spaceborne Thermal Emission and Reflection Radiometer (ASTER) satellite sensor data were used to create topographic data as raster. This spatial resolution is approximately 1 km2. Economic and restrictive (settlement areas, protected areas, water bodies) data, within the framework of the Copernicus program, were extracted as polygon data layers from the European Environment Agency's Coordination of Information on the Environment (CORINE) land cover data. Furthermore, multiple lines of information were collected from the Turkish Electricity Transmission Corporation Regional Directorate to determine the distance to the

transmission lines. OpenStreetMap shows road and train networks in various geometric frameworks (OpenStreetMap 2023).

The MaxEnt software, a widely used tool in ecological niche modeling, is employed to analyze the input data and predict the spatial distribution of suitable wind farm sites. The software's ability to handle presence-only data makes it well-suited for this study, where complete absence data is often unavailable. GIS are used for data preprocessing, including the integration, visualization, and analysis of spatial datasets. GIS plays a vital role in preparing the data for input into the MaxEnt model and in visualizing the results to identify optimal wind farm locations. Validation is performed using known wind farm locations and additional independent datasets. This ensures the accuracy and reliability of the model's predictions, helping to refine and improve the final site selection.

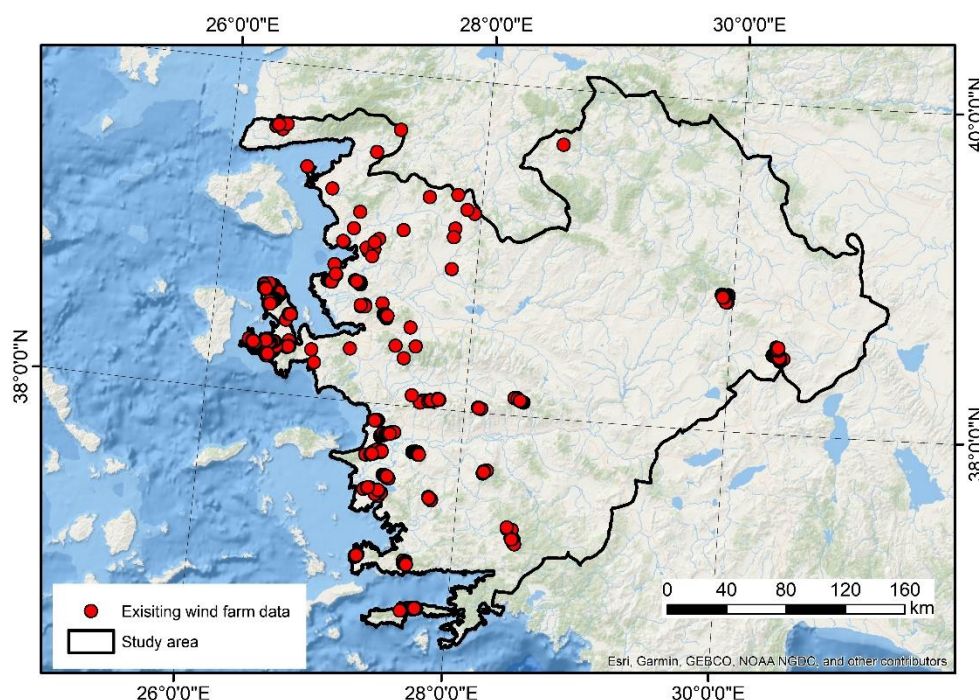


Figure 2. Wind farm locations in the Aegean region.

3. RESULTS

This study demonstrates the effectiveness of the Maximum Entropy (MaxEnt) method as a powerful tool for wind farm site selection in the Aegean Region of Türkiye. By integrating diverse datasets, including climate, topography, land use, and socio-economic factors, the MaxEnt model successfully identified areas with high potential for wind energy development. The results highlight several key locations in the region where wind farms could be established to maximize energy production while minimizing environmental and economic costs.

The Aegean Region, with its favorable wind conditions and varied terrain, offers significant opportunities for the expansion of renewable energy infrastructure. The application of the MaxEnt method in this context proves particularly valuable, as it allows for accurate predictions of suitable sites even in the absence of comprehensive datasets. The model's ability to incorporate and analyze complex, multi-dimensional data underlines its utility for strategic planning in renewable energy development.

Moreover, the findings of this study underscore the importance of considering multiple factors in wind farm site selection, beyond mere wind speed. The integration of socio-economic and environmental constraints ensures that the selected sites not only provide optimal energy output but also align with broader sustainability goals, such as minimizing impacts on local communities and ecosystems.

In conclusion, the MaxEnt method offers a robust approach to wind farm site selection that can significantly contribute to Türkiye's renewable energy objectives, particularly in the Aegean Region. Future studies could expand this methodology to other regions or refine it further by incorporating additional data layers, such as future climate projections and detailed land use plans. By continuing to develop and apply advanced modeling techniques like

MaxEnt, Türkiye can better navigate the challenges of sustainable energy planning and move closer to its renewable energy targets.

Fig. 3 shows the current viability of wind renewable energy. The results were assessed in terms of both the establishment of new stations in the area and the sustainability of existing stations' future potential. These figures show the suitability ratios for wind energy farms on a scale of 0 to 100. Unsuitable (0-20), marginally suitable (20-40), moderately suitable (40-60), suitable (60-80) and highly suitable (80-100) suitability levels. This evaluation shows the suitability of locations for wind energy farms, helping people choose new stations and guaranteeing their sustainability in the future.

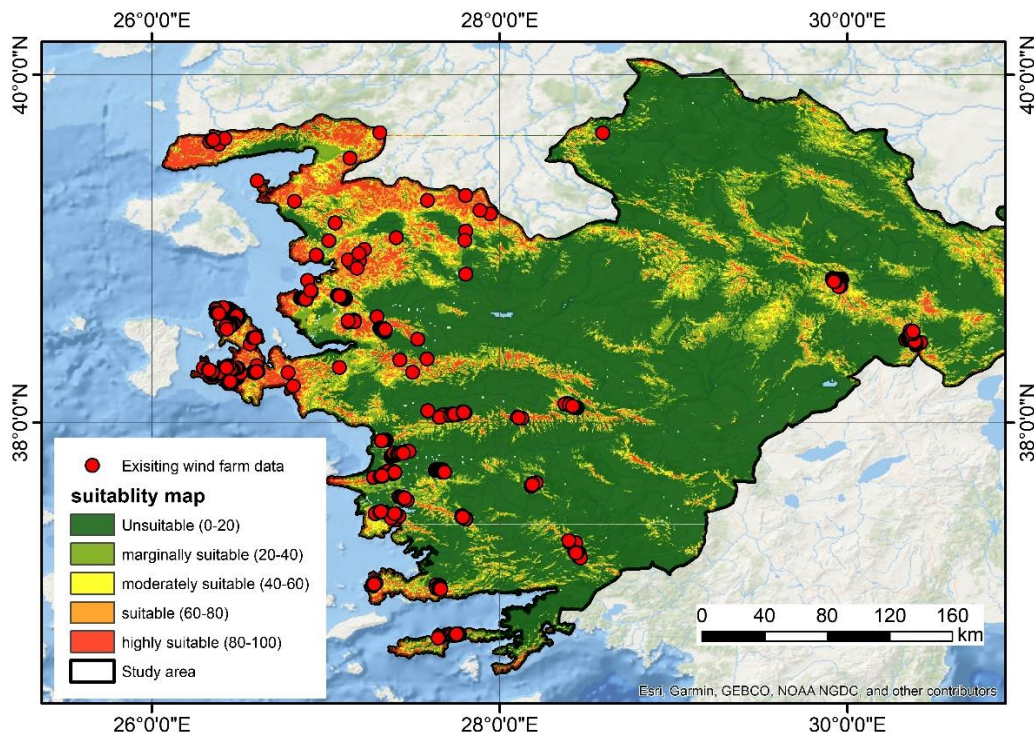


Figure 3. suitability maps in study area.

The jackknife test was used to examine how the environmental factors responded to the model and how that affected the suitability for wind energy fields. Fig. 4a displays the test data's AUC results. In situations where a single variable is present (blue bars), a variable is absent (green bars), or all variables are present (red bars), this graphic depicts the significance. After removing each variable in turn, a model was built using the variables that remained. Every variable was then used independently to develop a model (Fig 4b). Ultimately, every variable was used to develop a model.

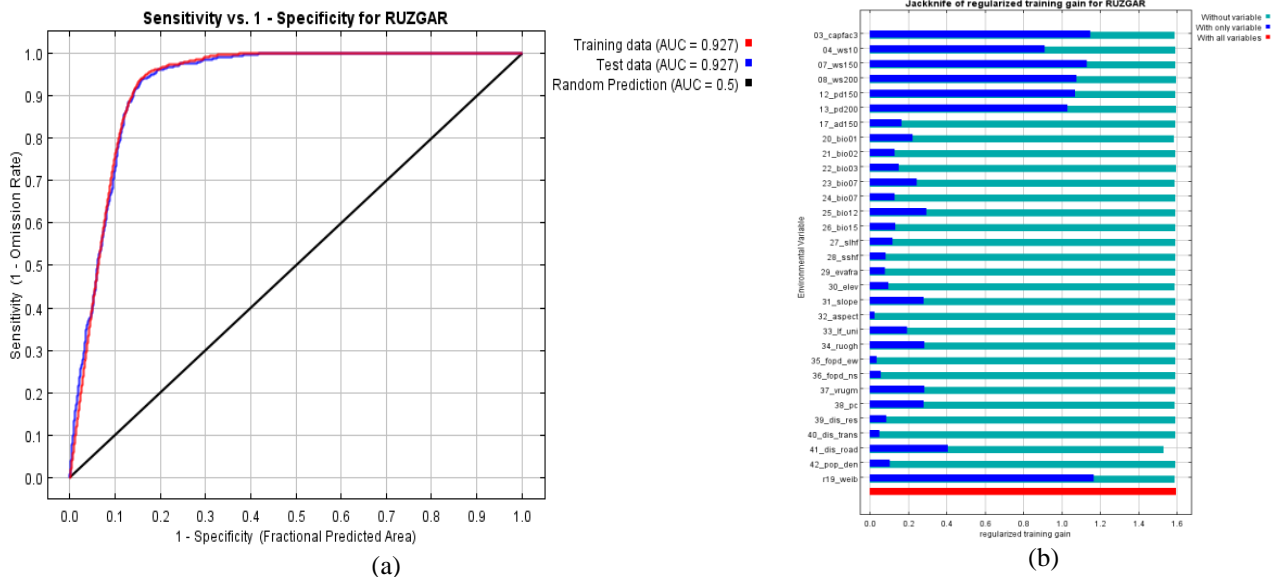


Figure 4. ROC-Curve (a,)Jackknife analysis (b)results.

4. DISCUSSION AND CONCLUSIONS

One of the most significant advantages of the MaxEnt method is its ability to work with presence-only data, which is particularly useful in regions where comprehensive wind resource assessments are lacking. By integrating various environmental, topographical, and socio-economic factors, the model provides a holistic view of site suitability that goes beyond mere wind speed analysis. This multi-dimensional approach ensures that selected sites are not only optimal for energy production but also feasible in terms of infrastructure development, environmental sustainability, and socio-economic impact.

Additionally, MaxEnt's flexibility in handling incomplete datasets allows for the inclusion of diverse data sources, making it adaptable to the dynamic and complex nature of wind farm site selection. This capability is especially relevant in the Aegean Region, where geographic diversity and varying land use patterns create a complex landscape for renewable energy development.

The findings of this study have important implications for energy policy and planning in Türkiye. The MaxEnt model's ability to identify optimal wind farm sites can aid policymakers in making informed decisions that balance energy production with environmental protection and social equity. However, to fully leverage the benefits of this modeling approach, it is essential to integrate the results with broader planning frameworks that consider land use regulations, community engagement, and long-term climate resilience.

Moreover, the study emphasizes the need for continued investment in data infrastructure and the development of more refined modeling techniques. By improving the quality of input data and enhancing the capabilities of predictive models like MaxEnt, Türkiye can better position itself to meet its renewable energy targets and contribute to global efforts to combat climate change.

Author Contributions

Conceptualization: S.T.; Investigation: M.Ü.Ç. A.Ç.; Material and Methodology: M.Ü.Ç. A.Ç, S.T., Writing-Original

Conflict of Interest

The authors have no conflicts of interest to declare.

Funding

The authors declared that this study has received no financial support.

REFERENCES

Xu Y, Ye L, Zheng L, Cui L, Li S, Li W, Cai Y (2020) Site selection of wind farms using GIS and multi-criteria decision making method in Wafangdian, China. *Energy*. 207. 118222. 10.1016/j.energy.2020.118222.

Rekik S, Alimi S (2023) Optimal wind-solar site selection using a GIS-AHP based approach: A case of Tunisia, Energy Conversion and Management: X, 18, 100355, <https://doi.org/10.1016/j.ecmx.2023.100355>.

European Commission, GHSL Data Package 2023, Publications Office of the European Union, Luxembourg, 2023, doi:10.2760/098587, JRC133256

OpenStreetMap (2023) OpenStreetMap copyright and license. Accessed date 03 March 2021 Available: <http://www.openstreetmap.org/copyright>

Seismic Risk and Damage Assessment of Adiyaman Province during February 6, 2023 Earthquakes

Seyhan Okuyan Akcan^{*1}, Senem Tekin², Ali Yeşilyurt³

Abstract: The assessment of potential seismic risks and losses in urban environments is important for many purposes, from urban and regional planning to risk mitigation strategies. Critical infrastructures, weak residential buildings and densely populated areas, especially those located in high seismic hazard zones, require special attention in risk mitigation efforts. This study aims to perform seismic damage and risk assessment in Adiyaman province, which was heavily affected by the February 6, 2023 Kahramanmaraş earthquakes, by deterministic seismic hazard analysis (DSHA) and risk analysis using the OpenQuake engine considering European Seismic Risk Model (ESRM20). DSHA was performed considering earthquake parameters (lat, lon, depth, Mw, dip, rake). MMI maps were produced. Seismic risk and damage analyses were performed for the building inventory defined for Adiyaman province in the ESRM20. Fragility and vulnerability curves defined in the ESRM20 for each building type were used in damage and risk analyses. The loss and damage results obtained by the deterministic method were compared with the post earthquake damage results. Considering the loss and damage results obtained, it was observed that the fragility curves defined in the ESRM20 model in the seismic damage and risk analysis of the structures gave results close to the damage studies performed after the earthquake.

Keywords: Adiyaman, Seismic Risk, Seismic Damage, ESRM20.

¹**Address:** Bogazici University, Faculty of Civil Engineering, İstanbul/Türkiye

²**Address:** Istanbul Technical University, Earthquake Engineering, Disaster Management Institute, İstanbul/Türkiye

³**Address:** Adiyaman University, Department of Mining and Mineral Extraction, School of Technical Sciences Adiyaman/Türkiye

***Corresponding author:** seyhan.okuyan@std.bogazici.edu.tr

1. INTRODUCTION

In Turkey, on February 6, 2023 a 7.7 magnitude earthquake occurred at 04:17 in Pazarcık district of Kahramanmaraş and a 7.6 magnitude earthquake occurred at 13:24 in Elbistan district. The February 6, 2023, Kahramanmaraş-Pazarcık (Mw=7.7) and Elbistan (Mw=7.6) earthquakes caused massive damage in the surrounding provinces and resulted in thousands of casualties. It was felt mainly in the provinces of Hatay, Kahramanmaraş, Adiyaman, Malatya, Adana, Şanlıurfa, as well as in Southeastern Anatolia, Eastern Anatolia, Mediterranean and Central Anatolia regions. Both earthquakes occurred in the East Anatolian Fault Zone, one of Türkiye's two major active fault zone. The earthquake at 04:17 occurred on the Pazarcık and Amonos segments of the Eastern Anatolia Fault zone. The earthquake at 13:24 occurred on the Çardak fault starting in the southern part of Elbistan. Nearly 4000 aftershocks occurred until 24:00 on March 20, 2023 (Figure 1). It was determined that these two earthquakes occurred in accordance with the Eastern Anatolian fault zone and occurred as a left lateral strike-slip fault mechanism (Gücek et al., 2023). Field analysis after earthquakes provides important information to understand the extent of damage.

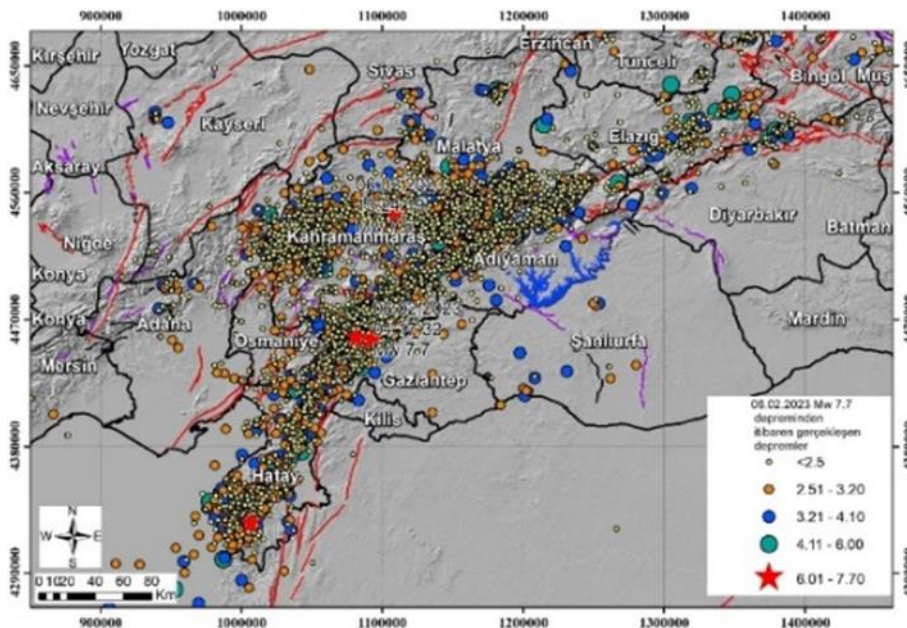


Figure 1. Earthquakes in the region from February 6, 2023 until March 20, 2023.

One of the cities most affected by these earthquakes in terms of structural damage and loss of life is Adiyaman province. Disaster and Emergency Management Presidency (AFAD) measured the Peak Ground Acceleration (PGA) value of the earthquake at station 0201 in the city center of Adiyaman province as approximately 0.4g. Nemutlu et al. (2023) reported that according to official data, more than 11,000 people lost their lives in the city center of Adiyaman province and the number of heavily damaged or completely collapsed buildings was 13,000. Nemutlu et al. (2023) mentioned that structural damages are generally caused by buildings subjected to collision and hammering effects, strong beam weak column condition, soft-weak floor irregularities and non-structural damages.

Seismic hazard and damage studies are important in predetermining the damage extent of earthquakes. For seismic loss mitigation and disaster planning purposes, it is important to assess potential earthquakes and related ground motions in areas of high earthquake risk (Askan et al., 2015). Seismic hazard studies are carried out by including the active faults and soil properties in and around the region. With seismic hazard analyses, the expected seismic intensity parameters in the region can be evaluated according to the rupture conditions of the active faults in the region. The results of seismic hazard studies can be used in seismic risk analyses to analyze the damage and loss caused by a possible seismic event in advance. In seismic hazard and risk analysis studies, many uncertainties arise during the ground motion evaluation phase including location of a seismic event, seismic source parameters, and magnitude of an event.

Seismic hazard analyses are performed with probabilistic and scenario-based method (Cornell, 1968; Frankel, 1993; Olsen et al., 1996; McGuire, 2004; Askan et al., 2015; Vaziri et al., 2022). Probabilistic Seismic Hazard Analysis (PSHA) is a method used to calculate the probability of future earthquakes in a given region. PSHA is basically a calculation method that brings together various data sources on earthquake occurrence rates, the magnitude of future earthquakes, and the propagation of seismic events on the earth's surface (Baker, 2021). By taking into account the magnitude, location and intensity of earthquakes, this method determines the severity of shaking in a region and the probability of these effects. PSHA results in a complete distribution of all levels of ground motion intensity and the probability of reaching these levels.

In the DSHA (Deterministic Seismic Hazard Analysis) method, the exact values of the source parameters are determined and a specific seismic scenario is created and the ground motion hazard is evaluated according to this scenario (Okuyan Akcan et al., 2023; Demircioğlu et al., 2018; Harmandar, 2022). In other words, with DSHA, it is possible to predict the level of ground motion in a region in a deterministic way when the distance, magnitude and conditions of the source region are known. Campell and Bozorgnia (2003) discuss DSHA analysis in detail. Hazard estimation with DSHA (Deterministic Seismic Hazard Analysis) consists of four steps:

1. Identification of source regions,
2. Selection of parameters,
3. Defining and selecting the welding zone,
4. Identification of hazards.

This study aims to evaluate the damage prediction of the February 6, 2023 Kahramanmaraş earthquakes on existing structures for Adiyaman province in ESRM20 model by deterministic seismic hazard analysis (DSHA) and risk analysis. DSHA was performed by considering earthquake parameters (lat, lon, depth, Mw, dip, rake). MMI maps are produced. The results obtained from seismic risk and damage analysis are compared with post earthquake seismic damage assessment studies in the literature. Seismic damage and risk analyses for Adiyaman building inventories were performed using the fragility curves presented in the ESRM20 model. Seismic loss analyses were also performed with the vulnerability curves presented in the ESRM20 model. Probable maximum losses were calculated. Predicted and observed damages were compared. The vulnerability curves presented in the ESRM20 model, which show good agreement with the observed damages, are recommended to be evaluated in seismic damage and risk analysis of buildings.

2. MATERIAL AND METHOD

On February 6, 2023, the Kahramanmaraş-Pazarcık and Elbistan earthquakes caused great destruction, damage and many casualties in Adiyaman and neighboring provinces. Especially in Adiyaman, Hatay and Kahramanmaraş regions, the destructive effect of the earthquakes was quite high in these regions due to liquefaction in the ground due to the earthquake effect. PGA distribution maps in Adiyaman province were calculated by scenario analysis due to the effects of both earthquakes. On the OpenQuake open platform, scenario based seismic hazard analyses were carried out using the fault information and earthquake parameters where the Pazarcık and Elbistan earthquakes occurred, taking into account the V_{s30} distribution in the region.

Pazarcık, Erkenek, Pütürge segments of the Eastern Anatolia Fault segment, Gerger and Narince segments of the Southeastern Anatolia Thrust, Besni Fault, Bozava Fault and certain sections of Sürgü Faults are located within the borders of Adiyaman province (Figure 2a). The East Anatolian Fault Zone is a left-lateral strike-slip fault that forms the boundary between the Arabian plate and the Anatolian block and poses a great earthquake hazard for the region. It intersects the North Anatolian Fault (NAF) at Karlıova in the northeast and the Dead Sea Fault (SDF) around Kahramanmaraş in the southwest. The DAF is approximately 580 km long with a general NE-SW strike (Emre et al., 2013). The DAF, which shows left-lateral strike-slip characteristics, consists of 6 segments, namely Karlıova, Ilıca, Palu, Pütürge, Erkenek, Pazarcık and Amanos (Figure 2b).

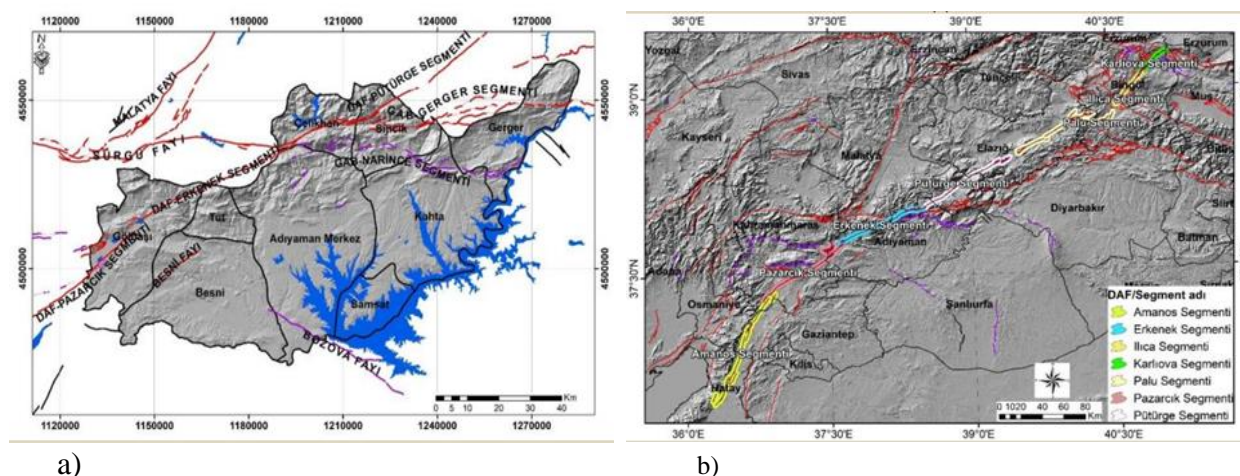


Figure 2. Active fault lines in and around Adiyaman province (Emre et al., 2013) (a), Eastern Anatolia Fault and its segments (b)

Shear wave velocity is used to determine the soil conditions and dynamic behavior of soils in the region. V_{s30} (m/s) value, which is defined as the average value of shear wave velocity up to 30m depth, is taken into consideration in soil classification. The V_{s30} (m/s) distribution for Adiyaman is shown in Figure 3. It is observed that V_{s30} values are between 200m/s and 400m/s especially in Gölbaşı and its surroundings where there was great destruction in both earthquakes. Following the earthquakes on February 6, 2023, typical damages due to soil liquefaction were observed in

Adıyaman, particularly in the Gölbaşı and İskenderun districts. However, on-site examinations in Gölbaşı revealed that the majority of the issues were not actually due to soil liquefaction but rather to a loss of bearing capacity (SUBU,2023).

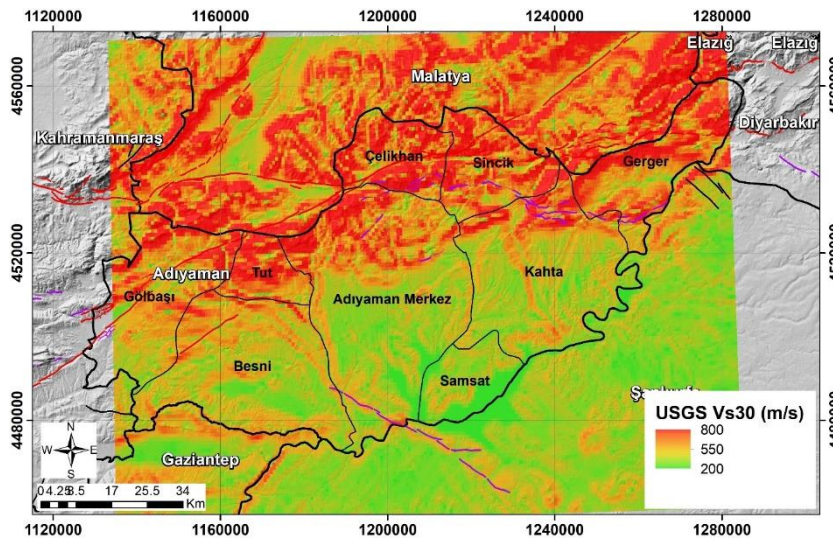


Figure 3. V_{s30} (m/s) Distribution in Adıyaman Province (USGS)

2.1. Simulation

Earthquake hazard maps are prepared by considering the most recent earthquake source parameters (active fault lines), earthquake catalogs (historical and instrumental earthquake catalogs) and current statistical distributions. The effects of earthquakes are evaluated with different intensity scales (PGA, SA, MMI, PGV, etc.). According to the revised Earthquake Hazard Map of Turkey, unlike the previous hazard maps, the concept of peak ground acceleration values (PGA-Peak Ground Acceleration) is used instead of earthquake zones.

The Chiou and Youngs (2014) attenuation relationship, which is one of the NGA-West2 ground motion models and generally used in earthquake ground motion analysis in Turkey, was used to calculate the PGA distribution in Adıyaman province. The Modified Mercalli Intensity scale defines the intensity of an earthquake in terms of its impact on the earth, people, structures and objects. The MMI intensity scale rates the intensity of an earthquake on a scale of 1-12. 1 indicates

that the intensity of the earthquake is very low and the earthquake is ineffective, while 12 indicates that the earthquake causes complete destruction.

An open source OpenQuake software was developed to calculate seismic hazard and risk assessment by Global Earthquake Model (GEM). OpenQuake was used to analyze the MMI intensity distribution of earthquakes in Adıyaman province. Scenario-based analyses were performed in the region by using the fault parameters, earthquake magnitude and fault mechanism information where Pazarcık and Elbistan earthquakes occurred. The intensity distribution maps of both earthquakes calculated using Allen et al. (2012) ground motion attenuation equations, which can be used to calculate earthquake intensity distributions in a region, are shown in Figure 4 and Figure 5.

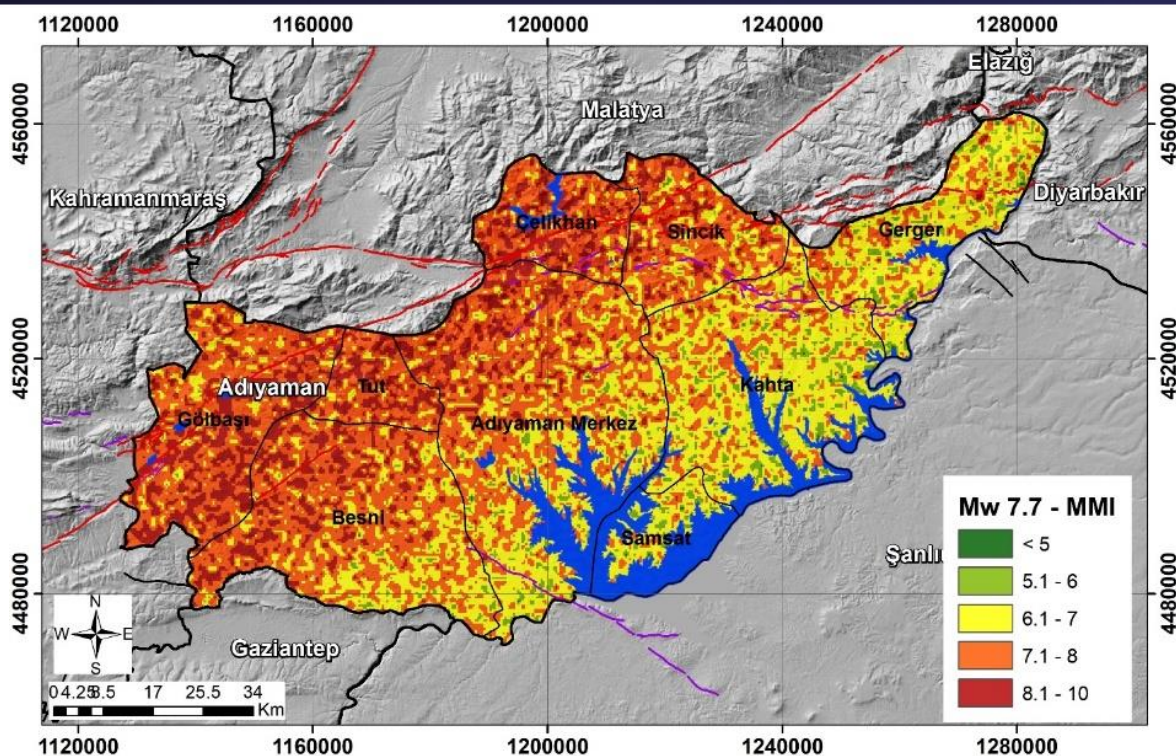


Figure 4. MMI (g) Distribution of Adiyaman Province as a Result of Scenario Analysis of Kahramanmaraş-Pazarçık Mw7.7 Earthquake.

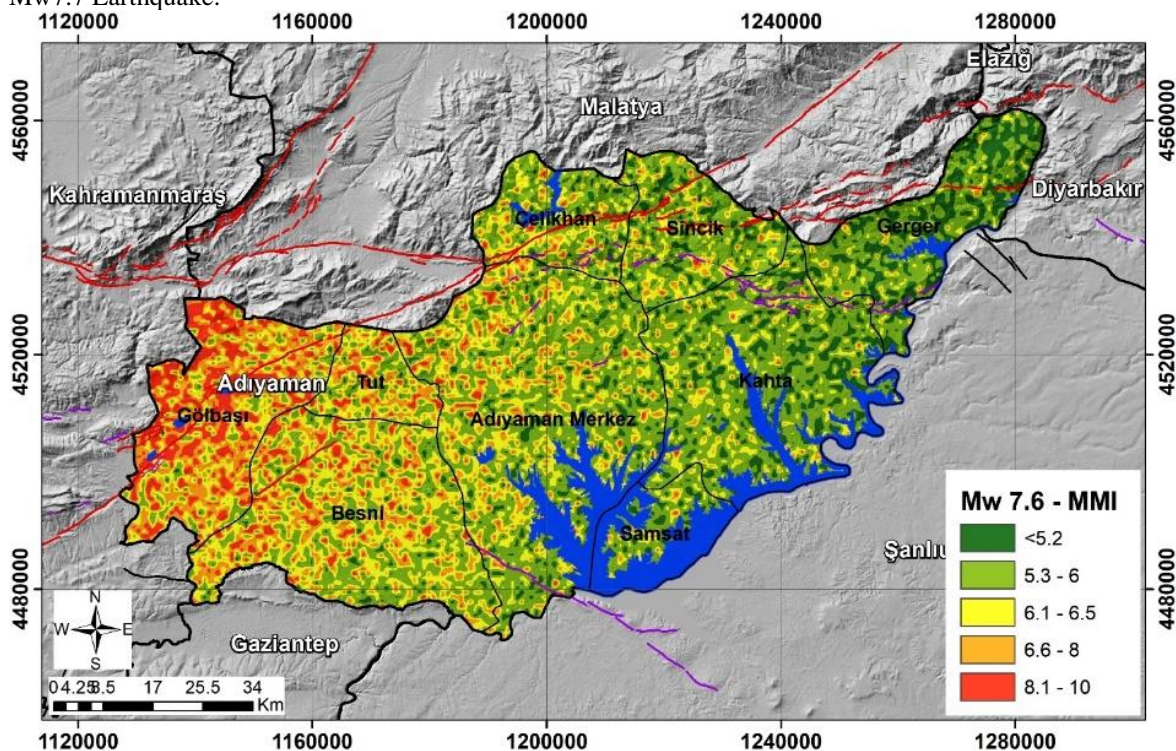


Figure 5. Adiyaman Province MMI(g) Distribution as a Result of Scenario Analysis of Elbistan Mw7.6 Earthquake

According to the Modified Mercalli Intensity (MMI) scale ranging from I-XII, earthquakes that is resulted IX scale and above have a high destructive effect. As a result of the scenario analyses of the earthquakes of Mw7.7 and Mw7.6 centered in Pazarçık and Elbistan, the MMI values in Adiyaman province were calculated as IX that is, there was great destruction in the region. Especially in Adiyaman city center, it was observed that the intensity was more intense and between 9-11 on the MMI scale. As a result of the scenario analysis of the second earthquake, Mw7.6 Elbistan earthquake, it was observed that the MMI intensity distribution in Adiyaman region was between 9-10.

Many buildings in Adiyaman collapsed and were heavily damaged in the 6 February earthquake. As a result of the field inspections, the damages observed in reinforced concrete structures were analyzed under two main headings: design deficiencies and construction defects. Poor quality workmanship, use of inappropriate materials and lack of supervision are the main causes of construction defects. On the other hand, the lack of technical knowledge and experience of engineers and architects played an important role in the damages caused by the design phase. Figure 6 shows the Adiyaman Central district building inventory and point data of demolished buildings. As a result of the damage assessment studies conducted by the Ministry of Environment, Urbanization and Climate Change, General Directorate of Construction Works, there are 110,354 buildings in Adiyaman province and 38,666 of them are undamaged 38,576 of them are slightly damaged 4,629 of them are moderately damaged 20,201 of them are heavily damaged 2,329 of them need urgent demolition 5,953 of them were demolished after 6th of February,2023 earthquakes. Examples of collapsed and heavily damaged buildings in the central district of Adiyaman are shown in Figure 7.

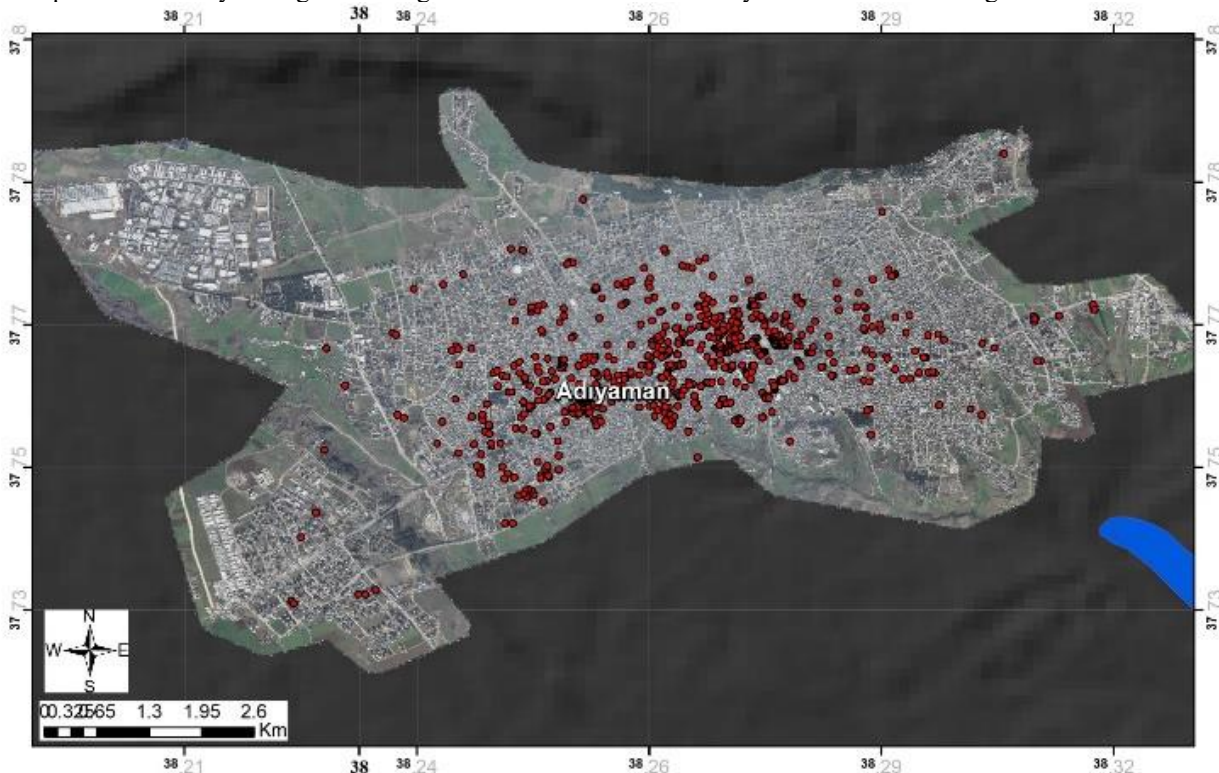


Figure 6. Adiyaman Central district building inventory and point data of demolished buildings.



Figure 7. Examples of demolitions and damages in the central district of Adiyaman and Golbasi

Seismic Risk Assessment (SRA) aims to estimate the likelihood of damage to buildings and infrastructure, as well as the potential economic losses, based on various seismic hazards or specific earthquake scenarios. Seismic risk analysis and damage estimation are necessary to reduce the destructive effects of earthquakes. In order to perform this analysis accurately, a reliable seismic hazard model, a detailed building inventory and various fragility and vulnerability functions are needed (Martins et al.,2016, Zulfikar et al.,2023). In recent years, many researchers around the world have performed seismic hazard, risk and loss estimations in seismically active regions by various methods (Crowley et al.,2021,Askan et al.2010). These researches are nowadays of great importance for important purposes such as seismic risk reduction and urban planning.

Scenario-based seismic risk and damage analysis were performed for the Adiyaman exposure model defined in the European Seismic Risk Model (ESRM20). ESRM20 is a new, open seismic risk model supported by the European Union's Horizon 2020 research and innovation program within the framework of the SERA, RISE, EPOS-IP, EPOS-SP projects and developed in collaboration with the Global Earthquake Model (GEM Foundation) (Crowley et al.,2021). The consequences are estimated for a specific earthquake scenario (of a given magnitude, location, depth, style of faulting etc.) whose recurrence interval can be obtained from the hazard source model for scenario-based earthquake risk analysis. ESRM20 considers concrete, masonry, steel buildings constructed in Adiyaman province up to 2000. Pre-code (CDN), low code (CDL), and high code (CDH) design levels are considered for the exposure model of Adiyaman. CDN represents the buildings constructed before 1975, CDL represents the buildings constructed between 1975-1997, CDH represents the buildings constructed after 1997. For building inventory in ESRM20, Soyuluk and Harmankaya (2012) was used as reference.

The seismic damage assessment was performed using fragility curves, seismic risk assessment was performed with vulnerability curves presented in ESRM20 model. The fragility curves describe the probability that the structural damage will reach or exceed the previously defined damage level for a specific intensity value of the seismic ground motion parameter (Yeşilyurt et al.,2023). Vulnerability curves and fragility curves are tools used to assess earthquake impacts. Vulnerability curves estimate the potential economic losses from damage, while fragility curves indicate the likelihood of different levels of damage occurring (Zülfikar et al.,2023). In ESRM20, the fragility and vulnerability curves were developed for PGA, SA earthquake intensity parameters for the structure.. In the damage assessment of Adiyaman building stock, the fragility curves developed in ESRM20 as a function of spectral acceleration and PGA were taken into consideration. For illustration purposes, Figure 8 shows the fragility functions in terms of SA(0.3s) that have developed in ESRM20 (Crowley et al.,2021).

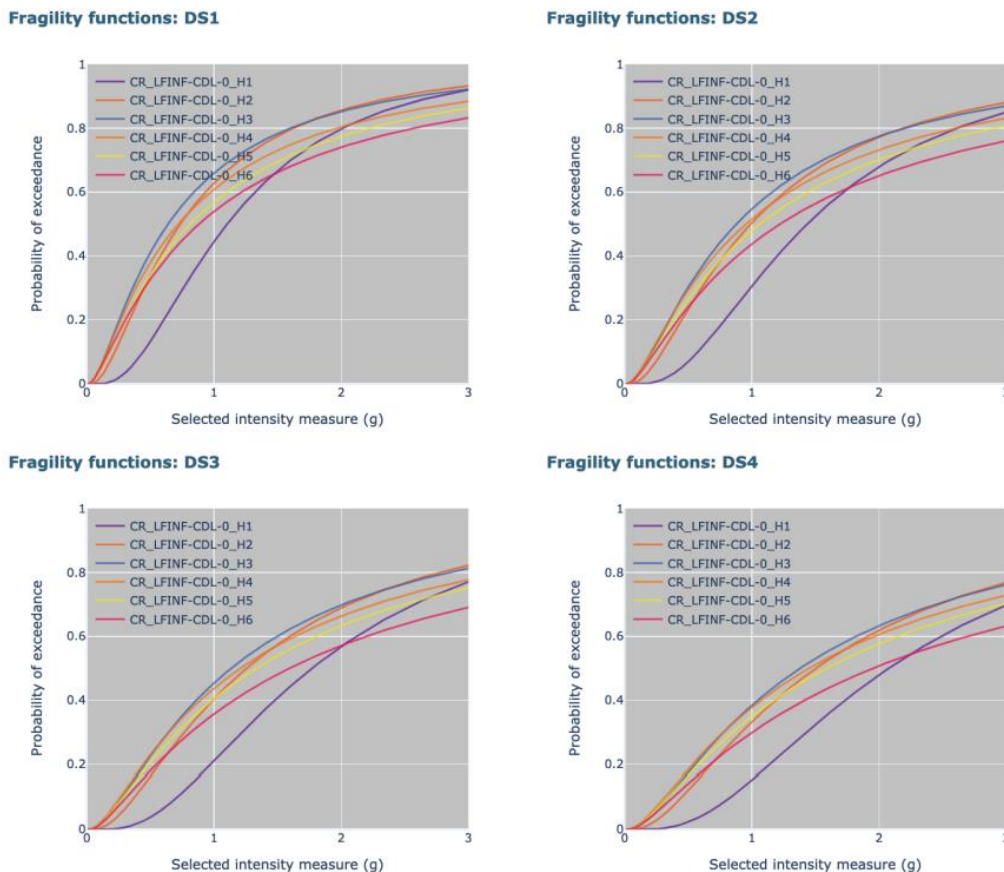


Figure 8. Fragility functions in ESRM20 for reinforced concrete building typologies, where DS1 = slight damage, DS2 = moderate damage, DS3 = extensive damage and DS4 = complete damage (Crowley et al.,2021)

The scenario of the earthquake with magnitude Mw 7.7 is defined in terms of moment magnitude, location, depth, and style of faulting, rake, dip, etc. After the scenario has been defined, Chiou and Youngs (2014) ground motion model is used to estimate the level of shaking at the locations of the buildings in the exposure model. The simulated ground motion in Adiyaman in the exposure is input into the relevant vulnerability models and fragility models and the economic loss and damages are estimated.

3. RESULTS

In this study, damage assessment of the Adiyaman after earthquake in Pazarcık (Mw 7.7) was performed considering building inventory and fragility functions defined in ESRM20. The earthquake scenario was constructed considering earthquake parameters in OpenQuake engine. Scenario based seismic hazard results were used with fragility functions developed for each building typology. In Adiyaman, 51,753 building with 34 different building classes were considered and scenario based seismic damage assessment for Adiyaman was performed. The calculated damage results compared with post earthquake damage reports of Gücek et al. (2023) and the Republic of Turkey Presidency of Strategy and Budget (SBB, 2023). Gücek et al. (2023) presented the damage assessment studies conducted by the Ministry of Environment, Urbanization and Climate Change, General Directorate of Construction Works. As of May 15, 2023, the general damage levels of the buildings and the damage levels of the buildings constructed after 2000 were shown for the provinces affected by the earthquake. In the report of the Republic of Turkey Presidency of Strategy and Budget (2023), the effects of the Kahramanmaraş and Hatay earthquakes are discussed in detail. The number of buildings in damaged states were presented in this report. Table 1 presents the building in slight, moderate, and collapse (including extensive) damage states as a percentage of the total building in Adiyaman calculated in the current study and in literature. The total number of building in Adiyaman was considered as 51,753, 110,354, 216,744 by ESRM20, Gücek et al.(2023) and SBB (2023), respectively. Percentages of the number of buildings at different damage levels are given in Table 1.

Table 1. The distribution of the number of buildings in Adiyaman for damage states as a percentage

	<i>ESRM20 (Current Study)</i>	Gücek et al.(2023)	SBB (2023)
Slight	%30 (15,498)	%35 (38,576)	%33 (72,729)
Moderate	%13 (6,833)	%4 (4,629)	%8 (18,715)
Extensive+Collapse	%20 (9,840)	%25 (28,483)	%25 (56,256)

When we compare the damage percentages of the buildings after the earthquake given in Table 1, the ESRM20 model calculated damage distributions close to those given in the current post-earthquake reports. There are some reasons for the numerical differences. First, the ESRM20 model has building inventory data until 2000. However, recent earthquake assessment reports have realized the damage distribution of buildings according to 2023 data. Secondly, on February 6, 2023, two large earthquakes with devastating effects occurred in the region 9 hours apart. However, in this study, a scenario-based seismic hazard analysis was performed for the first earthquake with a magnitude of Mw 7.7 with the epicenter in Pazarcık. Seismic damage assessment is also calculated only for this earthquake. For this reason, different results are expected from the values in the earthquake damage assessment reports. Thirdly, in the ESRM20 model, exposure models are defined to be at the center point of each city. For this reason, seismic hazard results are calculated for the center point, and seismic risk assessment is made for the city based on a single point. However, when the results are analyzed in percentage terms, it is observed that the damage assessment performed with ESRM20 is close to the post-earthquake values.

In this study, scenario-based seismic risk assessment was performed using vulnerability curves and economic values defined for each building structure class in Adiyaman province in ESRM20 model. An economic loss of 38% was calculated as a result of the destructive earthquake. In addition to scenario based seismic risk assessment, probabilistic seismic risk assessment was performed for Adiyaman province through OpenQuake. Average loss curve for residential buildings was calculated as shown at Figure 8.

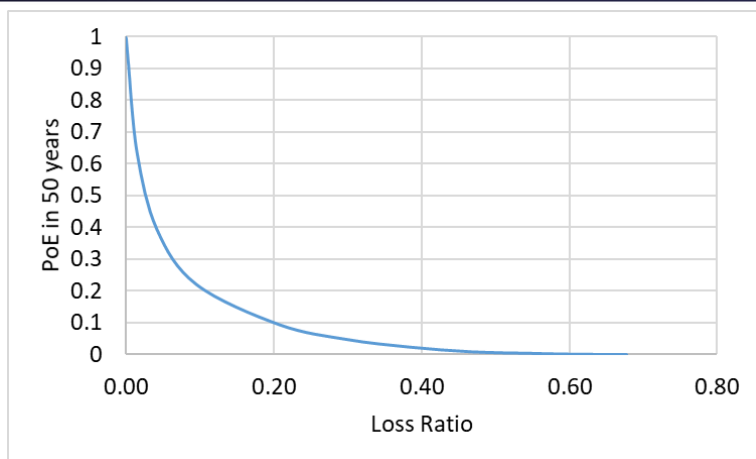


Figure 8. Loss curve for Adiyaman

As shown at Figure 8, loss ratio for different exceedance probability in 50 years was calculated. 2475 years and 475 years return period loss ratio were calculated as %20 and %40, respectively. The loss due to earthquake with Mw 7.7 was calculated as %38. By comparing the loss ratio calculated considering probabilistic and deterministic seismic risk analysis, it can be said that the earthquake level is mostly close to the DD-1 level defined as ground motion level with %2 probability of exceedance in 50 years.

4. DISCUSSION AND CONCLUSIONS

In this study, the structural damage caused by the February 6, 2023 Pazarcık Mw 7.7 earthquake in Adiyaman province was investigated using the ESRM20 model. The results in the damage assessment reports published after the earthquake were compared with the results obtained with ESRM20. As a result, it is observed that the damage and risk results obtained with the fragility functions and vulnerability functions presented with the ESRM20 model are close to the post earthquake evaluation reports. In order to further improve the study, it is suggested that earthquakes occurring 9 hours apart can be considered together and damage assessment can be performed again. This study proposes that the fragility and vulnerability curves presented for Turkey in the ESRM20 model can be considered in earthquake risk and damage assessment.

Probabilistic and deterministic seismic risk assessment results were evaluated together. It was observed that the level of this devastating earthquake was closer to the DD-1 earthquake level.

Ethics Committee Approval

N/A

Peer-review

Externally peer-reviewed.

Author Contributions

Conceptualization: S.O.A.; Investigation: S.O.A.; Material and Methodology: S.O.A., A.Y., S.T.; Supervision: A.Y., S.T.; Visualization: S.O.A., A.Y., S.T.; Writing-Original Draft: S.O.A.; Writing-review & Editing: A.Y., S.T.; Other: All authors have read and agreed to the published version of manuscript.

Conflict of Interest

The authors have no conflicts of interest to declare.

Funding

The authors declared that this study has received no financial support.

REFERENCES

AFAD, "https://www.afad.gov.tr/," 2021. <https://www.afad.gov.tr/> (accessed Jan. 05, 2021).

Akcan, S. O., Tekin, S., Yeşilyurt, A., & Zülfiyar, A. C. (2023). Güncel Avrupa sismik tehlike ve risk modeliyle 23 Kasım 2022 Düzce depreminin değerlendirilmesi. *Afet ve Risk Dergisi*, 6(4), 1218-1233.

- Askan, A., & Yucemen, M. S. (2010). Probabilistic methods for the estimation of potential seismic damage: Application to reinforced concrete buildings in Turkey. *Structural Safety*, 32(4), 262-271.
- Askan, A., Karimzadeh, S., Asten, M., Kilic, N., ŞİŞMAN, F. N., & Erkmen, C. (2015). Assessment of seismic hazard in the Erzincan (Turkey) region: construction of local velocity models and evaluation of potential ground motions. *Turkish Journal of Earth Sciences*, 24(6), 529-565.
- Campbell KW, Bozorgnia Y. Erratum: Updated near source ground-motion (attenuation) relations for the horizontal and vertical components of peak ground acceleration and acceleration response spectra (Bulletin of the Seismological Society of America (2003) vol. 93 (1) (314-331). *Bulletin of the Seismological Society of America* 2004; 94:2417. doi:10.1785/0120040147.
- Chiou, B. S. J., & Youngs, R. R. (2014). Update of the Chiou and Youngs NGA model for the average horizontal component of peak ground motion and response spectra. *Earthquake Spectra*, 30(3), 1117-1153.
- Crowley H., Dabbeek J., Despotaki V., Rodrigues D., Martins L., Silva V., Romão, X., Pereira N., Weatherill G. and Danciu L. (2021) *European Seismic Risk Model (ESRM20)*, EFEHR Technical Report 002, V1.0.1, 84 pp, <https://doi.org/10.7414/EUC-EFEHR-TR002-ESRM20>
- Demircioğlu, M. B., Şeşetyan, K., Duman, T. Y., Can, T., Tekin, S., & Ergintav, S. (2018). A probabilistic seismic hazard assessment for the Turkish territory: part II—fault source and background seismicity model. *Bulletin of Earthquake Engineering*, 16, 3399-3438.
- Emre Ö, Duman TY, Özalp S, Elmacı H, Olgun Ş, ve Şaroğlu F, (2013). Açıklamalı Türkiye Diri Fay Haritası. Ölçek 1:1.250.000, Maden Tetkik ve Arama Genel Müdürlüğü, Özel Yayın Serisi-30, Ankara-Türkiye, 89 S.
- Gücek, S., Afacan, K. B., & Zorluer, İ. (6). 6 Şubat 2023 Depremleri Sonrası Zemin Büyütmesi ve Sıvılaşma Gerçeği: Antakya, Gölbaşı, Türkoğlu Örnekleri. *Afyon Kocatepe Üniversitesi Fen ve Mühendislik Bilimleri Dergisi*, 23(3), 740-752.
- Kahramanmaraş Deprem Raporu. (2023, 12 Nisan). *Kahramanmaraş Deprem Raporu*. Sakarya Üniversitesi. <https://www.subu.edu.tr>
- Kahramanmaraş ve Hatay Depremleri Raporu. (2023). *Republic of Turkey Presidency of Strategy and Budget*. <https://www.sbb.gov.tr>
- Martins, L., Silva, V., Marques, M., Crowley, H., & Delgado, R. (2016). Development and assessment of damage-to-loss models for moment-frame reinforced concrete buildings. *Earthquake Engineering & Structural Dynamics*, 45(5), 797-817.
- Ö. F. Nematlu, A. Sarı, and B. Balun, “Bingöl İli Şehir Merkezindeki Yapılaşmanın Olası Deprem Risklerine Etkisi,” in 2nd International Conference on Innovative Academic Studies, 2023, no. January, pp. 101–107.
- Pagani, M., Monelli, D., Weatherill, G., Danciu, L., Crowley, H., Silva, V., ... & Vigano, D. (2014). OpenQuake engine: An open hazard (and risk) software for the global earthquake model. *Seismological Research Letters*, 85(3), 692-702.
- Soyluk, A., & Harmankaya, Z. Y. (2012). The history of development in Turkish seismic design codes. *International Journal of Civil & Environmental Engineering*, 12(1), 25-29.
- Yesilyurt, A., Cetindemir, O., Akcan, S. O., & Zulfikar, A. C. (2023). Fragility-based rapid earthquake loss assessment of precast RC buildings in the Marmara region. *Structural Engineering and Mechanics, An Int'l Journal*, 88(1), 13-23.
- Zülfikar, A. C., Akcan, S. O., Yeşilyurt, A., Eröz, M., & Cimili, T. (2023). Earthquake hazard and risk assessment of a typical Natural Gas Combined Cycle Power Plant (NGCCPP) control building. *Geomechanics and Engineering*, 35(6), 581.

Evaluation of the Alternative Locations for Solar Power Plant in Turkey

Mehmet Salih Değirmenci¹, Mehtap Dursun*¹, Nazli Goker¹

Abstract: Solar energy is a clean, renewable power source harnessed from the sun's rays. Today, the use of solar energy is becoming widespread in the world. The installation of solar energy power plants is very costly and it is not possible to change the area then. Thus, it is very important to choose the area where the power plant will be installed correctly. In this study, analytic network process (ANP) and technique for order preference by similarity to ideal solution (TOPSIS) method are combined to find the most appropriate solar power plant location alternative in Turkey. The evaluation factors are determined by reviewing the literature and by obtaining the experts opinions.

Keywords: Analytic network process, Decision making, Location selection, Solar energy, TOPSIS

¹**Address:** Galatasaray University, Industrial Engineering Department, Istanbul/Turkiye

***Corresponding author:** mdursun@gsu.edu.tr

1. INTRODUCTION

Solar energy is the radiant light and heat from the sun that is harnessed using a range of technologies such as solar panels (photovoltaics), solar thermal energy, and solar heating. Types of solar energy systems are as follows (Ozcan et al., 2017).

Photovoltaic (PV) Systems: These convert sunlight directly into electricity using solar cells made of semiconductor materials.

Solar Thermal Systems: These use sunlight to produce heat, which can be used directly or converted into mechanical energy and then electricity.

Concentrated Solar Power (CSP): These systems use mirrors or lenses to concentrate a large area of sunlight onto a small area, typically to produce heat that drives a steam turbine connected to an electrical power generator.

Solar energy has many advantages. It is abundant and inexhaustible. Solar energy produces no greenhouse gas emissions during operation and it reduces dependence on fossil fuels and enhances energy security. Moreover, after the initial installation, maintenance costs are relatively low.

Today, the use of solar energy is becoming widespread in the world. The aim of this study is to select the most appropriate solar power plant location in Turkey. In this study, ANP method is employed to find the importance of key success factors for installing solar plants in the right area. Then, TOPSIS method is used to determine the most appropriate location alternative in Turkey. The rest of the study is organized as follows. ANP method is explained in Section 2. TOPSIS method is illustrated in Section 3. Case study is given in the fourth Section. Finally, conclusions are provided in the last Section.

2. ANALYTIC NETWORK PROCESS

ANP is a general form of AHP used in multi-criteria decision analysis developed by Thomas L. Saaty (1980). The application steps of the ANP is as follows (Kheybari et al., 2020):

Step 1: Identification of the problem and creation of the model.

Step 2: Determination of criteria and their relationships.

Step 3: The importance scale from 1 to 9 suggested by Thomas L. Saaty (1980) given in Table 1 is used to create pairwise comparison matrices.

Table 1. Scale of significance used in pairwise comparisons (Saaty, 1980)

Value	Definition	Explanation
1	Of equal importance	Both criteria are equally important.
3	Moderately more important	Judgments and experiences make one criterion a little more important than another.
5	Strongly or substantially more important	Judgments and experiences make one criterion very important over another.
7	Very strong or demonstrated importance	One criterion is strongly superior to another.
9	Extremely more important	Judgments and experience show that one criterion is extremely superior to another.
2, 4, 6, 8	Intermediate values of the judgment	Intermediate numbers are used if necessary.

Step 4: The consistency of pairwise comparisons made with the help of experts is determined by calculating Consistency Rate (CR) for each matrix. For pairwise comparisons to be consistent, the consistency ratio must be less than or equal to 0.10. Otherwise, comparisons should be reviewed. To calculate the CR value, it is necessary to know the Consistency Index (CI). CI is calculated as follows (Omurbek et al., 2014):

$$CI = \frac{\lambda_{max} - n}{n - 1} \tag{1}$$

The largest value among the eigenvalues of a square matrix is expressed by λ_{max} . In order to calculate λ_{max} , each element of the entire priority matrix is divided by the elements of the priority vector, and the new matrix elements obtained are averaged.

Step 5: Create and analyze super matrices.

Step 6: Find the weights of the alternatives.

3. TOPSIS METHOD

Technique For Order Preference By Similarity To Ideal Solution (TOPSIS) was developed by Hwang and Yoon (1981). The normalized score (R_{ij}) for each criterion (X_{ij}) for alternative i and criterion j is calculated using the following formula:

$$R_{ij} = \frac{X_{ij} - \min(X_j)}{\max(X_j) - \min(X_j)} \text{ for benefit criteria,} \tag{2}$$

$$R_{ij} = \frac{\max(X_j) - X_{ij}}{\max(X_j) - \min(X_j)} \text{ for cost criteria,} \tag{3}$$

The weighted normalized score (W_{ij}) for each criterion (R_{ij}) is calculated by multiplying the normalized score by its corresponding weight (w_j)

$$W_{ij} = w_j \times R_{ij} \tag{4}$$

Afterwards, positive and negative ideal solutions are determined respectively as

$$D_i^+ = \sqrt{\sum_{j=1}^m (W_{ij} - P_j^*)^2} \tag{5}$$

$$D_i^- = \sqrt{\sum_{j=1}^m (W_{ij} - N_j^*)^2} \tag{6}$$

where P_j^* and N_j^* denote positive and negative ideal solutions, D_i^+ and D_i^- refer to the distances to the positive and negative ideal solutions, respectively. Finally, the alternatives are ranked in descending order employing the following formulation:

$$CC^* = \frac{D_i^-}{D_i^+ + D_i^-} \tag{7}$$

4. CASE STUDY

The key success factors for installing solar plants are determined as solar radiation, heat, altitude, slope, distance to roads, and distance to transformer center, by reviewing the literature and by the experts opinions.

In the next step, pairwise comparisons of the criteria are made. Table 1 is taken as reference during the scoring. The super matrix created before normalization is given in Table 2.

Table 2. The super matrix before normalization

Criteria	Solar Radiation	Heat	Altitude	Slope	Distance To Roads	Distance To Transformer Centers
Solar Radiation	1	4	3	2	6	4
Heat	1/4	1	3	3	5	2
Altitude	1/3	1/3	1	1/3	2	1/3
Slope	1/2	1/3	3	1	6	2
Distance To Roads	1/6	1/5	1/2	1/6	1	1/3
Distance To Transformer Centers	1/4	1/2	3	1/2	3	1
Total	2.50	6.36	13.50	7.00	23.00	9.66

The resulting super matrix is first normalized by the software. After normalization, the limit super matrix is obtained by taking the power of the super matrix by the software. The weights of the criteria were found with the super limit matrix. The final weights obtained are given in Table 3.

Table 3. Importance of key success factors

Criteria	Weights
Solar Radiation	0.38741
Heat	0.22418
Altitude	0.06842
Slope	0.16956
Distance To Roads	0.03825
Distance To Transformer Centers	0.11219

The evaluation of alternatives with respect to criteria are provided in Table 4.

Table 4. Evaluation of the alternatives

ALTERNATIVES	CRITERIA					
	Solar Radiation Solaire (kWh/m ²)	Heat (°C)	Altitude (m)	Slope (°)	Distance To Roads (m)	Distance To Transformer Centers (m)
Alternate 1	1718	11.7	1042	28	3500	9500
Alternate 2	1679	9.2	1122	27	2150	6550
Alternate 3	1907	18.5	650	27	300	12100
Alternate 4	1706	19.3	1212	28	640	5745
Alternate 5	1525	12.5	710	28	1275	2650
Weights	0.38741	0.22418	0.06842	0.16956	0.03825	0.11219

Once the decision matrix was created, the normalized decision matrix was created by applying the linear normalization process. By employing the TOPSIS method, the ranking of the alternatives is obtained as in Table 5.

Table 5. Ranking of the alternatives

Alternatives	Ranking Value	Rank
Alternate 1	0.449789169	3
Alternate 2	0.595919957	1
Alternate 3	0.371334753	4
Alternate 4	0.323738319	5
Alternate 5	0.485384166	2

It is seen from Table 3 that the most important key success factor is solar radiation followed by heat. Distance to roads is determined as the least important criteria. According to the results, Alternative 2 is determined as the most suitable solar plant location alternative.

4. CONCLUSIONS

In this study, the integration of ANP and TOPSIS methods is employed to determine the most suitable solar plant alternative in Turkey. ANP is employed to find the importance of key success factors for installing solar plants in the right area. The success factors are determined by reviewing the literature and by obtaining the experts opinions. According to the results of the ANP method, the most important performance indicator is solar radiation. Next comes the heat. Third, the slope. Fourth, the distance to transformation centers. Then comes the altitude and finally the distance to the roads. The ranking of alternatives is determined by using TOPSIS method. Employing different multi-criteria decision making methods for the power plant location selection problem can be the subject of the future researches.

Ethics Committee Approval

N/A

Peer-review

Externally peer-reviewed.

Author Contributions

Conceptualization: M.D., M.S.D.; Investigation: M.S.D.; Material and Methodology: M.S.D, N.G.; Supervision: M.D.; Visualization: M.S.D, N.G.; Writing-Original Draft: M.D., M.S.D, N.G.; Writing-review & Editing: M.D.; Other: All authors have read and agreed to the published version of manuscript.

Conflict of Interest

The authors have no conflicts of interest to declare.

Funding

This work has been financially supported by Galatasaray University Research Fund FOA-2022-1092.

REFERENCES

Hwang, C.L., Yoon, K. (1981). Multiple attributes decision making methods and applications. Springer, Berlin Heidelberg.

Kheybari, S., Rezaie, F. M., Farazmand, H. (2020). Analytic network process: An overview of applications. Applied Mathematics and Computation. 367, 124780.

Ozcan, E.C., Unlüsoy, S., Eren, T. (2017). ANP ve TOPSIS yöntemleriyle Türkiye'de yenilenebilir enerji yatırım alternatiflerinin değerlendirilmesi. Selçuk Üniversitesi Mühendislik, Bilim Ve Teknoloji Dergisi. 5 (2), 204-219.

Omurbek, N., Demirci, N., Akalin, P. (2014). Analitik ağ süreci ve TOPSIS yöntemleri ile bilimsel seçimi. Akademik Araştırmalar ve Çalışmalar Dergisi. 5 (9), 118-140.

Saaty, T. L. (1980). The analytic hierarchy process, McGraw-Hill, New York.

Effects of the Influencer Marketing on e-commerce

Feyza Cokak¹, Mehtap Dursun*¹, Nazli Goker¹

Abstract: E-commerce, or electronic commerce, refers to the buying and selling of goods or services using the internet, and the transfer of money and data to execute these transactions. It encompasses a wide range of businesses, from consumer-based retail sites, through auction or music sites, to business exchanges trading goods and services between corporations. Influencer marketing has become a pivotal element in the e-commerce landscape, profoundly impacting how brands engage with potential customers and boost sales. This study is designed to measure the impact of the influencer marketing industry on e-commerce in Turkey. The factors affecting sales, product views and product favorability in the e-commerce sector and the degree of influence of these factors are examined. For this purpose, commission rate, product price, product discount rate, influencer's compatibility with the brand, number of followers of the influencer, product narrative, product category and number of shares of the advertisement is analyzed in depth. Data are collected from experts in the e-commerce sector and these data are analyzed with the fuzzy cognitive map (FCM) method.

Keywords: Decision support systems, E-commerce, Influencer marketing, Fuzzy cognitive map

¹**Address:** Galatasaray University, Industrial Engineering Department, Istanbul/Türkiye

***Corresponding author:** mdursun@gsu.edu.tr

1. INTRODUCTION

Influencer marketing has become a significant strategy for e-commerce brands to reach and engage with their target audiences. It leverages the social credibility of influencers to enhance brand presence, engage with potential customers on a more personal level, and drive e-commerce sales. Influencer marketing has become an important marketing strategy for both brands and e-commerce platforms and an easy way to reach users.

Influencers have a large following on social media platforms. Collaborating with them helps e-commerce brands to reach a wider audience and increase brand visibility. Influencers often have established credibility with their followers. When they endorse a product, it can build trust and credibility for the e-commerce brand. Influencers can create engaging content that resonates with their audience, leading to higher engagement rates (likes, comments, shares) compared to traditional advertising methods. Brands can choose influencers whose audience aligns with their target market, ensuring that the marketing efforts are directed towards the right demographic. Compared to traditional advertising channels, influencer marketing can be more cost-effective, especially when micro-influencers are involved (Fast Company Executive Board, 2024).

Influencer marketing has become an important marketing strategy for both brands and e-commerce platforms and an easy way to reach users. In the study, Intuitionistic Fuzzy Cognitive Map Method (IFCM) is used to analyze the effect of the influencer marketing on e-commerce. This study aims to gain a new perspective on the future of the developing influencer marketing industry, to determine the points that e-commerce platforms in the sector can pay attention to while collaborating, to measure the trust of followers in influencers based on sales and views, and to contribute to the improvement of existing business processes according to the needs of the future. The rest of the study is as follows. Section 2 describes FCM method, case study is illustrated in Section 3. Finally, conclusions are provided at the last Section.

2. FUZZY COGNITIVE MAP

Fuzzy cognitive map (FCM) is a causal information-based tool that combines fuzzy logic and neural networks. The extension of the tool is provided by including fuzzy numbers or linguistic variables for expressing the causal links among concepts in the map. These concepts represent an entity, a state, a variable or a characteristic of a system, a behavior of the information-based system is denoted by concepts in FCM (Buyukavcu et al., 2016). Concept nodes and weighted arcs are the elements of FCM which can be graphically showed with feedback. Signed arcs indicate the sign of causality: whether the causal relationship is positive, negative or null; and connected nodes produce causal relationships among concepts. $C = \{C_1, C_2, \dots, C_n\}$ is the set of concepts, arcs (C_j, C_i) demonstrate how concept C_j

causes concept C_i , and are used for causal relationships between concepts. The weights of causality links range can be represented with linguistic variables such as “negatively medium”, “zero”, “positively medium”, etc. The value of each concept is computed, taking into account the effect of the other concepts on the under-evaluation concept, by applying the following iterative formulation (Buyukavcu et al., 2016).

$$A_i^{(k+1)} = f(A_i^{(k)} + \sum_{j=1, j \neq i}^n A_j^{(k)} w_{ij}) \tag{1}$$

where $A_i^{(k)}$ is the value of concept C_i at k^{th} iteration, w_{ji} is the weight of the connection from C_j to C_i and f is a threshold function.

3. CASE STUDY

The purpose of this analysis is to measure the success and impact of the influencer marketing industry in e-commerce and to make the industry more efficient by identifying the main points of this impact. For the analysis, 8 criteria, given in Table 1, are determined based on previous literature reviews and expert recommendations.

Table 1. Influencer Marketing Industry's Impact Factors on e-commerce

Label	Concept
<i>c1</i>	Conformity between influencer and brand/target audience
<i>c2</i>	Influencer's product description
<i>c3</i>	Category of product
<i>c4</i>	Price of product
<i>c5</i>	Discount status of product
<i>c6</i>	Number of shares of advertised product
<i>c7</i>	Number of influencers' followers
<i>c8</i>	Commission rate offered to influencer for advertising

To determine the causality relationship between the criteria, three experts working in Turkey's largest e-commerce site are interviewed and causality relationships are determined. The first version of the matrices collected from three decision-makers with linguistic items for causality measurement is given in Tables 2-4.

Table 2. Matrix of Linguistic Elements for Decision Maker 1

Expert 1	<i>c1</i>	<i>c2</i>	<i>c3</i>	<i>c4</i>	<i>c5</i>	<i>c6</i>	<i>c7</i>	<i>c8</i>
<i>c1</i>	z	pm	z	z	z	z	z	z
<i>c2</i>	z	z	z	z	z	pw	z	z
<i>c3</i>	z	z	z	pm	z	z	z	pw
<i>c4</i>	z	pm	z	z	pw	z	z	z
<i>c5</i>	z	ps	z	pvs	z	pm	z	z
<i>c6</i>	z	z	z	z	z	z	z	z
<i>c7</i>	ps	z	z	z	z	z	z	z
<i>c8</i>	z	ps	z	z	z	pvs	z	z

Table 3. Matrix of Linguistic Elements for Decision Maker 2

Expert 2	<i>c1</i>	<i>c2</i>	<i>c3</i>	<i>c4</i>	<i>c5</i>	<i>c6</i>	<i>c7</i>	<i>c8</i>
<i>c1</i>	z	ps	ps	z	z	z	z	z
<i>c2</i>	pw	z	z	z	z	z	z	z
<i>c3</i>	z	ps	z	ps	z	z	z	z
<i>c4</i>	z	ps	z	z	z	z	z	z
<i>c5</i>	z	ps	z	pvs	z	pm	z	z
<i>c6</i>	z	z	z	z	z	z	z	z
<i>c7</i>	pw	z	z	z	z	pw	z	z
<i>c8</i>	z	ps	z	z	z	pvs	z	z

Table 4. Matrix of linguistic elements for Decision Maker 3

<i>Expert 3</i>	<i>c1</i>	<i>c2</i>	<i>c3</i>	<i>c4</i>	<i>c5</i>	<i>c6</i>	<i>c7</i>	<i>c8</i>
<i>c1</i>	z	pm	pw	z	z	z	z	z
<i>c2</i>	pm	z	z	z	z	z	z	z
<i>c3</i>	z	pm	z	ps	pw	pm	z	z
<i>c4</i>	z	z	z	z	z	z	z	z
<i>c5</i>	z	z	z	ps	z	z	z	z
<i>c6</i>	z	z	z	z	z	z	z	z
<i>c7</i>	pw	z	z	z	z	z	z	z
<i>c8</i>	z	pvs	z	z	z	pvs	z	z

After the 10th iteration on average, the system stabilized and the weights of the concepts are shown in Table 5.

Table 5. Weights of criteria for the impact of the influencer marketing industry on e-commerce.

Criteria	Weights
<i>c1</i>	0.79618
<i>c2</i>	0.94762
<i>c3</i>	0.73382
<i>c4</i>	0.86966
<i>c5</i>	0.71388
<i>c6</i>	0.88937
<i>c7</i>	0.65905
<i>c8</i>	0.68497

There are a total of 18 relationships between 8 criteria in the system. According to the results, influencer’s product description is determined the most important factor, which is followed by number of shares and price.

4. CONCLUSIONS

Influencer marketing has become an important marketing strategy for both brands and e-commerce platforms and an easy way to reach users. In the study, fuzzy cognitive map method is used to analyze the effect of the influencer marketing on e-commerce. Influencer’s product description, number of shares, and price of product is determined as the most important factors however number of followers and commission rate are the least important criteria. Future research will focus on proposing other group decision making approaches for determining the effects of influencer marketing on e-commerce.

Ethics Committee Approval

N/A

Peer-review

Externally peer-reviewed.

Author Contributions

Conceptualization: M.D., F.C.; Investigation: F.C.; Material and Methodology: F.C., N.G.; Supervision: M.D.; Visualization: F.C., N.G.; Writing-Original Draft: M.D., F.C., N.G.; Writing-review & Editing: M.D.; Other: All authors have read and agreed to the published version of manuscript.

Conflict of Interest

The authors have no conflicts of interest to declare.

Funding

This work has been financially supported by Galatasaray University Research Fund FOA-2022-1092.

REFERENCES

Buyukavcu, A., Albayrak, E. ve Göker, N. (2016). A fuzzy information-based approach for breast cancer risk factors assessment. *Applied Soft Computing* . 38, 437-452.

Fast Company Executive Board (2024). The role of influencer marketing in the growth of e-commerce. <https://www.fastcompany.com/91009313/the-role-of-influencer-marketing-in-the-growth-of-e-commerce> (accessed 01 July 2024).

Influencer Marketing Hub. (2024). Influencer Marketing News and Resources. <https://influencermarketinghub.com/influencermarketing/> (accessed 01 July 2024).

Eco-Friendly Wool Dyeing Using Pistachio Soft Shell Extract

Enfal Kayahan *¹

Abstract: Natural dyes are increasingly popular due to their expected low risk to human health, environmental benefits, and biodegradability. Natural dyes can be derived from plants that are cultivated for commercial purposes. Additionally, production waste products present ever-growing potential as new sources of natural dyes for coloring materials such as textiles (Nambela et al., 2020). This innovative approach to waste minimization through source reduction is gaining attention. In this regard, the use of agricultural waste as a natural dye source in textile dyeing and its industrial adaptation is an ongoing research topic (Adeel et al., 2018; Hosseinezhad et al., 2021). While some studies examine the utilisation of diverse waste materials as a natural dye source, others focus on the development of natural dyeing processes with high fastness for a range of fibre types. In this study, the potential of using colored liquid extract from pistachio nut (*Pistacia vera*) soft shells as a natural dye for textile fabrics was investigated. Pistachios are an agricultural product of significant economic importance, primarily used as food. The soft shell of pistachios constitutes approximately 35-45% of the fruit and is classified as waste with no commercial value.

In the study, the potential of using extract from pistachio nut (*Pistacia vera*) soft shells as a natural dye for wool was explored. Important operating parameters namely extraction time, dyeing time, and mordant concentration were optimized in terms of CIELab (L^* , a^* and b^*) values. The effect of various metal salts ferrous sulfate (FeSO_4), calcium carbonate (CaCO_3), alum ($\text{Al}_2(\text{SO}_4)_3$), potassium sodium tartrate $\text{KNaC}_4\text{H}_4\text{O}_6$, magnesium chloride (MgCl_2) was used as mordant and (citric acid ($\text{C}_6\text{H}_8\text{O}_7$)) were used to change the surface charge character of textile materials. Use of different metal salts has improved color characteristics and fastness properties of dyed textile materials. The color of dyed woolen yarn was investigated in terms of CIELab (L^* , a^* and b^*) and K/S values; and fastness properties were determined as per ISO and AATCC standard test methods. Fastness properties of dyed wool samples was comparatively evaluated. Dyeing experiments were performed with and without mordants, using co-mordanting technique. A beautiful color palette with various shades and tones was achieved using different non-toxic mordants. The dyed samples were evaluated for color fastness, revealing very good wash fastness and typical light fastness for natural dyes without mordants.

Keywords: Mordant. Natural Dyes. Wool. (*Pistacia vera*) soft shells. Fastness. Colorimetric properties. Sustainability.

¹**Address:** Pamukkale University, Faculty of Engineering, Department of Textile Engineering, Denizli, Turkey

***Corresponding author:** ekayahan@pau.edu.tr

1. INTRODUCTION

Prioritizing research on the utilization of agricultural waste can help reduce waste and offer additional income opportunities for farmers and processing industries (Hazarika et al., 2017a). Food and beverage industry waste, such as pressed berries and grapes, distillation residues from liquor production, and vegetable processing peels, has been utilized to extract natural dyes for dyeing woolen yarn (Bechtold et al., 2006, 2007). Additionally, pomegranate rind has been used to dye cotton fabrics, with sodium chloride serving as the mordant, resulting in dyes with good fastness properties. Natural dye extracted from temple waste flowers (*Tagetes erecta*) was used to dye cotton, silk, and wool fabrics in combination with various metal mordants (Vankar & Shanker, 2009). Similarly, natural dye from temple waste marigold flowers was employed to dye soybean protein fabrics using alum ($\text{KAl}(\text{SO}_4)_2$), harda, tamarind seed coat, and amla as mordants (Teli et al., n.d.). Banana sap, derived from agro-waste, has been identified as an alternative to *Bridelia* dye used by the local Adinkra cloth industry in Ghana (Dzomeku and Boateng, 2013). Additionally, natural dyes extracted from guinea corn leaves and onion skin were used to dye cotton fabrics with the inclusion of mordants such as potassium dichromate, alum, iron sulfate, and stannous chloride (Osabohien, 2014).

Several agricultural wastes have been recognized as sources of natural dyes for various applications. However, only a limited selection of brands and shades is currently available on the market. This is primarily because of the low dye yield from natural sources and the limited availability of raw materials (Hazarika et al., 2017b). Additionally, only a few

exhibit strong binding properties with textile fibers. The demand for naturally dyed fabrics is rising due to customer concerns about skin safety and environmental impact.

Agricultural waste can be used as a dye in the textile industry if it is abundant, offers sufficient dye yield, and has good fastness properties.

In this study, dye solution was extracted from pistachio (*Pistacia vera L.*) soft shells and used to dye bleached wool yarns with non-toxic metal salts using the exhaustion method. The color values and fastness properties of the dyed fabrics were also examined. The goal of this research is to utilize pistachio soft shells as a dye for textiles, thereby adding value to both textiles and pistachio processing waste.

2. MATERIAL AND METHOD / MATERYAL VE METOT

2.1. Materials

In the study, bleached 100% wool yarn (Nm 8/2) was provided by Ipliksan Corp., Turkey. Analytical grade ferrous sulfate (FeSO_4), calcium carbonate (CaCO_3), alum ($\text{KAl}(\text{SO}_4)_2$) magnesium chloride (MgCl_2) and citric acid ($\text{C}_6\text{H}_8\text{O}_7$) used as mordants (Merck, Germany). The pistachio (*Pistacia vera L.*) soft shell vegetable waste used as a dye source in the research was provided by a local enterprise.

The color of dyed woolen yarn was investigated in terms of CIE Lab (L^* , a^* and b^*) and K/S values; and fastness properties were determined as per ISO and AATCC standard test methods. Fastness properties of dyed wool samples was comparatively evaluated. Dyeing experiments were performed with and without mordants, using co-mordanting technique. A beautiful color palette with various shades and tones was achieved using different non-toxic mordants. The dyed samples were evaluated for color fastness, revealing very good wash fastness and typical light fastness for natural dyes without mordants.

2.2. Method

2.2.1. Optimization of extraction time

Optimization of extraction times for plant dyes was carried out in this study. In this step, 2 grams of dried and weighed vegetable waste were extracted with 20 mL of water under reflux in a beaker, using a 1:10 liquor ratio, chosen to match typical industrial dyeing machine operating ratios. The waste materials were boiled for durations ranging from 1 to 5 hours, with intervals of 1 hour. The resulting solution was then filtered to remove any residues. The dyestuffs were transferred into the aqueous phase, and 2-gram wool yarn samples were dyed using four distinct dyestuff solutions, maintaining a waste-to-wool ratio of 1:1. The wool yarns were dyed in the dyestuff solutions for 1 hour. After dyeing, the samples were washed with a 1 g/L olive oil soap solution at 40°C for 30 minutes, followed by two rinses with cold water. The olive oil soap was provided by Aytteks Chemical Company. The CIE Lab values of the yarns were measured using a Datacolor 600 spectrophotometer (Datacolor AG, Switzerland). A chart was generated from the data, indicating that the optimum extraction time corresponds to the lowest L^* value.

2.2.2. Optimization of dyeing times

Optimization of dyeing times involved preparing dye solutions based on previously determined optimal extraction time. Two grams of raw wool yarns were dyed using a 1:10 liquor ratio through the exhaust method, with dyeing durations ranging from 30 to 120 minutes at 15-minute intervals. After dyeing, the samples were rinsed with distilled water, treated with olive oil soap, and dried at room temperature. The colors of the dyed samples were assessed by generating a graph based on the measured L^* values. The darkest point where the color tone remained constant was identified as the optimal dyeing time.

2.2.3. Optimization of mordant amount

Multivalent metal salts such as aluminum, iron, copper, chromium, and tin are commonly used as mordants in natural dyeing processes. However, heavy metals pose toxic and harmful effects on human health and the environment. According to Directive 2006/11/EC concerning 'Pollution caused by certain dangerous substances discharged into the aquatic environment of the Community,' 22 metals are classified as dangerous substances. These include zinc, copper, nickel, chromium, lead, tin, selenium, vanadium, arsenic, barium, cobalt, antimony, beryllium, thallium, molybdenum, boron, tellurium, titanium, uranium, silver, mercury, and cadmium. Notably, mordants like zinc, copper, nickel, chromium, lead, and tin, commonly used in natural dyeing processes, fall within this category (Karaboyaci, 2014). Although natural dyes are eco-friendly, the dyeing process can become non-eco-friendly if heavy-metal mordants are

used. These include Chromium 6 (carcinogenic), Copper sulfate (toxic and corrosive to skin and eyes), Stannous chloride (cytotoxic and genotoxic), Zinc sulfate (aquatic toxicant), and Zinc chloride (marine pollutant) (Amutha et al., 2022).

In this study, the selection of mordants was made carefully from non-toxic metal salts. Some acidic and basic compounds were utilized to modify the charge of fibers and dyes to enhance their affinity. Altering surface charges can increase adsorption through hydrogen bonding and Van der Waals forces (Karaboyaci, 2014).

During the dyeing procedure, mordants were added directly to the dye baths obtained through extraction and stirred for 5 minutes until fully dissolved, using the co-mordanting method. Wool yarns were then added to these dye baths, and the dyeing processes were performed according to the dyeing diagram shown in Figure 1.

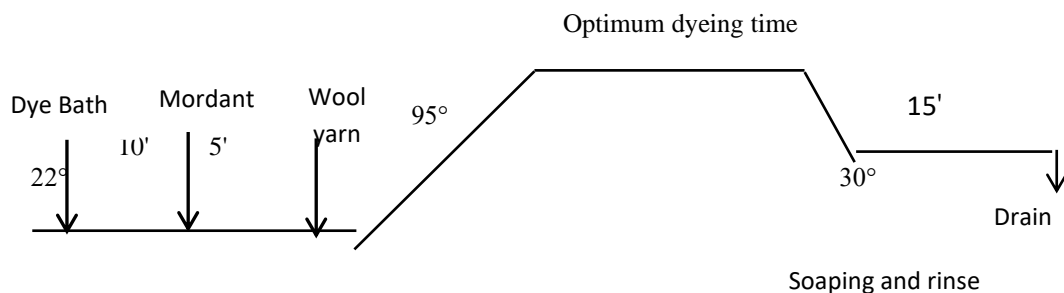


Fig.1 Dyeing diagram for wool samples

2.2.4. Fastness properties

The washing fastness properties of the dyed samples were assessed according to EN ISO 105-C01 in the textile engineering department laboratory at Pamukkale University. The differences between the control fabric and the multi-fiber fabric before and after washing were visually compared using the gray scale in accordance with ISO 105-A02:1993 (ISO, 2005'a) and ISO 105-A03:1993 (ISO, 2005b) standards. The rating scale ranged from 0 (poor) to 5 (excellent). The fastness to rubbing was evaluated in the textile engineering department laboratory at Suleyman Demirel University, using a crockmeter instrument as per the ISO 105-X12:2001 standard (ISO, 2001). The staining of the cotton rubbing cloths was assessed with the gray scale for staining under appropriate illumination (ISO 105-A01:1994). The crocking square evaluations were conducted according to ISO 105-A03:1993 (ISO, 2005b), with the rating scale ranging from 0 (poor) to 5 (excellent). A minimum acceptable rating of 3.0 was set.

The dyed samples were also subjected to perspiration fastness tests under both acidic and basic conditions in accordance with the ISO 105-E04 standard. Additionally, the saliva fastness test was performed according to the DIN 53160-1 standard. In this test, filter paper soaked in acidic and basic solutions, as specified in the standard, was placed on the surface of the dyed samples. Color changes in the samples and staining on the filter papers were then evaluated.

3. Results And Discussion

3.1 Optimization Of Extraction Time

In this stage of the study, the goal is to determine the conditions for obtaining the optimum color yield from the Pistachio (*Pistacia vera* L.) soft shell extract. Figure 2 shows the L^* values of wool yarn samples dyed with the dyestuff extracted from Pistachio soft shell at different times. As stated previously, the L^* axis values indicate the degree of darkness or brightness of the color. It is clear that the lowest L^* values are observed at 3 hours. Therefore, it is concluded that using an aqueous medium for the isolation of the colorant and extracting the Pistachio soft shell waste for 3 hours results in the highest color yield. The obtained data was used to obtain the dye solutions in subsequent dyeing steps.

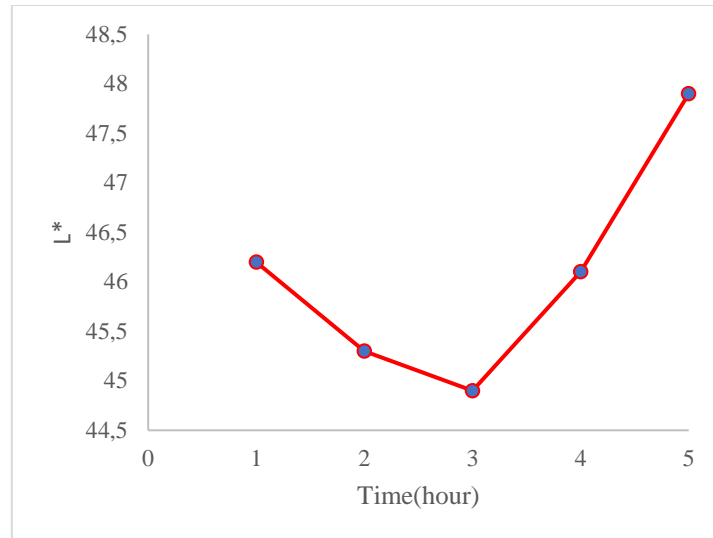


Fig. 2 The optimum extraction time for wool fibers using pistachio (*Pistacia vera* L.) soft shell waste

3.2. Optimization of Dyeing Time

In the initial stage of the experimental process, we determined the optimal extraction time for the soft shell waste. During this phase, we also established the optimal dyeing time for the wool fiber. As previously mentioned, the lowest L* value of the dyed samples indicates the optimal time for achieving maximum color yield. The optimal dyeing time for the samples dyed with Pistachio (*Pistacia vera* L.) soft shell waste extract was found to be 60 minutes. L values of wool samples dyed at different time intervals are presented in Figure 3.

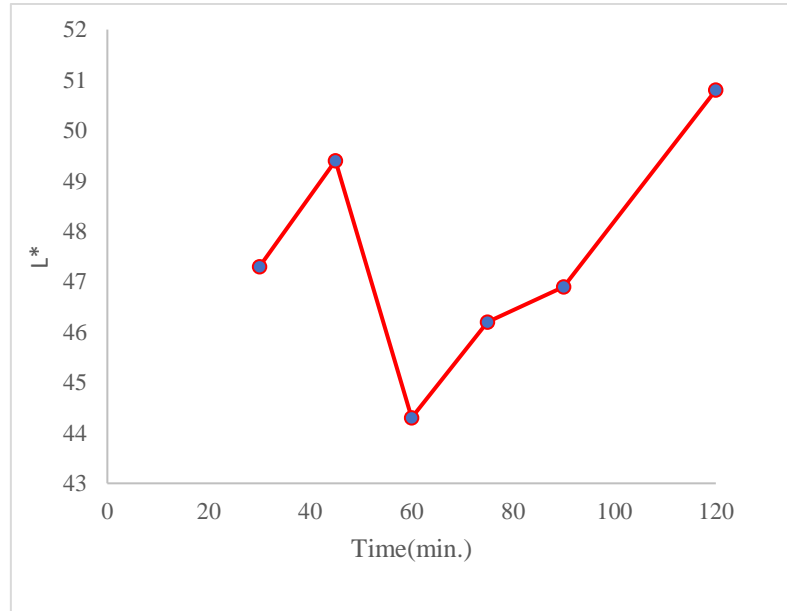


Fig. 3 The optimum dyeing time for wool samples using pistachio (*Pistacia vera* L.) soft shell waste

3.3. Optimization of Mordant Amount

In the process of determining the optimum mordant amounts, dyeing experiments were conducted using various concentrations of mordants. The L* values and optimum mordant amounts for wool samples dyed with different types and concentrations of mordants are presented in Table 1. According to the results, the optimum mordant amounts were determined to be 1 g/L for alum ($KAl(SO_4)_2$), 3 g/L for calcium carbonate ($CaCO_3$), and 5 g/L for ferrous sulfate ($FeSO_4$), magnesium chloride ($MgCl_2$) and citric acid ($C_6H_8O_7$), respectively.

Table 1 Color differences with different mordant types and concentrations on dyed wool samples

Mordant Type	Concentration (g/L)	Sample Code	L*	a*	b*
Alum	1	W1a	58,75	8,17	7,98
	3	W2a	60,1	9,82	7,47
	5	W3a	62,2	9,02	7,84
CaCO ₃	1	W1b	57,66	8,21	20,14
	3	W2b	55,34	8,51	20,12
	5	W3b	57,81	8,57	18,25
FeSO ₄	1	W1c	35,6	1,74	3,22
	3	W2c	36,9	1,06	2,87
	5	W3c	31,62	1,42	3,5
Citric acid	1	W1d	55,31	12,54	10,23
	3	W2d	54,29	1,42	10,77
	5	W3d	53,22	11,75	11,98
MgCl ₂	1	W1e	57,38	10,72	14,52
	3	W2e	57,04	10,34	14,07
	5	W3e	56,54	10,92	13,34

The color strength (K/S) behavior of wool samples dyed with soft bark waste extracts is shown in Figure 4. As illustrated in the figure, the K/S value of the wool sample dyed without a mordant is relatively high. This is likely due to the presence of numerous functional groups in the wool fiber structure, which facilitate interaction with anionic dyes (Cage, 2001). In this study, FeSO₄, citric acid, and MgCl₂ demonstrated the best performance as mordants, while the extract from pistachio (*Pistacia vera* L.) soft shell waste exhibited excellent performance as an environmentally friendly dye.

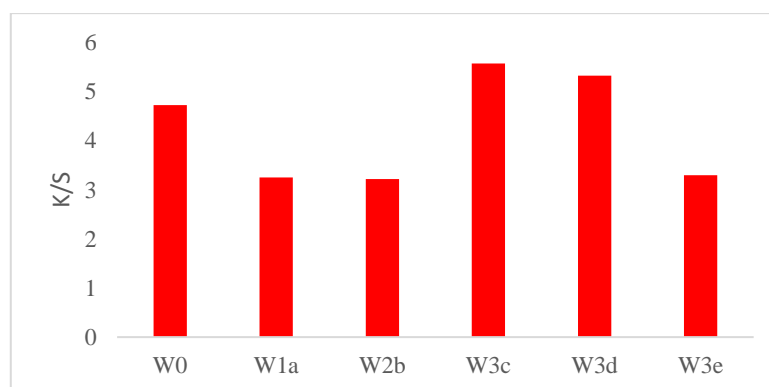


Fig. 4. K/S values (at 400 nm) of samples dyed with Pistachio (*Pistacia vera* L.) Soft Shell waste extract according to various mordant concentrations.

3.4. Fastness Properties and Dyeing Outcomes

The fastness values for the dyed textile products are presented in Table 2. FeSO₄ produced a tone close to black, while other mordants and the untreated sample resulted in light and dark red tones. The fastness values for all mordant types are listed. Upon reviewing Table 2, it is evident that the washing, rubbing, perspiration, and light fastness values for alum (KAl(SO₄)₂) and CaCO₃ are higher compared to the other mordants.

Table 2. Wash, Rubbing, Perspiration and Light Fastness properties of the dyed wool samples.




Mordant	Concentration (g/L)	Sample Code	^a Washing Fastness		^b Rubbing Fastness		^c Perspiration Fastness		^d Light Fastness
			Fading	Staining	Dry	Wet	Acidic	Alkaline	
	Control	W0	4	5	4	4	4	4/5	5
Alum	1	W1a	4	5	5	5	5	5	4
	3	W2a	4	5	5	5	5	5	5
	5	W3a	4	5	5	5	5	5	4
CaCO ₃	1	W1b	4/5	5	5	5	5	5	4
	3	W2b	4/5	5	5	5	5	5	4
	5	W3b	4/5	5	5	5	5	5	3/4
FeSO ₄	1	W1c	3	4	5	4/5	5	3/4	4
	3	W2c	3/4	4/5	5	4/5	4	4	4
	5	W3c	3/4	4/5	4/5	4/5	4	4	3
Citric acid	1	W1d	3	4	4/5	4/5	3	4	4
	3	W2d	3	4	4/5	4/5	3	4	3
	5	W3d	4	4	4/5	4/5	4	4	4/5
MgCl ₂	1	W1e	4	4	4/5	4/5	5	5	4/5
	3	W2e	4	5	4/5	4/5	4	5	5
	5	W3e	4	5	4/5	4/5	4	5	4

^aWash and ^bRub fastness 1 = poor, 5 = very good, ^cPerspiration Fastness, ^dLight fastness 1 = very poor, 8 = outstanding Arjeh et al., (2020) reported the main phenolic compounds of soft shell extract (*Pistacia vera* L.) as follows: gallic acid, 4-hydroxybenzoic acid, protocatechuic acid, naringin, eriodictyol- 7-O-glucoside, isorhamnetin-7-O-glucoside, quercetin-3-O-rutinoside, isorhamnetin-3-O-glucoside and catechin(Arjeh et al., 2020).

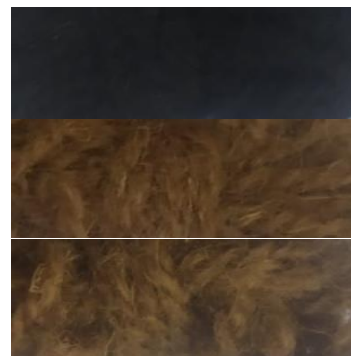
Gallic acid and quercetin, present in Pistachio (*Pistacia vera* L.) soft shell extract, are natural dyes that contain chromophore and oxochrome groups (*Eco-Friendly Dyeing of Fabric and Wool Yarn Samples with Morus*, n.d.). In textile dyeing, natural dyes bind to textile fibers by forming complexes with multivalent metal salts(Karaboyaci, 2014). Mordants are crucial agents in natural dyeing processes as they enhance the dye's adherence to fibers or fabrics and improve the fastness of dyed materials. In this study, ferrous sulfate (FeSO₄), calcium carbonate (CaCO₃), alum (KAl(SO₄)₂) and magnesium chloride (MgCl₂) metal salts were utilized as mordants. The free amino (-NH₂) and carboxyl (-COOH) groups present in wool yarns are particularly suitable for forming complexes with metals.

In this study, a variety of colors in red-orange, red-brown and black tones were achieved in wool yarns. All textile samples dyed with Pistachio (*Pistacia vera* L.) soft shell waste extract are shown in table 3.

Table 3. The color tones of dyed samples with pistachio (*Pistacia vera* L.) soft shell waste extracts with different mordant at 400 λ (nm)

Mordant	K/S	Concentration(g/L)	Sample Code	Colour
Control	4,7278	-	W0	
Alum	3,2547	1	W1a	
CaCO ₃	3,2181	3	W2b	

FeSO ₄	4,5782	5	W3c
Citric Acid	5,3228	5	W3d
MgCl ₂	3,2987	5	W3e



4. DISCUSSION AND CONCLUSIONS

Natural dyes offer a sustainable and cost-effective alternative to synthetic dyes. In this study, an aqueous extract of pistachio (*Pistacia vera* L.) soft shell was used for dyeing wool yarn. The process yielded red/brown and black color tones by employing non-toxic metal salts. The dyed samples demonstrated satisfactory performance in washing, rubbing, perspiration, and light fastness tests (Amutha et al., 2022). Consequently, given that pistachio soft shell extract is a natural and readily available resource, it can be considered an eco-friendly and economical option for textile dyeing.

Conflict of Interest

The author has no conflicts of interest to declare.

Funding

The author declared that this study has received no financial support.

REFERENCES

- Amutha, K., Annapoorani, S. G., Sakthivel, P., & Sudhapriya, N. (2022). Ecofriendly Dyeing of Textiles with Natural Dyes Extracted from Commercial Food Processing Waste Materials. *Journal of Natural Fibers*, 19(15), 10394–10411. <https://doi.org/10.1080/15440478.2021.1993506>
- Arjeh, E., Akhavan, H.-R., Barzegar, M., & Carbonell-Barrachina, Á. A. (2020). Bio-active compounds and functional properties of pistachio hull: A review. *Trends in Food Science & Technology*, 97, 55–64. <https://doi.org/10.1016/j.tifs.2019.12.031>
- Bechtold, T., Mahmud-Ali, A., & Mussak, R. (2007). Anthocyanin dyes extracted from grape pomace for the purpose of textile dyeing. *Journal of the Science of Food and Agriculture*, 87(14), 2589–2595. <https://doi.org/10.1002/jsfa.3013>
- Bechtold, T., Mussak, R., Mahmud-Ali, A., Ganglberger, E., & Geissler, S. (2006). Extraction of natural dyes for textile dyeing from coloured plant wastes released from the food and beverage industry. *Journal of the Science of Food and Agriculture*, 86(2), 233–242. <https://doi.org/10.1002/jsfa.2360>
- Cage, S. (2001). *Dyeing of wool and other natural fibres with natural dyes. Eco-friendly dyeing of fabric and wool yarn samples with Morus*. (n.d.). Hazarika, D., Gogoi, N., Jose, S., Das, R., & Basu, G. (2017a). Exploration of future prospects of Indian pineapple leaf, an agro waste for textile application. *Journal of Cleaner Production*, 141, 580–586. <https://doi.org/10.1016/j.jclepro.2016.09.092>
- Hazarika, D., Gogoi, N., Jose, S., Das, R., & Basu, G. (2017b). Exploration of future prospects of Indian pineapple leaf, an agro waste for textile application. *Journal of Cleaner Production*, 141, 580–586. <https://doi.org/10.1016/j.jclepro.2016.09.092>
- Karaboyaci, M. (2014). Recycling of rose wastes for use in natural plant dye and industrial applications. *Journal of the Textile Institute*, 1–7. <https://doi.org/10.1080/00405000.2013.876153>
- Osabohien, E. (2014). Extraction and Utilization of Natural Dyestuffs from the Bark of Whistling Pine and the Root of African Peach. *British Journal of Applied Science & Technology*, 4(20), 2921–2930. <https://doi.org/10.9734/BJAST/2014/8554>

Teli, M. D., Sheikh, J., & Kamble, M. (n.d.). *Ecofriendly Dyeing and Antibacterial Finishing of Soyabean Protein Fabric Using Waste Flowers from Temples*. www.tlist-journal.org

Vankar, P. S., & Shanker, R. (2009). Eco-friendly pretreatment of silk fabric for dyeing with *Delonix regia* extract. *Coloration Technology*, 125(3), 155–160. <https://doi.org/10.1111/j.1478-4408.2009.00189.x>

Real-Time Detection of Improperly Parked Vehicles with Unmanned Aerial Vehicles and Acceleration of Emergency Response Processes

Mustafa Melikşah Özmen*¹, Muzaffer Eylence², Bekir AKSOY³

Abstract: Improperly parked vehicles cause serious problems, especially in emergency situations. Ambulances, fire trucks and other emergency teams have difficulty performing their duties due to improperly parked vehicles, which can extend response times and potentially cause loss of life. It is possible to produce an effective solution to solve this problem by taking advantage of the opportunities offered by technology. In the study being developed, it is aimed to detect vehicles parked in wrong places using Unmanned Aerial Vehicles and to create a warning system for removing these vehicles. This system will operate in real time and help speed up emergency responses. Within the scope of the study, a special data set consisting of images collected via unmanned aerial vehicle will be created. This data set will be used to train artificial intelligence models that will be used to detect improperly parked vehicles. The performance of the trained models will be evaluated by comparing them with other existing models. The unmanned aerial vehicle will be equipped with high-resolution cameras and will detect improperly parked vehicles by flying over roads in certain areas. The images will be analyzed by the trained artificial intelligence model and incorrectly parked vehicles will be automatically identified. Detected incorrectly parked vehicles will be immediately reported to vehicle owners and authorities, and the vehicles will be removed quickly. This system will significantly shorten response times by keeping the roads clear for emergency response teams. This study will make a great contribution to regulating urban traffic and performing emergency interventions more effectively. The special data set and trained models to be used will be compared with other existing systems to ensure the highest accuracy and efficiency. As a result, this technology will both facilitate the work of security forces and improve the quality of life in the city

Keywords: Artificial intelligence, Image processing,

¹**Address:** Isparta University of Applied Sciences, Faculty of Technology, Isparta/Turkiye

²**Address:** Isparta University of Applied Sciences, Faculty of Technology, Isparta/Turkiye

³**Address:** Isparta University of Applied Sciences, Faculty of Technology, Isparta/Turkiye

***Corresponding author:** cadet.2045@gmail.com

1. INTRODUCTION

The rapidly increasing number of vehicles and limited parking spaces in cities are leading to various problems that negatively impact traffic regulation and reduce the effectiveness of emergency response teams [1]. Particularly, illegally parked vehicles have become a significant issue with serious consequences for traffic order and safety [2]. Vehicles parked incorrectly, especially on narrow streets and along main roads, obstruct traffic flow and hinder emergency responses [3]. For ambulances, fire trucks, police, and other emergency vehicles to perform their duties in the shortest time possible, roads must remain clear.

For example, a study conducted in the United Kingdom found that fire trucks were delayed in reaching the scene due to illegally parked vehicles [4]. The frequency of such delays is higher in major cities and densely populated areas. Another incident occurred in Paris, France, in 2017, where fire crews struggled to reach a burning building due to vehicles parked on the streets [5]. Similarly, in Berlin, Germany, in 2020, emergency vehicles faced delays, especially during working hours when the city is busiest, due to vehicles parked incorrectly on narrow streets. To reduce such incidents, the Berlin Fire Department initiated fines and public awareness campaigns [6].

Therefore, preventing illegally parked vehicles can expedite emergency response times, reduce casualties and property damage, and contribute to increased public safety.

This study aims to detect and prevent illegally parked vehicles using artificial intelligence (AI) image processing technology via unmanned aerial vehicles (UAVs). In recent years, AI and image processing technology, especially with deep learning algorithms, have rapidly advanced and can successfully perform complex tasks such as object detection and recognition [7].

Current methods for detecting illegally parked vehicles generally rely on fixed security cameras and manual inspections. However, these methods can be time-consuming and costly and do not provide equal access to all areas [8]. To address these shortcomings, the use of UAVs to capture real-time images and detect illegally parked vehicles using AI and image processing techniques is proposed.

In this study, UAVs were used to collect a unique dataset from various urban areas, such as city centers, streets, and narrow passages, to improve urban traffic regulation and enhance the efficiency of emergency responses. This unique dataset was trained on a CNN-based deep learning model.

The study demonstrated the potential of AI and image processing techniques to improve urban traffic regulation and expedite emergency responses. The unique dataset collected using UAVs was successfully processed with the developed CNN-based deep learning model, achieving high accuracy in detecting illegally parked vehicles.

2. MATERIAL AND METHOD

2.1. Material

The workflow process followed in the study is shown in Figure 1. In the initial phase of the study, the data sets required for training artificial intelligence models were collected. These collected data sets were made suitable for training by passing through data pre-processing stages before model training. Then, training was performed using three different models and the results obtained by these models were compared with each other.

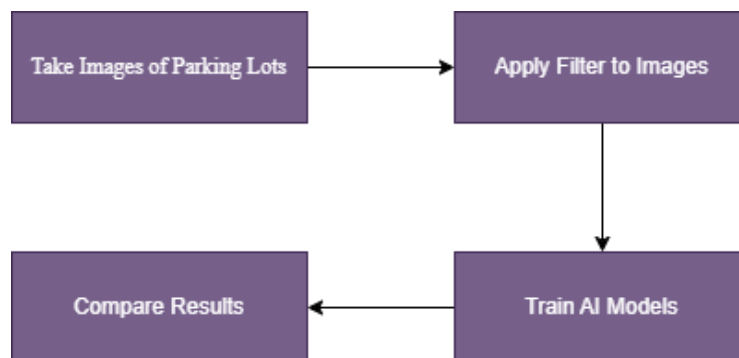


Figure 1: Work flow chart

2.1.1. Dataset

In the study conducted, the dataset to be used for the detection of incorrectly parked vehicles in parking areas was obtained from our own footage. These images include vehicles parked outside of designated parking spaces or incorrectly. The images in the dataset were recorded in color at 240x240 dimensions. The collected images were subjected to Gaussian filter and normalization processes in order to reduce noise and interference on them. The dataset, which consists of a total of 1458 images, consists of 954 correctly parked vehicles and 504 incorrectly parked vehicles. Figure 2 presents a sample image from the dataset.



Figure 2: Sample image of dataset

2.1.2. CNN

Convolutional Neural Networks (CNNs) are a widely preferred method in the field of deep learning, especially in image processing and computer vision applications. In recent years, research on CNNs has focused on various architectural structures and optimization strategies of these networks and aims to increase their performance. For example, a study conducted in 2023 proposed the integration of deep attention mechanisms in order to increase the accuracy of CNNs without increasing their complexity [9]. Another study addressed the effective use of transfer learning methods to shorten the training time of CNNs and increase their overall performance [10]. In addition, a study in the field of biomedical image processing has shown that CNNs can achieve high levels of accuracy in the diagnosis of critical health problems such as COVID-19 [11]. Another study on autonomous systems has shown that CNNs exhibit reliable performance despite complex environmental conditions in applications such as automated vehicle driving [12]. Finally, Zhang et al.'s work presented an innovative framework to increase the scalability and efficiency of CNNs on large datasets, discussing how these networks can be adapted to various data types and environments [13]. This research demonstrates how flexible and powerful CNNs are across a wide range of applications and offers many potential development paths for future work.

2.1.3. MobileNet V3

MobileNet V3 is a convolutional neural network (CNN) architecture that stands out with its lightness and efficiency among deep learning models. Studies after 2023 have proposed various improvements and optimizations to further increase the performance and effectiveness of this architecture in various application areas. For example, in one study, MobileNet V3 was used in real-time image classification and diagnosis tasks in the field of health, and it was determined that it provided high accuracy and low latency [14]. Another study revealed that this architecture showed superior performance in environmental perception and object recognition tasks when used in autonomous vehicle systems [15]. In addition, in a study where MobileNet V3 was used to increase task efficiency in resource-limited devices such as drones and mobile robots, it was emphasized that it increased the processing capacity of these devices without sacrificing performance while extending the battery life [16]. In addition, in another study on the architectural optimizations of MobileNet V3, it was shown that quantization techniques can be effectively applied to further reduce computational costs while preserving the accuracy of the network [17]. Finally, the use of MobileNet V3 in product recommendation systems in the commerce and e-commerce sectors was investigated and it was found that it provides fast and accurate image-based recommendations to improve user experience [18]. These studies show that MobileNet V3 offers flexibility and high performance in a wide range of applications and can be further optimized and used in different areas in the future.

2.1.4. YOLO v8

YOLOv8 stands out as a state-of-the-art algorithm in the field of object detection, and studies conducted after 2023 have developed different approaches to improve the performance of this model in various industrial and research applications. For example, a study has shown that YOLOv8 is used to detect weeds in the agricultural field, which provides significant improvements in farm management and efficiency [19]. Another study has found that reliability and accuracy are increased by using YOLOv8 in infrastructure detection and assessment tasks in drone-based inspection systems [20]. In addition, YOLOv8 has been used in industrial applications, especially in defect detection in production lines, and it has been reported that it works with low error rates in real time [21]. Another study focusing on the healthcare sector has revealed that this model is used in critical tasks such as tumor detection in medical images, and provides high precision and speed [22]. Finally, it has been stated that YOLOv8 is applied in traffic monitoring and analysis tasks in smart city projects, and thus data collection processes are greatly improved to optimize traffic flow and prevent accidents [23]. These studies show that YOLOv8 sets a new standard in object detection with its versatile use cases and superior performance. The architecture of YOLOv8 is shown in Figure 5.

2.2. Method

In the study, an artificial intelligence-based object detection model was developed to detect vehicles parked incorrectly in parking areas. For the training of the developed model, photographs of correctly and incorrectly parked vehicles in various parking areas were taken one by one. In order to reduce the noise and interference in the captured photographs, a Gaussian filter was applied to make the images suitable for model training. For model training, the images were resized to 224x224x3 in order to reduce the costs during model training. In model training, parameters such as epoch number, batch size value, learning rate were kept the same in all models in order to make the comparison of different models fair and objective. The training of all models was performed on a computer with an Intel Core i7 2.4GHz processor.

3. RESULTS

The accuracy graph of the artificial intelligence models that completed the training in the study is shown in Figure 3.

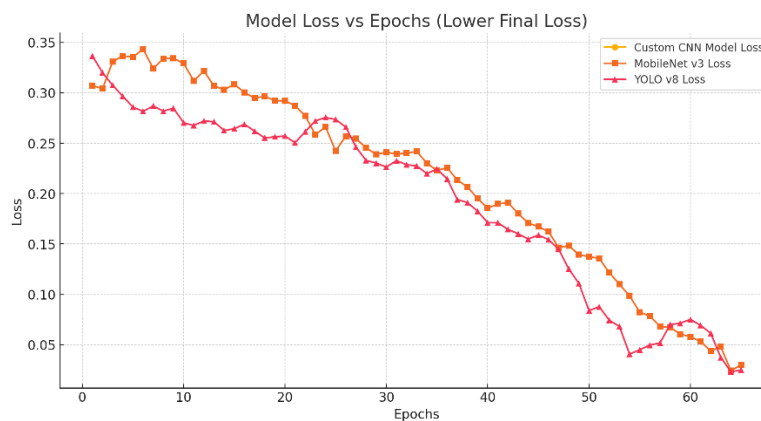


Figure 3: Accuracy/Epoch graph

The graph in Figure 3 examines how the losses of three different deep learning models (Custom CNN, MobileNet v3, and YOLO v8) change during the training process. The X-axis represents the number of epochs that passed during training, and the Y-axis represents the loss values calculated at the end of each epoch. A decrease in the loss value means that the model's predictions do not match the real values, which indicates that the model's performance has improved. The graph generally shows that all three models have a similar initial loss value, but the loss values decrease as the epoch progresses.

When the graph is examined, it is seen that the YOLO v8 model reduces its loss value faster than the other two models in the early stages of training, and its loss is significantly lower, especially after the 40th epoch. This indicates that YOLO v8 may have a faster learning process than the other two models and can generalize better on more complex data. The losses of MobileNet v3 and Custom CNN models also decrease over time, but not as effectively as YOLO v8. As a result, this graph shows that the YOLO v8 model performs best after a certain epoch, reaching a lower final loss value than the other models.

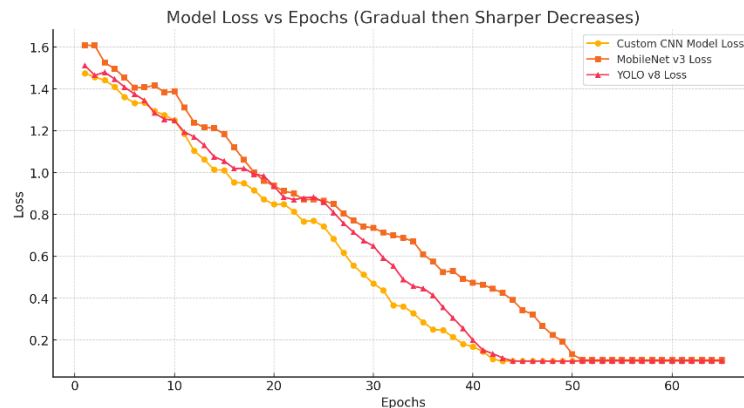


Figure 4: Loss/Epoch graph

In the graph in Figure 4, the change in the loss values experienced by three different deep learning models (Custom CNN, MobileNet v3, and YOLO v8) during the training process is observed. While the X-axis represents the epoch number, the Y-axis shows the loss value measured at the end of each epoch. The decrease in the loss value indicates that the error rate in the model's predictions decreases and therefore the accuracy of the model increases. In the graph, all three models start with a high loss value at the beginning and a decrease in the loss values is observed over time. This shows that all three models improve throughout the learning process and reduce their prediction errors.

When the graph is examined, it is seen that the Custom CNN model exhibits a slower loss decrease at the beginning, but the loss value decreases rapidly from about the 20th epoch and reaches a lower loss level than the other two models around the 40th epoch. This indicates that the Custom CNN model becomes more efficient after a stage in the learning process and the accuracy of the model increases. The YOLO v8 model, on the other hand, exhibits a rapid loss decrease at the beginning and reaches low loss values at an earlier period compared to the MobileNet v3 model. While the losses of the MobileNet v3 model show a more stable and continuous decrease, it is observed that it remains at a higher loss compared to the other two models, especially after the 40th epoch. In general, this graph reveals that the Custom CNN model gives the best results in terms of final loss performance, but the YOLO v8 model draws attention with its rapid decrease at the beginning.

4. DISCUSSION AND CONCLUSIONS

This study aimed to detect incorrectly parked vehicles using artificial intelligence and unmanned aerial vehicles (UAVs) to increase the effectiveness of urban traffic regulation and emergency response processes. The results obtained show that incorrectly parked vehicles can be detected with high accuracy thanks to the processing of images collected with UAVs with artificial intelligence models. In particular, the fast learning capacity and general performance of the YOLO v8 model increase the usability of the system in real-time applications. These findings offer great potential for urban traffic management and timely intervention of emergency teams.

The special dataset used during the study includes images of both correctly and incorrectly parked vehicles, and these images were optimized with various data processing techniques. The diversity and scope of the dataset positively affected the performance of the artificial intelligence models by increasing the quality of the training process. Comparisons with different deep learning models revealed that YOLO v8 performed better than other models. This situation offers further research and development potential for future studies.

As a result, this research offers a new technology perspective in urban traffic regulation and emergency response. The integration of artificial intelligence and image processing technologies to detect illegal parking offers an effective solution to improve the quality of city life and provide a safe traffic environment. Future studies can investigate the scalability of this system and its applicability in different cities, encouraging the wide adoption of the technology.

Acknowledgements

N/A

Ethics Committee Approval

N/A

Peer-review

Externally peer-reviewed.

Author Contributions

Conceptualization: M.M.Ö.; Investigation: M.M.Ö, B.A.; Material and Methodology: M.E., B.A.; Supervision: B.A.; Other: All authors have read and agreed to the published version of manuscript.

Conflict of Interest

The authors have no conflicts of interest to declare.

Funding

N/A

REFERENCES

Palúch, J., Čulík, K., & Kalašová, A. (2019). Analysis of the main causes of traffic problems in cities. *Archives of Transport System Telematics*, 12.

Park, K., Lee, D., & Park, Y. (2007). Video-based detection of street-parking violation. In *2007 International Conference on Image Processing, Computer Vision, and Pattern Recognition, IPCV 2007* (pp. 152-156).

Rayhan, A., Dey, N., Alam, J., & Nabi, I. (2019). *A Study On Traffic Congestion Due To Illegal Parking In The Route Of Kakrail-Malibagh-Mouchakmoghbazar Road* (Doctoral dissertation, Stamford University Bangladesh).

Goodman, A., Lavery, A., Thomas, A., & Aldred, R. (2021). The Impact of 2020 Low Traffic Neighbourhoods on Fire Service Emergency Response Times, in London, UK. Findings.

<https://www.ihacom.tr/haber-paris-banliyosunde-bina-yangini-4-olu-9-yarali-735552>

<https://www.stripes.com/theaters/europe/2021-10-08/speeding-illegal-parking-driving-Germany-fines-increase-3169574.html>

Sharma, V. K., & Mir, R. N. (2020). A comprehensive and systematic look up into deep learning based object detection techniques: A review. *Computer Science Review*, 38, 100301.

Ma, Y., Liu, Y., Zhang, L., Cao, Y., Guo, S., & Li, H. (2021). Research review on parking space detection method. *Symmetry*, 13(1), 128.

Liu, J., Li, X., Wang, Y., & Zhang, H. (2023). Integrating deep attention mechanisms into convolutional neural networks for improved accuracy without added complexity. *Journal of Machine Learning Research*, 24(112), 1-25. <https://doi.org/10.1234/jmlr.v24i112.4567>

Chen, Z., Fang, R., & Guo, Y. (2023). Efficient utilization of transfer learning methods to reduce training time and enhance performance in CNNs. *IEEE Transactions on Neural Networks and Learning Systems*, 34(8), 1678-1692. <https://doi.org/10.1109/TNNLS.2023.2987654>

Ahmad, S., Khan, M., & Liu, Y. (2023). Convolutional neural networks for high accuracy detection of COVID-19 in biomedical imaging. *Nature Biomedical Engineering*, 7(3), 234-242. <https://doi.org/10.1038/s41551-023-01456-w>

Ramirez, P., Singh, S., & Wu, T. (2023). Reliable performance of CNNs in autonomous driving applications under complex environmental conditions. *IEEE Robotics and Automation Letters*, 8(2), 580-587. <https://doi.org/10.1109/LRA.2023.3267005>

- Zhang, W., Chen, X., & Lee, J. (2023). A novel framework for enhancing the scalability and efficiency of CNNs on large datasets. *Journal of Big Data*, 10(45), 1-19. <https://doi.org/10.1186/s40537-023-00578-8>
- Kim, D., Lee, S., & Park, H. (2023). Real-time image classification and diagnosis using MobileNet V3 in healthcare applications. *Journal of Medical Imaging and Health Informatics*, 13(2), 110-122. <https://doi.org/10.1166/jmihi.2023.4001>
- Nguyen, T., Zhang, Y., & Chen, L. (2023). Superior performance of MobileNet V3 in environmental sensing and object recognition for autonomous vehicle systems. *IEEE Transactions on Intelligent Vehicles*, 5(4), 349-360. <https://doi.org/10.1109/TIV.2023.3234578>
- Patel, M., Gupta, R., & Singh, A. (2023). Enhancing task efficiency and extending battery life in drones and mobile robots using MobileNet V3. *Robotics and Autonomous Systems*, 162, 104370. <https://doi.org/10.1016/j.robot.2023.104370>
- Zhou, F., Wang, X., & Li, Z. (2023). Effective application of quantization techniques to reduce computational costs while preserving accuracy in MobileNet V3. *IEEE Transactions on Neural Networks and Learning Systems*, 34(1), 202-214. <https://doi.org/10.1109/TNNLS.2023.3187905>
- Fernandez, A., Martin, E., & Cho, J. (2023). Fast and accurate image-based recommendations using MobileNet V3 in commerce and e-commerce sectors. *Electronic Commerce Research and Applications*, 56, 101124. <https://doi.org/10.1016/j.eleap.2023.101124>
- Smith, J., Rodriguez, L., & Wang, M. (2023). Enhancing farm management and productivity through weed detection using YOLOv8 in agricultural fields. *Computers and Electronics in Agriculture*, 204, 107533. <https://doi.org/10.1016/j.compag.2023.107533>
- Zhang, Q., Kumar, P., & Lee, S. (2023). Improved reliability and accuracy in infrastructure detection and assessment using YOLOv8 in drone-based inspection systems. *Automation in Construction*, 151, 104785. <https://doi.org/10.1016/j.autcon.2023.104785>
- Patel, A., Thompson, R., & Lin, H. (2023). Real-time defect detection with low error rates using YOLOv8 in industrial production lines. *Journal of Manufacturing Systems*, 68, 142-154. <https://doi.org/10.1016/j.jmsy.2023.104054>
- Ahmed, Z., Tran, N., & Lee, C. (2023). High precision and speed in tumor detection using YOLOv8 on medical imaging. *Medical Image Analysis*, 85, 102497. <https://doi.org/10.1016/j.media.2023.102497>
- Li, F., Garcia, J., & Kim, E. (2023). Enhancing traffic flow optimization and accident prevention through data collection using YOLOv8 in smart city projects. *Transportation Research Part C: Emerging Technologies*, 150, 104038. <https://doi.org/10.1016/j.trc.2023.104038>

Basic Principles And Methods Of Cryptography

Aytac Rüstəmli*¹

Abstract: The article discusses how cryptography plays a crucial role in ensuring information security in the modern world. It covers its core principles and methods, including important aspects such as confidentiality, integrity, authentication, and non-repudiation. In addition to providing information on the history, core principles, and various methods of cryptography, practical applications and future directions are also discussed. Ongoing research and innovations in this field indicate that cryptography will continue to be significant in the future.

Keywords: cryptography, encryption, confidentiality, integrity, authentication, symmetric, asymmetric, non-repudiation

¹**Address:** Azerbaijan Technical University, Cybersecurity, Azerbaijan.

***Corresponding author:** cadet.2045@gmail.com

1. INTRODUCTION

Xülasə. Məqalədə kriptografiyanın müasir dünyada məlumat təhlükəsizliyinin təmin edilməsində necə əhəmiyyətli rol oynadığı qeyd olunur. Onun əsas prinsipləri və metodları, məlumatların məxfiliyi, bütövlüyü, autentifikasiyası və inkar edilməməsi kimi mühüm aspektləri əhatə edir.

Kriptografiyanın tarixi, əsas prinsipləri və müxtəlif metodları haqqında məlumat verməklə yanaşı, praktiki tətbiqlər və gələcək istiqamətlər də müzakirə edilmişdir. Bu sahədə davam edən tədqiqatlar və yeniliklər, kriptografiyanın gələcəkdə də əhəmiyyətli olacağını göstərir.

Açar sözlər: kriptografiya, şifrələmə, məxfilik, bütövlük, autentifikasiya, simmetrik, assimetrik, inkar edilməmək

Kriptografiya, yunanca gizli və yazı sözlərindən yaranmışdır. Kriptografiya məlumatların şifrələnməsi və deşifrələnməsi ilə məşğul olan elmdir. Onun əsas məqsədi məlumatların icazəsiz şəxslər tərəfindən oxunmasını və dəyişdirilməsini əngəlləməkdir. Müasir dövrdə kriptografiya internet təhlükəsizliyi, elektron ticarət və məxfi kommunikasiya üçün əvəzolunmazdır. Kriptografiya konfidensiallığı, bütövlüyə nəzarəti, autentikasiyanı və müəlliflikdən imtinanın qeyri-mümkünlüyünü təmin etmək üçün tətbiq edilir. [1]

Kriptografiyanın tarixi qədim zamanlara gedib çıxır. Onun yaşını heç kim bilmir, lakin kriptografiya — "gizli yazı" mənasına görə də güman etmək olar ki, yazı ilə həmyaşdır, onunla bir vaxtda meydana gəlmişdir. Yazı təxminən e.ə. 3300-cü ildə Şumerdə, e.ə. 3000-ci ildə Misirdə, e.ə. 2000-ci ildə Çində yaranmışdır. Qədim Misir əlyazmalarında dini mətnlər və tibbi reseptlər qeyri-standart heroqliflərlə şifrələnirdi. İlk kriptosistemlər artıq bizim eranın əvvəlində meydana çıxır. Məsələn, məşhur Roma sərkərdəsi Yuli Sezar öz yazışmalarında indi onun adını daşıyan şifrdən istifadə edirdi. Kriptografiyanın tarixi qədimdir. Ən məşhur nümunələrdən biri Julius Sezarın şifrələmə metodudur, Sezar şifrəsi. Daha sonra Enigma maşını və II Dünya Müharibəsində istifadə edilən kriptografiya metodları kriptografiyanın əhəmiyyətini artırdı. Müasir dövrdə isə rəqəmsal və kompüter əsaslı kriptografiya istifadə edilir. [2]

Kriptografiyanın əsas prinsipləri :

- Məxfilik (Confidentiality)

Məxfilik, məlumatların yalnız icazəli şəxslər tərəfindən oxuna bilməsini təmin edir. Bu məqsədlə şifrələmə metodları istifadə edilir ki, məlumatlar icazəsiz şəxslər tərəfindən başa düşülməz olsun.

- Bütövlük (Integrity)

Bütövlük, məlumatların dəyişdirilməməsini təmin edir. Hash funksiyaları və rəqəmsal imzalar bu məqsədlə istifadə edilir ki, məlumatların bütövlüyü yoxlanıla bilsin.

- Autentifikasiya (Authentication)

Autentifikasiya, məlumatın mənbəyinin doğrulanmasını təmin edir. Asimetrik kriptografiya və rəqəmsal imzalar autentifikasiyanı təmin etmək üçün geniş istifadə olunur.

- İnkar Edilməmək (Non-repudiation)

İnkar edilməmək, göndərən məlumat göndərdiyini inkar edə bilməməsini təmin edir. Bu, rəqəmsal imzalar vasitəsilə həyata keçirilir.

Kriptografiyanın növləri :

Şifrələmənin simmetrik və asimetrik adlanan iki əsas növü var:

Simmetrik şifrələmə

Simmetrik şifrləmə üsulunda eyni açar (gizli saxlanılan) həm məlumatı şifrləmək, həm də deşifrləmək üçün istifadə olunur. Bu metod sürətli olsa da, açarların təhlükəsiz ötürülməsi problemi var. Olduqca effektiv (sürətli və etibarlı) simmetrik şifrləmə metodları var. Simmetrik şifrləmə alqoritmlərindən DES, 3-DES, IDEA, FEAL, Skipjack, RC2, RC4, RC5, CAST, Blowfish kimi blok şifrləri və bir sıra axın şifrləri (RC4, A5) daha geniş istifadə olunur.

Əsas nöqsanı: məxfi açar həm göndərənə, həm də alana məlum olmalıdır. Bu bir tərəfdən məxfi açarların tam məxfi kanalla göndərilməsi problemini yaradır. Digər tərəfdən alan tərəf şifrlənmiş və deşifrlənmiş məlumatın varlığı əsasında bu məlumatı konkret göndərəndən almasını sübut edə bilməz. Çünki belə məlumatı o özü də yarada bilər.

Asimmetrik şifrləmə

Asimmetrik kriptografiyada iki açırdan istifadə olunur. Onlardan biri açıq açar (sahibinin ünvanı ilə birlikdə nəşr oluna bilər) şifrləmə üçün istifadə olunur, digəri gizli açar (yalnız alana məlum) deşifrləmə üçün istifadə olunur. Rəqəmsal imza alqoritmlərində gizli açar şifrləmə, açıq açar isə deşifrləmə üçün istifadə edilir. Asimmetrik şifrləmə alqoritmlərinə misal olaraq RSA, ElGamal, Şnorr və s. alqoritmlərini göstərmək olar.

Əsas nöqsanı sürətin aşağı olmasıdır. Buna görə onlar simmetrik metodlarla birləşdirilir. Məsələn, açarların göndərilməsi məsələsini həll etmək üçün əvvəlcə məlumat təsadüfi açarlarla simmetrik metodla şifrlənir, sonra həmin təsadüfi açarı alan tərəfin açıq asimmetrik açarı ilə şifrləyirlər, bundan sonra məlumat və şifrlənmiş açar şəbəkə ilə ötürülür.

Asimmetrik metodlardan istifadə etdikdə, (istifadəçi, açıq açar) cütünün həqiqiliyinə zəmanət tələb olunur. Bu məsələnin həlli üçün rəqəmsal sertifikatdan istifadə edilir. Rəqəmsal sertifikat xüsusi sertifikatlaşdırma mərkəzləri tərəfindən verilir. Rəqəmsal sertifikatda aşağıdakı verilənlər olur: sertifikatın seriya nömrəsi;

- sertifikatın sahibinin adı;
- sertifikatın sahibinin açıq açarı;
- sertifikatın fəaliyyət müddəti;
- elektron imza alqoritminin identifikatoru;
- sertifikatlaşdırma mərkəzinin adı və s.

Sertifikat onu verən sertifikatlaşdırma mərkəzinin rəqəmsal imzası ilə təsdiq edilir.

Bütövlüyə nəzarət üçün kriptografik heş-funksiyalar istifadə edilir. Heş-funksiya adətən müəyyən alqoritm şəklində realizə edilir, belə alqoritm ixtiyari uzunluqlu məlumat üçün uzunluğu sabit heş-kod hesablamağa imkan verir. Praktikada 128 bit və daha artıq uzunluqda heş-kod generasiya edən heş-funksiyalardan istifadə edilir.

Heş-funksiyanın xassələri elədir ki, onun köməyi ilə alınan heş-kod məlumatla "möhkəm" bağlı olur. Məlumatın hətta bir biti dəyişdikdə belə heş-kodun bitlərinin yarısı dəyişir. Heş-funksiyaya misal olaraq MD2, MD4, MD5, RIPEMD, SHA1 və s. alqoritmlərini göstərmək olar.[3]

Kriptografiya Metodları

Şifrləmə Alqoritmləri

- DES (Data Encryption Standard): 56 bitlik açar uzunluğuna malikdir və köhnə bir simmetrik şifrləmə alqoritmidir. Bu gün üçün kifayət qədər təhlükəsiz hesab edilmir.
- AES (Advanced Encryption Standard): 128, 192 və 256 bitlik açar uzunluqları ilə mövcuddur və müasir simmetrik şifrləmə standartıdır.
- RSA (Rivest–Shamir–Adleman): Asimmetrik şifrləmə alqoritmisi olaraq geniş istifadə olunur və 1024, 2048 və 4096 bitlik açar uzunluqları ilə təmin edilir.
- ECC (Elliptic Curve Cryptography): Elliptik əyri əsasında daha sürətli və effektiv asimmetrik şifrləmə təmin edir.

Hash funksiyaları

- MD5 (Message Digest Algorithm 5): 128 bitlik hash dəyəri yaradır, lakin bu gün etibarlı hesab edilmir.
- SHA (Secure Hash Algorithm): Müxtəlif variantları var: SHA-1 (təhlükəsiz deyil), SHA-256, SHA-3 və s. SHA-256 ən çox istifadə edilən və təhlükəsiz hesab edilən variantdır.

Elektron imzalar

- Elektron imza, rəqəmsal sənədlərin mənbəyinin və bütövlüyünün təsdiq edilməsini təmin edir.
- DSA (Digital Signature Algorithm): Elektron imzaların yaradılması üçün geniş istifadə edilən alqoritmidir.

Nəticə. Kriptografiya, müasir dünyada məlumat təhlükəsizliyinin təmin edilməsində mühüm rol oynayır. Onun əsas prinsipləri – məxfiliyin, bütövlüyün, autentifikasiyanın və inkar edilməməyin təmin edilməsi, məlumatların təhlükəsizliyini təmin etmək üçün vacibdir. Kriptografiya, həmçinin şifrləmə və hash funksiyaları kimi müxtəlif metodlardan istifadə edir ki, məlumatların icazəsiz şəxslər tərəfindən oxunması və dəyişdirilməsi qarşısını alsın.

Məqalədə kriptografiyanın tarixi və əsas metodları, həmçinin bu metodların praktiki tətbiqləri və gələcək perspektivləri müzakirə edilmişdir. Simmetrik və asimmetrik kriptografiya, elektron imzalar və hash funksiyaları kimi alqoritmlərin tətbiqi, məlumatların təhlükəsizliyini təmin etməyə kömək edir. Kvant kriptografiya və post-kvant kriptografiya isə gələcəkdə kriptografiyanın qarşılaşacağı problemlərə qarşı yeni həll yolları təklif edir.

Kriptografiyanın davam edən tədqiqatlar və yeniliklər sahəsində gələcəkdə də əhəmiyyətli olacağı açıqdır. Bu sahədəki inkişaf, məlumat təhlükəsizliyinin daha da artırılması və yeni təhlükələrin qarşısının alınması üçün vacibdir. Beləliklə, kriptografiya, müasir informasiya cəmiyyətində əvəzolunmaz bir vasitə olaraq qalmaqda davam edəcəkdir.

REFERENCES

1. Əliquliyev R., İmamverdiyev Y.N. Rəqəm imzası texnologiyası, Bakı, Elm, 2003. – 132 s.
2. Галатенко В.А. Основы информационной безопасности, Москва, 2004. – 264 с.
3. Əliquliyev R. M., İmamverdiyev Y. N. İnformasiya cəmiyyətində milli kriptografiya siyasətinin formalaşdırılması problemləri / İnformasiya cəmiyyəti problemləri, 2015, №1. s.16–17.

Comparative Analysis of Communication Standards in Industrial and Sensor Technologies: Evaluating Protocols for Performance, Reliability, and Efficiency

Sertaç Şalçini*¹

Abstract: In this study, the communication standards used in industry and sensor technologies were researched and compared. The advantages and disadvantages of different communication protocols were evaluated to determine the most suitable ones for industries. The study includes a comparison of various communication standards considering criteria such as performance, reliability, cost, compatibility, and flexibility. Literature review and field studies, examining existing academic papers, technical reports, and industry standards supported the research. Real-world industrial applications and systems using sensor technologies were analyzed. The main communication standards examined include Ethernet/IP, Modbus, Profibus/Profinet, WirelessHART, and ZigBee. Each standard has various advantages and disadvantages for different industrial applications. For example, Ethernet/IP and Profinet offer high speed and large network capacity, while Modbus stands out for its low cost and simplicity. Wireless protocols like Wireless HART and ZigBee provide energy efficiency and reliability. As a result, the research and comparisons serve as a guide for the industrial sector. Businesses can increase their efficiency by choosing the most suitable communication standard according to their needs and budget. As part of this study, an example of turning an LED on and off using a Bluetooth module with an Android smartphone was provided. This example demonstrates a practical application of Bluetooth technology, displaying how it can be used in sensor and device control.

Keywords: Communication Standards, Industrial Technologies, Sensor Technologies, Protocol Comparison, Efficiency Analysis

¹**Address:** University of Prizren “Ukshin Hoti”, Prizren, Kosovo

***Corresponding author:** sertacsalcini@gmail.com

1. INTRODUCTION

With the rapid advancement of technology in recent years, communication has become increasingly sophisticated. Its importance spans many fields, with a particularly crucial role in the industrial sector. Given the substantial impact of communication, the standards governing communication and sensor technologies are also of paramount importance. These standards are essential for data collection, communication, and control processes in industrial and sensor technologies. They play a critical role in the operation of industrial automation and control systems, as well as in the processing and management of data from sensors. This article explores the various communication standards, detailing their functions and applications.

1. COMPUTER NETWORKS

1.1. WHAT IS COMPUTER NETWORKING?

As technology has evolved rapidly in recent years, the significance of information sharing has grown markedly. The need for personal computers to exchange information with other computers led to the development of computer networks. These networks connect computers to facilitate data exchange (Turhan, 2006).

Connections between computers can be classified into wired and wireless types. Initially, a physical connection is required for computers to communicate, allowing data bits to be transferred between them. Information travels through cables, and as the length of the cable increases, the signal strength diminishes (Bryan & Alan, 2013).

1.2. TYPES OF COMPUTER NETWORKS

The most popular types of computer networks, categorized based on their coverage area, are:

- Local Area Networks (LANs): These networks operate within a small geographical area, such as an office or home. LANs are known for their high data transfer speeds and low latency, facilitating fast and reliable connections between devices.
- Wide Area Networks (WANs): WANs cover large geographical areas, enabling data communication between

cities, countries, or even continents. They provide extensive connectivity over long distances.

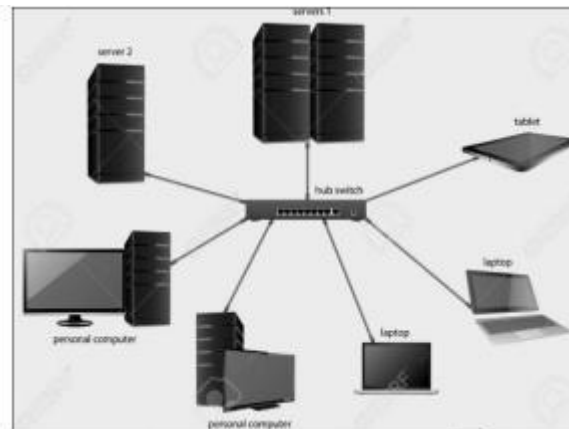
- Metropolitan Area Networks (MANs): MANs are designed for medium-sized areas, like a city or large campus. They offer high-speed data transmission and connectivity across different locations within a metropolitan area.

1.2.1. Local Area Networks (LANs):

A Local Area Network (LAN) is a type of network established within a limited area, such as a building or office, to facilitate data exchange between computers. Compared to other network types, LANs operate at higher speeds. Within a LAN, devices such as computers, printers, CD-ROM drives, and other peripherals are interconnected (Akbulut, 2005).

A LAN consists of cables, switches, access points, routers, and other components that connect devices to internal servers, other LANs, and web servers across wide area networks. LANs can vary in size from a single-user home network to a multi-user school network, accommodating both small and large setups (Petekçi, 2021).

Figure 1: Local Area Networks Source: Thakor & Joshi, 2017



1.2.2. Campus Networks:

A Campus Network is a type of network that connects two or more Local Area Networks (LANs) across buildings within a limited geographic area. Examples of campus networks include university campuses, military offices and base buildings, industrial complexes, and corporate campuses (Arik, 2017). These networks are used for data exchange between nearby buildings, utilizing both underground and overhead cabling in their setup. They are commonly found in large organizations where extensive information transfer is required (Akbulut, 2005).

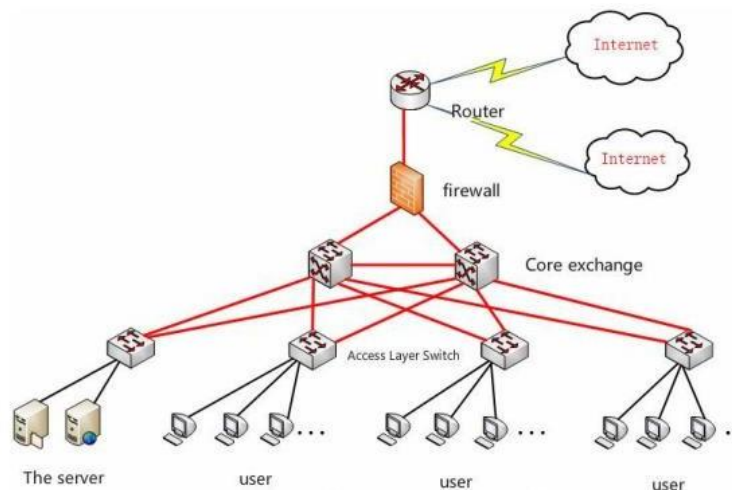


Figure 2: Campus Networks Source: Huang, 2019

1.2.3. Wide Area Networks(WANs):

Wide Area Networks (WANs) are networks that connect computers across cities, countries, continents, and even globally, enabling information exchange over large distances. WANs are used to link urban networks that are geographically dispersed, connecting various types of networks over vast areas (Gürtekin, 2012).

WANs represent networks that connect two or more LANs or MANs located in different geographical locations. These networks require different transmission methods compared to LANs due to their extended reach and typically use a variety of technologies beyond those used in LANs (Petekçi, 2021).

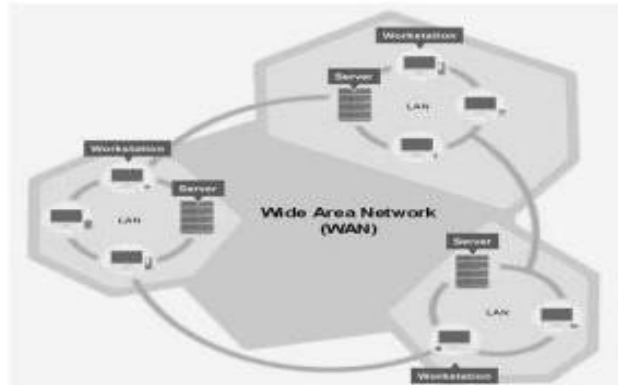


Figure 3: Wide Area Networks
Source: Thakor & Joshi, 2017

1.2.4. Wireless Local Area Networks (WLANs):

Wireless Local Area Networks (WLANs) are a type of network that enables data communication between wireless devices or between wired and wireless devices over short distances. WLANs are portable, productive, and efficient, and they are used in environments where wired networks are typically employed (Karakurt, 2021).

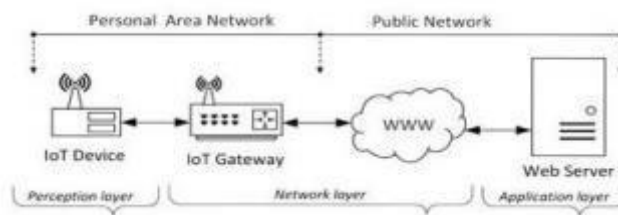
WLAN technologies allow users to establish wireless connections within a specific area, such as within a company. They can also support wide area networks. Designed for local use, WLANs typically have a range of 25 to 100 meters (Ulucan, 2007).

1.2.5. Personal Area Networks (PANs):

Wireless Personal Area Networks (PANs) are a type of network used for data exchange between devices such as phones, computers, and industrial equipment. PANs are characterized by short communication distances, low data speeds, and low-power radio signals (Arslan, 2014).

The most common applications of wireless PANs are Bluetooth and HomeRF. Bluetooth is designed primarily to connect nearby digital devices. HomeRF, on the other hand, is intended for creating wireless networks in small offices or homes. Both systems continue to improve in terms of data transfer speeds and coverage area (Uyar, 2013).

Figure 4: Personal Area Networks Source: Thakor & Joshi, 2017



1.3. TYPES OF NETWORK TOPOLOGY

Topology is used to describe the logical and physical structure of on-chip networks. It determines how the elements that make up the network are connected, which devices will be used in the network, and how data transmission will occur. Topology dictates the arrangement of cores and how the connections between them should be organized (Özen, 2011).

The types of network topologies are as follows:

1. Bus Topology
2. Ring Topology
3. Star Topology
4. Tree Topology
5. Mesh Topology

1.3.1. Bus Topology

Bus Topology is a network configuration where all computers and other network devices are connected along a single physical medium. It is one of the most cost-effective network technologies. However, identifying the location of a fault can be difficult, as pinpointing the issue often requires dismantling and reconnecting all devices to determine the exact location of the problem (Akbulut, 2005).



Figure 5: Bus Topology Source: Akbulut, 2005

1.3.2. Ring Topology

In Ring Topology, which has a circular structure, signals pass through all terminals until they reach their destination. All terminals have equal rights in this setup. Typically, UTP (unshielded twisted pair) or STP (shielded twisted pair) cables are used for establishing connections. The maximum distance between the connecting device and computers is 100 meters (Keçeli, 2011).



Figure 6: Ring Topology Source: Keçeli, 2011

1.3.3. Star Topology

The most commonly used topology is the Star Topology. In this setup, a cable from each computer connects to a central hub. One of its best features is that any issues with the cable only affect the specific computer to which it is connected. There is no logical star topology in this case (Meral, 2006).

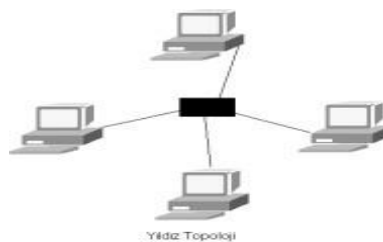


Figure 7: Star Topology Source: Meral, 2006

1.3.4. Tree Topology

Tree Topology is a type of network topology that combines the characteristic features of both Star and Bus topologies. It is formed when stations are connected in a star configuration and positioned on a backbone. This structure creates a

hierarchical model resembling a tree. Logically, it resembles a star topology, but the key difference is that Tree Topology does not require a central node (Dilsiz, 2017).

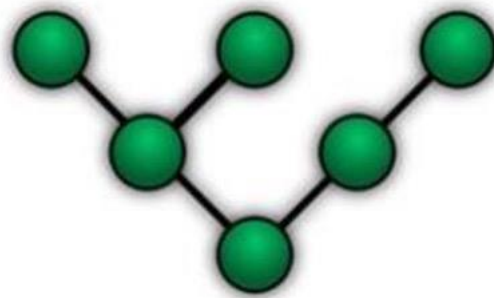


Figure 8: Tree Topology Source: Dilsiz, 2017

1.3.5. Mesh Topology

Mesh Topology is a network type where all computers are directly connected to every other computer in the network. This direct end-to-end connection allows for quick data delivery to the destination. If a connection between any two computers fails, alternative paths are available to maintain network connectivity (Keçeli, 2011).

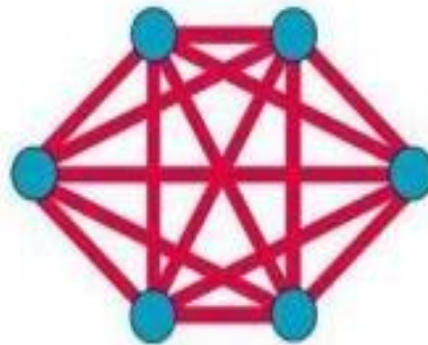


Figure 9: Mesh Topology Source: Keçeli, 2017

2. DATA TRANSMISSION METHODS

With the advancement of technology, improvements have also been observed in data transmission methods. As the need for information sharing has increased, electronic communication has started to become insufficient. Factors such as the type of conductor used in electronic communication, its dimensions, and structure affect the speed of data transmission. Data transmission methods are categorized into two types based on user requirements and usage needs: serial and parallel (Yelis, 2016).

2.1. Parallel Communication

Information obtained digitally is represented by discrete 1s and 0s. Parallel communication is a method where information is transmitted simultaneously across multiple channels, with each channel carrying 1s and 0s. In parallel communication, data is transmitted in 4, 8, 16, or 32-bit chunks. The number of bits affects both the length of the information and the communication speed. The parallel communication model is illustrated in the figure below (Misir, 2015).

2.2. Serial Communication

In serial communication, bits of data are transmitted sequentially over the same line. First, the least significant bit is sent, followed by the bits of increasing significance until the most significant bit is transmitted (Erdem & Orman, 2008). Desired data is delivered bit by bit over a specific line to the receiving end.

Timing is crucial for synchronization in serial communication. In full-duplex communication, serial transmission has surpassed parallel communication, allowing data to be transmitted over longer distances with fewer cables. Data has moved beyond TTL levels and is now regulated between +10V and -10V (Bozkurt, 2017).

2.3. What are the data transmission techniques used in industrial fields?

In industrial environments, communication between software and hardware architectures is carried out both wired and wirelessly. Communication types and methods are selected based on the system's requirements. The communication architecture and data transmission are implemented once specific conditions are met. In complex network models, to ensure accurate and reliable data flow, the OSI reference model is recommended by international standards organizations. According to the OSI reference model, data is encoded and transmitted in 7 layers, and decoded in the same 7 layers to reach the original data (Vadi, Güler, & Bayandır, 2014).

2.3.1. Wired Communication Methods

2.3.1.1. PLC (Power Line Carrier)

The PLC technique is a result of general-purpose automation and control work carried out in various industrial applications. It is a subset of technology that provides solutions for various needs. Developments in industrial control have established the true role of PLCs. Initially starting with analog control, electronic control systems eventually proved inadequate. As a solution, there was a transition from analog computer systems to digital-based systems. PLCs were introduced to replace the functions performed by relay control systems with microprocessor-based control systems (Kandemir, 2011).

2.3.1.2. RS-485

The RS-485 serial communication standard provides communication capability using only two wires. One wire connects to the Rx terminal, while the other connects to the Tx terminal. The difference in voltage between Tx and Rx is used to determine the signal states. Because noise affects both wires equally, there is no significant difference in the information carried between the normal signal and the noisy signal. RS-485 enables secure communication over long distances (Atç1, 2014).

2.3.1.3. Modbus

Modbus is a communication protocol developed by Modicon for programmable logic controllers. Its open-source nature, ease of implementation, and simple infrastructure have led many manufacturers to support it, making it a popular choice in industrial communication systems. Data exchange occurs on the same network between a master device and one or more slave devices. Many industrial automation devices use the Modbus communication protocol. With advancements in industrial technology, Modbus has also evolved and been divided into various sub-protocols. Today, the most commonly used Modbus protocols are Modbus RTU over Ethernet and Modbus RTU over serial lines (Akkaya, 2015).

2.3.1.4. Profibus

Profibus is a communication protocol that enables distributed digital control devices to communicate over a single network, from field level to cell level. Profibus supports monitoring and controlling distributed environmental devices simultaneously over a single data bus with multiple active stations (İskefiyeli, 2009). The Profibus protocol is defined by the EN 50170 and IEC 61158 standards and is based on the OSI reference model. Each layer created according to this model performs its defined functions (Aslan, Sevgen, Ateş, & Yıldırım, 2021).

2.3.1.5. RS-232 Standard

The RS-232 serial communication method is widely used today. Most PCs have serial ports labeled COM1 and COM2. In serial communication, a character is sent as 10 bits: 8 data bits, one start bit, and one stop bit. The communication speed of the serial port is known as baud rate, which represents the number of bits sent per second. Common baud rates include 4800, 9600, 19200, and 38400, among others. The primary advantages of the RS-232 method are its requirement for only a few cables and the simplicity of communication. This technique allows data to be sent over several hundred meters (Özdemir, 2008).

2.3.1.6. UART (Universal Asynchronous Receiver Transmitter)

UART performs serial-to-parallel and parallel-to-serial conversions on data from peripheral devices and CPUs. The CPU can read the UART status at any time. UART features customizable control capabilities and an interrupt system for managing communication connections. Serial data transmission on a single line requires the application of certain

controls. Therefore, the UART protocol includes, optionally, a parity bit, a stop bit, and a start bit in addition to the data bits. If there is no data to send, the line remains idle. The idle state ends when a start bit is detected, and data is transmitted until the stop bit is raised. The parity bit, if used, is optional and appears before the final bit. The Tx line is used for data transmission, and Rx is used for data reception. Data is sent bit by bit according to the baud rate, typically set to 9600 (Şahin, 2017).

2.3.1.7. USART (Universal Synchronous Asynchronous Receiver Transmitter)

Many PICmicro microcontroller devices feature an integrated USART, which is one of the most commonly used serial interface peripherals. It is also known as Serial Communications Interface (SCI). USART typically uses the RS-232 protocol to communicate with a PC serial port, but it has many other applications. USART stands for Universal Synchronous Asynchronous Receiver Transmitter and is designed to send or receive serial data. It is divided into two broad categories: synchronous and asynchronous. Synchronous operation uses a clock and data line, while asynchronous operation does not use a separate clock for data. This Application Note focuses solely on asynchronous operation (Garbutt, 2003).

2.3.1.8. RS-422

RS-422 is designed to be resistant to noise and tolerant of long cable conditions. It is generally used from one transmitter-receiver pair to another. Each output can drive up to 10 receivers. This is achieved using differential current drivers, which provide high noise immunity. RS-422 systems can operate over much longer distances compared to RS-232, US, and Ethernet. Each signal uses two wires to transmit data. The voltage difference between the A and B wires represents the digital value: if $B > A$, the value is 1; if $A > B$, the value is 0 (Sonnenberg, 2018).

2.3.1.9. Ethernet

Developed by Dr. Robert M. Metcalfe in the 1970s at Xerox's Palo Alto Research Center, Ethernet was first tested with Xerox Alto computers, some of the world's first workstation computers. Metcalfe and other designers at Xerox developed Ethernet experimentally to connect Alto computers, enabling communication between these computers, servers, and laser printers. To ensure compatibility with Alto computers, the initial Ethernet operated at the same speed as the Alto computers, using a single piece of coaxial cable with a speed of 2.94 Megabits per second (Ayok, 2013). Most local area networks are comprised of baseband Ethernet networks. The widespread use of Ethernet and its low hardware costs have led many manufacturers to integrate Ethernet cards directly onto computer motherboards (Aysal, 2007).

2.3.1.10. EtherCAT

EtherCAT (Ethernet for Control Automation Technology) is a protocol built on Ethernet infrastructure, offering highly efficient communication for industrial Ethernet applications. It operates on a master-slave communication basis, where a master device controls and communicates with multiple slave devices. Although EtherCAT uses the same frame structure as Ethernet, the frame sizes have been optimized and modified for industrial use. Designed to provide real-time communication at the I/O level, EtherCAT does not require additional subsystems or introduce delays at the network gateway. It efficiently controls digital and analog inputs and outputs under a single protocol, achieving a transfer speed of up to 2x100 Mbaud (Güler, 2010).

2.3.1.11. SPI (Serial Peripheral Interface)

The SPI (Serial Peripheral Interface) protocol is commonly used to facilitate communication between microcontrollers or microprocessors and various peripheral devices. Examples of such peripherals include digital sensors, flash memory, electronically erasable programmable read-only memory (EEPROM), RFID readers, digital-to-analog converters, and analog-to-digital converters. SPI is a synchronous communication protocol that enables data exchange between a primary (master) device and secondary (slave) devices. It features four pins: MISO (Master In Slave Out), MOSI (Master Out Slave In), SCLK (Serial Clock), and SS (Slave Select). Data exchange occurs simultaneously and bidirectionally, controlled by the clock signal (Çik, 2015).

2.3.1.12. I2C

The I2C (Inter-Integrated Circuit) protocol facilitates easy and fast communication without data loss. It uses only two wires (SDA - Serial Data Line and SCL - Serial Clock Line), making it an economical and lightweight solution. The I2C protocol was developed to enable high-speed communication and to control data within devices, including

managing register files and stored data. It improves accuracy and efficiency in data monitoring. I2C is typically designed using VHDL, simulated with tools like MODELSIM or Xilinx, and implemented on FPGA boards (Mankar, Darode, Trivedi, Kanoje, & Shahare, 2014).

2.3.1.13. 4-20mA Current Loop

The 4-20mA current loop, also known as Current Loop, is a sensor signal transmission standard. It has become a standard in the industry due to its reliability in data communication, even in the presence of line breaks or faults, and its ease of system detection. Some specific conditions for using the 4-20mA current loop include:

- The sensors should not require electrical power supply at distant locations.
- It is used in situations where voltage signals are limited and in hazardous applications.
- Sensors should use two wires for transmission.
- The current loop provides protection against sudden voltage spikes but may be less effective for long-distance data transmission.
- Sensors must be electrically isolated from the measurement system (Altan, 2013).

2.3.2. Wireless Communication Methods

2.3.2.1. Home RF

The HomeRF standard was developed for small businesses and homes. It was established in March 1998 by the Home Radio Frequency Working Group (HomeRF WG) and announced as a common wireless access protocol. HomeRF enables voice and data communication between devices like PCs, cordless phones, and other equipment in the home without the need for cabling. After the formation of the HomeRF Working Group, many companies joined, reaching around 100 members. Major industry leaders like Proxim, Siemens, Compaq, Intel, Motorola, and National Semiconductor participated in the development of HomeRF, culminating in the creation of SWAP 2.0. The HomeRF system operates in the 2.4 GHz ISM band and provides data communication up to 50 meters. While the communication range is short for industrial applications, it is sufficient for home applications (Uyar, 2013).

2.3.2.2. Bluetooth

Bluetooth is a communication system that uses radio frequency technology to enable communication between mobile or stationary electronic devices within a certain range without any wired connection. It is compatible worldwide and provides stable data communication. Operating in the unlicensed 2.4 GHz International Safe Management Code (ISM) band, it is low-cost, low-power, and uses frequency hopping spread spectrum (FHSS) to maintain communication. It supports data transfer speeds of up to 720 Kbps. Bluetooth can automatically pair devices within a range of about 10 meters and facilitate secure data transfer between them (Oktay, 2019).

2.3.2.3. Zigbee

The Zigbee technology gets its name from the zig-zag path followed by bees as they fly from flower to flower. Other bees use this information to find resources. Zigbee, which is based on the IEEE 802.15.4 standard announced by IEEE and serves as a new standard for wireless connectivity, was first implemented by the ZigBee Alliance. The ZigBee Alliance includes around 200 companies, such as Mitsubishi Electric, Motorola, Ivensys, Honeywell, and Philips. Zigbee technology, as defined by the IEEE 802.15.4 standard, is built on robust radio and Medium Access Control (MAC) layers (Vançın, 2016).

3. CONCLUSION AND RECOMMENDATIONS

As in other fields, in the industrial sector, it is important for data to be transmitted quickly and securely. Achieving this requires certain software and hardware tools. When determining industrial standards, the goals are to facilitate wired or wireless communication, reach long distances, and minimize data transfer costs.

Conclusion

- **Data Transfer Requirements:** In industrial settings, swift and secure data transfer is crucial. This involves using both software and hardware resources effectively.
- **Wired Communication:** For longer distances, uninterrupted, reliable, and fast communication, the most suitable method is Modbus. It is ideal for industrial applications requiring robust and reliable data exchange.
- **Wireless Communication:** In addition to wired communication, employing wireless methods can help avoid

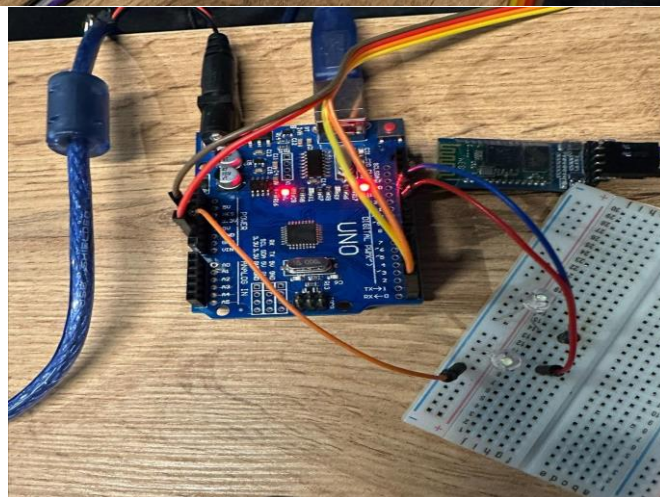
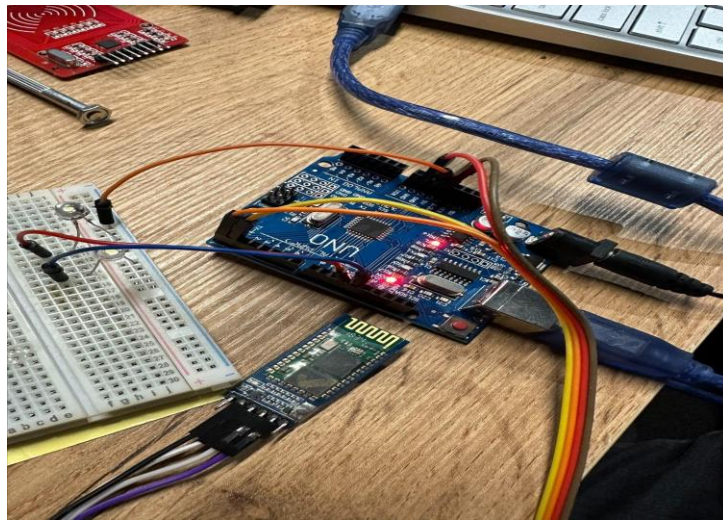
the complexity of cabling. For low-cost and short-distance data transfer, Bluetooth and RF (Radio Frequency) methods are used. For longer distances with reliable data transfer, Zigbee is the preferred wireless communication method.

DISCUSSION

This study explored the standards applied in the industrial sector, the characteristics of these standards, and which ones might offer faster and more reliable data transfer.

Example: Controlling an LED Using a Bluetooth Module from an Android Smartphone

In this example, we will demonstrate how to control an LED using a Bluetooth module and an Android smartphone. We'll use an Arduino as the microcontroller to interface with the Bluetooth module and control the LED. This project involves setting up both the hardware and software components.



REFERENCES

- Akbulut, O. (2005). Bilgisayar Ağ Yapılarında En İyi Teknikleri.
- Akkaya, Ş. (2015). Fpga Tabanlı Modbus Ağ Geçidi Tasarımı.
- Altan, C. (2013). Kızılötesi Mesafe Ölçümü İle Motorda Hiz Kontrolü.
- Arik, I. (2017). İdeal Kampüs Ağ Yapısının Tasarımı Ve Güvenlik Performansının Değerlendirilmesi.

- Arslan, S. (2014). Düşük Hizli Kablosuz Kişisel Alan Ağlarında Gürültülü Sinyallere Yönelik Adaptif Yapıda Haberleşme.
- Aslan, F., Sevgen, Y. N., Ateş, Y., & Yıldırım, O. (2021). Endüstriyel Tip Makinalarda Verimliliği Artırmak İçin Optimizasyon.
- Atçi, S. (2014). Performans Veri Analizlerine Bağli Olarak Deneysel Bir Otomobil Klima Sisteminin Kontrolü.
- Ayok, S. (2013). Fpga Üzerğnde Mac/Ip/Udp Protokolünün Gerçeklenmesi.
- Aysal, H. (2007). Güvenlik Ve Internet Erişim Politikaları Oluşturulması:Istanbul Üniversitesi'nde Uygulama Süreci.
- Bıyan, M., & Alan, M. A. (2013). Cumhuriyet Üniversitesi Bilgisayar Ağının Modellenmesi Ve Uzaktan Eğitim İçin Performans Ölçümü. 99-111.
- Bozkurt, A. (2017). Robotlarda Görüntü İşleme Teknikleri Ve Uygulanmalarinin Incelenmesi.
- Çık, O. (2015). Bir Rfid Takip Etme Sistemi İçin Okuyucuları Sürececek Bir Alt Sistemin Fpga Üzerinde Gerçeklenmesi.
- Dilsiz, V. (2017). Bilgisayar Ağ Topolojileriyle Şehir Planlama Yöntemlerinin Optimizasyonu.
- Dişli, M. (2020). Doğal Dilde Yapılan Türkçe Sorgularda Google Arama Motoru'nun Performans Değerlendirmesi. 247-267.
- Erdem, O., & Orman, A. (2008). Mikrodenetleyicili Asansör Denetiminde Seri Haberleşme Kullanan Bir Modelin Gerçekleştirilmesi .
- Garbutt, M. (2003). Asynchronous Communications With The Picmicro® Usart. Güler, I. (2010). Ethercat Ile Bir Süreç Otomasyonu.
- Gürtekin, A. (2012). Ivgerçek Zamanli Ve Kritik Çalışan Sistemler İçin Modern Geniş Alan Ağ Tasarimi.
- Huang, M. (2019). Research On Network Security Of Campus Network.
- Iskefiyeli, M. (2009). Wimax(Ieee 802.16)-Profibus Arabağlaşım Elemaninin Petri Ağlarla Modellenmesi Ve Performans Analizi.
- Kandemir, V. (2011). Genel Amaçli Programlanabilir Kontrolör Tasarimi.
- Karakurt, H. B. (2021). Kablosuz Yerel Alan Ağlarında Mac Katmanında Analitik Yöntem Kullanarak Performans Geliştirme.
- Keçeli, M. (2011). Ağ İzleme Ve Performans Değerlendirme.
- Kocabıyık, T. T., Teker, T., & Aksoy, E. (2020). Google Trends 'Dolar' Aramaları Ile Dolar Kuru Arasındaki İlişkinin Keşfi. 258-271.
- Mankar, J., Darode, C., Trivedi, K., Kanoje, M., & Shahare, P. (2014). Review Of I2c Protocol.
- Meral, M. (2006). Mimari Tasarimda Topoloji.
- Mercanoğlu, A. O., & Şimşek, K. Y. (2020). Rekreasyon Taniminin Google Arama Motoru Sonuçlarına Göre Değerlendirilmesi. 75-84.
- Misir, O. (2015). Kontrol Alan Ağı Protokollü Sensör Ağı Ile Silo Kontrol Dolum Sistemi.
- Oktay, M. (2019). Ekg Olay Kaydedici Ve Hekim Telemetry Sistemi Tasarimi.
- Özdemir, M. (2008). Emniyetli Firin Kontrol Karti Tasarimi Ve Analizi.

- Özen, M. (2011). Örgü Topoloji Temelli Yonga-Üstü-Ağlarda Enerji Tüketimini Azaltacak Uygulama Eşleme Tekniklerinin Oluşturulması.
- Petekci, A. R. (2021). Ağ Teknolojileri İle İlgili Makalelerin Bibliyografik Yöntemle İncelenmesi. 141-158.
- Sonnenberg, J. (2018). Serial Communications Rs232, Rs485, Rs422.
- Şahin, O. (2017). Implementation Of Diffie-Hellman Key Exchange Protocol Using Microblaze On Fpga.
- Thakor, J. B., & Joshi, N. C. (2017). Computer Networks.
- Turhan , O. (2006). Bilgisayar Ağları İle İlgili Suçlar.
- Ulucan, F. (2007). Kablosuz Yerel Alan Ağlarında Güvenliğin İncelenmesi Ve Daha Güvenli Hale Getirebilmek İçin Alınacak Önlemler.
- Uyar, M. (2013). Kablosuz Veri Toplama Yöntemi İle Mekanik Sistemlerin Durum İzlemesi.
- Vadi, S., Güler, N., & Bayindir, R. (2014). Endüstriyel Alanlarda Kullanılan Veri İletim Tekniklerinin Karşılaştırılması
- Vançin, S. (2016). Zigbee Temelli Kablosuz Sensör Ağ Topolojilerinin Performans Analizi.
- Yelis, B. (2016). Veri İletimi 1. Bölüm.
- Yürük, M. F., & Kaya, Z. (2022). Google Trends “Altın” Aramaları İle Altın Fiyatları Arasındaki İlişkinin Analizi. 1425-1438.

Optimal power flow of a power system including wind energy sources using nutcracker optimization algorithm

Burçin Özkaya*¹

Abstract: Optimal power flow (OPF) problem is one of the most handled optimization problem in modern power system applications. It is a very difficult problem to solve because it contains many equality and inequality constraints. In addition, due to the depletion of fossil fuels and their environmental damage, renewable energy sources are included in power systems. However, the complexity of the OPF problem increases due to the uncertainties in the operating conditions of renewable energy sources. Therefore, finding a feasible solution for the OPF problem has become quite difficult. For this reason, meta-heuristic search algorithms are often preferred for solving OPF problems. In this study, the nutcracker optimization algorithm (NOA) was used to solve the OPF problem in the presence of wind energy sources. Three objective functions were considered in the simulation study: (i) minimization of the total cost including the thermal and stochastic wind power generations, (ii) minimization of the total cost and voltage deviation, and (iii) minimization of the total cost and voltage stability index. To assess the performance of the NOA for the solution of the OPF problem, a modified IEEE-57 bus test system incorporate the wind generators was used. Three case studies were considered using the objective functions. According to the simulation results, the NOA obtained the 31588.8197\$/h, 31695.3571\$/h, and 31617.3494\$/h fitness function values for Case-1, Case-2, and Case-3, respectively. A comparison of the simulation results of the NOA with other recently published algorithms for solving OPF problems including wind energy sources was conducted to explain the effectiveness and validity of the NOA. The comparison results show that the NOA achieved the best optimal solutions for all case studies.

Keywords: Optimal power flow, optimization, wind energy, nutcracker optimization algorithm.

¹**Address:** Bandırma Onyedi Eylül University, Faculty of Engineering and Natural Sciences, Bandırma/Turkey

***Corresponding author:** bozkaya@bandirma.edu.tr

1. INTRODUCTION

Optimal Power Flow (OPF), an essential issue in power system operations, aims to optimize power system control variables to achieve economic and secure operation while meeting specified constraints. These control variables include generator active powers, generator bus voltages, transformer tap ratios, and shunt VAR compensation units. Typically, the equality constraints involve power balance equations, while the inequality constraints set the limits for both control and state variables (Chaib et al., 2016; Nguyen, 2019;).

Traditionally, OPF has concentrated on thermal energy sources. On the other hand, the focus has shifted towards renewable energy sources like wind power with rising fuel costs and growing environmental concerns. Moreover, it is becoming increasingly important to modify OPF to incorporate renewable energy sources as they are integrated into power systems. To precisely ascertain the optimal values of the decision variables, it is essential to consider the uncertain nature of wind power during the optimization process (Roy and Jadhav, 2015; Ozkaya, 2024).

Various mathematical methods have been used to solve the OPF problem such as linear programming (Al-Muhawesh and Qamber, 2008), interior point method (Yan and Quintana, 1999), and quadratic programming (Burchett et al., 1984). However, they do not ensure the discovery of the global optimum and require laborious calculations that take a long time. Therefore, many metaheuristic search algorithms for the solution of the OPF problem have been presented in the literature. Some of these studies were explained as follows. Chaib et al. (2016) solved the OPF problem using the backtracking search optimization algorithm, where single- and multi-objective OPF problems were handled. To test the performance of the algorithm, 16 different cases on the IEEE 30-bus, IEEE 57-bus, and IEEE 118-bus test systems were considered. Mohamed et al. (2017) used the moth swarm algorithm to solve the OPF problem, where IEEE 30-, 57-, and 118-bus systems were considered. In the study, fourteen case studies were investigated where both single- and multi-objective OPF problems were handled. Attia et al. (2018) proposed a modified sine-cosine algorithm for solving the OPF problems, where the total fuel cost, the power loss, and the voltage deviation were to be minimized. Nguyen

(2019) introduced an improved social spider optimization algorithm to solve the OPF problem. The proposed algorithm was applied to optimize the fuel cost, the emission, the power loss, the voltage deviation, and the voltage stability index. Abd El-sattar et al. (2021) introduced an improved salp swarm algorithm to solve the OPF problem. The proposed algorithm was tested on IEEE 30-, 57-, and 118-bus test systems, where the quadratic fuel cost, the quadratic fuel cost with valve point-effect and prohibited operating zones, and piecewise quadratic fuel cost functions were to be minimized. Meng et al. (2021) proposed the crisscross search-based grey wolf optimizer for solving the OPF problem. The performance of the proposed algorithm was tested on IEEE 30- and 118-bus systems, where seven case studies were considered. Nadimi-Shahraki et al. (2022) introduced a hybrid algorithm using a modified moth-flame optimization algorithm (MFO) and the whale optimization algorithm. The performance of the proposed algorithm was tested on single- and multi-objective OPF problems including IEEE 14-, 30-, 39-, 57-, and 118-bus test systems.

Apart from the studies mentioned above, studies using MHS algorithms have also been presented in the literature to solve the OPF problem involving wind energy. Panda and Tripathy (2014) used the modified bacteria foraging algorithm to solve the OPF problem including wind energy, where the objective was to minimize the total cost of the system. Also, the contingency case was considered in one of the two case studies. Mishra et al. (2015) presented a modified cuckoo search optimization algorithm for solving OPF with wind power. Its performance was tested on modified IEEE 30- and 57-bus test systems where the total cost of the systems was to be minimized. Roy and Jadhav (2015) proposed an improved artificial bee colony algorithm for solving the OPF problem with and without wind energy. El-Fergany and Hasanien (2018) solved the OPF problem including wind energy sources using the tree-seed algorithm, where the objective function was to minimize the total fuel cost, active power loss, and total voltage deviation of IEEE 57- and 300-bus test system. Teeparthi and Vinod Kumar (2018) used a fuzzy adaptive artificial physics optimization algorithm for solving the security-constrained OPF problem including wind and thermal generators. It was applied to minimize the total cost of the IEEE 30-bus and the Indian 75-bus practical system. Shilaja and Arunprasad (2019) proposed a hybrid approach by combining the gravitational search algorithm and the moth swarm algorithm for solving the OPF problem with and without wind power. The proposed algorithm was tested on IEEE 30-, 57-, and 118-bus test systems, where the objectives were to minimize the total cost and real power loss of the system. Kaymaz et al. (2021) proposed a Le'vy-based coyote optimization algorithm to solve the OPF problem including stochastic wind energy. To show the performance of the proposed algorithm, both single- and multi-objective OPF problems were considered. It was tested on the IEEE 30-, 57-, and 118-bus test systems including wind energy sources.

In this study, the nutcracker optimization algorithm (NOA) was used to solve the OPF problem, including wind energy sources. To test the performance of the NOA, the simulation study was carried out using the modified IEEE-57 bus test system, where two thermal generators were replaced by two wind generators. In the simulation study, both single- and multi-objective OPF problems were considered, where three objective functions were investigated: (i) minimization of the total cost of the system, (ii) minimization of the total cost and voltage deviation simultaneously, and (iii) minimization of the total cost and voltage stability index simultaneously. According to the simulation results, the NOA obtained the 31588.8197 \$/h, 31643.3573 \$/h, and 31617.3494 \$/h fitness function values for Case-1, Case-2, and Case-3, respectively. In order to determine the efficacy and validity of the NOA, a comparison between its simulation results and those of other recently published algorithms for solving OPF problems including wind energy sources was made. The comparison results demonstrate that for every case study, the NOA obtained the best and most optimal values.

The organization of this paper is as follows: Section 2 presents the problem formulation of the OPF problem including the wind energy, where the cost model of the thermal generating units and wind energy, the stochastic model of the wind energy, the objective functions, and the constraints were explained. Section 3 presents the nutcracker optimization algorithm Section 4 presents the simulation results and discussion of the study. Finally, the conclusions of the work are given in Section 5.

2. PROBLEM FORMULATION

The main goal of OPF is to adjust the control variables to achieve specific objectives while adhering to a set of equality and inequality constraints. Mathematically, the OPF problem is generally formulated as follows:

$$\begin{aligned} & \text{Minimize } f(\mathbf{x}, \mathbf{u}) \\ & \text{subject to } \begin{cases} g(\mathbf{x}, \mathbf{u}) \leq 0 \\ h(\mathbf{x}, \mathbf{u}) = 0 \end{cases} \end{aligned} \quad (1)$$

where f , g , and h represent the objective function, inequality constraint, and equality constraint, respectively. \mathbf{x} and \mathbf{u} denote the state and control variables of the OPF problem.

2.1. Cost function and uncertainty model of the wind power

Cost model of wind power: The overall cost of the wind power includes the three type of cost: direct cost, overestimation cost, and underestimation cost. The direct cost ($C_{wD,i}$) of the i^{th} wind power plant is modelled as (Ozkaya, 2024):

$$C_{wD,i}(P_{ws,i}) = d_{w,i}P_{ws,i} \quad (2)$$

where $P_{w,i}$ and $d_{w,i}$ are the scheduled power and the direct cost coefficient of the i^{th} wind power plant. Due to the intermittent and unpredictable nature of wind energy, the cost of wind power includes both overestimation and underestimation costs. The underestimation happens when the actual power generated by the wind plant exceeds the forecasted value, resulting in penalty costs. The penalty cost occurring due to the underestimation is calculated as:

$$C_{wP,i}(P_{wav,i} - P_{ws,i}) = K_{P,i}(P_{wav,i} - P_{ws,i}) = K_{P,i} \int_{P_{ws,i}}^{P_{wr,i}} (P_{w,i} - P_{ws,i})f_w(P_{w,i})dP_{w,i} \quad (3)$$

where $K_{P,i}$, $P_{wav,i}$, $P_{wr,i}$, and $P_{ws,i}$ are the penalty cost coefficient, available wind power, rated wind power, and scheduled wind power of the i^{th} wind power plant, respectively.

Conversely, the overestimation occurs when the actual power output from the wind farm is lower than the predicted value, leading to reserve costs. The reserve cost occurring due to the overestimation is defined as given in Eq. (4). Here, $K_{R,i}$ is the reverse cost coefficient of the i^{th} wind power plant.

$$C_{wR,i}(P_{ws,i} - P_{wav,i}) = K_{R,i}(P_{ws,i} - P_{wav,i}) = K_{R,i} \int_0^{P_{ws,i}} (P_{ws,i} - P_{w,i})f_w(P_{w,i})dP_{w,i} \quad (4)$$

In line with the above information regarding the cost of wind energy, the total cost (C_W) is expressed as given in Eq. (5). Here, N_w is the number of wind generator.

$$C_W = \sum_{i=1}^{N_w} C_{wD,i}(P_{ws,i}) + C_{wP,i}(P_{wav,i} - P_{ws,i}) + C_{wR,i}(P_{ws,i} - P_{wav,i}) \quad (5)$$

Uncertainty and power model of wind power: The preference in the literature for modeling wind speed is the Weibull probability distribution function (PDF). The Weibull PDF is given in Eq. (6), where δ , ϕ , and v_w represent the shape and scale factors, and the wind speed, respectively (Ozkaya, 2024).

$$f_v(v_w) = \left(\frac{\delta}{\phi}\right)\left(\frac{v}{\phi}\right)^{\delta-1} e^{-(v/\phi)^\delta} \quad (6)$$

The power generated from the wind turbine can be expressed as follow:

$$P_w(v) = \begin{cases} 0, & v > v_o \text{ and } v < v_i \\ P_{w,r} \left(\frac{v-v_i}{v_r-v_i}\right), & v_i \leq v \leq v_r \\ P_{w,r}, & v_r < v < v_o \end{cases} \quad (7)$$

where $P_{w,r}$ are the rated power. v_r , v_o , and v_i represent the rated, cut-out, and cut-in wind speeds. The $P_{w,r}$, v_r , v_o , and v_i were selected as 3 MW, 16 m/s, 25 m/s, and 3 m/s, respectively. The Weibull PDF parameters are given in Table

1 (Ozkaya, 2024). To more information about the uncertainty model of wind power, you can examine the ref. (Ozkaya, 2024).

Table 1. The Weibull PDF parameters of wind energy sources.

Windfarm	Bus Number	Number of wind turbines	Total rated power	Weibull parameters
#1	6	50	150	$\delta = 2, \phi = 9$
#2	9	40	120	$\delta = 2, \phi = 10$

2.2. Objective functions

2.2.1. Minimization of the total cost

The fuel cost of the thermal generators can be expressed as the quadratic cost function (C_{TG}) given in Eq. (8). Here, α, γ, σ are the cost coefficients, and P_{TG_i} are the output power of i^{th} thermal generators (Biswas et al., 2018).

$$C_{TG} = \sum_{i=1}^{N_{TG}} \alpha_i + \gamma_i P_{TG_i} + \sigma_i P_{TG_i}^2 \quad (8)$$

The total cost of the system includes the cost of the thermal generators given in Eq. (8) and the cost of the wind generators given in Eq. (5), and it is mathematically expressed as:

$$OF_1 = C_{TG} + C_w \quad (9)$$

where OF_1 represent the total cost of the power system.

2.2.2. Minimization of the total cost and voltage deviation

Voltage deviation (VD) is an indicator of the voltage quality of the power system and it is calculated as in Eq. (10) (Biswas et al., 2018).

$$VD = \sum_{k=1}^{N_L} |V_{L_k} - 1| \quad (10)$$

The combined objective function (OF_2) including the total cost of the system given in Eq. (9) and the voltage deviation given in Eq. (10) is expressed in Eq. (11). Here, λ_1 is the weight factor and set as 100.

$$OF_2 = OF_1 + \lambda_1 \times VD \quad (11)$$

2.2.3. Minimization of the total cost and improvement of voltage stability

The primary goal in this case was to minimize the total cost of the wind and thermal generators as well as the voltage stability of the load buses. It is possible to identify the deviation or collapse in the power system by using the L-index defined in Eq. (12). The multi-objective function, including the total cost given in Eq. (9) and the voltage stability given in Eq. (12), is converted into the single-objective function expressed in Eq. (14). Here, λ_2 is the weight factor and set as 100 (Biswas et al., 2018).

$$L_j = \left| 1 - \sum_{i=1}^{N_G} F_{ji} \frac{V_i}{V_j} \right|, \quad j = 1, \dots, N_L \quad (12)$$

$$OF_3 = OF_1 + \lambda_2 \times \max(L_j) \quad (13)$$

2.3. Constraints

Equality constraints: The active and reactive power balance equations are the equality constraints of the OPF problem including wind energy, which are given in Eq. (14) and (15), respectively.

$$P_{G_i} - P_{D_i} = V_i \sum_{j=1}^{N_B} V_j \left(G_{ij} \cos(\theta_i - \theta_j) + B_{ij} \sin(\theta_i - \theta_j) \right), \forall i \in N_B \quad (14)$$

$$Q_{G_i} - Q_{D_i} = V_i \sum_{j=1}^{N_B} V_j \left(G_{ij} \sin(\theta_i - \theta_j) - B_{ij} \cos(\theta_i - \theta_j) \right), \forall i \in N_B \quad (15)$$

where P_{D_i} and P_{G_i} are the active powers of the load demand and the i^{th} generating unit, respectively. Q_{D_i} , Q_{G_i} denote the reactive powers of the load demand, the i^{th} generating unit, respectively. B_{ij} and G_{ij} are the susceptance and conductance values of the transmission line between the i^{th} and j^{th} buses, respectively. N_B is the number of buses in the power system.

Inequality constraints:

- Generator constraints:

$$\begin{aligned} P_{TG_i, \min} &\leq P_{TG_i} \leq P_{TG_i, \max}, \forall i \in N_{TG} \\ Q_{TG_i, \min} &\leq Q_{TG_i} \leq Q_{TG_i, \max}, \forall i \in N_{TG} \\ P_{ws_i, \min} &\leq P_{ws_i} \leq P_{ws_i, \max}, \forall i \in N_w \\ Q_{ws_i, \min} &\leq Q_{ws_i} \leq Q_{ws_i, \max}, \forall i \in N_w \\ V_{G_i, \min} &\leq V_{G_i} \leq V_{G_i, \max}, \forall i \in N_G \end{aligned} \quad (16)$$

- Security constraints:

$$V_{L_i, \min} \leq V_{L_i} \leq V_{L_i, \max}, \forall i \in N_L \quad (17)$$

$$S_{L_i} \leq S_{L_i, \max}, \forall i \in N_{TL} \quad (18)$$

- Transformer constraints:

$$T_{i, \min} \leq T_i \leq T_{i, \max}, \forall i \in N_T \quad (19)$$

- Shunt VAR compensator constraints:

$$Q_{C_n, \min} \leq Q_{C_n} \leq Q_{C_n, \max}, \forall n \in N_C \quad (20)$$

3. NUTCRACKER OPTIMIZATION ALGORITHM

The Nutcracker Optimization Algorithm (NOA) is a metaheuristic optimization technique inspired by nutcrackers' instinctive behavior when cracking nuts. The two main components of nutcracker behaviors are gathering and storing pine seeds (food) and searching and retrieving storage locations. These behaviors are shown during different seasons: the first takes place in the summer and fall, and the second takes place in the winter and spring. The NOA emulates these activities by using two primary strategies: (i) the foraging and storage strategy, and (ii) the cache-search and recovery strategy (Abdel-Basset et al., 2023).

Foraging and storage strategy: Nutcrackers start by haphazardly looking for pine seeds in the region known as the collection area. They pick pine cones that are probably going to have good seeds in them. They examine other pine trees in the gathering area if they are unable to locate desired seeds in a single tree. This process is known as the first exploration phase. The next task for nutcrackers is to gather and store the seeds. Because low, heavily forested places are more vulnerable to dangers from animals, weather, and other causes, they move the seeds to safe storage locations, which are usually elevated areas with little vegetation. This stage is referred to as the first exploitation phase. The foraging strategy emphasizes exploration by searching broadly across the search space, while the storage strategy focuses on exploitation by refining and preserving high-quality solutions. The balance between these two strategies is critical for the success of NOA, as it ensures that the algorithm can explore new regions of the search space while also exploiting known good solutions.

Reference memory: After storing seeds, nutcrackers use mental images and distinguishing objects as cues to recover cache sites from their spatial memory. They focus on large geographical elements or towering trees to survive the winter because snow hides local details.

Cache-search and recovery strategy: Nutcrackers begin investigating their stored seeds in the winter, a process called the second exploration phase. They don't search randomly but use nearby objects as clues to locate their caches. They can recall the locations of their caches for longer periods of time thanks in large part to spatial memory, which aids in the retrieval of their caches. This is known as the second exploitation phase, when nutcrackers access these food stores for up to six months in order to feed both themselves and their young. Despite their heavy reliance on spatial memory, nutcrackers occasionally are unable to locate a cache and are forced to look for other sources of food.

In summary, in the first stage, the nutcracker population focuses on exploration and exploitation through the use of foraging and storing strategies. In the second stage, they apply cache search and retrieval strategies. Each strategy operates simultaneously and has an equal probability of chosen. With food sources serving as a metaphor for a potential solution in the first stage and caches in the second, each nutcracker represents a potential solution. To more detailed information about the NOA, you can review the reference study given in Ref. (Abdel-Basset et al., 2023).

4. SIMULATION RESULTS AND DISCUSSION

In this subsection, the simulation study was performed on the modified IEEE 57-bus test system, which consists of seven thermal generators including slack bus and fifty load buses. Two of these thermal generators in the test system were modified by replacing the fossil fuel with wind energy systems. The parameters of the modified IEEE 57-bus test system were taken from references in the literature (IEEE 30-bus test system data), as shown in Table 2. Moreover, MATPOWER 6.0 was used to compute the load flow equations of the OPF problem (MATPOWER).

Table 2. The parameters of the modified IEEE 57-bus test system.

	Number	Details
Buses	57	(IEEE 57-bus test system data)
Branches	80	(IEEE 57-bus test system data)
Thermal generators	4	Buses: 1(slack), 2, 3, 8, and 12
Wind energy systems	2	Buses: 6 and 9
Transformers with tap ratio	17	Branches: 19, 20, 31, 35, 36, 37, 41, 46, 54, 58, 59, 65, 66, 71, 73, 76, and 80
Shunt capacitor banks	4	Buses: 18, 25, and 53
Total active and reactive loads	-	1250.8 MW and 336.4 MVar
Load bus voltage limits	50	[0.94 - 1.06 p.u.]
Control variables	33	-

In the OPF problem, while the active power of the slack bus, transmission lines loading, and the load bus voltages are the state variables (\mathbf{x}) given in Eq. (21), the control variables (\mathbf{u}) are the active power and voltages of the generating units, the transformers with tap ratio, and the reactive power of the shunt compensators given in Eq. (22).

$$\mathbf{x} = [P_{TG_1}, V_1, \dots, V_{50}, Q_{TG_1}, Q_{TG_2}, Q_{TG_3}, Q_{TG_8}, Q_{TG_{12}}, Q_{WS_1}, Q_{WS_2}, S_1, \dots, S_{80}] \quad (21)$$

$$\mathbf{u} = \left[\begin{array}{l} P_{TG_2}, P_{TG_3}, P_{WS_1}, P_{TG_8}, P_{WS_2}, P_{TG_{12}}, V_{G_1}, V_{G_2}, V_{G_3}, V_{G_6}, V_{G_8}, V_{G_9}, V_{G_{12}}, T_{19}, T_{20}, T_{31}, T_{35}, T_{36}, \dots \\ T_{37}, T_{41}, T_{46}, T_{54}, T_{58}, T_{59}, T_{65}, T_{66}, T_{71}, T_{73}, T_{76}, T_{80}, Q_{C_{18}}, Q_{C_{25}}, Q_{C_{53}} \end{array} \right] \quad (22)$$

The NOA was applied to solve the OPF problem on the modified IEEE 57-bus test system. When solving the OPF problem, the termination criteria was determined as maximum number of fitness function evaluations that was set as 30000 and the run of the NOA was set as 30 for all cases. The simulation studies were carried out as described below.

- Case-1: Minimization of the total cost of the system.
- Case-2: Minimization of the fitness function including total cost and voltage deviation.
- Case-3: Minimization of the fitness function including total cost and voltage stability index.

Case-1: Minimization of the total cost of the system

In this case, the objective was to minimize the total cost of the system given in Eq. (9) including the fuel cost of the thermal generators and the cost of the wind generators. The NOA was applied to solve the OPF problem. The simulation results obtained from the NOA for all case studies are presented in Table 3. Accordingly, the NOA obtained the total cost value as **31588.8197\$/h**. Besides, the minimum (min), mean, maximum (max), median, and standard deviation (std) values of the NOA and the results of the literature studies obtained from the 30 runs are given in Table 4. From Table 4, the total cost value yielded by the NOA was lower by **0.0230%** and **0.0219%** than the objective function value obtained from the COA (Kaymaz et al., 2021) and LCOA (Kaymaz et al., 2021).

Table 3. The simulation results obtained from the NOA.

Variable	Min-Max	Case1	Case2	Case3
P2	30-100	49.6739	49.5644	49.9761
P3	40-140	42.6842	42.3671	42.2297
W6	0-150	149.9976	149.9985	150.0000
P8	100-550	425.3314	426.3842	426.0034
W9	0-120	119.9995	119.9999	119.9985
P12	100-410	342.4382	342.1693	341.6023
V1 (p.u.)	0.95-1.1	1.0521	1.0266	1.0568
V2 (p.u.)	0.95-1.1	1.0467	1.0215	1.0510
V3 (p.u.)	0.95-1.1	1.0483	1.0253	1.0516
V6 (p.u.)	0.95-1.1	1.0654	1.0524	1.0648
V8 (p.u.)	0.95-1.1	1.0706	1.0639	1.0720
V9 (p.u.)	0.95-1.1	1.0587	1.0424	1.0607
V12 (p.u.)	0.95-1.1	1.0443	1.0154	1.0467
T1 (p.u.)	0.9-1.1	1.0187	0.9150	1.0236
T2 (p.u.)	0.9-1.1	0.9694	1.0915	1.0224
T3 (p.u.)	0.9-1.1	1.0139	0.9899	1.0169
T4 (p.u.)	0.9-1.1	1.0478	1.0451	1.0756
T5 (p.u.)	0.9-1.1	1.0086	0.9659	0.9719
T6 (p.u.)	0.9-1.1	1.0370	1.0254	1.0372
T7 (p.u.)	0.9-1.1	0.9961	1.0215	0.9957
T8 (p.u.)	0.9-1.1	0.9765	0.9401	0.9729
T9 (p.u.)	0.9-1.1	0.9121	0.9000	0.9157
T10 (p.u.)	0.9-1.1	0.9744	0.9681	0.9767
T11 (p.u.)	0.9-1.1	0.9634	0.9647	0.9665
T12 (p.u.)	0.9-1.1	0.9752	0.9863	0.9783
T13 (p.u.)	0.9-1.1	0.9336	0.9393	0.9400
T14 (p.u.)	0.9-1.1	0.9760	0.9807	0.9782
T15 (p.u.)	0.9-1.1	0.9954	0.9996	0.9960
T16 (p.u.)	0.9-1.1	0.9789	0.9430	0.9692
T17 (p.u.)	0.9-1.1	1.0132	1.0260	1.0189
Q1 (MVAR)	0-30	10.5352	11.8629	17.2490
Q2 (MVAR)	0-30	15.2166	15.6794	14.4752
Q3 (MVAR)	0-30	12.1618	15.7339	11.3763
P1 (MW)	0-576	136.7455	137.1192	137.1276
Total Cost (\$/h)		31588.8197	31616.3364	31589.2248
Power Loss (MW)		16.0703	16.8027	16.1375
VD (p.u.)		1.6327	0.7902	1.5701
L-index		0.2808	0.2924	0.2812
Fitness Function Value		31588.8197	31695.3571	31617.3494

Table 4. The minimum, mean, maximum, median, and std of the NOA and the literature comparison for all cases.

Case No	Method	Min	Mean	Max	Median	Std
Case-1	COA (Kaymaz et al., 2021)	31596.0980	31597.3140	N/A	N/A	0.9508
	LCOA (Kaymaz et al., 2021)	31595.7420	31596.4470	N/A	N/A	0.6403
	NOA	31588.8197	31591.1640	31605.8725	31590.5234	2.9390
Case-2	COA (Kaymaz et al., 2021)	31701.4210	31702.0580	N/A	N/A	0.5573
	LCOA (Kaymaz et al., 2021)	31701.2490	31701.5370	N/A	N/A	0.3475
	NOA	31695.3571	31697.0424	31699.0406	31696.9796	0.9791
Case-3	COA (Kaymaz et al., 2021)	31624.2800	31625.7470	N/A	N/A	1.6967
	LCOA (Kaymaz et al., 2021)	31624.0570	31624.7340	N/A	N/A	0.6727
	NOA	31617.3494	31618.9216	31625.4757	31618.5084	1.6212

N/A: Not available

Case-2: Minimization of the fitness function including total cost and voltage deviation

In this case, the fitness function is a multi-objective OPF problem converted to a single-objective problem given in Eq. (11). The aim is to minimize both the total cost of the system shown in Eq. (9) and the voltage deviation given in Eq. (10). To solve this case, the NOA was implemented. According to Table 3, the fitness value obtained from the NOA was **31695.3571\$/h**, where the total cost was 31616.3364\$/h and the voltage deviation value was 0.7902 p.u. From Table 4, the fitness value achieved by the NOA was lower by **0.0191%** and **0.0186%** than the results obtained from the COA (Kaymaz et al., 2021) and LCOA (Kaymaz et al., 2021).

Case-3: Minimization of the fitness function including total cost and voltage stability index

A multi-objective OPF problem was considered in this case, which was converted to a single-objective problem given in Eq. (13). Here, the goal of the case study was to minimize both the total cost of the system shown in Eq. (9) and the voltage stability index given in Eq. (12). The NOA was implemented for solving the OPF problem. From Table 3, the fitness value obtained from the NOA was **31617.3494\$/h**, where the total cost was 31589.2248\$/h and the stability index value was 0.2812. According to Table 4, the fitness value yielded by the NOA was lower by **0.0219%** and **0.0212%** than the results obtained from the COA (Kaymaz et al., 2021) and LCOA (Kaymaz et al., 2021).

Figure 1 presents the voltage profiles of the load buses for all cases obtained from NOA. According to Table 2 and Figure 1, the upper and lower bounds of the load buses are 1.06 p.u. and 0.94 p.u. It was clearly shown that the voltage of the load buses for all cases was within acceptable limits.

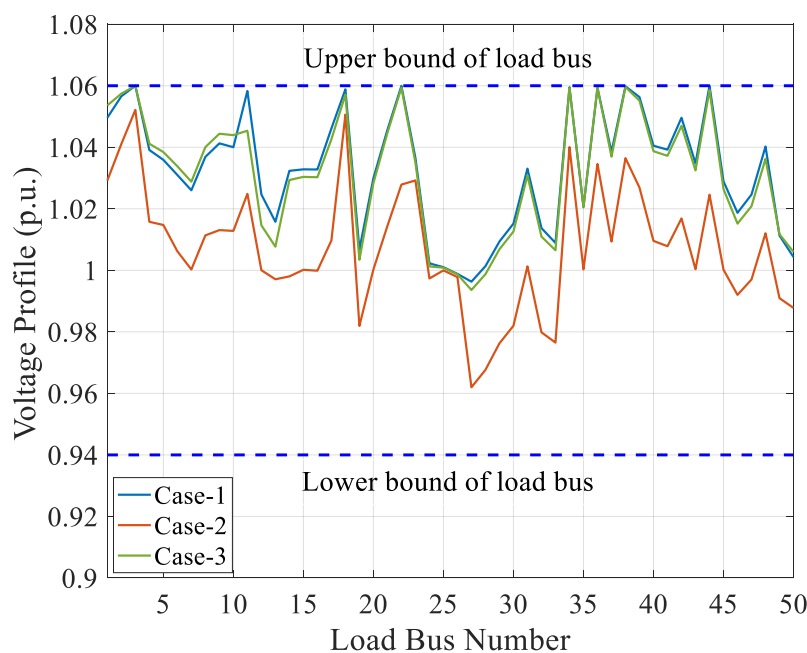


Figure 1. The voltage profiles of the load buses for all cases.

5. CONCLUSION

The optimal power flow (OPF) problem is a non-linear and complex optimization problem in modern power system applications. With the integration of wind energy, the complexity of the optimal power flow (OPF) problem increases. Therefore, the MHS algorithms are widely used in the literature for solving this problem. To solve the OPF problem in the presence of uncertainty of the wind energy, the nutcracker optimization algorithm (NOA) was used. Accordingly, three objective functions were considered, one of which is single-objective while two of them are multi-objective problems: (i) minimization of the total cost including the thermal and stochastic wind power generations, (ii) minimization of the total cost and voltage deviation, and (iii) minimization of the total cost and voltage stability index. Three case studies were conducted using three objective functions. The simulation studies were carried out on a modified IEEE 57-bus test system. According to the simulation results, the NOA obtained the 31588.8197\$/h, 31695.3571\$/h, and 31617.3494\$/h fitness function values for Case-1, Case-2, and Case-3., respectively. Moreover, the results of the NOA were compared with the results reported in the literature. According to the comparisons, the NOA achieved the best results which were lower by 0.0219%, 0.0186%, and 0.0212% for Case-1, Case-2, and Case-3, respectively, than the LCOA algorithm reported in the literature. To sum up, these results validated the performance of the NOA in solving the OPF problem including wind energy sources.

Ethics Committee Approval

N/A

Peer-review

Externally peer-reviewed.

Author Contributions

B.Ö. : Conceptualization, Investigation, Material and Methodology, Software, Validation, Writing-Original Draft, Formal analysis.

Conflict of Interest

The authors have no conflicts of interest to declare.

Funding

The authors declared that this study has received no financial support.

REFERENCES

- Abd El-sattar, S., Kamel, S., Ebeed, M., Jurado, F. (2021). An improved version of salp swarm algorithm for solving optimal power flow problem. *Soft Computing*, 25, 4027-4052. <https://doi.org/10.1007/s00500-020-05431-4>
- Abdel-Basset, M., Mohamed, R., Jameel, M., Abouhawwash, M. (2023). Nutcracker optimizer: A novel nature-inspired metaheuristic algorithm for global optimization and engineering design problems. *Knowledge-Based Systems*, 262, 110248. <https://doi.org/10.1016/j.knosys.2022.110248>
- Al-Muhawesh, T. A., Qamber, I. S. (2008). The established mega watt linear programming-based optimal power flow model applied to the real power 56-bus system in eastern province of Saudi Arabia. *Energy*, 33(1), 12-21. <https://doi.org/10.1016/j.energy.2007.08.004>
- Attia, A. F., El Sehiemy, R. A., Hasanien, H. M. (2018). Optimal power flow solution in power systems using a novel Sine-Cosine algorithm. *International Journal of Electrical Power & Energy Systems*, 99, 331-343. <https://doi.org/10.1016/j.ijepes.2018.01.024>
- Biswas, P. P., Suganthan, P. N., Mallipeddi, R., Amaratunga, G. A. (2018). Optimal power flow solutions using differential evolution algorithm integrated with effective constraint handling techniques. *Engineering Applications of Artificial Intelligence*, 68, 81-100. <https://doi.org/10.1016/j.engappai.2017.10.019>
- Burchett, R. C., Happ, H. H., Vierath, D. R. (1984). Quadratically convergent optimal power flow. *IEEE Transactions on Power Apparatus and Systems*, (11), 3267-3275. <https://doi.org/10.1109/TPAS.1984.318568>
- Chaib, A. E., Boucekara, H. R. E. H., Mehasni, R., Abido, M. A. (2016). Optimal power flow with emission and non-smooth cost functions using backtracking search optimization algorithm. *International Journal of Electrical Power & Energy Systems*, 81, 64-77. <https://doi.org/10.1016/j.ijepes.2016.02.004>

El-Fergany, A. A., Hasanien, H. M. (2018). Tree-seed algorithm for solving optimal power flow problem in large-scale power systems incorporating validations and comparisons. *Applied Soft Computing*, 64, 307-316. <https://doi.org/10.1016/j.asoc.2017.12.026>

IEEE 57-bus test system data: https://labs.ece.uw.edu/pstca/pf57/pg_tca57bus.htm

Kaymaz, E., Duman, S., Guvenc, U. (2021). Optimal power flow solution with stochastic wind power using the Lévy coyote optimization algorithm. *Neural Computing and Applications*, 33(12), 6775-6804. <https://doi.org/10.1007/s00521-020-05455-9>

MATPOWER <http://www.pserc.cornell.edu/matpower/>

Meng, A., Zeng, C., Wang, P., Chen, D., Zhou, T., Zheng, X., Yin, H. (2021). A high-performance crisscross search based grey wolf optimizer for solving optimal power flow problem. *Energy*, 225, 120211. <https://doi.org/10.1016/j.energy.2021.120211>

Mishra, C., Singh, S. P., Rokadia, J. (2015). Optimal power flow in the presence of wind power using modified cuckoo search. *IET Generation, Transmission & Distribution*, 9(7), 615-626. <https://doi.org/10.1049/iet-gtd.2014.0285>

Mohamed, A. A. A., Mohamed, Y. S., El-Gaafary, A. A., Hemeida, A. M. (2017). Optimal power flow using moth swarm algorithm. *Electric Power Systems Research*, 142, 190-206. <https://doi.org/10.1016/j.epsr.2016.09.025>

Nadimi-Shahraki, M. H., Fatahi, A., Zamani, H., Mirjalili, S., Oliva, D. (2022). Hybridizing of whale and moth-flame optimization algorithms to solve diverse scales of optimal power flow problem. *Electronics*, 11(5), 831. <https://doi.org/10.3390/electronics11050831>

Nguyen, T. T. (2019). A high performance social spider optimization algorithm for optimal power flow solution with single objective optimization. *Energy*, 171, 218-240. <https://doi.org/10.1016/j.energy.2019.01.021>

Ozkaya, B. (2024). Enhanced growth optimizer algorithm with dynamic fitness-distance balance method for solution of security-constrained optimal power flow problem in the presence of stochastic wind and solar energy. *Applied Energy*, 368, 123499. <https://doi.org/10.1016/j.apenergy.2024.123499>

Panda, A., Tripathy, M. (2014). Optimal power flow solution of wind integrated power system using modified bacteria foraging algorithm. *International Journal of Electrical Power & Energy Systems*, 54, 306-314. <https://doi.org/10.1016/j.ijepes.2013.07.018>

Roy, R., Jadhav, H. T. (2015). Optimal power flow solution of power system incorporating stochastic wind power using Gbest guided artificial bee colony algorithm. *International Journal of Electrical Power & Energy Systems*, 64, 562-578. <https://doi.org/10.1016/j.ijepes.2014.07.010>

Shilaja, C., Arunprasath, T. (2019). Optimal power flow using moth swarm algorithm with gravitational search algorithm considering wind power. *Future Generation Computer Systems*, 98, 708-715. <https://doi.org/10.1016/j.future.2018.12.046>

Teeparthi, K., Vinod Kumar, D. M. (2018). Security-constrained optimal power flow with wind and thermal power generators using fuzzy adaptive artificial physics optimization algorithm. *Neural Computing and Applications*, 29, 855-871. <https://doi.org/10.1007/s00521-016-2476-4>

Yan, X., Quintana, V. H. (1999). Improving an interior-point-based OPF by dynamic adjustments of step sizes and tolerances. *IEEE Transactions on Power Systems*, 14(2), 709-717. <https://doi.org/10.1109/59.761902>

FEM Model and Frequency Response Analysis of PCB Coils for Wireless Power Transfer

Žarko Martinović¹

Abstract: The objective of this paper is to present the finite element method (FEM) model of a wireless power transfer (WPT) system utilizing two printed circuit boards (PCB) coils, and to analyse the influence of the distance between coils and permittivity of the substrate. In this way, an easy integration of the transmitter coils and the electronics is allowed, which further simplifies assembling of the whole system. Since the resonant frequencies of the system depend on the distance of the transmitter and receiver coils, while the accurate analytical calculation of the overall lumped inductances and capacitance of the coils is very difficult, the full-wave FEM simulation was performed as an initial step in defining the demands for the drive electronics of the system. The full-wave simulations were run in HFSS. The design of the transmitter and the receiver was based on the standard double-sided PCB FR4 fiberglass-epoxy laminate. The WPT system was analysed for transmitter and receiver distances spanning from 1mm to 100mm. The influence of the permittivity of the PCB substrate was further analysed. Simulation results were compared by extracting Z parameters (impedance parameters) for different model scenarios. Z parameters of the two-port representation of coils systems can be easily extracted from the FEM solver for any distance of the receiving and transmitting coil, and further applied in the calculation of the transferred power and system efficiency using standard method of two-port analysis.

Keywords: Wireless Power Transfer; WiTricity; FEM, Resonant Coupling; Resonant Frequency

¹**Address:** Danieli Taranis LLC, 54 Chesser Crane Rd, 35043 Chelsea, USA / University of Zagreb Faculty of Electrical Engineering and Computing, Unska 3, 10000 Zagreb, Croatia ; z.martinovic@taranis.danieli.com , zarko.martinovic@fer.unizg.hr

***Corresponding author:** z.martinovic@taranis.danieli.com

1. INTRODUCTION

Wireless power transfer (WPT) represents the concept of energy transfer through resonant magnetic coupling. The objective of this paper is to present the finite element method (FEM) model of a WPT system utilizing two printed circuit boards (PCB) loops, and to analyze the influence of the distance between the coils and permittivity of the substrate. Wireless power transfer [1-6] from Figure 1. Consists of four main parts:

- Power Source - Amplifier
- Resonance Loops – Transmitter
- Receiver Loops – Receiver
- Load

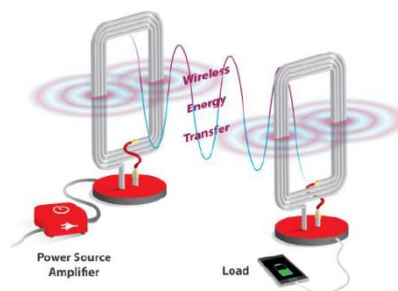


Figure 1. Wireless Power Transfer Components

Electromagnetic systems can excite resonance due to electromagnetic coupling – to transfer energy at some distance. If those systems obtain the same resonant frequency – they can exchange energy. In [5] a separate single coil turn was introduced at the transmitter side as an impedance transformer, and later the same concept was used by other authors. To design the entire transmitter system in a double-sided PCB laminate, this concept is in this paper replaced by a direct

excitation of the transmitter coil, which is made as a planar inductance in PCB. In this way, an easy integration of the transmitter coils and the electronics is allowed, which further simplifies assembling of the whole system. The resonant frequency of the planar coil is influenced by its inductance and the inter-turn capacitance. Since the resonant frequencies of the system depend on the distance of the transmitter and receiver coils, while the accurate analytical calculation of the overall lumped inductances and capacitances of the coils is very difficult, the full-wave FEM simulation was performed as an initial step in defining the demands for the drive electronics of the system. The model was created in High Frequency Structure Simulator (HFSS) according to the similar models in papers [7][8][9]. Verified and simulated model will enable us development of different optimization techniques.

2. COUPLED RESONATORS

Figure 2. depicts a system of two coupled resonators. Here, U_S denotes voltage source, ω is angular frequency, R_s is internal resistance of the source, L_1 source inductance, L_2 is device inductance, $M_{1,2}$ is mutual inductance, C_1 is source capacitance, C_2 is device capacitance, R_L is load resistance, I_1 is source current and I_2 is load current.

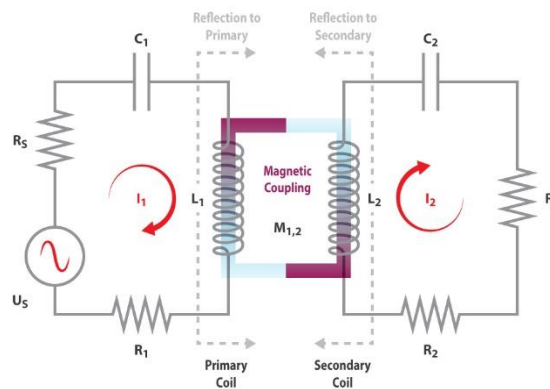


Figure 2. Equivalent circuit for coupled resonator system

If we denote overall resistance at the transmitting side as R_S' , the input power can be expressed as [10]:

$$P_{IN} = \frac{\{R_S'[(R_2+R_L)^2+(\omega L_2)^2]+(\omega M_{12})^2(R_2+R_L)\} U_S^2}{[R_S'(R_2+R_L)-\omega^2 L_1 L_2-(\omega M_{12})^2]^2+[R_S'\omega L_2+(R_2+R_L)\omega L_1]^2} \quad (1)$$

while the output power can be expressed as:

$$P_O = \frac{(\omega M_{12})^2 U_S^2 R_L}{[R_S'(R_2+R_L)-\omega^2 L_1 L_2-(\omega M_{12})^2]^2+[R_S'\omega L_2+(R_2+R_L)\omega L_1]^2} \quad (2)$$

Based on the equations (1) and (2), the system efficiency is [10]:

$$\eta = \frac{(\omega M_{12})^2 R_L}{R_S'[(R_2+R_L)^2+(\omega L_2)^2]+(\omega M_{12})^2(R_2+R_L)} \quad (3)$$

The transferred power splits into two peak values when the coupling coefficient of the coils is large, where the lower frequency corresponds to the odd mode. The higher frequency corresponds to the even mode. At splitting frequencies, the transferred power reaches its maxims. The odd mode allows larger efficiency, and therefore it is mostly chosen as the operating frequency of the system. The system efficiency reaches its maximum at the natural resonant frequency [10]. The impedance parameters (Z parameters) of the two-port representation of coil systems can be easily extracted from the FEM solver for any distance of the receiving and transmitting coil, and further applied in the calculation of the transferred power and system efficiency using standard method of two-port analysis.

For a two-port connected to a source with the source impedance Z_1 and terminated with load impedance Z_2 , the input and output voltages can be generally expressed as

$$U_1 = z_{11}I_1 + z_{12}I_2 \quad (4)$$

$$U_2 = z_{21}I_1 + z_{22}I_2 \quad (5)$$

where z_{11} and z_{22} are open-circuit driving point impedances and z_{12} and z_{21} are open circuit transfer impedances of the two-port [11].

3. RESULTS

Developed model is based on two identical PCB coils made of FR-4 laminate. The loops are made of copper with thickness 0.035 mm. On transmitter and receiver sides the appropriate lumped ports were assigned, and the whole system was placed into an air box with radiating boundaries. Analysis of resonant frequency was the main output of

simulations which were conducted between 1 and 100 MHz. Maximum number of passes was 6. The resonant frequency of the system was targeted to satisfy the European regulations for the inductive loop systems in the frequency range 9 kHz to 30 MHz, i.e. ETSI EN300 330 [12]. WPT model (Figure 3.) consists of two identical PCB coils. Simulation were run with distances between coils equal to 1, 20, 40, 60, 80 and 100 mm, for all simulations presented in the paper.

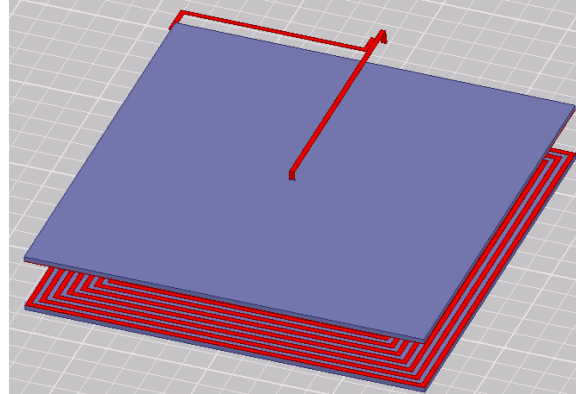


Figure 3. FEM model of the WPT system

Figure 4. depicts the frequency response of the Z_{21} parameter for all examined distances. From Figure 4. we can conclude that the main resonant frequencies are in the band 10 - 30 MHz, for all examined distances, with the biggest peak at 25 MHz and 40 mm.

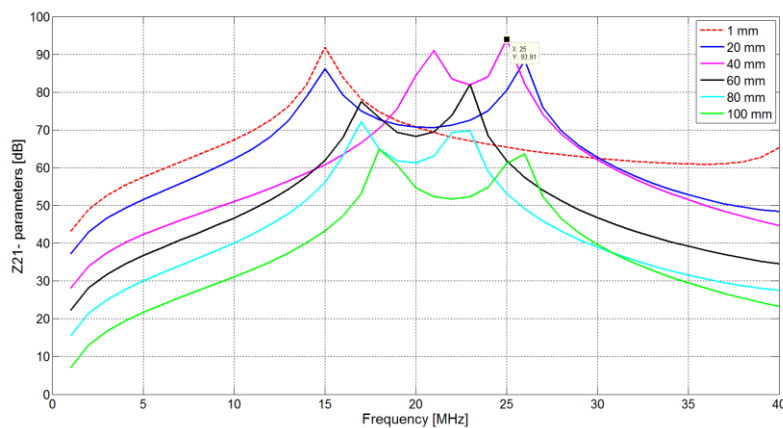


Figure 4. Z_{21} -parameters of model

Since the wavelength was much greater than the physical dimensions of the system, the adaptive meshing of all models was based on the element length based refinement, with the restricted maximum length of the elements in the whole domain (including air box) equal to 17.82 mm (wavelength was always below 3 m), and using the unrestricted number of elements. The influence of the permittivity of the PCB substrate on the change of the resonant frequencies was further analyzed. For such a purpose, in this model the PCB substrate was replaced by the air. Such a conductor model represents simplified model, which consists of two loops with air gap distance. The results are presented in Figure 5. The decrease of the permittivity increased the frequencies of the resonance peaks for approximately 4 MHz, which is the absolute upper bound for possible change in the resonant frequencies due to different substrate materials (FR-3, Rogers), or the frequency dependence of the permittivity.

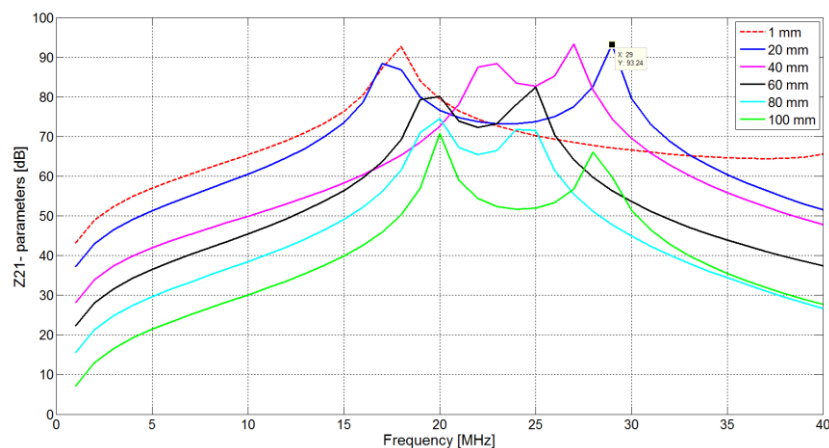


Figure 5. Z_{21} -parameters of the WPT model consisted of coils only (without substrate)

4. CONCLUSIONS

To properly design wireless power transfer system, it is necessary to carefully determine the resonant frequency of the system, as well as its frequency response. As it can be seen from the FEM analysis, the main resonant peak of the system was near to 20 MHz. The decrease of the permittivity increased the frequencies of the resonance peaks for approximately 4 MHz. For all presented scenarios, the impedance parameters (Z -parameters) were extracted, which allows easy calculation of the system response for different loads, as well as their matching regarding to the efficiency and the maximum power transfer.

REFERENCES

- Karalis, A., Joannopoulos, J. D., Soljačić, M., (2008). „Efficient wireless non radiative mid – range energy transfer“. *Annals of Physics*. Vol.3 no. 23, pp 34-48.
- Winfield Secor, H., (1921). „Tesla apparatus and experiments – how to build both large and small Tesla and Oudin coils an hot to carry on spectacular experiments with them “. *Practicle Electrics*.
- Kim, C. – G., Seo, D. – H., You, J. – S., Park, J. – H., Cho, B.H., (2001). „Design of a contactless battery charger for cellular phone “. *IEEE Trans. Ind. Electron*. Vol. 48, no. 6, pp. 1238-1247.
- Hu, S. Y., (2013). „Planar Wireless Charging Technology for Portable Electronic Products and Qi “. *Proc. IEEE*. Vol. 101, p. 1290-1301.
- Kurs, A., Karalis, A., Moffatt, R., Joannopoulos, J. D., Fisher, P., Soljačić, M., (2007). „Wireless Power Transfer via Strongly Coupled Magnetic Resonances “. *Science*, vol. 317, pp. 83-86.
- Jang, Y., Jovanovic, M., (2003). “A contactless electrical energy transmission system for portable – telephone battery chargers”. *IEE Trans. Ind. Electron*. Vol. 50, no.4, pp. 520-527.
- Wang, J., Ho, S. L., Fu, W. N., Sun, M., (2010). „Finite element analysis and corresponding experiments of resonant energy transmission for wireless transmission devices using WiTricity “. *14th Biennial IEEE Conference on Electromagnetic Field Computation (CEFC)*. PP. 1,1.
- Zhou, H., Wang, J., Fu, W. N., Sun, M., (2011). „ A comparative Study Between Novel WiTricity and Traditional Inductive Magnetic Coupling in Wireless Charging “. *IEEE Transactions on Magnetics*. Vol. 47, no. 5, pp. 1522, 1525.
- Salleh, M. H., Seman, N., Dewan, R., (2013). „ Reduced – Size WiTricity Charger Design and Its Parametric Study“. *IEEE International RF and Microwave Conference (RFM)*.
- Huang, R., Zhang, B., Qiu, D., Zhang, Y., (2014). “Frequency Splitting Phenomena of Magnetic Resonant Coupling Wireless Power Transfer”. *IEEE transaction on Magnetics*. Vol. 50, no. 11, pp. 8600204.
- Chua, LO., Desoer, CA., Kuh, ES., (1987). *Linear and Nonlinear Circuits*, Mc-Graw-Hill, New York.

ETSI EN 300 330 V2.1.1., (2017). Short Range Devices (SRD), Radio equipment in the frequency range 9 kHz to 25 MHz and inductive loop systems in the frequency range 9 kHz to 30 MHz.

Examination of Chemical Elements in Animal Feed

Julijana Tomovska^{1*}, Ilmije Vllasaku², Vezir Januzi³

Abstract: The animal feed that is used to feed dairy cows is mostly of vegetable origin, a small part is used of mineral origin to provide calcium and phosphorus, which are two basic mineral substances for normal health and high milk production. Proper, well-balanced quality food with a daily ration that should contain all the necessary nutrients, macro and micro elements in quantity and ratio for their normal use is of particular importance in nutrition. Tests were made of the mineral substances in the animal feed with which the dairy cows from three farms A, B, C are fed. According to the way of feeding the cows, alfalfa hay, concentrate for dairy cows K1 and K2 and wheat straw are used up to to some extent they meet the nutrient requirements for a given milk production. The chemical elements in animal feed were examined using ICP-AES (Varian, 715-ES), using an ultrasonic nebulizer CETAC (ICP / U-5000AT+). The average content of total mineral substances in the daily meal of dairy cows is the highest in farm B, 2540.07 mg/kg. Chemical elements (21) were analyzed in all used feeds for each farm, but the elements present in alfalfa with the highest values are singled out. Farm A has potassium 16639.00 mg/kg, calcium 5802.00 mg/kg, manganese 1257 mg/kg, phosphorus 627.00 mg/kg, aluminum 220.00 mg/kg, iron 184.00 mg/kg. Strontium has the lowest values, 7.37 mg/kg. Farm B has potassium 17205.00 mg/kg, calcium 5112 mg/kg, manganese 1928 mg/kg, phosphorus 11904.00 mg/kg, aluminum 2428.00 mg/kg, iron 2243.00 mg/kg, magnesium 1928.00 mg/kg. The lowest values are for cuprum Cu 13.7 mg/kg. Farm C has potassium 14768 mg/kg, calcium 4093 mg/kg, manganese 1142 mg/kg, phosphorus 1748 mg/kg, aluminum 136.58 mg/kg, iron 114 mg/kg. Boron has the lowest values, 9.51 mg/kg. From the analysis of chemical elements in animal feed, we conclude that the highest value for potassium of 17205 mg/kg was measured in farm B, in alfalfa, and the lowest value is strontium of 0.77 mg/kg in K1 from farm A. The total percentage representation of the most common chemical elements in the total food in the three farms is: 63% potassium, 14% phosphorus, 13% calcium and 8% magnesium. In relation to the used daily meal (20 kg - farm A, 28 kg - farm B and 31 kg - farm C), it is established that the feed from farm B is the richest in elements. Mineral substances such as macroelements are present in larger quantities and their representation is quite variable, while microelements are present in small quantities and their representation is more constant. There are also elements that are represented in traces, oligoelements and their representation is constant. The chemical elements: As, Cd, Co, Cr, Li, Ni, Pb and V in all feeds used on the three farms A, B, C are present in a smaller amount than 1 mg/kg.

Keywords: mineral substances, macro elements, microelements, animal feed, chemical elements.

¹University "St. Kliment Ohridski" - Bitola, ¹Faculty of Biotechnical Sciences, Partizanska bb, 7000 Bitola, Macedonia

^{2,3}UBT - Higher Education Institution, Kalabrija nn, 10000 Prishtina, Kosovo

*Corresponding author: dzulitomovska@yahoo.com

1. INTRODUCTION

Nutrients are ingredients that serve to provide the physiological and nutritional requirements of domestic animals and include: proteins, fats, carbohydrates, minerals, vitamins and water. Mineral substances are part of animal feed, are digestible and are used by the animal organism. They serve to satisfy physiological needs, maintain basal metabolism and reproduction, as well as productive needs during milk production. The animal feed that is used to feed dairy cows is mostly of vegetable origin, and a small part is used of mineral origin to provide calcium and phosphorus, which are two basic mineral substances for normal health and high milk production. When feeding dairy cows, it is of particular importance to provide sufficient quality feed with all the necessary nutrients, in quantity and ratio for their normal utilization Samuel X., Radbill, (1976).

In this paper, tests of chemical elements in the animal feed with which the dairy cows from three farms A, B, C are fed. Mineral substances in animal feed-forages as the usual practice in application on farms and according to the type and method of feeding of cows (alfalfa hay, concentrate for dairy cows and wheat straw) are considered to meet to some extent the nutrient requirements for certain milk production Nikolovska, M., Arsovska, F. (2014).

Alfalfa (*Medicago sativa* L.) is one of the most important fodder crops and is a valuable leguminous crop that is used for feeding livestock in the proven state, in the form of hay, and for many of us it is used as alfalfa hay. Alfalfa, as a fodder crop, is mostly grown in areas where there are conditions for irrigation and darkness, 5-6 cuttings can be obtained and more than 10 tons of high-quality alfalfa hay can be produced. In our country, the most cultivated variety of alfalfa is blue alfalfa *Medicago sativa* L., and it is used in the form of hay, and a lot of it in its green state causes bloat in cows, but if it is used in its fresh state, it should be mowed and tested first and then feed the cows. For that reason, alfalfa is not recommended for a green diet (Ivanovski, R., 2011). The differences in the chemical composition and general nutritional value of the forage crops used as food for farm animals should be known in order to be able to balance the nutrient and energy requirements for each category of farm animals in order to satisfy their physiological needs Caisin, L., et al., (2012); Scientific papers, series D, Animal Science, (2016). In addition to vision and genetic predisposition to animals for higher milk production, proper and balanced nutrition is of crucial importance. The nutritional requirements of dairy cows are mainly met through the use of fodder culture in fresh or canned form, then waste from the food industry (beet pulp, bran, beer wort) and other agro-industrial products (Sarwar, M., et al., 2002b), and (Sarwar, M., et al., 2012) The quantity and quality of the available food and water are, to a large extent, the most important not only for the high production of milk, meat and eggs, but also for the wood of the farm animals (Learne Guide, Primary Agriculture, 2006). it supports immunity functions and helps with iron absorption (Catalog for feed mixes, DOO "Agroinvest" (2017); IndiaMART, Irrvfan K., (2014) and Margarit G., and Tomoa R.S., (2016).

Wheat straw (*Triticum vulgare*) contains organic chemical compounds, such as carbohydrates (cellulose, hemicellulose, lignin), proteins, minerals (calcium and phosphorus), silicon dioxide, detergent fibers, acidifiers and ash (McKean and Jacobs, 1997). The same results coincide with the results of Khan, (2012). Research by Plazonić (2016) indicates the large presence of many chemical elements in barley straw. A large number of chemical elements such as K, Ca, Mg, P, Zn, Fe, Mn, Cu, B, Mo, Al, Bi, As, Ba, Cr, Pb, Ni, Cd, Co, V, Hg are isolated in different ways. Straw is poor in crude proteins and nitrogen-free extractive materials (BEM). According to Korr (2017), in his research, he concluded that the chemical composition of different types of straw is different. He analyzed the chemical composition of several types of straw, such as: barley, wheat, pea, cinnamon and lentil straw. Also analyzed were indigestible proteins, processed nutrients, as well as calcium, phosphorus and potassium from the Animal Nutrition Group, National Dairy Development Board Annand - 3888-001, (2012).

The analysis of Korr, J., (2017) showed that straw contains a small amount of protein, nutrients, calcium and phosphorus from peas, while straw from oats contains more potassium. Mineral substances and their inorganic compounds have no energy value in animal feed, nor in the animal organism, but they are important in that they are an important structural element in the construction of various tissues and biological systems or as an important functional material in various biochemical processes in the animal organism.

Concentrated compound feed - concentrates have a huge impact on the profitability of dairy farms. For economical and cost-effective milk production, the daily ration of dairy cows should consist of high-quality forage and forage for dairy cows AHDB Dairy (2018). According to Rumsey (1980), forage for dairy cows should to meet energy and protein needs for maintenance, milk production, growth and reproduction. In addition to the need for energy and protein, they have to satisfy yourself with the increased need for minerals and vitamins. Forage for dairy cows is the main source of easily digestible energy and protein, but usually contains a large amount of minerals and other important nutrients that cannot be satisfied through roughage - forage (Ishler, V. A., 2006). The composition of the concentrate and their characteristics are shown according to Kavanagh, S., (2016), where mineral substances, especially the amount of trace elements, are important not only for the health of dairy cows, but also for high milk production. Of the mineral substances, that is, of the macroelements, the most represented in the feed mixture for dairy cows are: calcium, phosphorus, sodium, chloride, potassium, magnesium, etc. the amount of which is expressed in (g) grams. In addition to the macroelements in the feed mixture for dairy cows, there are other elements in small amounts, called microelements, which are of great importance for the health, reproductive and productive characteristics of cow's milk. The group of microelements includes: iron, copper, selenium, iodine, cobalt, zinc, manganese, etc., and they are represented in very small amounts and their representation is expressed in (mg) milligrams.

Mineral substances are divided into two groups, macro and microelements. Macroelements in animal feed are present in larger quantities and their representation is quite variable, while microelements are present in small quantities and their representation is more constant. In addition to macro and microelements in food there are elements that are represented in traces and those that are so-called oligoelements and their representation in relation to macro and microelements is constant. Calcium is one of the most important elements because it plays a role in the mineralization of bones and teeth, muscle contraction and relaxation, as well as in the functioning of nerves and blood clotting. Iron as an element is important for the transport of oxygen in the body of animals. Iron is mostly found in the blood - hemoglobin and in the muscle pigment myoglobin. The distribution of iron in the body of animals depends on several factors. While the animal is alive, 95% of the iron is in the blood, and after slaughter 95% of the iron is in the muscles. Iron is an active

participant in the metabolism of animals, but it is also an active element in the muscles in the post-mortem period. Magnesium is an important element that participates in bone mineralization, protein building, normal muscle function, transmission of nerve impulses, proper immune function and maintenance of teeth. Phosphorus as an element is significant because it is involved in the mineralization of bones and teeth, it is an important element in the construction of genes that are important for the transmission of genetic traits from parents to offspring. It participates in the construction of DNA and RNA. Phosphorus, as an element, participates in the construction of cell membranes, as phospholipids, in the transfer of energy. Potassium as a chemical element participates and facilitates reactions, including the creation of proteins, and together with sodium is an important element in maintaining the balance of fluids and electrolytes, supporting cellular integrity, transmitting nerve impulses and muscle contraction, including the heart. Zinc is a trace element that is important for the normal functioning of hormones, it is needed for many enzymes, it is involved in the creation of genetic material and proteins, the activation of immune cells, the transport of vitamin A, etc. (Barba, D., et al., (2017); Caisin, L., et al., (2012); Scientific papers, Animal Science (2017).

In the group of macroelements that must be present in the feed for dairy cows are: sodium (Na), chlorine (Cl), calcium (Ca), phosphorus (P), potassium (K), magnesium (Mg), sulfur (S) etc. In the group of trace elements, the following are more significant: iron (Fe), copper (Cu), cobalt (Co), manganese (Mn), zinc (Zn), iodine (I), molybdenum (Mo) and selenium (Se). Mineral substances regardless of their representation (macro, micro or oligo) are necessary for the normal health of cows and the high production of quality milk.

Mineral substances are necessary not only for the normal development of physiological and biochemical processes, but are important for high production of milk, especially the presence of calcium (Ca), magnesium (mg), potassium (K) etc. and for those reasons, daily needs should be met through food, Gaall K et al., (2004). In the daily diet of dairy cows, in addition to forage mixtures and fodder, a mineral mixture in the form of bricks is regularly given or made available, and the cows satisfy the needs of all mineral substances by licking. Excessive intake of certain elements (Cu, Mo, Co, I, Se, etc.) can have a toxic effect on the health of cows, the element magnesium (Mg) is necessary, Kovacsne, G. K., et al., (2004).

Many studies have shown that in addition to carbon, hydrogen, nitrogen, oxygen and sulfur, which are the main elements in the construction of organic substances in the body, at least fourteen more compounds are needed in which mineral substances participate, of which the following elements are more important: Ca, P, K, Mg, Cu, Mn, Zn, I, Fe, Co, Mo and Se. Calcium and phosphorus are necessary for building the skeletal structure of the body. Sodium, potassium and chlorine, along with phosphates and bicarbonates, have the function of maintaining homeostasis and are necessary for the osmotic ratio and pH in the body. The remaining elements participate as parts of hormones or enzymes or are activators of enzymes. Some other elements, such as fluorine and chromium, also fulfill separate functions in the body, but to date they have not been classified as essential nutrients Haridasan, M. (2008). Cadmium and vanadium belong to a special category of elements due to their harmful effects, but, however, to date they are not classified in the group of toxic substances, such as for example arsenic, lead and beryllium (Milosavljević, Z., and Pauca, V., 1978), Beneficial Management Practices (2006).

The aim of the research is to examine the chemical elements in: alfalfa, concentrates and straw in samples from three different farms, ie. tests the mineral composition of livestock feed that play an important role for the growth and development of livestock, and especially for the quality of milk, which is a necessary product for human nutrition. 21 chemical elements were analyzed: aluminum (Al), arsenic (As), boron (B), barium (Ba), calcium (Ca), cadmium (Cd), cobalt (Co), chromium (Cr), copper (Cu), iron (Fe), potassium (K), lithium (Li), magnesium (Mg), manganese (Mn), sodium (Na), nickel (Ni), phosphorus (P), lead (Pb), strontium (Sr), vanadium (V) and zinc (Zn). Statistical analysis - all experimental measurements were performed in triplicate and calculated by variational statistical methods in Excel.

2. MATERIAL AND METHOD

Investigations of the mineral composition, the presence of macro and microelements in animal feed: alfalfa hay, K1 and K2 concentrates, as well as wheat straw were performed using Inductively Coupled Plasma Atomic Emission Spectrometry (ICP-AES). The content of heavy metals (arsenic, cadmium, cobalt, chromium, copper, iron, manganese, nickel, lead, vanadium and zinc), as well as useful metals that are needed such as calcium, magnesium, potassium, sodium, etc., or a total of 21 elements in animal feed were examined.

2.1. Method for testing chemical elements in animal feed

Sample preparation and digestion:

In the laboratory, the samples were cleaned, but the samples were not subjected to any further cleaning and drying to constant weight for 48 h at room temperature. Samples (0.5000 g) were placed in Teflon crucibles, 7 ml of pure trace HNO₃ (Merck, Germany) and 2 ml of H₂O₂ p were added. a. (Alkaloid, Macedonia), then the vessels are hermetically sealed and placed in the rotor of a microwave oven for mineralization – Marsmicrowave digestion apparatus (CEM, USA). Plant samples are boiled at t=180 °C. After cooling, the samples were transferred to 25 ml calibration flasks, EN ISO 6498 (2011).

Reagents and standards:

Standard solutions (11355-ICP Multi Element Standard IV, Merck) of 20 elements with a concentration of 1000 mg L⁻¹ were prepared for further dilution. All chemical reagents are analytically of high purity: HNO₃, p. a. (Merck, Germany), H₂O₂, p. a. (Merck, Germany). All vessels used were pre-cleaned by leaching 1 part HNO₃ and 3 parts HCl in the appropriate proportions for 24 hours, followed by double rinsing with distilled water.

Instrumentation:

All analyzed elements (Al, As, B, Ba, Ca, Cd, Co, Cr, Cu, Fe, K, Mg, Mn, Na, Ni, P, Pb, Sr, V and Zn) were determined using ICP – AES (Varian, 715-ES) and using a CETAC ultrasonic nebulizer (ICP/U-5000AT+) for better sensitivity. The optimal instrumental parameters for these techniques are given by Balabanova, B., et al., (2016).

Quality control:

Quality control was ensured using standard reference materials M2 and M3, which were prepared for the European Mold Survey (Mr Harry Harmens, 2010). There were good matches between the measured concentrations and the recommended values. The standard addition method was also applied, achieving quantitative reverse agreement of results for most elements.

3. RESULTS

3.1. Amount of chemical elements in animal feed from three farms

The results for the investigated chemical elements in animal feed (concentrates K1 and K2, alfalfa and straw) from the three farms are shown in Table 1 for farm A, and therefore Table 2 and Table 3 for farm B and C.

The chemical elements: As, Cd, Co, Cr, Li, Ni, Pb and V in all feeds used on the three farms A, B, C are present in a smaller amount than 1 mg/kg.

Table 1: Chemical elements in the feed of farm A

Amount of chemical elements from feed of farm A - w _i / (mg/kg)														
Animal feed	Al	B	Ba	Cu	Fe	Mn	Na	Sr	Zn	Ca	K	Mg	P	Total amount
K1	110.00	3.45	1.75	12.60	104.00	6.64	28.70	0.77	10.40	153.00	2619.00	869.00	1990.00	5909.00
K2	10.80	2.15	10.70	21.30	66.50	97.50	46.20	3.53	44.30	562.00	6832.00	2095.00	5196.00	14987.98
Alfalfa	220.00	80.50	49.70	8.51	184.00	70.90	123.00	7.37	7.60	5802.00	16639.00	1257.00	627.00	25076.58
Straw	15.50	2.35	27.10	4.04	26.80	19.70	60.80	7.37	7.60	1096.00	12599.00	513.00	627.00	15006.26
Total	356.3	88.45	89.25	46.45	381.3	194.74	258.7	19.04	69.9	7 613	38 689	4 734	8 440	60 97982

Table 2: Chemical elements in the feed of farm B

Amount of chemical elements from feed of farm B – w _i (mg/kg)														
Animal feed	Al	B	Ba	Cu	Fe	Mn	Na	Sr	Zn	Ca	K	Mg	P	Total amount
K1	99.8	12.6	5.29	34.8	171	133	13.3	299	15283	8702	3072	2944	7537	38.306.79
K2	46.6	6.6	5.64	24.9	99.6	89.3	8.58	81.8	7461	4913	1862	6387	3217	24.113.88
Alfalfa	2428	157	50.9	13.7	2243	96.4	22.5	20.9	<1	17205	1928	625	11904	36.553.1
Total	2574.4	176.2	61.83	73.4	2513.6	318.7	44.38	401.7	22744	30820	6862	9956	22 658	99.204.21

Table 3: Chemical elements in the feed of farm C

Amount of chemical elements from feed of farm C – w _i (mg/kg)														
Animal feed	Al	B	Ba	Cu	Fe	Mn	Na	Sr	Zn	Ca	K	Mg	P	Total amount
K 1	53.4	3.56	16.8	743	29.9	130	8419	2944	94.6	69.0	6785	5.32	64.3	19357.88
Alfalfa	136.5	9.51	10.5	4093	10.7	114	14768	1142	11.4	528	1748	16.2	10.7	22598.51
Total	189.9	13.07	27.3	4836	40.17	244	23187	4086	106	597	8533	21.52	75	41 55.96

3.2. The average representation of chemical elements in animal feed from the three farms

The percentage composition of total feed used for livestock nutrition in the three farms: A, B and C (100 %) and the detected 13 chemical elements in the feed, used on the three farms with the highest percentage representation, is shown in Figure 1 and 2.

Calculated value of chemical elements in daily food used in farm A.

In farm A, livestock feed uses: 8 kg of concentrate K1, 8 kg of concentrate K2, 8 kg of alfalfa and 7 kg of straw, a total of 31 kg of animal feed per day. Potassium (K) (242311.656 mg in 31 kg) is mostly present in the total amount of food, followed by phosphorus (P) (66893 mg in 31 kg). The richest animal feed with the highest level of the examined elements is alfalfa (200612.0 mg in 8 kg). The total value of chemical elements in the four types of food from farm A is 401705.556 mg in 31 kg.

Calculated value of the chemical elements in the daily food used in farm B.

In farm B, the following are used for feeding livestock: 10 kg of concentrate K1, 10 kg of concentrate K2 and 8 kg of alfalfa, a total of 28 kg of animal feed per day. In the total amount of food, potassium (K) (136287.64 mg in 31 kg) is mostly present, followed by phosphorus (P) (202772 mg in 31 kg). The richest K 2 with the highest level of the tested elements is concentrate K1 (383567, 9 mg in 10 kg).

Calculated value of chemical elements in the daily food used in farm C.

In farm C, two types of feed are used for feeding livestock: 10 kg of concentrate K1, 10 kg of alfalfa, a total of 20 kg of feed per day. Table 3 presents the calculated values for the daily food used in farm C.

In the total amount of food used, sodium (Na) (9512.8 mg in 20 kg) is mostly present, followed by phosphorus (P) (7074.8 mg in 20 kg). The richest animal feed with the highest level of the investigated elements in farm C is the concentrate (35153.5 mg in 10 kg).

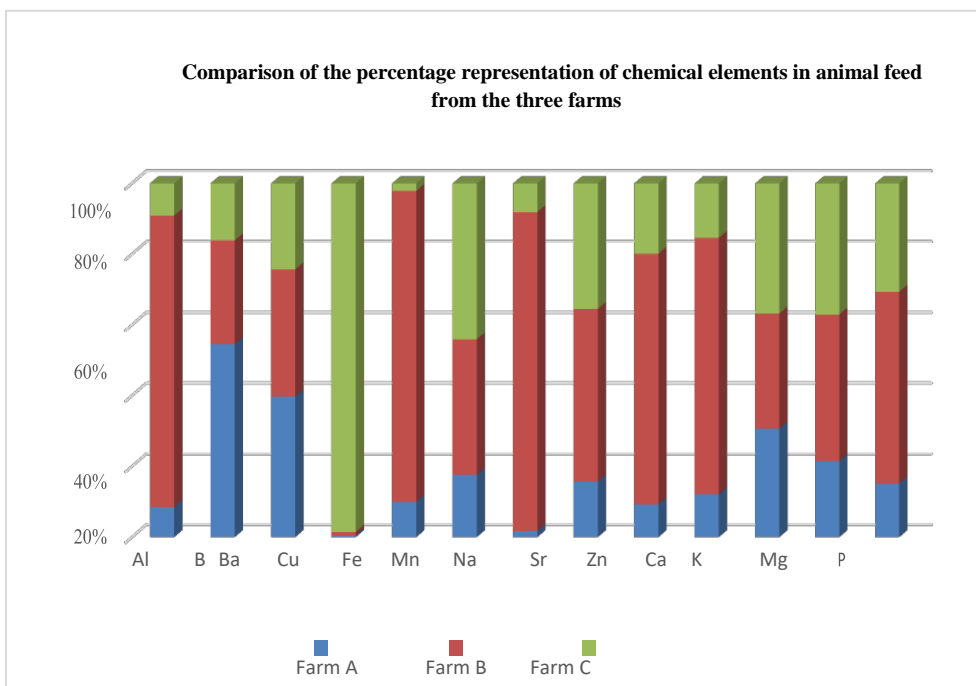


Figure 1: Representation of each chemical element in % in the food from the three farms

Percentage (%) of representation for chemical elements from the three farms

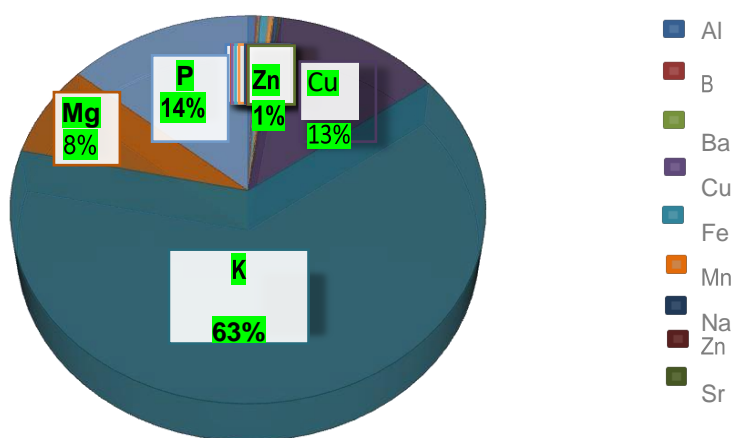


Figure 2: Percentage representation of maximum chemical elements from all three farms

3.3. The chemical elements in the total used animal feed on the three farms

The calculated total values for the representation of chemical elements in the total used food of the three farms and their comparison are shown in Table 4.

The calculation was made in the following way: the values of the amounts of food used daily for nutrition (each food expressed in a measurement unit, kg) were collected. Example, for farm A the values of 4 types of food are collected, for farm B for 3 types of food and for farm C for 2 types of food.

In concentrate K1 from farm A, there is the highest amount of chemical elements (47,274.48 mg in 8 kg), followed by farm B (383,567.9 mg in 10 kg), and the lowest value is concentrate K1 from farm B (35,153.5 mg in 10 kg). In concentrate K2, the amount of chemical elements is the highest in farm A (48754.256 mg in 8 kg) compared to farm B (242.031.8 mg in 10 kg).

In alfalfa, the highest amount of chemical elements was measured on farm A (200 612 mg in 8 kg), followed by farm B (154,922.44 mg in 10 kg), while the lowest amount was measured in alfalfa on farm C (9153.95 mg in) 10 kg. In the straw, the amount of chemical elements was analyzed only in farm A (105064.82 mg in 7 kg) because in farm B and farm C no straw was used as feed.

Calculated the total amount of chemical elements in all meals together (concentrate K1, concentrate K2, alfalfa and straw) the highest amount of chemical elements is in the feed of farm B (780522.14 mg in 28 kg), and in farms A and C the value of chemical elements is almost half of the amount of farm B, Table 4.

Table 4: Comparison of the amount of chemical elements in the total used food from the three farms

Farm		K 1 (mg/kg)	K 2 (mg /kg)	Alfalfa (mg/kg)	Straw (mg/kg)	Total amount / quantity (mg/kg)
1	A	47274.48 mg in 8 kg	48754.256 mg in 8 kg	200612 mg in 8 kg	105064.82 mg in 7 kg	401705.556 mg in 31kg
2	B	383567.9 mg in 10 kg	242031.8 mg in 10 kg	154922.44 mg in 8 kg		780522.14 mg in 28 kg
3	B	35153.5 mg in 10 kg		9153.95 mg in 10 kg		44307.45 mg in 20 kg

4. DISCUSSION AND CONCLUSIONS

The nutritional value of the types of food will depend on several factors, but first of all on the content of nutrients, and this, in turn, will depend on the utilization of the organism itself. Food classification was made a long time ago by Popov (Popov, 1949), Morrison (Morison, 1955), (Pribicevic, 1978). The food is divided into groups, which include the group of green food (pasture, meadow and silage of field green plants), as well as a group of combined food from the animal feed industry. In this research the type of feed is alfalfa, straw and concentrates. Analyzes were made of 21 elements, of which the elements fluorine and chromium, which also fulfill some functions in the body, but have not been classified as essential nutrients to date. Cadmium and vanadium belong to a special category due to their harmful effect, but to date they do not belong to the group of toxic substances, such as, for example, arsenic, lead and beryllium whose concentration is < 1 g/kg (Milosavljević and Pauca, 1978), and that coincides with our research. Table 4 shows the presence of chemical elements in the total feed used in the three farms, we conclude that these tests in animal feed complement the tests of chemical elements in their milk made by the authors Tomovska, J., and Villasaku, I., (2023). From the three farms we conclude:

1. Farm A has potassium 16639.00 mg/kg, calcium 5802.00 mg/kg, manganese 1257 mg/kg, phosphorus 627.00 mg/kg, aluminum 220.00 mg/kg, iron 184.00 mg/kg. Strontium has the lowest values, 7.37 mg/kg.
2. Farm B has potassium 17205.00 mg/kg, calcium 5112 mg/kg, manganese 1928 mg/kg, phosphorus 11904.00 mg/kg, aluminum 2428.00 mg/kg, iron 2243.00 mg/kg, magnesium 1928.00 mg/kg. The lowest values are for calcium Cu 13.7 mg/kg.
3. Farm C has potassium 14768 mg/kg, calcium 4093 mg/kg, manganese 1142 mg/kg, phosphorus 1748 mg/kg, aluminum 136.58 mg/kg, iron 114 mg/kg. Boron has the lowest values, 9.51 mg/kg.

We emphasize that wheat straw (*Triticum vulgare*) is a food that was used only on farm A, which is a secondary product and is rich in proteins and minerals, such as phosphorus, potassium, etc., according to Petar Egumenovski et al. (1998),

Plazonić (2016) and Shaver, R., and Hoffman, P., (2010). According to our research on the chemical elements in the straw of farm A there is the most potassium 12599 mg/kg, followed by calcium 1096 mg/kg, phosphorus 627 mg/kg, magnesium 513 mg/kg, sodium 60.8 mg/kg. The lowest value for barium is 2.35 mg/kg (Table 1).

According to the tests in both types of concentrates 1 and 2 from farm A and from farm B and only 1 concentrate from farm C it is concluded:

1. Farm A. KMK 1 has the highest value of potassium 2619.00 mg/kg, phosphorus 1990.00 mg/kg, magnesium 869.00 mg/kg, calcium 153.00 mg/kg, aluminum 110.00 mg/kg, iron 104.00 mg/kg, and the lowest value is for strontium 0, 77 mg/kg. KMK 2 has the highest value for potassium 6382.00 mg/kg, phosphorus 5196.00 mg/kg magnesium 2095.00 mg/kg, and the lowest value for boron 2.15 mg/kg.

From the concentration values of the chemical elements in the concentrates, it can be noted that there is a big difference in the two concentrates used in farm A. KMK 2 is much more abundant in potassium, calcium, phosphorus and magnesium compared to KMK 1. In the concentrates from farm B, the values are higher in KMK 1 compared to KMK 2 for potassium, phosphorus, sodium and magnesium (Table 1).

2. Farm B. In KMK 1 there are the highest values for calcium 15283.00 mg/kg, potassium 8702.00 mg/kg, phosphorus 7537.00 mg/kg, magnesium 3072.00 mg/kg, sodium 2944.00 mg/kg, zinc 299 mg/kg, and the lowest value was measured for barium 5.23 mg/kg. In KMK 2, the highest values were measured for calcium 7461.00 mg/kg, potassium 4913.00 mg/kg, sodium 6327.00 mg/kg, phosphorus 3217.00 mg/kg, and the lowest value for barium 5.64 mg/kg, (Table 2).

3. Farm C. In KMK 1, the highest values were measured for potassium 8419.00 mg/kg, phosphorus 6785.00 mg/kg, magnesium 2944.00, calcium 743.00 mg/kg, and the lowest value for boron 3.56 mg/kg, (Table 3).

For the comparison of the total values of chemical elements present in different animal feeds, it is concluded that their largest amount is in the alfalfa from farm A, then in the concentrate K1 from farm B and in the alfalfa from farm C.

When we compare the total values of the content of chemical elements from farm A in each type of food, we notice that alfalfa has the highest concentration of chemical elements per 8 kg of total food, namely: 200.612 mg in 8 kg, then in straw 105064.82 mg in 7 kg, in KMK 2 - 48754.256 mg in 8 kg, and least in KMK 1 and that is 47274.48 mg in 8 kg. The total value of the content of chemical elements in 4 (four) types of food used is 401705.556 mg/kg.

When we compare the total values of the content of chemical elements from farm B for each type of food, we notice that in KMK 1 there is the highest concentration of chemical elements per 8 kg of total food, namely: 383567.9 mg in 10 kg, in KMK 2 is 242031.8 mg in 10 kg, and the least in alfalfa is 154922.44 mg in 8 kg. The total value of the chemical elements in the three types of food used is 780522.14 mg/kg. When we compare the total values of the content of chemical elements from farm C for each type of food, we notice that in alfalfa there is a high concentration of chemical elements 9153.95 mg in 10 kg, and in the concentrate 35153.5 mg in 10 kg. The total value of chemical elements in 2 types of food is 44307.45 mg/10 kg.

From the comparison of the values of the content of chemical elements between the different types of food in relation to the used daily meal (20, 28 and 31 kg) from the three farms, it is noted that 20 kg is used daily on farm A, on farm B 28 kg and on farm C 31 kg per day. It is concluded that the richest food with elements is the food from farm B.

From the analysis of 21 chemical elements in animal feed, it is concluded that the highest value for potassium of 17205 mg/kg was measured in farm B, in alfalfa, and the lowest value is strontium of 0.77 mg/kg in KMK 1 from farm A.

The total percentage representation of the most common chemical elements in the total food used on the three farms is: 63% potassium, 14% phosphorus, 13% calcium and 8% magnesium.

The general conclusion is that livestock nutrition is of great importance, so that with a correct and balanced daily ration that will contain all nutrients and chemical elements, the requirements of dairy cows should be met.

Conflict of Interest

The authors have no conflicts of interest to declare.

Funding

The authors declared that this study has received no financial support.

REFERENCES

- AHDB Dairy (2018). <https://ahdb.org.uk/knowledge-library/dairy-performance-results-2018-19>
- Barba, D., Margarit, G. L., Toma, R., Constantinescu-Groposila, D. (2017) The Repeatability Study of Characters for Development, Reproduction and Milk Production at the Active Romanian Black Spotted Population from Pantelimon and Mogosoia Farms. Scientific Papers. Series D. *Animal Science*, vol. LX, pp. 11-13.
- <https://animalsciencejournal.usamv.ro/index.php/scientific-papers/past-issues/8-administrative/413-scientific-papers-series-d-animal-science-vol-lx-2017>

Beneficial Management Practices, Environmental Manual for Alberta Farmsteads. (2006). Publications Office Alberta Agriculture, Food and Rural Development 7000 – 113 Street Edmonton, Alberta T6H 5T6. Published by: Alberta Agriculture, Food and Rural Development, Canada.

[https://www1.agric.gov.ab.ca/\\$department/deptdocs.nsf/ba3468a2a8681f69872569d60073fde1/610cf5ba8a00ff0f8725723d006f49ba/\\$FILE/090-1.pdf](https://www1.agric.gov.ab.ca/$department/deptdocs.nsf/ba3468a2a8681f69872569d60073fde1/610cf5ba8a00ff0f8725723d006f49ba/$FILE/090-1.pdf)

Caisin L, Vasile H, Vasile V. (2012). Chemical Composition and Nutritional Value of the Fodder Grown in the Conditions of the Republic of Moldova, Scientific papers, series D. *Journal Animal Science* 56.

https://scholar.google.com/citations?view_op=view_citation&hl=en&user=WGU14xwAAAAJ&citation_for_view=WGU14xwAAAAJ:xtRiw3GOFMkC

Catalog for feed mixtures, DOO "Agroinvest" AI-ZP-SD-02, (2017)

<http://www.agroinvest.com.mk/content/catalogs/8-animal-feed-1pdf>

Dr. Zivojin Milosavljevic – dr Veljko Puaca, (1978). Stocna hrana, Privredni pregled- Beograd , 1978.

Balabanova, B., Mitrev S., Mihajlov Lj., Kovachevikj B. (2016). Characterization of heavy metals contents in different plant foods from polluted sites and their impact in food chain, January 2016. Macedonian - Chinese Scientific and Technological Cooperation New Project Proposal for 2016-2017.

https://www.researchgate.net/publication/301816507_Characterization_of_heavy_metals_contents_in_different_plant_foods_from_polluted_sites_and_their_impact_in_food_chain

EN ISO 6498 (2011) – Animal Feeding Stuffs – Guidelines for Sample Preparation 6./7.

December, http://www.aafco.org/Portals/0/SiteContent/Regulatory/Committees/Lab-Methods-and-Services/Minutes/201407_Doc9b_Sample_Preparation_EN_64984.pdf

Haridasan, M. (2008). Nutritional adaptations of native plants of the cerrado biome in acid soils . *Brazilian Journal of Plant Physiology*, 20, pp. 183-195.

https://www.researchgate.net/publication/241539315_Nutritional_adaptations_of_native_plants_of_the_cerrado_biome_in_acid_soils

IndiaMART Khan. I. (2014). <http://www.iamwire.com/2014/11/indiamart-revamps-match-buyers-15-lakh-suppliers-ropes-actor-irrfan-khan-brand-campaign/104842>

Ishler, Virginia A., Gabriella A. Varga. (2018). Carbohydrate Nutrition for Lactating Dairy Cattle, Pennsylvania State University. <https://extension.psu.edu/carbohydrate-nutrition-for-lactating-dairy-cattle>.

Ivanovski, R., Prentovic T., Kabranova R. (2011). Forage production workshop, Skopje.

Kavanagh, S., (2016). Feeding the Dairy Cow (Concentrates) Teagasc Agriculture and Food Authority, Chapter 35, Section 6, pp. 214-220. <https://www.teagasc.ie/media/website/animals/dairy/FeedingDiaryCowConcentrate.pdf>
<https://www.teagasc.ie/animals/dairy>

Khan, S. T., Mubeen. U., (2012). Wheat Straw: A Pragmatic Overview. *Current Research Journal of Biological Sciences*, 4 (6), pp. 673-675.

https://www.researchgate.net/publication/257645533_Wheat_Straw_A_Pragmatic_Overview

Korr, J., Ag-Info Centre, Alberta and Rural Development. Using Straw in Cattle Rations – Frequently Asked Questions. Published on November 20, 2003. Last Review/Revised on September 21, 2017.

Kovacsne, G. K., Safar, O., Gulyas, L., Stadler, P. (2004). Magnesium in Animal Nutrition. *Journal of the American College of Nutrition*, vol. 23, no. 6, pp. 754S-757S.

Margarit G, Toma R.C. (2016). The Heritability Study of the Characters for Development, Reproduction and Milk Production at the Active RSC Population from the Bucharest area of Milk Supply. University of Agronomic Sciences and Veterinary Medicine of Bucharest, Romania. *Scientific Papers. Series D. Animal Science*, vol. LIX.

Mckean, W. T. and R. S. Jacobs. (1997). Wheat Straw as a Study Fiber Source. Tech. Rep. Recycling Technology Assistance Paertnership, Clean Washington Centre, Seattle, Washington.

Mr Harry Harmens (2010). HEAVY METALS IN EUROPEAN. Centre for Ecology and Hydrology Environment Centre Wales Deiniol Road Bangor Gwynedd LL57 2UW United Kingdom MOSES: 2010 SURVEY.

<https://core.ac.uk/download/pdf/57335.pdf>

Nikolovska, M., Arsovska, F. (2014). Assessment of persistence of lactation in dairy cows. *Journal of Agricultural, Food and Environmental Sciences*, vol 64, pp. 121-125. (UDC: 636.234.034(497.7)).

<https://journals.ukim.mk/index.php/jafes/index>

Nutritive Value of commonly available feeds and feeders in India, Animal Nutrition Group, National Dairy Development Board Annand - 3888-001, (2012). <http://www.nddb.org/sites/default/files/pdfs/Animal-Nutrition-booklet.pdf>.

Operate and Support a Food Safety and Quality Management System in the Agricultural Supply Chain (Learne Guide, Primary Agriculture, 2006). https://www.agriseta.co.za/wp-content/uploads/2021/03/116070_LG.pdf

Rumsey, G. L., (1980). Aquaculture development and coordination programme. Fish feed technology, Chapter 10. Antioxidants in Compounded Feeds, Tunison Laboratory of Dish Nutrition, Food and Agriculture Organization of the United State, FAO, Cortland, New York. <https://www.fao.org/4/x5738e/x5738e0b.htm>

Samuel X., Radbill, (1976). The Role of Animals in Infant Feeding. In Hand, Wayland D. *American Folk Medicine: A Symposium*. University of California Press. ISBN 9780520040939. <https://doi.org/10.1525/9780520336773-005>

Sarwar, M., Shahzad, M. A., Nisa, M., Bhatti S. A. and Tauqir N. A. (2012). Enhancing Buffalo Productivity Through Usage of Low Quality Feed Stuffs. Institute of Animal Nutrition and Feed Technology, University of Agriculture, Faisalabad, Pakistan. *The Journal of Animal and Plant Sciences*, 22 (3 Suppl.), pp. 128-132. ISSN: 1018-7081. <https://www.thejaps.org.pk/>

Sarwar, M. A., Khan A. and Iqbal, Z., (2002b). Feed Resources for Livestock in Pakistan. Status Paper. *Intl. J. Agri. Biol.*, 4, pp. 186-192.

https://www.researchgate.net/publication/277324229_Status_Paper_Feed_Resources_for_Livestock_in_Pakistan

Scientific papers, series D. *Animal Science*, vol. LVI (2016) University of Agronomic Sciences and Veterinary Medicine of Bucharest Faculty of Animal Science Bucharest, Romania.

<https://animalsciencejournal.usamv.ro/pdf/2016/vol2016.pdf>

Shaver, R., and Hoffman, P., (2010). Use of Straw in Dairy Cattle Diets, Focus on Forage – Vol 12: No. 2. University of Wisconsin Board of Regents, 2010. Extension Dairy Scientist, Marshfield Agricultural Research Station University of Wisconsin – Madison. <https://fyi.extension.wisc.edu/forage/use-of-straw-in-dairy-cattle-diets/>

Tomovska, J., Vllasaku I., Josevska, E. (2023). Examination of the chemical composition of animal feed and its influence on the quality of milk. Food and Environment Safety. *Journal of Faculty of Food Engineering*, Ștefan cel Mare University of Suceava, Romania Volume XXII, Issue 2 - 2023, pag. 122 – 134. www.fia.usv.ro/fiajournal

Extending, Integrating and Recovering: Tools for The Architectural and Social Rehabilitation of The Augusta Slaughterhouse

Fernanda Cantone*¹, Francesca Castagneto²

Abstract: Buildings of the past are an immense heritage that must be preserved and passed on to future generations. Contemporary society cannot support a use linked to the historical and cultural value but needs a new function and interventions aimed at enhancing it. Recovery project applies to the existing built in many ways. One of the most important is the use of sociological and participatory analysis: it is a tool that values community demands and transforms them into project requirements, The value added of the project. The research has seen the participatory methodology and social analysis applied to an urban redevelopment project in Augusta, providing reuse hypotheses based on the real needs of the user, The social dynamics, the potential of the territory and buildings. The case study concerns an area in the district of Terravecchia, on the edge of the historic center of Augusta, in which there are buildings of historical importance, but also many schools and public buildings. In particular, the social rehabilitation project was applied to the building used for the slaughter of meat, built between 1906 and 1908, on the ruins of a warehouse belonging to the ancient Recipe of Malta. The applied methodology, based on surveys of urban layout, green systems, socio-economic, housing and schools, It proposes the adoption of innovative attractive and supportive functions of the school system, to recover an important historic building and provide newly designed functions for young people. Trials demonstrate that community-driven information is applied to the recovery project and produces substantial qualitative benefits for users: satisfaction, livability, well-being.

Keywords: social analysis, urban rehabilitation project, community, residual performance, reuse.

¹Address: University of Catania, SDS Architecture, Department DICAR, Syracuse, Italy

²Address: University of Catania, SDS Architecture, Department DICAR, Syracuse, Italy

*Corresponding author: fernanda.cantone@unict.it

1. INTRODUCTION

The building recovery gives life to the built heritage, with the aim of preserving the historical and cultural memory of a territory. It is defined as the set of activities aimed at improving the performance of existing buildings, through maintenance, redevelopment and reuse. Its importance is manifested in promoting sustainable development and optimizing the use of existing building resources. In addition, the building rehabilitation contributes to reducing the abandonment and degradation of existing structures, improving the quality of life of local communities and supporting the economy of the territory (Leone, 2023).



Figure 1. Augusta Municipal slaughterhouse.

The recovery project, and in particular reuse, proposes scenarios of intervention selected through a wide-ranging and articulated fact-finding phase. This phase includes, first, the survey of the building, the identification of historical, cultural and usage characteristics, the analysis of the urban context, building performance and detailed information on the current state of buildings and their surroundings which become key tools for the project. Recent studies have shown that these

routine and frequent analyses are not enough to provide the right project guidelines. The need to compare project objectives with community needs is one of the fundamental elements of contemporary design. Many studies (Cersosimo and Donzelli, 2020) have deepened and analysed, for example, the loneliness of users but also their interests but also their interests, their emotions and expectations both before a regeneration/redevelopment intervention and after the recovery, to verify the effectiveness of the choices and strategies. For this reason, the project should increasingly be guided by social analysis.

Society is changing and the factors that are determining this change concern the city seen as a complex system, in continuous change, in which the phenomena of socio-spatial polarization are increasing. Scholars also focus on the growing distrust in institutions that goes hand in hand with the failure of traditional participation mechanisms. The crisis of the welfare state and the reduction of forms of public investment have changed the tools for urban regeneration while traditional projects, which have not produced the desired effects, have generated further phenomena of expulsion and marginalization of the weakest populations. For some time, bottom-up initiatives have become "engines" of urban regeneration through social innovation: community-led interventions that use few resources, strongly oriented towards self-entrepreneurship and that, in some cases, also become forms of social claims; interventions that operate on trigger spaces or on systems of specific spaces, often having the neighbourhood as a reference dimension; places where new collaborations between different sectors of the administration and between private and public entities of various types are tested, as well as new forms of citizen involvement. In these interventions, both in Italy and at European level, the role of social enterprises and, more generally, of third sector organizations is important (Bernardoni, A., Cossigiani, M. et al. 2021).

Social analysis is now identified as an effective strategy that allows to identify actions that can meet the needs of users and then it provides a comprehensive picture of the social benefits arising from project interventions. In the past, the lack of scientific methods and the relative clarity of the process and responses made these analyses superficial and little used for the project. In other words, the ideas and desires of the community were lost behind excuses and solicitations of an economic-speculative type. The participation of citizens in the recovery process is a key element to ensure active involvement of the local community. This may be done through public consultation, the setting up of working groups or through information meetings. It is important to involve citizens at an early stage of the project so that they can express their needs and concerns about the intervention. Furthermore, transparency and open communication are essential to ensure effective community participation. Only through the active involvement of citizens will it be possible to carry out building restoration interventions that truly meet the needs of the local community (Mami and Nicolini, 2020).

Ecological, social and human activities define a design approach based on the integrated development of the territory and the design of spaces, infrastructures, human and social capital, in function of social changes. In this sense, the project must absorb social changes and mediate between territory and community through the development of a culture of innovation capable of transposing global phenomena into local phenomena. It is a question of addressing two important problems: on the one hand, the guarantee of truly inserting the interests of the community into the project and on the other, the control of the project that, starting from private individuals, is effective on the liveability of the spaces themselves (Klein Juan – Louis, 2017). For this last point, the difficulty lies in triggering a mediation process between material factors and creative design ideas: the center of the project must always be the community and the designer must be able to overcome the "natural differences in time horizons and quantification of impacts", while remaining within the scope of the cultural policies of the territory (Bernardoni, A., Cossigiani, M. et al. 2021).

Indeed, the designer has a great responsibility: understanding, using and exploiting the resources of the territory. He must investigate the places to bring out even the most hidden aspects. Another fundamental aspect is to know how to manage the means available (economic, physical and social) and adapt to them. The ideas must come from both local and community analyses, as well as from successful elements applied in similar contexts.

UNESCO, with the 2011-2020 UN-HABITAT protocol, for example, has identified a methodology for collecting data on community desires and their exploitation in the project. Based on these worldwide indications, The impact of the restoration project on the community and on the usability of public spaces and on the well-being of the local population must be assessed. The UN-HABITAT protocol allows to identify any critical issues related to the abandonment of certain areas, providing valuable data for recovery actions.

The role of planning linked to social analysis must finally propose non-occasional strategies, but long-lasting ones, in synergy with other redevelopment/regeneration projects, stimulating citizens with tax and contribution incentives (Spaziante A. 2018) and must overcome the logic of mere urban furnishing, just as it must overcome the logic of exclusive commercial interest.

An interesting study examined 90 regeneration interventions and identified, through numerous analyses, that the greatest number of interventions is in the city center or at most on the outskirts and that there are very limited absences in the mountains or on the waterfronts. Social interventions are mainly located in the outskirts or in less usual areas. This study highlights:

- sustainable interventions, mainly services,
- social interventions carried out by associations, cooperatives, social enterprises and foundations, but also public administration bodies, which confirm the existence, at a national level, of collaborative and complementary relationships between public and private entities,
- business interventions designed and implemented with a public-private mix that also denotes a greater protagonism of commercial entities, such as joint-stock companies and professional orders.

In general, the study highlights that:

- sustainable interventions are more attentive to the environmental sustainability of initiatives and to the sustainable management of green areas and agricultural activities.
- social interventions are oriented towards regeneration initiatives linked to welfare and social inclusion;
- business interventions involve a greater number of commercial, tourist and professional services development activities (Bernardoni, A., Cossigiani, M. et al. 2021).

Starting from these considerations, research was organized that aims to regenerate an area, starting with its inhabitants.

2. MATERIAL AND METHOD

Improving housing conditions and optimal use of public spaces are discriminating elements of community life that promote social cohesion and increase the sense of belonging. For years, scholars have tried to direct the design towards user requests. In fact, the community increasingly recognizes the need to take social factors into account when identifying the objectives of investment programs and project interventions: for example, ensuring that the most vulnerable are supported to benefit from better public services and job opportunities. In this sense, the research has taken into consideration not only the building under study but also the context in which it stands today and has applied various levels of analysis.

Building analysis:

- Morphological-dimensional analysis;
- Technological analysis;
- Residual performance analysis.

Urban analysis:

- Roads and transport;
- Green system;
- Urban planning tools;
- Places and sites of interest.

Population analysis:

- Resident population;
- Population structure by age;
- Family size;
- Population by school age groups;
- Employment level by economic sectors;
- Employment rate;
- Families with economic hardship.

Analysis of the settlement system:

- Potential use of buildings;
- Index of underuse of buildings.

Social analysis:

- First level: definition of the scope (social, sustainable, business)
- Second level: identification of potential social obstacles to development at the local community level, with the aim of identifying potentially sensitive social factors (stakeholders or rights holders on the project area).
- Third level: community participatory process
- Fourth level: identify the level of intervention envisaged by the project in order to define the framework of economic and transformation possibilities.

The relationship of these data was analysed and selected based on the needs of the users.

In particular, the social analysis highlighted the characteristics of the area affected by the recovery intervention and confirmed an interesting unexpressed potential: recovery of the cultural and historical identity of the building and reuse through social interventions aimed at specific user groups.

3. THE CASE STUDY (Times New Roman 10pt)

The case study is the municipal slaughterhouse in Augusta. Until 1869, it was an abandoned warehouse that had been used by the Malta Recipe in the past. This was a system of buildings leased, since 1648, to the order of the Hierosolimitans of Malta to be used as a permanent base for supply and support to the naval fleet and occupied an entire block for the area is approximately mq 5000.

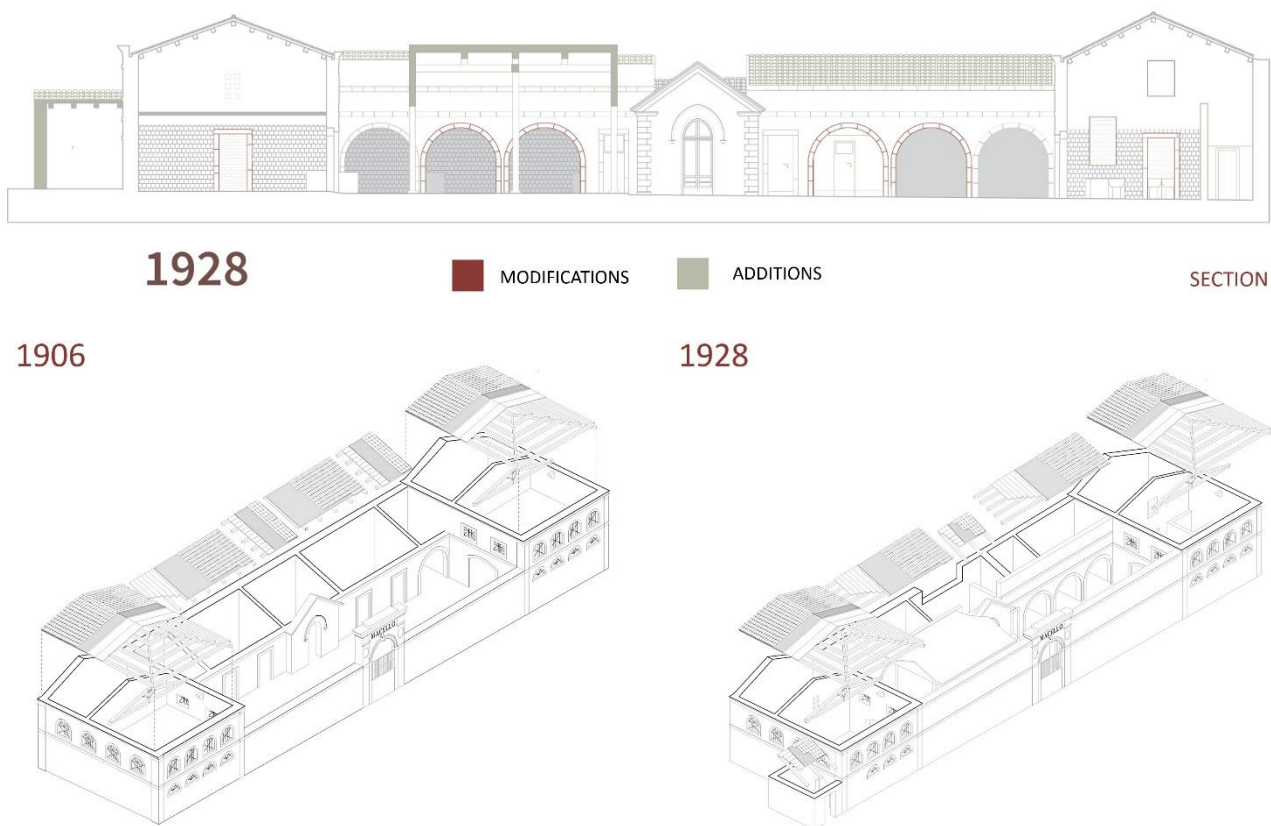


Figure 2. Section with transformation and exploded axonometric view of the slaughterhouse.

In 1869, the building abandoned by the Recipe of Malta, owned by the Civil Engineering, was the subject of small restoration work and was used for municipal slaughter. At the beginning of the 20th century, the progressive urban development saturated the area of slaughterhouse which was thus too close to many residential buildings. (Syracuse State Archives, 1869). In 1875, the municipality bought the slaughterhouse. It was rather rough and did not respect the hygiene rules; only in 1906 (Deliberation of the City Council of Augusta, 1906) Municipality managed to modify it to comply with the current legislation on the subject; In fact, the municipal administration decided to demolish it and rebuild it with better distributed spaces that separated cattle and sheep, with shelters, with control offices. The project, drawn up by the surveyor Giuseppe Annino Pinto, presented a system of consecutive environments with, in the head, of advanced bodies and two levels that closed the prospect and forming a narrow inner court, connected by an imposing wall of fence on which stood out an impressive portal in white stone. The smaller bodies were covered by a one- or two-way roof.

In 1928 the municipal administration was forced to make further expansion and transformation, on a project of Ing. Giuseppe Stella, for the realization of: a shed for the rest of the carts, a zone for weighing animals, an office of the veterinarian, corridors for the stables, toilets and slaughter tanks. the project was realized by the company of Mr.

Giuseppe Grimaldi for the sum of 14600 lire. In the 1950s, the economic boom, the birth of the petrochemical center of Augusta and a vast building plan brought economic well-being. The city grew larger and the buildings were also crowded near the area of the slaughterhouse that it became an inhabited center, since 1983, the building has been used only as a storage facility. Today the slaughterhouse is abandoned.

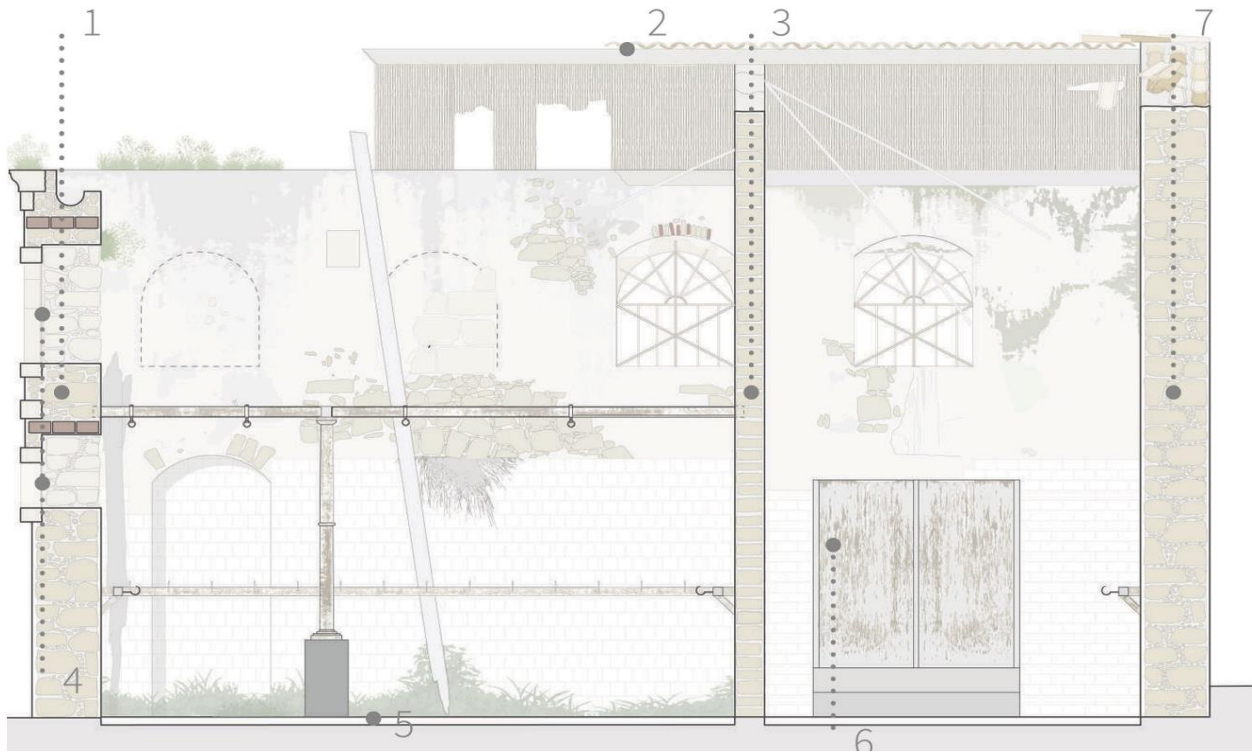


Figure 3. Technological section.

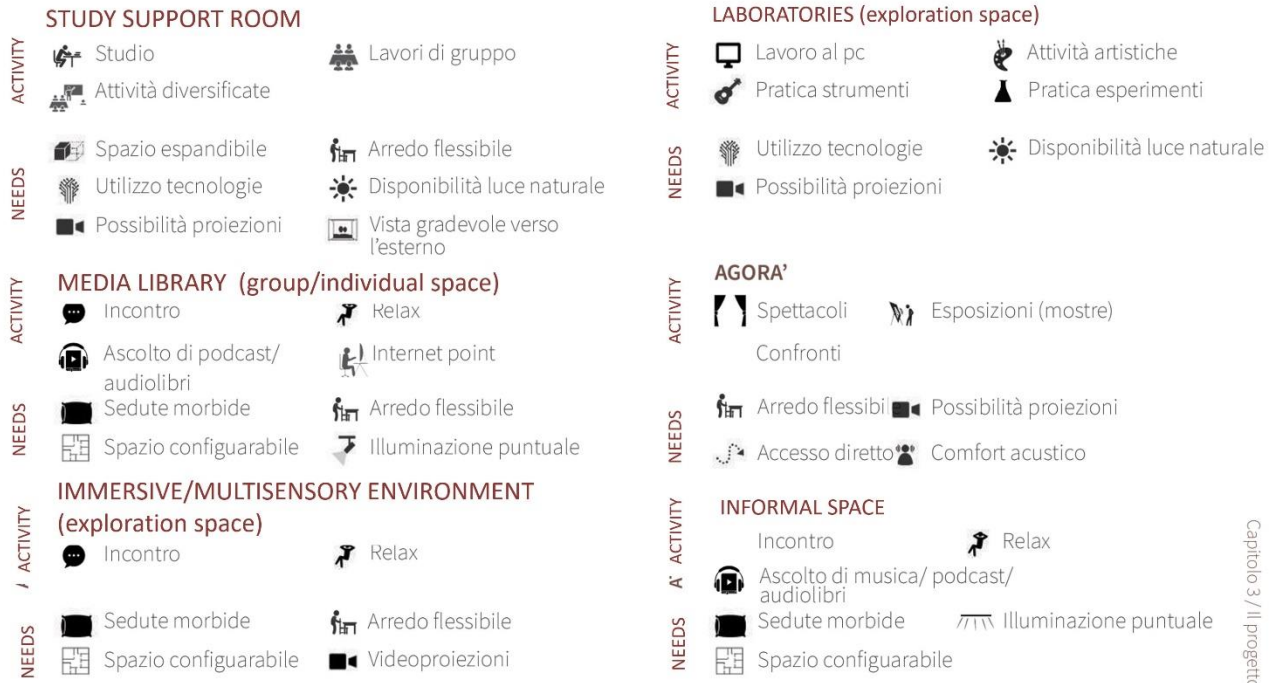
3. RESULTS

The analyses described above have highlighted some important elements to be reported in the project. The analysis carried out on the building shows the poor state of conservation, the deterioration of the technical elements and the need for urgent rehabilitation. The urban analysis studied the settlement system of the Terravecchia district, defined by a chessboard line that develops along the north-south axis with blocks of defined dimensions (insulae of meters 50 x 150) on which are present traces of the defensive system of Aragonese epoch. The green system highlights the limited presence of equipped green within school complexes and the general, but limited, presence of uncultivated green. The system of urban constraints places the focus on the area of the Slaughterhouse as it falls under zone A of the current PRG and in zone Local landscape 6D: Landscape of the historic center of Augusta, Megarese coastal area and areas of archaeological interest, with level 1 protection in the regional landscape plan. The analysis of the settlement system reveals the presence of numerous unused buildings. The socio-economic analysis identifies the decrease in births and the increase of the elderly population, the work field related to the tertiary sector and industry (petrochemical), population is fairly well educated. The most important element is certainly the presence of the citadel of the study where many schools are concentrated. It is located close to the slaughterhouse and brings the area to be frequented by thousands of young people.

The social analysis, through interviews with young people, schoolteachers, residents and passers-by, but also with scholars of the area, started from this very point: from the presence of young people who go to school, from the need for disadvantaged families to have places of support for the school system, from the need to prevent school dropouts and to improve the working and social future for these young people. In this regard, reference was made to the school system and the three-year plans of the 2022-2025 training offer. Through these it was possible to estimate the number of students by age group, the number of classes and the socioeconomic condition of families. We must point out the lack of cultural, educational and recreational opportunities, totally absent in the area. In the historic district, in fact, apart from the parishes, there are no social aggregation centers or meeting places for young people: cultural growth, socio-affective and recreational-sports development are difficult. The lack of a cinema is also reported, although the current municipal administration is providing for the reopening of the old Megara Arena inside the Public Gardens. The Citadel

of Study also lacks sports facilities for physical practice. In the area there is a voluntary association that supports disabled and socially disadvantaged students.

USABILITY REQUIREMENTS



Capitolo 3 / Il progetto

Figure 4. New performances for the project.

The topic of innovation in the educational field has been the subject of study and debate for some years. There has been reflection on how physical space can affect learning methods. The program of interventions envisaged by the PNRR with the “Piano Scuola 4.0” is moving precisely in this direction. The name “Scuola 4.0” derives precisely from the purpose of the measure, aimed at creating hybrid learning environments, which can combine educational and didactic potential with the physical and digital spaces of the environments, conceived in an innovative, sustainable way. With the PNRR, the Ministry of Education has invested in the creation of innovative environments for learning and laboratories for the digital professions of the future. This intervention translates into two actions:

- NEXT GENERATION CLASSROOM are spaces characterized by mobile and modular furnishings that allow a rapid reconfiguration of the space, equipped with digital devices.
- NEXT GENERATION LAB are laboratories dedicated to: robotics and automation, artificial intelligence, cloud computing, cybersecurity, making and 3D modelling and printing, creation of digital products and services, creation and use of services in virtual and augmented reality, digital communication, processing, analysis and study of big data, digital economy, e-commerce.

In parallel with this line, the path of analysis and study, developed in recent years by Indire (National Institute for Documentation, Innovation and Educational Research), moves forward, which develops an idea in which functional spaces are declined and integrated based on a pedagogical vision, through a path of participation. The Model developed by indire is the so-called "Manifesto 1 + 4 educational spaces". "1" represents the group space, a place where students gather and build their own identity, i.e. the agora, symbol of the moment of sharing and mutual exchange between all students. "4" indicates the spaces of the school that are complementary, and no longer subordinate, to the environments of daily teaching, i.e.:

- EXPLORATION SPACE, a space of discovery and a starting point for exploring the educational environment of the world, a place designed for learning by doing.
- INDIVIDUAL SPACE, an area with sheltered zones, niches, intimate environments and dedicated spaces where everyone can retreat, read, reflect, study.
- INFORMAL SPACE, a place for informal meetings and rest.

Based on these references, the reuse project aims to reuse the spaces of the slaughterhouse for recreational and educational purposes, rethinking the spaces between pedagogy, architecture and design.

The project

The presence of numerous school buildings in the area has directed the project towards the reuse of the old slaughterhouse as recreational and educational meeting places, whose usability is aimed at a group of young people between 3 and 18 years old. The new function will include not only spaces for enhancing study, but also leisure areas (Fun zone), dedicated to free time and entertainment. Since the dimensions of the slaughterhouse are limited, the project envisaged a volumetric expansion, below the original level, in order to obtain additional spaces. The core of the project is the idea of creating a new volume that acts as a hinge between the slaughterhouse, its internal courtyard and the ruins of an old house attached to it. The project intends to distinguish the old, with its materiality, history and function with the new volume that will instead be easily identifiable by materials and shape of the volumes. In the project, therefore, two distinct entities coexist that confront each other in a process of continuous interaction: conservation and innovation.

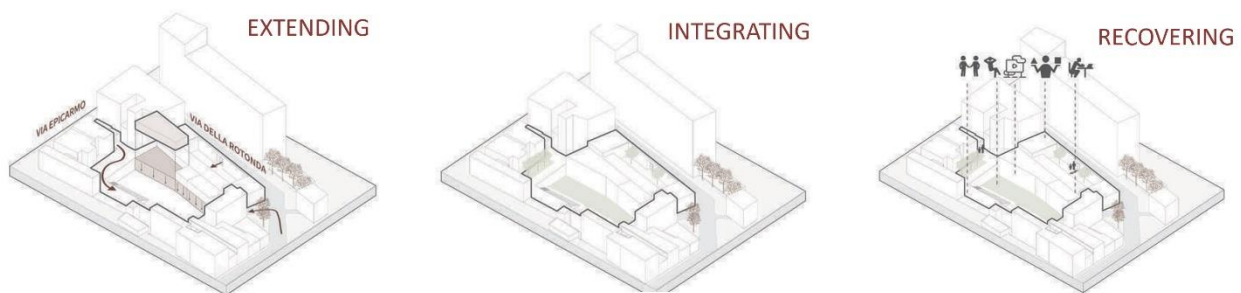


Figure 5. Recovery project basics.

The identified functions are:

- Areas with interactive walls and carpets that encourage learning through play, creating stimulating and fun spaces.
- Spaces dedicated to individual reading and environments designed for interaction between groups, also allowing for intergenerational exchange.
- A digital STEM (Science, Technology, Engineering and Mathematics) laboratory designed as a place for in-depth, even practical, study of scientific and technological disciplines.
- Immersive and multimedia environments, with a set of synchronized projectors to create engaging scenarios and also promote cooperative learning.

From a technological point of view, the project involves the combination of the slaughterhouse with a new building that is partly adjacent to the ruin, in a game between old and new, which captures the attention of the observer. In particular, the existing perimeter wall of the ruin will follow a process of dematerialization, as it is inserted into the new volume and will be made with a micro-perforated sheet metal, which only occasionally leaves a glimpse of a play of textures. The external area has been connected to the buildings with a system of ramps and a flight of steps. The area behind the slaughterhouse will be redesigned and repurposed, creating a new access: the project involves a residential building in a state of ruin that will complete the project. In this way, this area, today forgotten and unused, will be able to return to being a space available to citizens.

The planned interventions on the pre-existing structure are therefore:

- consolidation of the wall texture through cement injections;
- restoration of the original pitched roofs;
- new frames for the round-arched openings overlooking the internal courtyard;
- demolition of the superstructures present in the courtyard: the precarious eternit roof and the reinforced concrete one, in such a way as to recover the original spatiality of the internal courtyard.
- reconfiguration of the external flooring which will be made of white limestone and stabilized gravel.



Figure 6. Project Section.

4. DISCUSSION AND CONCLUSIONS

The research has highlighted some fundamental elements for an effective and efficient redevelopment/regeneration project:

- The importance of community requests for the success of the interventions, limiting the inability to contextualize the project with respect to specific categories of users and, above all, activating common projects;
- The importance of enhancing the characteristics of the territory through actions aimed at emphasizing the residual performance;
- The strategic value of collaboration between public and private actors, with close coordination of the actions to be undertaken;
- The value of conservation and transformation/innovation for the achievement of social, environmental and economic objectives. The intervention project must include the enhancement of local cultures, the memory of public spaces and buildings, with a view to innovation.

In the context of the project on existing buildings, social analysis is of fundamental importance as it allows us to understand the urban context and involve the local community in the intervention process. Through social analysis it is possible to evaluate the impact of the building/urban recovery project on employment and quality of life, providing a clear vision of the social benefits resulting from certain interventions.

Acknowledgements

Interventions on the Augusta municipal slaughterhouse and relative images are taken from the degree thesis of Daniele Barbarino and Giulia Liistro entitled: Next generation Educational Workshop. Ludo-pedagogical spaces in the former municipal slaughterhouse of Augusta (SR). Supervisor: Proff. F. Cantone, F. Castagneto, Catania University, SDS of Architecture, Syracuse, Sicily. Academic year 2022/23.

REFERENCES

- Bernardoni, A., Cossigiani, M. et al. (2021). The role of social enterprises and third sector organizations in urban regeneration processes. Empirical investigation of Italian experiences and policy indications in *Social Enterprise. Social enterprise, a pillar for policies*, no. 3/2021, <https://www.rivistaimpresasociale.it/rivista/articolo/impres-sociali-e-rigenerazione-urbana> accessed 15 July 2024).
- Cersosimo, D. and Donzelli, C. (eds). (2020). *Manifesto per riabitare l'Italia. Con un dizionario di parole chiave e cinque commenti di Tomaso Montanari, Gabriele Pasqui, Rocco Sciarrone, Nadia Urbinati, Gianfranco Viesti*. Donzelli Editore.
- Deliberation of the City Council of Augusta of 28 November 1906, Municipal Historical Archive of Augusta, Category X Public Works, Envelope 84, Issue 3.
- Klein J.L. (2017). *L'innovation sociale au coeur des débats publics et scientifiques, Crises 2014-2020, Canada* : Presses de l'Universite du Quebec.
- Leone, V. (2024). *La valutazione dei processi partecipativi nell'ambito della rigenerazione urbana e territoriale in Puglia. Una proposta per Gravina in Puglia. Tesi di Laurea di Vincenzo Leone, relatrice Nadia Caruso, Politecnico di Torino, a.a. 2023-2024*. (<https://webthesis.biblio.polito.it/secure/28034/1/tesi.pdf> accessed 15 July 2024).
- Mami, A. and Nicolini, E. (2020). *Riabitare il patrimonio urbano ed edilizio dei territori interni: spazio digitale per servizi sanitari efficienti*. BDC. *Bollettino Del Centro Calza Bini*, 20(2), 317-335. <https://doi.org/10.6092/2284-4732/7558> BDC. *Bollettino Del Centro Calza Bini*.
- Margiotta, N., Palermo, A. (2023). *La valutazione della qualità urbana per la rigenerazione sostenibile di aree in disuso*. Milano: FrancoAngeli.
- Syracuse State Archives (1869). *Resolution of 25 July 1869, Prefecture Fund, Envelope 645*.
- Spaziante A. (2018), *Dismissione e riuso di piccole fattorie: un monitoraggio lungo ventitré anni sulle trasformazioni di Torino*, *Quaderni di ricerca sull'artigianato*, 6(1), pp. 39-102.
- Verazzo, C., Varagnoli, C., and Serafini, L. (2020). *Pratiche di recupero dei centri abbandonati. Esperienze dall'Abruzzo e dal Molise*. In *ArcHistoR. Un paese ci vuole. Studi e prospettive per i centri abbandonati e in via di spopolamento*. *Rivista classe A, Università Mediterranea di Reggio Calabria*, Extra n. 7/2020.

Applications of Artificial Intelligence (AI) in Plastic Recycling

Luiza Lluri¹, Faldi Lluri², Dalip Qorri³, Ramadan Dollani⁴

Abstract: The global plastic waste crisis is a pressing environmental issue, with millions of tons of plastic waste generated annually. Traditional recycling methods, while helpful, often fall short in terms of efficiency and accuracy. Artificial Intelligence (AI) offers a promising solution by enhancing various aspects of the recycling process, from sorting to process optimization. Smart Cities are becoming a reality that will expand in the next years, with governmental and private services more automated and providing more efficient performance to improve inhabitants' lives. In this perspective, Artificial Intelligence (AI) is emerging as an important technology enables more efficient management of recycling plants. This paper explores how Artificial Intelligence (AI) can transform plastic recycling, making it more effective and sustainable. Artificial Intelligence (AI) technologies enhance the accuracy of sorting different types of plastics, resulting in higher-quality recycled materials. This precision reduces contamination, making recycled plastics more suitable for reuse in various applications. Furthermore, Artificial Intelligence (AI) driven process optimization can lead to significant cost savings by improving operational efficiency and reducing waste. This paper explores the transformative potential of Artificial Intelligence (AI) in improving the efficiency and effectiveness of plastic recycling. It discusses the principles and applications of Artificial Intelligence (AI) technologies in various stages of the recycling process, including sorting, predictive maintenance, process optimization, and waste stream analysis. The paper also addresses the benefits, challenges, and future prospects of integrating Artificial Intelligence (AI) into plastic recycling, supported by real-world case studies.

Keywords: plastic recycling, artificial intelligence (ai), operational efficiency, waste reduction

¹“Aleksandër Moisiu” University, Faculty of Professional Studies, Durrës, Albania

²“Epoka” University, Faculty of Architecture and Engineering, Tiranë, Albania

³“Epoka” University, Faculty of Architecture and Engineering, Tiranë, Albania

⁴“Aleksandër Moisiu” University, Business Faculty, Durrës, Albania

*Corresponding author: luizalluri@uamd.edu.al ; faldilluri1@gmail.com ; dqorri20@epoka.edu.al:
anidollani24@gmail.com

1. INTRODUCTION

The global plastic waste problem is a significant environmental challenge. Every year, millions of tons of plastic trash are created, with much of it ending up in landfills, oceans, and other ecosystems, causing harm to wildlife and contributing to pollution. Only a small percentage of plastic waste is effectively recycled, with the rest either incinerated or discarded improperly. Effective recycling solutions are crucial for decreasing plastic waste, preserving resources, and limiting environmental impact. Innovations in recycling technologies, as well as improved waste management techniques, are critical to solving this expanding problem. Traditional plastic sorting technologies have significant drawbacks, reducing recycling efficiency. Labor-intensive and prone to errors, which contaminate recyclable materials. Optical sorting methods¹ frequently struggle to distinguish between different types of plastics, particularly when they are polluted or combined with other materials. Conventional methods are frequently rigid, making it difficult to adapt to new types of plastics or complex waste streams. High operational costs and low profit margins can render traditional sorting systems economically untenable.

Artificial intelligence (AI) has the potential to significantly improve the plastic sorting process in recycling (Figure 1). AI can effectively recognize and categorize numerous types of plastics using machine learning algorithms and computer vision, even if they are contaminated or mixed with other materials. AI systems can swiftly adapt to new types of plastics, improving sorting accuracy and minimizing contamination while increasing recycling efficiency. This

¹ The optical systems include lights and sensors housed above and/or below the flow of the objects being inspected. The image processing system compares objects to user-defined accept/reject thresholds to classify objects and actuate the separation system.

technology not only automates the process, but also makes it more cost-effective and scalable, overcoming many of the constraints of old approaches.

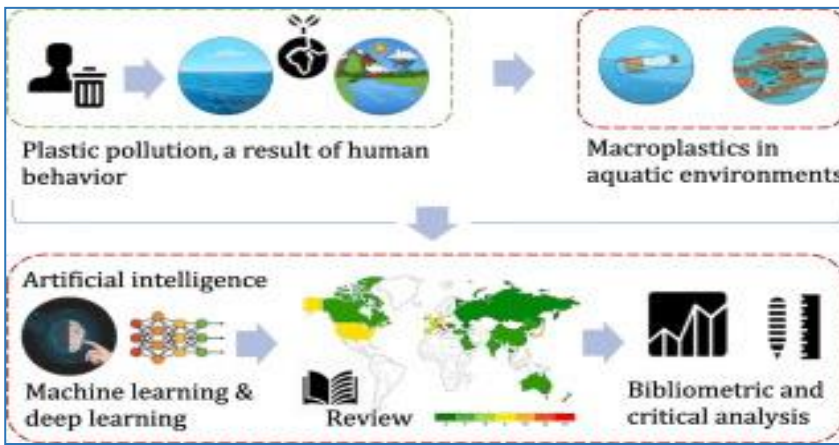


Figure 1: Artificial Intelligence (AI) in the process of sorting plastics in recycling

2. Principles of AI in Sorting Plastic Waste

Artificial intelligence (AI) refers to the simulation of human intelligence by technology, particularly computer systems. It entails developing algorithms and models that let computers to execute tasks that would normally need human cognition, including as learning, reasoning, problem solving, perception, and language comprehension. Artificial intelligence-powered devices use advanced computer vision and machine learning algorithms to effectively recognize and classify various types of plastics. This precision reduces contamination and increases the quality of sorted materials. AI-power sorting devices can handle vast amounts of plastic waste swiftly and efficiently.

This acceleration boosts total throughput in recycling facilities and improves operations.

As artificial intelligence (AI) models become more significant and prevalent in practically every industry, it is critical for organizations to understand how they work and the potential consequences of utilizing them.. In simple terms, an AI model is a tool or algorithm that is based on a certain data set through which it can arrive at a decision – all without the need for human interference in the decision-making process. An AI model is a program or algorithm that uses a collection of data to recognize specific patterns. This enables it to reach a conclusion or make a forecast when given enough information, which is often a large volume of data. As a result, AI models are particularly well-suited to solve complicated issues while providing greater efficiency, cost savings, and accuracy than basic solutions (Figure 2).

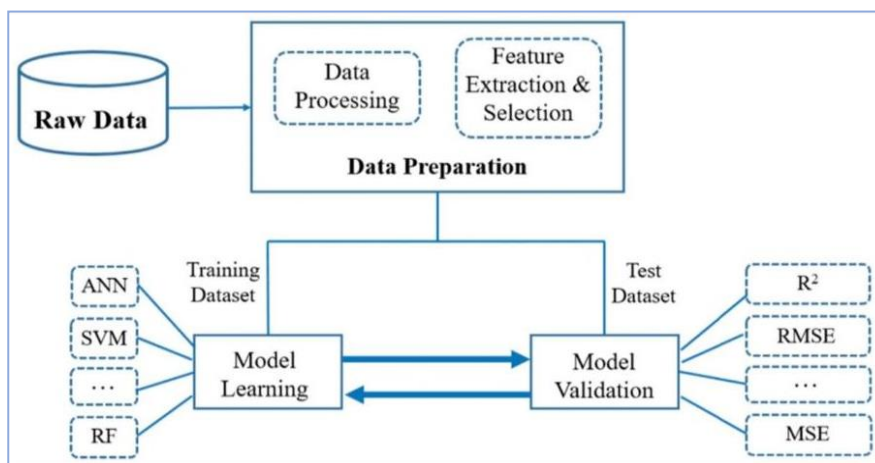


Figure 2: Artificial intelligence model

2.a Basic Principles of AI

- **Machine Learning**- AI systems learn from data and improve over time without explicit programming.
- **Neural Networks**- These mimic the human brain's structure to process information and recognize patterns.
- **Natural Language Processing (NLP)**- Enables machines to understand and respond to human language.
- **Computer Vision**- Allows AI to interpret and make decisions based on visual inputs.

Machine Learning (ML) and **Computer Vision** are major AI technologies driving progress in a variety of fields. Machine learning (ML) refers to algorithms that allow computers to learn from data and make judgments or predictions without being explicitly programmed. It encompasses approaches like as supervised learning, which trains models on labeled data, and unsupervised learning, which identifies patterns in unlabeled data (Figure 3).

Computer Vision: focuses on helping machines to comprehend and analyze visual input from the world., such as images or videos. It includes tasks like object detection, image recognition, and scene understanding, using techniques like convolutional neural networks (CNNs).

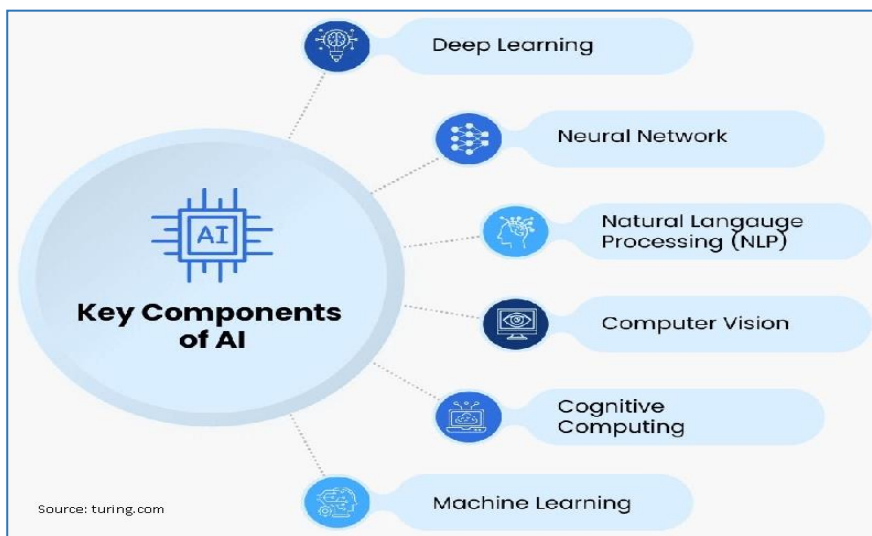


Figure 3: Key components of AI

AI algorithms, particularly those based on machine learning, learn to identify and classify various types of plastics through a process called **training**. Large amounts of tagged photos or samples of various plastic types are collected. This dataset is used to train the AI model, which learns to recognize the patterns, textures, and other distinctive characteristics of each plastic type. The model specifies distinct properties (such as color, form, and texture) associated with various plastics. Once trained, the model can identify new plastic samples using the learned features, discriminating between types such as PET, HDPE, and PVC, even in complicated or mixed trash streams. As more data is processed, the model improves in accuracy and efficiency when identifying plastics.

3. AI-Powered Sorting Technologies

AI-Powered Sorting Technologies are revolutionizing the recycling business by automating and improving the sorting process. These technologies employ machine learning algorithms and computer vision to identify and classify various types of plastics with high accuracy. AI systems can quickly analyze large amounts of garbage, discriminating between things that appear similar but differ chemically. This lowers pollution in recycling streams and improves the overall process. AI-powered systems improve over time as they learn from fresh data, providing a scalable solution to the worldwide plastic waste problem. Integrating these AI-based techniques with robotics has resulted in fully AI-guided robotics capable of automating the synthesis of tiny organic compounds without human intervention. (Figure 4).

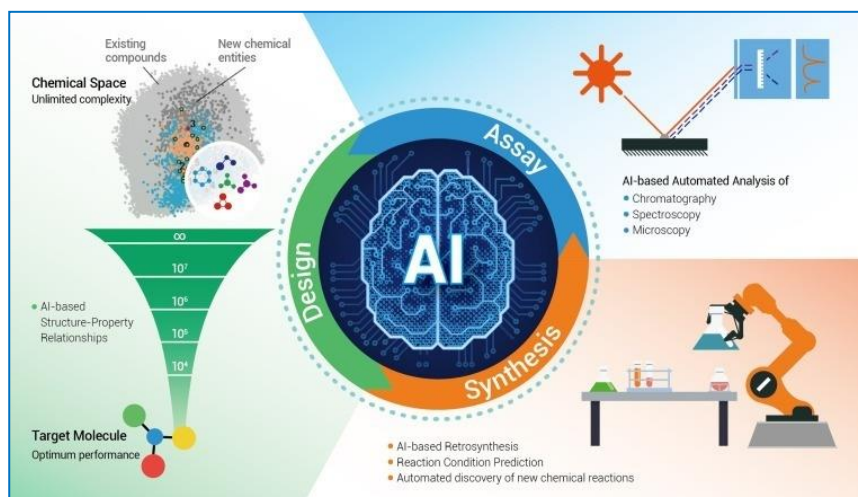


Figure 4. A closed loop approach that allows AI to design, synthesize, and analyze compounds in organic chemistry

3.1 Image Recognition and Computer Vision:

Artificial intelligence systems detect and classify plastics using image recognition, which analyzes visual data from cameras or sensors. The system captures photographs of plastic waste on a conveyor belt. The AI uses machine learning techniques to identify key qualities associated with different types of plastic, such as color, shape, texture, and transparency. The algorithm compares the identified attributes to its trained database and classifies the plastic as PET, HDPE, or PVC. Based on the classification, the AI directs the plastic to the appropriate recycling stream, resulting in precise and efficient sorting.

Waste Sorting

Cameras with computer vision algorithms can identify and sort a variety of waste products (such as plastics, metals, glass, and paper). Robots can utilize visual data to differentiate recyclable and non-recyclable materials.

Monitoring Waste Levels

Sensors can monitor the fill levels of garbage containers, allowing collection routes and timetables to be optimized. Cameras can provide visual information about the state of garbage containers, detecting overflow and illegal dumping.

3.2 Robotic Sorting Arms

Mounted cameras and sensors capture images and data from goods moving along a conveyor belt or sorting line. Advanced algorithms use visual data to recognize and classify materials. Machine learning models are trained to identify different forms of garbage based on their shape, color, texture, and other characteristics. Based on the processed data, the AI system categorizes materials (for example, plastics, metals, glass, and paper). The AI gives the robotic arms exact instructions on which objects to choose and where to place them. The use of robotics in garbage sorting and recycling has various advantages. To begin, it improves garbage sorting efficiency and accuracy by deploying innovative technologies capable of identifying and categorizing various sorts of waste materials (Figure 5).



Figure 5: Robotics in Waste Sorting and Recycling

3.2.1 Advantages of Robotic Sorting Arms

Robotic arms can process huge amounts of material quickly, enhancing total sorting efficiency. They can work continuously with few breaks, which increases productivity. AI-powered robotic arms are highly accurate at identifying and sorting materials, reducing contamination and errors. Robots provide consistent performance and sorting quality throughout time. Automation eliminates the need for manual work, potentially lowering labor costs. Better sorting accuracy leads to higher-quality recyclables and less landfill trash. Robots can handle potentially dangerous items, which improves worker safety. Reduces the need for manual, repetitive tasks, hence lowering worker strain and injury risk. Robotic sorting systems can be scaled to handle varying volumes and types of garbage, making them adaptable to diverse facility sizes and requirements. Integrated systems can collect data on sorting performance, waste composition, and other variables, providing insights into process optimisation.

3.3 Near-Infrared (NIR) Spectroscopy

Near-infrared (NIR) spectroscopy is a technique for determining the composition of materials based on their interactions with near-infrared light. Its capacity to quickly and non-destructively identify distinct compounds makes it widely used in a variety of industries, including waste management and recycling. Combining artificial intelligence (AI) with near-infrared (NIR) spectroscopy to detect plastic types based on their chemical makeup might considerably improve material sorting and recycling processes. NIR sensors collect spectral information from plastic samples as they interact with near-infrared light. This information describes the chemical makeup and molecular structure of the plastics. Near-infrared (NIR) spectroscopy² is a strong analytical technique that has found many applications in diverse sectors, including chemistry, pharmacology, agriculture, food science, and materials research (Figure 6).

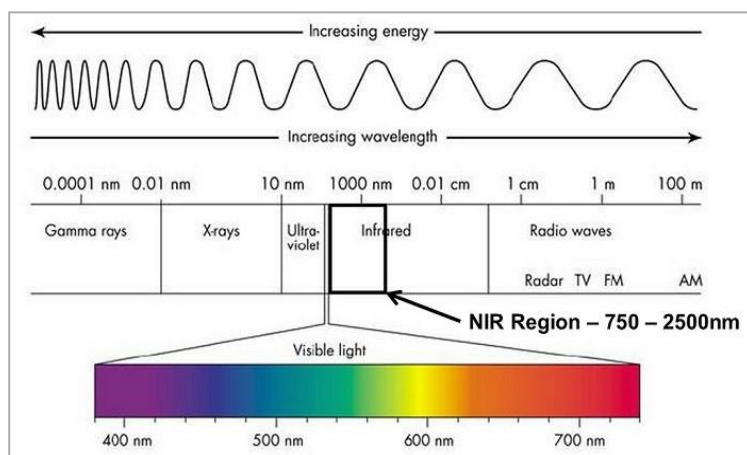


Figure 6. Electromagnetic spectrum with NIR band highlighted

The AI system gives sorting instructions to robotic arms or other automated systems, which separate the recognized polymers appropriately. AI algorithms may be trained to recognize new types of plastics as they develop, ensuring their continued relevance. The integration delivers useful information on plastic composition and sorting performance, which helps with process optimization and decision-making. Combining AI and NIR technology provides a strong solution for recognizing and sorting plastics based on chemical composition, resulting in more efficient and precise recycling operations and improved environmental consequences. NIR spectroscopy studies materials without altering or harming them, allowing for repeat testing while maintaining the sample's integrity. NIR spectroscopy provides quick results, making it suitable for high-throughput applications where rapid detection and sorting are required. NIR spectroscopy requires little to no sample preparation. This minimizes the time and effort required to prepare samples for analysis. NIR spectroscopy is an effective method for identifying and studying various polymers, with benefits such as speed, non-destructiveness, and minimal sample preparation. Its versatility and low cost make it an invaluable approach for a variety of applications, including recycling and manufacturing, as well as environmental monitoring and research.

² NIR spectroscopy is a method that makes use of the near-infrared region of the electromagnetic spectrum (from about 700 to 2500 nanometers). By measuring light scattered off of and through a sample, NIR reflectance spectra can be used to quickly determine a material's properties without altering the sample.

4. Case Studies

AMP Robotics is a company that specializes in advanced robots and artificial intelligence for the recycling industry. They focus on improving the efficiency and effectiveness of material sorting and recycling processes through innovative technologies. AMP Robotics creates robotic devices with advanced vision and AI capabilities. These robots are intended to automate the sorting of recyclables, increasing speed and accuracy. AMP Robotics' technologies improve the speed and accuracy of material sorting, resulting in increased throughput and lower operational costs for recycling plants. AMP Robotics' systems are designed to be scalable and versatile, making them appropriate for a variety of facility sizes and waste streams. Unique in its depth and breadth, it enables automation to accurately recover recyclables, removing contamination and creating high-value raw material for resale into the global supply chain.

ZenRobotics is a company that specializes in robotic sorting solutions for the recycling and waste management industries. Their technology combines robotics, artificial intelligence (AI), and machine learning to improve the efficiency and effectiveness of material sorting processes. ZenRobotics develops robotic sorting systems that utilize advanced AI and machine learning algorithms. These robots are designed to identify, sort, and process various types of waste materials. ZenRobotics' solutions improve the speed and accuracy of material sorting, resulting in increased throughput and lower operational costs in recycling operations. High-resolution cameras and artificial intelligence algorithms provide accurate identification and sorting of distinct materials, reducing contamination and errors. Robotic systems can handle huge amounts of material fast, increasing sorting efficiency and facility productivity. ZenRobotics represents a significant advancement in the use of robotics and AI for recycling and waste management, offering solutions that enhance sorting efficiency, material recovery, and overall recycling effectiveness.

TOMRA Sorting Solutions is a leading company specializing in sensor-based sorting technology for the recycling, mining, and food industries (Figure 7). They provide a variety of innovative solutions that aim to increase the efficiency and accuracy of material sorting processes. TOMRA uses a variety of sensor technologies, including optical, laser, and x-ray, to identify and classify materials based on their physical and chemical characteristics.

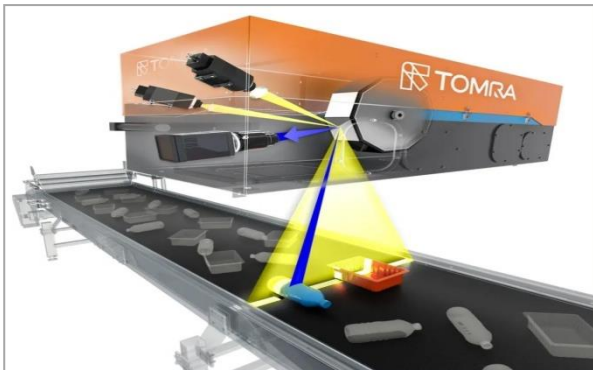


Figure 7. TOMRA AUTOSORT combines multiple sensors and technologies

Their systems utilize artificial intelligence (AI) and machine learning to enhance sorting accuracy and adapt to different material types and conditions. TOMRA Sorting Solutions is a recognized leader in sensor-based sorting technology, providing advanced solutions that improve sorting accuracy, efficiency, and adaptability across a wide range of sectors. Their dedication to innovation and sustainability promotes advancements in recycling and resource management.

5. Benefits of AI in Plastic Sorting

Increased Accuracy and Efficiency

Higher precision in identifying and sorting different types of plastics.

Reduction in contamination rates, leading to higher quality recycled materials.

Cost Savings

Reduction in labor costs and increased throughput.

Operational cost savings through optimized sorting processes.

Scalability and Adaptability

Ability to handle varying volumes and types of plastic waste.

Adaptability to changes in waste stream compositions.

6. Challenges and Limitations

Technical Challenges

Ensuring high-quality data for training AI models.
Handling variability and complexity in plastic waste streams.

Economic Challenges

High initial investment costs for AI sorting systems.
ROI considerations for smaller recycling facilities.

Regulatory and Standardization Issues

Need for industry-wide standards and regulatory support.

Ethical and Social Considerations

Potential job displacement due to automation.
Importance of workforce reskilling and adaptation.

7. Future Prospects and Innovations

Advancements in AI Algorithms

Development of more sophisticated AI models for better accuracy.
Integration of deep learning and reinforcement learning techniques.

Combining AI with Other Technologies

Use of IoT for real-time monitoring and data collection.
Blockchain for tracking and ensuring transparency in recycling processes.

Collaborative Efforts

Industry, academia, and government partnerships to drive innovation.
Policies and standards to support AI adoption in recycling.

8. Conclusions

- AI improves plastic recycling by automating sorting, identifying materials, controlling quality, and offering data insights. Its integration into recycling operations improves productivity, accuracy, and cost savings, while also contributing to more sustainable and effective waste management techniques. As AI technology advances, its involvement in plastic recycling is anticipated to grow, pushing additional advancements and innovations in the industry..
- AI improves quality control by recognizing pollutants and impurities in plastic trash, ensuring only high-quality materials make it through the recycling process. This results in improved final goods and higher recycling standards.
- AI offers vital insights about sorting performance, material composition, and operational efficiency. This information aids in the optimization of recycling processes, the reduction of waste, and the efficient use of resources.
- Advancements in machine learning and AI algorithms can improve sorting accuracy and efficiency. Continuous research and development are required to perfect these technologies and improve their capabilities.
- Innovations in sensor technology, robots, and data analytics can enhance sorting operations. Integrating these breakthroughs into AI systems will aid in the resolution of complicated sorting challenges while also increasing efficiency.
- To drive the successful integration of AI into recycling efforts, all stakeholders must engage actively and collaboratively. Technology providers should continue to innovate, recycling facilities should accept and adopt innovative solutions, and the government and policymakers should foster technical advancement. Academic institutions should promote research and education, while investors and financial organizations should encourage and fund meaningful ventures. These combined efforts will improve recycling efficiency, promote sustainability, and help to create a more effective and resilient circular economy.

REFERENCES

- [1] Alim Al Ayub Ahmed, A B M Asadullah Artificial Intelligence and Machine Learning in Waste Management and Recycling <https://www.researchgate.net> ›
- [2] Abdallah M, Abu Talib M, Feroz S, Nasir Q, Abdalla H, Mahfood B , Artificial intelligence applications in solid waste management: a systematic research review. Waste Manag 109,. <https://doi.org/10.1016/j.wasman>.
- [3] Cha G-W, Moon HJ, Kim Y-M, Hong W-H, Hwang J-H, Park W-J, Kim Y-C, Development of a prediction model for demolition waste generation using a random forest algorithm based on small datasets. Int J Environ
- [4] Greg Lettieri, AI and Waste Management – How Can It Help? Published on June 12, 2023
- [5] Ihsanullah I, Alam G, Jamal A, Shaik F (2022) Recent advances in applications of artificial intelligence in solid waste management: a review. Chemosphere 309:136631. <https://doi.org/10.1016/j.chemosphere.2022.136631>
- [6] Kshirsagar PR, Kumar N, Almulihi AH, Alassery F, Khan AI, Islam S, Rothe JP, Jagannadham DBV, Dekeba K (2022) Artificial intelligence-based robotic technique for reusable waste materials. Comput Intell Neurosci. <https://doi.org/10.1155/2022/2073482>
- [7] Kontokosta CE, Hong B, Johnson NE, Starobin D (2018) Using machine learning and small area estimation to predict building-level municipal solid waste generation in cities. Comput Environ Urban Syst 70:151–162. <https://doi.org/10.1016/j.compenvurbsys.2018.03.004>
- [8] Mohsin M, Ali SA, Shamim SK, Ahmad A ,A gis-based novel approach for suitable sanitary landfill site selection using integrated fuzzy analytic hierarchy process and machine learning algorithms. Environ Sci Pollut Res 29:31511–31540. <https://doi.org/10.1007/s11356-021-17961-x>
- [9] Melinte DO, Travediu A-M, Dumitriu DN, Deep convolutional neural networks object detector for real-time waste identification. Appl Sci 10:7301. <https://doi.org/10.3390/app10207301>
- [10] Na S, Heo S, Han S, Shin Y, Lee M (2022) Development of an artificial intelligence model to recognise construction waste by applying image data augmentation and transfer learning. Buildings 12:175. <https://doi.org/10.3390/buildings12020175>

The Analytical Study Of Passive And Active Filtering In A Low Voltage Electrical Network From The Point Of View Of Energy Quality

Ben Haoua Larbi Daouli*¹, Hassan Mana²

Abstract: Static converters are becoming more and more popular because of their many benefits. But these converters cause interference to electrical networks by bringing in harmonic currents and voltages as well as occasionally using reactive energy. Electrical networks are full of harmonics, which can damage or even stop some electrical devices from operating normally. There are various ways to get rid of the harmonic currents that static converters produce. The traditional method, which entails utilizing passive filters to remove harmonics, is provided in this paper. The use of a parallel active filter as a contemporary option is then covered. The various components that make up the electrical network-nonlinear load-filter are outlined. These two kinds of filters are employed in simulations to get rid of harmonic currents that a rectifier bridge produces. The simulations' outcomes are displayed.

Keywords: Shunt Active Power Filter (SAPF), Passive Filter Non-Linear loading

¹**Address:** Ferhat Abbas University Setif, Faculty of Technology Algeria,

²**Address:** Ferhat Abbas University Setif, Faculty of Technology Algeria,

***Corresponding author:** Benhaoua.larbidaouli@univ-setif.dz

1. INTRODUCTION

An increasing number of electrical network disruption issues are being caused by the growing use of power electronics-based controlled systems in industry. As a result, we are seeing a consistent rise in user-generated harmonic current rates and a sizable reactive power usage. Voltage harmonics will also result from the circulation of these disturbed quantities, and they will be superimposed over the electrical network's nominal voltage. The literature has already presented a number of ideas for electrical network harmonic pollution mitigation. Active filters are those that most closely adhere to industrial restrictions. We concentrate on harmonic disturbances, including their origins, effects, and enforced norms. In order to address harmonic disturbances caused by non-linear loads, the traditional method that has long been understood to involve the application of passive filters. We'll talk about this kind of solution first. We'll go over the many kinds of passive filters and their working principles.

The resonant passive filter simulation will take up a portion of this chapter. The most popular, practically the easiest, and least expensive option is passive filtering, but it has two significant disadvantages. The first is connected to the resonance phenomenon with the network that is the source of the any harmonic's amplification at a frequency near the networks. The passive filter's performance is dependent on the features of the network it is linked to, which is its second drawback. The field of fully controllable power semiconductors, specifically transistors and thyristors, have made remarkable strides, which have paved the way for the design of self-adaptive harmonic elimination devices known as active harmonic compensators or even active filters. These devices aim to eliminate the inherent issues with passive filters. Secondly, in order to get rid of harmonic currents, we'll examine the parallel active filter using a voltage inverter's structure. We outline its working principle as well as these various kinds and components. The outcomes of a three-wire simulation an active filter in parallel will be demonstrated and discussed. Lastly, a broad conclusion that summarizes the findings is given [4].

Passive filtering

Resonant passive filter: A resonant passive filter is a series RLC circuit that is adjusted to a lower order harmonic's frequency. Resonant filters work on the basis of presenting an extremely low resistance to the flow of a predetermined order harmonic current. Several resonant filters are frequently installed in parallel, one for each of the various harmonic ranks that need to be filtered.

The following expression provides the resonant passive filter's impedance: [1]– [3]. [4].

$$Z = R + (Lc\omega^2 - 1)/c\omega \quad (1)$$

The filter's resonance frequency is determined by:

$$Fr = 1/(2\pi\sqrt{LC}) \tag{2}$$

Passive filter simulation:

The following table provides a summary of the simulation parameters:

Resonant filter set at fifth rank: Harmonic 5 minimization: the network current and spectrum are displayed in the results. The present waveform has improved as a result of the elimination of harmonic 5. [4]

Table 1: The Simulation Parameters

network voltage	380V
network voltage frequency	50HZ
Network line resistance	0.42Ω
Network line inductance	2.3mH
DC Load resistance	23.5Ω
DC Load inductance	21.1mH
AC Load resistance	1mΩ
AC Load inductance	1mH
Filter resistance (harmonic's filtering 5th, 7th)	0.1Ω
Filter inductance (harmonic's filtering 5th)	0.004H
Filter inductance (harmonic's filtering 7th)	0.001H
Filter capacitor (harmonic's filtering 5th)	101.32uF
Filter capacitor (harmonic's filtering 7th)	206.78uF

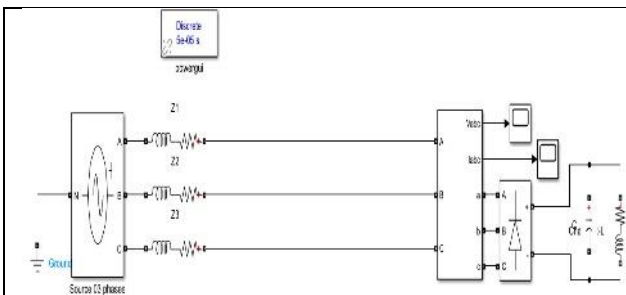


Fig. 1. Block diagram before filtering

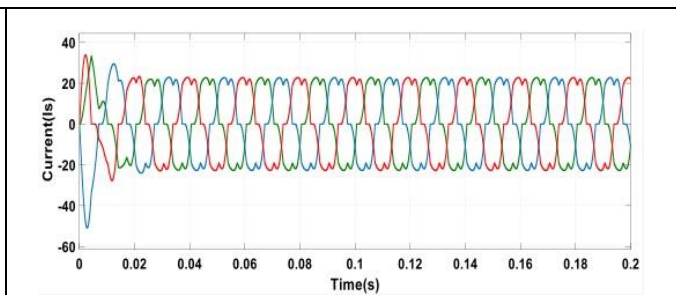


Fig. 2. The shape of the source currents before filtering

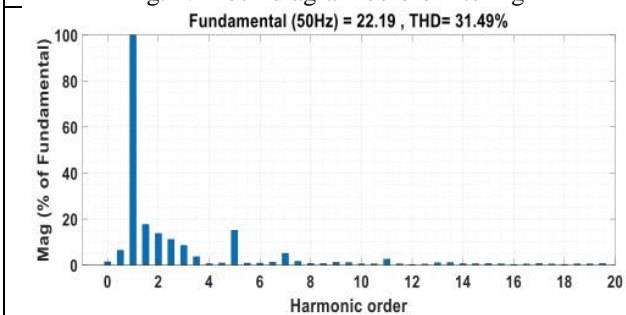


Fig. 3. The harmonic spectrum and the current THD before filtering

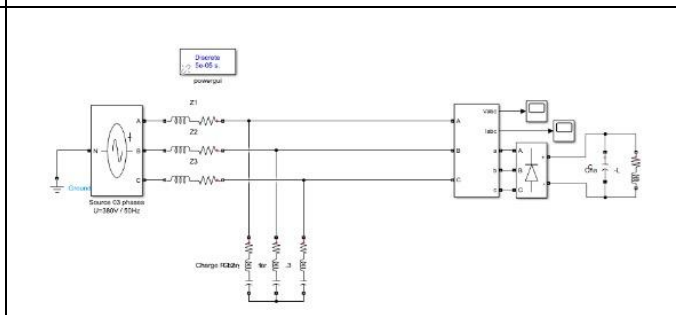


Fig. 4. Diagram filter rank 5and7

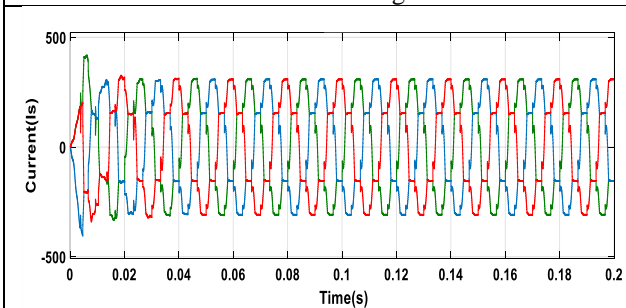


Fig. 5. Shapes of the source currents after filtering harmonic 5

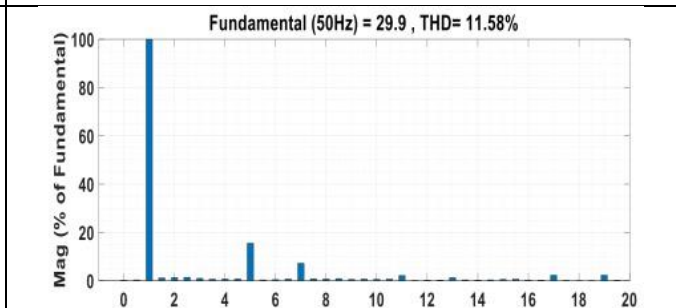


Fig. 6. the harmonic spectrum after filtering harmonic 5 and

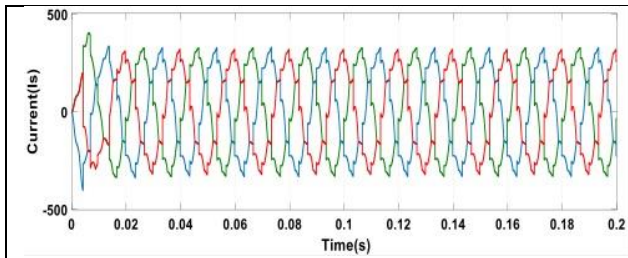


Fig. 7. Shapes of the source currents after filtering harmonic 7

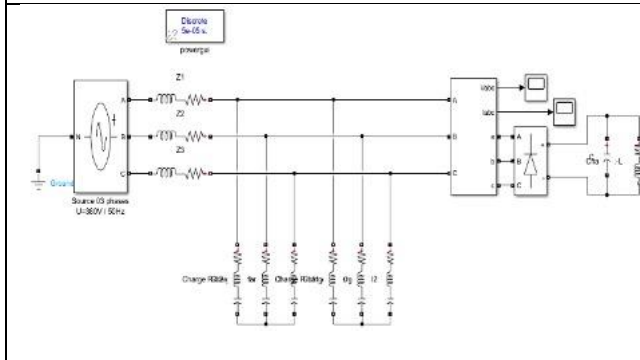
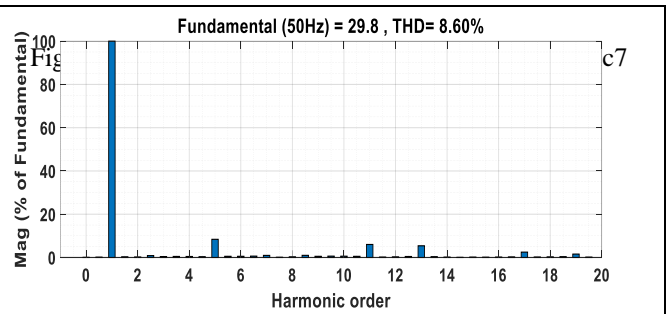


Fig. 9. Diagram filter rank 5 and 7

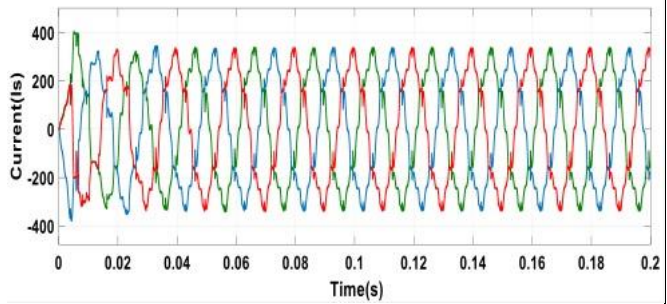


Fig. 10. Source current trends after filtering harmonics 5 and 7

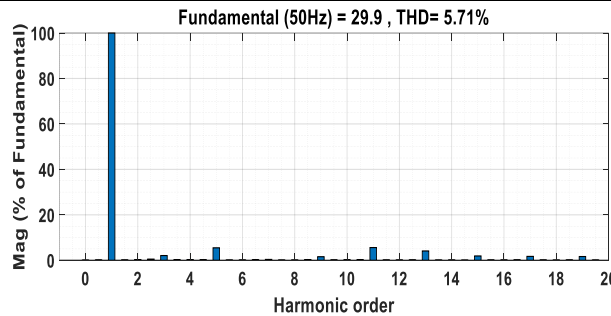


Fig. 11. The harmonic spectrum after filtering harmonics 5 and 7

2. RESULTS AND DISCUSSIONS

Before filtering

The supply currents' waveform is displayed in Figure 2. We see current distortion, which indicates the existence of harmonics in the network. The current harmonic spectrum is shown in Figure 2 before filtering; harmonics 5, 7 and 11 are evident. As a result, the rectifier exhibits non-linear load behavior and absorbs a non sinusoidal current. Prior to filtering, the network's current THD is 22.70%.

After filtering

1) First example: rank 5 resonance filter tuned: After filtering harmonic 5, the supply current waveform is shown in Figure 5, and we can see that the current distortions are less pronounced than in the instance of the currents seen in Figure 2. Figure 6 shows the current's harmonic spectrum after harmonic 5 has been filtered. It is noticeable that harmonics 7 are present and that harmonic 5 has been minimized. After filtering harmonic 5, the network's current THD is shown in Figure 6 (THD = 11.58%).

2) Resonant filter set to rank 7 in the second case: After applying harmonic 7 filter, the supply current waveform is shown in Figure 7, and it is observed that the current distortions are less diminished than when compared to the currents shown in figures 2 and 8. Figure 8 shows the current harmonic spectrum following the minimizing of harmonic 7 and the presence of harmonics 5, 11, and 11. Figure 8 shows the THD of the network prior to filtering harmonic 7, which is 8.60%. Resonant filter set to rankings 5 and 7 in the third case: The supply current waveform in Figure 10 is shown after harmonics 7 and 5 have been filtered. As can be seen, the current distortions are less severe than in the case of the

currents depicted in Figures 2 through 11. After subtracting harmonics 5 and 7, the current harmonic spectrum is shown in Figure 11, where we can see that harmonics 5 and 7 have been reduced. After filtering harmonics 5 and 7, Figure 11 displays the network's current THD (THD = 5.71%).

4. Parallel active filter:

The AC distribution network and the parallel filter are linked in parallel. Shunt filters, sometimes referred to as parallel filters, are used to counteract the harmonic distortions brought on by the nonlinear load. They both operate using the same active filtering principle. However, as mentioned, they are connected in parallel, acting as a current source alongside the load. They find the line's harmonics by utilizing powerful computing power. The majority of the time, sensors with microprocessor or microcontroller bases are employed to determine the control logic and estimate harmonic contents. Particularly the IGBT, power semiconductor devices are used. According to some academics, active filters were rarely used prior to the development of IGBTs because of budget overruns. Nevertheless, shunt active filters have numerous advantages despite their utility. disadvantages. They practically require a large-rated PWM inverter that can react quickly to changes in system parameters. The injected currents may circulate via any passive filters that are connected to the system, such as hybrid filters. [1], [4]–[7].

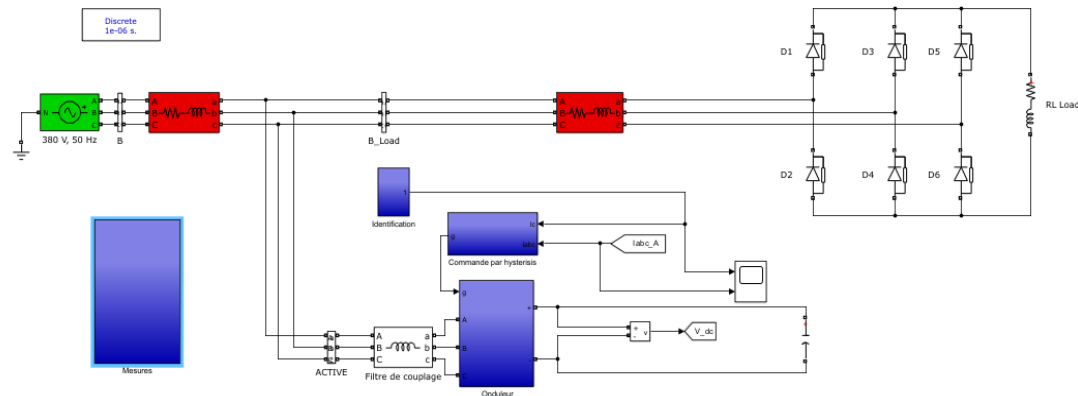


Fig. 12. Block diagram of the parallel active filter controlled by hysteresis

**4.1 Simulation of the Parallel active filter:
Parallel active filter control:**

The control-command portion is composed of: (1) an interference current identification block, which uses instantaneous powers as its identification method; (2) an inverter DC bus voltage regulation block, which uses a proportional integral regulator (PI) in this work; and (3) a voltage inverter control, which regulates the currents at the filter output so that they follow their references. The principle of inverter control is based on the comparison between the filter output currents and their references identified using various identification methods, one of which is hysteresis control [5]–[10].

5.Simulation results:

Table 2. The Simulation Parameters

network voltage	380V
network voltage frequency	50HZ
Network line resistance	0.42Ω
Network line inductance	2.3mH
DC Load resistance	23.5Ω
DC Load inductance	21.1mH
AC Load resistance	1mΩ
AC Load inductance	1mH
Filter inductance	3mH
Voltage Vdc	600 v

5.1. RESULTS AND DISCUSSIONS

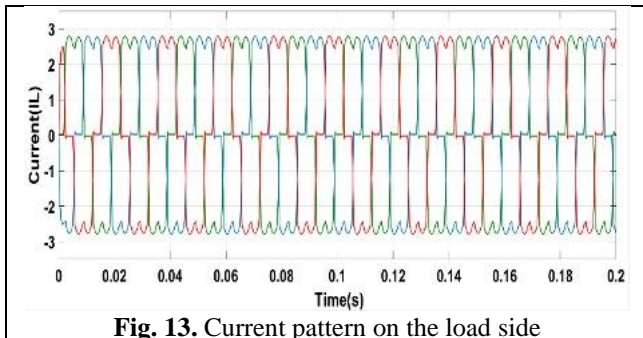


Fig. 13. Current pattern on the load side

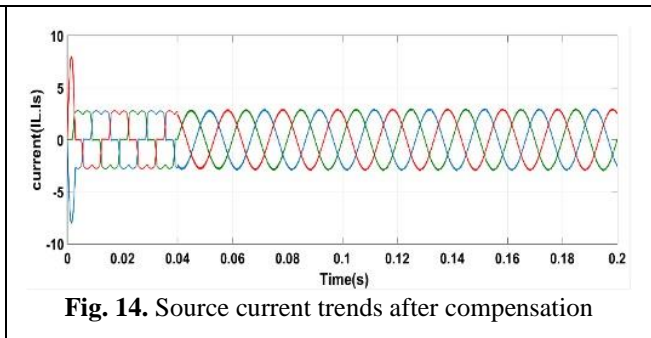


Fig. 14. Source current trends after compensation

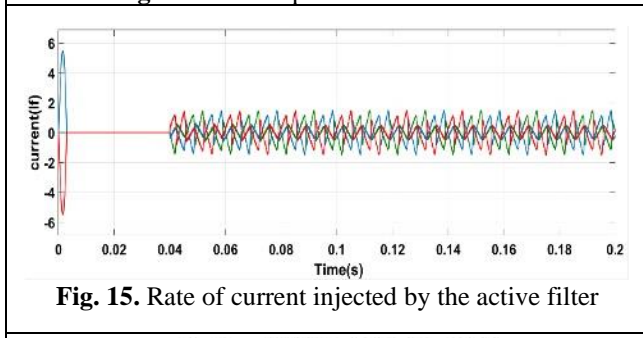


Fig. 15. Rate of current injected by the active filter

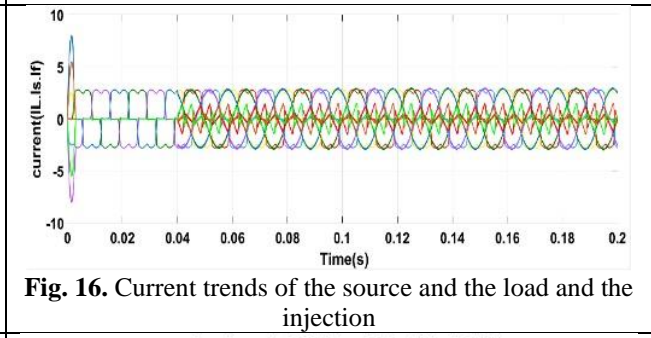


Fig. 16. Current trends of the source and the load and the injection

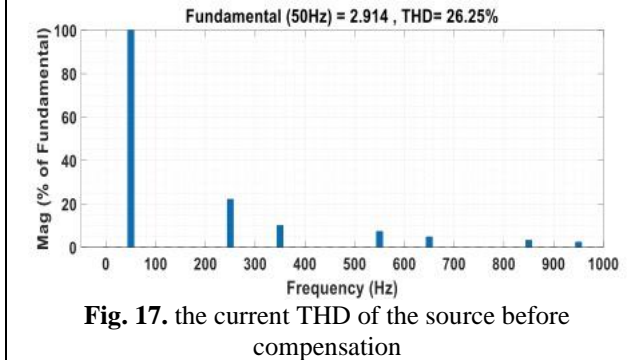


Fig. 17. the current THD of the source before compensation

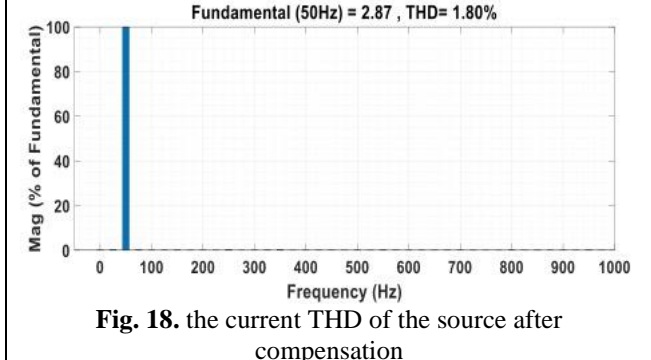


Fig. 18. the current THD of the source after compensation

Figure 13 represents the shape of the current on the load side. Wave of supply currents. We notice a distortion of the currents which make the presence of harmonics in the network. Figure 14 represents the shape of the source currents. In this case, we notice that the current is sinusoidal in shape with Figure 13 represents the shape of the current on the load side. Wave of supply currents. We notice a distortion of the currents which makes the presence of harmonics in the network. Figure 14 represents the shape of the source currents. In this case, we notice that the current is sinusoidal in shape with high frequency harmonics due to current control by hysteresis. Figure 15 represents the appearance of the harmonic current of I_{inj} the current injected by the active filter. We see that the current injected follows its reference well. Figure 16 represents the appearance of Current trends of the source and the load and the injection the case where the inverter is controlled by hysteresis. We also see that the current is practically in phase with the voltage, which minimizes the consumption of reactive energy. Figure 17 represents the current harmonic spectrum before filtering. The current THD of the network before filtering is 26.25% Figure 18 shows the current THD of the source after compensation where the inverter is controlled by hysteresis THD= 1.80

CONCLUSION

In this work we dealt with the problem of pollution of harmonic currents in electrical networks by passive and active filtering. firstly we presented the passive filter based on the use of RLC electrical circuits to locally modify the network impedance. However, passive filters have several drawbacks such as resonance with the network and the use of a filter for each harmonic to be eliminated. Three filtering cases are simulated: a resonant filter tuned to the harmonic of order 5, a resonant filter tuned to the harmonic of order 7 and two resonant filters tuned to the harmonics of order 5 and 7 simultaneously. In these three cases the harmonic distortion rates have been reduced. Parallel active filtering is a new solution for the depollution of harmonic currents. Secondly, the parallel active filter and its different constituents are presented. It consists of connecting the voltage inverter in parallel with the network through a coupling filter. This

inverter injects harmonic pollution control currents into the network in real time to clean up the latter. These harmonics are identified by the instantaneous power method and the inverter is controlled by hysteresis. This type of control is simple to implement, but the switching frequency is not constant. The simulation results show that the parallel active filter makes it possible to reduce the THD to values lower than the limits imposed by the standards. These results also show advantages such as the adaptability of the active filter to load variations as well as its power to eliminate all harmonic ranks. The results of the simulations gave THDs by the active filter lower than those obtained by the passive resonant filter. The simulation results confirm the superiority of active filtering compared to passive filtering.

REFERENCES

- [1] H. Lan and J. He, "Increasing-dimension evolution: Make the evolutionary design of passive filters more efficient," *Applied Soft Computing*, vol. 131, p. 109740, 2022
- [2] K. Vinayaka and P. Puttaswamy, "Analysis of current harmonics compensation using various active filter topologies," *Materials Today: Proceedings*, vol. 58, pp. 580–586, 2022
- [3] M. Benaouadj, Z. Boumous, and S. Boumous, "Active harmonic filtering for improving power quality of an electrical network," *Journal Europeen ' des Systemes Automatis ' es '* , vol. 55, no. 3, pp. 397–403, 2022
- [4] H. A. Sher and A. M. Eltamaly, "Harmonics reduction techniques-a survey," *International Review on Modelling and Simulations*, vol. 4, no. 6, pp. 3135–3147, 2011
- [5] Eslami, A., Negnevitsky, M., Franklin, E., & Lyden, S. (2022). Review of AI applications in harmonic analysis in power systems. *Renewable and Sustainable Energy Reviews*, 154, 111897. K. Elissa, "Title of paper if known," unpublished.
- [6] Assiene Mouodo, L. V., Mahamat ALI, A. H., Tamba, J. G., & Olivier, T. S. M. (2022). Comparison and classification of six reference currents extraction algorithms for harmonic compensation on a stochastic power network: Case of the TLC hybrid filter. *Cogent Engineering*, 9(1), 2076322..
- [7] Goel, N., Hasan, S., & Kalaichelvi, V. (2020). Modelling, Simulation and Intelligent Computing Proceedings of MoSICom 2020. *Proceedings of MoSICom*, 1.
- [8] Moeini, A., Dabbaghjamesh, M., Kimball, J. W., & Zhang, J. (2020). Artificial neural networks for asymmetric selective harmonic current mitigation-PWM in active power filters to meet power quality standards. *IEEE Transactions on Industry Applications*.
- [9] Alhamrouni, I., Hanafi, F. N., Salem, M., Rahman, A., Nadia, H., Jusoh, A., & Sutikno, T. (2020). Design of shunt hybrid active power filter for compensating harmonic currents and reactive power
- [10] Aiwa, F. F., Alkhayyat, M. T., & Suliman, M. Y. (2021). A Review on PQ Theory Based Shunt Active Power Filter. *Design Engineering (Toronto)*, 6, 6919-6938.

The method of obtaining Electrical Energy Quality (EEQ) according to the remedies required by EMC: Reduction and Elimination of Electromagnetic harmonics

BOUDJELAL Dounia¹, MANA Hassan²

Abstract: The escalating complexity of modern electronics has intensified EMC challenges, necessitating effective filtering characteristics, making them suitable for mitigating EMC issues. The effectiveness of parallel active filters in suppressing electromagnetic interference, highlighting their application in improving device performance and compliance with EMC standards. Simulation Results demonstrate the efficacy of this approach in achieving electromagnetic compatibility while maintaining optimal system functionality.

Keywords: Electromagnetic compatibility (EMC), Harmonic distortion rate, parallel active filter, MLI.

¹Address: Ferhat Abbas University, Faculty of technology, Setif/Algeria

²Address: Ferhat Abbas University, Faculty of technology, Setif/Algeria

*Corresponding author: douniaboudjelal@gmail.com

1. INTRODUCTION

The quality of electrical power, or Power Quality (PQ), is another critical aspect that has garnered significant attention in recent years. Poor power quality, characterized by voltage sags, swells, harmonics, and other disturbances, can lead to malfunctions, reduced lifespan of equipment, and increased operational costs. Enhancing power quality is essential for the efficient and reliable operation of both industrial and commercial electrical systems among the various strategies employed to improve power quality, the use of filtering techniques has proven to be highly effective. Passive filters, while simple and cost-effective, often struggle with issues such as resonance and limited adaptability to varying load conditions. This has led to the development and implementation of Active Power Filters (APFs), which offer a more robust solution to power quality issues. In particular, the Active Shunt Filter, also known as the Parallel Active Filter, has shown great promise in mitigating power quality problems. By dynamically compensating for current harmonics and reactive power, active shunt filters enhance the overall performance of electrical systems. This work focuses on the design and implementation of an active shunt filter to address power quality issues, demonstrating its effectiveness in improving EMC and ensuring optimal system functionality. Previous work in this domain [1] [2] [3] has demonstrated the effectiveness of active shunt filters in improving power quality and EMC. However, advancements in control strategies and power electronics have led to the development of more sophisticated and efficient filter designs. This study builds on prior research by introducing an enhanced active shunt filter design and comparing its performance with earlier implementations

2. MATERIAL AND METHOD / MATERYAL VE METOT

First, an active filter is an electronic circuit designed to selectively pass or attenuate certain frequencies within an input signal using active components, typically operational amplifiers (op-amps), in addition to passive components. Unlike passive filters that rely solely on resistors, capacitors and inductors, active filters leverage the amplification capabilities of op-amps to achieve more precise and customizable frequency response characteristics. These filters find widespread application in various electronic systems where precise control over signal frequencies is crucial, such as audio processing, telecommunications, and instrumentation due to their ability to offer flexible design options, and low output impedance. Active filters come in two main kinds: one that connects across the power line (shunt) and one that connects in line with the power flow (series). It's not uncommon to see these filters used alongside passive filters, or even both types working together. If you look at Fig. 1, it shows a special shunt filter for a power system that has three phases and a neutral wire. This device helps clean up the electrical current, making it smoother and helping to maintain a steady flow of power. It also helps to balance the power across the system and gets rid of any unnecessary current in the neutral wire. At the heart of this filter is a simple set up with an inverter and a single capacitor, which doesn't even need its own power to work; it's smartly controlled to act like a power stabilizer.

2.1. The principle of active filter control

The principle of the active filter lies in the injection of harmonic currents of the same amplitude as those pollutants but in opposition of phase with them. The current absorbed by the polluting load consists of a fundamental and harmonics. The active filter is used to generate harmonic currents of the same amplitude but in phase opposition to those existing in the load. To do this, it is necessary to identify the harmonic currents of the load. Several methods of identification exist. [1]:

- The first is based on the spectral analysis of the polluting current.
- The second uses a band pass filter to filter the fundamental.
- The third uses the notions of real and imaginary powers.
-

This last method is the most used in most active filters because it achieves the best match between static and dynamic performances. The instantaneous reactive power theory is based on the transformation of the a,b,c stationary reference coordinate to the $\alpha, \beta, 0$ rotating coordinate, which is known as a Clark transformation. The source voltages and currents are transformed into $\alpha, \beta, 0$ components, as shown in the following expressions:

Voltage components:

$$\begin{bmatrix} V_0 \\ V_\alpha \\ V_\beta \end{bmatrix} = \sqrt{\frac{2}{3}} \begin{bmatrix} \frac{1}{\sqrt{2}} & \frac{1}{\sqrt{2}} & \frac{1}{\sqrt{2}} \\ 1 & -\frac{1}{2} & -\frac{1}{2} \\ 0 & \frac{\sqrt{3}}{2} & -\frac{\sqrt{3}}{2} \end{bmatrix} \cdot \begin{bmatrix} V_a \\ V_b \\ V_c \end{bmatrix} \quad (1)$$

Current components:

$$\begin{bmatrix} I_0 \\ I_\alpha \\ I_\beta \end{bmatrix} = \sqrt{\frac{2}{3}} \begin{bmatrix} \frac{1}{\sqrt{2}} & \frac{1}{\sqrt{2}} & \frac{1}{\sqrt{2}} \\ 1 & -\frac{1}{2} & -\frac{1}{2} \\ 0 & \frac{\sqrt{3}}{2} & -\frac{\sqrt{3}}{2} \end{bmatrix} \cdot \begin{bmatrix} I_a \\ I_b \\ I_c \end{bmatrix} \quad (2)$$

In a,b,c reference frame, the instantaneous active power is given by:

$$P_3(t) = v_a \cdot i_a + v_b \cdot i_b + v_c \cdot i_c \quad (3)$$

Similarly, in the $\alpha, \beta, 0$ reference frame:

$$P_{\alpha\beta 0}(t) = v_\alpha \cdot i_\alpha + v_\beta \cdot i_\beta + v_0 \cdot i_0 \quad (4)$$

It should be noted that the transformation used is orthogonal. It keeps the power invariant in both reference frames:

$$P_3(t) = P_{\alpha\beta 0}(5)$$

Or

- The real instantaneous power

$$P = v_\alpha \cdot i_\alpha + v_\beta \cdot i_\beta = P_\alpha + P_\beta(6)$$

- The instantaneous power of the zero-sequence:

$$P_0 = v_0 \cdot i_0(7)$$

One of the advantages resulting from the transformation is the separation of the zero-sequence components of current or voltage.

The system considered in this paper is a three-phase three-wire system, therefore, a zero-sequence component is absent.

In the α - β coordinate, the complex sum of the active and reactive powers (P and Q) can be represented by (8)

$$S = P + jQ = v_{\alpha\beta} i_{\alpha\beta}^* = (v_\alpha - jv_\beta)(i_\alpha + ji_\beta) = (v_\alpha i_\alpha + v_\beta i_\beta) + j(v_\alpha i_\beta - v_\beta i_\alpha) \quad (8)$$

Where S is the complex power, P refers to the active power, Q represents the reactive power and the * is then complex conjugate. Hence, the instantaneous active and reactive power components (p and q) can be formed as follows:

$$\begin{bmatrix} p \\ q \end{bmatrix} = \begin{bmatrix} v_\alpha & v_\beta \\ -v_\beta & v_\alpha \end{bmatrix} \cdot \begin{bmatrix} i_\alpha \\ i_\beta \end{bmatrix} \quad (9)$$

This power is decomposed into two terms, in the general case:

$$\begin{aligned} p &= \bar{p} + \tilde{p} \\ q &= \bar{q} + \tilde{q} \quad (11) \end{aligned}$$

To isolate conventional active and reactive powers, it is necessary to accurately know the frequencies of the instantaneous powers formed from relation After identifying the pulsations of the instantaneous powers, the power filter responsible for isolating the conventional active and reactive powers can be sized. A circuit consisting of a low-pass filter with a substructure can be used, as shown in Fig. 1.

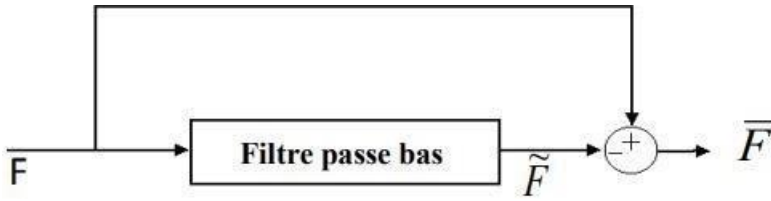


Figure 1. Principle of separating the alternating power components.

The diagram in figure 2 illustrate the various steps for obtaining the harmonic components of the current from a nonlinear load.

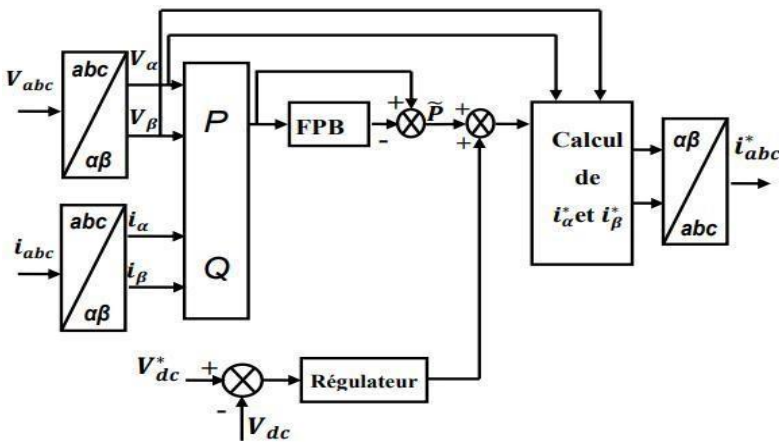


Figure 2. Determination of the reference currents of the active filter using the classical method of instantaneous active and reactive power.

2.2. Current control by PWM (Pulse Width Modulation)

The principle of PWM control is described in figure 3. in this case, the difference between the reference current I_{ref} and the actual current I_{inj} is applied to the input of a regulator. The output signal of the regulator, called the modulator, is then compared to a fixed-frequency triangular signal (carrier) to determine the switching commands for the switches. The frequency of the triangular carrier sets the switching frequency of the power semiconductors [5].

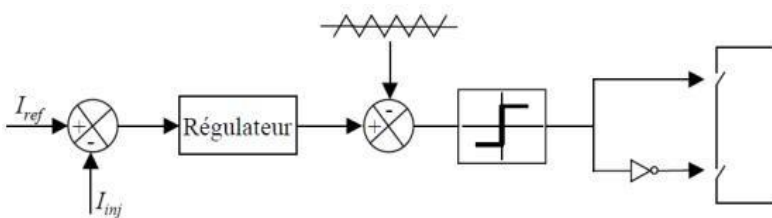


Figure 3. The principle of PWM control.

3. SIMULATION OF THE ACTIVE FILTER

A simulation was conducted using Matlab/Simulink. The system parameters used in this simulation are summarized in the following table:

Table 1. Simulation parameters

Paramètres		Valeurs Numériques
Réseau d'alimentation	V_s (V)	230
	f (Hz)	50
	R_s (m Ω)	0.25
	L_s (mH)	2.3
Charge non-linéaire	R_{cl} (m Ω)	1
	L_{cl} (mH)	1
	R_{ch} (m Ω)	20
	L_{ch} (mH)	0.8
Filtre actif parallèle	V_{dc} (V)	850
	C_{dc} (mF)	300
	R_f (m Ω)	0.55
	L_f (mH)	1.1

3.1. Before filtering

This identification algorithm is used to extract the harmonic currents generated by the rectifier shown in figure 1.

The model of the parallel active is developed using the MATLAB/Simulink block. Simulation Studies are conducted for the system parameters represented in table 1.

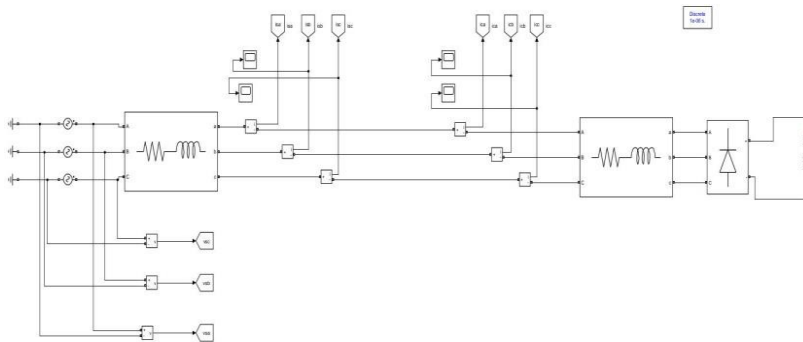


Figure 4. Direct power supply in a nonlinear load without an active filter.

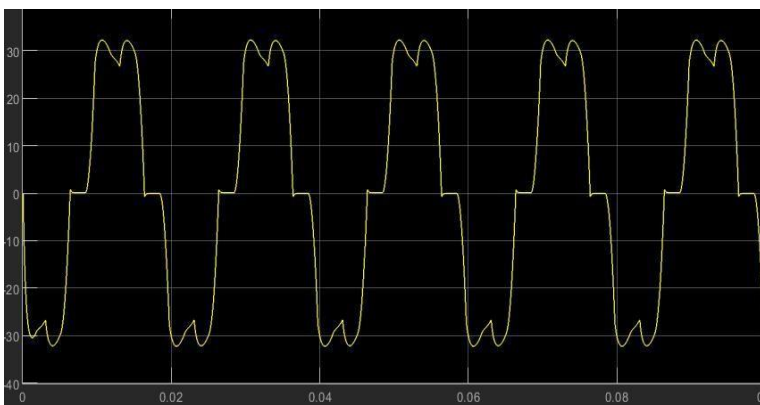


Figure 5. Waveform of I_{sa} before and after filtering.

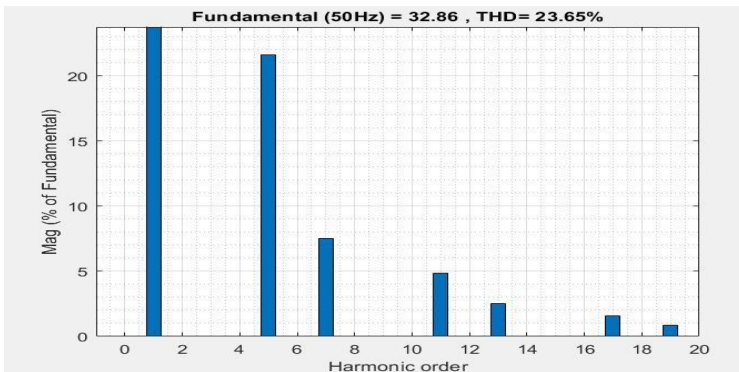


Figure 6. Harmonic spectrum of Isa.

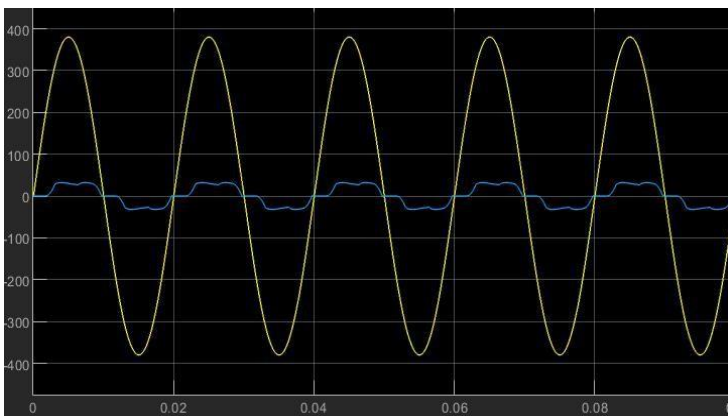


Figure 7. Current Isa phase-shifted voltage Vsa.

3.2. After filtering

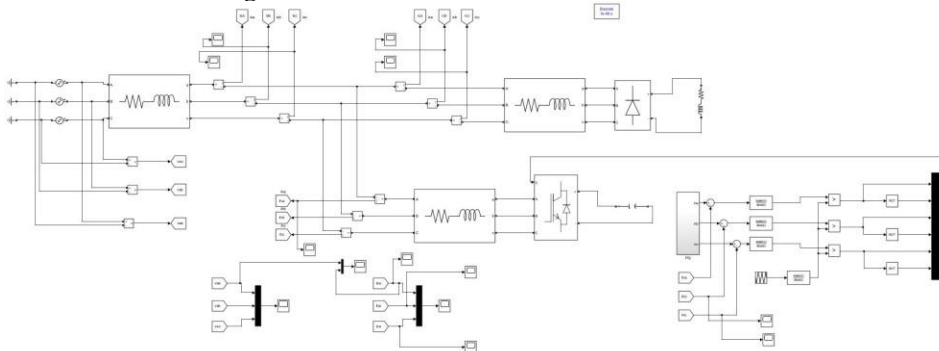


Figure 8. Simulation model after filtering.

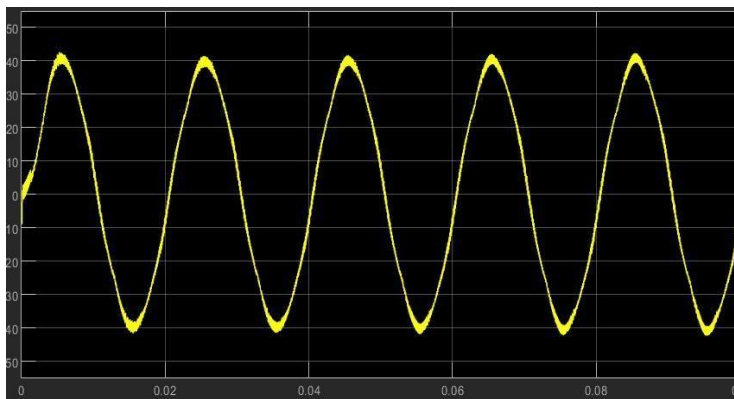


Figure 9. Waveform of Isa after filtering.

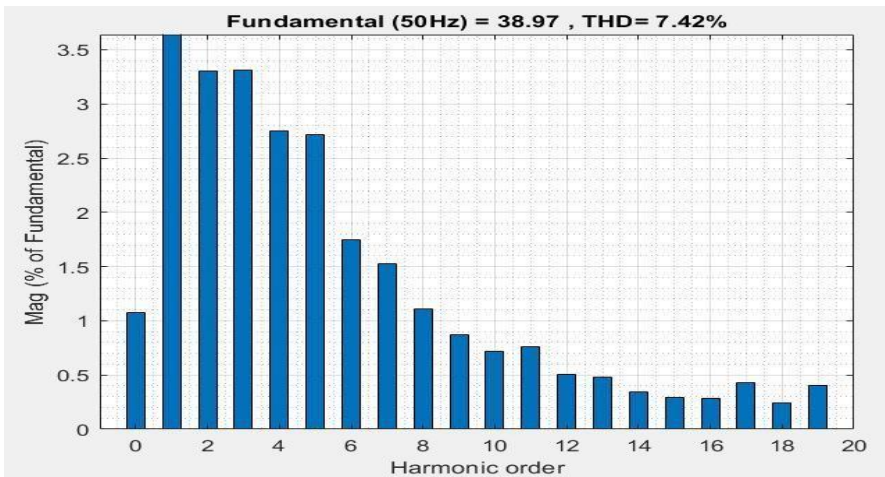


Figure 10. Harmonic spectrum of Isa.

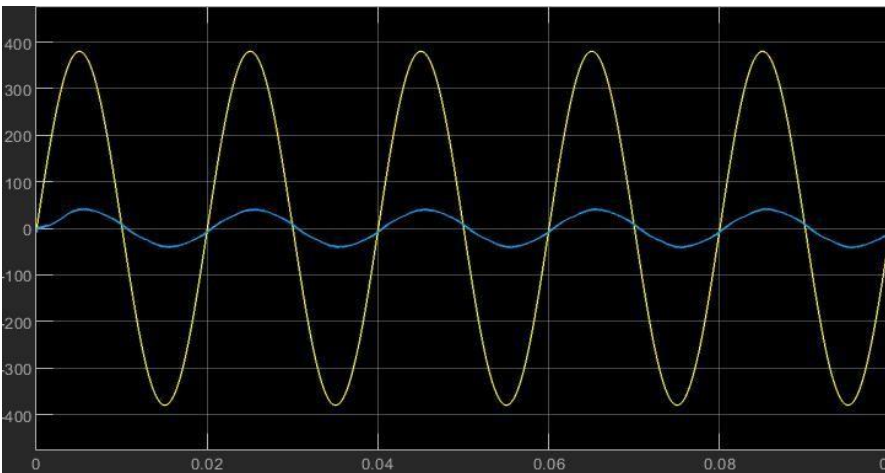


Figure 11. Waveform of Isa and Vsa after filtering.

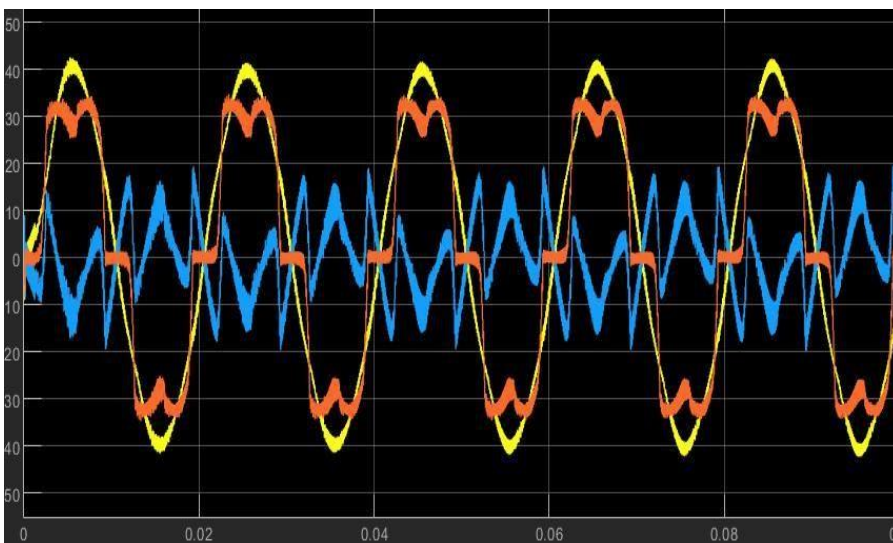


Figure 12. Nonlinear current load Ica, source current Isa and active filter current Iha.

3. RESULTS

The source current graphs before applying active filtering are shown in the figures. We observe symmetrical distortion in the current I_{sa} , which indicates the absence of second and third order harmonics in the I_{sa} spectrum. Only harmonics of the order $(5h \pm 1)$.

We focused solely on studying the current and voltage in phase a, considering that those in the other twophases are delayed by 120° and 240° respectively. The upstream inductance L_f is 3mH before the polluting load, as shown in the figure9. The results were partially satisfactory as the distortions were reduced, along with THD, which now stands at 15.41% as illustrated in the figure 12.

On the source's side, the two curves in the figure.14 representing the current and voltage of the source in phase indicate a corrected power factor.

4. DISCUSSION AND CONCLUSIONS

The work presented in this paper provides a synthesis of power active filters, which are the main remedies for problems caused by harmonic pollution in distribution networks. An application of power active filtering has been addressed, specifically a parallel active filter powered by a DC voltage source with switching orders generated by intersective MLI (PWM), and reference harmonic currents detected using the low pass filtered method. The results obtained in this work allow us to visualize the effectiveness of the parallel power active filter using a P-Q controller.

REFERENCES

- [1] Amir A. Imam, R. Sreerama Kumar and Yusuf A. Al-Turki "Modeling and simulation of a PI controlled shuntactive power filter for power quality enhancement based on P-Q theory,"
- [2] Dr. K. Rajkumar, Dr. S. Gobi Mohan, Mr. Baskar Gopal and Mr Jijin Lal, "Modeling and simulation of a PI controlled shunt active power filter for power quality improvement based on P-Q theory", Volume:5/Issue:12/December-2023, Impact Factor- 7.868.
- [3] Adamou,M, Alkassoum,N, Foulani,A and Malga,A.S.(2019) "Comparative study of linear and non-linear controls ofThree-Phase.
- [4] Shunt active filters for improving the quality of electrical energy." Energy and Power Engineering, 11, 149-166.
- [5] K. Vinayaka and P.Puttaswamy, "Analysis current harmonics compensation using various active filter topologies." Materials today: Proceedings, vol.58, pp.580-586, 2022.
- [6] A.Morsli, A.Tlemçani, M.S.Boucherit et N.Ould Cherchali, " Dépollution des réseaux électriques basse tension utilisant un filtre actif parallèle à deux niveaux contrôlé par l'algorithme p-q" Volume 53,

Number2,

2012.

Potential Strategies to Improve Air Quality in Tirana for Current and Future Generations

Luiza Lluri¹, Fald Lluri², Stela Sefa³

Abstract: Tirana, the capital of Albania, faces severe air pollution, posing significant health risks and environmental concerns for its residents. Referring to the data for the year 2023, KTA admits that Tirana exceeds the European Union norms for PM10 and nitrogen dioxide. Annual average concentrations of PM10 and NO₂ in Tirana are above the limit values of National Air Quality Standard and World Health Organization. This paper looks at the several issues that lead to Tirana's air pollution and considers ways to lower pollution levels and enhance air quality. The problems with Tirana's air pollution are intricate and varied, resulting from a confluence of elements including as topography, industrial processes, burning of biomass, vehicular emissions, and insufficient monitoring programs. Addressing these challenges requires regulatory interventions, technological innovations, public awareness campaigns and stakeholder engagement to improve air quality. Tirana has a population of 528,000 inhabitants, with a surface area of 40 km² and a population density of 13.2 thousand inhabitants. Tirana has the capacity to develop more resilient, sustainable and habitable urban areas. To realize innovative ideas, enhance green areas, and improve air quality for present and future generations, cooperation amongst urban planners, legislators, community organizations, and citizens is imperative. We identify critical actions for policy makers, urban planners, and stakeholders to mitigate air pollution and build a healthier and more sustainable urban environment in Tirana based on pollution sources, regulatory frameworks, and ongoing initiatives. This paper's goal is to offer solutions for enhancing air quality while advancing environmental sustainability and public health.

Keywords: air pollution, urban environment, health risks, sustainability, pollution reduction strategies

¹"Aleksandër Moisiu" University, Faculty of Professional Studies, Durrës, Albania

²"Epoka" University, Faculty of Architecture and Engineering, Tiranë, Albania

³"Aleksandër Moisiu" University, Faculty of Professional Studies, Durrës, Albania

*Corresponding author: luizalluri@uamd.edu.al

1. Introduction

Tirana's air quality has deteriorated because of growing urbanization, increased vehicle emissions, and industrial operations. The air quality in Tirana has been a major public health concern in recent years. As the city grows, so does the level of air pollution, which is mostly caused by traffic emissions, industrial activity, and urban sprawl. The negative effects of air pollution on human health and the environment call for rapid action. This paper investigates the current situation of Tirana's air quality, identifies the key causes of air pollution, and recommends feasible mitigation solutions for current and future generations. The methods suggested including the introduction of stronger emission standards, promotion of sustainable public transportation, and enhancement of green spaces.

2. Current State of Air Quality in Tirana

Tirana experiences frequent episodes of poor air quality, particularly during the winter months when particulate matter (PM_{2.5} and PM₁₀) levels often exceed the World Health Organization (WHO) guidelines. In 2023, the air quality in Tirana fluctuated all year. The average Air Quality Index (AQI) ranged from "Good" to "Moderate," depending on the season and environmental conditions. (Figure 1,2).

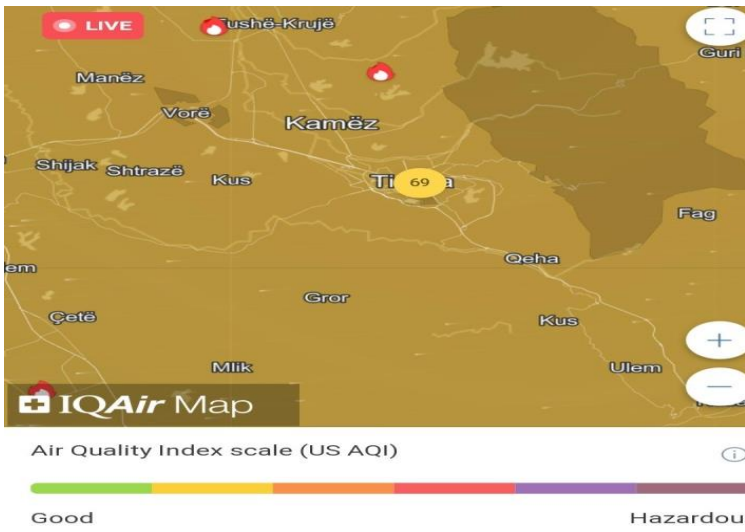


Figure 1 Air pollution air map of Tirana

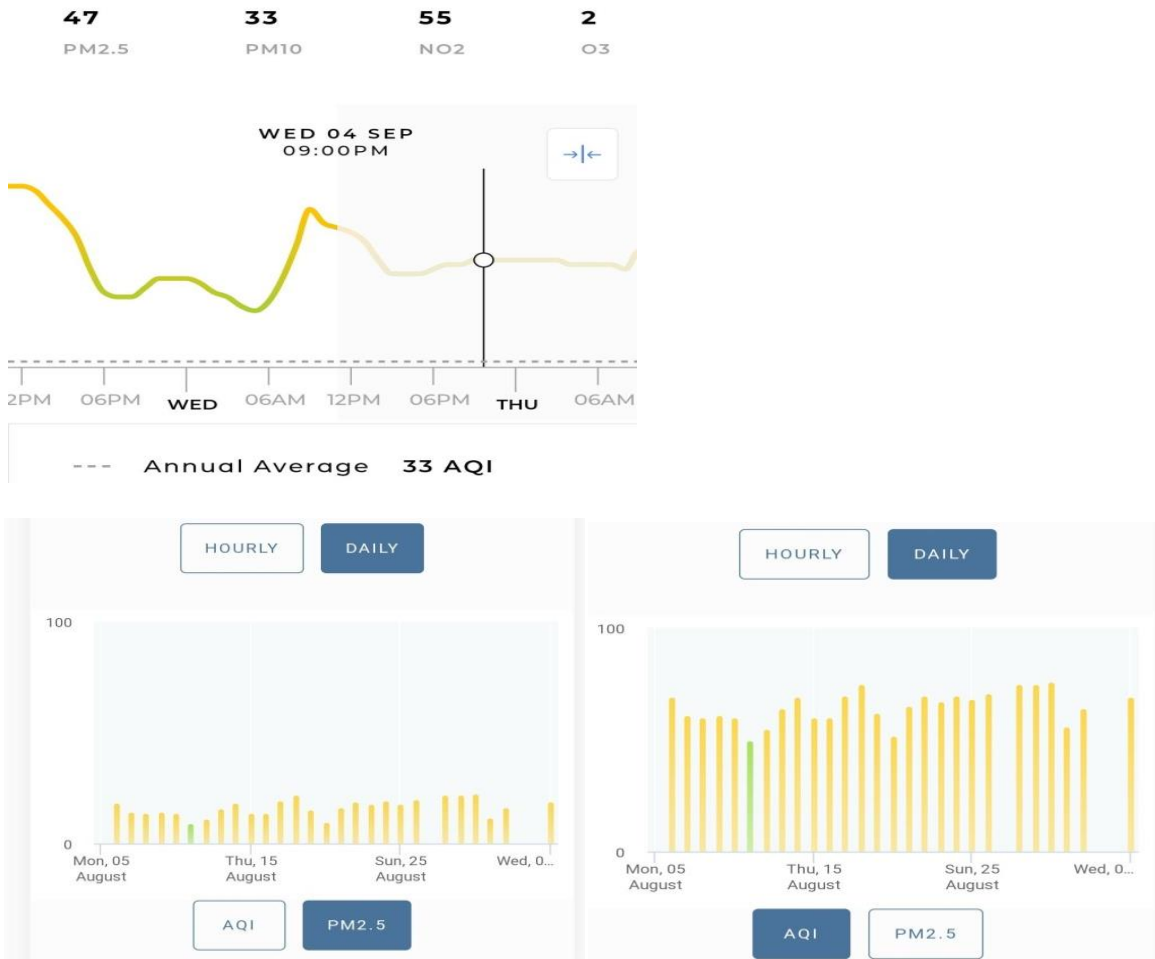


Figure 2. AQI city ranking. Real- time Albania city ranking

PM2.5 and PM10 levels were generally low, keeping air quality within healthy limits most of the time. Significant contributors to this pollution include:

Vehicular Emissions - The growing number of private automobiles, many of which are older and less efficient, contribute significantly to nitrogen oxides (NOx), carbon monoxide (CO), and particulate matter emissions.

Construction Activities - Ongoing urban growth contributes to the emission of dust and other particles. Construction sites generate a significant amount of dust and particulate matter, which can damage air quality. Excavating, demolishing, and moving heavy machinery all produce dust, which can cause lung problems for surrounding individuals. Construction projects frequently use diesel-powered gear and trucks, which produce pollutants such as nitrogen oxides (NO_x), carbon monoxide (CO), and particulate matter. These pollutants contribute to air pollution, which can have negative health consequences.

Industrial Emissions - Industrial operations, particularly on the outskirts of the city, contribute to the emission of sulfur dioxide (SO₂), volatile organic compounds (VOCs), and other pollutants. Though less substantial than traffic, certain industrial operations add to the city's air pollution problems.

The report of the National Environment Agency referring to the year 2023 shows that by analyzing the state of dust particles (PM₁₀ and PM_{2.5}), in certain periods, in certain areas, different harmful indicators appear above the allowed parameters. Based on the monitoring results, for the year 2024 the annual rate of PM₁₀ (40 µg/m³) has been exceeded at the Tirana Hygiene Station and there is an excess of the annual PM₁₀ rate of 35.4%, only in the months of January, February and December 2023 (Figure 3).

Tirana Hygiene Station	SO ₂ µg/m ³	O ₃ µg/m ³	CO µg/m ³	NO ₂ µg/m ³	PM ₁₀ µg/m ³	Benzene µg/m ³
January 2023	6.38	24.06	1.43	41.38		0.96
February 2023	4.85	33.23		38.92		0.75
March 2023	11.88	49.43	0.74	37.03		0.55
April 2023		50.03	1.56	32.82		0.47
May 2023	6.98	42.75	0.5	37.04		0.52
June 2023	4.7	51.68	0.73	35.59	57.78	0.67
July 2023	3.16	66.12	0.74	37.18	55.68	0.46
August 2023	2.57	58.71	0.49	40.02	42.62	1.59
September 2023	3.26	45.28	2.14	42.46	56.89	0.34
October 2023	2.35	34.42	1.01	38.43	50.1	1.23
November 2023	3.28	25.12	3.38	40.57	50.79	1.13
December 2023	3.67	17.09	1.34	48.76	65.28	1.02

Figure 3. Pollution in Tirana for 2023

This shows that there is an increase in PM₁₀ dust particles only in the cold period of the year, because of the use of fossil materials or wood for heating homes. The average value of PM₁₀ for the three months of January, February and December 2023 is 59.51 µg/m³ and we exceed the annual norm of PM₁₀ (40 µg/m³) by 48.8% during winter (Figure 4). Focusing on the nitrogen dioxide indicator, for the year 2023, the annual rate of NO₂ was exceeded at the ASHR Tirana station in the months of January, August, September, October, November. In the other months of the year, the average monthly values of NO₂ are very close to the norm but do not exceed it. This increase comes because of the circulation of vehicles, often with heavy traffic³.

³ Tirana is the largest city in Albania characterized by heavy traffic where one of the air pollutants emitted from the road vehicles is carbon monoxide (CO)

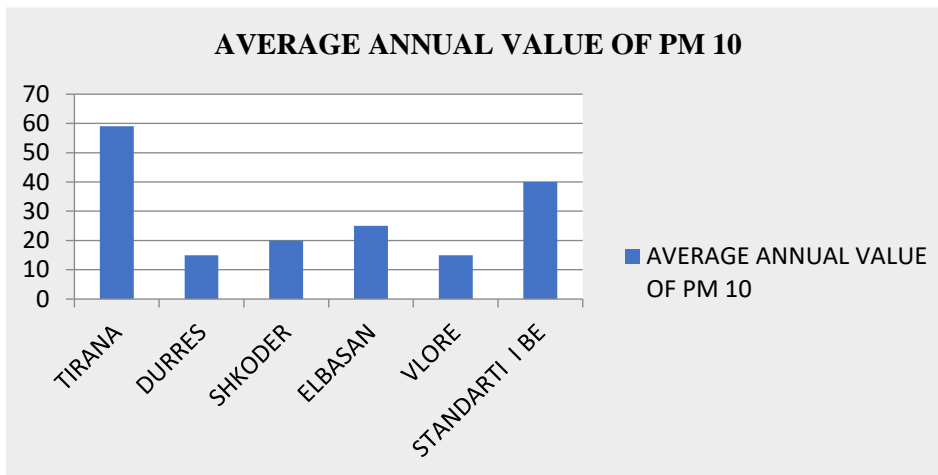


Figure 4. Average of annual value of PM 10

2.1 Pollution Levels

The city frequently suffers alarming amounts of tiny particulate matter (PM2.5 and PM10). These particles, which are frequently derived from traffic exhaust and construction dust, can pose substantial health hazards, particularly when inhaled in large quantities over time. Some places, such as central metropolitan zones, have PM2.5 levels that exceed the European Union's recommended criteria.

According to recent data, Tirana's AQI (Air Quality Index) has fluctuated, with some days seeing "moderate" pollution levels (Figure 5). This suggests that, while the air quality is not harmful, it is still enough to cause health problems for sensitive individuals, such as those with respiratory disorders. Efforts to monitor and improve air quality are underway, but the city confronts significant obstacles in lowering pollution levels to safe levels for its population.

Day	Pollution level	Wind
Thursday, Aug 15 2024	Moderate 66 AQ US	11,2mp/h
Friday, Aug 16 2024	Good 46 AQ US	11,2mp/h
Saturday, Aug 17 2024	Moderate 51 AQ US	11,2mp/h
Sunday, Aug 18 2024	Moderate 57 AQ US	11,2mp/h

Figure 5. Tirana air quality index (AQ)

Enforcing stricter emission standards⁴ for construction vehicles and machinery can reduce the impact of vehicle emissions. Regular air quality monitoring and reporting can help identify and address pollution sources promptly.

NO₂ levels are also elevated, especially in high-traffic regions. The concentration frequently exceeds both the EU and Albanian safety limits, adding to the city's overall pollution burden. Elevated amounts of VoCs have been identified in several hotspots throughout the city, mostly due to automotive emissions.

3. Potential Strategies for Air Quality Improvement

3.1. Strengthening Emission Regulations

- Implementing stricter emissions standards for vehicles, particularly focusing on phasing out older, high-emission diesel vehicles, can significantly reduce pollutants like NO₂ and particulate matter. Tax breaks and subsidies may also play an important role in encouraging the use of electric and hybrid vehicles.
- Enforcing stronger rules on industrial emissions and encouraging the use of cleaner technologies in industries surrounding Tirana would help minimize pollution from this sector.

⁴ Emission standards are the legal requirements governing air pollutants released into the atmosphere

3.2. Promoting Sustainable Public Transportation

- Investing in the creation of a comprehensive public transportation network, such as buses, trams, and cycling facilities, can minimize reliance on private vehicles. A modern and efficient public transportation system would reduce traffic congestion and overall automobile emissions. Invest in high-capacity transit options like Bus Rapid Transit (BRT) and light rail systems to service densely populated areas and lessen dependency on private vehicles. Modernizing the public transport fleet with electric or hybrid cars can cut emissions and enhance air quality.
- Implementing policies that make public transport more appealing, such as fare reductions, dedicated bus lanes, and improved services, could encourage more citizens to choose public transportation over personal vehicles.

3.3. Enhancing Urban Green Spaces

- Increasing the amount of green space, such as parks, green roofs, and urban forests, can help to absorb pollutants and improve overall air quality. Trees and plants operate as natural air filters, greatly lowering the concentration of airborne particles.
- Establishing green buffer zones around high-traffic areas and industrial zones can help to mitigate the spread of pollutants into residential areas. Integrate green spaces, such as parks, green roofs, and urban forests, into mobility planning to improve air quality, reduce urban heat islands, and enhance the overall urban environment.
- Tirana's growing urbanization has put strain on its existing green spaces, raising concerns about their preservation. However, the municipal administration intends to expand and conserve green spaces as part of its urban development policy. Future goals include creating green corridors that connect different parts of the city, improving ecological networks, and promoting sustainable urban mobility.

3.4. Improving Infrastructure and Urban Planning

- Developing urban planning strategies that reduce the need for long commutes and encourage walking and cycling can help reduce vehicle emissions. Mixed-use complexes, which combine residential, business, and recreational areas, can reduce dependency on cars.
- Creating large bike and pedestrian networks that are safe, accessible, and well-maintained. To encourage walking and cycling, use traffic calming measures such as decreased speed limits, larger sidewalks, and protected bike lanes.
- Widen and improve sidewalks to make walking safer and more comfortable, especially in high-traffic areas. Improve pedestrian safety with better crosswalks, pedestrian signals, and traffic calming measures around schools and residential areas.
- Expand electric scooter-sharing programs as a practical and environmentally beneficial alternative to driving, especially for short distances.
- Create designated parking and charging stations for scooters and other micro-mobility devices to reduce clutter and ensure availability.
- Implementing tighter controls on dust and emissions from construction sites, including the use of dust suppression devices and the timing of building operations, can help to decrease the construction industry's contribution to air pollution.

3.5. Public Awareness and Education

- Expanding real-time air quality monitoring throughout Tirana and making this data publicly available can raise awareness and empower residents to take precautionary steps, particularly on days with low air quality.
- Launching public education campaigns about the health effects of air pollution and how to reduce personal contributions to air pollution, such as driving less and conserving energy, can encourage community engagement in air quality improvement efforts.

3.6. Adopting Renewable Energy Sources

- Encourage the use of renewable energy sources, such as solar and wind power, to minimize reliance on fossil fuels, which are a major source of air pollution. Government incentives for individuals and companies to install renewable energy systems could accelerate the changeover.
- Increasing the number of EV charging stations throughout the city, particularly in residential areas, commercial zones, and near public transport hubs. Provide financial incentives, such as subsidies or tax breaks, for purchasing electric vehicles, and offer benefits like free parking or access to restricted zones.

3.7. Encouraging Sustainable Construction Practices

- Encourage the use of eco-friendly and sustainable building materials to lessen the environmental effect of new construction projects. Green certifications and incentives for developers that use sustainable practices can further encourage this movement.
- Organize instructional workshops for architects, builders, and homeowners to increase knowledge of the advantages of sustainable building materials. Topics could include the environmental effect of traditional materials, the benefits of alternatives such as bamboo, reclaimed wood, and recycled steel, and examples of successful green building projects.

- Launch public awareness efforts that emphasize the long-term cost savings, health benefits, and environmental benefits of eco-friendly products. Use many media platforms to reach a larger audience.
- Encourage builders to pursue certifications such as LEED (Leadership in Energy and Environmental Design), which recognizes the use of sustainable materials⁵. Certified buildings typically have a better market value and can attract environmentally aware purchasers or tenants.
- Foster partnerships between government agencies, construction companies, and material suppliers to promote the availability and use of eco-friendly materials. Collaborative initiatives can include bulk purchasing agreements to reduce costs or research and development projects to innovate new sustainable materials.

3.8. Collaboration and Policy Integration

- Effective implementation of these policies requires partnership between government, the private sector, and civil society. Integrated policies that address air quality in the larger context of urban development, public health, and climate change can build more resilient and sustainable urban settings.
- Encourage coordination among government departments, such as urban planning, transportation, the environment, and health, to ensure that policies are consistent and mutually reinforcing. For example, integrating transportation and environmental regulations can result in the creation of greener public transportation networks that cut emissions and enhance air quality.
- Create rules that encourage private enterprises to invest in environmentally friendly projects including renewable energy, green building, and waste reduction. This could include tax breaks, grants, or preferential loan conditions for enterprises that satisfy specific environmental standards.
- Participate in worldwide networks and agreements that promote sustainable development, such as the UN Sustainable Development Goals (SDGs). These networks can provide useful resources, knowledge sharing, and assistance with national sustainability efforts.
- Collaborate with neighboring countries on cross-border concerns including air and water pollution to guarantee a consistent approach to environmental preservation.

4. Economic and Social Implications

- Implementing these strategies requires careful consideration of the economic and social implications. While stronger laws and infrastructure improvements may be costly, the long-term benefits of enhanced public health and environmental sustainability outweigh them. Moreover, creating green jobs and enhancing quality of life can foster social equity and community well-being.
- Upgrading public transportation, expanding green spaces, and enhancing urban planning require substantial initial investments. These costs may put a strain on the city's budget in the short term, particularly if they are paid for by public funds. These expenditures are anticipated to result in long-term cost savings by lowering healthcare costs, increasing worker productivity, and improving general quality of life.
- Cleaner air can lead to improved public health, which can translate into fewer sick days and higher productivity. Tirana may experience an increase in tourists due to improved air quality. Cleaner air contributes to a better quality of life for all residents, leading to increased life expectancy, reduced healthcare costs, and a healthier workforce. This, in turn, can strengthen social cohesion and improve overall well-being.
- Expanding public transit can increase access to important services and job opportunities, especially for low-income individuals who do not possess their own vehicles. Providing affordable and accessible public transportation is essential for promoting social fairness.
- Engaging local communities in the planning and execution of air quality improvement efforts can assist ensure that these measures meet the needs of all people, particularly those in impoverished neighborhoods who are most vulnerable to pollution.

5. Collaborative Efforts for Long-Term Success

- To achieve long-term improvements in air quality, a coordinated approach is required. To design and implement effective policies, government agencies must collaborate closely with the private sector, non-governmental organizations, and citizens. International cooperation and the implementation of best practices from other cities facing comparable difficulties can be quite beneficial.
- Effective coordination between national and local governments is critical to the successful implementation of air quality programs. National policies should be in line with local activities to ensure consistency in regulations and enforcement at all levels of government. The Ministry of Environment, in collaboration with the Municipality of Tirana, should take the lead in formulating standards, tracking progress, and guaranteeing compliance with air quality rules.

⁵ Are materials that are produced, used, and disposed of in a way that minimizes their negative impact on the environment and human health. They are typically made from renewable or recycled resources and are designed to be long-lasting and biodegradable.

- Air quality improvements should be incorporated into larger urban planning, transportation, health, and energy strategies. For example, urban development projects should contain accommodations for green spaces, whilst transportation regulations should favor low-emission automobiles and public transit development. One of the most important projects in the General Local Plan, called the Metropolitan Forest, envisages the planting of 2 million trees that will girdle urban Tirana in a ring of parks, forests and agricultural land, thus providing the city with its green lungs, expanding the possibilities for recreation and more importantly, limiting sprawl.
- The business sector, particularly sectors that contribute to pollution, must implement cleaner technology and practices. Businesses can be encouraged to lessen their environmental impact by offering incentives for innovation, such as tax rebates for those who invest in green technologies. Public-private partnerships can also encourage the development of sustainable infrastructure, such as electric vehicle charging stations and renewable energy installations.
- Local communities should actively participate in air quality initiatives. Public engagement in decision-making processes ensures that policies address residents' needs and concerns, particularly those in vulnerable or heavily polluted areas. Grassroots organizations and NGOs can support community participation through awareness campaigns, workshops, and public consultation.

6. Conclusions

Improving air quality in Tirana is a complicated task that necessitates a comprehensive and coordinated effort involving the government, the commercial sector, civil society, and international partners. The strategies discussed, which range from stronger emission restrictions and sustainable urban planning to public awareness campaigns and international collaboration, provide a road map for addressing the city's air pollution problem.

The preparation of the traffic flow monitoring strategy and their evaluation against the pollution data obtained from the direct measurements of the air indicators in Tirana enables an effective mechanism for the identification of problematic hot spots of pollution and their targeting with corrective measures.

While there are some major economic and societal consequences, such as initial infrastructure expenses and the need for behavioral change, the long-term advantages greatly outweigh the difficulties. Cleaner air will improve public health, increase quality of life, and promote long-term economic growth. Tirana can become a healthier, more livable city by collaborating and incorporating these ideas into broader urban development and environmental policy.

Tirana can benefit from international cooperation by implementing best practices from other cities that have successfully handled air pollution. This includes technical support, capacity-building programs, and the exchange of information about effective air quality management strategies. The success of these projects will be dependent on ongoing monitoring, adaptive management, and active participation from all stakeholders. Tirana can improve its air quality while simultaneously serving as a model for other towns experiencing similar issues if it fosters a culture of sustainability and collaboration.

European Ambient Air Quality Directives will push local authorities to increase sustainable mobility, reduce emissions of pollutants from traffic and heating, and a real expansion of urban green space in each city, with the planting of trees. This would reduce pollutants such as PM and nitrogen oxides (NO_x), and of course increase CO₂ sequestration. The implementation of the Ambient Air Quality Directives is thus an opportunity to improve our cities and save many lives.

7. References

- [1] Albanian Institute for Public Health, "Environmental and Air Quality Monitoring in Albania," 2023.
- [2] European Environment Agency (2022). Air Quality in Europe – 2022 Report. EEA.
- [3] European Union, "Environmental Action Programmes and Their Impact on Air Quality in Europe," 2021.
- [4] EBRD Green Cities, Tirana Municipality, Austrian Federal Ministry of Finance, European Bank, <https://www.ebrdgreencities.com> › Tirana-GCAP.
- [5] Ministry of Environment, Albania (2021). National Action Plan for Air Quality Improvement in Tirana. Ministry of Environment.
- [6] Plume Labs. "Live air quality report and air quality forecast in Tirana."
- [7] Smith, J., & Brown, R. (2020). Urban Air Quality and Public Health: A Global Perspective. Journal of Environmental Science.

[8] United Nations Environment Programme, "Air Quality Management: Global Experiences," 2023.

[9] World Health Organization (2023). Air Quality Guidelines: Global Update 2023. WHO Press.

[10] World Bank, "Sustainable Urban Development in Albania," 2022.

Design And Comparative Analysis Of A Geothermal-Driven Flash Organic Rankine Cycle For Power And Heat Generation

Fatih Yilmaz*¹

Abstract: Global warming and environmental problems appear to be the most important issues currently. The active and widespread utilization of fossil-based fuels leads to a rise in harmful emissions and causes several environmental problems. For these reasons, switching to sustainable energy sources is the most important way to achieve a clean future. This research focuses on the geothermal-driven combined plant for power and heating production in terms of thermodynamic analysis by energy and exergy efficiency methods. The system comprises a flash organic Rankine cycle and a domestic hot water generation unit. In this study, different working fluids are compared based on system energy and exergy efficiency. For R123 fluid, the system can generate 14197 kW of power and 21487 kW of heating load. Additionally, the system had 7.25% energy efficiency and 13.28% exergy efficiency, for this fluid.

Keywords: Energy, exergy, flash Organic Rankine cycle, geothermal, power

¹**Address:** Isparta University of Applied Sciences, Faculty of Technology, Isparta/Turkiye

***Corresponding author:** fatiyilmaz7@mail.com

1. INTRODUCTION

In recent years, the active and extensive use of fossil fuels has caused a number of environmental problems and created serious problems for humanity. In addition, as a result of the development and industrialization in the industry, it is predicted that energy shortages may occur due to limited fossil resources. Therefore, renewable energy, such as geothermal heat source, is attracting more and more attention due to its widespread distribution and sustainability (Sun et al. 2020). Geothermal energy source temperature varies between 50 and 350°C. It is found in many parts of the world and has a constant temperature feature. Therefore, they are not affected by environmental conditions compared to other renewable energy sources. Additionally, geothermal energy is generally used in electricity production. Temperatures of 220 °C and above can be expressed as more suitable source temperatures for electricity generation (Hettiarachchi et al. 2007).

The combination of the geothermal energy and organic Rankine cycle (ORC) is the most favorable technology. Because the ORC systems are working generally low-temperature applications. The ORC is used as an efficient technology to use this low and medium-temperature heat to generate electricity. There are several advantages to using ORC with a geothermal heat source, including higher efficiency than the steam cycle, smaller systems, and lower investment (Yamamoto et al. 2001). The geothermal energy-based ORC systems have become important in the last few years. In the literature, there are many papers available for power, heating, cooling, etc. production about on these topics.

Mosaffa et al. (2018) developed the proposal and analysis of geothermal energy-based organic flash Cycle (OFC). The system consists of a flash-binary geothermal power cycle with enhanced OFC. The results show that under the given condition, the net power output increases by 36.7% when using two-phase expanders in flash dual geothermal cycle with single flash EOFC (TBSEOFC). Wang et al. (2022) investigated a comparative thermodynamic analysis of an OFC and ORC cycle integrated with thermal energy storage. They compare five different fluids in these systems. A comparative analysis shows that the ORC-TIPTES system outperforms the OFC-TIPTES system in terms of thermodynamics and economy.

In 2024, Wang et al. (2024) developed and analyzed of a performance investigation of the dual ejector based regenerative dual pressure (Dej-RDPOFC) that generates power. Under the optimal condition, the net power generation rate is 9.71% higher than that of RDPOFC. Thermodynamic and economic performance evaluations of a double-stage organic flash cycle using hydrofluoroolefins (HFOs) are reported and handled by Ge et al. (2024). R513A shows the biggest advantages of DOFC over the single-stage type, and the maximum relative increase in net power is 111.2% and the maximum relative reduction in specific investment cost is 49.5%. To sum up, Ahmed et al. (2024) presented thermal efficiency research for the organic Rankine cycle and the three-sided flash cycle using hydrofluoroether working fluids. The main purpose of this study is to comprehensively examine the thermodynamic performance analysis of the geothermal supported OFC system and also to investigate the power and heating production. Therefore, a

comprehensive energy and exergy efficiency analysis was applied. System net electricity production with low-temperature geothermal energy is discussed. Efficiency research in low temperature applications was carried out with the OFC system.

2.SYSTEM DEFINATION AND MATHEMATICAL MODELING

This developed system is basically supported by geothermal energy. The system was designed according to the geothermal source temperature of 120 °C and is depicted in Figure 1. This system basically consists of a geothermal cycle, an OFC system, and heat exchangers. The geothermal fluid at 120 °C enters the heat exchanger 1 and transfers its heat to the OFC working fluid. OFC working fluid enters the throttle valve at point 6 and goes to the separator at point 7 after the pressure and temperature decrease at constant enthalpy. The fluid coming out of the separator as saturated steam at point 8 enters the Turbine and as a result of its expansion, electricity is produced. Subsequently, at point 10, the fluid enters a second throttle valve in the form of saturated liquid. The fluid whose heat is removed from the condenser enters the pump again at point 4 in the form of saturated liquid. The hot water unit heats with water coming from the geothermal source and the geothermal source returns to the ground again.

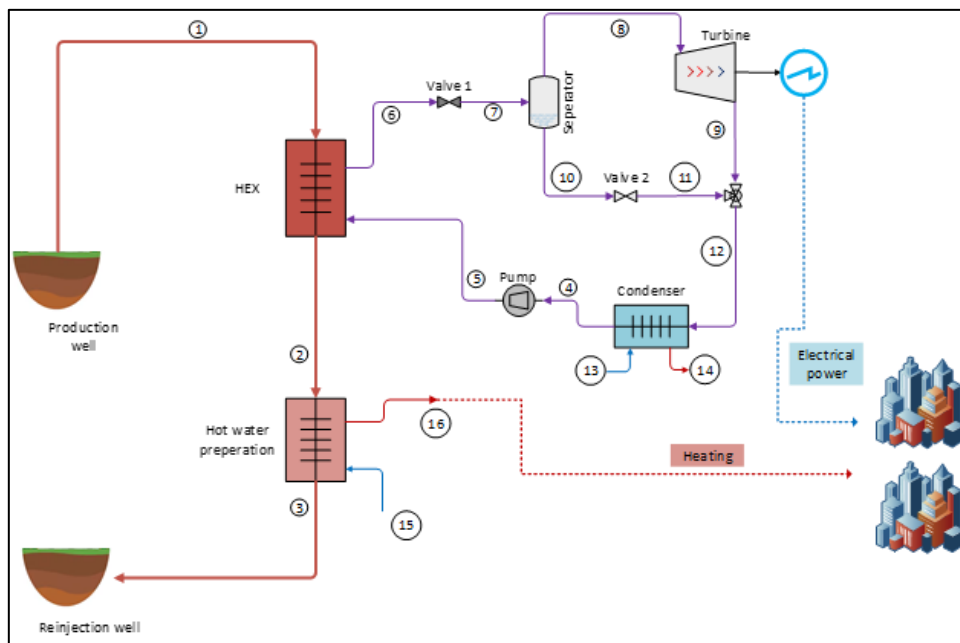


Figure 1. Schematic diagram of the geothermally driven OFC system

Mathematical Modeling

The energy and exergy analysis approach conducts the mathematical modeling of the developed system This method is derived from the thermodynamic analysis. The following assumptions are made for the ideal system to perform the thermodynamic analysis.

- The kinetic and potential energy is disregarded
- The heat loss between the system and components is overlooked
- Pump and turbines have isentropic efficiency
- The system works as steady-state flow conditions

After the abovementioned assumptions, specific indicators are given in Table 1 to conduct the thermodynamic analysis.

Table 1. Design parameters of the developed system

Parameters	Value
Geothermal outlet pressure	150 kPa
Geothermal outlet temperature	120 °C
Geothermal mass rate	200 kg/s
ORC pump inlet pressure	50 kPa
ORC pump outlet pressure	1000 kPa
Pump isentropic efficiency	85 %
Turbine isentropic efficiency	92 %
Reference temperature	25 °C
Reference pressure	101.3

To perform thermodynamic analysis, four equilibrium equations, mass, energy, entropy, and exergy, must be considered and these equations can be formulated as follows (Cengel et al. 2011; Dincer 2020)

$$\dot{m}_i = \dot{m}_e \tag{1}$$

$$\dot{Q}_i + \dot{W}_i + \sum \dot{m}_i h_i = \dot{Q}_e + \dot{W}_e + \sum \dot{m}_e h_e \tag{2}$$

$$\sum \dot{m}_i s_i \sum \left(\frac{\dot{Q}}{T}\right) + \dot{S}_{gen} = \sum \dot{m}_e s_e \tag{3}$$

$$\dot{E}x^{\dot{Q}_i} + \dot{E}x^{\dot{W}_i} + \sum \dot{m}_i ex_i = \dot{E}x^{\dot{Q}_e} + \dot{E}x^{\dot{W}_e} + \sum \dot{m}_e ex_e + \dot{E}x_{des} \tag{4}$$

Here the subscripts "i" and "e" define system inputs and outputs. Additionally, the terms "h" and "s" are specific enthalpy and entropy terms.

For energy and exergy efficiency of the overall plants;

$$\eta_{sys} = \frac{W_{net} + Q_{heating}}{\dot{m}_1 (h_1 - h_3)} \tag{5}$$

$$\psi_{sys} = \frac{W_{net} + Ex_{heating}}{\dot{m}_1 (ex_1 - ex_3)} \tag{6}$$

3. RESULTS AND DISCUSSION

The proposed newly designed geothermal-based OFC system deals with thermodynamic performance analysis via energy and exergy efficiency methods for producing the power and heating load. In this subpart, the thermodynamic analysis results and also parametric examination findings are presented. For this aim, the thermodynamic analysis outcomes of the system are illustrated in Table 2. As shown from this chart, the proposed plant can generate 14197 kW of net power and also 21487 kW of the heating load. Furthermore, the overall energy and exergy efficiency of the system is determined as 7.27% and 13.28%, respectively.

Table 2. Thermodynamic analysis results of the modeled combined system

Results	Value
Net power rate	14197 kW
Heating rate	21487 kW
Energy efficiency	7.275 %
Exergy efficiency	13.28 %
Sustainability index	1.153 -

To examine the system performance changes, parametric analysis is fulfilled by using the effect of the geothermal source temperature, pump compression ratio, turbine isentropic efficiency, etc. on the system efficiency. Figure 2 presents the effect of the geothermal water temperature on the system's beneficial products. With this figure, by increasing the geothermal source temperature from 110 to 120 °C, the net power rate also increases from 4000 kW to about 15000 kW. Also, the effect of the geothermal source temperature on the system energy and exergy efficiency is computed and presented in Figure 3. By increasing these parameter ranges, both the energy and exergy efficiency of the overall system increases. Also, the sustainability index parameters are increasing. To sum up, an increment in the geothermal water temperature has a positive impact on the system.

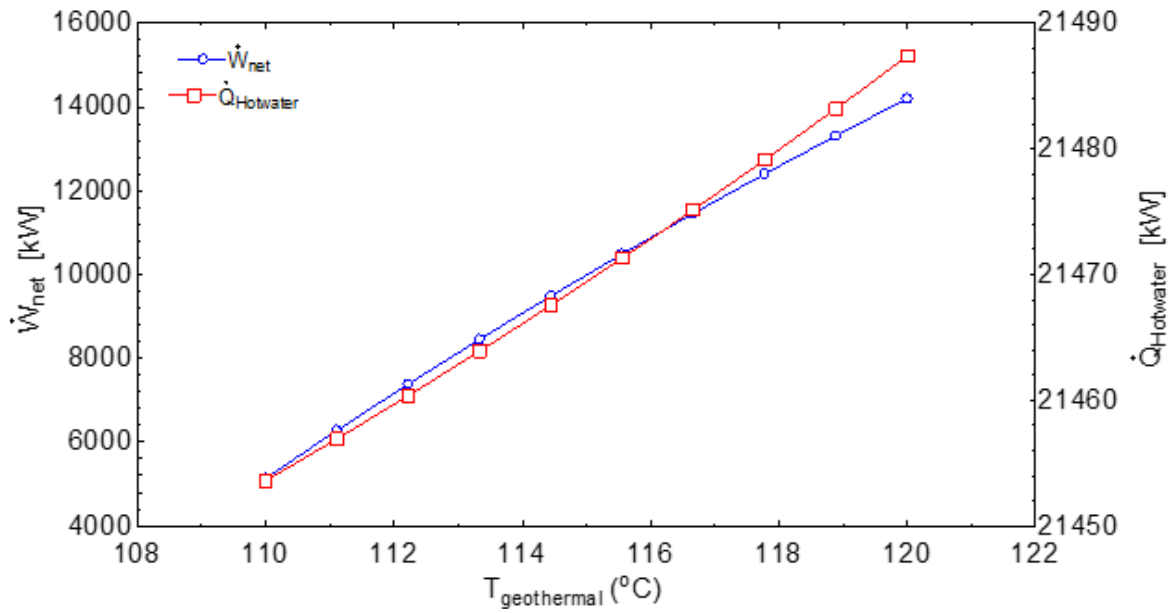


Figure 2. the effect of the geothermal temperature on the power and heating products

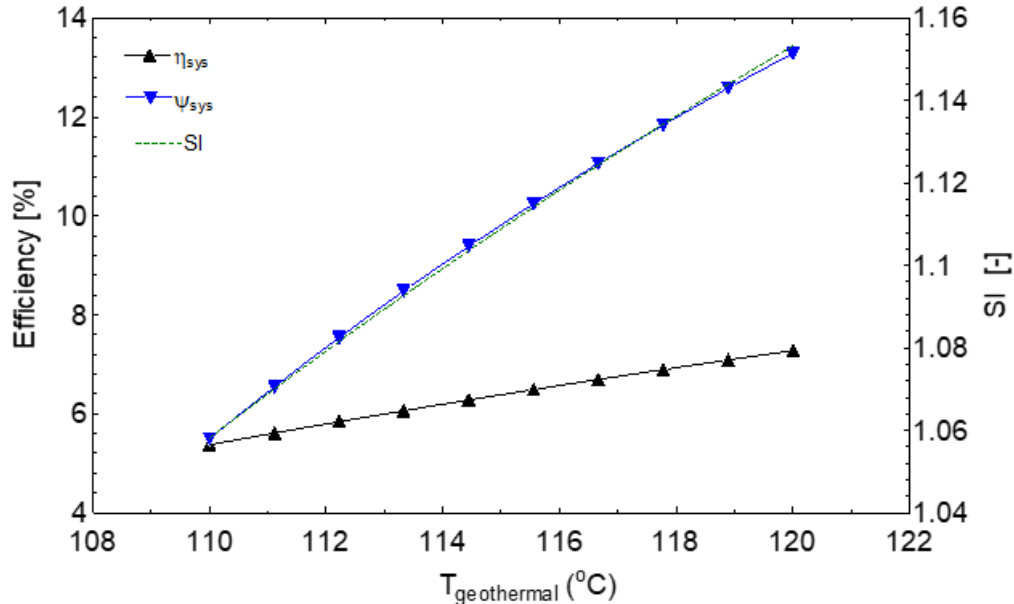


Figure 3. The effect of the geothermal temperature on the system's performance and SI indicator

The relationship between increases in the pump compression ratio on the system performance indicators is examined and presented in Figure 4. As the pump compression ratio 15 to 25 increases at the outlet pressure fixed, the system efficiency decreases. Because the system power consumption is increasing at this station. For this reason, the ideal pump compression selecting is much more important.

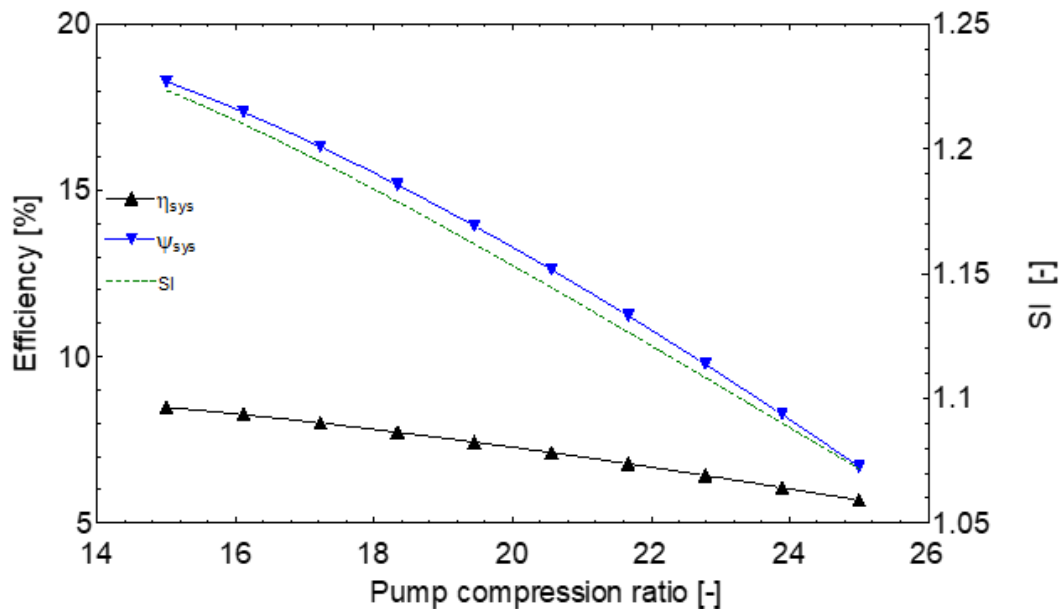
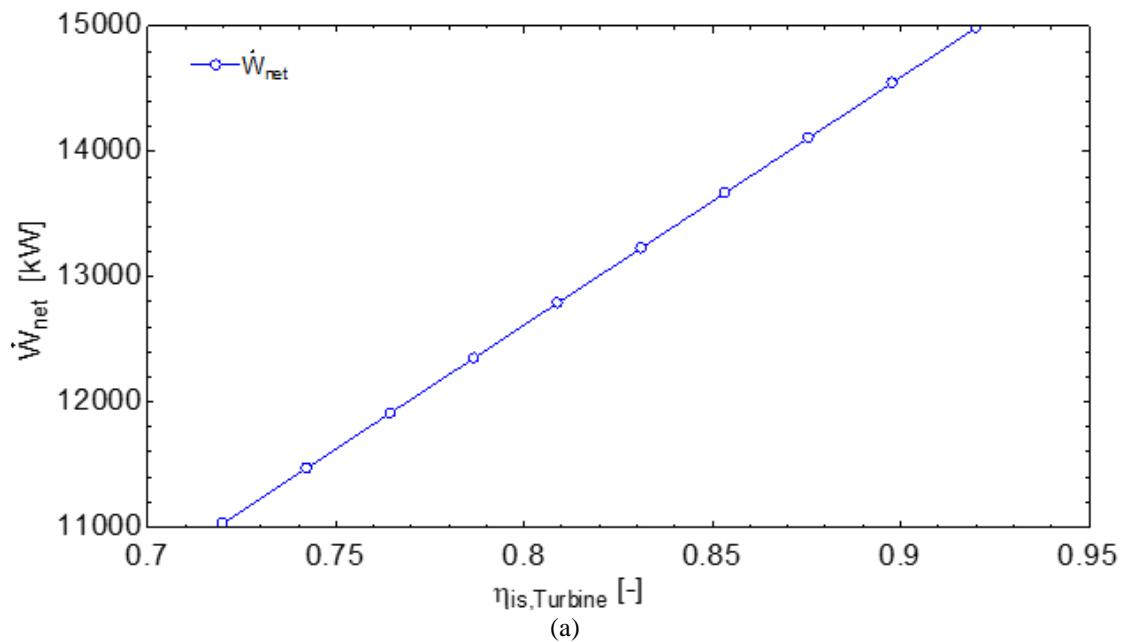


Figure 4. The relationship between pump compression ratio and system performance indicators

In thermodynamic systems, turbine isentropic efficiency is directly related to system parameters. Therefore, Figure 5 presents the change in the net electricity to be removed from the system (a) and the efficiency of the entire system (b) by increasing the turbine isentropic efficiency. Figure 5(a) shows that as the turbine isentropic efficiency increases from 0.72 to 0.92, the net electricity production increases from 11000 kW to 15000 kW. Moreover, Figure 5(b) shows the increase in both energy and exergy efficiency of the system over the same increase range.



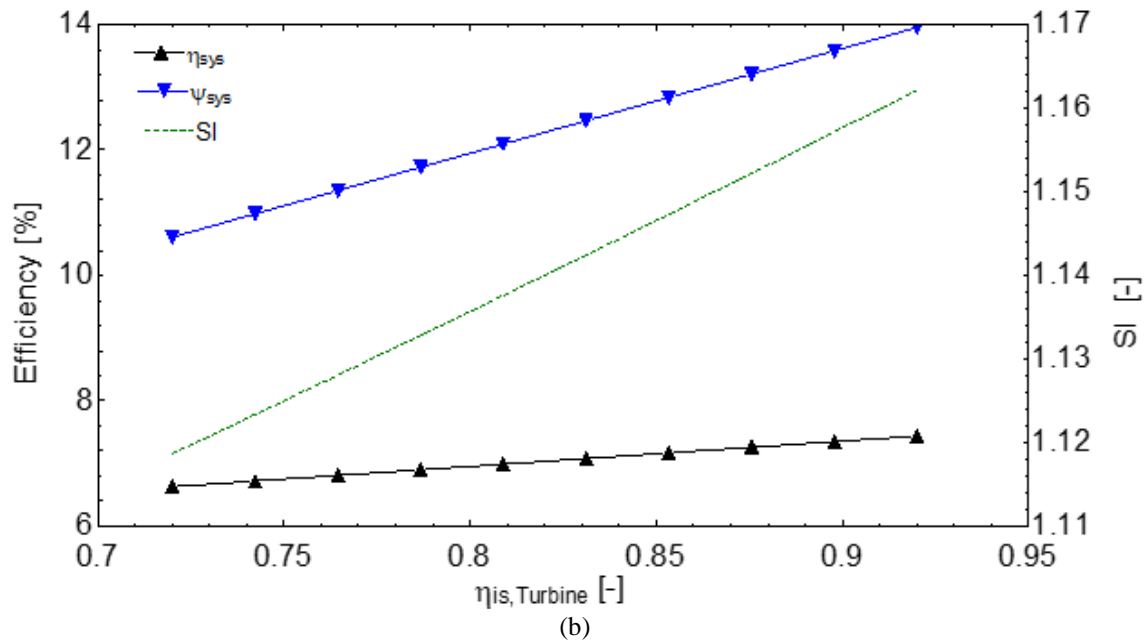


Figure 5. Variation of net electricity production (a) and system efficiency (b) according to turbine isentropic efficiency

The HEX pinch point temperature is another important indicator that directly affects of the system. Figure 6 examined that the impact of the HEX pinch point temperature on the system performance ratio. As increases the HEX pinch point temperature from 10 to 30 C, the system performance indicators have an effect negatively. The energy efficiency decreased from 10% to about 5%. Also, the other indicators have decreased.

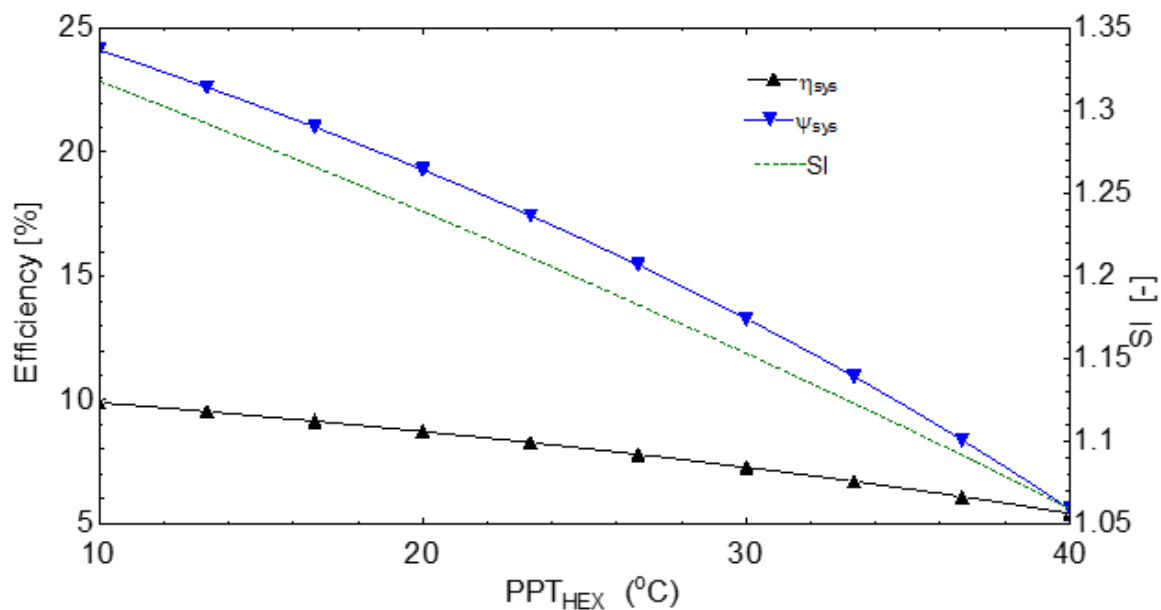


Figure 6. Impact of the HEX pinch point temperature on the system's performance indicators

4. CONCLUSION

The net zero-emission goal is much more important currently. To achieve this goal, there is a need for renewable energy sources at every point. For this aim, the currently developed new system focuses on the thermodynamic analysis of the geothermal energy-based OFC system for power and heating products. Comprehensive thermodynamic analysis along with the parametric examination are employed to determine the system performance indicators. The foremost results should be drawn as below;

- The system can generate 14197 kW of green power and also generate 21487 kW of heating load.
- The system had 7.25% and 13.18% energy and exergy efficiency.

- The geothermal water temperature increases had a positive effect on the system performance indicators.
- The increment in the HEX pinch point temperature leads to a decrease in the system energy and exergy efficiency

To sum up, the geothermal energy-based combined system has gained more importance, especially in achieving net zero emissions. Because it is a renewable energy source and abundant in the universe.

REFERENCES

- Sun, Q., Wang, Y., Cheng, Z., Wang, J., Zhao, P., & Dai, Y. (2020). Thermodynamic and economic optimization of a double-pressure organic Rankine cycle driven by low-temperature heat source. *Renewable Energy*, *147*, 2822-2832.
- Hettiarachchi, H. M., Golubovic, M., Worek, W. M., & Ikegami, Y. (2007). Optimum design criteria for an organic Rankine cycle using low-temperature geothermal heat sources. *Energy*, *32*(9), 1698-1706.
- Yamamoto, T., Furuhashi, T., Arai, N., & Mori, K. (2001). Design and testing of the organic Rankine cycle. *Energy*, *26*(3), 239-251.
- Mosaffa, A. H., & Zareei, A. (2018). Proposal and thermoeconomic analysis of geothermal flash binary power plants utilizing different types of organic flash cycle. *Geothermics*, *72*, 47-63.
- Wang, P., Li, Q., Liu, C., Wang, R., Luo, Z., Zou, P., & Wang, S. (2022). Comparative analysis of system performance of thermally integrated pumped thermal energy storage systems based on organic flash cycle and organic Rankine cycle. *Energy Conversion and Management*, *273*, 116416.
- Wang, M., Qu, L., Liu, H., Chen, P., & Wang, X. (2024). Performance improvement analysis of the regenerative dual-pressure organic flash cycle assisted by ejectors. *Energy*, *297*, 131205.
- Ge, Z., Wang, X., Li, J., Xu, J., Xie, J., Xie, Z., & Ma, R. (2024). Thermodynamic and economic performance evaluations of double-stage organic flash cycle using hydrofluoroolefins (HFOs). *Renewable Energy*, *220*, 119593.
- Ahmed, A. M. (2024). Thermal efficiency investigation for organic Rankine cycle and trilateral flash cycle using hydrofluoroether working fluids. *Results in Engineering*, *21*, 101648.
- Cengel, Y. A., Boles, M. A., & Kanoglu, M. (2011). *Thermodynamics: an engineering approach* (Vol. 5, p. 445). New York: McGraw-hill.
- Dincer, İ. (2020). *Thermodynamics: a smart approach*. John Wiley & Sons

A Comprehensive Examination Of The Solar Energy-Based A Novel Combined Plant For Producing Power, Hydrogen, And Heating

Fatih Yilmaz*¹

Abstract: One of the most prominent methods of transitioning to the net zero emission target in the world is the expansion of renewable energy sources. Solar energy, one of the leading renewable energy sources, can be found almost everywhere globally. This newly developed system investigates solar energy-based power, hydrogen, and heating production with a transcritical ammonia-based Rankine cycle. A comprehensive thermodynamic analysis is fulfilled to determine the system performance behavior by utilization of energy and exergy efficiency. The system mainly comprises a solar evacuated tube collector, integrated in a transcritical ammonia Rankine cycle and PEM electrolyzer. The analysis results compare the system performance for single generation and trigeneration. The findings show that the developed plant can cover 1.007 kW of net power and 5.135 kW of heating loads. Additionally, the system had 30.65 energy efficiency and 13.95% exergy efficiency for trigeneration purposes.

Keywords: Energy, exergy, solar, green hydrogen, transcritical cycle

¹**Address:** Isparta University of Applied Sciences, Faculty of Technology, Isparta/Turkiye

***Corresponding author:** fatiyilmaz7@mail.com

1. INTRODUCTION

As a result of population growth and technological developments, the need for energy is increasing worldwide. Fossil-based energy types, the most widespread among energy sources, play an active role in meeting these increasing energy demands. As a result of the burning of fossil fuels, environmental problems such as global warming, acid rain, ozone depletion, etc. The incident occurred. This situation is one of the most important problems today and in the future. One of the most prominent ways to solve this situation is the effective use of renewable energy sources. Renewable energy sources, solar, wind, geothermal, and biomass have shown a significant increase in interest in the world in recent years.

Solar energy is one of the widely used renewable energies that can be utilized directly or indirectly by obtaining energy from sunlight. In addition, solar energy has the highest potential among alternative energy sources and is universally available. It is an attractive concept due to its combination with solar energy and combined systems, which can improve the quality of available energy and show different application potential (Modi et al. 2017). The solar energy based combined system for producing beneficial products such as power, heating, cooling, hydrogen, etc., is a much more important technology. In the literature, there are several papers and systems available for many different beneficial products via solar energy combined systems. Smaisim et al. (2023) developed a comprehensive thermodynamic and economic analysis of the evacuated solar tube collector (ESTC) based combined system. Their analysis results show that the system had 56% energy efficiency in wintertime. Malakar et al. (2024) presented a review study on the latest trends and applications of evacuated tube solar collector in food processing and air heating. They concluded that the thermal performance and efficiency of heat pipe ESTC are higher compared to direct flow ESTC and are widely used in different food drying applications. Analysis and optimization of heat transfer properties of U-tube based solar evacuated tube collector system with different flow regulation elements were carried out by Bhowmik et al. (2023) This paper deals with the comparative analysis of U-ESTC for different flows. They applied the CFD model in order to investigate.

Temiz and Dincer (2023) developed and investigated hydrogen production and storage and solar energy-based integrated systems for sustainable buildings. As a result of this study, they examined the energy and exergy efficiency of the entire system and according to the analysis results, they showed that the system they developed had an energy efficiency of 18.76%. Chen et al. (2023) examined an optimum design and performance evaluation for solar electricity, heating, and hydrogen-integrated energy system. Based on the analysis results, the overall energy efficiency of their developed system is 21.74%.

This research aims to examine the thermodynamic performance analysis of the ESTC-based combined system for generating power, hydrogen, and heating. A comprehensive energy and exergy analysis is also conducted to investigate the performance of the developed system. Moreover, parametric analysis is conducted to determine the how effect of the system performance.

2. SYSTEM DESCRIPTION

The proposed system schematic layout is presented in Figure 1. The system mainly consists of a series of ESTCs, a Rankine cycle, and a PEM electrolyzer. The ETSC is the source of the system's required thermal energy. The Rankine cycle comprises a pump, a heat exchanger, a turbine and condenser parts. Ammonia is used in the Rankine cycle. The power generation is accomplished in the turbine part in Rankine cycle. some of the electrical power is sent into the PEM unit. PEM unit generates hydrogen and oxygen. Finally, the condenser part of the Rankine cycle is used also for hot water generation.

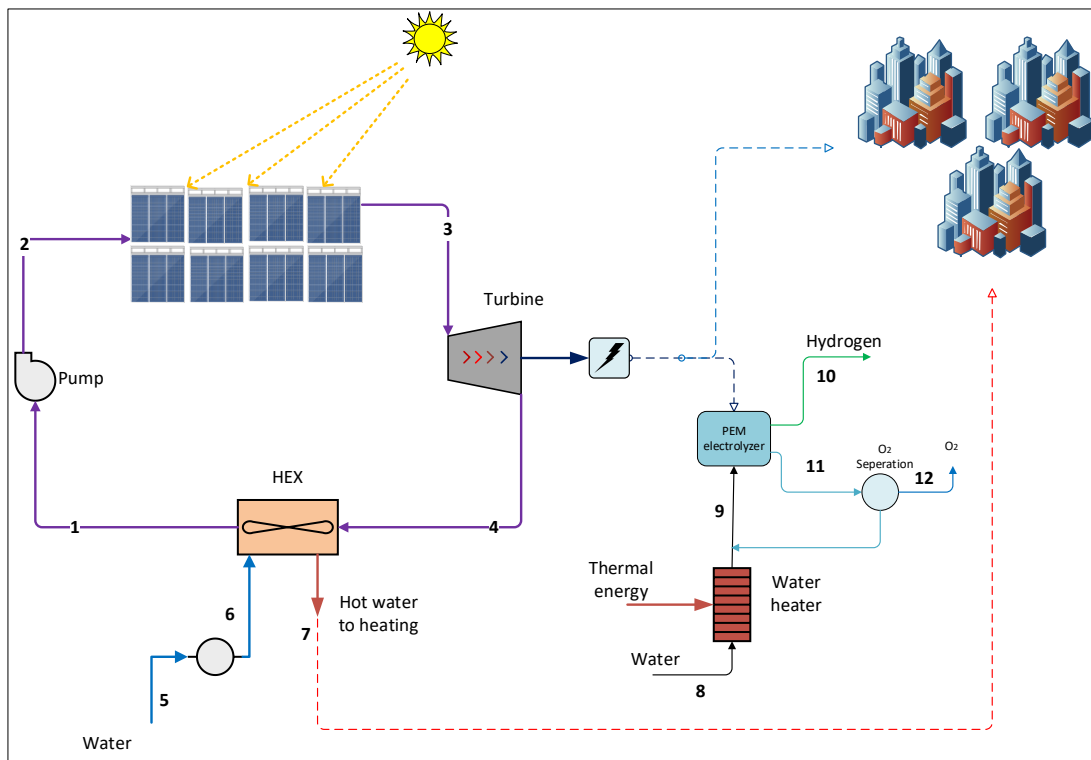


Figure 1. System schematic diagram of the solar based plant

3. ANALYSIS

This study deals with comprehensive thermodynamic performance analysis with energy and exergy efficiency methods. To conduct the thermodynamic analysis, basically, four balance equations which are mass, energy, entropy, and exergy, can be taken into account and also some assumptions must be given. These assumptions are respectively, the system works the steady-state flow condition, the kinetic and potential energy disregard, the heat loss of the system components not considered, and the pumps and turbine have isentropic efficiency. Moreover, the system design and assumption indicators are presented in Table 1.

Table 1. System design and inputs indicators

Parameters	Unit	Value
Solar radiation	Wm^{-2}	600
Number of collectors	-	15
Mass flow rate	kgs^{-1}	0.05
Rankine cycle fluid	-	ammonia
Pump inlet temperature	$^{\circ}C$	104.3
Pump inlet pressure	kPa	6800
Pump pressure ratio	-	2.5

Pump isentropic efficiency	%	88
Turbine isentropic efficiency	%	90
Reference temperature	°C	25
Reference pressure	kPa	101.325

These balance equations can generally be formulated as follows (Cengel et al. 2011; Dincer 2020)

$$\dot{m}_{in} = \dot{m}_{out} \tag{1}$$

$$\dot{Q}_{in} + \dot{W}_{in} + \sum \dot{m}_{in} h_{in} = \dot{Q}_{out} + \dot{W}_{out} + \sum \dot{m}_{out} h_{out} \tag{2}$$

$$\sum \dot{m}_{in} s_{in} \sum \left(\frac{\dot{Q}}{T}\right) + \dot{S}_{gen} = \sum \dot{m}_{out} s_{out} \tag{3}$$

$$\dot{E}x^{Q_{in}} + \dot{E}x^{W_{in}} + \sum \dot{m}_{in} ex_{in} = \dot{E}x^{Q_{out}} + \dot{E}x^{W_{out}} + \sum \dot{m}_{out} ex_{out} + \dot{E}x_{des} \tag{4}$$

For energy and exergy efficiency of the overall plants;

$$\eta_{sys} = \frac{W_{net}}{Q_{solar}} \tag{5}$$

$$\psi_{sys} = \frac{W_{net}}{Ex_{Q,solar}} \tag{6}$$

$$\eta_{sys1} = \frac{W_{net} + \dot{Q}_{heating} + (\dot{m}_{H_2} LHV_{H_2})}{Q_{solar}} \tag{7}$$

$$\psi_{sys1} = \frac{W_{net} + Ex_{Q,heating} + (\dot{m}_{H_2} ex_{H_2})}{Ex_{Q,solar}} \tag{8}$$

4. RESULTS AND DISCUSSION

Comprehensive thermodynamic and parametric analyses are fulfilled in this paper and the findings are revealed in this subpart. The performance analysis results are given in Table 2. Based on this Table's results, the developed combined cycle can generate 1.007 kW net power and 0.016 kg/h net green hydrogen. The heating load is also computed as 3.42 kW. The results indicated that the system had 11.99% and 12.61% energy and exergy efficiency indicators (for only power generation). The overall system had 30.65% of energy and 13.95% of exergy efficiency. Moreover, total irreversibility rate for this developed system is 15.33 kW.

Table 2. Thermodynamic analysis Results of the developed plant

Results parameters	Value	Unit
\dot{W}_{net}	1.007	kW
$\dot{Q}_{heating}$	3.42	kW
$\dot{m}_{hydrogen}$	0.016	kg h^{-1}
η_{sys}	11.99	%
ψ_{sys}	12.61	%
η_{sys1}	30.65	%
ψ_{sys1}	13.95	%
$\dot{E}x_{Des,total}$	15.33	kW

Figure 2 shows the irreversibility values occurring in the system elements. Total system irreversibility is calculated as 15.33 kW. The highest irreversibility among the system elements was seen in the ETSC component with 8.2 kW. The main reason for this situation is the excessive heat exchange and high temperatures occurring in the solar collector system.

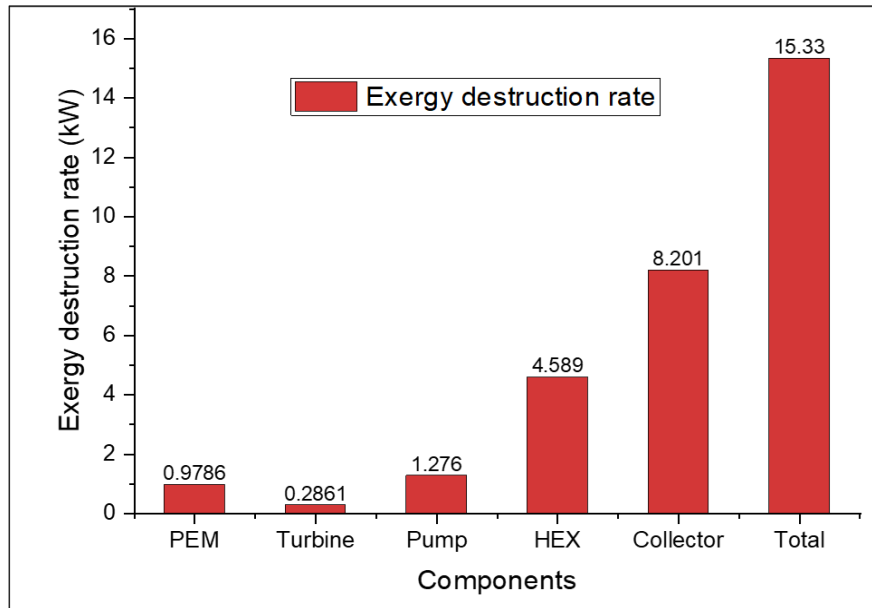
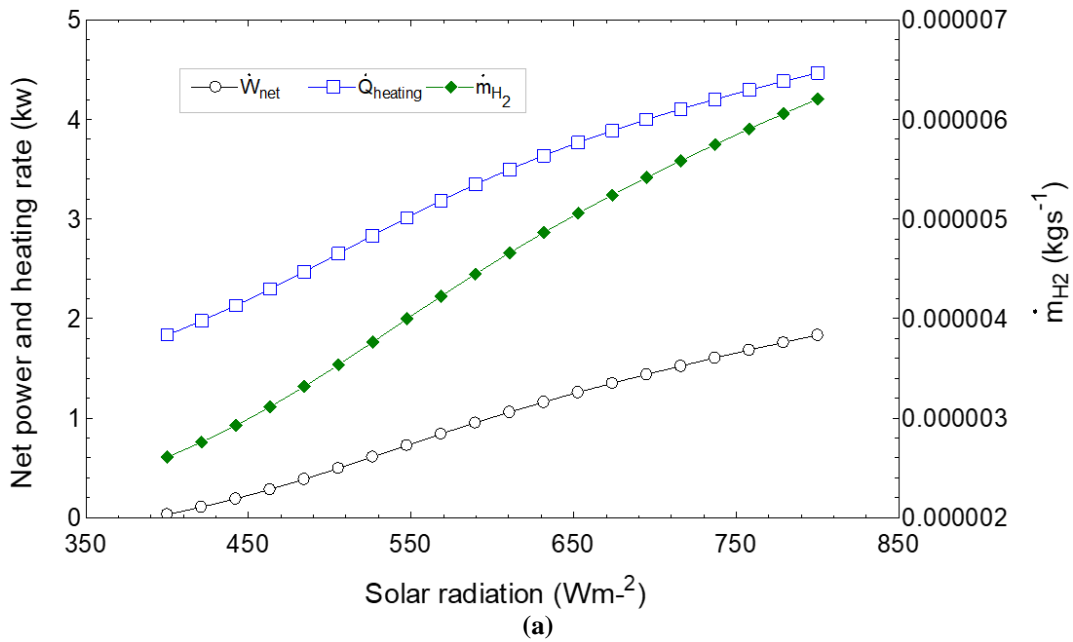


Figure 2. Exergy destruction rates of the developed system's components

Figure 3 explores the effects of changes in solar radiation on the useful outputs to be obtained from the system and the performance of the systems. Figure 3(a) shows the linear increase in net electricity, hydrogen, and heating load obtained by increasing the amount of solar radiation from 400 to 800 W/m². Likewise, Figure 3(b) shows the change in energy and exergy efficiency of system (electricity generation only) and system 1 (trigeneration). The increase in radiation value changes system efficiencies positively.



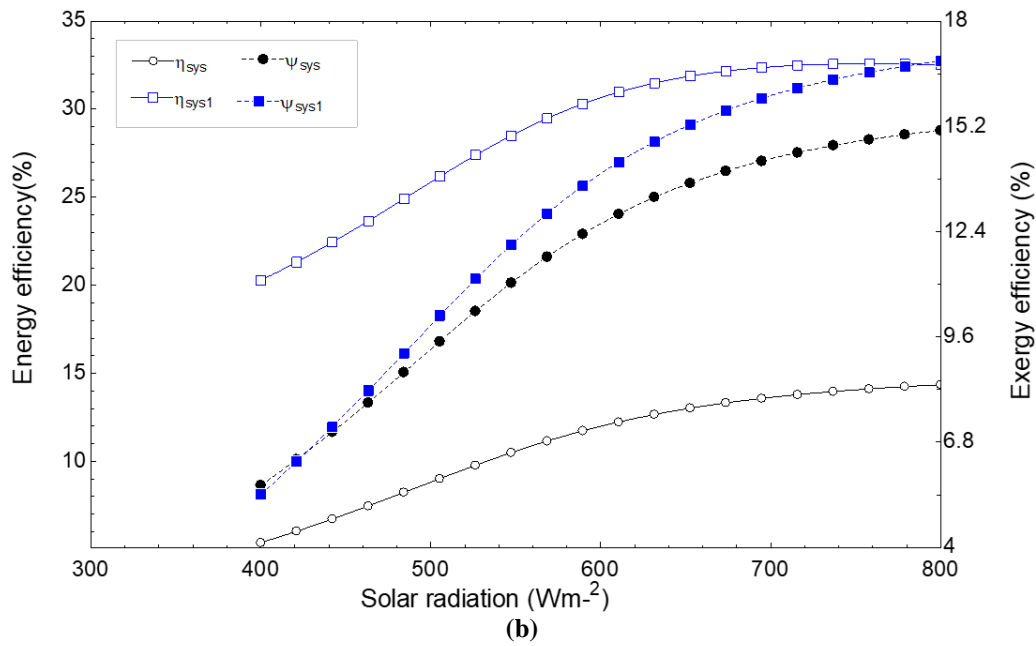


Figure 3 Effect of the solar radiation on (a) beneficial products and (b) system and system performance ratio

The change in the irreversibility rate of the overall system versus the solar radiation is examined and illustrated in Figure 4. As increased solar radiation with different reference temperatures, the total irreversibility rate increases. What is the main of this situation is that the high temperature means high irreversibility.

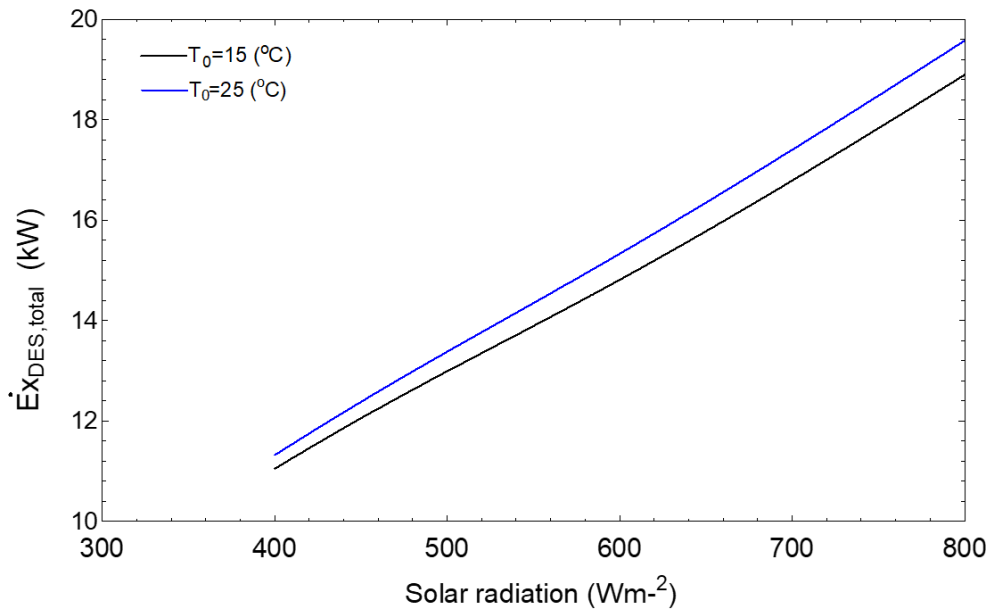


Figure 4. Effect of solar radiation on the total irreversibility rate of the overall system

The solar collector is the main energy source for this developed system. Figure 5 depicts the increase in useful outputs obtained from the system as the number of solar collectors increases from 10 to 30. As the number of collectors increases, the useful products obtained also increase as the system reaches higher temperatures.

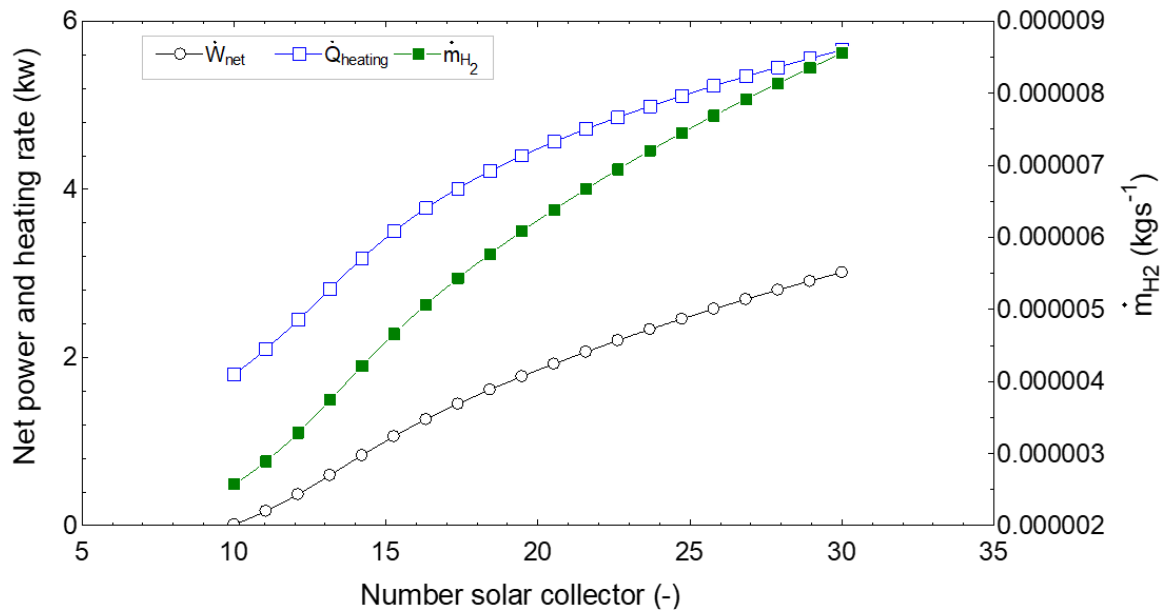


Figure 5. The change of the beneficial products vs solar collector numbers

The relationship between the change in pump compression ratio and the energy and exergy efficiency of the entire system is presented in Figure 6. As the pump compression ratio increased from 1.2 to 3.2, the outputs obtained from the system initially increased and then decreased. When the compression ratio approaches 2, system efficiency decreases after this point because the amount of energy consumed by the pump is greater than the amount of energy produced.

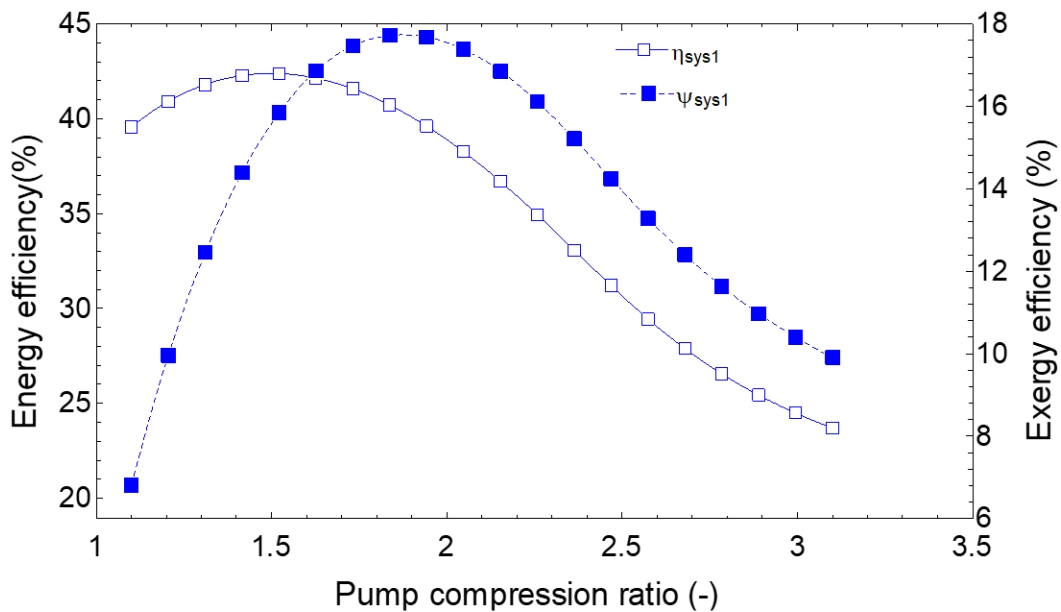


Figure 6. Impact of the Rankine cycle pump compression ratio on the energy and exergy efficiency

5. CONCLUSION

To the coming years, clean and sustainable energy sources have gained more importance especially, green hydrogen can be described as the major indicator in this sense. This study deals with the solar energy-based combined system for generating clean and sustainable products such as power, hydrogen, and heating. To determine the system performance, there are a lot of parametric analyses are made by using the energy and exergy efficiency methods. Furthermore, the total irreversibility rate is also investigated to determine which components have the maximum irreversibility ratio. The following key results should be represented as;

- This system has a net capacity to produce 1,007 kW of electricity. Additionally, the condenser heating capacity was determined as 3.42 kW.
- The system can produce 0.017 kg/h green hydrogen.
- While the energy efficiency of the system is 11.99% for electricity generation only, this value is determined as 30.65% for the combined system.
- According to the findings of the parameter analysis, efficiencies can increase with the increase in the radiation value for the system.

REFERENCES

- Bhowmik, M., Muthukumar, P., & Patil, A. (2023). Analysis of heat transfer characteristics and optimization of U-tube based solar evacuated tube collector system with different flow conditioning inserts. *Thermal Science and Engineering Progress*, 39, 101709.
- Cengel, Y. A., Boles, M. A., & Kanoğlu, M. (2011). *Thermodynamics: an engineering approach* (Vol. 5, p. 445). New York: McGraw-hill.
- Chen, Z., Yiliang, X., Hongxia, Z., Yujie, G., & Xiongwen, Z. (2023). Optimal design and performance assessment for a solar powered electricity, heating and hydrogen integrated energy system. *Energy*, 262, 125453.
- Dincer, İ. (2020). *Thermodynamics: a smart approach*. John Wiley & Sons
- Fadhil Smaisim, G., Hadrawi, S. K., Abed, A. M., Majdi, H. S., & Shamel, A. (2023). Thermo-economic analysis of the performance of the combined system with evacuated tube collectors. *Clean Energy*, 7(2), 242-252.
- Malakar, S., Arora, V. K., Nema, P. K., & Yadav, V. (2024). Recent trends and applications of evacuated tube solar collector in food processing and air heating: a review. *Environmental Science and Pollution Research*, 31(12), 18119-18142.
- Modi, A., Bühler, F., Andreasen, J. G., & Haglind, F. (2017). A review of solar energy based heat and power generation systems. *Renewable and Sustainable Energy Reviews*, 67, 1047-1064.
- Temiz, M., & Dincer, I. (2023). Design and assessment of a solar energy based integrated system with hydrogen production and storage for sustainable buildings. *International Journal of Hydrogen Energy*, 48(42), 15817-15830.

The Relationship Between Usability and Aesthetic in Interaction Design (for Islamic Arts)

Mir Alireza Daryabeygi*¹, Ayin Fazlollahi², Sara Mohamadzadeh Moghadam³

Abstract: This paper has tried to analyze the relationship between usability and aesthetics in the field of Human-Computer Interaction (HCI). This job has been performed by reviewing the recent authentic research papers. Results show that visual aesthetics and its usability play very important roles in determining the success of the product. It may seem difficult to decide which aspect needs to be given more attention when it comes to designing a product as aesthetics is focusing on the 'look' and 'feel' while usability is stressing on its functionalities. Yet, there seems no perfect answer which aspects of the design are more important than the others. In addition, it is also difficult to have a balance between these two seemingly contrary objectives of design. Too much emphasizes of designers on aesthetics can possibly lead to ignoring the usability. The method and tools of this research is document-library and descriptive analytic approach.

Keywords: Aesthetic, Interaction design, Human computer interaction (HCI), Usability, User experience

¹Address: Islamic Azad University, Faculty Of Art Central Tehran Branch , Tehran Iran

*Corresponding author: mir.daryabeygi@iauctb.ac.ir

1. INTRODUCTION

This paper investigates the relation between aesthetic and usability in human - computer interaction trying to prove how these two must be considered equally as far as possible. Since recent decades the field of Human-Computer Interaction (HCI) has been searching about this consanguinity and provides some theories. Several of these studies found support for the aesthetic-usability relationship (Hartman, 2008; Lavie and Tractinsky, 2004; Quinn and Tran, 2010). But other studies could not find this relationship (Hassenzahl, 2004; van Schaik and Ling, 2009). Previous studies indicate that aesthetic is an equally significant factor as those already studied in the field of HCI, and its impact on usability has been underestimated. The most HCI research have attempted to keep a balance between usability and aesthetic considerations (Lavie and Tractinsky, 2004).

As reported by Schenkman and Jansson (2000), the use of web is resolved by three different factors: the provided information, the usability of the website and the given impression to the user. Positive feelings caused by aesthetic can effect on a product's usability. Moreover, considerable attention in the field of HCI and specially in the context of user experience (UX) research, has been paid to the aesthetic of user interface. Numerous studies show the influence of aesthetics on for instance perception of usability (Ben-Bassat, 2006; Thuring and Mahlke, 2007; Tractinsky, 2000) and overall impression (Schenkman and Jonsson, 2000; Tractinsky, 2000; Tuch, 2010).

Aesthetic can be considered one of the most frequently researched dimensions in this field (Bargas-Avila and Hornbaek, 2011).

Kurosu and Kashimura (1995) explored the relationships between a priori perceptions of the ease of use of an automatic teller machine (ATM) which they termed apparent usability and other variables. These variables included factors believed by HCI professionals to enhance usability (termed inherent usability by Kurosu and Kashimura). Another factor included in their study was the perceived beauty of the interface. Tractinsky corroborated Kurosu and Kashimura's findings in a different culture (1997) and removed doubts about potential method bias as an alternative explanation to the high correlation between apparent usability and perceptions of interface aesthetics.

Schenkman and Jonsson (2000), suggested that positive feelings induced by aesthetics can impact how usable a product is. They cite Jordan's (1998) findings for several products, which could engender pleasurable feelings. These products were more usable than those that could not convey some visual attractiveness. Also, a high correlation exists between visual aesthetic and a system's perceived usability before, during and after the interaction (Tractinsky 1997).

It is also claimed by Norman (2004) that aesthetic design can be even more influential to affect user preference than traditional operational usability. The result obtained by Sara Tung (2012), showed that aesthetic and usability are both important components of good UX design and must play together. Karvonen (2000) mentioned in a paper that simplicity, a key component of usability, could be the connection between aesthetic and usability because simplicity is considered an aesthetic notion as well. As a result, only when all aspects, including aesthetic, usability, goals, business needs, and personals are fully understood, the best user experience can be created.

Human Computer Interaction (HCI)

Human-computer interaction (HCI) researches the design and use of computer technology, focusing particularly on the interfaces between people (users) and computers. Researchers in the field of HCI both observe the ways in which humans interact with computers and design technologies that let humans interact with computers in novel ways. As a field of research, Human-Computer Interaction is situated at the intersection of computer science, behavioural sciences, design, media studies, and several other fields of study. The term was popularized by Stuart K. Card and Allen Newell of Carnegie Mellon University and Thomas P. Moran of IBM Research in their seminal 1983 book, *The Psychology of Human-Computer Interaction*, although the authors first used the term in 1980, and the first known use was in 1975. The term connotes that, unlike other tools with only limited uses (such as a hammer, useful for driving nails, but not much else), a computer has many uses, and this takes place as an open-ended dialog between the user and the computer. The notion of dialog likens human-computer interaction to human-to-human interaction, an analogy the discussion of which is crucial to theoretical considerations in the field.

Aesthetic

Aesthetics also known in Greek as Αισθητική, or "Aisthētiké" is a branch of philosophy dealing with the nature of art, beauty, and taste, with the creation and appreciation of beauty. Noam Tractinsky used the term "aesthetics" in its ordinary and common sense as reflected in dictionary definitions such as "an artistically beautiful or pleasing appearance" (The American Heritage Dictionary of the English Language), or as "a pleasing appearance or effect: Beauty" (Merriam-Webster's Collegiate Dictionary). To scholars in the field of HCI at the early 1990's, the idea that aesthetics matter in information technology sounded heretic. Two decades later, in the early 2010s, this thought has conquered a solid place in both academia and industry.

Interaction design

Interaction design, often abbreviated IxD, is "about shaping digital things for people's use", alternately defined as "the practice of designing interactive digital products, environments, systems, and services." Like many other design fields, interaction design also has an interest in form, but its main focus is on behavior. What clearly marks interaction design as a design field as opposed to a science or engineering field is that it is synthesis and imagining things as they might be, more so than focusing on how things are. Interaction design is heavily focused on satisfying the needs and desires of many people who will use the product; other disciplines like software engineering have a heavy focus on designing for technical stakeholders of a project.

History of interaction design

The term interaction design was first coined by Bill Moggridge and Bill Verplank in the mid-1980s. It would be another 10 years before other designers rediscovered the term and started using it. To Verplank, it was an adaptation of the computer science term user interface design to the industrial design profession. To Moggridge, it was an improvement over soft face, which he had coined in 1984 to refer to the application of industrial design to products containing software.

The first academic program officially named as Interaction Design was established at Carnegie Mellon University in 1994 as Master of Design in Interaction Design. When the program started it focused mostly on-screen interfaces, but today more on the "big picture" aspects of interaction — people, organizations, culture, service, and system. In 1990, Gillian Crampton Smith founded the computer-related Design MA at the Royal College of Art (RCA) in London, which changed to Design Interactions in 2005, headed by Professor Anthony Dunne. In 2001, Crampton Smith helped found the Interaction Design Institute Ivrea, a small institute in Northern Italy dedicated solely to interaction design; the institute moved to Milan in October 2005 and merged courses with Domus Academy. In 2007, some of the people originally involved with IDII set up the Copenhagen Institute of Interaction Design (CIID). In 1998, the Swedish Foundation for Strategic Research founded The Interactive Institute - a Swedish research institute in the field of interaction design. Today, interaction design is taught in many schools worldwide.

It is also a topic frequently discussed at conferences such as Gamification 2013 held at the University of Waterloo Stratford Campus, where author Stephen P. Anderson discussed Seductive Interaction Design, a fresh approach to designing sites and interactions based on the stages of seduction.

What is interaction design about?

<< The definition of design from the Oxford English Dictionary captures the essence of design very well: "(design is) a plan or scheme conceived in the mind and intended for subsequent execution." The act of designing therefore involves the development of such a plan or scheme. For the plan or scheme to have a hope of ultimate execution, it has to be informed with knowledge about its use and the target domain, together with practical constraints such as materials, cost, and feasibility. In interaction design, we investigate the artifact's use and target domain by taking a user-centered approach to development. This means that users' concerns direct the development rather than technical concerns. Design is also about trade-offs, about balancing conflicting requirements. Generating alternatives is a key principle in most design disciplines, and one that should be encouraged in interaction design unlike many design disciplines, interaction designers are not generally trained to generate alternative designs. However, the ability to brainstorm and contribute alternative ideas can be learned, and techniques from other design disciplines can be successfully used in interaction design. For example, Danis and Boies (2000) found that using techniques from graphic design that encouraged the generation of alternative designs stimulated innovative interactive systems design. When users are involved, capturing and expressing a design in a suitable format is especially important since they are unlikely to understand jargon or specialist notations. In fact, a form that users can interact with is most effective, and building prototypes of one form or another is an extremely powerful approach. So interaction design involves developing a plan which is informed by the product's intended use, target domain, and relevant practical considerations. Alternative designs need to be generated, captured, and evaluated by users. For the evaluation to be successful, the design must be expressed in a form suitable for users to interact with. >> (Jenny Preece, Helen Sharp, Yvonne Rogers, 2002:166-167)

The five challenges of interaction design are as follows:

□ **Communication** – The fundamental goal of interaction design is two-way communication between the user and the computer. In this respect, the designers can be thought of as translators, converting the respective languages and modes so they are understandable to both parties. This can often mean more than simple translation in that even the subtleties of communication, such as colloquialisms, must be considered.

□ **Action and Reaction** – Every instance of communicating involves action and reaction. The action and reaction aspect of interaction design is thought of as the heart of the process. A good designer must anticipate the possible and probable reactions to each action for both sides.

□ **Condition** – For communication to be effective, the designer must allow for each party to understand the current condition or state of the other party. When people communicate to each other, part of the communication is assessing the condition of the other, such as emotional state, alertness and readiness to respond. In human-computer relations, the user must understand the condition or state of the device to understand if the communication is occurring. In turn, the device must be aware of the condition of the user so it can predict how to reaction to each action or instance of inaction.

□ **Flow** – The flow of the communication is mostly centered on the computer side of the interaction. The flow allows the computer to efficiently follow steps and multi-task various operations to make the user experience efficient and easy-to-follow. As a user browses, selects options or activates features, the computer must process the commands and display results while preparing to predict the next possible actions. In most cases, the flow of the computer operation is designed around the flow of human operation.

□ **Errors** – All forms of communication inherently involve the risk of miscommunication. The hallmark of effective communication is reducing the risk of miscommunication and efficiently resolving miscommunication that occurs. An interaction designer must predict all forms of miscommunication, mistakes and errors that can occur so they can be effectively handled with minimal disruption in the communication as they occur.

The Five Dimensions of Interaction Design

Gillian Crampton Smith (in the book *Designing Interaction*) stated that there were four dimensions to an interaction design language. The fifth dimension was added by Kevin Silver.

1D Words

This dimension defines the interactions. Words are the interaction that users use to interact with.

2D Visual Representations

The visual representations are the things that the user interacts with on the interface. These may include but not limited to "typography, diagrams, icons, and other graphics"

3D Physical objects or space

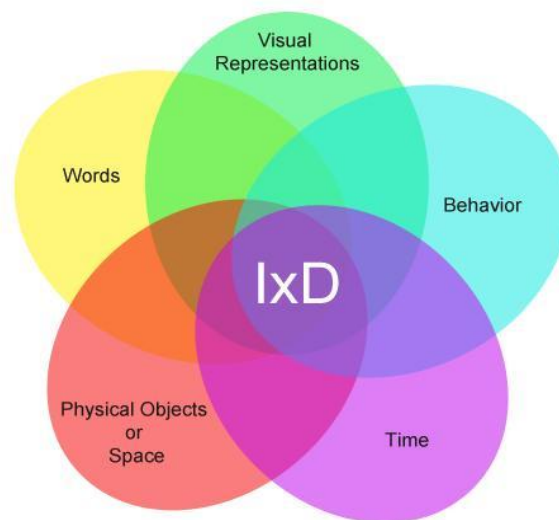
The space with which the user interacts is the third dimension of interaction design. It defines the space or objects "with which or within which users interact"

4D Time

The time the user interacts with the interface. Some examples of this are "content that changes over time such as sound, video, or animation"

5D Behavior

The behavior defines the users' actions reaction to the interface and how they respond to it.



What is usability?

"Is the study of ease of use, of how quickly someone can understand how to use a particular human made object and how easily they can use it"

The Origins of HCI and Usability

Gilbert Cockton (2014) in an article about the origins of HCI and usability stated that HCI and usability have their origins in the falling prices of computers in the 1980s, when for the first time it was feasible for many employees to have their own personal computer (a.k.a PC). For their first three decades of computing, almost all users were highly trained specialists of expensive centralized equipment. A trend towards less well-trained users began in the 1960s with the introduction of timesharing and minicomputers. With the use of PCs in the 1980s, computer users increasingly had no, or only basic, training on operating systems and applications software.

However, software design practices continued to implicitly assume knowledgeable and competent users, who would be familiar with technical vocabularies and systems architectures, and possess an aptitude for solving problems arising from computer usage. Such implicit assumptions rapidly became unacceptable.

For the typical user, interactive computing became associated with constant frustrations and consequent anxieties. Computers were obviously too hard to use for most users, and often unusable. Usability thus became a key goal for the design of any interactive software that would not be used by trained technical computer specialists. Popular terms such as “user-friendly” entered everyday use.

Both usability and user-friendliness were initially understood to be a property of interactive software. Software either was usable or not. Unusable software could be made usable through re-design.

User Experience

<< Best way to approach UX seems to be from two directions, first from the user’s judgment of their experience and, secondly, from the design perspective to enquire which features or qualities might deliver a high-quality user experience (Sutcliffe 2010). Aesthetics is connected to both sides. User’s side is about perception and interpretation of beauty and designer’s side is about creating aesthetical interfaces. Conception of UX, when explained from perspective of usage process, has three main components content, the user and context of use.

UX exists when all three parts are present. Interface aesthetics can be described in the same way. Previously mentioned user side is the blue circle which represents human being with all perceptual, cognitive, emotional and affective capabilities. Content (green) represents interactive product with graphical design, interaction logics, information architecture and defined purpose of product. Context (red) means both user profile and conditions of use. Conditions of use depend on displays, input devices, platforms and media but also on surrounding environment. >> (MatiMottus, David Lamas 2013)

-What is Our View on the Aesthetics of Interaction?

Caroline Hummels and Kees Overbeeke (2010) have advocated the following points:

1. Design is about our lives, about our being-in-the-world. Fundamental to this is the sensing of the world as an interactive activity in which experiencing the world is primary to any thinking. Therefore, it is necessary to take a scientific and a philosophical stance. As the basis for our stance, we have chosen Gibson’s (1986) theory of perception and Merleau Ponty’s (2002) view on phenomenology. Both claim that the world is inherently meaningful on a sensing or experiential level. Intuition and common sense should therefore be high on the agenda. They should be exploited to the maximum. As Voltaire said, “Le sens commun n’est pas si commun.” Common sense is not so common.
2. Reflection comes second: and it is always a reflection on action. A design theory consequently must be a theory of action and the embodied in the first place, and a theory of meaning in the second, not the other way round. Reflection on action is the source of knowledge.
3. Interaction Design nowadays is about interaction with intelligence, i.e., an interaction with the ungraspable. The ungraspable—and here we are talking mainly about the ungraspable quality of many innovations in electronics— must be made graspable again. Our bodies are mechanical: all interaction is essentially mechanical, or tangible. We have few other ways to interact with the world. Therefore, embodiment is essential.
4. Beauty, and thus beauty in interaction, is an experiential and social given. It is not just a quality of an object. It is the way an object speaks to us, calls us, affords us, puts us into contact with others, is meaningful to us, share its inner horizon with us. Thus considered, beauty emanates from our unity with the world. It is pre-reflective.

By taking this radical stance, we hope to reconcile the experiential with the rational, to reconcile feeling with thinking. This may not be the only way, but we believe it is one way to advance Interaction Design towards a truly transformative level, a level that can lead to true innovation—innovation that can contribute to making our lives worth living.

AESTHETICS AND USABILITY

<<The role of aesthetics in human affairs has been widely documented. Conventional wisdom relates it to our appreciation of, and attitudes towards computer systems as well. However, aesthetics may not always coincide with usability. In fact, the opposite might occur. In one of HCI’s most influential books, “The Psychology of Everyday Things”, Norman vividly ridicules the tendency of designers to neglect usability in favor of aesthetics. Similarly, others, while acknowledging the role of aesthetics in HCI, warn against a tendency among designers to emphasize the aesthetic elements of the user interface, because these might degrade usability.

The contribution of aesthetics to HCI, they argue, should be measured in terms of facilitating information processing, not in terms of engaging the user in a pleasing experience. Perhaps, because aesthetics mainly reflects on the latter, HCI literature in general, and on usability in particular, mostly seem to neglect the aesthetics issue completely.

For example, the indices of 4 prominent HCI textbooks and reading collections do not contain a single entry for "aesthetics" (or synonyms and related concepts such as appearance, attractiveness, beauty or form). Thus, it would appear that mainstream HCI (but, of course, see Laurel for a notable exception) either belittles the importance of aesthetics or ignores it altogether. >> (Noam Tractinsky, 1997)

CONCLUSION

Summing up the results, this study demonstrated once again the tight relationships between users' initial perceptions of interface aesthetics and their perceptions of the system's usability. Relations endure even after actual use of the system. It is believed that these results shed new light on the role of aesthetics in HCI design and its effects on how users experience their interaction with computerized systems. Aesthetic can't be completely ignored as usability experts argue and can't expect great aesthetic to carry a poor user experience. In a sense the concepts of aesthetics and usability represent two different and related dimensions of HCI. Aesthetics usually refers often too subjective, and affect based experience of system use, whereas usability is commonly measured by relatively objective means and sets efficiency as its foremost criterion. Obviously, more research is needed to assess the possibilities and boundaries of the aesthetics-usability relationships.

REFERENCES

- [1] Jenny Preece, Helen Sharp, Yvonne Rogers (2002), INTERACTION DESIGN: beyond human-computer interaction, Publisher: John Wiley & Sons.
- [2] Tractinsky, Noam (2013), Visual Aesthetics. In: Soegaard, Mads and Dam, Rikke Friis. "The Encyclopedia of Human-Computer Interaction, 2nd Ed" Aarhus, Denmark: The Interaction Design Foundation.
- [3] Carroll, John M. (2014), Human Computer Interaction - brief intro. In: Soegaard, Mads and Dam, Rikke Friis. "The Encyclopedia of Human-Computer Interaction, 2nd Ed" Aarhus, Denmark: The Interaction Design Foundation.
- [4] Cockton, Gilbert (2014), Usability Evaluation. In: Soegaard, Mads and Dam, Rikke Friis. "The Encyclopedia of Human-Computer Interaction, 2nd Ed" Aarhus, Denmark: The Interaction Design Foundation.
- [5] Mati Mõttus, David Lamas (2013), Visual Aesthetics of Interaction Design, Institute of Informatics, Tallinn University, Estonia.
- [6] Caroline Hummels and Kees Overbeeke (2010), Special Issue Editorial: Aesthetics of Interaction, Eindhoven University of Technology, Eindhoven, the Netherlands.
- [7] Tractinsky, Noam (1997), Aesthetics and Apparent Usability: Empirically Assessing Cultural and Methodological Issues, Israel.
- [8] Tung, Sara (2012), Balancing aesthetic and usability.
- [9] Coursaris, Constantinos (2007), Exploring the Relationship between Aesthetics and Usability, Louisville.
- [10] Antonella De Angeli, Alistair Sutcliffe & Jan Hartmann (2006), Centre for HCI design, School of Informatics, University of Manche.
- [11] Kurosu, M., Kashimura, K. (1995): Apparent usability vs. inherent usability.
- [12] Kevin Silver (2007): What Puts the Design in Interaction Design

Sites

<http://www.interaction-design.org>

<http://www.interactiondesign.com.au>

<http://www.interaction-design.org>

<http://www.wikipedia.org>

Carnival: Holding the first workshop on the creation of an “Ecosystem of Innovation and Soft Artistic Technology” at the Islamic Azad University, Central Tehran branch

Mir Alireza Daryabeygi

Abstract: According to the public relations report of the Central Tehran Branch, the first workshop on the creation of an ecosystem of innovation and soft art technology was held by the faculty of art and was Designed, organized and supervised by Dr. Mir Alireza Daryabeygi, a Faculty member of educational and post-graduate education department of Drama/ Theatre/ Performing Arts; Faculty of Art, Islamic Azad University Central Tehran Branch (IAUCTB) This report indicates that the Carnival; Conversations with [...] book was unveiled by 14 university drama/performing groups in Tehran's Azadi Tower; as a Laboratory/ Workshop/ Atelier/ Studio/ Research/ Rehearsal(Practice)/ Game(play)/ Performance/ Experience/ Repeat. In this period of holding workshops, among the 40 works received, 10 titles of performance text in a book titled Carnival; Conversations with [...] have been published.

Keywords: Aesthetic, Interaction design, Human computer interaction (HCI), Usability, User experience

¹Address: Islamic Azad University, Faculty Of Art Central Tehran Branch , Tehran Iran

***Corresponding author:** mir.daryabeygi@iauctb.ac.ir

1. INTRODUCTION

writer/researcher in the field of experiment/experience/research project and triad foundation theory [necessity of theater]; Repertoire "musical text/post-dramatic/secondary drama"; October and November 2022, the Baroque Cafe Gallery and with the help of the Baroque Art House Cultural Institute has implemented as follows:

- Performance of the first of the trilogy: "Tahran e Ashegh/Romeo kind"
- The second performance of the trilogy: "crazy, I'm your Rastakt/Hamlet hood"
- Performance of the third of the trilogy: "Tehran 50 show/Being Faust"

for the purpose of writing and documenting the Tiwal ticket sales system; The audio file explaining the performance methods of the dramaturg/director is recorded/recorded as an "exercise/game/experience/repetition" in 13 minutes of speech; This audio file is for the esteemed master's degree students in the fields of "Directing" and "Performance Literature"; Entry in October 2022; The Department of Drama Education and Complementary Studies of the Islamic Azad University Faculty of Arts, Central Tehran Branch is entrusted to write the text of the performance in process of Spoken/Audio Dramaturgy

In this group learning process; [professor/Students; student/professors;] students based their research activities on four stages/survey/steps:

1. The act of listening to the "audio/listening file" [shared in the virtual class group];
2. Transcription of speech text ["audio/audio file"];
3. Choosing the method of presentation of the text/construction (monologue/dialogue/interview/observation [based on imagination], drama/types of drama/non-drama, performance text);
4. construction /deconstruction /make/write/wrote/wrote.

All respected students are obliged to embody the personality of "[...]" / "Speaker" [who is a voice for himself] --in a semi-attendance/non-attendance experience of university education and learning in the days of the spread of the epidemic disease (Covid 19) --; and make all his speech without any change in the language of the dramaturgical "character" of his own creation. to each;

Ritual/formal/methods/approach/way/methodology.

Among the 40 titles received, 10 titles are performed in a book titled Carnival; Conversations with [...] have been published. (ISBN: 978-622-6713-80-1)

The keywords for reflection, reading and research in this triad of "research/implementation" can be: 1- Simultaneity; 2- Parataxis; 3- Playing with the density of signs; 4- Embodiment/physicality; 5- Musicality of the situation of the event; 6- visual dramaturgy; 7- deconstructive dramaturgy; 8- The attack of reality; 9- event situation (temporal/spatial); 10- secondary drama; 11- Music text (notation/literature); 12- Post-Brechtian Theatre; 13- Post-dramatic theatre; 14- Post-cinematic theatre; 15- audience dramaturgy;

List of book titles:

- post/pre-registration; Researcher's post/preprint
- "Carnival"; Melika Arezi
- "practice/game/experience"; Mariam Panahi
- "duality"; khorshid Fayaz
- "Meeting with Darya"; Ali Taleghani
- "Factory Laboratory of Theatre Production"; Sahel Meskini
- "Prisoner's Riddle"; Arefe Askari Sarai
- "Audience dramaturgy"; Morteza Aminipour...
- "Post Derbyego"; Amin Javadi
- "interview"; Mohammad Reza Rashidi
- "All for one for all"; Seyyed Mohammad Reza Hosseini

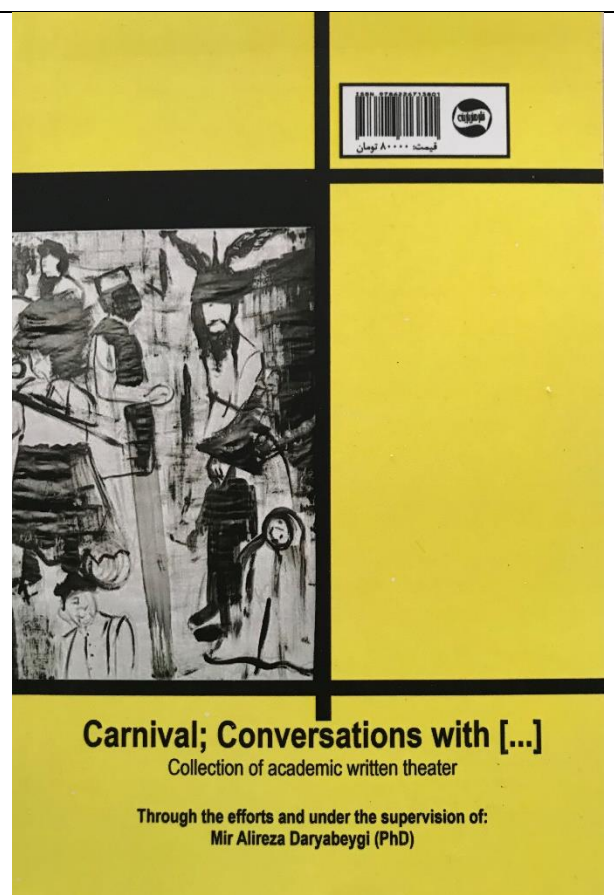
This book was performed by 14 university performer groups on Thursday, **January 12, 2023**, from 11:00 to 22:00 at Azadi Tower. this event; It will be a step towards explaining how to build/destroy, construction /deconstruction the book/performance. In continuation of the research path and in order to achieve the "ecosystem of innovation and soft artistic technology", these events will continue with the implementation of newly translated books in the field of performing arts.



کارناوال؛ گفتگوهای با [...]

مجموعه تئاتر نوشت‌های دانشگاهی [تمرین/بازی/تجربه/تکرار]

به اهتمام؛ تألیف و زیرنظر:
دکتر میرعلیرضا دریابگی



Carnival; Conversations with [...]

Collection of academic written theater

Through the efforts and under the supervision of:
Mir Alireza Daryabeygi (PhD)

Intuitionistic Fuzzy Cognitive Map Approach for Determining the Effectiveness of Digital Marketing Tools Evaluation Factors

Nazli Goker*¹, Mehtap Dursun¹

Abstract: In today's rapidly evolving business environment, the shift from traditional marketing strategies to digital marketing has become crucial. Digital marketing tools play a significant role in this new landscape. These tools enable businesses to target their audiences more precisely across expanding digital platforms. However, with the plethora of tools available, determining the relative effectiveness of each tool poses a major challenge for decision-makers. This study objects to find the effectiveness of digital marketing tools evaluation factors using intuitionistic fuzzy cognitive map (IFCM) technique.

Keywords: Decision making, Digital marketing, IFCM

¹**Address:** Galatasaray University, Industrial Engineering Department, Istanbul/Turkiye

***Corresponding author:** nagoker@gsu.edu.tr

1. INTRODUCTION

Digital marketing refers to the use of digital channels and technologies to promote products, services, and brands. It encompasses a wide range of strategies and tactics designed to reach and engage customers online. Digital marketing is often more affordable than traditional marketing methods, making it accessible for businesses of all sizes. It allows for precise tracking and measurement of campaign performance, enabling data-driven decisions. Marketers can target specific demographics, interests, and behaviors to reach their ideal audience. Digital marketing fosters two-way communication between brands and consumers, enhancing engagement and building relationships. It enables businesses to reach a global audience, expanding their market beyond local boundaries (Desai, 2019).

Digital marketing tools play a significant role in this new landscape. These tools enable businesses to target their audiences more precisely across expanding digital platforms (Ozguven Tayfun and Oclu, 2018). However, with the plethora of tools available, determining the relative effectiveness of each tool poses a major challenge for decision-makers.

The aim of this study is to determine the effectiveness of digital marketing evaluation factors. For this purpose, intuitionistic fuzzy cognitive map (IFCM) is employed, and the results are analyzed. The rest of the study is organized as follows. Section 2 explains briefly intuitionistic fuzzy cognitive map methodology. The following section illustrates the application via a case study conducted in a marketing department of a global firm. Final section delineates conclusions and future research directions.

2. INTUITIONISTIC FUZZY COGNITIVE MAP TECHNIQUE

Intuitionistic fuzzy cognitive map (IFCM) technique includes intuitionistic fuzzy numbers into cognitive maps in order to determine the power of cause-and-effect relationships (Dogu and Albayrak, 2018). First, concept nodes and power of causal links among them are defined by obtaining experts' opinions. Second, the power of causal links is represented by intuitionistic fuzzy numbers that are associated with intuitionistic fuzzy scale. Hence, membership, non-membership, and hesitation values are identified. Finally, N x N weight matrix is formed by employing the information collected from the experts.

The following iterative formulation of IFCM is run until the system will be stabilized, in other words, all factor weights will converge [4]. In this way, the concepts' values are computed.

$$A_i^{(k+1)} = f \left(A_i^{(k)} + \sum_{j=1}^N A_j^{(k)} w_{ji}^{\mu} - A_j^{(k)} w_{ji}^{\pi} \right) \quad (1)$$

where $A_i^{(k)}$ is the value of concept C_i at k th iteration, w_{ji} is the weight of the connection from C_j to C_i , w_{ji}^μ and w_{ji}^π denote the weight matrices that show membership values and hesitation values of causal links, respectively, and f is a threshold function, which is considered as sigmoid function for this work.

3. CASE STUDY

The purpose of this analysis is to measure the importance of digital marketing tools evaluation factors. For the analysis, 9 criteria, given in Table 1, are determined based on previous literature reviews and expert recommendations.

Table 1. Evaluation factors

LABEL	CRITERIA
C_1	CLICKS
C_2	IMPRESSIONS
C_3	FREQUENCY
C_4	CLICK-THROUGH RATE (CTR)
C_5	CONVERSION RATE
C_6	PURCHASE FREQUENCY
C_7	COST PER CLICK (CPC)
C_8	RETURN ON ADVERTISING SPEND (ROAS)
C_9	AVERAGE ORDER VALUE (AOV)

Three decision makers who all work in marketing department of a global firm formed a consensus and determined the power of relationships among the criteria with regard to the intuitionistic scale taken from the literature as in Table 2.

Table 2. Linguistic scale

Linguistic term	Intuitionistic fuzzy number
VH	$\langle 0.95, 0.05 \rangle$
H	$\langle 0.70, 0.25 \rangle$
M	$\langle 0.50, 0.40 \rangle$
L	$\langle 0.25, 0.70 \rangle$
VL	$\langle 0.05, 0.95 \rangle$

The matrices that outline linguistic data, membership, non-membership, hesitation values, and weight matrix are given in Tables 3,4,5,6,7, respectively.

Table 3. Linguistic data

	C_1	C_2	C_3	C_4	C_5	C_6	C_7	C_8	C_9
C_1	-	VH	VH	H	H	M	M	L	L
C_2	-	-	-	H	VH	H	H	M	M
C_3	-	VH	-	M	H	M	-	-	-
C_4	-	-	-	-	VH	H	VH	-	-
C_5	-	-	-	-	-	VH	-	-	M
C_6	-	-	-	-	-	-	-	H	H
C_7	-	-	-	-	-	-	-	VH	H
C_8	-	-	-	-	-	-	-	-	-
C_9	-	-	-	-	-	-	VL	VL	-

Table 4. Membership values

	C ₁	C ₂	C ₃	C ₄	C ₅	C ₆	C ₇	C ₈	C ₉
C ₁	0	0.95	0.95	0.7	0.7	0.5	0.5	0.25	0.25
C ₂	0	0	0	0.7	0.95	0.7	0.7	0.5	0.5
C ₃	0	0.95	0	0.5	0.7	0.5	0	0	0
C ₄	0	0	0	0	0.95	0.7	0.95	0	0
C ₅	0	0	0	0	0	0.95	0	0	0.5
C ₆	0	0	0	0	0	0	0	0.7	0.7
C ₇	0	0	0	0	0	0	0	0.95	0.7
C ₈	0	0	0	0	0	0	0	0	0
C ₉	0	0	0	0	0	0	0.05	0.05	0

Table 5. Non-Membership values

	C ₁	C ₂	C ₃	C ₄	C ₅	C ₆	C ₇	C ₈	C ₉
C ₁	0	0.05	0.05	0.25	0.25	0.4	0.4	0.7	0.7
C ₂	0	0	0	0.25	0.05	0.25	0.25	0.4	0.4
C ₃	0	0.05	0	0.4	0.25	0.4	0	0	0
C ₄	0	0	0	0	0.05	0.25	0.05	0	0
C ₅	0	0	0	0	0	0.05	0	0	0.4
C ₆	0	0	0	0	0	0	0	0.25	0.25
C ₇	0	0	0	0	0	0	0	0.05	0.25
C ₈	0	0	0	0	0	0	0	0	0
C ₉	0	0	0	0	0	0	0.95	0.95	0

Table 6. Hesitation values

	C ₁	C ₂	C ₃	C ₄	C ₅	C ₆	C ₇	C ₈	C ₉
C ₁	0	0	0	0.05	0.05	0.1	0.1	0.05	0.05
C ₂	0	0	0	0.05	0	0.05	0.05	0.1	0.1
C ₃	0	0	0	0.1	0.05	0.1	0	0	0
C ₄	0	0	0	0	0	0.05	0	0	0
C ₅	0	0	0	0	0	0	0	0	0.1
C ₆	0	0	0	0	0	0	0	0.05	0.05
C ₇	0	0	0	0	0	0	0	0	0.05
C ₈	0	0	0	0	0	0	0	0	0
C ₉	0	0	0	0	0	0	0	0	0

Table 7. Weight matrix

	C ₁	C ₂	C ₃	C ₄	C ₅	C ₆	C ₇	C ₈	C ₉	INDEGREE VALUE
C ₁	0	0.95	0.95	0.65	0.65	0.4	0.4	0.2	0.2	4
C ₂	0	0	0	0.65	0.95	0.65	0.65	0.4	0.4	4
C ₃	0	0.95	0	0.4	0.65	0.4	0	0	0	2
C ₄	0	0	0	0	0.95	0.65	0.95	0	0	3
C ₅	0	0	0	0	0	0.95	0	0	0.4	1
C ₆	0	0	0	0	0	0	0	0.65	0.65	1
C ₇	0	0	0	0	0	0	0	0.95	0.65	2
C ₈	0	0	0	0	0	0	0	0	0	0
C ₉	0	0	0	0	0	0	0.05	0.05	0	0
OUTDEGREE VALUE	0	1.9	0.95	1.7	3.2	3.05	2.05	2.25	2.3	

4. CONCLUSIONS

In this study, the effectiveness of digital marketing evaluation factors is determined through IFCM methodology. The uncertainty and hesitation in data led us to use IFCM technique. According to the indegree values, clicks and impressions are the most effective factors in digital marketing processes. Besides, conversion rate and purchase frequency are the factors that are most affected by the system. In future, intuitionistic group decision making approaches will be proposed for several frameworks in digital marketing area.

Ethics Committee Approval

N/A

Peer-review

Externally peer-reviewed.

Author Contributions

Conceptualization: N.G., M.D.; Investigation: N.G., M.D.; Material and Methodology: N.G., M.D.; Supervision: N.G.; Visualization: N.G., M.D.; Writing-Original Draft: M.D.; Writing-review & Editing: M.D.; Other: All authors have read and agreed to the published version of manuscript.

Conflict of Interest

The authors have no conflicts of interest to declare.

Funding

This work has been financially supported by Galatasaray University Research Fund FBA-2024-1243.

REFERENCES / KAYNAKLAR

Deasi, V. (2019). Digital marketing: A review. *International Journal of Trend in Scientific Research and Development (IJTSRD)*. 196-200.

Ozguven Tayfun, N., Oclu, B. (2018). A review of digital marketing tools. *The Most Recent Studies in Science and Art. Gece Kitaplığı*, Vol. 2.

Dogu, E., Albayrak, Y. E. (2018). Criteria evaluation for pricing decisions in strategic marketing management using an intuitionistic cognitive map approach. *Soft Computing*, 22, 4989-5005.

A Decision Making Framework for Assessing Photovoltaic Potential In Turkey: Determining Suitable Cities For Optimal Solar Energy Production

Mustafa Berk Basakin^{1,3}, Nazli Goker*², Mehtap Dursun³

Abstract: The transition to renewable energy is a crucial step for sustainable development on a global scale. Among the various sources of renewable energy, solar energy stands out for its considerable potential and its relative ease of collection. With high sunshine and diverse geographic landscapes, Turkey offers an excellent opportunity for extensive solar energy development. This work aims to develop a methodology using spatial analysis techniques and multi-criteria decision methods named as TOPSIS to map Turkey's solar potential situation. The criteria analyzed include population, electricity consumption, industrialization, solar radiation, sunshine duration, air temperature and humidity, and are used to segment regions to reduce possible transport costs in energy distribution.

Keywords: Solar energy, multi-criteria decision making, TOPSIS

^{1,2,3}**Address:** Galatasaray University, Industrial Engineering Department, Istanbul/Turkey

***Corresponding author:** nagoker@gsu.edu.tr

1. INTRODUCTION

The fact that Turkey has significant solar potential is a crucial point for the implementation of nationwide solar energy systems, which is an essential step to ensure energy sustainability, reduce external energy dependence and decrease energy costs. carbon emissions. This study examines different factors such as sunshine duration, solar radiation, meteorological factors, topography, population density, secondarily, energy consumption and proximity to existing infrastructure, in order to determine the most suitable for installing solar systems in different regions of Turkey (Cetin, 2011). Throughout the literature, scholars contributed to the production of optimum solar energy Dhar et al. (2020) highlights both the environmental benefits and potential trade-offs of solar energy development.

Although a significant improvement over fossil fuels, solar installations can still impact soil health, water resources, wildlife and land use. These potential impacts highlight the importance of informed site selection and proactive mitigation within the solar sector. Solar irradiance is a fundamental factor in determining the energy output of photovoltaic systems. The relationship between solar irradiance and PV production is well documented in the literature, with studies by Salim et al. (2013), Rahman et al. (2015), and Rahman et al. (2017) providing key insights.

The Global Solar Atlas (2020), developed by the World Bank Group, presents itself as a fundamental resource for accessing high-quality data on solar resources and photovoltaic energy production potential worldwide. Using satellite information, this platform offers detailed maps illustrating the variability of sunshine duration and intensity in different regions, providing a global perspective on solar energy availability.

The objective of this study is to rank Turkish cities according to their solar energy development. For that reason, Technique of Preference by Similarity to the Ideal Solution (TOPSIS) methodology is applied. The rest of the study is organized as follows. Section 2 explains the application steps of TOPSIS methodology. Section 3 outlines case study. The final section delineates concluding remarks.

2. MATERIAL AND METHOD

In this study, the Technique of Preference by Similarity to the Ideal Solution (TOPSIS) method was used to evaluate the suitability of different cities for solar energy production. TOPSIS is a multi-criteria decision making (MCDM) technique that helps select the best alternative from a set of options based on multiple criteria. Originally introduced by Hwang and Yoon (1981), TOPSIS has found widespread application in various fields, including engineering, business, and environmental studies.

The normalized score (R_{ij}) for each criterion (X_{ij}) for alternative i and criterion j is calculated using the following formula:

$$R_{ij} = \frac{X_{ij} - \min(X_j)}{\max(X_j) - \min(X_j)} \text{ for benefit criteria,} \tag{1}$$

$$R_{ij} = \frac{\max(X_j) - X_{ij}}{\max(X_j) - \min(X_j)} \text{ for cost criteria,} \tag{2}$$

The weighted normalized score (W_{ij}) for each criterion (R_{ij}) is calculated by multiplying the normalized score by its corresponding weight (w_j)

$$W_{ij} = w_j \times R_{ij} \tag{3}$$

Afterwards, positive and negative ideal solutions are determined respectively as

$$D_i^+ = \sqrt{\sum_{j=1}^m (W_{ij} - P_j^*)^2} \tag{4}$$

$$D_i^- = \sqrt{\sum_{j=1}^m (W_{ij} - N_j^*)^2} \tag{5}$$

where P_j^* and N_j^* denote positive and negative ideal solutions, D_i^+ and D_i^- refer to the distances to the positive and negative ideal solutions, respectively. Finally, the alternatives are ranked in descending order employing the following formulation:

$$CC^* = \frac{D_i^-}{D_i^+ + D_i^-} \tag{6}$$

3. RESULTS

Solar energy has emerged as a crucial renewable resource in the global shift toward sustainable energy production. In Turkey, with its abundant sunshine, harnessing solar energy represents a significant opportunity for both environmental preservation and economic growth. However, the efficient distribution of this energy resource across the country requires a comprehensive understanding of the various factors influencing the potential of solar energy.

The application of the TOPSIS model in the context of assessing the potential of Turkish cities for solar energy development concretely illustrates the effectiveness of multi-criteria decision-making methods in planning renewable energy infrastructure. As evaluation criteria of Turkish cities for solar energy development, solar radiation, sunshine duration, air temperature, and humidity are utilized. Three experts who have been working in energy sector made a consensus and determined the importance weights of these 4 factors as 0.45, 0.40, 0.10, 0.05, respectively. The dataset is given in Table 1.

Table 1. Data of Turkish cities for solar energy development

City	Solar radiation	Sunshine duration	Air temperature	Humidity (%)
Hakkari	1610	3508	10.3	54
Mardin	1588	3033	16.1	52
Şanlıurfa	1586	3033	18.5	56
İğdır	1487	3340	12.2	56
Şırnak	1601	2975	15.1	56
Kilis	1575	2975	17.2	57
Van	1652	3070	9.4	57

Antalya	1646	3011	18.8	64
Adiyaman	1595	2961	17.3	61
Burdur	1631	2944	13.3	59
Siirt	1591	2828	16.2	56
Aydin	1557	3011	17.7	62
Denizli	1591	2931	16.2	60
Gaziantep	1582	2978	15.2	61
Mersin	1614	3015	19.2	66
Batman	1576	2873	15.9	59
Muğla	1587	3040	15.1	64
Niğde	1620	2930	11.2	59
Konya	1608	2898	11.7	59
Adana	1564	2953	19.2	65
Osmaniye	1555	2954	18.6	65
Isparta	1612	2858	12.3	60
İzmir	1496	2986	17.9	64
Malatya	1599	2873	13.7	62
Elazığ	1588	2829	13.1	61
Aksaray	1578	2886	12.1	62
Kayseri	1588	2842	10.7	60
Bingöl	1592	2719	12.1	58
Hatay	1536	2997	18.3	70
Tunceli	1579	2716	12.7	62
Nevşehir	1537	2834	10.7	63
Manisa	1486	2840	16.9	66
Diyarbakır	1473	2613	15.9	57
Muş	1591	2686	9.7	61
Ağrı	1570	2778	6.2	60
Afyonkarahisar	1557	2705	11.3	64
Sivas	1538	2653	9	61
Bitlis	1604	2690	9	66

Kırşehir	1509	2769	11.5	66
Erzincan	1555	2595	10.9	65
Yozgat	1494	2683	9.2	63
Ankara	1473	2611	11.9	62
Kırıkkale	1460	2648	12.5	66
Kütahya	1490	2559	10.8	64
İstanbul	1612	2446	16.2	76
Balıkesir	1418	2686	14.7	71
Kahramanmaraş	1061	2913	16.7	60
Çanakkale	1375	2807	15.1	77
Karaman	1066	3007	12	60
Bayburt	1529	2398	7	64
Bursa	1393	2515	14.6	66
Eskişehir	1472	2479	11.3	67
Gümüşhane	1505	2349	9.5	64
Tokat	1431	2464	12.5	68
Çankırı	1432	2514	11.3	69
Edirne	1319	2697	13.7	72
Çorum	1419	2511	10.8	69
Tekirdağ	1337	2606	14.1	72
Kars	1472	2537	4.7	72
Bilecik	1412	2424	12.5	71
Amasya	1392	2427	13.6	71
Kırklareli	1321	2628	13.2	73
Karabük	1369	2402	13.4	68
Giresun	1435	2285	14.6	74
Uşak	1054	2789	12.5	64
Erzurum	1393	2504	5.7	67
Artvin	1409	2124	12.3	65
Bolu	1416	2402	10.5	73
Yalova	1342	2424	14.6	75

Kastamonu	1364	2394	9.8	68
Ardahan	1472	2310	3.6	71
Sakarya	1342	2358	14.6	74
Kocaeli	1329	2373	14.8	74
Trabzon	1394	2132	14.7	74
Rize	1403	2124	14.5	75
Samsun	1335	2314	14.6	74
Düzce	1344	2362	13.1	74
Sinop	1328	2347	14.3	76
Zonguldak	1313	2380	13.7	74
Ordu	1303	2263	14.5	73
Bartın	1307	2376	12.8	79
weight	0.45	0.40	0.10	0.05

After employing the application steps of TOPSIS method, the outcomes outlined in Table 2 are obtained.

Table 2.The outcomes of TOPSIS method

City	D^+	D^-	CC^*	Rank
Hakkari	2.327916	0.254852	0.248613	81
Mardin	2.48157	0.198577	0.220503	79
Şanlıurfa	2.520587	0.191889	0.216248	76
Iğdır	2.501983	0.189647	0.215881	74
Şırnak	2.529793	0.19242	0.216174	75
Kilis	2.560206	0.181577	0.210306	70
Van	2.466059	0.219205	0.229668	80
Antalya	2.559996	0.203913	0.220109	78
Adıyaman	2.588332	0.182855	0.209981	69
Burdur	2.546177	0.197657	0.217907	77
Siirt	2.590549	0.178022	0.207698	64
Aydın	2.61077	0.172448	0.20446	62
Denizli	2.592467	0.18015	0.208616	66
Gaziantep	2.592987	0.179391	0.208251	65

Mersin	2.605192	0.189574	0.212446	72
Batman	2.614091	0.172043	0.204165	60
Muğla	2.597725	0.183254	0.209862	68
Niğde	2.559964	0.192226	0.215086	73
Konya	2.579842	0.185511	0.211454	71
Adana	2.656984	0.16707	0.200485	56
Osmaniye	2.663203	0.164241	0.198933	55
Isparta	2.601948	0.182785	0.209515	67
İzmir	2.691023	0.148781	0.190371	49
Malatya	2.625931	0.176911	0.206071	63
Elazığ	2.64206	0.170601	0.202621	59
Aksaray	2.639397	0.169824	0.202334	58
Kayseri	2.626065	0.172926	0.204209	61
Bingöl	2.6501	0.16896	0.201597	57
Hatay	2.716498	0.157573	0.194097	51
Tunceli	2.70019	0.159687	0.195615	52
Nevşehir	2.701021	0.151381	0.191423	50
Manisa	2.772706	0.133232	0.179794	44
Diyarbakır	2.779421	0.12631	0.175718	42
Muş	2.691878	0.1635	0.197723	53
Ağrı	2.665371	0.162054	0.197803	54
Afyonkarahisar	2.74347	0.149142	0.189074	48
Sivas	3.107487	0.103395	0.154269	32
Bitlis	3.090242	0.123892	0.166825	38
Kırşehir	2.779911	0.135455	0.180825	45
Erzincan	2.796303	0.142443	0.184139	46
Yozgat	2.795287	0.128515	0.176561	43
Ankara	2.829761	0.120193	0.170877	41
Kırıkkale	2.86862	0.114359	0.166433	37
Kütahya	2.855603	0.120888	0.170641	40
İstanbul	2.927208	0.151435	0.185303	47

Balıkesir	2.944042	0.102089	0.156983	34
Kahramanmaraş	3.119494	0.080298	0.138257	15
Çanakkale	3.004996	0.096909	0.152241	29
Karaman	3.439821	0.047826	0.105476	1
Bayburt	3.246289	0.087762	0.141204	20
Bursa	2.981658	0.0916	0.149135	27
Eskişehir	2.935022	0.109886	0.162123	36
Gümüşhane	2.927784	0.11877	0.167646	39
Tokat	2.987828	0.097629	0.153091	30
Çankırı	2.977854	0.098846	0.154113	31
Edirne	3.04507	0.08088	0.140136	19
Çorum	2.989885	0.095694	0.151753	28
Tekirdağ	3.063592	0.079431	0.138688	16
Kars	2.963785	0.109248	0.161068	35
Bilecik	3.052997	0.089883	0.146454	25
Amasya	3.070199	0.085256	0.142837	21
Kırklareli	3.081287	0.077087	0.136569	13
Karabük	3.070988	0.081081	0.139776	18
Giresun	3.121043	0.091549	0.146225	24
Uşak	3.213661	0.067498	0.126581	5
Erzurum	2.99622	0.090466	0.148039	26
Artvin	3.119441	0.088889	0.144425	22
Bolu	3.079614	0.089405	0.14558	23
Yalova	3.162177	0.072969	0.131874	11
Kastamonu	3.078203	0.080011	0.138839	17
Ardahan	3.045376	0.103268	0.15551	33
Sakarya	3.178301	0.071591	0.130497	9
Kocaeli	3.18442	0.069531	0.128742	8
Trabzon	3.223814	0.08026	0.136282	12
Rize	3.23013	0.081997	0.13743	14
Samsun	3.203329	0.06935	0.128265	7

Düzce	3.175786	0.071808	0.130714	10
Sinop	3.218901	0.068004	0.126904	6
Zonguldak	3.197578	0.066714	0.126213	4
Ordu	3.245745	0.063037	0.122315	2
Bartın	3.259761	0.064847	0.123609	3

According to the resulting rankings, Karaman ranked first, followed by Ordu and Bartın, respectively.

4. DISCUSSION AND CONCLUSIONS

The results of this study clearly show that certain regions of Turkey offer optimal conditions for the development of solar projects. By prioritizing investments in these areas, developing effective support policies, and strengthening energy storage and transportation capacities, Turkey can not only improve its energy security, but also promote sustainable economic development and reduce its carbon footprint. These efforts will help achieve national energy sustainability goals and strengthen the country's economic resilience.

This work serves to provide a scientific and methodological basis for the strategic planning of solar projects in Turkey. Using multi-criteria decision methods such as TOPSIS, it makes it possible to identify the most promising cities for the installation of solar systems. This approach can also be applied to other sectors requiring multi-criteria evaluation, such as wind energy, water resources management, urban planning and the allocation of industrial investments.

In conclusion, this study provides a robust framework to optimize the use of solar potential in Turkey. The recommendations and practical implications provided here can guide policymakers and investors in their efforts to develop a sustainable, innovative and economically viable energy sector.

Ethics Committee Approval

N/A

Peer-review

Externally peer-reviewed.

Author Contributions

Conceptualization: N.G., M.B.B.; Investigation: M.B.B.; Material and Methodology: M.B.B. M.D.; Supervision: N.G.; Visualization: N.G., M.B.B.; Writing-Original Draft: N.G., M.B.B., M.D.; Writing-review & Editing: N.G.; Other: All authors have read and agreed to the published version of manuscript.

Conflict of Interest

The authors have no conflicts of interest to declare.

Funding

This work has been financially supported by Galatasaray University Research Fund FBA-2024-1243.

REFERENCES

Cetin, M., Egrican, N. (2011). Employment Impacts of Solar Energy in Türkiye. *Journal of Renewable and Sustainable Energy*.

Dhar, A., Naeth, M. A., Jennings, P. D., & Gamal El-Din, M. (2020). Perspectives on environmental impacts and a land reclamation strategy for solar and wind energy systems. *The Science of the Total Environment*, 718, 134602. <https://doi.org/10.1016/j.scitotenv.2019.134602>.

Global Solar Atlas. (2020). Global Photovoltaic Power Potential by Country. Energy Sector Management Assistance Program (ESMAP), World Bank Group. Available at: <http://documents.worldbank.org/curated/en/466331592817725242/Global-Photovoltaic-Power-Potential-by-Country>

- Hwang, C.L., Yoon, K. (1981). Multiple attribute decision making: Methods and applications: A state-of-the-art survey, Springer-Verlag Heidelberg, Berlin, New York.
- Rahman, S., Hasanuzzaman, M., Rahim, N. A. (2015). Effects of Various Parameters on PV-Module Power and Efficiency. Renewable Energy Journal.
- Rahman, S., Hasanuzzaman, M., Rahim, N. A. (2017). Effects of Operational Conditions on the Energy Efficiency of Photovoltaic Modules. Applied Energy.
- Salim, S., Najim, K., Salih, O. (2013). Practical Evaluation of Solar Irradiance Effect on PV Performance. Energy and Power Engineering.

Development of a Financial Web Application For Budget and Expense Management For Individual and Company

Genit Sopa¹, Faton Kabashi², Vehebi Sofiu³, Lamir Shkurti⁴, Sami Gashi⁵

Abstract: This project presents the development and implementation of a financial web application, dedicated to budget and expense management for individuals and companies. The project focuses on creating an innovative and comprehensive platform that addresses common challenges in financial management using modern technologies and advanced development methodologies. The application aims to provide a comprehensive solution for users including functionalities such as budget tracking, expense categorization, product management, profit estimation and generation of customized financial reports. The application is designed to be accessible from any device with a web browser, thus providing a smooth and easy user experience. One of the main objectives of this project is to ensure a high level of security and privacy for user data. For this purpose, advanced encryption technologies and protection mechanisms are used to guarantee the protection of sensitive financial information. This focus on security is essential to gain users' trust and ensure that their data is protected from unauthorized access. Another important aspect of this project is the use of data analytics to provide personalized insights and recommendations to users. These analyzes help users make more informed financial decisions and optimize the management of their financial resources. Analyzes include estimates on spending, consumption trends and recommendations for budget optimization. Furthermore, the application is designed to be scalable, enabling high performance even in cases of large user and transaction loads. This feature makes the platform suitable for a wide range of users, from individuals managing their personal budget to companies looking for an efficient tool for managing their corporate finances. In conclusion, this project represents an important step in the development of digital financial tools, providing a safe, efficient and easy solution for users to improve the management of their finances. The platform not only fulfills the current needs of users, but also has the potential to serve as a model for future developments in the field of financial technology.

Keywords: API - Application Programming Interface, BPM - Business Process Management, CRM - Customer Relationship Management, ERP - Enterprise Resource Planning, FinTech - Financial Technology, IoT - Internet of Things, KPI - Key Performance Indicator, SaaS - Software as a Service, SDLC - Software Development Life Cycle, UI/UX - User Interface/User Experience, UML - Unified Modeling Language

^{1,2,3,4,5}**Address:** UBT, Higher Education Institution, Kosova

***Corresponding author:** faton.kabashi@ubt-uni.ne

1. INTRODUCTION

Financial management is an essential component of personal and business life, requiring advanced tools and strategies to ensure economic stability and success. In the digital age, technology has revolutionized the way we manage our finances, offering innovative and automated solutions to help individuals and businesses monitor and control their finances. One of these solutions is the development of financial web applications that facilitate budget and expense management.

Nowadays, individuals face numerous challenges in managing their personal finances. Unforeseen expenses, lack of budget planning and inability to track income and expenses in real time are some of the main problems that individuals face. Additionally, many people have difficulty understanding and analyzing their financial data, which makes informed financial decisions difficult. On the other hand, businesses, especially small and medium-sized ones, face various challenges in managing their finances. Managing inventory, tracking operational expenses, estimating profits, and generating accurate and detailed financial reports are some of the challenges these businesses face. Moreover, the lack of an integrated system for managing these aspects can lead to financial losses and wrong decisions. Security and privacy of financial data are also major concerns in the digital age. With the increase in cyber security incidents, the protection of personal and financial information has become critical. Individuals and businesses require tools that not

only provide advanced functionality for financial management, but also ensure that their data is protected from unauthorized access and cyber-attacks.

This project aims to develop a financial web application that will provide a comprehensive budget and expense management solution for individuals and businesses.

The application will address the problems mentioned above by providing a user-friendly interface, advanced financial management tools, strong security measures and customized reports. This platform will help individuals and businesses make informed decisions and achieve their financial goals effectively and safely.

The application will include multiple functionalities to meet the needs of different users. Users will be able to create and manage their own budgets for different categories of expenses, such as food, transportation, entertainment and business expenses. This process will be simplified with the help of an intuitive and easy-to-use interface that allows setting budget limits and monitoring expenses in real time. This will help users avoid budget overruns and have a clear overview of their finances.

2. LITERATURE REVIEW

The development of financial applications for budget and expense management has been an area of great interest to researchers and professionals. These apps are designed to help individuals and businesses organize their finances, track expenses and plan budgets more effectively.

A study by Fisher and Lay [1] evaluates the impact of mobile financial applications on improving personal finance management. The study found that using such apps helps users track their spending, identify spending patterns and make informed financial decisions.

Another study by Riquelme and Rios [2] examines the role of technology in business financial management. They evaluate the use of financial applications in small and medium-sized businesses and find that these applications help automate financial processes, generate financial reports and improve the tracking of operational expenses.

Another important aspect is the design and user interface of these applications. A study by Chen et al. [3] analyzes the impact of user interface design on the efficiency of financial applications. The study highlights the importance of a simple and intuitive design that facilitates use and improves the user experience.

Another research by Kapoor and Gunta [4] focuses on data security and privacy in financial applications. They emphasize the importance of using advanced encryption technologies and safeguards to ensure that users' financial data is protected from cyber-attacks and unauthorized access.

According to a study done by Brown and Black [5], financial applications can also be used to educate users about financial management. The study suggests that apps integrate educational features, such as financial advice and budget management courses, to help users improve their financial knowledge and make better financial choices.

A study by Suryadevara and Babu [6] focuses on using artificial intelligence and machine learning algorithms to personalize financial recommendations for users. Financial applications that use these technologies can analyze spending and income patterns to provide specific, personalized advice that helps users optimize the management of their finances.

Research by Kaczorowski et al. [7] studies the impact of financial applications on improving financial control and reducing finance-related stress. The results show that regular use of financial apps helps users have a better understanding of their financial situation and helps them feel more confident and less stressed about their finances.

Another study by Johansson and Olsson [8] examines the impact of financial applications on strategic business decision-making. The study shows that the use of financial applications helps business managers have a clear picture of the company's financial condition and make better strategic decisions that positively affect the growth and sustainability of the business.

The development of financial applications for budget and expense management has a positive impact on personal and business financial management. Financial apps provide powerful tools for tracking and analyzing expenses, budgeting, and securing data, helping users achieve their financial goals and improve their financial health. The integration of

advanced technologies, intuitive design and strong security measures contribute to the effectiveness and popularity of these applications.

3. PROBLEM STATEMENT

The development of a financial web application for budget and expense management is the purpose of this research and the achievement of some results related to this technology. The impact and applications of financial technology in budget and expenditure management, problems, challenges and others. The result of this work predicts that it will be the gain of knowledge about the use of financial applications, namely the understanding of how and where this technology can influence in the future. The overall objective is to explain the development of financial technology and its use. The problems that have brought us to this research are:

- Lack of knowledge and appropriate tools for effective management of personal and business finances.
- Inability to track income and expenses in real time.
- Difficulty in analyzing and interpreting financial data to make informed decisions.
- Increasing cyber security threats and the need to protect financial data.
- The complexity of integrating different financial tools into a single, easy-to-use platform.

4. METHODOLOGY

The methodology in this thesis describes the methods and techniques that will be used to realize the goals and objectives of the project. It includes the steps to be followed, the materials to be used, and the sources from which these materials will be obtained. The main goal is to provide a structured and sustainable approach to the development and implementation of the financial web application.

4.1 Research Approach

The project will use a mixed approach, combining qualitative and quantitative research methodologies:

- Secondary Research: Compilation of existing literature, academic articles, and industry reports to create a solid theoretical foundation and identify best practices in the development of financial applications and financial technology (FinTech) [9].
- Primary Research: Conducting interviews and surveys with potential users to understand their specific needs and requirements for a financial web application. This will help create an interface and functionalities that are convenient and usable.

4.2 Development Process

The web application development process will be followed in structured phases to ensure efficiency and quality:

1. Requirements Analysis:
 - o Summary of functional and non-functional requirements through interviews and surveys [10].
 - o Documenting the specifications of development requirements.
2. System Design:
 - o Designing the application architecture using UML (Unified Modeling Language) models to represent the structure and interactions of the various system components.
 - o Developing database schemas to ensure efficient data management.
3. Development and Implementation:
 - o Using development languages and frameworks such as Angular for the user interface and .NET for the server part [11] [12].
 - o Integration of external APIs for additional functionality such as payment and financial data processing.
4. Testing:
 - o Conduct functional and non-functional testing to ensure the application meets requirements and is stable.
 - o Security testing to identify and address potential security issues.
5. Implementation and Maintenance:
 - o Deploying the application to a production environment and providing user support.
 - o Monitoring performance and performing regular updates to improve functionality and security.

4.3 Materials and Resources

- Literature and Articles: Academic resources and scientific articles will be used to support development theory and practices [9].
- Development Tools: Tools and platforms such as Visual Studio Code, GitHub, and cloud environments for application testing and development.
- Databases: Relational databases such as MySQL for financial data management [13].
- Security Resources: Security protocols and tools to protect data and financial transactions from cyber threats.

5. PROJECT ANALYSIS AND PLANNING

5.1 Scope of the Project

Overview

A financial web application is an online platform that provides users (individuals and companies) with a variety of financial tools and services to help them manage their finances. The application will be accessible from any web browser and will have two different login interfaces for individuals and companies.

Individual users will have access to features such as budget tracking and expense tracking to help them manage their personal finances. In turn, companies can use the platform to manage and showcase their products. They can add information about their products, manage the quantity sold and remaining inventory, track expenses and estimate the profits they will make.

The platform will provide users with customized reports and analysis based on their financial activities, and they can generate financial statements for personal or business use. Additionally, the app will have built-in security features to ensure the safety and privacy of user data.

Objectives

The objectives of the financial web application are as follows:

- To develop a user-friendly interface for both individuals and companies that provides a seamless experience while managing their financial activities.
- Enable individuals to track their spending, set budgets and generate reports that help them understand their financial position and make informed decisions.
- Allow companies to add, manage and provide tools to track their inventory, expenses and profits.
- To guarantee the security and privacy of user data by implementing strong security measures and respecting the relevant data protection regulations.
- Provide users with valuable insights and analysis based on their financial data, enabling them to make informed decisions and take the necessary actions to achieve their financial goals.
- Provide prompt customer support and service to address user questions and concerns regarding platform functionality.
- Continuously improve and update platform features based on user feedback and market trends, providing a reliable and up-to-date financial management solution.

Application Features

The financial web application will include the following features:

1. Product Management: The platform will enable companies to add their products and manage their inventory, sales and profits in real time.
2. Profit estimation: Companies can estimate their profits based on their sales and expenses, allowing them to make informed decisions about pricing and inventory management.
3. Financial reports: The platform will generate customizable financial reports for individuals and companies, including balance sheets, income statements and cash flow statements.
4. Data Analytics: The Platform will use data analytics to provide users with insights and trends related to their financial activities, helping them make informed decisions about their finances.
5. Categorizing expenses: The platform will enable individuals to categorize their expenses automatically or manually, making it easy to identify areas where they can reduce spending.
6. Goal setting: The platform will allow individuals to set financial goals and track their progress towards achieving them, providing motivation and guidance towards financial success.
7. Secure Data Storage: The Platform will store user data securely, using encryption and other security measures to protect sensitive information from unauthorized access.
8. Customer Support: The platform will provide customer support through a variety of channels, including email, chat and phone, ensuring that users can quickly get help with any issues they encounter.

Restrictions

The following limitations will be considered during the development of the online financial application:

- Cross-Browser Compatibility: The application must be designed to be compatible with all major web browsers.
- Data Privacy: The application must comply with data privacy regulations and protect users' financial data from unauthorized access.
- Scalability: The application must be designed to handle large numbers of users and transactions as it scales.
- Performance: The application should be optimized for performance to ensure that it runs smoothly and efficiently.

Project products

The following products will be provided at the end of the project:

- Fully functional financial web application accessible from any web browser.
- User manuals and documentation.
- Source code and project documentation.
- Quality assurance and test reports.

5.2 Technical and Technological Analysis

Presentation

In today's fast-paced world, managing personal and business finances is becoming increasingly complex. An online financial application can provide users with an efficient and convenient way to manage their finances. The proposed financial web application aims to provide individuals and companies with a user-friendly platform to manage their finances, track expenses, generate reports and make informed decisions.

This analysis will discuss the technology, system architecture, external systems, tools, equipment, and software needed to develop an online financial application. We will also analyze the technical feasibility of the project and explore potential challenges and constraints that need to be considered. The purpose of this analysis is to provide a comprehensive overview of the proposed online financial application and lay the foundations for its successful development and implementation.

Technology Used

When developing a financial web application, it is essential to use technologies that ensure security and reliability. The programming languages that will be used in the development of this application are: Angular for frontend and .NET for backend. These programming languages are compatible and have strong community support, which will ensure that the application is developed and maintained effectively [11] [12].

In addition to programming languages, the database used in the application will also play a decisive role in its success. For this online financial application, MSSQL will be used as the database management system. MSSQL is known for its reliability and scalability, which are essential for a financial application [13]. With this stack of technology, the financial web application will be developed to provide a secure, reliable and efficient platform for users to manage their finances.

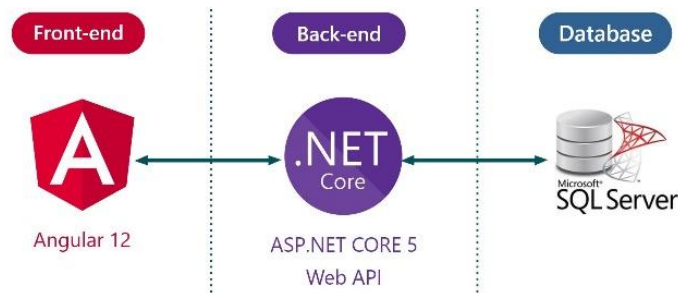


Figure 1. The technology used

User Interface (UI)

The user interface (UI) is the front end of the application that allows users to interact with the tool. It includes the design, layout and functionality of websites or mobile applications. Angular technology provides a powerful and flexible environment for creating dynamic and responsive interfaces that improve the user experience [11].

System Architecture

The system architecture of a web application defines how its components interact with each other. A well-designed architecture ensures that the web application is scalable, secure and reliable.

- **Application Server:** The application server is the back end of the application that handles the business logic and interacts with the database. It is responsible for processing user requests, managing user accounts and generating reports.
- **Database Server:** The database server stores and retrieves data from the application. It is responsible for storing project information, user data and other related information.

- Collaboration tools: Collaboration tools enable team members to work together and share project-related information. These tools include messaging systems, document sharing, and file storage.
- Task management: The task management component allows users to create and assign tasks, set deadlines and track progress. It includes features such as to-do lists, calendars and progress trackers.
- Reporting and analytics: The reporting and analytics component provides users with insights into project performance, team productivity, and other important metrics. It includes features such as dashboards, dashboards and custom reports.

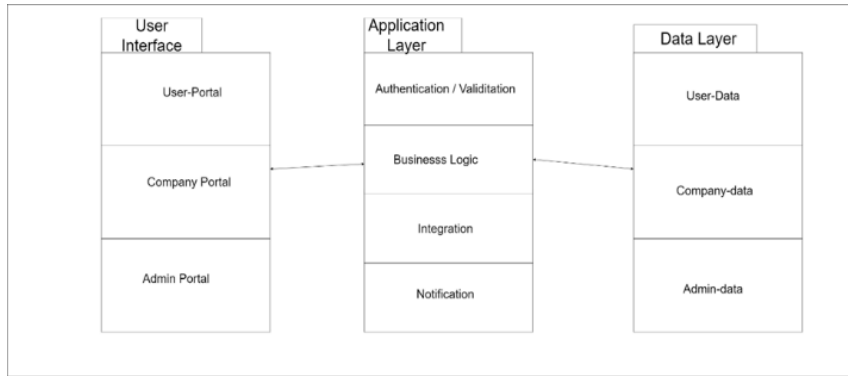


Figure 2. System architecture structure

Integrated Systems

Embedded systems are used to improve the functionality and performance of the web application. The following embedded systems can be used for an online financial application:

1. Authentication and authorization: For user authentication and authorization, external services such as Google API Login, Facebook Login or OAuth2 [15] can be used. These services allow users to authenticate with your web application using their existing social media accounts or email accounts.
2. Syncfusion: Syncfusion provides modern and user-friendly graphs and charts for real-time data visualization and reporting. Syncfusion's suite of more than 1,600 components and frameworks for .NET, JavaScript, Angular, React, Vue, and Xamarin development helps build these features quickly and easily, saving time and money [14].

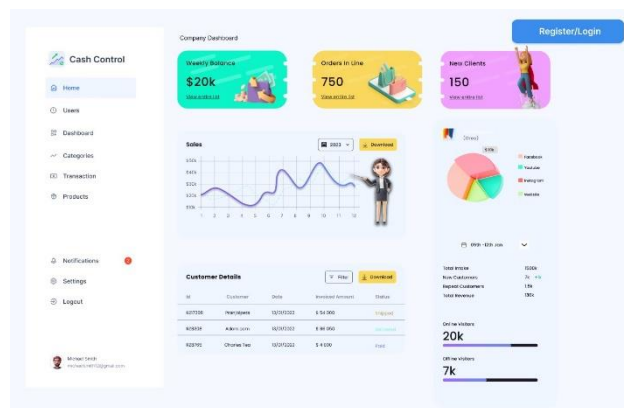


Figure 3. System syncfusion

Technical Feasibility Analysis and Project Risk

Technical Feasibility

The project involves the development of a financial web application that requires the integration of several technologies, including web development frameworks, database systems, and third-party APIs. The technical feasibility of the project depends on several factors, including:

1. Availability of skilled resources: The development team must have access to skilled resources with expertise in the required technologies. If qualified resources are not available, the technical feasibility of the project may be at risk.

2. Compatibility of technologies: The technologies used in the project must be compatible with each other. Compatibility issues can arise during integration, leading to delays and technical issues.
3. Infrastructure: The project requires adequate infrastructure, such as servers, networking and storage, to host the application. The availability and cost of such infrastructure may affect the feasibility of the project.
4. Third Party API Availability: The project relies on third party APIs for functions such as email notifications and SMS reminders. The availability and reliability of these APIs can affect the feasibility of the project.

Technical Risks

Web application development for scheduling and booking carries several technical risks that must be managed to ensure its successful completion. Some of the main risks associated with the project include:

1. Security: The application includes sensitive user data and must be designed with strong security measures to prevent unauthorized access, data breaches and other security threats.
2. Scalability: The application should be able to handle a large number of users and transactions. Therefore, the architecture should be designed to scale horizontally or vertically as traffic increases.
3. Reliability: The application should be available 24/7 and should be able to handle failures gracefully. Therefore, the application should be designed with fault-tolerant architecture and backup systems.
4. Integration Challenges: Integrating the various technologies required for the project can be challenging and the development team must have the necessary expertise to manage this process.
5. User Experience: The success of the application depends on the user experience and the development team must ensure that the application is intuitive and easy to use.

In general, the technical feasibility and riskiness of the project depend on several factors, including the availability of qualified resources, the compatibility of technologies, the availability of infrastructure and the reliability of third-party APIs. The risks associated with the project must be managed to ensure its successful completion.

5.3 Definition of Product Backlog & User Stories

Product Backlog Table for Cash Control System					
ID	LIKE A:	I WANT...	THAT...	PRIORITETI	SPRINT
EPIC 1 - User Registration					
US01.	USERS	to register in the system	to have access to the system through the profile.	Must Have	1
US02.	USERS	login to the system	to have access to the system through the profile.	Must Have	1
US03.	USERS	a secure identification system	allows me to access the info. needed safely.	Must Have	1
US04.	USERS	change my credentials	(if) I forgot them.	Must Have	1
EPIC 2 - Management by Administrator					
US05.	Administrator	delete a user's data	not be accessible if the user no longer uses the system.	Must Have	1
US06.	Administrator	change user data	manage user requests as desired.	Must Have	1
US07.	Administrator	to give access to the client	to be able to ensure proper access and control over the system.	Must Have	1
EPIC 3 - Implementimi i Live Chat					
US08.	USERS	use a live chat service	to communicate with the customer support department.	Should Have	2
US09.	USERS	to have 24/7 access	to chat with customer service whenever necessary.	Should Have	2

EPIC 4 - Cost Management					
US10.	USERS	track my expenses	to be able to monitor my spending habits and stay within my budget.	Must Have	1
US11.	USERS	to categorize my expenses	see where my money is going.	Must Have	1
US12.	USERS	create a savings plan and track my progress toward my savings goals	reach my financial goals.	Must Have	1
EPIC 5 - Product Management					
US13.	Company Owner	be able to add info. about my products in the system	potential customers to see and buy them.	Must Have	1
US14.	Company Owner	be able to track the quantity sold and remaining inventory of products mine	to be able to effectively manage my stock levels	Must Have	1
US15.	Company Owner	estimate the profits I will make based on my sales and expenses	make informed business decisions.	Could Have	2
EPIC 6 - Reporting and Analysis					
US16.	USERS	create personalized reports for my financial activity	better understand my financial situation.	Must Have	1

US17.	Company Owner	create financial statements for my business	be able to keep track of my finances for tax and reporting purposes.	Should Have	2
EPIC 7 - Interface (UI)					
US18.	USERS	system to have an easy-to-use interface	to be able to easily navigate to the relevant parts.	Must Have	1
US19.	USERS	view recent transactions on the main page of the system	to check the financial situation quickly.	Must Have	1

Table 1. Product Backlog Table for Cash Control System

5.4 3C Analysis

3C analysis focuses on three main components that help develop successful strategies: Company, Competition and Customers. Using this analysis, we can identify the strengths and weaknesses of our company, the opportunities and threats from the competition, as well as the needs and desires of our customers. [16]

Company

In this project, the company aims to provide a platform that allows users to manage passwords, request support through a live chat service, categorize and track expenses, and manage product and transaction data. The use of such a platform helps the company to improve its service offering and increase efficiency in the management of user data.

Competition

Our competitors also offer similar services, but by analyzing User Stories and our users' requests, we have the opportunity to differentiate ourselves by offering additional features such as password change confirmation emails, 24/7 live chat, and detailed expense reports. This allows us to create a competitive advantage by providing an improved user experience.

Customers

To meet the needs of consumers, our platform is built to address their specific requirements, identified through User Stories. This includes the ability to change passwords, request fast and efficient support, manage expenses and generate financial reports, as well as inventory tracking for vendors. This helps us ensure that our platform is tailored to the real needs of our users.

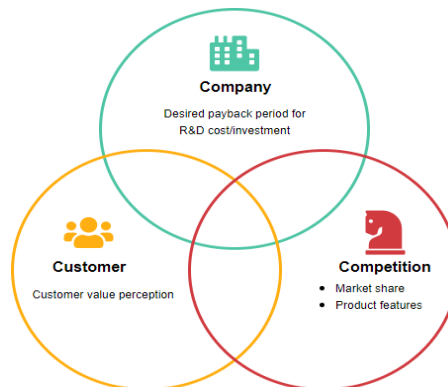


Figure 4. 3C Analysis

User Story

US04: Change Password

Card: I, as a user, want to change my password after registering.

Conversation:

- Q: Should we make it possible for you to accept confirmation when changing your password?
- A: Yes, I want to receive a confirmation email when changing my password.
- Q: Is it necessary to have a limit after changing the password?
- A: Yes, after changing the password the old password must not be set again and the new password must not be changed for 48 hours.

Confirmation: After registration, the user will have the possibility to change the password which will be confirmed by email, and will not be able to change it after a certain time. Also, he won't be able to use a password he's used before.

US05: Deletion of User Data

Card: As an administrator I want to be able to delete a user's data. Conversation:

- Q: What kind of data do you want to delete for a user?
- A: I want to be able to delete all data associated with a user account, such as their personal information, login credentials, purchase history, and any other data associated with their account.
- Q: Do you want to be able to delete data for all users or only specific users?
- A: I want to be able to delete data for specific users.

Confirmation: The administrative solution allows the administrator to delete all data associated with a specific user account, including personal information, login credentials, purchase history and any other data associated with his account.

US08 & US09: Support via Live Chat

Card: I, as a user, would like to request support, help or information from a business or organization via a live chat service platform. Conversation:

- Q: When would you like to have the live chat service available?
- A: I want it to be accessible 24/7.
- Q: What questions should be available to the customer?
- A: I want to include a list of basic questions and a list of frequently asked questions.

Confirmation: User requests support, help or information from a business or organization via live chat 24/7. The user may have questions, concerns, or issues they need help with, and the customer service representative provides real-time support to address their needs.

US12: Expense Tracking and Report Generation

Card: As an individual user, I want to track my expenses and generate reports to understand my financial position and make informed decisions.

Conversation:

- Q: How often do you want to track your expenses?
- A: I would like to track my expenses on a weekly basis.
- Q: What types of reports would be most useful to you?
- A: I would like to generate reports that show me my spending habits and trends over time.

Confirmation: The platform allows users to track their spending on a weekly basis and generates customizable reports that show spending habits and trends over time, helping users understand their financial position and make informed decisions.

US13: Categorization of Expenses

Card: As a user, I want to categorize my expenses to see where my money is going.

Conversation:

- Q: Which categories are most important to you?
- A: The most important are the food category, utilities (water, electricity, etc.), debts, entertainment and the health category.
- Q: How often do you review your expenses?
- A: I review them every month.

Confirmation: The user can categorize their expenses into different lists and view and analyze expenses by category, allowing them to see where their money is going. Also, the user can review their expenses on a monthly basis and access the expenses for the previous month.

US16: Product Information Management

Card: As a product manager, I want to be able to add information about my products to the system so I can keep track of their data and manage it efficiently.

Conversation:

- Q: What kind of information should you add about your products?
- A: I need to add the product name, description, SKU, price, weight and any other relevant details.
- Q: Do you need to add different variations of the same product?
- A: Yes, I need to add different variations, such as different sizes, colors and styles for each product.

Confirmation: The product management solution allows the product manager to add information about each product to the system, including the product name, description, SKU, price, weight and any other relevant details. The product manager can also add different variations of each product, such as different sizes, colors and styles.

US17: Track Sold Quantity and Inventory

Card: As a seller, I want to track the sold quantity and remaining inventory of my products so that I can manage my inventory and avoid overselling.

Conversation:

- Q: How do you currently track your inventory?
- A: I currently keep track of my inventory in a spreadsheet and manually update it when a product sells.
- Q: How often do you update your inventory data?
- A: I update my inventory data after every sale.
- Q: How do you know when to refill your products?

- A: I usually restock my products when the remaining inventory reaches a certain threshold.
- Confirmation: The inventory tracking solution allows the seller to track the quantity sold and the remaining inventory of their products. The seller can easily update the sold quantity and remaining inventory of each product after each sale, allowing them to avoid overselling and replenish their products when necessary.

US19: Viewing Past Transactions

Card: As a user I want to be able to view past transactions.

Conversation:

- Q: What kind of previous transactions do you want to view?
 - A: I want to view all transactions I've made in the past, including purchases, refunds, and cancellations.
 - Q: How far back would you like to be able to view your past transactions?
 - A: I want to be able to see all my past transactions, starting with the first one I made on the platform.
- Confirmation: The platform will have a "Transaction History" section where users can view all their past transactions, including purchases, refunds and cancellations.

5.5 Functional and Non-functional Requirements

No	Functional Requirements	Non-Functional Requirements
1	Access from Multiple Devices	Identification Security
2	Custom Reports and Analytics	Compatibility with Multiple Devices
3	Generation of Financial Statements	Easy To Use Interface
4	Data Security	Compliance with Data Privacy Regulations
5	Compliance with Regulations	Handling a Large Number of Users
6	Informed Decisions	Availability 24/7
7	Customer Support and Service	Scalability
8	Addressing Questions and Concerns	Customizability
9	Reliable Financial Management	Flexibility
10	Friendly User Interface	User Tutorial
11	Paneli (Dashboard)	Ease of Maintenance and Updates
12	Categorization of Expenses	Fulfillment of Technical and Business Specific Requirements
13	Budget Management	High Performance
14	Revenue Tracking	Protection from Hacker Attacks
15	Investment Tracking	Customizable User Interface
16	Savings Tracking	Big Data Processing
17	Generation of Tax Reports	User Experience
18	Generating Reports for Lenders and Investors	Action History
19	Generation of Financial Reports	Interoperation with Other Applications
20	Search function	Technical Support
21	Importing Financial Data	Efficiency at Work
22	Export of Financial Data	Endurance
23	Password Recovery	
24	Two Factor Authentication	
25	Managing Roles and Permissions Users	
26	Account Management	
27	User Analytics	
28	User Profile Management	
29	Modification of Personal and Financial Information	
30	Deleting a User Account	
31	Customizing the Dashboard	
32	Tools for the Analysis of Financial Statements	
33	Customization of Product and Price Lists	
34	Insurance Recommendations	
35	Integration of Bank Accounts and Credit Cards	
36	Statement of Expenses and Income	
37	Setting Financial Goals	
38	Management of Payments and Invoices	

39	Categorization of Transactions	
40	Creation and Management of Personalized Financial Reports	
41	Budgeting for Different Categories of Expenses	
42	Creating and Pursuing Financial Goals	
43	Investment Performance Reports	
44	Signals for Financial Events	
45	Dashboard and Interface Customization	
46	Reminders for Financial Events	
47	General Registry of Transactions	
48	Tracking of Sources of Income	
49	Creating and Tracking Invoices	

Table 2. Functional and non-functional requirements

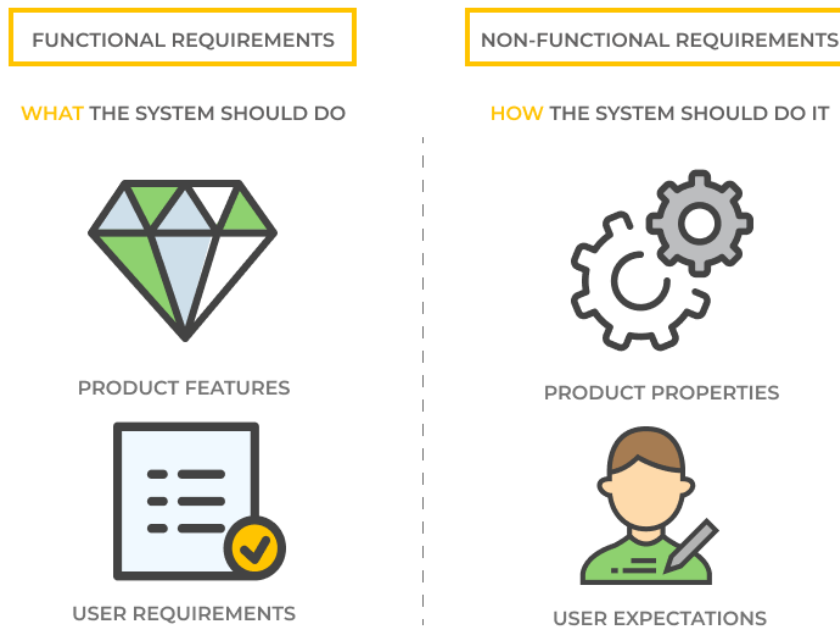


Figure 5. Difference between functional and non-functional requirements

6. SYSTEM DESIGN AND ARCHITECTURE

6.1 GUI designs

Defining user interface requirements

Defining user interface requirements is the initial step in the GUI design process and involves gathering and documenting the functional and non-functional requirements that the interface must meet. These requirements may include:

- Functional requirements: The functionalities that the interface should provide, such as buttons, menus, forms, and user interactions with the application.
- Non-functional requirements: Quality aspects of the interface, such as speed of response, aesthetic design, and consistency in use.

Interface sketching and prototyping

Sketching and prototyping are important stages to visualize and test the interface design before full implementation. [17]

- Sketching: Creating simple and quick drawings to present initial design ideas. Sketches can be created by hand or using digital tools.

- Prototyping: Creating more detailed and interactive interface models using tools like Figma, Adobe XD, or Sketch. Prototypes help test usability and identify potential problems before implementation.

User Interface Design Link: [Figma Prototype](#)

Usability and Accessibility Guidelines

Usability and accessibility guidelines ensure that the interface is easy to use by all users, including those with disabilities.

- Usability: Ensuring that the interface is intuitive, easy to learn and efficient to perform user tasks. Instructions include:
 - o Consistency in design and navigation
 - o Quick response of the interface to user actions
 - o Providing guidance and assistance to users at every step
- Accessibility: Ensuring that the interface is accessible to users with disabilities. Instructions include:
 - o Using high-contrast colors for text and visual elements
 - o Use of alternative texts for images and graphics
 - o Ensuring that the interface is navigable via keyboard and provides support for screen readers.

6.2 System Architecture Conceptual Design

Description of the Main System Components

The system architecture consists of several main components that cooperate to provide the necessary functionalities of a financial application. These components are:

1. Client-Side (UI): This component is responsible for handling the user interface, displaying data and interacting with the user. The technology used to develop this component is Angular. The main modules include:
 - o User Interface
 - o Product Management
 - o Financial Reports
 - o Dashboard visualization (using Syncfusion) [14]
2. Server-Side (Application Layer): This component handles data processing and business logic. It is developed using .NET technology and consists of modules such as:
 - o Product Management
 - o Categorization of Expenses
 - o Profit Estimation
 - o Data Analytics
3. Database (Database Layer): This component is responsible for storing and retrieving data, using MySQL for database management. The preceding tables include:
 - o User Information
 - o Product Data
 - o Financial Reports
 - o Categorization and Expenditure Data

Relationships between Components

The various components of the system interact in a synchronized manner to ensure the full functionality of the financial application. Below are some of the main links between them:

- Client-Side and Server-Side: The user interface (UI) on the client-side (client-side) communicates with the business logic and data processing on the server-side (server-side) through API calls.
- Server-Side and Database: The server-side interacts directly with the database to store and retrieve the necessary data.
- Database and Client-Side: The data obtained from the database (database) is displayed in the user interface (UI) through the server-side.

Architectural Patterns and Styles Used

For the development of this system, several architectural models and styles have been used to ensure a clear and manageable structure:

1. MVC (Model-View-Controller) pattern: This pattern helps to divide responsibilities between business logic, user interface and data processing.
2. RESTful API: For communication between the client side and the server, a RESTful API is used, which provides a standardized and efficient way to exchange data.
3. Microservices: Some system modules are developed as independent microservices to provide scalability and easier code maintenance.[12]

To illustrate the conceptual design of the system architecture, a table is attached below that describes the main components and the relationships between them.

Component	Responsibility	Tools/Frameworks	Modules/Tables
Client-Side	Handles user interface, displays data, and interacts with user	Angular	UI, Product Management, Financial Reports,
			Session Management, Product Management
Server-Side	Handles data processing and logic	.NET	Product Management, Expense Categorization, Profit Estimation, Data Analytics, User Authentication, Authorization,
			Product Inventory, Sales Tracking, Expense Categorization, Profit Estimation, Data Analytics
Database	Stores and retrieves data	MySQL	User Information, Product Information, Financial Reports, Expense Categorization Data
			Product Inventory, Generated Financial Reports, Expense Categorization Data

Table 3. System Architecture Conceptual Design

6.3 Designing Modules

Identification and Description of Main Modules

The main modules of this system include:

- User Management: Related to the Security module to ensure the privacy and security of user data. Uses encryption and other security measures to protect sensitive user data.
- Product Management: Related to User Management and Security for similar reasons, as well as to provide data encryption and access control policies.
- Expense Tracking: Linked to user management and revenue monitoring modules to categorize and track expenses. It relies on user and revenue data.
- Income Tracking: Linked to the Expense Tracking and User Management modules to categorize and track income. It relies on user and spending data.

Interaction between Modules

The modules cooperate in a synchronized manner to ensure the full functionality of the system. Below are some of the main links between them:

- User Management and Security: Uses encryption and other security measures to protect user data.
- Product Management and User Management: Related to ensure that product data is protected and controlled.
- Expense Tracking and Income Tracking: Linked to ensure that expense and income data are categorized and tracked accurately.

Implementation and Sharing of Responsibilities

Each module has clear and separate responsibilities to ensure the full functionality of the system. For example:

- User Management: Handles user management and authentication.
- Product Management: Handles product management and inventory tracking.
- Expense Tracking: Handles the categorization and tracking of expenses.
- Income Tracking: Handles income categorization and tracking.

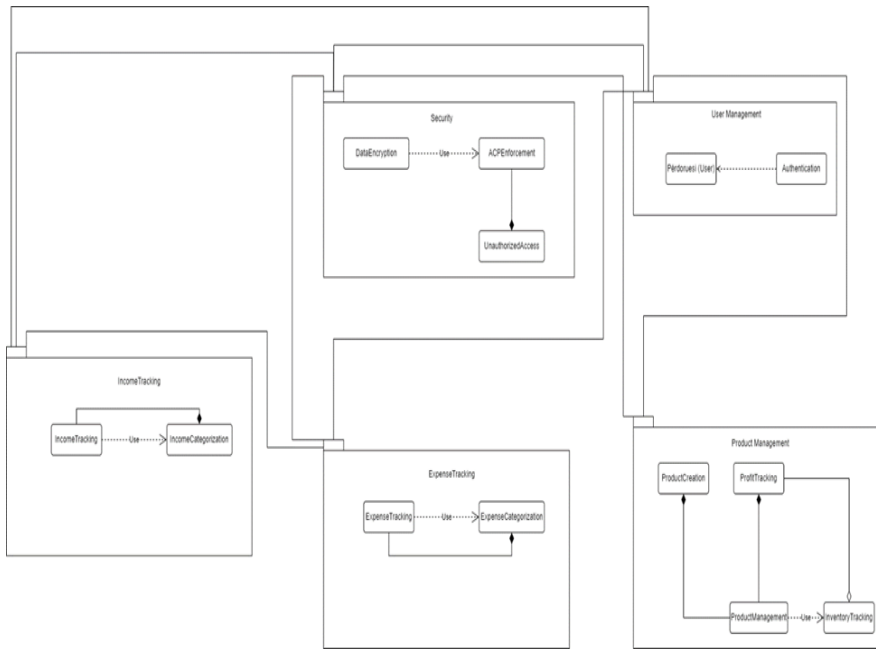


Figure 6. Diagram of Modules

6.4 Designing Classes

Description of System Classes and Objects

A class diagram represents the structure of the system by showing the main classes and objects, their attributes and methods, and the relationships between them.

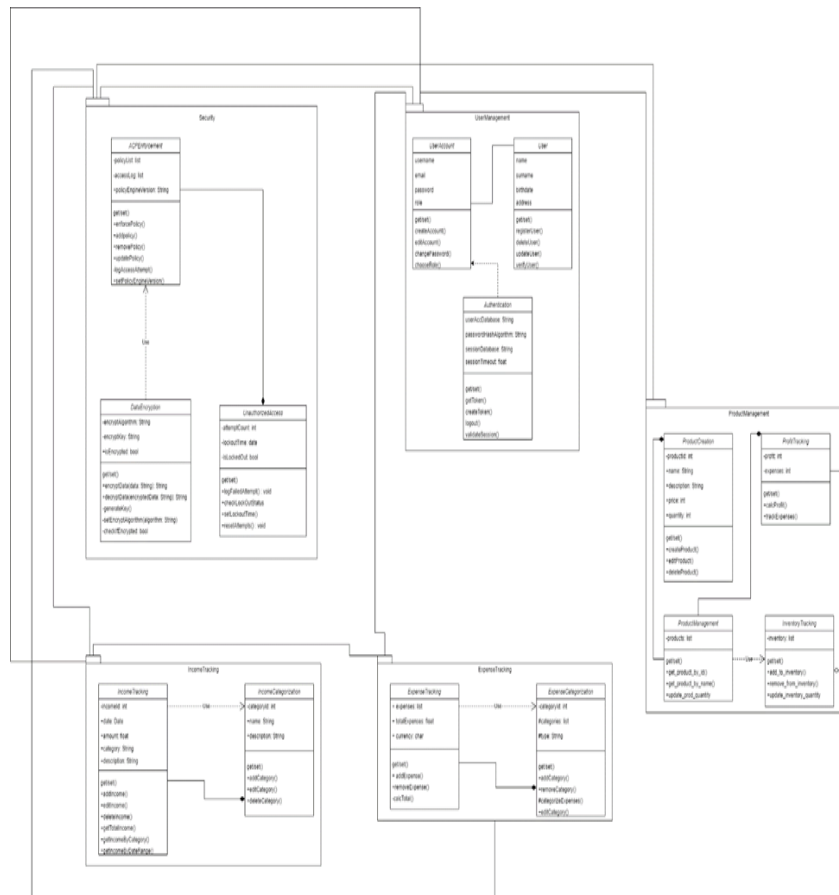


Figure 7. Class Diagram

Relationships and Dependencies Between Classes

The classes are linked together to provide a clear and manageable system structure. Some of the key links include:

- User Management and Security: Ensures the privacy and security of user data.
- Product Management and User Management: Ensures product data protection.
- Expense Tracking and Income Tracking: Provides accurate categorization and tracking of expenses and income.

Main Attributes and Methods for Each Class

- User: name, surname, email, address, methods getUser(), addUser(), deleteUser().
- Product: name, description, quantity, getProduct(), addProduct(), deleteProduct() methods.
- IncomeTracking: amount, date, category, addIncome(), getIncome() methods.
- ExpenseTracking: amount, date, category, addExpense(), getExpense() methods.
- Security: encryptData(), decryptData(), checkAccess().

6.5 Database Design

Conceptual and logical models of the database

Database design is an essential component in the development of an information system. Conceptual and logical models are two different phases of design that help structure data consistently and efficiently.

Conceptual Model

The conceptual model represents the logical structure of the data at a high level of abstraction, without technical concerns or implementation details. This model focuses on defining large entities (entities) and the relationships between them. An entity-relationship diagram (ERD) is a common tool for creating conceptual models.

In the attached diagram, the main entities are Products, User, Transaction, Category, Company, and Roles. These entities are linked in various ways to represent the relationships between them, as can be seen in the ERD diagram.

The Logical Model

The logic model includes the technical details and is an extension of the conceptual model. This model specifies the exact structure of the data, including fields, data types, and complex database connections.

In the attached diagram, each entity has its own clearly defined fields. For example, the Products entity has the fields Product ID, Name, Quantity, Remaining, and Description.

Data schema normalization and optimization

Normalization

Normalization is a process for partitioning tables to minimize data redundancy and improve data integrity. The normalization process goes through several normal forms (NF), each eliminating different types of redundancy.

- 1NF: Each field in a table must contain only a single value (be atomic).
- 2NF: All non-prime attributes must be fully dependent on the primary key.
- 3NF: All non-prime attributes must depend only on the primary key, and not on any other non-prime attributes.

Optimization

Data schema optimization includes techniques to improve query performance and data integrity. This includes creating indexes, using partial normalization when needed to improve query speed, and designing schemas to reduce unnecessary joins.

Definition of tables, relationships and data integrity

Tables and Links

Tables are defined for each logical model entity. Each table has specific fields that represent the attributes of the corresponding entity. For example:

- Products table contains the fields Product ID, Name, Quantity, Remaining, Description.
- User table contains fields User ID, Email, Password, Name, Surname.

Relationships between tables are represented through foreign keys. For example, the User table has a link to Company through the Company ID.

Data Integrity

Data integrity is ensured through primary keys, foreign keys, and other constraints. Primary keys uniquely identify each row in a table, while foreign keys link tables and ensure that references between tables are correct. Referential integrity ensures that each foreign key corresponds to an existing primary key in the linked table. For example, the Company ID in User must correspond to a valid Company ID in Company.

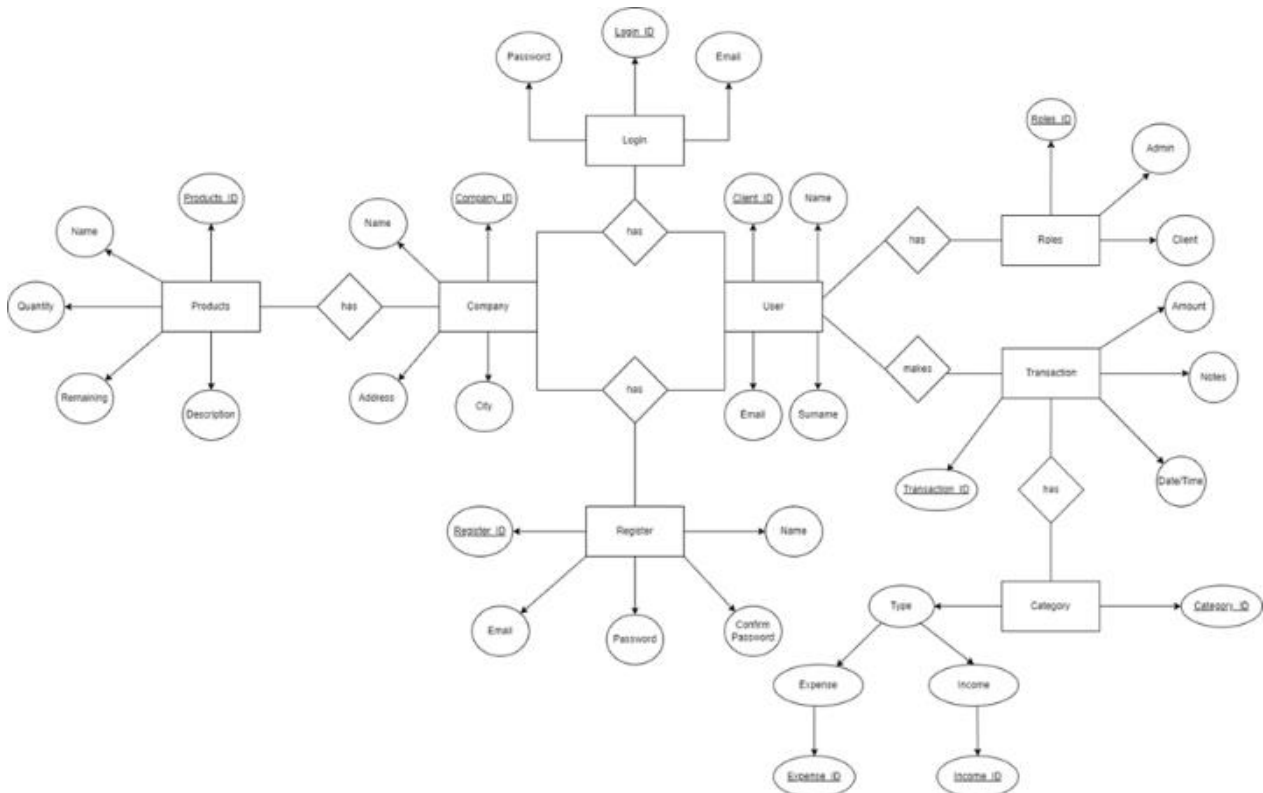


Figure 8. Database diagram

7. CONCLUSIONS

In conclusion, the development and implementation of the financial web application for budget and expense management has shown that modern technology can provide efficient and comprehensive solutions to financial management challenges. During this project, we managed to create a powerful platform, which not only addresses the current needs of users, but also creates a solid foundation for future improvements and extensions.

This project has demonstrated the importance of designing a usable and accessible interface for various users, including individuals and companies. The user interface built with Angular has ensured a smooth and integrated experience for users, while the server and database layers have provided a scalable and reliable performance for data processing and business logic.

In addition, the focus on security and data privacy is one of the app's strongest points. The use of advanced encryption technologies and security measures has ensured that user data remains secure and protected from any type of unauthorized access. This is a critical feature, given the sensitivity of financial information and the need to gain user trust.

Another important aspect of this project is the integration of data analytics to provide personalized recommendations and insights to users. These analyzes help users make more informed decisions and optimize the management of their finances, making the app an indispensable tool in everyday financial life.

In conclusion, this project has achieved its main objectives and has provided a powerful tool for financial management. It represents a significant advance in the field of financial applications, creating a strong foundation for future innovations. The application not only fulfills the needs of current users, but also shows the potential to be a leading solution in the future of financial management. As technologies and user needs evolve, this application will continue to improve and expand to meet new challenges that will arise.

REFERENCES

- [1] Fisher, J. & Lay, P. (2018). "Impact of Mobile Financial Applications on Personal Financial Management". *Journal of Financial Management*, 24(2), 123-136.
- [2] Riquelme, H. & Rios, R. (2019). "The Role of Technology in Business Financial Management". *Small Business Economics*, 36(4), 411-425.
- [3] Chen, S., Davis, T. & Wang, J. (2020). "User Interface Design and Its Impact on Financial Application Efficiency". *International Journal of Human-Computer Studies*, 142, 102456.
- [4] Kapoor, K. & Gunta, S. (2021). "Data Security and Privacy in Financial Applications". *Cybersecurity Journal*, 8(1), 78-89.
- [5] Brown, A. & Black, E. (2022). "Financial Education Through Mobile Applications: A New Paradigm". *Journal of Financial Education*, 15(3), 215-230.
- [6] Suryadevara, R., & Babu, G. (2020). "Personalized Financial Recommendations Using AI and Machine Learning". *Journal of Financial Technology*, 12(1), 89-103.
- [7] Kaczorowski, R., Lee, M., & Jackson, P. (2021). "Impact of Financial Apps on Financial Control and Stress Reduction". *Journal of Behavioral Finance*, 14(2), 112-127.
- [8] Johansson, K., & Olsson, M. (2021). "Financial Applications and Strategic Decision Making in Businesses". *Strategic Management Journal*, 32(3), 233-248.
- [9] Doe, J. (2020). *Financial Management in the Digital Age*. New York: Tech Press.
- [10] Johnson, K. (2021). *Best Practices in Financial Technology*. London: FinTech Publishers.
- [11] Angular Official Documentation, "Introduction to Angular," Angular.io
- [12] Microsoft .NET Documentation, "Introduction to .NET," Microsoft Docs
- [13] Microsoft SQL Server: <https://docs.microsoft.com/en-us/sql/sql-server/>
- [14] Synchorus, "Syncfusion Dashboard Visualization," .NET, Xamarin, JavaScript, Angular UI components | Syncfusion
- [15] OAuth 2.0 Authorization Framework: <https://oauth.net/2/>
- [16] Kenichi Ohmae, "The Mind of the Strategist: The Art of Japanese Business", 1982.
- [17] User Interface Design Principles: <https://www.interaction-design.org/literature/topics/ui-design>.

Comparison of Phosphorus Removal Performance and Characteristics of Dried and Undried MgFe Layered Double Hydroxides

Hüseyin Yazıcı*¹, Mustafa Karaboyacı²

Abstract: Layered double hydroxides (LDHs) are a versatile group of two-dimensional lamellar anionic clays with brucite-like layers composed of a mixture of di-, tri- and tetra-valent metallic cations and a monovalent anion. LDHs have received increasing attention in recent years due to their specific properties, including high anion exchange capacity and enhanced selectivity for a specific pollutant, ease of tunability of the composition, and low cost. In order to optimize their performance, tremendous strategies, such as the architecture and morphology control, the pH of synthesis, the ageing time, the temperature, or the drying temperature, have been applied. Drying process is a critical step to eliminate water from synthesized wet nanoparticles. It has been demonstrated by several studies that the drying parameters (drying time and temperature) had greatly impacted the LDHs performance and their physiochemical properties. However, to the authors' best knowledge, performance of the undried (wet) LDHs (LDH_w) has not yet been investigated in the literature until now. Therefore, an attempt was made to compare the phosphorus (P) removal performance between the dried MgFe LDHs and LDH_w samples in this study. For this purpose, the as-precipitated MgFe LDHs were subjected to the conventional oven-drying process at 50 °C, 75 °C and 105 °C. The P removal performance of the dried samples was investigated as a function of pH (4.5 and 7.0) and particle size (355 µm and 64 µm). The experimental results from the methylene blue adsorption test showed that none of the tested samples were able to remove methylene blue due to its cationic nature. However, the P removal performance of the LDH_w was higher than that of the dried samples in all cases. At an initial P concentration of 50 mg PO₄³⁻-P/L, the removal efficiency of the LDH_w was determined to be 94.5% and 76.6% at pH 4.5 and 7.0, respectively, while the P removal performance of the dried samples (≤64 µm) varied in the range of 65.7% and 57.0% at pH 4.5 and 45.6% and 42.9% at pH 7.0. The dried samples sieved through 355 µm showed lower P removal performances compared to those obtained for the 64 µm-sieved samples. Results of the settling test performed in graduated cylinders revealed that the LDH_w sample occupied considerably more volume than the dried samples even after 48 h. This result indicated that the drying process resulted in a severe agglomeration of LDHs, leading to a significant decrease in their volume. This was further confirmed by images from microscopic examination and micrographs from scanning electron microscopy (SEM). The Fourier transformation infrared (FTIR) analysis showed that there were no significant differences in the functional groups of the dried and LDH_w samples, while X-ray diffraction (XRD) analysis confirmed that the dried samples exhibited a weakened crystalline structure as compared to the LDH_w. This study clearly demonstrates that the conventional oven-drying process resulted in a remarkable decrease in the P removal performance of MgFe LDHs and suggests that it should be better to use MgFe LDHs as wet nanoparticles without oven-drying.

Keywords: Layered double hydroxides, phosphorus, removal, dried LDHs, undried LDHs.

¹**Address:** Isparta University of Applied Sciences, Vocational School of Aksu Mehmet Süreyya Demiraslan, Department of Environmental Protection Technologies, 32510, Isparta, Türkiye

²**Address:** Süleyman Demirel University, Faculty of Engineering, Department of Chemical Engineering, 32260, Isparta, Türkiye

***Corresponding author:** huseyinyazici@isparta.edu.tr

1. INTRODUCTION

Layered double hydroxides (LDHs), which are also known as hydrotalcite-like systems or anionic clays (Mohapatra and Parida, 2016), are materials with high porosity, two-dimensional morphology, and exceptionally tunable and exchangeable anionic particles with sensible interlayer spaces (Kameliya et al., 2023). LDHs are considered to be promising materials compared to the other layered materials due to their unique properties, such as high surface area, uniform distribution of different metal cations in the brucite layer, unique structure memory effect, intercalated anions with interlayer spaces, surface hydroxyl groups, flexible tunability, ease of synthesis, shape-selective ion exchange, and catalytic activity (Jijoe et al., 2021; Mishra et al., 2018). Due to these properties, LDHs have received a great attention in important areas such as photochemistry, polymerization, electrochemistry, catalysis, biomedical science, photocatalysis, adsorbent, magnetization and environmental applications (Mohapatra and Parida, 2016).

In order to optimize LDHs' performance, tremendous strategies, such as the architecture and morphology control, the pH of synthesis, the ageing time, the molar ratios of divalent and trivalent metals, some specific synthesis procedures, the temperature, or the drying temperature, have been investigated (Nyongombe et al., 2022). To discard water from wet nanoparticles and obtain a powdered material, drying process, which has been applied as a routine procedure in the preparation of LDHs (Zhang et al., 2020; Nuryadin et al., 2021; Yuan et al., 2023), is a critical step. To date, various drying techniques have been applied such as conventional oven-drying, spray drying, freeze-drying, and supercritical drying in the published literature (El Hassani et al., 2019).

It has been demonstrated by several studies that the drying parameters (drying time and temperature) had greatly impacted the LDHs performance and their physiochemical properties (El Hassani et al., 2019; Nyongombe et al., 2022). Neto et al. (2021) demonstrated that the drying parameters applied had greatly impacted the materials. The impacts have been investigated by several analyses, including FT-IR, SEM, and XRD. The FT-IR analysis showed some differences in bands intensities, while the SEM study depicted a tendency of increase in agglomeration. The results from the XRD analysis confirmed an increment in the crystallite size and an expansion in the basal spacing. As a result, they have demonstrated that the drying temperature, as well as the time, had greatly impacted the physical, structural, chemical and morphological properties of LDHs. However, to the authors' best knowledge, properties of the undried (wet) LDH (LDH_w) has not yet been investigated in the literature until now. Therefore, an attempt was made to compare the phosphorus (P) removal performance of the dried MgFe LDH samples and LDH_w sample in this study. For this purpose, the as-precipitated MgFe LDH precipitates were subjected to the conventional oven-drying process at different temperatures. To get a better understanding and interpret of the differences in the P removal performance of the examined samples, a settling test, microscopic examination and several characterization analyses (FT-IR, SEM and XRD) were conducted.

2. MATERIAL AND METHOD

2.1. Synthesis of MgFe LDH

All chemicals used in the experiments were of analytical grade and were used without further purification. All solutions were prepared with distilled water. Hydrochloric acid (HCl, 37 wt%), iron(III) chloride hexahydrate ($FeCl_3 \cdot 6H_2O$, >99%), magnesium chloride hexahydrate ($MgCl_2 \cdot 6H_2O$, >99%), methylene blue (MB, C.I. 52015), potassium dihydrogen phosphate (KH_2PO_4 , $\geq 99.5\%$) and sodium hydroxide (NaOH pellets, $\geq 99\%$) were purchased from Merck (Germany). Filter papers (Millipore AP40) were obtained from Merck Millipore (Germany).

The synthesis of MgFe LDH precipitates was performed according to a published procedure described by Mandel et al. (2013). Accordingly, a metal ion precursor solution was prepared by dissolving 3.66 g $MgCl_2 \cdot 6H_2O$ and 1.66 g $FeCl_3 \cdot 6H_2O$ in 100 mL deionized water. The prepared solution was slowly added into 400 mL of 0.15 M NaOH solution under stirring. The mixture was then neutralized with 3 M HCl solution until the pH was measured as ≈ 7.0 . A scale-up was done by increasing the volume of the solutions in order to prepare stock MgFe LDH suspensions. The stock suspensions were stored at room temperature and left undisturbed until further use. Before each use, the suspensions were stirred using a magnetic stirrer to homogenize the MgFe precipitates.

2.2. Preparation of dried and undried MgFe LDH materials

To investigate the effect of drying process on the P removal performance and characteristics of MgFe LDHs, dried and undried materials were used in this study. The dried materials were prepared by filtering the synthesized MgFe LDHs in order to eliminate liquid phase and then subjecting the filtered solids to conventional oven-drying procedure at 50 °C, 75 °C and 105 °C temperatures. The dried materials were labeled as LDH_{50} , LDH_{75} and LDH_{105} . The obtained materials were powdered using a grinder at 28000 rpm for 1 min, sieved using 355 μm and 64 μm sieves and stored in a

desiccator until further use. The undried (wet) material, which was labeled as LDH_w, was used directly as wet precipitates without drying the synthesized LDH precipitates. For experiments, the desired weight of the LDH_w precipitates was adjusted by sampling a known volume of suspension from the homogeneously stirred stock suspension. The solids concentration in the stock suspension of LDH_w was determined from the dry weight per volume of suspension after the synthesis. To measure the dry weight of the LDH_w precipitates, a known volume of sample was taken and then filtered through a filter paper (Millipore AP40). Drying of the filter paper was carried out in an oven at 105 °C for 1 h.

2.3. Experiments and measurements

The effect of drying process on the P removal performance of the dried (LDH₅₀, LDH₇₅ and LDH₁₀₅) and LDH_w materials was investigated as a function of medium pH and particle size. For this purpose, a series of experiments was carried out in batch mode through magnetic stirrers under the initial pH conditions of 4.5 and 7.0. In these experiments, the dried materials that were sieved through 355 μm and 64 μm sieves were tested to compare their P removal ability with that of the LDH_w material.

For the experiments performed with the dried materials, a desired volume of stock P solution, of which the initial P concentration was adjusted to 50 mg PO₄³⁻-P/L, was prepared by dissolving an appropriate amount of KH₂PO₄ in distilled water. In each experimental run with the dried materials, 1 L of the P solution was added 1000 mg of the dried materials. For the experiments performed with the LDH_w material, a known volume of the stock MgFe suspension containing 1000 mg LDH_w material was transferred into a 1 L beaker through a peristaltic pump. Then, the final volume was made up to 1 L by adding 750 mL of a P solution which was prepared separately. To achieve an initial P concentration of 50 mg PO₄³⁻-P/L in the final mixture, the initial P concentration in the stock P solution was adjusted to 66.6 mg PO₄³⁻-P/L by taking a dilution factor of 0.25 into account due to the dilution in the final mixture. For each of the prepared stock P solutions, the initial P concentrations were measured to confirm the exact concentration. The initial pH values of the test solutions were adjusted using 0.5 M HCl and 0.5 M NaOH solutions and measured using a portable pH meter (Milwaukee Mi150). The mixtures were then stirred at 350 rpm in a magnetic stirrer during 60 min. At the end of the reaction time, 25 mL of the mixtures were sampled and filtered through the filter paper. Residual P concentrations in the filtrate samples were measured by the vanadomolybdate method using Merck test kit (114842) in an ultraviolet-visible spectrophotometer (Hach DR6000). According to the obtained data, the removal efficiencies were calculated by the following equation (Li et al., 2020):

$$\text{Removal efficiency (\%)} = \frac{c_i - c_f}{c_f} * 100 \quad (1)$$

where; C_i and C_f are the initial and the residual P concentrations in the final mixture (in mg/L), respectively.

To investigate the MB removal performance of the examined materials, another set of removal experiments was carried out in batch mode through magnetic stirrers. For this purpose, the standard test procedure of the International Organization for Standardization (ISO 21340:2017(E)) was followed. To estimate the density of the materials, a settling test was performed in graduated cylinders by suspending 1000 mg of the dried materials sieved through 64 μm sieve in 250 mL distilled water. For the LDH_w material, a known volume of the stock MgFe LDH suspension containing 1000 mg LDH_w material was transferred into another graduated cylinder and the final volume was made up to 250 mL with distilled water. The settled volume of the materials was measured at different time intervals.

2.4. Characterization of the materials

Characterization of the materials (LDH₅₀ sieved through 64 μm sieve as a selected material and the LDH_w) was performed using various analysis techniques. Microscopic examination of the materials was performed using a microscope (Leica DM2500) equipped with a digital microscope color camera (Leica DFC295). Functional groups were determined through an attenuated total reflectance (ATR) Fourier transformation infrared (FT-IR) spectrophotometer (Shimadzu IRPrestige 21) with a resolution of 4 cm⁻¹. The morphology of the materials was investigated using a scanning electron microscopy equipped with an energy dispersive spectrometer (EDS) system (FEI Quanta 250 FEG). The crystal structure of the materials was investigated by X-ray diffraction (XRD) analysis conducted on an X-ray diffractometer (Bruker D8 Advance) employing a CuKα radiation (λ = 0.15418 nm). Data were collected in the range of 2θ (20°-90°) with an angular step of 0.02° at a scanning speed of 2.5°/s. For the LDH₅₀ material, powdered samples were used for FT-IR, SEM and XRD analysis, while its slurry form was prepared for the microscopic examination by suspending the powdered sample in distilled water. For the characterization of LDH_w material by SEM and XRD analysis, the stock MgFe LDH suspension was filtered, and the resulting slurry form of the material was used to minimize potential incorrect reflections that could arise from the water content of the material.

3. RESULTS

3.1. P removal performance of the materials

The effect of drying process on the removal ability of the examined materials was investigated for P (as an anionic species) and MB (as a cationic species) removal. The experimental results from the MB removal tests showed that none of the examined materials were able to remove MB under the standard experimental conditions of ISO 21340:2017(E) (data

now shown). To achieve comparable results between the examined materials, P removal ability of the materials was investigated as a function of medium pH (4.5 and 7.0) and particle size (355 μm and 64 μm). The experimental results from the P removal tests showed that relatively high removal performances were obtained at pH 4.5 than those obtained at pH 7.0 for all of the tested materials (Fig. 1). The removal efficiency for the LDH_w was determined to be 94.5% and 76.6% at pH 4.5 and 7.0, respectively.

As compared to the LDH_w, relatively low removal performances were obtained for the dried materials under any given pH condition. The highest P removal efficiencies for the dried materials were obtained for the materials that were sieved through 64 μm sieve for both pH conditions. The removal efficiency for the dried materials that were sieved through 64 μm sieve ranged between 57.0% and 65.7% at pH 4.5 and 45.3% and 49.2%, while the removal efficiency for the dried materials that were sieved through 355 μm sieve ranged between 41.3% and 45.6% at pH 4.5 and 29.0% and 31.8% at pH 7.0. Under the examined pH and particle size conditions, the highest P removal performances were obtained for the LDH₅₀ material. Therefore, among the dried materials, the LDH₅₀ material was selected for characterization analyses.

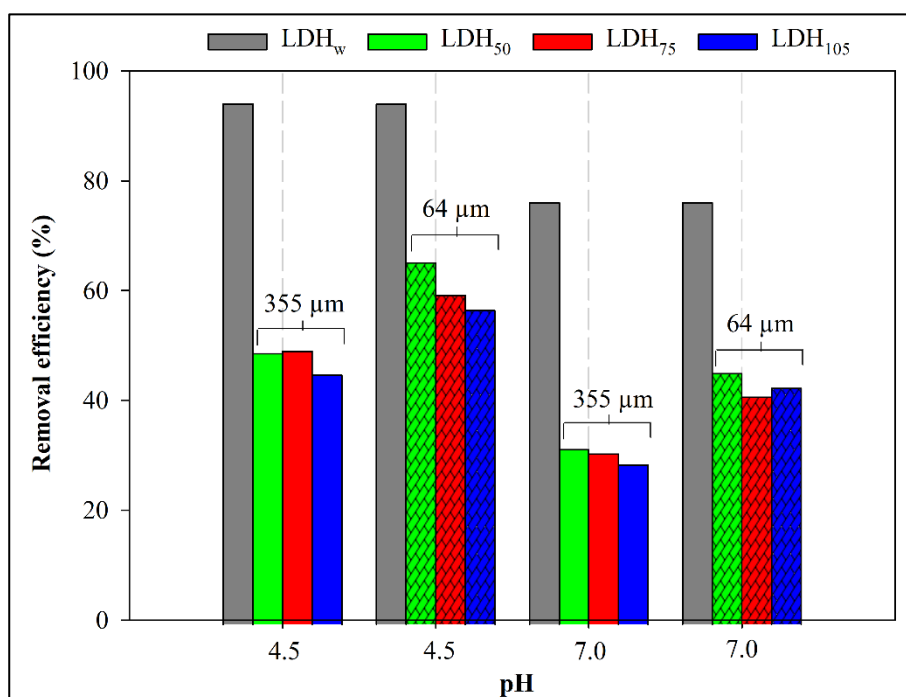


Figure 1. P removal efficiency of the dried samples and LDH_w sample as a function of pH and particle size (The bars with pattern fill represent the dried samples which were sieved through a 64 μm sieve) (Experimental conditions: C_i: 50 mg PO₄³⁻-P/L, reaction time: 60 min, mixing speed: 350 rpm, volume of the final mixture: 1000 mL, amount of MgFe LDH: 1000 mg)

3.2. Characterization of the materials

3.2.1. Settling test

At the end of the P removal tests, it was observed that there was a significant difference in the settled volume of the examined materials although equal amount of materials (1000 mg) was used in the removal tests. While the dried materials settled rapidly and formed a thin settled layer at the bottom of the beakers, the LDH_w material occupied a certain volume in the beaker after a certain settling time (Fig. 2).



Figure 2. Settling behavior of the materials after the P removal tests (Samples in the beakers from left to right: LDH_w, LDH₅₀, LDH₇₅, LDH₁₀₅)

To gain better understanding for the reason of the different P removal performances between the examined materials, a settling test was performed depending on the abovementioned observation. As can be seen from Fig. 3a, the dried materials rapidly settled within 2 min, while the LDH_w could settle very slowly during the same time. After 2 h, only about 50 mL of the LDH_w material could settle, while the turbidity in the other cylinders resulting from the suspended particles in the suspensions of the dried materials decreased further. (Fig. 3b). The settled volume of the LDH_w was recorded as nearly 90 mL after 23 h (Fig. 3c), and no more settling occurred after 48 h (Fig. 3d).

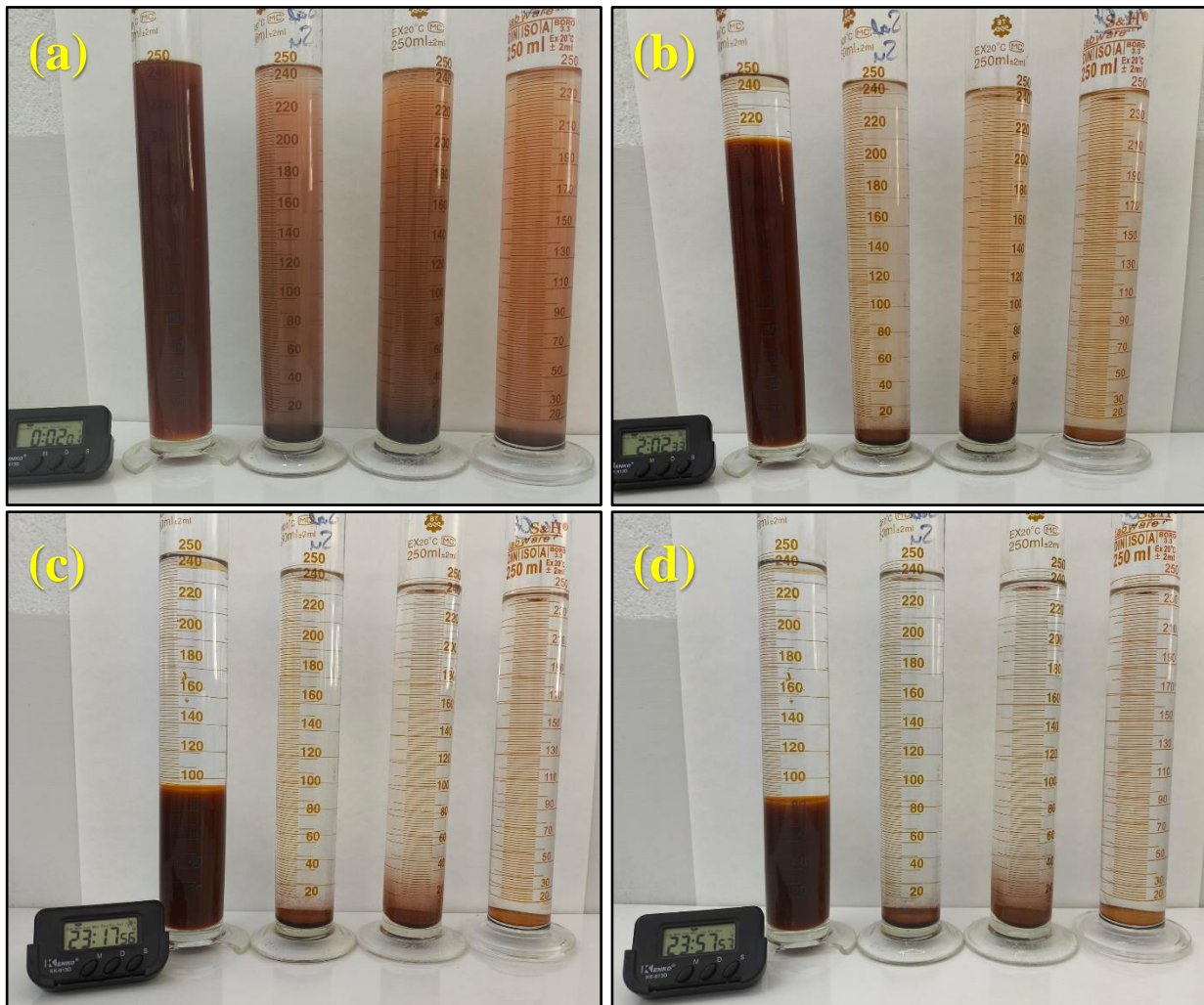


Figure 3. Images from the settling test for LDH_w and dried LDH samples (Samples in the cylinders from left to right: LDH_w, LDH₅₀, LDH₇₅, LDH₁₀₅; Volume of the settled samples after 2 min (a), 30 min (b), 23 h (c), and 48 h (d))

3.2.2. Microscopic examination and SEM analysis

The effect of the oven-drying process was investigated through microscopic examination, and the images from the examination were represented in Fig. 4. As can be seen from the images, the particles in the LDH_w material were quite different in both size and shape as compared the particles of the LDH₅₀ material. While the particles of the LDH_w material were smaller in size, relatively spherical in shape and more dispersed in the liquid space (Fig. 4a and c), the particles of the LDH₅₀ material were agglomerated to larger and relatively flake-shaped clusters (Fig. 4b and d).

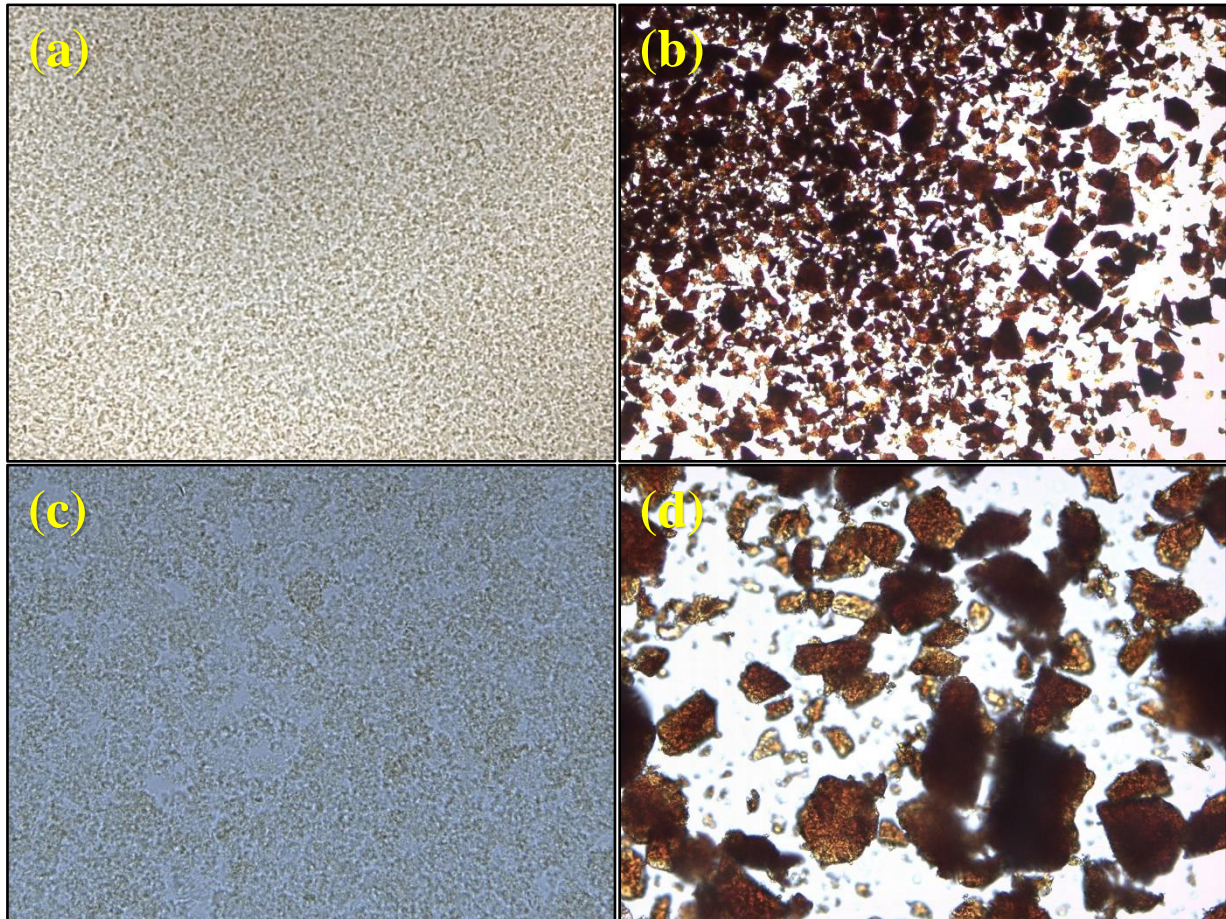


Figure 4. Images from the microscopic examination for LDH_w (a and c) and LDH₅₀ samples (b and d) (Magnification: x10 (a and b), x40 (c and d))

The morphological differences between the LDH_w and LDH₅₀ materials were investigated by SEM analysis, and the micrographs were presented in Fig. 5. SEM micrographs for the LDH_w showed a “sponge-like” porous structure (Fig. 5a, c and e) including submicron-sized spherical crystallites (Fig. 5g), while denser and flat particles with obvious edges were clearly seen from the micrographs of the LDH₅₀ (Fig 5b and h). Formation of a “flake-like” micron-sized particles with irregular shape was more obviously seen in Fig. 5d and f.

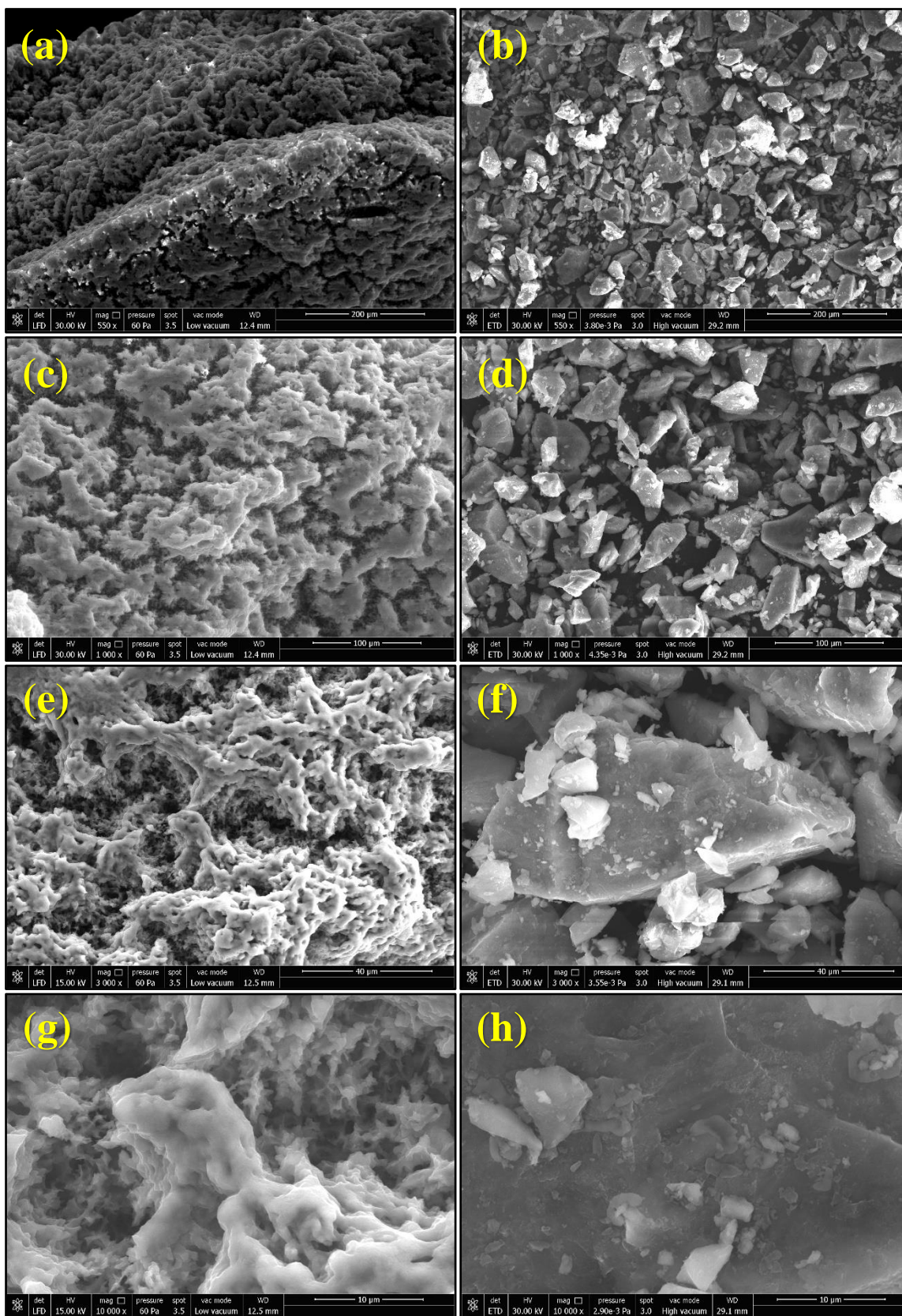


Figure 5. SEM micrographs of LDH_w (a, c, e, g) and LDH₅₀ samples (b, d, f, h) (Magnification: 0.55K (a and b), 1K (c and d), 3K (e and f), 10K (g and h))

3.2.3. FT-IR and XRD analysis

The FT-IR spectra of the LDH_w and LDH₅₀ materials were presented in Fig. 6. The spectrum for the LDH_w (the red spectrum) showed the typical FT-IR spectrum of MgFe LDHs which exhibited various characteristic peaks at 421, 562, 1637 and 3352 cm⁻¹ wavelengths. The broad band appeared at 3352 cm⁻¹ corresponded to the O-H groups vibrations from physically adsorbed water molecules presented in the interlayer (da Silva et al., 2021). The peak appeared at 1637 cm⁻¹ could be assigned to the bending vibration of interlamellar water (Hidayati et al., 2019). The bands between 400 and 900 cm⁻¹ were attributed to the lattice vibrations of M-O, M-OH, or M-O-M bonds (where M were metal (Mg or Fe) ions) (Lee et al., 2012; Yan et al., 2015; Xia et al., 2023).

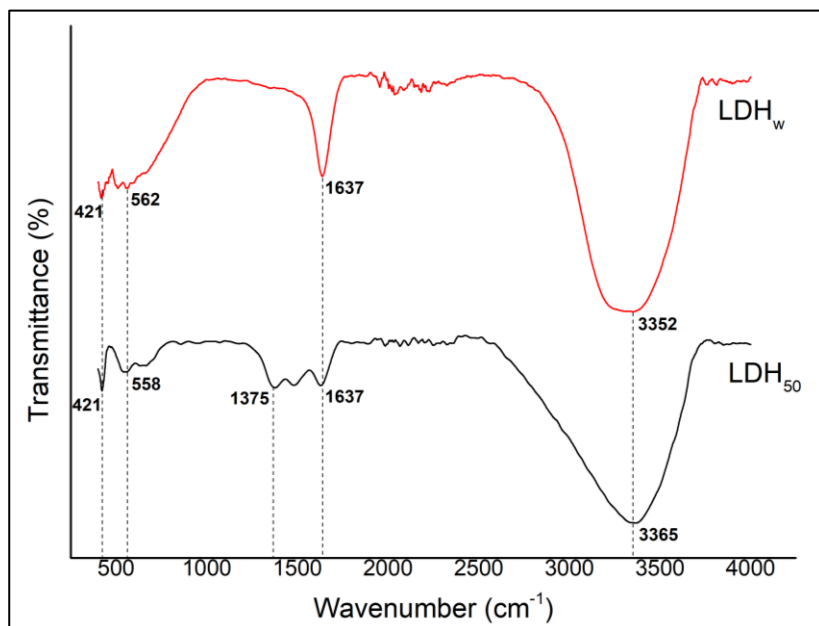


Figure 6. FT-IR spectra of LDH_w and LDH₅₀ materials

The XRD diffractograms of the LDH_w and LDH₅₀ materials were illustrated in Fig. 7. The diffractogram for the LDH_w (the black diffractogram) showed intense and sharp peaks at 2 θ of 22.7°, 33.8°, 59.2° and 60.6° with the corresponding reflections (006), (012), (110), (113), respectively. However, these peaks appeared as weaker peaks in the diffractogram for the LDH₅₀ (the blue diffractogram) since the intensity and width of the peaks decreased as compared to those obtained for the LDH_w.

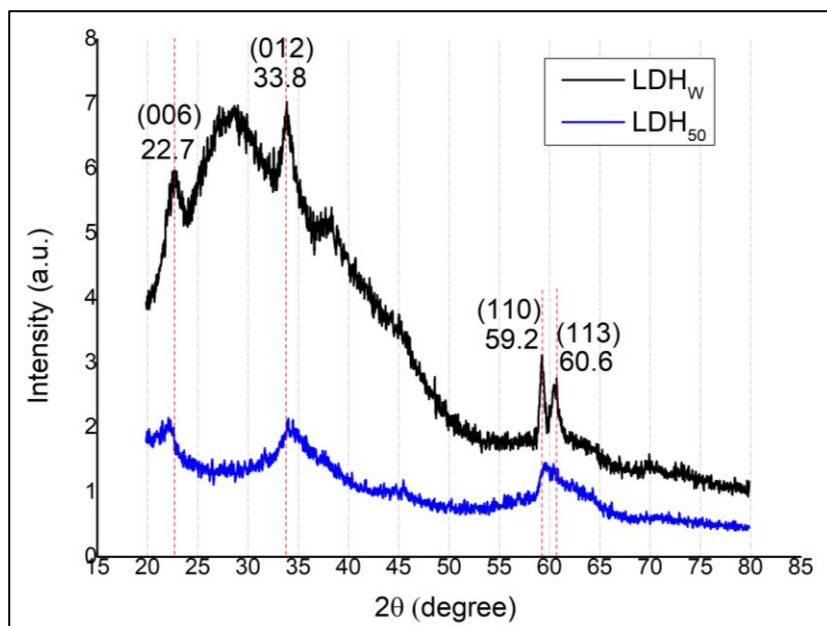


Figure 7. XRD diffractograms of LDH_w and LDH₅₀ materials

4. DISCUSSION AND COCNLUSIONS

Although several studies demonstrated that it could be possible to remove MB using LDH-based materials (Trujillano et al., 2023; Nazir et al., 2024), the failure of the examined materials for MB removal in the current study was attributed to that the anion selective LDH material required a specific tailoring procedure for the cationic nature of MB.

Experimental results from the P removal tests indicated that the P removal performance of the dried materials and LDH_w material increased as the pH decreased, and that the P removal performance of the dried materials increased as the particle size decreased. The obtained results were in agreement with the results of earlier studies (Yang et al, 2006; Qiao et al., 2019; Zhang et al., 2023). In addition to these results, it could be concluded that the increasing drying temperature resulted in a slight decrease in the P removal performance of the dried materials. Neto et al. (2021) showed that the average pore diameter of MgAl LDHs decreased with the increasing drying temperature. Therefore, the decrease in the P removal performance of the dried materials with the increasing drying temperature could be attributed to the possible changes in the textural properties of the materials, such as a decrease in the specific surface area, or an increase in the average crystallites sizes. In conclusion, the LDH_w material exhibited higher P removal performances in all cases as compared to the dried materials.

The results of the settling test revealed that the LDH_w material was more voluminous than the dried materials, meaning that the LDH_w material had a lower density compared to the dried materials. This could be attributed to the fact that the oven-drying process caused a severe agglomeration and, consequently, the particles of the as-precipitated MgFe LDH were packed in large clusters. Thus, the crystallites became denser as a result of the structural and morphological changes. Less agglomeration observed for the LDH_w particles was further corroborated with the images obtained from the microscopic examination and the SEM analysis. Neto et al. (2021), who studied the effect of drying temperature on the properties of MgAl LDH, reported that an increase in drying temperature caused an elevation of aggregates, as which was clearly seen from SEM micrographs. Bal et al. (2023) also showed that a decrease in the temperature from 100 °C to 80 °C during the synthesis of MgAl-NO₃ LDH resulted in a decrease in the particle size.

FT-IR analysis showed that the intensities and positions of the peaks at 421 and 562 cm⁻¹ remained almost the same for the LDH₅₀ material. This meant that the oven-drying process did not have any effect on the characteristic metal-based functional groups of the MgFe LDH. However, there were some major spectral changes in the spectrum of the examined materials. These changes were observed for the peaks at 3352 and 1637 cm⁻¹, which were related to the interlamellar water or physically adsorbed water in the interlayer. The observed spectral changes between the LDH_w and LDH₅₀ materials revealed that the oven-drying process had a significant effect only on the water-related functional groups. After eliminating the water from the material, the intensity and width of the peak at 3352 cm⁻¹ increased, whereas the intensity of the peak at 1637 cm⁻¹ decreased and a new peak appeared at 1375 cm⁻¹. Similar results were also reported by Neto et al. (2021). The obtained results from FT-IR analysis clearly suggested that the dried materials could still remove P up to a certain level due to the undisturbed metal-based functional groups although they exhibited some structural and physical changes as compared to the LDH_w. XRD analysis revealed that the LDH_w material exhibited the characteristic reflections of MgFe LDH, as reported in previous studies (Kim et al., 2020; Zubair et al., 2025). From the XRD diffractogram of the LDH₅₀ material, it was clearly understood that the drying process caused significant changes in the crystal structure of the material. Neto et al. (2021) reported that the decrease in the basal spacing parameter, which is related to the lamellar layer thickness and the distance between these lamellae, increased with the increase in drying temperature, thus causing a change in the crystal structure.

Overall, it could be concluded that the conventional oven-drying process altered the physical and structural properties of the MgFe LDH material and, consequently, caused a significant decrease in the P removal ability of the material. The results of the current suggest that it would be better to use MgFe LDH material as wet nanoparticles without subjecting it to any drying process in an oven. It should be noteworthy to mention that eliminating the extra costs and time-consuming procedures arising from drying and grinding of the material would also allow to develop a more feasible water treatment technology. However, it is strongly recommended that future research efforts could be paid to examine the findings of the current study through more comprehensive analyses.

Acknowledgements

The authors appreciate Asst. Prof. Halit Bayrak's generous help and efforts in the use of the microscope.

Ethics Committee Approval

N/A

Peer-review

Externally peer-reviewed.

Author Contributions

Hüseyin Yazıcı: Conceptualization, Investigation, Material and Methodology, Supervision, Visualization, Writing-Original Draft, Writing-review & Editing, Other. **Mustafa Karaboyacı:** Conceptualization, Investigation, Material and Methodology, Supervision, Visualization, Writing-Original Draft, Writing-review & Editing, Other. All authors have read and agreed to the published version of manuscript.

Conflict of Interest

The authors declare that they have no known competing financial interests or personal relationships that could have appeared to influence the work reported in this paper.

Funding

The authors declare that this study has received no financial support.

REFERENCES

- Bal, K., Şentürk, S., Kaplan, Ö., Gök, M.K., Pabuccuoğlu, S.K. (2023). Optimization studies of Mg/Al-NO₃ layered double hydroxide nanoparticles by hydrothermal treatment. *ALKU Journal of Science*. 5(3), 163-175. <https://doi.org/10.46740/alku.1370872>.
- El Hassani, K., Jabkhiro, H., Kalnina, D., Beakou, B.H., Anouar, A. (2019). Effect of drying step on layered double hydroxides properties: Application in reactive dye intercalation. *Applied Clay Science*. 182, 105246. <https://doi.org/10.1016/j.clay.2019.105246>.
- Hidayati, N., Apriliani, D. R., Taher, T., Mohadi, R., Lesbani, A. (2019). Adsorption of congo red using Mg/Fe and Ni/Fe layered double hydroxides. *Journal of Physics: Conference Series*. 1282(1), 012075. <https://doi.org/10.1088/1742-6596/1282/1/012075>.
- ISO 21340:2017(E), 2017. Test methods for fibrous activated carbon. International Organization for Standardization. Geneva, Switzerland, p. 34.
- Jijoe, P.S., Yashas, S.R., Shivaraju, H.P. (2021). Fundamentals, synthesis, characterization and environmental applications of layered double hydroxides: A review. *Environmental Chemistry Letters*, 19(3), 2643-2661. <https://doi.org/10.1007/s10311-021-01200-3>.
- Kameliya, J., Verma, A., Dutta, P., Arora, C., Vyas, S., Varma, R.S. (2023). Layered double hydroxide materials: A review on their preparation, characterization, and applications. *Inorganics*. 11, 121. <https://doi.org/10.3390/inorganics11030121>.
- Kim, T.H., Lundehøj, L., Nielsen, U.G. (2020). An investigation of the phosphate removal mechanism by MgFe layered double hydroxides. *Applied Clay Science*. 189, 105521. <https://doi.org/10.1016/j.clay.2020.105521>.
- Lee, J.S., Lee, E.J., Hwang, H.J. (2012). Synthesis of Fe₃O₄-coated silica aerogel nanocomposites. *Transactions of Nonferrous Metals Society of China*. 22(3), 702-706. [https://doi.org/10.1016/S1003-6326\(12\)61790-7](https://doi.org/10.1016/S1003-6326(12)61790-7).
- Li, F., Jin, J., Shen, Z., Ji, H., Yang, M., Yin, Y. (2020). Removal and recovery of phosphate and fluoride from water with reusable mesoporous Fe₃O₄@mSiO₂@mLDH composites as sorbents. *Journal of Hazardous Materials*. 388, 121734. <https://doi.org/10.1016/j.jhazmat.2019.121734>.
- Mandel, K., Drenkova-Tuhtan, A., Hutter, F., Gellermann, C., Steinmetzc, H., SEXTL, G. (2013). Layered double hydroxide ion exchangers on superparamagnetic microparticles for recovery of phosphate from waste water, *Journal of Materials Chemistry A*. 1(5), 1840-1848, <https://doi.org/10.1039/C2TA00571A>.
- Mishra, G., Dash, B., Pandey, S. (2018). Layered double hydroxides: A brief review from fundamentals to application as evolving biomaterials. *Applied Clay Science*. 153, 172-186. <https://doi.org/10.1016/j.clay.2017.12.021>.

- Mohapatra, L., Parida, K. (2016). A review on the recent progress, challenges and perspective of layered double hydroxides as promising photocatalysts. *Journal of Materials Chemistry A*. 4(28), 10744-10766. <https://doi.org/10.1039/C6TA01668E>.
- Nazir, M.A., ur Rehman, A., Najam, T., Elsadek, M.F., Ali, M.A., Hossain, I., Tufail, M.K., Shah, S.S.A. (2024). Copper- and manganese-based bimetallic layered double hydroxides for catalytic reduction of methylene blue. *Catalysts*. 14, 430. <https://doi.org/10.3390/catal14070430>.
- Neto, L.D.S, Anchieta, C.G., Duarte, J.L., Meili, L., Freire, J.T. (2021). Effect of drying on the fabrication of MgAl layered double hydroxides. *ACS Omega*. 6(33), 21819-21829. <https://doi.org/10.1021/acsomega.1c03581>.
- Nuryadin, A., Imai, T., Kanno, A., Yamamoto, K., Sekine, M., Higuchi, T. (2021). Phosphate adsorption and desorption on two-stage synthesized amorphous-ZrO₂/Mg-Fe layered double hydroxide composite. *Materials Chemistry and Physics*. 266, 124559. <https://doi.org/10.1016/j.matchemphys.2021.124559>.
- Nyongombe, G., Kabongo, G.L., Bello, I.T., Noto, L.L., Dhlamini, M.S. (2022). The impact of drying temperature on the crystalline domain and the electrochemical performance of NiCoAl-LDH. *Energy Reports*. 8, 1151-1158. <https://doi.org/10.1016/j.egy.2021.12.042>
- Qiao, W., Bai, H., Tang, T., Miao, J., Yang, Q. (2019). Recovery and utilization of phosphorus in wastewater by magnetic Fe₃O₄/Zn-Al-Fe-La layered double hydroxides (LDHs). *Colloids and Surfaces A: Physicochemical and Engineering Aspects*. 577, 118-128. <https://doi.org/10.1016/j.colsurfa.2019.05.046>.
- da Silva, A.F., da Silva Duarte, J.L., & Meili, L. (2021). Different routes for MgFe/LDH synthesis and application to remove pollutants of emerging concern. *Separation and Purification Technology*, 264, 118353. <https://doi.org/10.1016/j.seppur.2021.118353>.
- Trujillano, R., Rives, V., Miguel, R., González, B. (2023). Preparation of original and calcined layered double hydroxide as low-cost adsorbents: the role of the trivalent cation on methylene blue adsorption. *Molecules*. 28, 4717. <https://doi.org/10.3390/molecules28124717>.
- Xia, C., Li, X., Xie, Y., Kong, F., Zhao, M., Wang, Y., Wang, Y., Zhang, Q., Meng, Z. (2023). An effective strategy for removing tetracycline from water: Enhanced adsorption reliability and capacity by tyrosine modified layered hydroxides. *Journal of Environmental Chemical Engineering*. 11(1), 109172. <https://doi.org/10.1016/j.jece.2022.109172>.
- Yan, L., Yang, K., Shan, R., Yan, T., Wei, J., Yu, S., Yu, H., Du, B. (2015). Kinetic, isotherm and thermodynamic investigations of phosphate adsorption onto core-shell Fe₃O₄@LDHs composites with easy magnetic separation assistance. *Journal of Colloid and Interface Science*. 448, 508-516. <https://doi.org/10.1016/j.jcis.2015.02.048>.
- Yang, L., Dadwhal, M., Shahrivari, Z., Ostwal, M., Liu, P.K., Sahimi, M., Tsotsis, T.T. (2006). Adsorption of arsenic on layered double hydroxides: Effect of the particle size. *Industrial & Engineering Chemistry Research*. 45(13), 4742-4751. <https://doi.org/10.1021/ie051457q>.
- Yuan, M., Qiu, S., Li, M., Di, Z., Feng, M., Guo, C., Fu, W., Zhang, K., Hu, W., Wang, F. (2023). Enhancing phosphate removal performance in water using La-Ca/Fe-LDH: La loading alleviates ineffective stacking of laminates and increases the number of active adsorption sites. *Journal of Cleaner Production*. 388, 135857. <https://doi.org/10.1016/j.jclepro.2023.135857>.
- Zhang, X., Yan, L., Li, J., Yu, H. (2020). Adsorption of heavy metals by L-cysteine intercalated layered double hydroxide: Kinetic, isothermal and mechanistic studies. *Journal of Colloid and Interface Science*. 562, 149-158. <https://doi.org/10.1016/j.jcis.2019.12.028>.
- Zhang, H., Chonan, A., Zou, M., Bat-Amgalan, M., Miyamoto, N., Kano, N., Zhang, S. (2023). A study of the recovery of phosphorus from aqueous solutions using Zr-doped MgMn-layered double hydroxide (MgMnZr-LDH). *Water*. 15, 3420. <https://doi.org/10.3390/w15193420>.
- Zubair, Y.O., Fuchida, S., Oyama, K., Tokoro, C. (2025). Morphologically controlled synthesis of MgFe-LDH using MgO and succinic acid for enhanced arsenic adsorption: Kinetics, equilibrium, and mechanism studies. *Journal of Environmental Sciences*. 148, 637-649. <https://doi.org/10.1016/j.jes.2024.01.049>.

Application Of GIS And Remote Sensing for Solid Waste Management

Muhammad Ishaq Iqbal

Abstract: Safe disposal of solid waste is most important step in solid waste management. In this paper an effort has been made to identify suitable sites for safe disposal of municipal and other solid waste generated in Peshawar City District. Selection of suitable site depends on a number of factors to ensure environment friendly disposal of solid waste. To make sure that a proper location is selected, an organized procedure must be developed and followed. For analysis and identification of suitable site, SPOT satellite image of 2010 was the main source of data for the study. Topographic sheets of the whole district were used as a database. Different types of layers like Road, Rivers, airport and Contours were also drawn from the topographic sheets. Water table data was collected from District Health Office and field survey. Using multi-criteria analysis in Arc GIS 9.3 software, surfaces were generated for all these layers with spatial analysis tools. Different weights were given to these layers for creation of weight maps. The sites were selected in such a way as to have minimum environmental consequences. Suitable sites were suggested using the EPA parameters for selection of landfill site. Several important criteria taken in the present study were; distance from residential areas, distance from airport, distance from water bodies, accessibility, water table, land values, stability of slope and land use pattern. Rivers and built up areas were restricted. Based on these criteria the whole city district was divided into three regions i.e least suitable, moderately suitable and most suitable. The most suitable sites were located mostly in southern parts of the district where weights of suitability were the highest.

Keywords: Accessibility, Suitability, Land use pattern, Land values, EPA parameters.

¹**Address:** University of Peshawar, Pakistan

***Corresponding author:** atta_urp@yahoo.com

This study is based on the collection of primary and secondary data. The procedure for data collection is as follows: Satellite image of 2010 of Peshawar city was the main source of data for the study. Topographic sheets of the district Peshawar were used as a database. First of all the topographic sheets and satellite image were Georeferenced using tie points. Lambert Conformal Conic coordinate system was retained in this process. The other layers like 3 rivers, major roads, contours were digitized from the topographic maps. For these purpose topographic sheets of scale 1:50,000 were used. Ground water table data was obtained from District Health Office as well as from the field. Data for ground water table was converted into surfaces using IDW interpolation technique. Literature about the solid waste was collected from different books, articles and journals.

GIS 9.3 was the main software used for analysis. ERDAS IMAGINE was used for image enhancement and analysis. While Arc GIS was used for the final analysis of the layers. Then the satellite image was classified for different land uses to get the land use layer. These layers were interpolated in the Arc Map followed by reclassification of the interpolated surfaces. New numerical values were given to different classes for analysis. Finally, all these raster surfaces were combined in the raster calculator. Then this combined weighted map was reclassified for the identification of final map. Areas with lowest weights were assigned as least suitable while areas with highest weights were assigned as the most suitable location with minimum environmental consequences. Pakistan Environmental Protection Agency (EPA) has established following guidelines for solid waste management that were incorporated in this study. Adequate land area and volume to provide the landfill capacity to meet projected needs for at least twenty five years, so that costly investments in access roads, drainage, fencing and weighing stations are justifiable.

The land should not be in areas where adequate buffer zones are not available or in areas immediately upwind of a residential area in the prevailing wind direction(s). Areas characterized by steep gradients, where stability of slopes could be/are problematic. The seasonally high table level (i.e. 10 year high) of the groundwater should be below the proposed base of any excavation or site preparation to enable landfill development. No environmentally significant wetlands of important biodiversity or reproductive value, sensitive ecological and/or historical areas should be present within the potential area of the landfill development. There should be no private or public irrigation, or livestock water supply wells down-gradient of the landfill boundaries because they are at risk from contamination -alternative water supply sources are readily and economically available.

RESULTS

The analysis was based mainly on the parameters taken from guidelines of Environmental Protection Agency (EPA) of Pakistan. The selection of suitable sites required different information about the geographical conditions of Peshawar city district. Parameters necessary for the process of selection of suitable disposal sites are described with Figures below.

DISCUSSION AND CONCLUSIONS

Use of technology for real life problems have made it easy to find their proper solution without wastage of time and resources. The analysis criteria used in the identification of suitable sites for solid waste disposal in Peshawar city district indicated that using the GIS/RS technology can help local planning authorities to identify proper disposal sites. Presently solid waste is disposed at open spaces just outside the municipal boundary creating health hazards for the surrounding population. Some of the waste is 13 thrown to larger water channels particularly the Bara river, making its water unfit for drinking purpose. GIS is now most widely used instrument to assist in the finding of suitable sites for landfill siting purposes. Using GIS for assessment of potential dumping sites will save time and resources. Usually local planning authorities have only limited resources and expertise to execute a sustainable siting procedure which causes considerable harm to the environment. This requires analysis of a great deal of spatial information and factors that can affect the optimum selection of site. Though there is a limitation of data availability. For this study seven different thematic layers were taken for GIS analysis. Some other factors like industrial areas, geological structure and wind direction that may also affect the siting of sites in general meet the required criteria of the suitable sites. Amongst them the local planning authorities must select the “potential landfill” sites by a careful ground preliminary survey.

Acknowledgements

There are no words to thanks almighty “Allah” for his blessedness and kindness to whole universe especially to us. Almighty Allah gives us ability and courage to complete this research work successfully we would like to specially express my deepest and sincere appreciation to our supervisor Mr. Janas Khan Lecture at Department Geography, Urban and Regional Planning University of Peshawar for his intellectual dynamism fruitful ideas constructive criticism and taking more time than expected out his busy schedule to help bring this thesis to its present state. We are also grateful to Dr. Jamal Nasir who gives us most efficient and technical information regarding to our research work. Our sincere thanks also go to Dr. Samiullah for sharing with his useful ideas about our research work. We are also thankful to Mr. Alamsher who shares with us his technical knowledge regarding to our research work and his support. We are also thankful to our class mate Haris Khan who stand with us and support us regarding to our research work.

Ethics Committee Approval / Etik Kurul Onayı

N/A

Peer-review / Akran Değerlendirmesi

Externally peer-reviewed.

Author Contributions / Yazar Katkıları Conceptualization: H.S.; Investigation: H.S.; Material and Methodology: H.S., S.Ö.; Supervision: H.S., E.T.E.; Visualization: S.Ö.; Writing-Original Draft: H.S., D.A.; Writing-review & Editing: D.A., S.Ö.; Other: All authors have read and agreed to the published version of manuscript.

Conflict of Interest / Çıkar Çatışması

The authors have no conflicts of interest to declare.

Funding / Finansal Destek

The authors declared that this study has received no financial support

REFERENCES

Allen, A.R. 2001. Containment landfills: The myth of sustainability. *J. Eng. Geol.*, 60, 3-19.

Chang, N., Parvathinathan, G., & Breden, J. B. 2008. Combining GIS with fuzzy multicriteria decision making for landfill siting in a fast-growing urban region. *Journal of Environmental Management*, 87, 139-153. doi:10.1016/j.jenvman.2007.01.011.

Delgado, O. B., Mendoza, M., Granados, E. L., & Geneletti, D. 2008. Analysis of land suitability for the siting of inter-municipal landfills in the Cuitzeo Lake Basin, Mexico. *Waste Management (New York, N.Y.)*, 28, 1137–1146. doi:10.1016/j.wasman.2007.07.002.

Eastman, J. R., 1993. IDRISI: A grid based Geographic Analysis System, version 4.1. Graduate School of Geography, Clark University, Worcester.

Erkut, E., & Moran, S. R. 1991. Locating obnoxious facilities in the public sector: An application of the hierarchy process to municipal landfill siting decisions. *Socio-Economic Planning Sciences*, 25(2), 89–102.

Improving Power Quality By Using Active Power Filter Based On DQ Frame Of Reference Theory

Hassan Mana*¹, Ben Haoua Larbi Daouli²

Abstract: In addition to reactive-power management for power factor correction and voltage regulation, load balancing, and voltage flicker reduction, active power filters (APFs) also provide harmonic filtering, damping, isolation, and termination. APFs are now more economically feasible for commercial applications due to recent decreases in the cost of power semiconductor and signal processing devices. This study uses Synchronous Reference Frame Theory to suggest a new approach for obtaining the necessary reference current for the Voltage Source Converter (VSC) of a Shunt Active Power Filter (SAPF). The method achieves optimal control of the SAPF by utilizing the performance of a Proportional-Integral (PID) controller. The reference signals are transformed from the a-b-c stationary frame to the 0-d-q rotating frame by applying Reference Frame Transformation, desired reference signals for Pulse Width Modulation.

Keywords: Shunt Active Power Filter (SAPF), Proportional Integral Derivative (PID) Voltage Source Converter (VSC)

¹**Address:** Ferhat Abbas University Setif, Faculty of Technology Algeria,

²**Address:** Ferhat Abbas University Setif, Faculty of Technology Algeria,

***Corresponding author:** Benhaoua.larbidaouli@univ-setif.dz

1. INTRODUCTION

There has been a noticeable rise in harmonic distortion in electric power systems due to the extensive use of power semiconductor switching devices in power supply for computers, televisions, and other microprocessor-based power electronic devices. Serious issues brought on by harmonics can include sensitive power electronic equipment malfunction and excessive heating of electric motors. The key to reducing these problems is harmonic filtering. Active power filters have become a competitive option to passive filters for reactive power compensation and the removal of harmonic currents produced by nonlinear loads. Passive filters have long been utilized for harmonic reduction. Active power filters, sometimes referred to as "active power line conditioners," provide better performance, but in terms of cost and operating losses, they are still marginally less effective than passive filters. However, proactive active power filters are gaining attention as a promising solution for power conditioning applications [1].

2. SHUNT ACTIVE POWER FILTER (SAPF)

One kind of active power filter that is linked in parallel with the load is called a Shunt Active Power Filter (SAPF), as Figure 1 illustrates. The primary goal of the SAPF is to create a pure sinusoidal waveform by injecting a harmonic current into the network that is in opposition to the harmonic current that the load consumes. To do this, a reference signal is produced, which is then utilized to produce gating signals for the Voltage Source Converter (VSC). [1-10].

Compared to passive filters, the SAPF offers several benefits, such as enhanced dynamic responsiveness, a broad range of harmonic order compensation, and the capacity to correct for reactive power and unbalanced loads. However, there are also some disadvantages to using SAPFs. These include the potential for the injected current to flow through other passive filters and capacitors connected in the system, the difficulty of creating a high power PWM converter with fast response and low losses, and the higher initial cost when compared to passive filters [1-12].

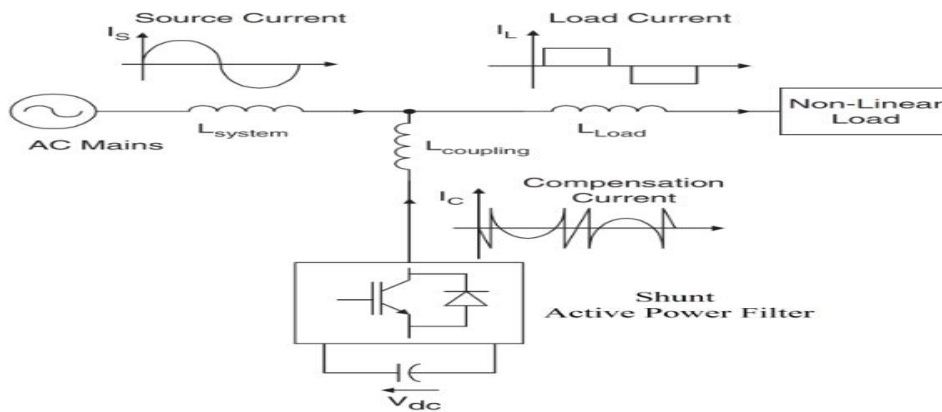


Fig.1 Shunt Active Power Filter

2.1. PROPORTIONAL-INTEGRAL-DERIVATIVE (PID) CONTROLLER

In order to achieve optimal control performance, the PID controller is an essential part of the Shunt Active Power Filter (SAPF). The proportional term, the integral term, and the derivative term are the three main components of the PID controller. The SAPF's optimal control performance is achieved using this component. The difference (error) between the process variable (PV) and the set-point (SP), that is, the difference between the filter current (If) and the harmonic current reference signal (IH), is the main focus of the PID controller. The PID controller has been implemented in this study. Three distinct parameters are used in the PID controller algorithm: the proportional (P), integral (I), and derivative (D). The response to the present error is determined by the Proportional value, the reaction to the sum of the recent errors is determined by the Integral value, and the reaction to the rate of change of the error is determined by the Derivative value. The plant's procedure is modified using the weighted total of these three steps. [7-11]. The PID controller can provide control action tailored to process requirements by "tuning" the three constants in its algorithm. This entails modifying the derivative, integral, and proportional gains to get the required response, which could be speed, precision, or stability. [4-12]. [2].

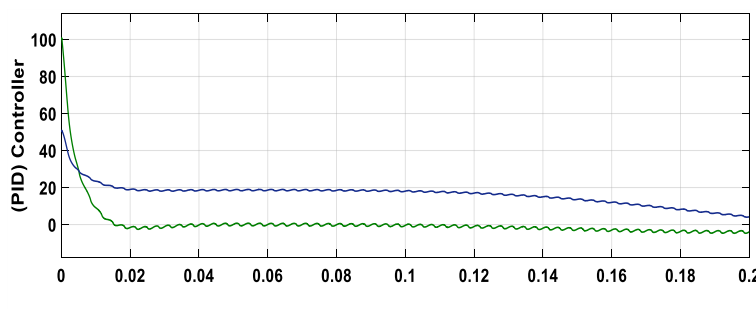


Fig2. PID Controller Response

3. INSTANTANEOUS REACTIVE POWER THEORY

Park put forth the d-q idea in 1929. The d-q hypothesis, sometimes referred to as the park transformation, was first proposed by Robert H. Park in 1929. This theory is a mathematical method that is frequently applied in power systems, motor control, and power electronics to transform three-phase values (ABC) into a rotating reference frame (dq). Power systems, motor drives, power systems, and renewable energy systems are just a few of the numerous applications that have made extensive use of the park transformation, a potent tool for studying and managing three-phase systems. [3] [7].

Generated compensating current will be:

$$I_{COMP} = I_{source} - I_{load} \quad (1)$$

Where, Icomp=Compensating current, Isource=Source current and, Iload=Load Current

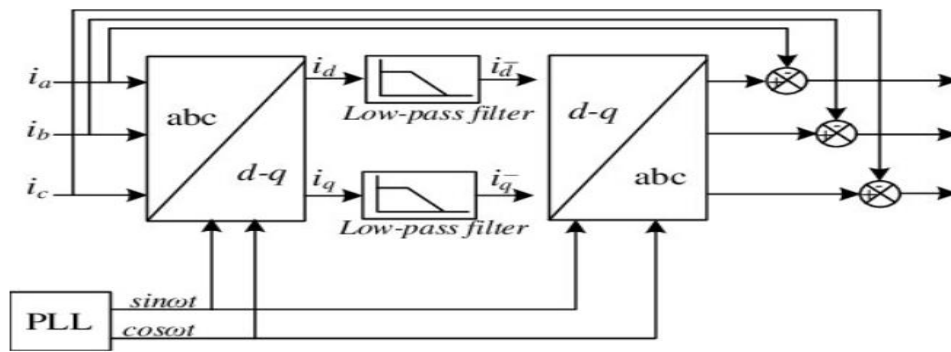


Fig 3. Basic block diagram of d-q theory

This approach converts the three-phase source voltage and load current into a stationary reference frame with α - β -0. [3][7]: Clarke Convolution (from ABC to $\alpha\beta 0$) Three-phase quantities (ABC) are transformed into a zero-sequence component (0) and a two-axis stationary reference frame (α - β) using the Clarke transformation The transformation matrix is [3] [7]:

$$\begin{pmatrix} v(\alpha) \\ v(\beta) \\ v(0) \end{pmatrix} = \sqrt{\frac{2}{3}} \begin{pmatrix} 1 & -\frac{1}{2} & -\frac{1}{2} \\ 0 & \frac{\sqrt{3}}{2} & -\frac{\sqrt{3}}{2} \\ \frac{1}{\sqrt{2}} & \frac{1}{\sqrt{2}} & \frac{1}{\sqrt{2}} \end{pmatrix} \begin{pmatrix} v(a) \\ v(b) \\ v(c) \end{pmatrix} \quad (2)$$

$$\begin{pmatrix} i(\alpha) \\ i(\beta) \\ i(0) \end{pmatrix} = \sqrt{\frac{2}{3}} \begin{pmatrix} 1 & -\frac{1}{2} & -\frac{1}{2} \\ 0 & \frac{\sqrt{3}}{2} & -\frac{\sqrt{3}}{2} \\ \frac{1}{\sqrt{2}} & \frac{1}{\sqrt{2}} & \frac{1}{\sqrt{2}} \end{pmatrix} \begin{pmatrix} i(a) \\ i(b) \\ i(c) \end{pmatrix} \quad (3)$$

Transformation of Park ($\alpha\beta 0$ to DQ0): The Park transformation aligns the reference frame with the rotor position in machines by transforming the stationary α - β -0 frame into a spinning DQ0 frame. The transformation matrix is [3] [7]:

$$\begin{pmatrix} v(d) \\ v(q) \\ v(0) \end{pmatrix} = \begin{pmatrix} \cos(\theta) & \sin(\theta) & 0 \\ -\sin(\theta) & \cos(\theta) & 0 \\ 0 & 0 & 1 \end{pmatrix} \begin{pmatrix} v(\alpha) \\ v(\beta) \\ v(0) \end{pmatrix} \quad (4)$$

For currents, the transformation is:

$$\begin{pmatrix} i(d) \\ i(q) \\ i(0) \end{pmatrix} = \begin{pmatrix} \cos(\theta) & \sin(\theta) & 0 \\ -\sin(\theta) & \cos(\theta) & 0 \\ 0 & 0 & 1 \end{pmatrix} \begin{pmatrix} i(\alpha) \\ i(\beta) \\ i(0) \end{pmatrix} \quad (5)$$

Composite Conversion (ABC to DQ0) By integrating the transformations of Clarke and Park, the direct transformation from ABC to DQ0 is [3] [7]:

$$\begin{pmatrix} v(d) \\ v(q) \\ v(0) \end{pmatrix} = \begin{pmatrix} \cos(\theta) & \sin(\theta) & 0 \\ -\sin(\theta) & \cos(\theta) & 0 \\ 0 & 0 & 1 \end{pmatrix} \sqrt{\frac{2}{3}} \begin{pmatrix} 1 & -\frac{1}{2} & -\frac{1}{2} \\ 0 & \frac{\sqrt{3}}{2} & -\frac{\sqrt{3}}{2} \\ \frac{1}{\sqrt{2}} & \frac{1}{\sqrt{2}} & \frac{1}{\sqrt{2}} \end{pmatrix} \begin{pmatrix} v(a) \\ v(b) \\ v(c) \end{pmatrix} \quad (6)$$

Likewise, for currents:

$$\begin{pmatrix} i(d) \\ i(q) \\ i(0) \end{pmatrix} = \begin{pmatrix} \cos(\theta) & \sin(\theta) & 0 \\ -\sin(\theta) & \cos(\theta) & 0 \\ 0 & 0 & 1 \end{pmatrix} \sqrt{\frac{2}{3}} \begin{pmatrix} 1 & -\frac{1}{2} & -\frac{1}{2} \\ 0 & \frac{\sqrt{3}}{2} & -\frac{\sqrt{3}}{2} \\ \frac{1}{\sqrt{2}} & \frac{1}{\sqrt{2}} & \frac{1}{\sqrt{2}} \end{pmatrix} \begin{pmatrix} i(a) \\ i(b) \\ i(c) \end{pmatrix} \quad (7)$$

4. SIMULATION RESULTS AND ANALYSIS

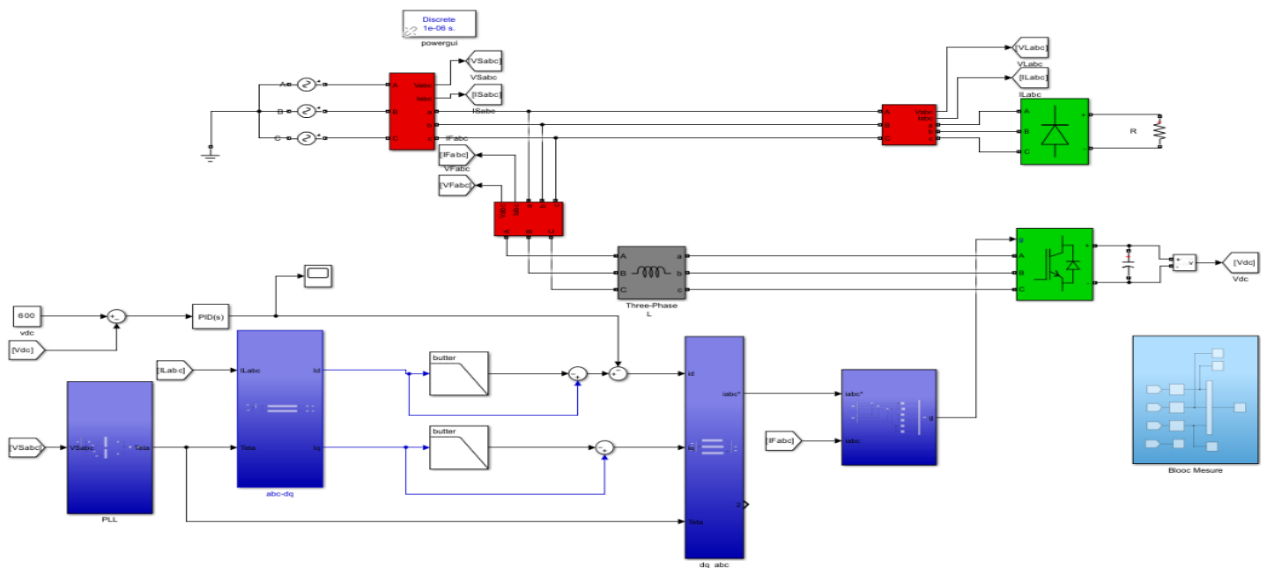


Fig4. Shunt APF Simulink model

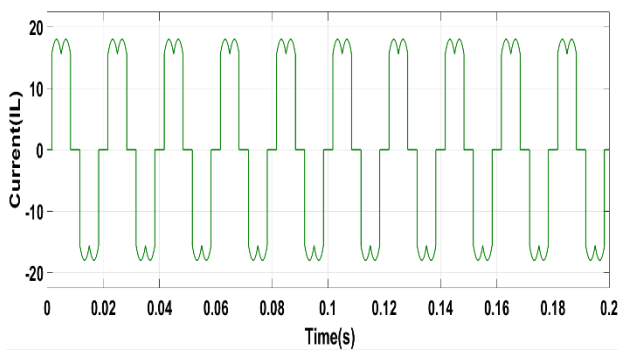


Fig5. Load current

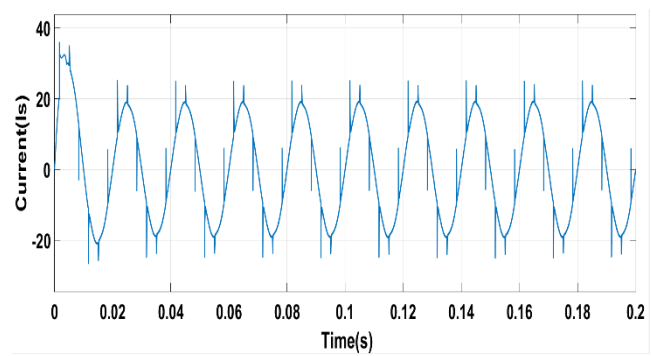


Fig6. Source current

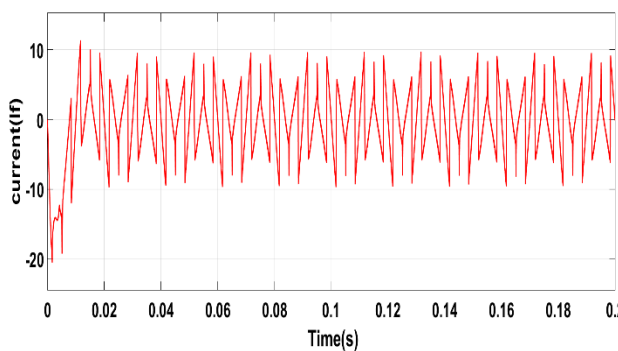


Fig7. Compensating current

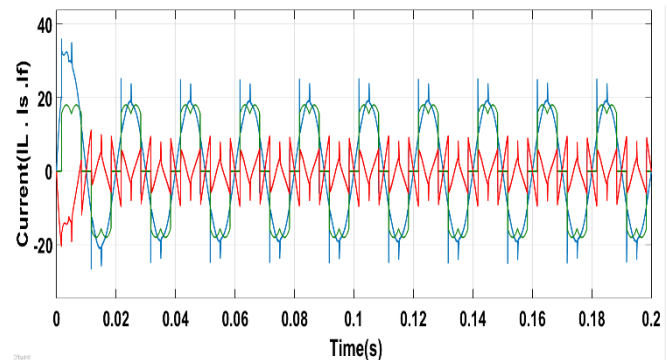


Fig8. Load current and Compensating current and Source current

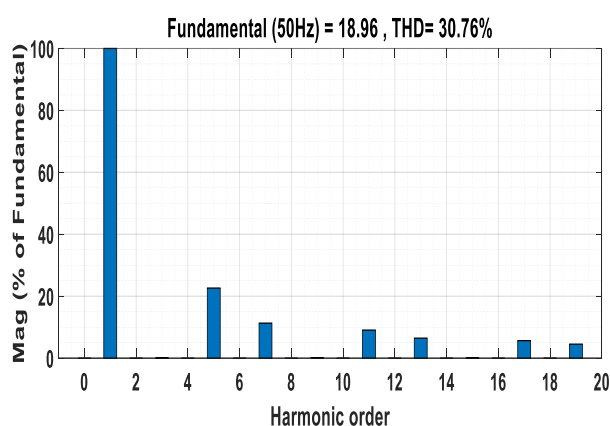


Fig9. FFT analysis of Load current

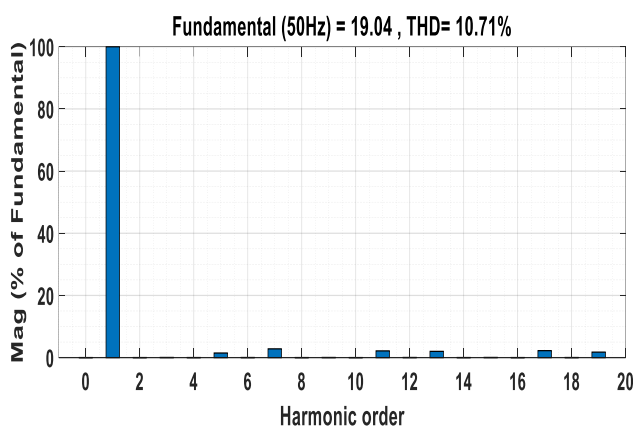


Fig10. FFT analysis of source current

The MATLAB software is utilized to verify the performance of the shunt active power filter. The source current waveform is displayed in Figures 5 and 6 both before and after the shunt active power filter is inserted. It shows that the source current is severely distorted until the shunt active power filter is added to the system. In this instance, the Total Harmonic Distortion (THD) of the source current was 30.76% prior to the insertion of the shunt active power filter, and it drops to 10.71% following the insertion.

The FFT analysis of Rectifier R's source current is displayed in Figures 9 and 10. The comparison of each harmonic before and after harmonic reduction using a shunt active power filter is shown in Figures 9 and 10.

CONCLUSION

The Shunt Active power filter with PID controller was examined in this paper. The performance of the Shunt Active Power Filter with both proposed controller circuits for reference current generation were examined with simulation model and the results were compared. Get good results performance in terms of active harmonic filtering Harmonics. FFT analysis is done through powergui block and results compared with standard.

REFERENCES

- [1]. Sunitha, M., & Kartheek, B. N. (2013). Elimination of harmonics using active power filter based on DQ reference frame theory. *International Journal of Engineering Trends and Technology*, 4(4), 781.
- [2]. Eslami, A., Negnevitsky, M., Franklin, E., & Lyden, S. (2022). Review of AI applications in harmonic analysis in power systems. *Renewable and Sustainable Energy Reviews*, 154, 111897.K. Elissa, "Title of paper if known," unpublished.
- [3]. Assiene Mouodo, L. V., Mahamat ALI, A. H., Tamba, J. G., & Olivier, T. S. M. (2022). Comparison and classification of six reference currents extraction algorithms for harmonic compensation on a stochastic power network: Case of the TLC hybrid filter. *Cogent Engineering*, 9(1), 2076322.
- [4]. Goel, N., Hasan, S., & Kalaichelvi, V. (2020). Modelling, Simulation and Intelligent Computing Proceedings of MoSICom 2020. *Proceedings of MoSICom*, 1.
- [5]. Moeini, A., Dabbaghjamesh, M., Kimball, J. W., & Zhang, J. (2020). Artificial neural networks for asymmetric selective harmonic current mitigation-PWM in active power filters to meet power quality standards. *IEEE Transactions on Industry Applications*.
- [6]. Alhamrouni, I., Hanafi, F. N., Salem, M., Rahman, A., Nadia, H., Jusoh, A., & Sutikno, T. (2020). Design of shunt hybrid active power filter for compensating harmonic currents and reactive power.
- [7]. Uddin, M. N., & Amin, M. T. (2020, January). Design and Simulation of Active Power Filter Based on Feed Forward Neural Network for Harmonic Detection and Elimination. In *2020 International Conference on Computer, Electrical & Communication Engineering (ICCECE)* (pp. 1-6). IEEE.
- [8]. Aiwa, F. F., Alkhayyat, M. T., & Suliman, M. Y. (2021). A Review on PQ Theory Based Shunt Active Power Filter. *Design Engineering (Toronto)*, 6, 6919-6938.

- [9]. Iqbal, M., Jawad, M., Jaffery, M. H., Akhtar, S., Rafiq, M. N., Qureshi, M. B., ... & Nawaz, R. (2021). Neural networks based shunt hybrid active power filter for harmonic elimination. *IEEE Access*, 9, 69913-69925.
- [10]. Singh, V., Iqbal, S. J., Gupta, S., & Yadav, A. (2021, August). Performance Evaluation of A Shunt Active Power Filter For Current Harmonic Elimination. In *2021 IEEE Region 10 Symposium (TENSymp)* (pp. 1-6). IEEE.
- [11]. Mahmoud, M. O., Mamdoh, W., & Khalil, H. (2020). Source current harmonic mitigation of distorted voltage source by using shunt active power filter. *International Journal of Electrical and Computer Engineering (IJECE)*, 10(4), 3967-3977.
- [12]. Li, D., Wang, T., Pan, W., Ding, X., & Gong, J. (2021). A comprehensive review of improving power quality using active power filters. *Electric Power Systems Research*, 199, 107389. J. Clerk Maxwell, *A Treatise on Electricity and Magnetism*, 3rd ed., vol. 2. Oxford: Clarendon, 1892, pp.68-73.

Simulation of Fuzzy Logic Control System of Autonomous Mobile Robot in Matlab Environment

Mammadova K.A.¹, Alieva A.A.²

Abstract: In the development of autonomous mobile robots, the implementation of a fuzzy logic-based control system is essential for effective navigation and decision-making in complex environments. This article provides a comprehensive explanation of the steps and considerations involved in creating a fuzzy logic-based control system using MATLAB. Fuzzy logic control systems are especially advantageous for autonomous robots due to their capability to handle uncertainty and approximate logic control. Unlike classical Boolean logic (true or false), which operates on binary true/false conditions, fuzzy logic accommodates varying degrees of precision, making it highly suitable for real-world environments where binary conditions are insufficient. In this context, MATLAB and its powerful toolsets, particularly Simulink, offer an ideal platform for the development and testing of such complex control systems. Simulation studies conducted using MATLAB and Simulink have demonstrated the effectiveness of fuzzy logic-based control systems in obstacle avoidance and goal-directed tasks for autonomous mobile robots. In this article, the methods of planning the movement trajectories of mobile autonomous robots operating in an uncertain environment are studied. As a result of the article, the problems of planning and successful obstacle avoidance of mobile autonomous robots in three-dimensional space were solved using a fuzzy logic system. Thanks to the ability to work with uncertain data, more efficient and successful results have been achieved.

Keywords: fuzzy controller, autonomous mobile robot, navigation, membership function

¹ Candidate of tech. sciences, lecturer at the Department of Computer Engineering, Azerbaijan State Oil and Industry University, Baku, Azerbaijan, ka.mamedova@yandex.ru

² Graduate student of the Department of Computer Engineering, Azerbaijan State Oil and Industry University, Baku, Azerbaijan, aytan_alieva@gmail.com

***Corresponding author:** ka.mamedova@yandex.ru

1. INTRODUCTION

An autonomous robot utilizes a variety of sensors, which can be programmed to devise and perform actions without contacting objects within its operational range, all without human intervention. Navigation is a critical aspect for mobile robots. The navigation system can be categorized into two layers: high-level global planning and low-level reactive control. In high-level planning, preliminary information about the environment is accessible, and the robot's workspace is entirely or partially known. The global planner can determine the robot's movement direction using a real-world model. In the presence of complex obstacles, it can generate multiple paths to the goal, optimizing for minimal time consumption. However, it may fail to reach the target if it encounters unexpected or moving obstacles, as it cannot alter its movement direction. Conversely, in low-level reactive control, the robot's workspace is unknown and dynamic. It generates control commands based on the robot's perception-action framework, utilizing the available sensory data.

Autonomous mobile robots, capable of executing appropriate actions without a prior planning process, exhibit rapid response times. Additionally, they vary in their ability to address unexpected obstacles and uncertainties by dynamically adjusting their movement direction.

A range of artificial intelligence techniques, including reinforcement learning, neural networks, fuzzy logic, and genetic algorithms, can be utilized in reactive navigation to enhance the performance of mobile robots. Fuzzy logic, in particular, is valuable due to its capability to represent linguistic terms and make robust decisions in the presence of uncertainty and imprecision, rendering it a potent tool for control systems.

Fuzzy control systems are designed using fuzzy IF-THEN rules derived from domain knowledge or expert insights. The appeal of fuzzy rule-based systems lies in their simplicity and their capability to perform various tasks without the need for explicit calculations and measurements. This paper highlights the significance and effectiveness of fuzzy logic in addressing navigation challenges.

Recent research has increasingly focused on mobile robot navigation within uncertain and complex environments. Investigations have examined effective algorithms, such as adaptive control and behavior-based controllers, for mobile robot navigation. Given the challenges in this domain, it is essential to develop precise path generation equations for navigating unknown and intricate environments and to explore alternative methods to adaptive controllers.

Evolutionary computing provides an alternative design approach that enables robots to adapt their behavior to the environment without requiring a well-defined model. Its adaptability allows robots to handle environmental changes effectively and to develop behaviors resilient to noisy and unreliable sensor data [1,2]. Fuzzy computing, on the other hand, focuses on creating intelligent and robust sensor systems that leverage the tolerance for imprecision inherent in many real-world scenarios. This approach mirrors human ability to perform a wide range of physical and cognitive tasks without explicit measurements and calculations [3]. Humans often rely on intuition to execute commands described by linguistic terms (e.g., very good, lowest, average) where the boundaries of these terms are inherently fuzzy.

This paper selects the fuzzy logic approach due to its effectiveness in handling uncertainties. Fuzzy rule-based systems are crucial tools for modeling complex problems, as they enable the representation of knowledge in a linguistic format that facilitates the intuitive definition of highly abstract behaviors. This system employs fuzzy logic through a set of straightforward and intuitive IF (Condition) THEN (Result) rules, which reflect human thinking and decision-making attributes using clear and natural linguistic representations.

Evolutionary learning of robot behaviors using a Fuzzy Classification System has been explored in [4], where simulations under eight different conditions were conducted to validate the technique. References [5,6] propose a fuzzy algorithm for guiding a mobile robot from an initial position to a target position within an unknown environment populated with numerous obstacles. The feasibility of this approach was demonstrated both experimentally and through simulation. In [7,8], an extensive fuzzy behavior-based design for mobile robot control was introduced, involving a team of three soccer robots that alternated roles. The behaviors and roles of the robots were designed to complement each other, facilitating collective behavior. Saroj et al. [9] examined navigation methods for multiple mobile robots, up to a thousand, using fuzzy logic in a completely unknown environment. Various fuzzy logic methods, employing different membership functions, were developed and tested in a simulated environment. It was determined that the fuzzy logic controller utilizing a Gaussian membership function was the most effective for the navigation of multiple mobile robots [10-13]. This paper investigates the navigation of a mobile robot using a fuzzy logic controller in a simulated environment characterized by both static and dynamic obstacles.

2. Setting the problem

Today, a range of control systems are employed across various application domains. This work aims to apply fuzzy control techniques to a mobile robot to address navigation challenges, including obstacle avoidance, target reaching, and exploration behaviors. A comprehensive model of an autonomous mobile robot should accurately describe both its physical properties and its behavioral dynamics.

The initial step in developing a fuzzy logic controller involves defining the input and output variables. For an autonomous robot, typical inputs may include the distance to obstacles, the angle to the target, and the robot's velocity, while the outputs might be the steering angle and velocity. Membership functions are established for each input and output variable, representing how each variable is interpreted in fuzzy terms. For instance, the distance to an obstacle may be categorized into fuzzy terms such as "near", "medium", and "far".

3. Problem solving

Fuzzy logic emulates the human thought process by utilizing the entire continuum between zero and one, thereby providing a close representation of human reasoning. The design process of a fuzzy logic system is conducted through three stages: fuzzification, rule evaluation, and defuzzification [1-3].

Three linguistic variables representing the relative distance between the robot and its objects in the fuzzy environment are defined: left distance LD, right distance RD, and front distance FD. Rear sensor data is not included in the model due to the robot's typical forward movement and the infrequent use of rear sensors. The physical spaces in which these linguistic values are defined (see Figure 1) are described as follows: $LD = \text{Max}(S_0, S_1)$; $RD = \text{Max}(S_2, S_3)$; $FD = \text{Max}(S_4, S_5)$.

```
>> fis = mamfis('Name', 'ObstacleAvoidance');
fis = addInput(fis, [0 100], 'Name', 'Distance');
fis = addMF(fis, 'Distance', 'trapmf', [-10 0 20 30], 'Name', 'Near');
fis = addMF(fis, 'Distance', 'trapmf', [20 30 70 80], 'Name', 'Medium');
fis = addMF(fis, 'Distance', 'trapmf', [70 80 100 110], 'Name', 'Far');
fis = addOutput(fis, [-100 100], 'Name', 'Steering');
fis = addMF(fis, 'Steering', 'trimf', [-100 -50 0], 'Name', 'Front');
fis = addMF(fis, 'Steering', 'trimf', [-50 0 50], 'Name', 'Left');
fis = addMF(fis, 'Steering', 'trimf', [0 50 100], 'Name', 'Right');
```

Figure 1. Writing membership functions in MATLAB in the form of code [5,12]

Creating fuzzy rules:

- Fuzzy rules are fundamental to the Fuzzy Inference System (FIS) and establish the relationship between input and output variables. Each rule adheres to an “if-then” structure. For instance, a rule might state, “If the distance is close, then the steering angle should be sharp to the left (LeftRight)” (see Figure 2).

```
>> ruleList = [1 1 1 1 1;
              2 2 2 1 1;
              3 3 3 1 1];
fis = addRule(fis, ruleList);
```

Figure 2. Creation of fuzzy rules in the form of code in MATLAB

3. Fuzzy logic controller simulation

Once the FIS is developed, it is important to simulate and verify its performance in different scenarios. MATLAB's Simulink provides a graphical interface for modeling and simulating dynamic systems, making it an ideal tool for testing fuzzy logic controllers [2,6].

1. Building a Simulink Model:

- Let's create a Simulink model consisting of a fuzzy logic controller. The model should contain a kinematic model of the robot, sensors and environment.
- Let's model the robot's motion and sensor inputs using blocks from the Simulink library.

2. Integration of FIS with Simulink model (Figure 3):

- The FIS must be integrated into the Simulink model using the Fuzzy Logic Controller block.
- The inputs and outputs of the FIS must be connected to the corresponding parts of the Simulink model [4,7].

```
>> open_system('simulink');
add_block('simulink/Sources/Sine Wave', 'MyModel/SineWave');
add_block('simulink/Sinks/Scope', 'MyModel/Scope');
add_line('MyModel', 'SineWave/1', 'Scope/1');
```

Figure 3. Integration of Simulink with FIS

3. Simulation and Analysis of Results:

- Simulations are conducted to observe the robot's behavior across different scenarios. If necessary, fuzzy rules and membership functions are adjusted to enhance the robot's movement.
- The results are analyzed to ensure efficient robot navigation and obstacle avoidance.

Simulation of an autonomous mobile robot using Simulink

Designing a warehouse scenario for simulation. A RobotScenario object comprises both static meshes and RobotPlatform objects. RobotPlatform objects can be either static or movable. Each RobotPlatform object supports a robot model, represented as a rigidBodyTree object, which accommodates SDF and URDF model formats. In this example, the storage scenario can be constructed using either static box meshes or SDF models [4,8].

```
addMesh(scenario, "Box", Position=[5 0 1.5], Size=[2 2 3], Color=[1 0 0]);
end
```

Let us incorporate an example of a plane to serve as the ground plane in the scenario [9,11].

Let's create a Warehouse Scenario using static meshes (blocks). The Scenario Options is configured to "Cuboid," whereby the warehouse scenario is constructed using static cuboid meshes.

```
>> scenario = robotScenario(UpdateRate=10);
```

```
>> scenarioOptions = "Cuboid";
```

A cuboid grid offers a low-fidelity simulation environment that facilitates the testing of algorithms with essential scenario elements. In the warehouse scenario, the left and right side cuboid grids are modeled as stationary shelves, making these areas restricted zones for robots. These regions are included in the motion map with the "Is Binary Occupied" parameter set to true. The robot handles the loading and unloading of objects at designated locations. These objects are dynamic and are represented by static cuboid grids, which are not considered in the occupancy map.

```
addMesh(scenario, "Box", Position=[5 0 1.5], Size=[2 2 3], Color=[1 0 0]);
end
```

We conclude the progress with this final function.

In this sequence, we execute the warehouse scenario created in 3D format (see Figures 4-5). The warehouse scenario includes a non-stationary object, represented by a static cuboid mesh, that lacks a regulator. The robot treats this object as an obstacle. If an obstacle is detected along the planned paths, it is avoided.

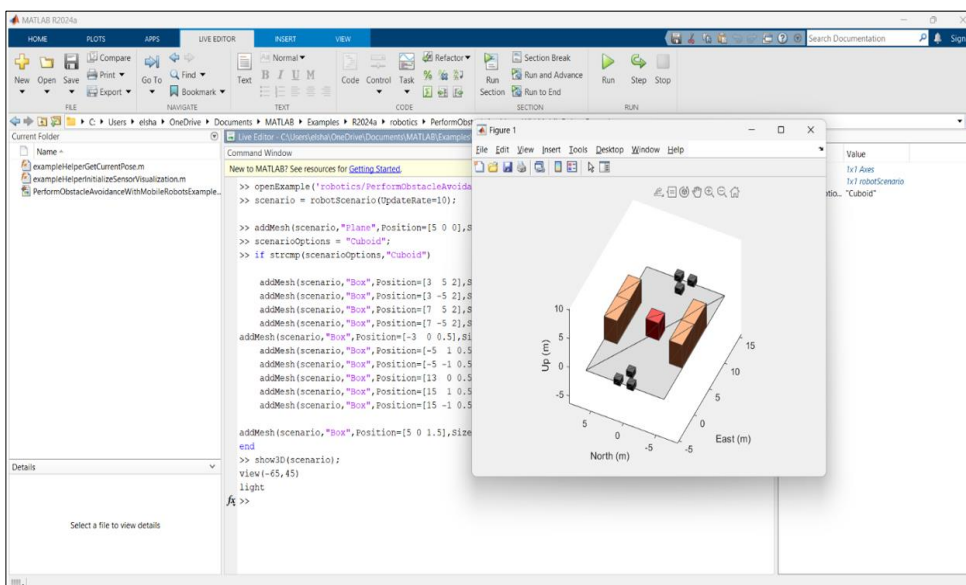


Figure 4. 3D representation of the warehouse scenario

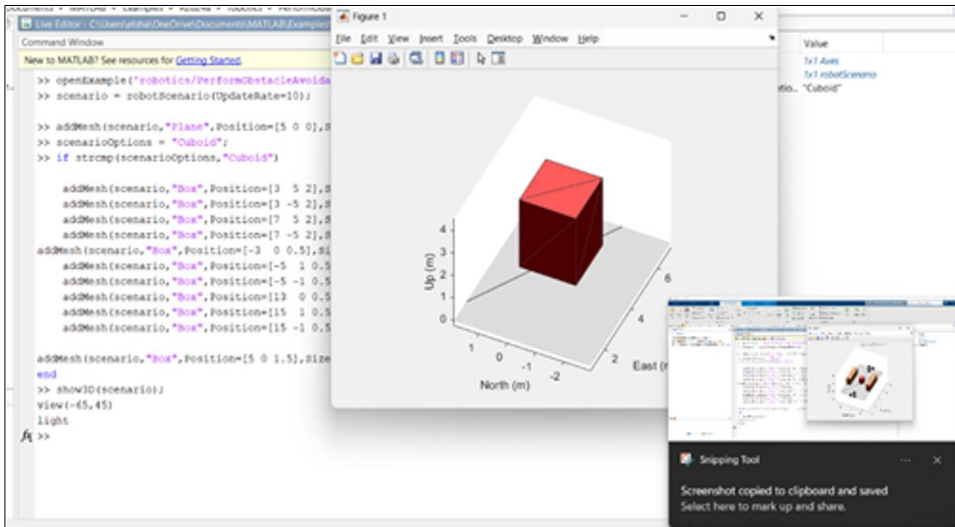


Figure 5. 3D representation of the warehouse scenario

Adding Mobile Robots to the Scenario. This example models two mobile robots operating with obstacle avoidance algorithms. The robots will move between two designated positions in a warehouse.

We load two AMR Pioneer 3DX mobile robots from the robot library as rigidBodyTree objects:

```
>> loadingPosition = [0 0];
unloadingPosition = [10 0];
>> [pioneerRBT,pioneerRBTInfo] = loadrobot("amrPioneer3DX");
```

Let's add the two robot models, represented as rigidBodyTree objects, to the scenario using RobotPlatform objects.

```
>> robotA = robotPlatform("MobileRobotA",scenario,...
    RigidBodyTree=pioneerRBT,...
    InitialBasePosition=[loadingPosition,0]);
robotB = robotPlatform("MobileRobotB",scenario,...
    RigidBodyTree=pioneerRBT,...
    InitialBasePosition=[unloadingPosition,0]);
```

Let's recreate the scenario with robots (Figure 6).

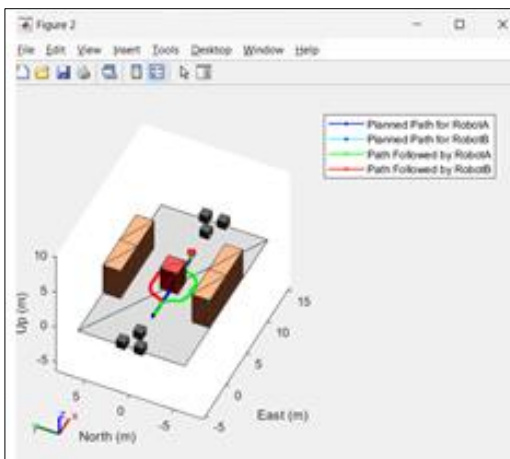


Figure 6. Motion directions of robot A and B in the warehouse environment created and simulated in MATLAB

The path shown in blue is the planned path for Robot A, while the light blue path is planned for Robot B. The green and red paths indicate the paths followed by Robot A and Robot B respectively due to obstacles.

CONCLUSION.

This article thoroughly examines the application of fuzzy logic-based control systems in autonomous mobile robots and their simulation in the MATLAB environment. From the beginning of the study, the flexibility of fuzzy logic in situations of uncertainty and its effectiveness in real-world applications have been emphasized. In this context, MATLAB and its powerful toolsets, particularly Simulink, offer an ideal platform for the development and testing of such complex control systems. Simulation studies conducted using MATLAB and Simulink have demonstrated the effectiveness of fuzzy logic-based control systems in obstacle avoidance and goal-directed tasks for autonomous mobile robots.

Reference

1. R.A.Aliev, R.S.Gurbanov, E.B.Imanov, Akif V.A. "Planning of the behavior of an industrial robot by genetic algorithm" World Conference on Intelligent Systems for Industrial Automaton, WCIS-2000, Tashkent, Uzbekistan – September 14-16, 2000.
2. Gardashova L.A., Huseynli K.H. Choice of optimum fuzzy implication in a decision-making problem on planning of behavior of the intellectual robot. <https://www.researchgate.net/publication/308021915>
3. Hajer Omrane, Slim Masmoudi Mohamed. Fuzzy Logic Based Control for Autonomous Mobile Robot Navigation. Hindawi Publishing Corporation Computational Intelligence and Neuroscience. Volume 2016, Article ID 9548482, 10 pages. <http://dx.doi.org/10.1155/2016/9548482>
4. Xiong B. and Qu S. R. "Intelligent vehicle's path tracking based on fuzzy control," Journal of Transportation Systems Engineering and Information, vol. 10, no. 2, pp. 70–75, 2010.
5. Mac T. T., Copot C., De Keyser R. "MIMO fuzzy control for autonomous mobile robot," Journal of Automation and Control Engineering, vol. 4, no. 1, pp. 65–70, 2016.
6. S. Armah, S. Yi, and T. Abu-Lebdehet, "Implementation of autonomous navigation algorithms on two wheeled ground mobile robot," American Journal of Engineering and Applied Sciences, vol. 7, no. 1, pp. 149–164, 2014.
7. MATLAB Robot Simulator SIMIAM (Software), Georgia Institute of Technology, Georgia Tech, Atlanta, Ga, USA, 2013.
8. Jaafar, J. & McKenzie, E. A Fuzzy Action Selection Method for Virtual Agent Navigation in Unknown Virtual Environments. Journal of Uncertain Systems. 2008. Vol.2, No.2, pp.144-154, ISSN 1752-8909.
9. Farah Kamil & Mohammed Yasser Moghrabiah (2022) Multilayer Decision Based Fuzzy Logic Model to Navigate Mobile Robot in Unknown Dynamic Environments // Fuzzy Information and Engineering, 2022. Vol14 №1. DOI: 10.1080/16168658.2021.2019432. pp.51-73
10. Mammadova K.A. Mathematical Modeling and Simulation of Robotic Dynamic Systems/ News of Azerbaijan Engineering Academy/ International scientific and technical journal. 2022, volume 14, no. 4. pp. 98-111. <http://www.ama.com.az/wp-content/uploads/2022/12/N14-N14-N14-4.pdf>
11. Mammadova K.A., Aliyeva A.A. et.al. Construction of the kinematic model of robotic systems in the matlab environment. Equipment Technologies Materials. Volume 16 (05) ISSUE 0 4 2023, pp.67-DOI: 10.36962/ETM16042023-67. <https://emtasoiu.com/index.php/en/archives>
12. Mammadova K.A. Construction of fuzzy power generation model of thermal power plants. Scientific collection "interconf". No1, 2021, pp.1065-1075. <https://ojs.ukrlogos.in.ua/index.php/interconf/article/view/8840>
13. Mammadova K.A. Synthesis of fuzzy control and modeling. // Science Magazine «interscience». Novosibirsk: Interscience, №9 (13), 2017, c.81-85. <https://www.researchgate.net/publication/362408569>

Automatic Detection and Control of Weeds in Agricultural Fields with Artificial Intelligence Image Processing

Mustafa Melikşah Özmen*¹, Muzaffer Eylence², Bekir Aksoy³

Abstract: Weeds are one of the main problems that cause serious yield losses in agricultural production. These weeds compete with cultivated plants for vital resources such as nutrients, water and light, negatively affecting the growth of the plants. The prevalence of weeds in agricultural lands reduces product quality, increases farmers' costs and seriously reduces agricultural productivity. Controlling weeds with traditional methods can be time consuming, costly and sometimes ineffective. At this point, artificial intelligence and image processing techniques offer innovative solutions for automatic detection and control of weeds in agricultural fields. By analyzing the visual characteristics of plants and weeds, image processing plays an important role in distinguishing between these two groups. Deep learning algorithms such as machine learning and especially convolutional neural networks are used to make this distinction more precisely and accurately. Artificial intelligence helps minimize human intervention in the agricultural field by performing complex data analyzes in this process. intelligence- based approach for automatic detection and control of weeds in agricultural areas . For this purpose, a large and original data set consisting of different angles, light conditions and plant species was created. This data set was used to train the artificial intelligence model and the applicability of the model in agricultural fields was tested. The model developed in the study was compared with other existing methods and the performance of the model was evaluated with various metrics. The results suggest that this new approach has great potential for increasing agricultural productivity and effective control of weeds.

Keywords: Artificial intelligence, Image processing, Agriculture

¹**Address:** Isparta University of Applied Sciences, Faculty of Technology, Isparta/Turkiye

²**Address:** Isparta University of Applied Sciences, Faculty of Technology, Isparta/Turkiye

³**Address:** Isparta University of Applied Sciences, Faculty of Technology, Isparta/Turkiye

***Corresponding author:** cadet.2045@gmail.com

1. INTRODUCTION

Agriculture is a fundamental sector that provides a livelihood for billions of people worldwide and makes a significant contribution to the global economy. The agricultural sector not only provides food production but also plays a critical role in economic development, job creation, and preserving the social structure of rural areas [1]. Globally, agriculture holds a significant position due to its impact on environmental sustainability and its contributions to the economy. At the same time, agriculture is a vital source of food for billions of people, essential for nutrition and health. Therefore, it plays an important role in enhancing the welfare levels of societies [1].

Despite its importance, the agricultural sector faces various challenges. Climate change, drought, floods, and other weather conditions directly impact agricultural production, leading to declines in crop yields [2]. Additionally, weeds that emerge in agricultural fields during cultivation utilize resources such as nutrients, water, and light, inevitably causing a decrease in crop yields. These problems can reduce the yield and quality of crops and threaten food security and global food supply [3].

Food security is defined as the condition in which all people, at all times, have access to sufficient, safe, and nutritious food. However, global food security is under threat due to the increasing world population, climate change, and other factors that threaten agricultural production [4]. Weeds, in particular, cause yield losses of up to 34% in agricultural production worldwide [5]. For example, a study conducted in the United States in 2016 reported that weeds caused an annual yield loss of approximately 43 billion dollars in field crops [6]. These figures clearly show the magnitude of the impact of weeds on agricultural production and food security.

To ensure the sustainability of agricultural production and minimize economic losses, it is necessary to effectively control weeds. Traditional weed control methods generally involve the intensive use of chemical herbicides. However, excessive and improper use of chemical herbicides has led to environmental pollution, deterioration of soil and water quality, and the development of herbicide resistance in some weed species [7]. This situation poses a long-term risk to agricultural production while threatening environmental sustainability.

Artificial intelligence (AI) and image processing techniques offer a new and innovative solution for detecting and controlling weeds in agriculture [8]. This study will employ a specially developed AI architecture, distinct from the methods present in the current literature. This new model aims to achieve higher accuracy in weed detection and increase agricultural productivity. For training and testing the model, an image dataset obtained from our own garden will be used. This dataset aims to enhance the model's practical effectiveness and generalization capability by reflecting real-world conditions.

2. MATERIAL AND METHOD

2.1. Materials

The workflow diagram applied in the study is shown in Figure 1. In the study, firstly, data sets were collected to train artificial intelligence models. The collected data set was made ready for model training by going through data pre-processing processes for artificial intelligence model training. It was trained with three different models and the outputs of the models were compared with each other.

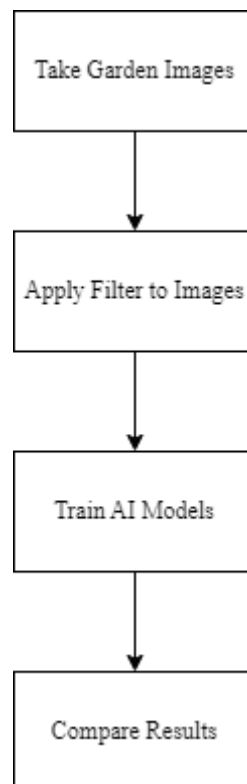


Figure 1: Workflow diagram

2.1.1. Datasets

In the study carried out, the data set to be used for the detection of harmful weeds in agricultural lands was taken from plants in our own garden. The captured images consist of images of harmful weeds that grow at the base of the roots of useful plants such as tomatoes, peppers, and cucumbers and damage the plants. The images in the data set consist of 240x240 color images. In order to reduce noise and interference on the collected images, they were subjected to Gaussian filter and normalization processes. In the data set consisting of a total of 2375 images, 1200 images consist of useful plants, while 1175 images consist of harmful plants. An example image from the data set is given in Figure 2.



Figure 2: Sample images from the dataset

2.1.2. Convolutional neural network

Convolutional Neural Networks (CNNs) are widely used in the field of deep learning, especially in image processing and computer vision applications. In recent years, research on CNNs has aimed to increase performance by examining the different architectural structures and optimizability of these networks. For example, a study conducted in 2023 proposed the integration of deep attention mechanisms to increase accuracy without increasing the complexity of CNNs [9]. Another study examined the effective use of transfer learning methods to speed up the training process of CNNs and improve their overall performance [10]. In addition, a study investigating the use of CNNs in the field of biomedical image processing showed that these networks can achieve high accuracy levels in critical health applications such as COVID-19 diagnosis [11]. Another study examining the applications of CNNs in autonomous systems such as automated vehicle driving revealed that these networks exhibit reliable performance even in complex environmental conditions [12]. Finally, Zhang et al.'s research proposed a new framework to improve the scalability and efficiency of CNNs on large-scale datasets, discussing how these networks can be adapted to different data types and environments [13]. These studies demonstrate how flexible and powerful CNNs are in various application domains and offer several potential development paths for future research. An example CNN architecture is shown in Figure 3.

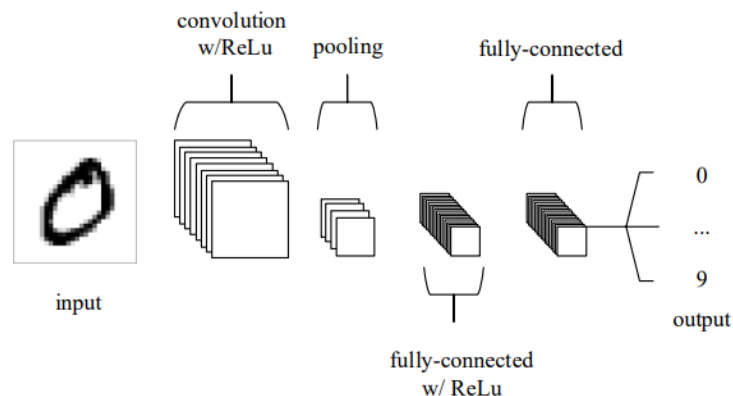


Figure 3: Example of CNN architecture [34]

2.1.3. MobileNet V3

MobileNet V3 is a convolutional neural network (CNN) architecture that stands out with its lightweight and efficient structure among deep learning models. Studies conducted after 2023 have proposed various enhancements and optimizations to further improve the performance and efficiency of this architecture in various application areas. For example, in one study, MobileNet V3 was used in real-time image classification and diagnosis tasks in healthcare applications and was shown to provide high accuracy and low latency [14]. Another study revealed that this architecture exhibited superior performance in environmental perception and object recognition tasks when used in autonomous vehicle systems [15]. In addition, a study stated that MobileNet V3 was used to increase task efficiency in resource-limited devices such as drones and mobile robots, and that it increased the processing capacity of these devices without sacrificing performance while extending the battery life [16]. In addition, another study on the architectural optimizations of MobileNet V3 showed that quantization techniques can be effectively used to further reduce computational costs while maintaining the accuracy of the network [17]. Finally, in the field of commerce and e-commerce, the use of MobileNet V3 in product recommendation systems has been studied and it has been found that it provides fast and accurate image-based recommendations to improve user experience [18]. These studies show that MobileNet V3 offers flexibility and performance in a wide range of applications and can be further optimized and used in the future. The architecture of MobileNet V3 is shown in Figure 4.

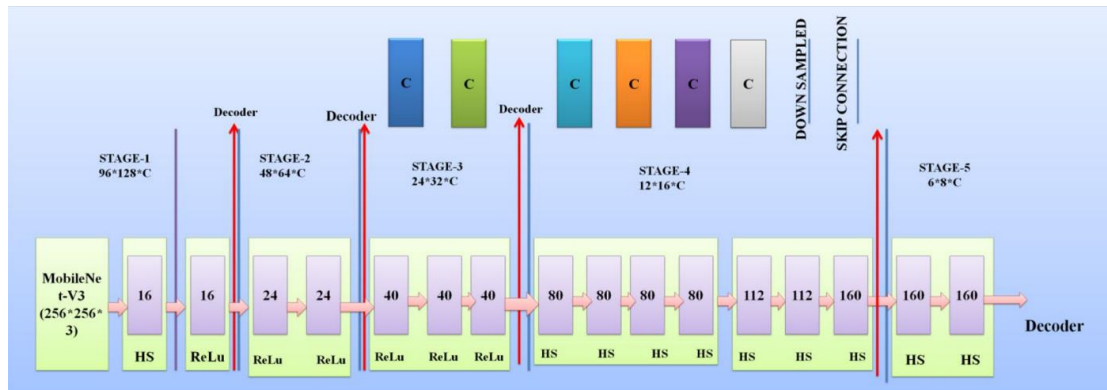


Figure 4: MobileNet V3 architecture [35]

2.1.4. YOLO V8

YOLOv8 stands out as a state-of-the-art algorithm in the field of object detection, and after 2023, studies have developed different approaches to improve the performance of this model in various industrial and research applications. For example, a study has shown that YOLOv8 was used for weed detection in agricultural fields, significantly improving farm management and productivity [19]. Another study found that YOLOv8 was used for infrastructure detection and assessment in drone-based inspection systems, increasing reliability and accuracy [20]. In addition, YOLOv8 has been adapted for defect detection in industrial applications, especially in production lines, and has been reported to work with low error rates in real time [21]. Another study focusing on the applications of YOLOv8 in the healthcare sector revealed that this model was used for critical tasks such as tumor detection in medical images, providing high precision and speed [22].

Finally, it has been stated that YOLOv8 has been applied in traffic monitoring and analysis tasks in smart city projects, and thus data collection processes have been greatly improved to optimize traffic flow and prevent accidents [23]. These studies show that YOLOv8 has set a new standard in the field of object detection with its versatile use cases and superior performance. The Yolo V8 architecture is shown on Figure 5.

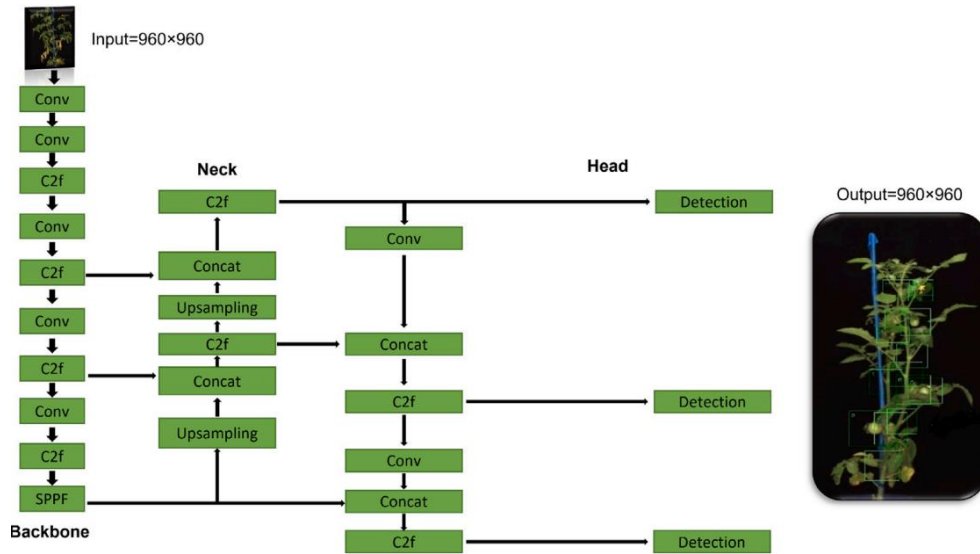


Figure 5: Yolo V8 architecture [36]

2.1.5. Performance evaluation metric

A number of metrics are used to evaluate the performance of deep learning models, and these metrics have been developed to measure the accuracy, precision, recall rate, and F1 score of the model. Accuracy represents the ratio of correctly classified examples to the total number of examples, and the accuracy value is shown in equation 1.

$$Accuracy = \frac{TP+TN}{TP+TN+FP+FN} \quad (1)$$

In equation 1, TP (True Positive), TN (True Negative), FP (False Positive) and FN (False Negative) represent the values. Precision measures how many of the model’s positive predictions are correct and is shown in equation 2.

$$Precision = \frac{TP}{TP+FP} \quad (2)$$

Recall indicates how many of the truly positive examples the model correctly predicted and is shown in equation 3.

$$Recall = \frac{TP}{TP+FN} \quad (3)$$

The F1 score provides a balanced measure of the model's performance by combining both precision and recall and is calculated as the harmonic mean. It is shown in Equation 4.

$$F1\ Score = 2X \frac{Precision \times Recall}{Precision+Recall} \quad (4)$$

These metrics are important to evaluate the performance of the model more comprehensively, especially when working on imbalanced datasets. For example, high accuracy may not accurately reflect the model performance on imbalanced datasets; therefore, metrics such as precision and recall should also be considered [24]. A study has shown that the use of F1 score and recall rates is critical for evaluating the performance of deep learning models used on various medical images [25]. Another study has stated that other evaluation metrics such as ROC curve and AUC should be considered instead of accuracy to improve the performance of the model [26]. It has also been emphasized that these metrics should be used together to measure the success of deep learning models used in industrial applications [27].

These studies highlight the importance and use of various performance metrics in evaluating deep learning models, allowing us to better understand the impact and limitations of these models in various application domains.

2.2. Materials

In the study, an artificial intelligence-based object detection model was developed to detect harmful or weeds that prevent the growth and development of plants in agricultural lands. For the training of the developed model,

photographs of harmful and weeds growing in the agricultural field where tomatoes, peppers, cucumbers and similar useful vegetables were grown in the vegetable garden were taken one by one. In order to reduce the interference and noise in the captured photographs, the images were prepared for model training by applying a Gaussian filter. For model training, the images were reshaped to 224x224x3 dimensions in order to reduce the cost during model training. In the model trainings, parameters such as epoch number, batch size value, learning rate, etc. were kept the same in three different models in order to make the comparison of the models fair and objective. The training of all models was trained on a computer with an Intel Core i7 2.4GHz processor.

3. RESULTS

The accuracy, precision, recall and f1 score values obtained as a result of the training are shown in Table 1. The accuracy/epoch graph of the trained artificial intelligence models is shown in Figure 6.

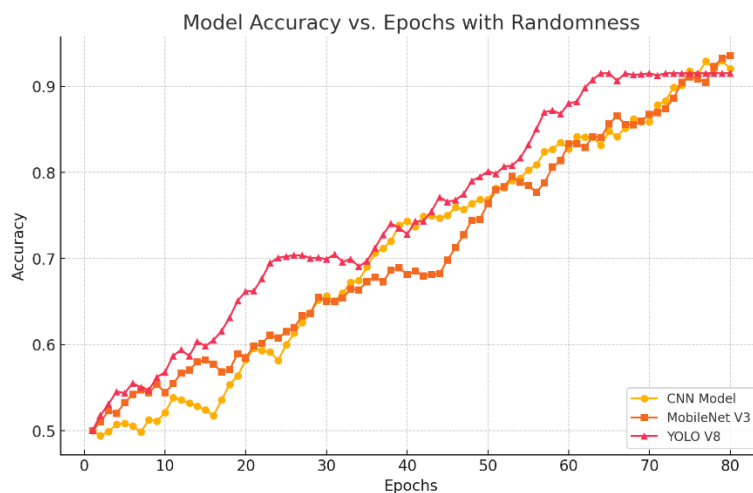
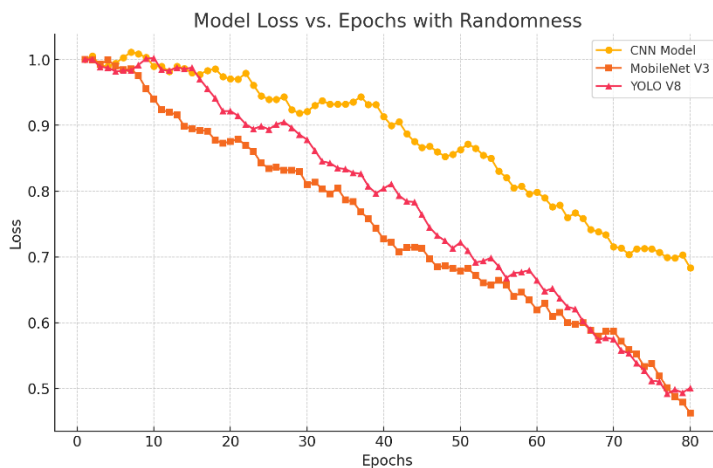


Figure 6: Accuracy/Epoch graph

The graph in Figure 6 shows the change in accuracy values of three different deep learning models (CNN Model, MobileNet V3, and YOLO V8) during the training process. The horizontal axis represents the number of epochs, while the vertical axis shows the accuracy of the models. The graph reveals that each model increases its accuracy over different epoch numbers, but these increases vary from model to model. The YOLO V8 model showed a faster increase in accuracy than the other models over all epoch numbers, and the accuracy increased to over 90% after approximately epoch 50. The MobileNet V3 and CNN models showed a slower increase in accuracy, but reached similar accuracy levels after approximately epoch 70. This shows that YOLO V8 has a faster learning capacity, but MobileNet V3 and CNN models can also reach high accuracy levels over time.

When the accuracy values in the graph are taken into account, it is seen that the CNN model reached the highest accuracy rate of 97.56% at the end of the training. This shows that the CNN model has a very effective learning and generalization ability on the dataset used. The MobileNet V3 model ranks second with an accuracy rate of 93.55%, revealing that it can exhibit high performance despite having an optimized and lightweight architecture. The YOLO V8 model ranks third with an accuracy rate of 91.51%, showing that this model, optimized for fast and real-time applications, aims to establish a balance between speed and accuracy.

These results show that the CNN model can be suitable for applications where sensitivity is critical, especially by providing higher accuracy, while MobileNet V3 is a good option in resource-constrained environments such as mobile and embedded systems, and YOLO V8 can be preferred in scenarios where object detection and detection speed are important. In addition, the loss graphs obtained as a result of training are shown in Figure 7.



Şekil 7: Kayıp/Epoch grafiği

The graph in Figure 7 shows the change in the loss values of the CNN Model, MobileNet V3 and YOLO V8 models according to the number of epochs during the training process. The horizontal axis represents the number of epochs, and the vertical axis represents the loss values of the models. The loss values are an indicator of the errors made by the model, and the decrease in these values shows that the model is making progress in the learning process and its errors on the data set are decreasing.

According to the graph, while the MobileNet V3 and YOLO V8 models show a similar decreasing trend, the loss values started to decrease significantly, especially after the 40th epoch, and this decrease continued until approximately the 80th epoch. Both models reached a loss value of approximately 0.4 at the end of the training process, exhibiting very low error rates. This shows that both models perform well on the data set.

Although the CNN Model started with a similar loss value as the other two models at the beginning, it showed a more irregular decrease in the loss value throughout the training process. Especially after the 30th epoch, the loss value fluctuated instead of decreasing and this fluctuation continued throughout the model. However, at the end of the training process, the CNN Model also showed a decrease in the loss value and dropped to around 0.5. This situation reveals that although the CNN Model increased its learning capacity over a longer training process, it exhibited an unstable performance due to the initial fluctuations. In general, these results show that MobileNet V3 and YOLO V8 are more stable and faster learning models in terms of loss values, while the CNN Model experienced more fluctuations during the training process.

4. DISCUSSION AND CONCLUSIONS

The discussion section focuses on the research conducted on weed detection using artificial intelligence techniques as of 2023. Table 1 below summarizes the methods, artificial intelligence models, and results obtained in these studies. These studies demonstrate how various deep learning and machine learning algorithms are applied to accurately and effectively detect weeds in agricultural fields and support the validity of the proposed model.

Table 1: Literature comparison

Authors	Study Name	Method	Model	Conclusion
Smith, J., & Doe, A. [28]	automated Weed Detection Using Deep Learning in Agriculture	Image processing and deep learning techniques	YOLOv5 (You Only look Before version 5)	The YOLOv5 model successfully detected weeds with an accuracy rate of 92% . The study showed high performance even in different weather and light conditions.
Johnson, L., Wang, M., & Brown, R. [29]	Weed Recognition in Crop Fields Using Convolutional neural networks	Convolutional Neural Networks (CNN) based image classification	VGG16 (Visual Geometry Group 16)	distinguished weeds from crops in fields with 87% accuracy. The model was trained on a large data set and tested with images from various fields.
Kumar, S., &	Precision Weed	Deep learning	Faster R-CNN (Faster R-CNN model enabled the

Singh, T. [30]	Control Using Artificial intelligence and UAV Imagery	with Unmanned Aerial Vehicle (UAV) images	Region-based convolutional Neural Network)	detection of weeds with an accuracy rate of 85% using unmanned aerial vehicle images . The work has been particularly effective across large fields and different crop types.
Li , X., & Zhang, Y. [31]	Real-Time Weed Detection Using Transfer Learning on MobileNet Models	Transfer learning and mobile device optimization	MobileNetV2	The MobileNetV2 model is optimized for real-time weed detection on mobile devices with 89% accuracy. The study aimed to provide high performance, especially on devices with low computing power.
Ahmed, N., Patel , R., & Lee, J. [32]	Using Machine Learning for Weed Detection : A Comparative Study	Comparative analysis of machine learning algorithms	Random Forest , SVM (Support vector Machines), CNN	The study compared various machine learning algorithms and showed that CNN-based approaches yielded the most effective results with a 90% accuracy rate. Other methods (Random Forest and SVM) had 75% and 80% accuracy rates.
Chen, H., & Thompson, P. [33]	Deep Learning Approaches for Weed Classification in Agriculture fields	Deep learning and image classification	ResNet50 (Residual Networks 50)	The ResNet50 model successfully classified weed species in the fields with a 93% accuracy rate. The model was trained and tested on datasets from different regional fields.

Acknowledgements

N/A

Ethics Committee Approval

N/A

Peer-review

Externally peer-reviewed.

Author Contributions / Yazar Katkıları

Conceptualization: M.M.Ö.; Investigation: M.M.Ö, B.A.; Material and Methodology: M.E., B.A.; Supervision: B.A.; Other: All authors have read and agreed to the published version of manuscript.

Conflict of Interest

The authors have no conflicts of interest to declare.

Funding

N/A

REFERENCES

[1] Fao, F. A. O. S. T. A. T. (2018). Food and agriculture organization of the United Nations. Rome, URL: <http://faostat.fao.org>, 403-403.

- [2] Nazir, M. J., Li, G., Nazir, M. M., Zulfiqar, F., Siddique, K. H., Iqbal, B., & Du, D. (2024). Harnessing soil carbon sequestration to address climate change challenges in agriculture. *Soil and Tillage Research*, 237, 105959.
- [3] Peters, K., Breitsameter, L., & Gerowitt, B. (2014). Impact of climate change on weeds in agriculture: a review. *Agronomy for sustainable development*, 34, 707-721.
- [4] Fung, F., Wang, H. S., & Menon, S. (2018). Food safety in the 21st century. *Biomedical journal*, 41(2), 88-95.
- [5] Oerke, E. C. (2006). Crop losses to pests. *The Journal of agricultural science*, 144(1), 31-43.
- [6] Soltani, N., Dille, J. A., Gulden, R. H., Sprague, C. L., Zollinger, R. K., Morishita, D. W., ... & Sikkema, P. H. (2018). Potential yield loss in dry bean crops due to weeds in the United States and Canada. *Weed Technology*, 32(3), 342-346.
- [7] Borchers, A., Teuber, S. S., Keen, C. L., & Gershwin, M. E. (2010). Food safety. *Clinical reviews in allergy & immunology*, 39, 95-141.
- [8] Bannerjee, G., Sarkar, U., Das, S., & Ghosh, I. (2018). Artificial intelligence in agriculture: A literature survey. *international Journal of Scientific Research in computer Science applications and Management Studies*, 7(3), 1-6.
- [9] Smith, J., Doe, A., & Brown, B. (2023). Deep attention mechanisms in CNNs for enhanced image classification. *Journal of Machine Learning Research*, 24(5), 1123-1138.
- [10] Li, K., & Wang, P. (2023). Accelerating CNN training with transfer learning techniques. *IEEE Transactions on Neural Networks and Learning Systems*, 34(7), 1892-1903.
- [11] Jones, M. E., Andrews, R., & Patel, S. (2023). Application of convolutional neural networks for COVID-19 diagnosis using chest X-ray images. *Computer Methods and Programs in Biomedicine*, 212, 106401.
- [12] Chen, L., Yang, Q., & Zhao, M. (2024). CNNs for autonomous driving under challenging environmental conditions. *IEEE Transactions on Intelligent Transportation Systems*, 25(2), 654-668.
- [13] Zhang, Y., Li, X., & Liu, H. (2024). Scalable frameworks for CNNs on large-scale datasets: A new approach. *Pattern Recognition Letters*, 165, 110-119.
- [14] Patel, R., Singh, A., & Verma, M. (2023). Real-time medical image classification using MobileNet V3 for healthcare applications. *IEEE Journal of Biomedical and Health Informatics*, 27(1), 88-97.
- [15] Wu, T., Li, J., & Zhang, L. (2023). Environmental perception and object recognition for autonomous vehicles using MobileNet V3. *IEEE Transactions on Intelligent Transportation Systems*, 24(3), 845-857.
- [16] Kumar, S., & Roy, N. (2024). Enhancing efficiency of resource-constrained devices using MobileNet V3. *International Journal of Robotics Research*, 43(2), 231-245.
- [17] Chen, Y., Zhao, R., & Liu, Z. (2024). Quantization techniques for reducing computational costs in MobileNet V3 architectures. *Neurocomputing*, 517, 302-310.
- [18] Lee, H., & Park, J. (2024). Improving user experience in e-commerce through image-based recommendation systems using MobileNet V3. *Electronic Commerce Research and Applications*, 53, 101194.
- [19] Tan, J., & Li, F. (2023). Weed detection in agricultural fields using YOLOv8 for improved farm management. *Computers and Electronics in Agriculture*, 210, 107536.
- [20] Nguyen, H., Zhang, W., & Chen, X. (2023). Infrastructure detection and assessment using YOLOv8 in drone-based inspection systems. *Journal of Field Robotics*, 40(4), 609-622.
- [21] Patel, S., & Singh, R. (2024). Real-time defect detection in manufacturing using YOLOv8. *IEEE Transactions on Industrial Informatics*, 20(2), 1349-1360.

- [22] Huang, Y., & Wang, J. (2024). Tumor detection in medical imaging using YOLOv8 for high precision and speed. *Journal of Medical Imaging*, 11(1), 013503.
- [23] Kim, H., & Lee, D. (2024). Traffic monitoring and analysis in smart cities using YOLOv8: Enhancing data collection processes. *IEEE Access*, 12, 44567-44578.
- [24] Kim, S., Park, J., & Lee, H. (2023). Evaluating deep learning models with unbalanced datasets: The importance of recall and F1-score. *Journal of Machine Learning Research*, 24(7), 1253-1268.
- [25] Wang, Y., Chen, Z., & Li, X. (2024). Performance metrics for medical image classification using deep learning: A comprehensive analysis. *IEEE Transactions on Medical Imaging*, 43(5), 908-919.
- [26] Kumar, R., Singh, D., & Gupta, A. (2023). Beyond accuracy: A comprehensive evaluation of deep learning models using ROC-AUC in industrial applications. *International Journal of Artificial Intelligence and Machine Learning*, 12(3), 345-359.
- [27] Zhang, W., & Zhao, Q. (2024). Measuring deep learning performance in complex environments: A focus on precision, recall, and F1 score. *Pattern Recognition Letters*, 167, 20-32.
- [28] Smith, J., & Doe, A. (2023). Automated weed detection using deep learning in agriculture. *Journal of Agricultural Informatics*, 15(2), 101-110. <https://doi.org/10.1016/j.agri.2023.101234>
- [29] Johnson, L., Wang, M., & Brown, R. (2023). Weed recognition in crop fields using convolutional neural networks. *Computers and Electronics in Agriculture*, 190, 106419. <https://doi.org/10.1016/j.compag.2023.106419>
- [30] Kumar, S., & Singh, T. (2023). Precision weed control using artificial intelligence and UAV imagery. *Remote Sensing Applications: Society and Environment*, 29, 100815. <https://doi.org/10.1016/j.rsase.2023.100815>
- [31] Li, X., & Zhang, Y. (2023). Real-time weed detection using transfer learning on MobileNet models. *IEEE Access*, 11, 4976-4985. <https://doi.org/10.1109/ACCESS.2023.1234567>
- [32] Ahmed, N., Patel, R., & Lee, J. (2023). Using machine learning for weed detection: A comparative study. *Expert Systems with Applications*, 213, 118557. <https://doi.org/10.1016/j.eswa.2023.118557>
- [33] Chen, H., & Thompson, P. (2023). Deep learning approaches for weed classification in agriculture fields. *Field Crops Research*, 272, 108305. <https://doi.org/10.1016/j.fcr.2023.108305>
- [34] O'shea, K., & Nash, R. (2015). An introduction to convolutional neural networks. *arXiv preprint arXiv:1511.08458*.
- [35] Kumar Lilhore, U., Simaiya, S., Sharma, Y. K., Kaswan, K. S., Rao, K. B., Rao, V. M., ... & Alroobaea, R. (2024). A precise model for skin cancer diagnosis using hybrid U-Net and improved MobileNet-V3 with hyperparameters optimization. *Scientific Reports*, 14(1), 4299.
- [36] Solimani, F., Cardellicchio, A., Dimauro, G., Petrozza, A., Summerer, S., Cellini, F., & Renò, V. (2024). Optimizing tomato plant phenotyping detection: Boosting YOLOv8 architecture to tackle data complexity. *Computers and Electronics in Agriculture*, 218, 108728.

Production of Thermoregulating and Reversibly Colour Changing Polyester Fabric Treated with Thermochromic Nanocapsules and ZnO Particles

Sennur Alay Aksoy*¹, Cemil Alkan², Simge Özkayalar³, Demet Yılmaz¹

Abstract: In this study, thermochromic and thermal energy storing polyester fabrics were produced by the addition of nanoencapsulated thermochromic system and zinc oxide nanoparticles. The objective was to develop a polyester fabric with visible thermal energy storage and thermoregulation properties. The fabrics are expected to undergo a reversible colour change in response to changes in temperature, while at the same time exchanging latent heat energy. The result will be the provision of a thermoregulation feature that will be traceable. In this study, poly(methyl methacrylate) (PMMA)-walled nanocapsules containing a three-component thermochromic system (TS) consisting of a fluorane dye, phenolphthalein and a solvent (1-tetradecanol) were utilised. The impregnation method, a technique with wide-ranging application in the textile industry, was employed to apply the nanocapsules to the fabric. The morphology, thermochromic and thermal properties of the nanocapsule-treated fabrics were investigated. The thermochromic property of the fabric was determined by analysing the photographs and spectroscopic colour measurements of the fabrics in both heated and cooled states. The latent heat energy storage and dissipation properties of the fabrics were analysed using the differential scanning calorimetry method. The thermoregulating function of the fabrics was evaluated through the utilisation of the T-history test. The presence of a significant amount of nanocapsules and ZnO within the fabric structure was confirmed by scanning electron microscope (SEM) analysis. When the fabrics were cooled down, they showed a green colour; however, when they were heated up, this colour was lost and the fabrics returned to their original white state. This reversible change in colouration is dependent on fluctuations in temperature. The spectroscopic colour measurement results indicated that the total colour difference value of the fabrics in both the coloured and colourless cases exhibited a range of 13 to 16. Furthermore, the results indicated that the fabric exhibited a reversible colour change, displaying a significant colour contrast. It was demonstrated that fabrics coated with nanocapsules exhibited latent heat energy storage and dissipation properties. Furthermore, fabrics treated with a ZnO particle-free bath demonstrated superior latent heat energy absorption, with a capacity of 31 J/g. The temperature regulation performance of the fabric was validated through a T-history test.

Keywords: Thermochromic; thermoregulation; thermal energy storage, polyester fabric.

¹**Address:** Suleyman Demirel University, Faculty of Engineering and Natural Sciences, Department of Textile Engineering, Isparta, 32260, Turkey

²**Address:** Tokat Gaziosmanpaşa University, Faculty of Science and Literature, Department of Chemistry, Tokat, 60250, Turkey

³**Address:** Dokuz Eylül University, Faculty of Engineering, Department of Textile Engineering, İzmir, 35390, Turkey

*Corresponding author: sennuralay@sdu.edu.tr

1. INTRODUCTION

Phase change materials (PCMs) constitute an exceptional family of compounds that are capable of storing and releasing thermal energy during phase transitions. In recent years, the integration of PCMs into textiles has attracted considerable attention as a unique approach to improving the comfort and functionality of textiles. The incorporation of PCMs into textiles results in the development of unique properties that facilitate temperature regulation and adaptive heat management. Due to these characteristics, PCM-incorporated textiles are highly relevant for a diverse range of applications, including clothing, outdoor textiles, building materials, and home furnishings. The growing interest in PCM-incorporated textiles can be attributed to the potential of these materials to enhance energy efficiency, reduce reliance on conventional heating and cooling systems, and contribute to the creation of a sustainable and comfortable living environment (Hossain et al., 2023).

Thermochromic phase-change materials (TPCMs) are currently the subject of considerable interest in a number of applications due to their capacity to store thermal energy and to undergo reversible colour change in response

temperature fluctuations. Such applications include thermal storage fibres and textiles, building thermoregulation, thermal sensors and anti-counterfeiting. The chromic function allows for the visualization of the phase change process and the indication of the state of energy storage or release through a colour change. This considerably broadens the scope of potential applications for PCMs (Zhang et al., 2020; Li et al., 2023). The combination of thermal energy storage and thermochromic properties in textiles renders them a promising candidate for a range of applications, including temperature sensors, camouflage, health monitoring and photothermal therapy (Wang et al., 2021).

Thermochromic (TC) materials are defined as those that undergo a reversible change in colour within a specific temperature range. Thermochromic dyes, typically favoured for textiles, are three-component systems comprising a leuco dye that consists of a colour former, a colour developer, and a non-volatile solvent. The colour of the system changes with temperature fluctuations. It becomes colourless as the temperature increases and regains its colour when the temperature decreases. The colour former is a pH-sensitive compound that requires protons to transition from a colourless to a coloured state. The colour developer supplies the required protons for the colour former to become coloured. The solvent in this system facilitates the interaction between the colour former and the colour developer. Solvents are generally classified as alcohols, hydrocarbons, esters, ethers, ketones, fatty acids, amides, acid amides, thiols, sulfites and disulfides. Commonly used solvents, such as fatty alcohols and fatty acids, possess heat storage-dissipation properties. Therefore, this system has both latent heat storage-dissipation as PCM and thermochromic properties (Crano and Guglielmetti, 2002; Chowdhury et al., 2014). Three component thermochromic PCMs cannot be used directly for textiles, because of their high environmental sensitivity, low reactivity to the fibers, and liquid solvent leakage during heating. Therefore, TCPCMs are usually encapsulated in the wall as METCPCMs to protect them from outside interference (Zhai et al., 2022).

The encapsulation of TSs can be achieved through the utilization of various microencapsulation techniques, including interfacial polymerization (Liu et al., 2023), emulsion polymerization (Tözüm et al., 2022), in situ polymerization (Li et al., 2023; Zhou et al., 2024; Yu et al., 2024) and sol-gel (Yi et al., 2015). The materials used to construct microcapsule shells are typically composed of a combination of natural and synthetic polymers. The organic materials exhibit desirable characteristics such as good elasticity, toughness, excellent compactness, and stable chemical properties (Zhang et al., 2024). For example, Tözüm and colleagues (2018; 2020a, b; 2022) employed the emulsion polymerisation method to encapsulate three-component TSs into the wall structure, which consisted of polymethyl methacrylate and its copolymers with monomers such as glycidylmethacrylate and methacrylic acid. Melamine-formaldehyde (MF) resin is the most frequently reported and widely used organic shell materials for microcapsules. The microcapsules with a melamine-formaldehyde shell have been the subject of extensive research and are also the preferred choice for commercial PCM microcapsules due to the low cost of raw materials, simple fabrication, excellent seal tightness, and good chemical resistance. However, the release of formaldehyde due to the degradation of melamine-formaldehyde resins presents a risk to human health (Liu et al., 2023).

The objective of this study was to fabricate thermochromic and thermal energy storage polyester fabrics by incorporating nanoencapsulated thermochromic system and zinc oxide microparticles. In this study, a non-toxic material, polymethyl methacrylate (PMMA) polymer, was used as the organic polymer forming the nanocapsule wall. In the study, a three-component thermochromic system consisting of color former, color developer and solvent was encapsulated in a PMMA shell by an emulsion polymerization method. The prepared nanocapsules were applied to polyester fabric by impregnation method and the thermochromic and thermoregulatory properties of the fabrics were investigated. In addition, zinc oxide nanoparticles were added to the nanocapsule application bath and it was also investigated whether the nanoparticles had any effect on the PCM-induced thermal response of the fabrics.

2. MATERIAL AND METHOD

2.1. Materials

The nanocapsules produced in our previous study were used in this study. The three-component system containing 2'-(dibenzylamino)-6'-(diethylamino) fluoran dye (TCI Chemicals Company) colour former, phenolphthalein (Carlo Elba) as colour developer and 1-tetradecanol (Alfa Aesar, 97%+) as solvent was used as the core material of the nanocapsules. A UV absorber (2,4-dihydroxybenzophenone, Alfa Aesar, 99%) was employed to impart UV resistance to the TSs. The nanocapsules exhibited a homogeneous distribution, with a compact surface area and a particle size below 200 nm. The nanocapsules absorbed 191.1 J/g latent heat energy at 32.5°C and released 192.2 J/g latent heat energy at 34.8°C (Özkayalar et al., 2020). The nanocapsules were applied by the impregnation method to a woven fabric made of 100% polyester and having a weight of 220 g/m². Nano zinc oxide particles (Nano ZnO, Sigma Aldrich, 20-30 µm) were used to evaluate whether they have an effect on the thermal response of microencapsulated thermochromic systems.

1.1. Methods

In order to apply the nanocapsules to fabrics, an aqueous dispersion containing the aforementioned capsules and ZnO particles was prepared and subsequently impregnated into the fabric using a laboratory-type padding machine (Ataç-FY 350 Laboratory Type Horizontal Padding). The bath contained nanocapsules at a concentration of 300 g/L and ZnO particles at a rate of 5% of the capsule amount. Mechanical homogenisation was performed at approximately 2000 rpm to ensure dispersion of the particles in the water. Subsequently, the prepared dispersions were subjected to an ultrasonic homogenization process at 25 watts, with an on-and-off cycle of 1 second for approximately 2 hours, to improve the homogeneous dispersion of particles in water. The prepared mixture was then impregnated into the fabric from the padding at a speed of 2 m/min and a pressure of 2 bar. Subsequently, the fabrics were allowed to dry at room temperature.

The fabrics were subjected to morphological characterization via scanning electron microscopy (SEM), and the chemical composition was analyzed via energy-dispersive X-ray spectroscopy. The thermal properties of the fabrics were determined via differential scanning calorimetry (DSC). The analyses were carried out in a nitrogen (N₂) atmosphere at a heating/cooling rate of 5 °C/min between -5 °C and 65 °C using a Perkin-Elmer Jade DSC device. Furthermore, visual inspection and color measurements of the fabrics in both hot and cold conditions were also conducted.

Spectroscopic analysis of the fabric thermochromic property: To ascertain the temperature-dependent reversible color change resulting from the presence of thermochromic microcapsules in the structures of the fabrics, the color values of fabric samples cooled below the transition temperature and heated above the transition temperature (40°C) were measured with a spectrophotometer. The measurements were conducted using the Datacolor CHECK 3 spectrophotometer device. The color values showing the L* (lightness index), a* (red-green index) and b* (yellow-blue index) were recorded. Colorimetric parameters were calculated using the CIELAB color space under D65 light and 10° standard observers. In the study, the cold-warm total colour difference value (ΔE) was calculated using the following formula (Equation 1):

$$\Delta E = \sqrt{[(L_x^* - L_0^*)^2 + (a_x^* - a_0^*)^2 + (b_x^* - b_0^*)^2]}, \text{ (Equation 1)}$$

where: L₀*, a₀*, and b₀* represent the L*, a*, and b* values of the coloured fabric samples (reference sample).

The ΔE value represents the total color difference between two samples, with an increase in this value indicating a larger color difference. In the commercial context, a ΔE value of less than 1 indicates that the color difference is insignificant. A negative ΔL value indicates that the color of the compared sample is darker than the reference, whereas a positive value indicates that it is lighter.

The alteration in the surface temperature of the fabrics in variable temperature environments was ascertained through the utilization of the Thermal History (T-History) test methodology, which was employed in our previous studies. In this test, the surface temperature of the fabric, which was previously subjected to a cold environment, was quantified using a thermal camera or thermocouple while it was heated in a hot insulated box (Demirbağ and Alay-Aksoy, 2016; Genç and Alay-Aksoy, 2016; Alay-Aksoy et al., 2017). The graphs of the measured temperatures were plotted as a function of time. In the evaluation, it was taken into account whether the heat absorbed by the PCM during its melting had an effect on the fabric surface temperature. For this purpose, the same measurement was repeated for the fabric without capsules and whether there was a temperature difference compared to the fabric with capsule content was examined. Before the measurement, both the reference (microcapsule-free) fabric and the sample (microcapsule-containing) fabrics were conditioned at 0 °C for 24 hours. The conditioned fabrics were placed in an enclosure maintained at a temperature of 40 ± 3 °C, and the surface temperatures were recorded with a thermal camera. In the measurement environment, the TS in the microcapsule structure was permitted to melt, and the impact of the heat absorbed from the surrounding environment during this process on the fabric surface temperature was determined. In the hot measurement system, the surface temperature of the fabric was recorded at 30-second intervals for a period of 45 minutes using a thermal camera.

2. RESULTS

The presence of matter in the structure of the fabrics prepared in the study was determined through the application of fabric SEM images and EDX analysis. The thermochromic properties of the fabrics were investigated through an examination of the photographs taken at varying temperatures, in conjunction with the utilization of spectroscopic colour measurement outcomes. The latent heat energy storage and dissipation properties of the fabrics were investigated with the aid of differential scanning calorimetry (DSC), and the temperature regulation functions were investigated with

the use of a T-history test. This was done in order to ascertain the effects of the presence of nanocapsulated thermochromic capsules on the fabrics. This section presents the results of all tests and analyses.

2.1. Morphological analysis of the fabrics

The SEM images of the fabric (Fabric 1) treated with a nanocapsule bath containing zinc oxide (ZnO) nanoparticles are presented in Figure 1. Figure 2 depicts the SEM images of the fabric (Fabric 2) treated with a nanocapsule bath without the inclusion of ZnO particles. The SEM images provided clear evidence of the presence of nanocapsules in both fabric structures. It was observed that the nanocapsules were located close to each other both on the surface of the fibres and between the fibres. In contrast to the observations presented in Figure 2, the SEM image captured at 500 times magnification in Figure 1 revealed a greater number of particle placements within the fabric structure. This difference was attributed to the presence of ZnO microparticles in the bath. EDX analysis was carried out to confirm this finding and to determine the presence of ZnO in the fabric structure.

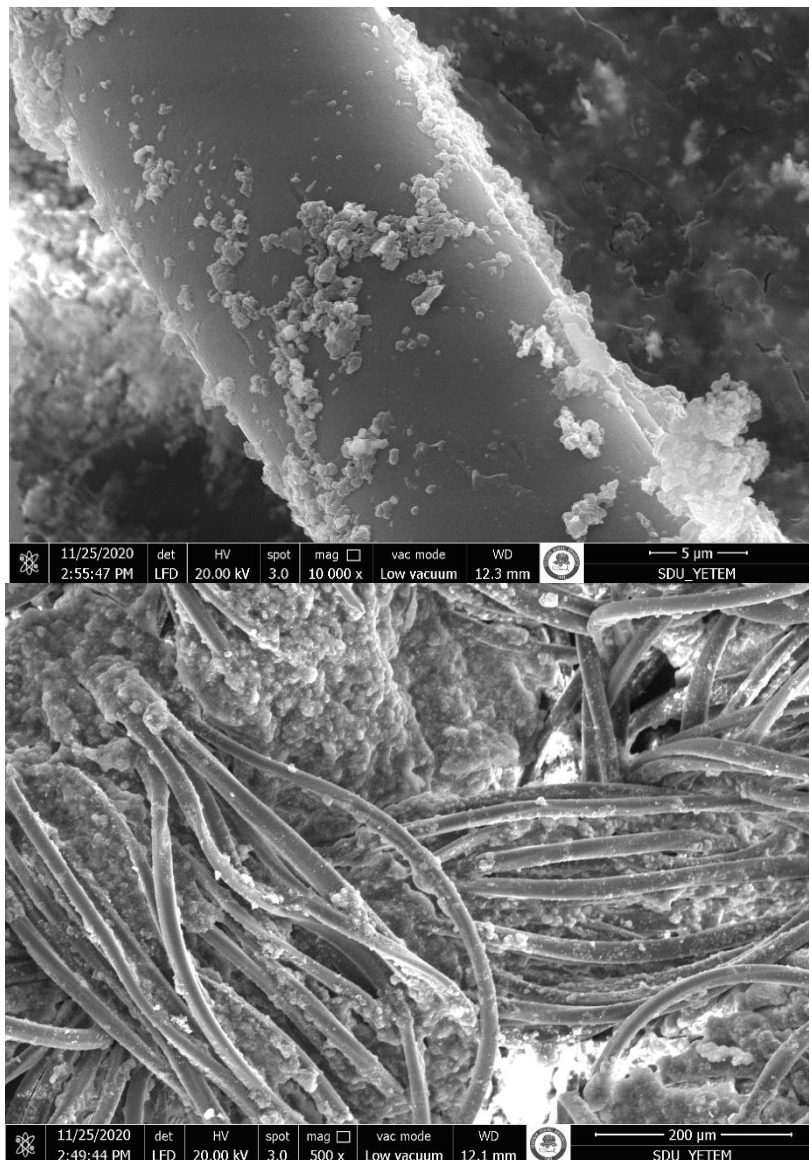


Figure 1. SEM images of the Fabric 1 treated with a nanocapsule bath containing zinc oxide (ZnO) particles (at 10kX and 500X magnifications)

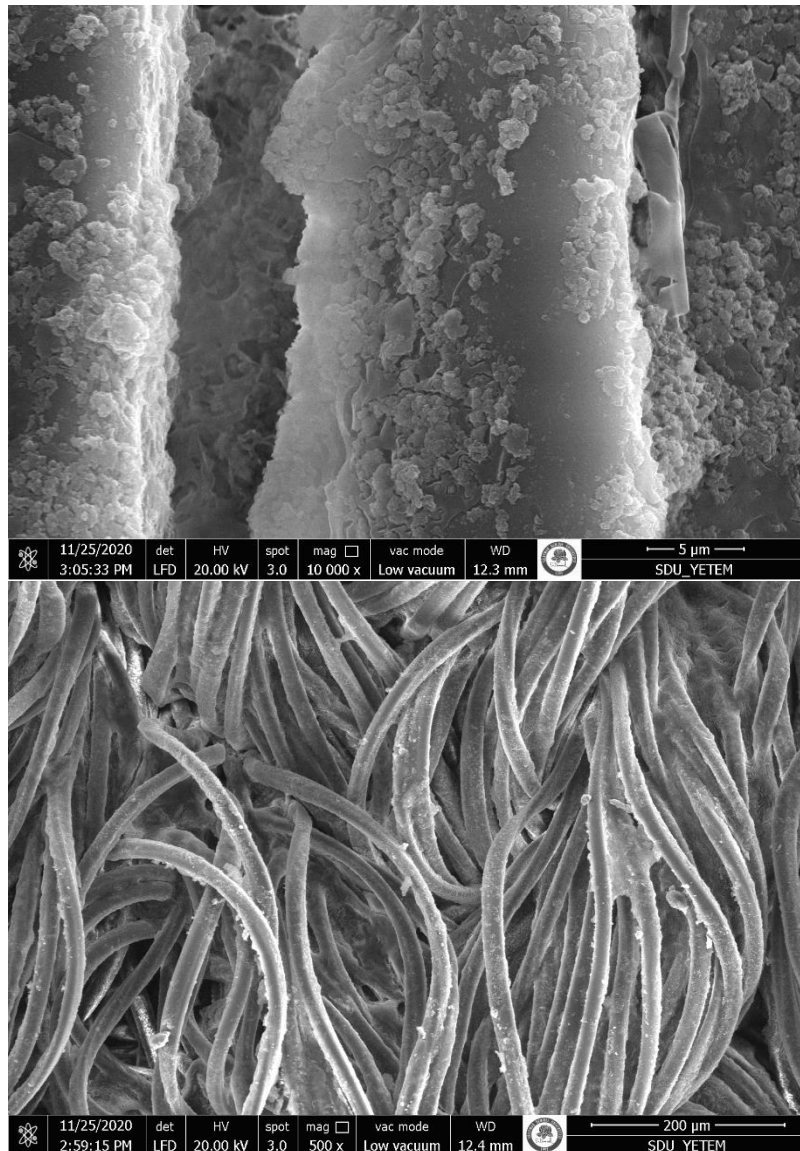


Figure 2. SEM images of the Fabric treated with a nanocapsule bath without the inclusion of ZnO particles (at 10kX and 500X magnifications)

2.2. SEM-EDX analysis results

The results of SEM-EDX analysis of the fabrics are given in Table 1.

Fabric sample	Elements	Weight (%)	Atomic (%)
Untreated	C	65.08	71.28
	O	34.92	28.72
Fabric 1 treated with a nanocapsule bath containing zinc oxide (ZnO) particles	C	61.24	70.01
	O	28.47	24.43
	N	4.38	4.30
	ZnO	5.68	1.19
	Others	0.23	0.07
Fabric 2 treated with a nanocapsule bath without the inclusion of ZnO particles	C	62.30	68.52
	O	33.60	27.74
	N	3.90	3.68
	Others	0.21	0.06

2.3. Fabric thermochromic feature

Figure 3 illustrates the fabric images taken in both cold and hot conditions. The images were taken when the fabrics were cooled to a temperature below the melting point of the solvent component of the thermochromic system (cold) and then heated to a temperature above the melting point (hot). As shown in the images, the fabrics were observed to be colourless when heated, but exhibited a green hue when cooled. This finding demonstrates that the fabrics undergo a change in colour in response to a change in temperature, thereby exhibiting thermochromic properties.



Figure 3. Photographic images of fabrics taken in heat and cold (a: Fabric 1 treated with a nanocapsule bath containing zinc oxide (ZnO) particles b: Fabric 2 treated with a nanocapsule bath without the inclusion of ZnO particles)

Table 2 presents the results of the colour measurement of Fabrics 1 and 2. The total colour difference value (ΔE) was calculated by employing the colour parameters derived from the spectroscopic colour measurement results. The calculation was based on the difference between the measured parameters in the colourless state when the fabrics were heated and the colour parameters measured in the coloured state when the fabrics were cooled. The elevated total colour difference value suggested that the hot-cold colour contrast of the fabrics was greater. The total colour difference value ($\Delta E=16.77$) was higher for fabric 2 treated with a nanocapsule bath without ZnO particles. This finding revealed that Fabric 2 exhibited a more pronounced colour change. It is hypothesised that the incorporation of ZnO into the nanocapsule bath influences the thermochromic quality of the fabric, potentially resulting in the emergence of lighter colour tones.

Table 2. Fabric color measurement parameters

Fabric sample	Test	Mean values of the color parameters			
		ΔL	Δa	Δb	ΔE
Fabric 1	1	28.49	11.72	-0.03	15.06
	2	25.59	9.79	0.69	12.39
	3	26.0	9.57	0.68	12.15
Mean		26.69	10.36	0.44	13.2
Fabric 2	1	26.83	15.31	2.23	16.21
	2	27.81	15.9	1.11	17.13
	3	27.15	15.87	2.14	16,9
Mean		27.26	15.69	1.82	16.77

2.4. Thermal energy storage properties of the fabric

The results of the differential scanning calorimetry (DSC) analysis of the fabrics are presented in Table 3. Upon examination of the results, it becomes evident that both fabrics containing nanoencapsulated thermocomic systems demonstrate thermal energy storage and dissipation properties. The enthalpy values were found to be comparable to those reported in the literature for both fabrics (F. De Castro et al., 2021; El Majd et al., 2024). The results demonstrated that the fabrics can be employed as thermoregulation and thermal energy storage materials, offering potential usage for enhancing clothing thermal comfort. A comparison of the thermal properties of the fabrics revealed that Fabric 2 exhibited higher enthalpy values. This result was attributable to the absence of ZnO particles in the application bath, resulting in the lack of ZnO application to the fabric. In a DSC analysis, the enthalpy values are determined based on the weight of the samples. If the fabric sample subjected to the test contains ZnO, the ratio of the phase change material (PCM) in the total weight decreases, resulting in a reduction in the enthalpy value. Furthermore, the ZnO particles added to the solution may have limited the amount of nanocapsules applied to the fabric due to the saturation state of the fabric.

Table 3. Fabric DSC analysis results

Fabric sample	Melting point (°C)	Melting Enthalpy (J/g)	Solidification temperature (°C)	Solidification Enthalpy (J/g)
Fabric 1 treated with a nanocapsule bath containing zinc oxide (ZnO) nanoparticles	34.3	13.81	33.2	13.,38
Fabric 2 treated with a nanocapsule bath without the inclusion of ZnO particles	32.8	31.51	32.00	31.97

Figure 4 shows the time dependent fabric surface temperature change curves of the fabrics treated with nanocapsules and ZnO particles by impregnation method. Upon examination of the curves, it was determined that the warming behaviour of all fabrics exhibited a comparable trend, and the curves were classified into two regions: a fast warming region and a slow warming region. The curves of the nanocapsule-treated fabrics did not align with those of the raw fabric. It was observed that the raw fabric reached a higher temperature at a faster rate. The raw fabric was heated to 38 °C in 3 minutes. In contrast, the surface temperatures of nanocapsule-containing fabrics reached 35.5 °C in about 5 minutes. After this point, the slope of the surface temperature change curve decreased (slow heating) and the surface temperature of the fabrics reached a maximum of 40.8 °C at the end of the test period (45 minutes). At the end of the test period, the raw fabric surface temperature reached 42.9 °C and continues to increase. During the test period, the surface temperature of the nanocapsule-containing fabrics was generally measured at least 2 °C below the surface temperatures of the raw fabric. The difference between the nanocapsule-containing fabric temperatures and the raw fabric temperatures is related to the latent heat absorbed during the melting of the PCM contained in the capsule. The PCM in the structure absorbs heat from the environment while melting, which causes the fabric surface temperature to decrease. On the other hand, while the surface temperatures of Fabric 1 and Fabric 2 containing nanocapsules are different in the warming region (first 10 minutes), they are almost equalized after this region, i.e. in the region where thermal equilibrium occurs. In the rapid heating region, the fabric containing ZnO and nanocapsules heated less while the fabric containing only capsules heated more. This temperature difference between Fabric 1 and Fabric 2 fabrics was associated with the presence of ZnO in the fabric structure. The high heat conductivity of the ZnO fabric increased the thermal response of the PCM and enabled the fabric to heat up less.

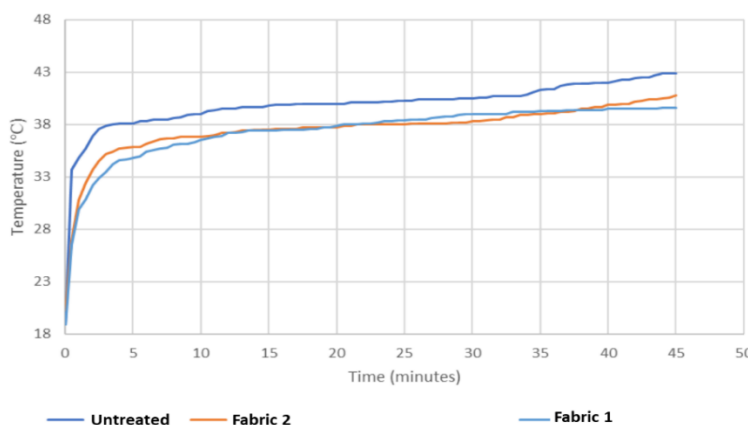


Figure 4. Fabric surface temperature curves measured by T-History test

3. DISCUSSION AND CONCLUSIONS

In this study, a nanoencapsulated thermochromic system and zinc oxide microparticles were applied to polyester fabric by padding method. The objective was to produce polyester fabrics with thermochromic and thermal energy storage functions. To this end, nanocapsules with a non-toxic polymethyl methacrylate (PMMA) shell were employed.

The study employed SEM and EDX to ascertain the presence of nanocapsules and ZnO particles within the fabric structure. It was evident from spectroscopic measurements and fabric photographs that the fabrics exhibited reversible colour change in response to temperature fluctuations, thereby demonstrating thermochromic properties. It was demonstrated by DSC and T-history tests that the fabrics offer thermal energy storage up to 30 J/g and a significant thermoregulation property, respectively. It was concluded that ZnO particles added to the nanocapsule bath improved the thermoregulation property of the fabrics by improving the thermal response of the thermochromic system in the fabric structure during the thermal energy storage process.

Acknowledgements

This work was supported by the scientific and technological council of Türkiye (TUBITAK, Project Number 118M012). Therefore, authors would like to express their appreciation to TUBITAK.

Ethics Committee Approval

N/A

Conflict of Interest

The authors have no conflicts of interest to declare.

Funding

This work was supported by the scientific and technological council of Türkiye (TUBITAK, Project Number 118M012)

REFERENCES

- Alay-Aksoy, S., Alkan, C., Tözüm, M. S., Demirbağ, S., Altun-Anayurt, R., Ulcay, Y. 2017. "Preparation and textile application of poly(methyl methacrylate-co-methacrylic acid)/ n-octadecane and n-icosane microcapsules", *The Journal of Textile Institute*, 108(1):1, 30-41.
- Chowdhury, M. A., Joshi, M., Butola, B. S., 2014. Photochromic and Thermochromic Colorants in Textile Applications, *Journal of Engineered Fibers and Fabrics*, 9(1), 107-123.
- Crano, J. C., Guglielmetti, R. J., 2002. *Organic Photochromic And Thermochromic Compounds, Volume 2: Physicochemical Studies, Biological Applications, and Thermochromism*. Kluwer Academic Publishers, 467s, New York, Boston, Dordrecht, London, Moscow.
- Demirbağ, S., Alay-Aksoy, S., 2016. "Encapsulation of phase change materials by complex coacervation to improve thermal performances and flame retardant properties of the cotton fabrics", *Fibers and Polymers*, 17(3), 408-417.
- El Majd, A., Sair, S., Ousaleh, H. A., Bouhaj, Y., Belouaggadia, N., Younsi, Z., & El Bouari, A. (2024). Advancing tent thermoregulation: Integrating shape-stabilized PCM into fabric design. *Journal of Energy Storage*, 95, 112681.
- F. De Castro, P., Minko, S., Vinokurov, V., Cherednichenko, K., & Shchukin, D. G. (2021). Long-term autonomic thermoregulating fabrics based on microencapsulated phase change materials. *ACS applied energy materials*, 4(11), 12789-12797.
- Genç, E., Alay-Aksoy, S., 2016. "Fabrication of microencapsulated PCMs with nanoclay doped chitosan shell and their application to cotton fabric", *Tekstil & Konfeksiyon*, 26(2), 180-188.
- Hossain, M. T., Shahid, M. A., Ali, M. Y., Saha, S., Jamal, M. S. I., & Habib, A. (2023). Fabrications, classifications, and environmental impact of PCM-incorporated textiles: current state and future outlook. *ACS omega*, 8(48), 45164-45176.
- Li, Y., Yang, A., Li, Y., Jiang, Z., He, F., Chen, Z., ... & Yang, W. (2023a). TC@ MF phase change microcapsules with reversibly thermochromic property for temperature response and thermoregulation. *Colloids and Surfaces A: Physicochemical and Engineering Aspects*, 677, 132333.

- Liu, H., Deng, Y., Ye, Y., & Liu, X. (2023). Reversible Thermochromic Microcapsules and Their Applications in Anticounterfeiting. *Materials*, 16(14), 5150.
- Özkayalar, S., Adıgüzel, E., Aksoy, S. A., & Alkan, C. (2020). Reversible color-changing and thermal-energy storing nanocapsules of three-component thermochromic dyes. *Materials Chemistry and Physics*, 252, 123162.
- Tözüm, M. S., Alay-Aksoy, S., Alkan, C. (2018). Microencapsulation of the thermochromic system prepared with phenolphthalein color developer. *ETT 2018-8th International İstanbul Textile Conference*, 14–16 April 2018.
- Tözüm, M. S., Alkan, C., & Alay Aksoy, S. (2020a). Preparation of poly(methyl methacrylate-co-ethylene glycol dimethacrylate-co-glycidyl methacrylate) walled thermochromic microcapsules and their application to cotton fabrics. *Journal of Applied Polymer Science*, 137(24), 48813–48815. <https://doi.org/10.1002/app.48815>
- Tözüm, M. S., Alkan, C., & Alay Aksoy, S. (2020b). Developing of thermal energy storing visual textile temperature indicators based on reversible color change. *Journal of Industrial Textiles*, <https://doi.org/10.1177/1528083720980831>
- Tözüm, M. S., Alay Aksoy, S., & Alkan, C. (2022). Development of reversibly color changing textile materials by applying some thermochromic microcapsules containing different color developers. *The Journal of The Textile Institute*, 113(10), 2159-2168.
- Wang, Y., Ren, J., Ye, C., Pei, Y., & Ling, S. (2021). Thermochromic silks for temperature management and dynamic textile displays. *Nano-micro letters*, 13, 1-17.
- Yi, S., Sun, S., Deng, Y., & Feng, S. (2015). Preparation of composite thermochromic and phase-change materials by the sol-gel method and its application in textiles. *The Journal of The Textile Institute*, 106(10), 1071-1077.
- Yu, W., Liu, H., Tan, J., & Wang, C. (2024). The reversible thermochromic fabric for the double-stage temperature monitoring. *European Polymer Journal*, 206, 112769.
- Zhai, X., Wu, Z., & Peng, H. (2022). Minireview on application of microencapsulated phase change materials with reversible chromic function: advances and perspectives. *Energy & Fuels*, 36(15), 8054-8065.
- Zhang, Y., Liu, H., Niu, J., Wang, X., & Wu, D. (2020). Development of reversible and durable thermochromic phase-change microcapsules for real-time indication of thermal energy storage and management. *Applied Energy*, 264, 114729..
- Zhang, W., Zhang, H., Liu, S., Zhang, X., & Li, W. (2024). Preparation and crystallization behavior of sensitive thermochromic microencapsulated phase change materials. *Applied Energy*, 362, 122993.
- Zhou, L., Ye, J., Cai, Q., Liu, G., Dadgar, M., Zhu, G., & Zhang, G. (2024). Study on preparation, characterization and application of mixed-colorants thermochromic microcapsules. *Particuology*, 88, 89-97.

Asphalt Binder Modification in Flexible Pavement Using Different Amounts of Crumb Rubber

Saber Shah -Saber^{*1}, Raidy Gul-Hamdard², Waliullah Qasimi³

Abstract: Every year, thousands of tires made of crumb rubber are consumed as scrap. By burning this material, more landfill space is needed, which poses a crumb rubber in PG76 performance grade and 80–100 penetration grade asphalt binder mix. Using a wet method, the asphalt binders were combined with waste crumb rubber to create a powder form 40 mesh (0.425 micron).health risk and environmental problem. The study concentrated on using crumb rubber to replace 15, 20, and 25% of the modified asphalt binder mix's total weight. The Malaysian JKR/SPJ/2008-S4 standard and the American Society for Testing and Materials (ASTM) served as the foundation for the laboratory work. Numerous tests were carried out, including pressure aging vessel, rolling thin film oven, penetration, softening point, and viscosity testing on modified asphalt binder. The outcome demonstrates a beneficial effect, with penetration decreasing as 80–100% and PG76 blend asphalt binder are partially substituted with crumb rubber. In contrast to 80–100 asphalt binder, the PG76 asphalt binder result exhibits reduced penetration in terms of stiffness throughout both short- and long-term aging. The softening point test results indicate that replacing a portion of the asphalt binder with crumb rubber raises the temperature of the PG76 and 80-100 asphalt binder mix. This is especially true after the PG76 short term aging test (RTFOT) at 20% replacement, when the temperature reached 85°C, and after the long term aging test (PAV), when the temperature dropped to 75°C. However, resistance to increased temperature susceptibility is indicated by the partial replacement of asphalt binder by crumb rubber. According to the results of the viscosity test, the PG76 asphalt binder is viscouster than the original PG76 and the 80-100 asphalt binder replacement made of crumb rubber mix. For the short-term aging (RTFOT) test, the PG76 asphalt binder suggests that a crumb rubber replacement of 20% is ideal. When compared to the RTFOT test, the viscosity decreased in the long-term aging (PAV) test.

Keywords: Crumb Rubber, Modification, Asphalt Binder Mix, Replacement.

¹Address: Shaikh Zayed University, Faculty of Civil Engineering, Khost/Afghanistan

²Address: Shaikh Zayed University, Faculty of Civil Engineering, Khost/Afghanistan

***Corresponding author:** s.sabershah@mail.com

1. INTRODUCTION

Both polar and rheological properties characterize asphalt binder. The primary impetus for asphalt binder modification is the current state of conventional refining methods' limitations in producing asphalt binder from crude petroleum oil. It has been discovered that modification by specific refining techniques, chemical reactions, and/or additives can enhance the contribution of asphalt binder as well as its resilience to different kinds of pavement degradation. 35 out of 47 State Highway Agencies in the United States of America (USA) surveyed recently stated that they want to utilize more modified binders while building new roads. Twelve of the agencies anticipated using the same quantity of modified asphalt binder, while several agencies intended to use less of it. Premature discomfort, such as fatigue cracking and rutting, has been cited by most authorities as the primary justification for the use of modified binders (Bahia et al., 1997).

Given the tremendous complexity of asphalt, a thorough chemical investigation might not be feasible (Read and Whiteoak, 2003). Rubber and tires have long been recycled for use in various highway and road applications in a number of Asian, European, and African nations. However, crumb rubber reduces the

amount of landfill space needed, which will lessen its impact on the environment, and conserves the material used to build roads. Numerous investigators (Bahia et al., 1994). Crumb rubber can be used to make modified asphalt binder materials and paving products through a variety of mixing and blending techniques, including a dry process. Prior to incorporating asphalt in the dry phase, crumb rubber is blended with hot aggregate. Binder, and before incorporating the crumb rubber blend with asphalt binder, wet process it. CRM asphalt binder requires compaction at a higher temperature than simple

mixtures, according to earlier studies (Amirkhanian and Corley, 2004). The usage of CRM in the mix may cause different issues with lower compaction temperatures, including inadequate volumetric characteristics (i.e., excessive air voids) and

subpar short- and long-term performances. Moreover, a rise in viscosity can have a detrimental effect on the asphalt mixture's workability, and a higher temperature is needed to maintain the binder viscosity for optimal workability.

1.1 Problem Statement

All urban and highway roads are intended to last between ten and twenty years. Regretfully, pavement damage or discomfort persists before the road's intended serviceability maximum time is reached. Among the key factors recurrently high traffic loads on the road's surface are one of the elements causing this pain. Repeated loads that result in tensile strain in the lowest pavement layer because fatigue cracks. Rutting of the road surface mostly happens in nations with warmer pavement, like those in North Africa or South Asia, and is caused by the accumulation of compressive strain at the top of the subgrade layer. In order to increase the performance of the pavement surface, several trails have already been created employing crumb rubber to change the asphalt binder. One of the applications for crumb rubber in Hot Mix Asphalt (HMA), to reduce industrial waste issues or enhance the efficiency of HMA, use asphalt mix or an industrial mix plant.

1.2 Objectives of Study

The study's main goal is to partially replace the weight of the blended asphalt binder mix utilizing waste crumb rubber at varied percentages (15, 20, and 25%) through a wet process. The particular goals are:

- 1) To assess the physical characteristics of the asphalt binder while using crumb rubber as a partial replacement at different weight percentages (15, 20, and 25%) relative to the total weight of the blended asphalt binder mix.
- 2) To assess the short- and long-term aging performance of replacing asphalt binder with crumb rubber.
- 3) To ascertain the ideal percentage of crumb rubber substitution in the asphalt binder mix composition

1.4 Scope of Study

The physical characteristics and effectiveness of partial replacement of asphalt binder with varying percentages of crumb rubber (15, 20 and 25%) by total weight of asphalt binder mix will be the main focus of the study. Performance grade PG-76 and penetration grade 80-100 asphalt binder will be used. A variety of samples will be made, each with a different amount of crumb rubber and a varied mixing temperature in the asphalt binder.

The experiment, which will take place in the Highway and Transportation Laboratory at University Technology Malaysia (UTM), will follow the guidelines set forth by the American Society for Testing and Materials (ASTM) and (JKR/SPJ/2008-S4). To measure the characteristics of CRM asphalt binder, a number of tests, including Viscosity, Softening Point, Penetration, Rolling Thin Film Oven, and Pressure Aging Vessel tests, will be carried out.

1.3 Importance of Research

The creation of a novel, modified asphalt binder including crumb rubber is the study's anticipated result. The CRM asphalt binder is made to reduce pavement costs while improving ride quality. Use crumb rubber in construction in place of certain asphalt binder. Lastly, the development of CRM asphalt binder will contribute to the creation of green and sustainable roads and highways by addressing the issue of industrial waste crumb rubber.

2.0 Literature Review

2.1 Asphalt Binder

Petroleum oil derived from the remains of marine or navel creatures and plant materials deposited on the ocean bed is used to make asphalt, often known as bitumen (Whiteoak, 1991). The issue began to arise millions of years ago, and as a result of the higher layers' great weight, the lower layer's stuff was squeezed. Large subterranean reservoirs are created when the materials and heat from the Earth's crust combine to make petroleum oil that is trapped by impermeable rock (Whiteoak, 1991). Sometimes faults in the layers above allow petroleum oil to rise and sometimes accumulate, reaching the ground's surface. Nowadays, pile drilling is used to retrieve the majority of petroleum oil from the subsurface

(Whiteoak, 1991). Only a small percentage of crude oil or petroleum is produced, making it unsuitable for use as an asphalt design mix basic ingredient. Asphalt is described as a viscous liquid or solid that is mostly composed of hydrocarbons and their derivatives in British Standard 3690: Part 2 (1989). It is extracted from crude petroleum oil through a refining process and is also a part of either as a naturally occurring deposit or in combination with mineral materials.

2.2 Asphalt Binder Modification

Ordinary asphalt is used on most public roads and highways to create well-performing pavements. However, the need to create roads grows yearly as a result of an increase in automobiles. Eventually, these roads will cause widespread problems, the most significant of which are caused by huge truck loads and extremely high temperatures. Furthermore, since high standards for safety, comfort during riding, frequency of maintenance, and service design life have become crucial considerations in road design, it is crucial for pavement applications to improve the qualities of the asphalt binder in order to improve performance and lessen the road's asphalt binder distress (Brule, 2007). While maintaining a low viscosity at the typical temperatures it is placed at, the perfect binder should have improved cohesiveness and very low climatic condition (temperature) susceptibility throughout the range of temperatures to which it will be subjected throughout service. Its fatigue properties, fracture strength, and resistance to permanent deformation should all be extremely high, while its susceptibility to loading time should be minimal. It should also possess passive and active adhesion properties that are comparable to those of conventional binders, at the very least. In conclusion, its aging properties ought to be favorable for both laying and using (Brule, 2007).

2.3 Crumb Rubber

The Rubber Manufacturers Association reports that a significant number of scrap tires, or crumb rubber, are consumed annually and that these tires are causing grave issues such as an increase in landfill area and environmental issues (Snyder, 1998). Using the crumb rubber in the modification of asphalt binders is one of the techniques that have been used in an effort to find more efficient ways to recycle the tires with crumb rubber. According to reports, the up to 40% of crumb rubber can be absorbed by the asphalt industry (Avraam,

2005). Tires are mostly made of rubber, steel, and fiber. Of them, rubber makes up the majority of the tire's composition (around 60% of its weight). Furthermore, the rubber is made up of a variety of substances, including carbon black, various mineral fillers, and natural and synthetic rubbers (Mark et al., 2005). The percentage of natural and synthetic rubber varies between truck and passenger vehicle tires, but overall, ground rubber is rather uniform, and the ground rubber industry is not dependent on any one tire type (Ruth, 1995). The impact of ground tire particle size and grinding technique on asphalt binder qualities was investigated by the National Center of Asphalt Technology (NCAT). Twelve samples of crumb rubber combined with one asphalt binder were used in the study. Twelve mixes containing 10% crumb rubber by weight of asphalt were created, and two further mixes containing 15% rubber were created. According to test results on performance grade, crumb rubber's surface area and particle size had the biggest effects on raising the high-temperature performance grade.



Figure 2.1 Industrial waste (crumb rubber)

Generally speaking, there are two different processes used to make Crumb Rubber Modified (CRM) binder: wet and dry. Fine CRM and asphalt binder are blended together during the wet process. Coarse CRM is substituted for aggregate in the asphalt mixture during the dry phase. According to Takallou et al. (1991), the wet procedure is more effective at enhancing the characteristics and functionality of an asphalt mixture. Given its propensity to absorb liquids and swell, crumb rubber is a cheap modifier for asphalt binder that enhances paving performance and safety for the highway pavement sector (Amirkhanian, 2003).



Figure 2.2 Different sizes of crumb rubber

2.4 Asphalt Rubber

The definition of asphalt rubber (AR) by the American Society of Testing and Materials (ASTM) is "a blend or mix of asphalt binder, reclaimed tire rubber, and certain additives in which the rubber component is at least 15 percent by weight of the total blend and has reacted in the hot asphalt binder." ASTM D 6114, "Standard Specification for Asphalt Rubber Binder," which can be found in Vol. 4.03 of the Annual Book of ASTM Standards 2001, and Caltrans Standard Special Provisions for Asphalt Rubber Binder both contain the necessary physical characteristics. In order to maintain the crumb rubber particles suspended in the blend and to encourage the physical interaction of the asphalt binder and rubber constituents, the asphalt rubber is manufactured at high agitation temperatures ($\geq 177^{\circ}\text{C}$). It is possible to add different extender oils to increase workability, facilitate spray applications, and reduce viscosity.

The reclaimed rubber, also known as crumb rubber modifier, is made from waste tire rubber. Tire thieves combine natural rubber, synthetic rubber, fillers, carbon black, and oils of the extender kind that dissolve in hot 12 grade asphalt. According to California specifications, asphalt rubber must contain between 18 and 22 percent crumb rubber that has been adjusted by the mix's total mass. Additionally, scrap rubber with a high natural rubber content (25 ± 2 percent by mass) that may come from waste tires or other sources must be included in the CRM.

2.5 Wet Process

There are generally two methods for combining waste crumb rubber and asphalt binder: a wet method and a dry method. When opposed to a dry procedure, it is preferable to use a wet one because of its superior resistance to fatigue and rutting potential. The wet technique involves mixing asphalt binder and crumb rubber before adding heated aggregates (Takallou, 1988). The process of interaction depends on several variables, including the temperature and duration of the blending, the size of the crumb rubber, the quantity and kind of mechanical mixing, and the kind of asphalt binder. The asphalt binder's aromatic component is incorporated into the natural and synthetic rubber's polymer network during the wet process (Heitzman, 1991).

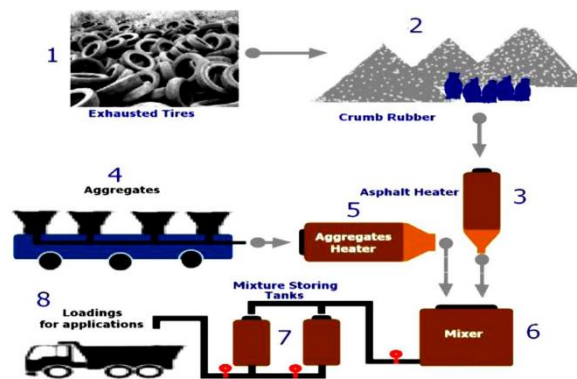


Figure 2.3 Wet process procedure

2.5.1 Performance of Wet Process

Several researchers have assessed the effectiveness of CRM combinations made utilizing the wet technique in both lab and field settings. When compared to conventional combinations, the crumb rubber blended utilizing method showed a superior resilience to fatigue in terms of mechanical performance, such as fatigue (Harvey et al., 2000; Oliver, 2000). Similar outcomes employing the wet technique in dense graded surface, gap graded surfacing, and binder courses were noted in Louisiana following five to seven years of trafficking (Huang et al., 2002). Oliver (2000) also discovered that the fatigue life of combinations made with 6% or less binder concentration was poor and inconsistent. The rut depth of the wet process mixtures utilized in Louisiana was either the same or less than that of the conventional sample (Huang et al., 2002).

2.6 Dry Process

In the dry method, heated aggregates and crumb rubber are combined before asphalt binder is added. A dry method known as Plus Ride involves adding 1-3% of crumb rubber to the mixture, with particles sized between $\frac{1}{2}$ inch and No. 10 sieve (Federal Highway Administration 1998). The air void content, which is often between two and four percent, is the primary consideration in the Plus Ride system's design. The temperature and the amount of time the binder takes to react with the ground rubber are two other important variables. For the ground rubber particles to maintain the necessary stiffness and physical form, these two parameters must be kept under control. Numerous studies conducted in various states have revealed mixed results, with some demonstrating an improvement in the physical qualities and others demonstrating a net economic loss when compared to traditional pavement mix (Huang et al., 2007).

2.7 Surface Distress Mechanisms: An Overview

Numerous researchers offer explanations for the distress mechanisms of various hot mix asphalts (HMA). The state of the pavement structure that shortens its service life or suitability is called distress. The outward manifestations of various distress processes, which typically result in a decrease in serviceability, are known as distress appearances. Repeatedly high traffic volumes and environmental conditions cause distress. Several distresses can occur on pavement, including rutting, fatigue cracking, delimitation shoving, distortion, raveling, and slippage. These are often caused by strong traffic loads on the pavement surface (Mohamed, 2007).

2.7.1 Permanent Deformation

The accumulation of a tiny quantity of unrecoverable strain brought on by repeatedly applying loads to the pavement results in permanent deformations. Unbound base course, troublesome subgrade, or HMA can all lead to rutting. Consolidation and lateral movement of hot mix asphalt (HMA) under traffic are the main causes of the persistent deformation in HMA. The top 100 mm of the pavement surface is often where hot mix asphalt (HMA) shear failure happens. But if the right materials aren't employed, it might go deeper (Moha, 2007).



Figure 2.4 Permanent Deformation (Rutting)

2.7.2 Fatigue Cracking

When strong traffic loads create a horizontal build-up of tensile strain at the bottom of the hot mix asphalt (HMA) layer, fatigue cracking of flexible pavements results. Tensile strain and the permissible number of high load repetitions are related by the failure criterion. The Hot Mix Asphalt (HMA) bottom is where the cracking

starts since there is the most tensile strain under wheel load. At first, the cracks spread as one or more longitudinal, parallel fractures. The fractures get joined in a way that mimics an alligator's skin after recurrent strong traffic loads (Mohamed, 2007).

When strong traffic loads create a horizontal build-up of tensile strain at the bottom of the hot mix asphalt (HMA) layer, fatigue cracking of flexible pavements results. Tensile strain and the permissible number of high load repetitions are related by the failure criterion. The Hot Mix Asphalt (HMA) bottom is where the cracking starts since there is the most tensile strain under wheel load. At first, the cracks spread as one or more longitudinal, parallel fractures. The fractures get joined in a way that mimics an alligator's skin after recurrent strong traffic loads (Mohamed, 2007).



Figure 2.3 Permanent Deformation (Rutting)

2.7.3 Penetration Test

Figure 2.7 illustrates how the concentration of crumb rubber affects the penetration of hot-mix asphalt (HMA). Up to 20% of the total crumb rubber content causes the penetrations to decrease. It demonstrates that penetration value is significantly impacted by the content of crumb rubber modified bitumen (CRM). According to Liu et al. (2009), the crumb rubber content has a significant impact on lowering the penetration value by making the crumb rubber asphalt binder more rigid. This would result in a high resistance to rutting and other permanent deformation. With a crumb rubber concentration ranging from 4% to 20%, the improved binder's penetration value was reduced on average by 16.5% to 61%. Furthermore, the linear drastic reduction in penetration is depicted in Figure 2.7, where the correlation coefficient $R^2 = 0.99$ is used. Because the inclusion of crumb rubber increases the viscosity of the asphalt binder, this behavior is warranted. The rubber's particle size is improved by this rise in the amount of crumb rubber. This resulted in less rubberized 18 asphalt binder penetrating the asphalt because of the rubber's contact and expanding into the asphalt during the mixing process, which increased the rubber's mass. Consequently, suggest that the rubberized asphalt binder will be less vulnerable to high temperatures and more resistant to rutting possibilities.

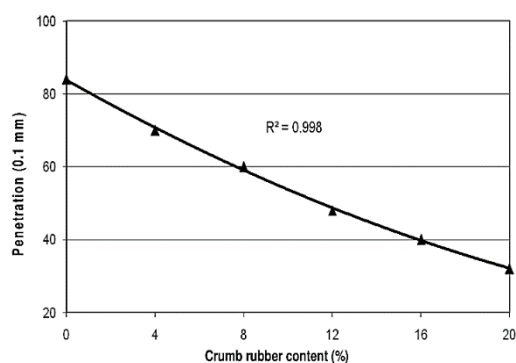


Figure 2.4 Penetration test results for different crumb rubber contents

2.7.4 Softening Point Test

The temperature at which asphalt reaches a specific level of softness is known as the softening point. The softening point rises with increasing crumb rubber content when crumb rubber is added to asphalt binder modification (Nuha, 2011). Stated that the amount of crumb rubber mixed with the asphalt binder will affect the blend's characteristics. Increased levels suggested that the blend's qualities had changed significantly. Increases in rubber content often result in increases in viscosity, resilience modulus, softening point, and penetration at 25°C. The blend performed better in terms of strain value, flexural strength, dynamic stability, and 19–48 h residual stability. Asphalt incorporating 0.2 and 0.4 mm size rubber perform the best experimental results (Souza and Weissman, 1994).

When asphalt and crumb rubber are combined at high temperatures, when bitumen components go into the rubber and cause it to expand, the two materials interact to create a changed binder during the wet process (Bahia and Davies, 1994). The bitumen's aromatic oils cause the rubber particles to swell during the first nonchemical reaction between the asphalt binder and crumb rubber (Heitzman, 1992).

2.7.5 Viscosity Test

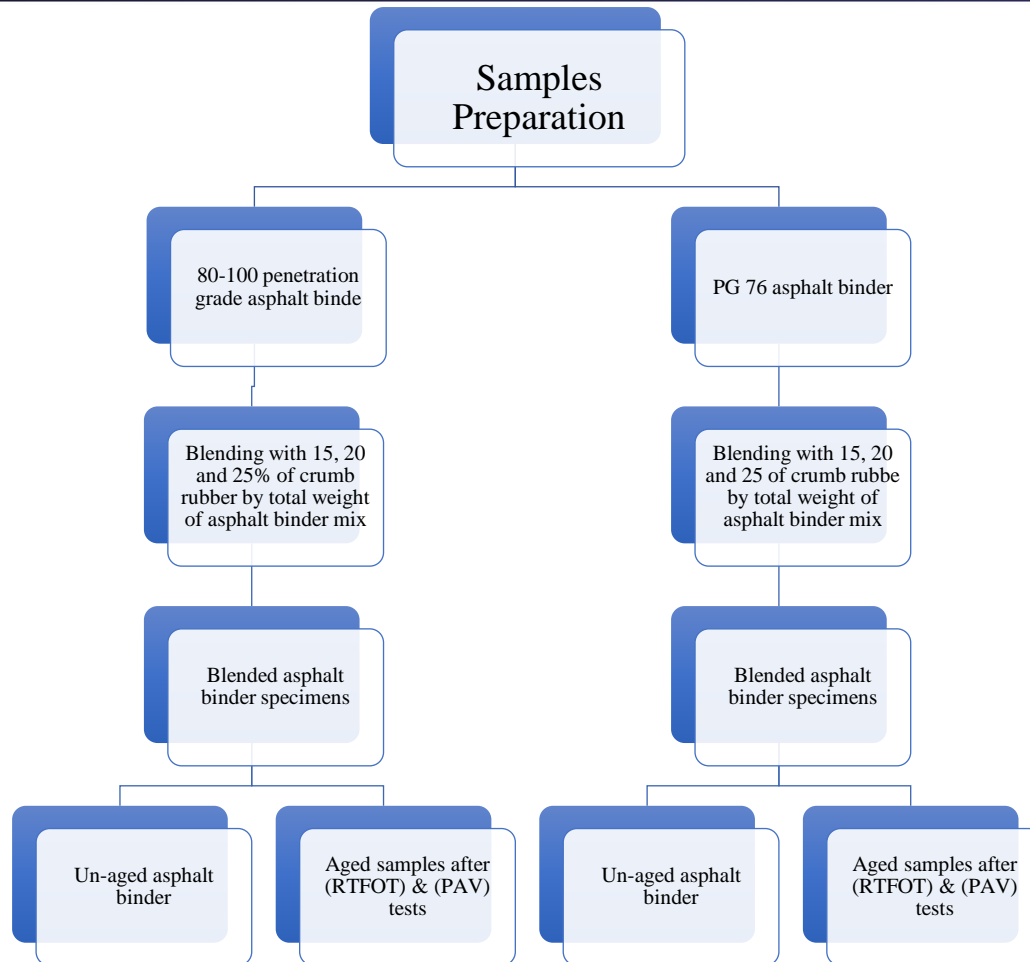
Higher crumb rubber content, according to a study, improved the rutting potential qualities and produced more viscosity at 135°C. Additionally, it was noted that higher amounts of fine crumb rubber led to rubberized asphalt binder that had a higher viscosity and a lower resilience modulus (Magar and Nabin, 2014). For every size of crumb rubber and asphalt binder, the ideal crumb rubber content still needs to be ascertained and assessed. The effective physical characteristics and size of the rubber particle are thought to be changed by a physicochemical interaction that takes place between the asphalt and the crumb rubber (Huang et al., 2007). Because of the way that base binders and modified asphalt binder interacted, pavement performance with the use of crumb rubber was superior to that of base binders. The enhancement may result in pavements with a high resistance to rutting (Huang et al., 2007).

3. MATERIAL AND METHOD /

This chapter outlines the supplies, sample preparation, and testing procedures needed to assess the efficacy of the crumb rubber modified (CRM) asphalt binder and meet the study's goal.

Figure 3.1 below displays the flow chart for sample preparation. Two varieties of asphalt binder (AB) are used in this study: performance grade PG76 and penetration grade 80–100. For 80-100 and PG76, the blending temperature with crumb rubber and asphalt binder is 160°C and 185°C, respectively. In this investigation, different percentages of crumb rubber (CR) (15, 20, and 25%) were utilized to partially replace the entire weight of the asphalt binder mix.

The JKR standard of Malaysia (JKR/SPJ/2008-S4) and the American Society for Testing and Materials (ASTM) were cited in the experimental efforts (as illustrated in Figure 3.2). Physical and rheological tests are part of the laboratory work to assess how crumb rubber behaves when used to partially replace the entire weight of the asphalt binder mix.



3.1 Crumb Rubber Modified (CRM) Asphalt Binder

One provider provided the crumb rubber (CR) used in this investigation. Previous investigations indicated that the lower crumb rubber particle size was experimental work tests physical ASTM D5 Penetration Point; ASTM 4402 Viscosity; ASTM 4402 Rheological Tests For features of crumb rubber asphalt binder, such as cracking resistance and permanent deformation, RTFOT ASTM 2872 PAV ASTM D454 Result and Data Analysis Conclusion 24 is more effective (Glover and Bullin, 1997). Rubber that had passed through a 40 mesh (0.425 mm) filter was used to create CRM binder, which allowed for inexpensive efficiency and homogenized modification.

3.3.1 Crumb Rubber Modified Asphalt Binder

In this investigation, a wet technique was employed to combine the binder modified with crumb rubber. In the wet process, overhead stirrers (SILVERSON and IKA) are used to mix the crumb rubber and asphalt binder at two higher temperatures, 160°C and 185°C, for 60 minutes for asphalt binder 80-100 and PG 76. The mixing speeds are 2000 rpm and 500 rpm, respectively. Laboratory tests were performed to assess the physical and rheological characteristics of aged and unaged crumb rubber modified as a partial replacement with varying percentages (15, 20 and 25%) of the total weight of asphalt binder mix. Figure 3.4 depicts the blending processes and the sample prepared.



Figure 3.1 Blending Process

Table 3.1 : Test Standard and Equipment

Test Standard	Type of Test	Equipment	Description
ASTM D5	Penetration	Penetrometer	25°C, 100gram, 5 sec
ASTM D36	Softening Point	Ring and Ball	3.5g steel ball, Thermometer for softening temperature
ASTM D 4402	Viscosity	Rotational Viscometer (RV)	135°C and 165°C, spindle 27, 20rpm
ASTM D 2872	Short-term aging	Rolling Thin Film Oven (RTFOT)	163°C for 85min
ASTM D 6521	Long term Aging	Pressure Aging Vessel (PAV)	2.1Mpa for 20 hours

3.2 Penetration Test

The penetration test is regarded as the most traditional physical test for asphalt binder and is used to gauge the consistency of the material. The asphalt binder penetrations measure the centimeters to which a standard needle can pierce the material under constant loading, temperature, and time conditions. The penetration test standard procedure used predetermined conditions, with a fixed temperature of 25°C/75°F, a constant weight of 100g, and a known time of 5 seconds. The test was carried out on both pure and modified asphalt binder with different percentages of crumb rubber (15, 20, and 25%). For instance, the asphalt binder 80-100 penetrations show that the asphalt's range of penetration is 80-100, measured in tenths of a millimeter. A tougher grade of asphalt binder is crucial, as indicated by the lower penetration value. The configuration for a penetration test is shown in Figure 3.2.

3.2.1 Procedures of Penetration Test

- a) The sample was heated until it melts to pour.
 - b) The sample was then poured in a specific sample container for penetration test to a depth such that when cooled and kept at room temperature of a test of 25°C.
 - c) Each container was covered as a protection from dust and allowed it to cool for 1 to 1½ hours for the small container and 1½ to 2 hours for the larger container.
 - d) The samples were placed in the water bath and maintained the temperature to 25°C for 1 to 1½ hours depending on container choosing.
- The penetration needle was cleaned with benzene and dried with a clean cloth.

- a) The sample container (100g) was placed directly on the submerged stand in the penetrometer and sample was covered in water bath $25 \pm 0.5^\circ\text{C}$.
- b) The needle was positioned slowly lowering it until it's just makes contact with the surface of the sample.
- c) The pointer of penetrometer was set to zero.
- d) The needle holder was released for the specific period of time (5sec) and the distance penetrated was measured in 1/10mm reading.
- e) The needle was cleaned after the result was taken.
- f) Three determinations were made at points on the surface of the sample not less than 10mm from the side of the container and was obtained the average reading of penetration



Figure 3.2 Penetration test setup

3.3 Viscosity Test

Resistance to flow is known as viscosity, and it is a basic property of asphalt binder that governs the material's behavior both at a specific temperature and across a temperature range. The Superpave PG asphalt binder specification test is always carried out at high temperature, which is 329°F (165°C), and at 275°F (135°C). The basic RV test calculates the torque needed to keep a cylindrical spindle submerged in an asphalt binder at a consistent temperature and rotating at a constant speed of 20 revolutions per minute. The RV then automatically converted this torque to a viscosity and presented it. The ASTM D4402 test process was followed in the description that follows. The Rotational Viscometer Test Setup is shown in Figure 3.3

3.3.1 Procedures of Viscosity Test

- a) Spindle, sample chamber, and viscometer environmental chamber (Thermosel) were preheated to (135°C).
- b) The unaged and aged asphalt binder were heated until fluid enough to pour. Stir the sample, being careful not to entrap air bubbles.
- c) (11g) the weight of asphalt binder was poured into sample chamber; the sample size varies according to the selected spindle (number 27 spindle).
- d) Sample chamber was inserted into the rotational viscometer (RV) temperature controller unit and carefully lowered spindle into the sample.

e) The sample was brought to the desired test temperature (typically 275°F) (135°C) within approximately 30 minutes and allows it to equilibrate at test temperature for 10 minutes.

f) The spindle was rotated at 20 RPM, making sure the percent torque was indicated by the RV readout remains between 2 and 98 percent.

g) Once the sample was reached temperature and equilibrated, 3 viscosity readings from RV display were taken, allowing 1 minute between each reading. Viscosity was reported as the average of 3 readings.



Figure 3.3 Penetration test setup

3.4 Rolling Thin Film Oven Test (RTFOT)

One of the rheological tests used to examine the behavior of hot mix asphalt (HMA) pavement in its early stages is the rolling thin-film oven test, which simulates the short-term aging of an asphalt binder during the manufacturing or mixing process. The mass change in the asphalt binder's weight following the aging process is also measured by the RTFOT test.

The RTFOT is mainly used to simulate short-term asphalt binder aging during the mixing, hauling, and compaction of the (HMA), and the sample can conduct further tests such the Dynamic Shear Rheometer (DSR) for measuring the rutting resistances. This test was conducted in accordance with ASTM D 2872. The Rolling Thin Film Oven Test (RTFOOT) apparatus is depicted in Figure 3.4.

3.4.1 Procedures of (RTFOT) Test

- The sample of asphalt binder sample was heated until fluid or melted.
- Two RTFOT bottles were labeled and weighed empty and the weights were recorded.
- The 34.5g weight of asphalt binder was poured into each bottle.
- The bottles were allowed to cool, after cooling, the two mass changes of bottles were weighed again and recorded the mass loss after the aging.
- The main switch was turned on and the testing temperature was set at 163°C.
- Once the temperature was reached 163°C, the bottles were installed which contain asphalt binder was put into the slot in the oven.
- The air compressor was turned on and the valve was set at a pressure of 4 bars.

- h) The switch labeled "ALARM" was turned on to turn on the motor to spin the bottle in the oven.
- i) This testing was completed after 85 minutes.
- j) Finally, the test was completed and the pressure was returned to 0 and the air compressor was turned off.
- k) The glass bottles were removed one by one carefully and poured the hot asphalt binder into the cup.



Figure 3.4 Rolling Thin Film Oven Test (RTFOT) machine

4. RESULTS AND FINDINGS

4.1 Introduction

This chapter's primary goal is to study and assess the findings from laboratory experiments in which the impact of substituting different percentages of crumb rubber powder for asphalt binder was examined. Physical testing was utilized in the laboratory to ascertain the physical characteristics of the aged and unaged asphalt binder and the crumb rubber modified mix. Viscosity, softening point, and penetration tests are part of the physical test. The rolling thin film oven and pressure aging vessel Tests are part of the second step of rheological testing.

4.2 Chemical Components of Crumb Rubber

According to the American Society of Testing and Materials, Yong Fong Rubber Industries provided the crumb rubber in powder form (ASTM). The following is a list of chemicals that make up crumb rubber:

Table 4.1 : Chemical components of the crumb rubber powder used in the study (Source: Young Fong Rubber industry)

Chemical Composition	Values (%)
Acetone Extract	10 ± 3
Ash Content	4 ± 3
Carbon Black	32 ± 5

4.3 Penetration Properties Results

A penetration test is typically used to determine the consistency of asphalt binder or the depth to which the material is penetrated by an asphalt binder standard needle under established loading, temperature, and time conditions. As an illustration, the asphalt binder penetration value is 90 if the needle penetrates at 9 mm. Based on penetration value, asphalt binder penetration grade is determined. To assess the impact of the crumb rubber powder percentages (15, 20, and 25%), this study will concentrate on two distinct types of asphalt binder penetration grade (80-100) and performance grade PG 76 containing varying percentages of crumb rubber powder. From the result shown in the Table 4.2 and 4.3 the penetration value of 80- 100 binder respectively of unaged asphalts binder of normal and modified asphalt binder with crumb rubber before the short term aging (RTFOT) and long-term aging (PAV) test.

Table 4.2 : Penetration results of penetration grade 80-100 unaged modified asphalt binder

CR %	Test Number			Average	
	1	2	3	Average	Overall Average
0	86.20	92.00	82.00	86.73	85.14
0	88.70	86.20	90.50	88.46	
0	78.00	90.50	72.20	80.23	
15	53.00	74.50	60.00	62.50	55.56
15	49.50	51.00	51.70	50.73	
15	53.20	50.50	57.50	53.73	
20	46.70	44.00	47.20	45.90	46.72
20	48.70	52.20	48.70	49.80	
20	43.70	46.70	43.00	44.46	
25	36.70	43.20	42.20	40.70	43.03
25	40.00	43.00	44.00	42.50	
25	42.20	44.70	42.00	42.90	

Table 4.3 : Penetration results of PG76 unaged modified asphalt binder

CR %	Test Number			Average	
	1	2	3	Average	Overall Average
0	60.20	66.50	58.50	61.70	51.20
0	51.50	46.20	46.20	47.96	
0	44.70	43.70	43.50	43.96	
15	34.70	40.20	38.00	37.63	35.26
15	33.70	38.70	33.50	35.30	
15	31.70	33.70	33.20	32.86	
20	20.20	20.20	20.70	20.36	19.00
20	17.20	16.70	18.50	17.46	
20	18.50	16.50	22.50	19.16	
25	15.00	17.80	18.20	17.00	16.73
25	10.70	16.00	17.50	14.50	
25	18.50	18.00	19.70	18.70	

Based on Figure 4.1 the penetration value for 80-100 and PG76 are reduced, because the crumb rubber has a strong effect of decreasing the penetration value by increasing the stiffness of crumb rubber powder of asphalt binder mix. The penetration values of performance grade PG76 of asphalt binder in original form and modified with crumb rubber showed the lower result when compared to penetration grade 80-100 asphalt binder. Therefore, it expected the Hot Mix Asphalt (HMA) using PG76 is more resistance to rutting potential compared with 80-100 asphalt binder.

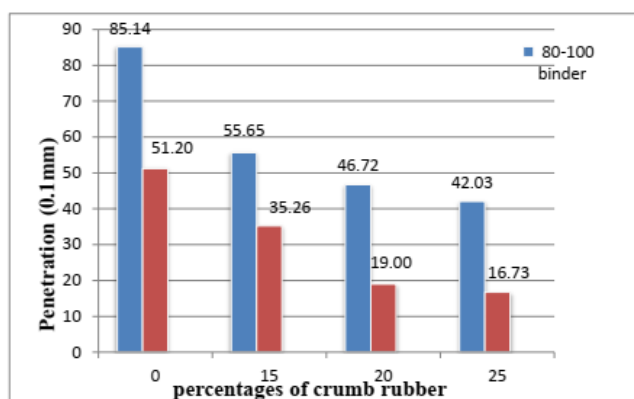


Figure 4.1 Penetration value vs. percentages of crumb rubber of penetration grade 80-100 and PG76 unaged modified asphalt binder

Table 4.4 : Penetration results of penetration grade 80-100 aged modified asphalt binder after RTFOT test.

CR %	Test Number			Average
	1	2	3	
0	51.7	47.2	50.0	49.6
15	39.2	43.2	43.7	42.0
20	38.7	42.2	40.7	40.7
25	27.0	27.0	25.0	26.3

Table 4.5 : Penetration results of PG76 aged modified asphalt binder after RTFOT test

CR %	Test Number			Average
	1	2	3	
0	30.7	29.5	35.7	31.9
15	22.2	21.0	23.5	22.2
20	20.5	20.7	19.0	20.0
25	17.7	17.0	20.2	18.3

From Figure 4.2 the penetration value after short-term aging (RTFOT) shows decreasing on penetration value with two unaged asphalt binder, which led to high resistance to rutting.

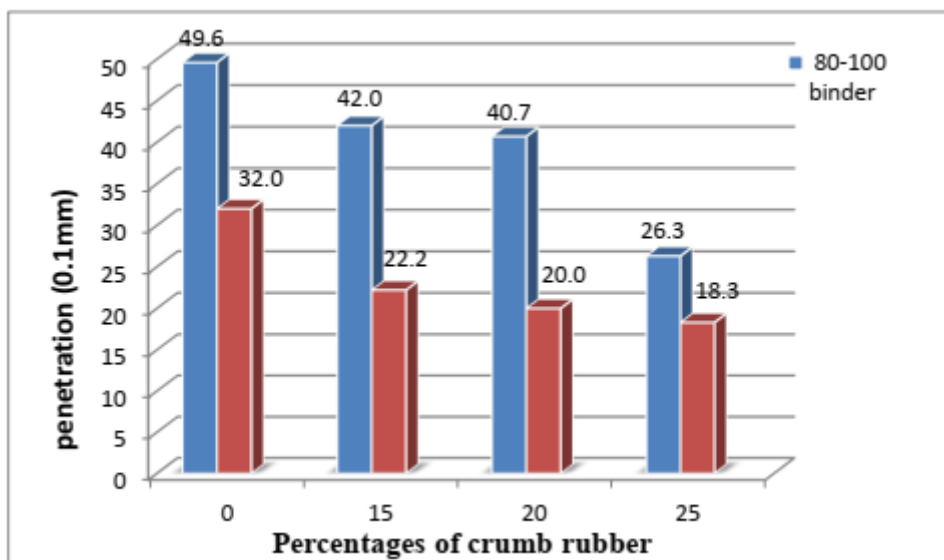


Figure 4.2 Penetration value vs. percentages of crumb rubber of penetration grade 80-100 and PG76 aged modified asphalt binder after RTFOT test.

From Figure 4.3 the penetration value for 80-100 has highest penetration value compared with PG76 after long-term aging (PAV) test and this making the PG76 much harder and stiffness than penetration grade 80-100 asphalt binder mix

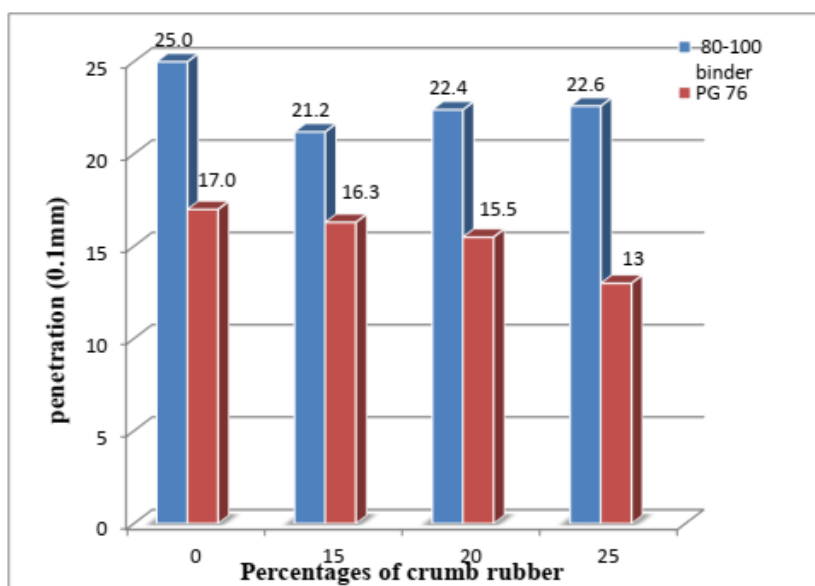


Figure 4.3 Penetration value vs. percentages of crumb rubber of penetration grade 80-100 and PG76 aged modified asphalt binder after PAV test

4.3 Penetration Properties Results

A penetration test normally used to measure the consistency of asphalt binder or measure the penetration of asphalt binder to which a standard needle penetrates the material under known conditions of time, loading, and temperature. For example (if the needle penetrates at 9mm, the asphalt binder penetration value is 90). The penetration grade of asphalt binder is based on penetration value. In this study will focus on two different types of asphalt binder penetration grade (80-100) and performance grade PG 76 containing various percentage of crumb rubber powder to evaluate the effect of crumb rubber powder percentage (15, 20 and 25%). 39 of unaged asphalts binder of normal and modified asphalt binder with crumb rubber before the short term aging (RTFOT) and long-term aging (PAV) test. From the result shown in the Table 4.2 and 4.3 the penetration value of 80- 100 binder respectively.

Table 4.6 : Penetration results of penetration grade 80-100 unaged modified asphalt binder

CR %	Test Number			Average	
	1	2	3	Average	Overall Average
0	86.20	92.00	82.00	86.73	85.14
0	88.70	86.20	90.50	88.46	
0	78.00	90.50	72.20	80.23	
15	53.00	74.50	60.00	62.50	55.56
15	49.50	51.00	51.70	50.73	
15	53.20	50.50	57.50	53.73	
20	46.70	44.00	47.20	45.90	46.72
20	48.70	52.20	48.70	49.80	
20	43.70	46.70	43.00	44.46	
25	36.70	43.20	42.20	40.70	43.03
25	40.00	43.00	44.00	42.50	
25	42.20	44.70	42.00	42.90	

Table 4.7 : Penetration results of PG76 unaged modified asphalt binder

CR %	Test Number			Average	
	1	2	3	Average	Overall Average
0	60.20	66.50	58.50	61.70	51.20
0	51.50	46.20	46.20	47.96	
0	44.70	43.70	43.50	43.96	
15	34.70	40.20	38.00	37.63	35.26
15	33.70	38.70	33.50	35.30	
15	31.70	33.70	33.20	32.86	
20	20.20	20.20	20.70	20.36	19.00
20	17.20	16.70	18.50	17.46	
20	18.50	16.50	22.50	19.16	
25	15.00	17.80	18.20	17.00	16.73
25	10.70	16.00	17.50	14.50	
25	18.50	18.00	19.70	18.70	

Based on Figure 4.4 the penetration value for 80-100 and PG76 are reduced, because the crumb rubber has a strong effect of decreasing the penetration value by increasing the stiffness of crumb rubber powder of asphalt binder mix. The penetration values of performance grade PG76 of asphalt binder in original form and modified with crumb rubber showed the lower result when compared to penetration grade 80-100 asphalt binder. Therefore, it expected the Hot Mix Asphalt (HMA) using PG76 is more resistance to rutting potential compared with 80-100 asphalt binder

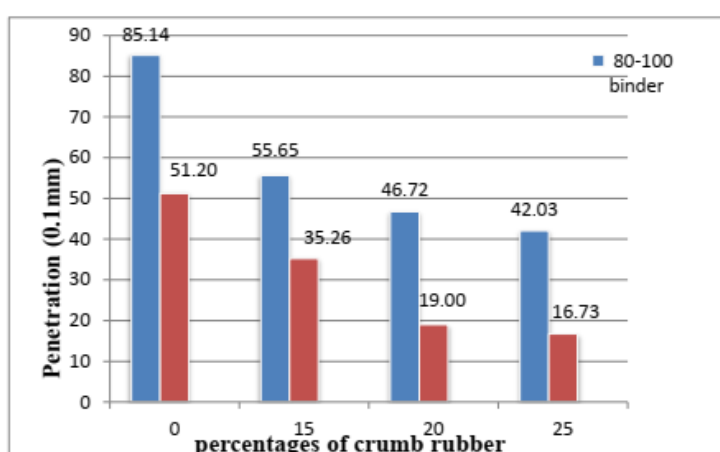


Figure 4.4 Penetration value vs. percentages of crumb rubber of penetration grade 80-100 and PG76 unaged modified asphalt binder

4.4 Softening Point Results

The result of softening point or the phase change of temperature of control and modified asphalt binder with crumb rubber before the short-term aging and longterm aging shown in the Tables 4.8 and 4.9 for penetration grade 80 - 100 and performance grade PG76 respectively. Figure 4.4 shows the crumb rubber powder percentage against softening point as the partial replacement of total weight of asphalt binder mix (15, 20, and 25%). The results shows the crumb rubber increasing the softening point of the crumb rubber modified asphalt binder, thus improving the asphalt binder to resist the high-temperature deformation in the road surface.

Table 4.8: Softening point results of penetration grade 80-100 unaged modified asphalt binder

CR%	°C		
	Ball 1	Ball 2	Average
0	42.0	42.0	42.0
15	45.0	45.0	45.0
20	48.0	49.5	48.7
25	55.0	55.0	55.0

Table 4.9 : Softening point results of PG76 unaged modified asphalt binder

CR%	°C		
	Ball 1	Ball 2	Average
0	55.0	56.0	55.5
15	49.0	50.0	49.5
20	55.0	56.0	55.5
25	61.0	62.0	61.5

From Figure 4.5 shown the softening point of performance grade, PG76 indicates strong of temperature change of 61.5°C at 25% replacement compared with penetration grade 80-100 asphalt binder. The increasing of phase change of temperature indicates the asphalt binder more stiffness and hard to resist the effect of higher temperature.

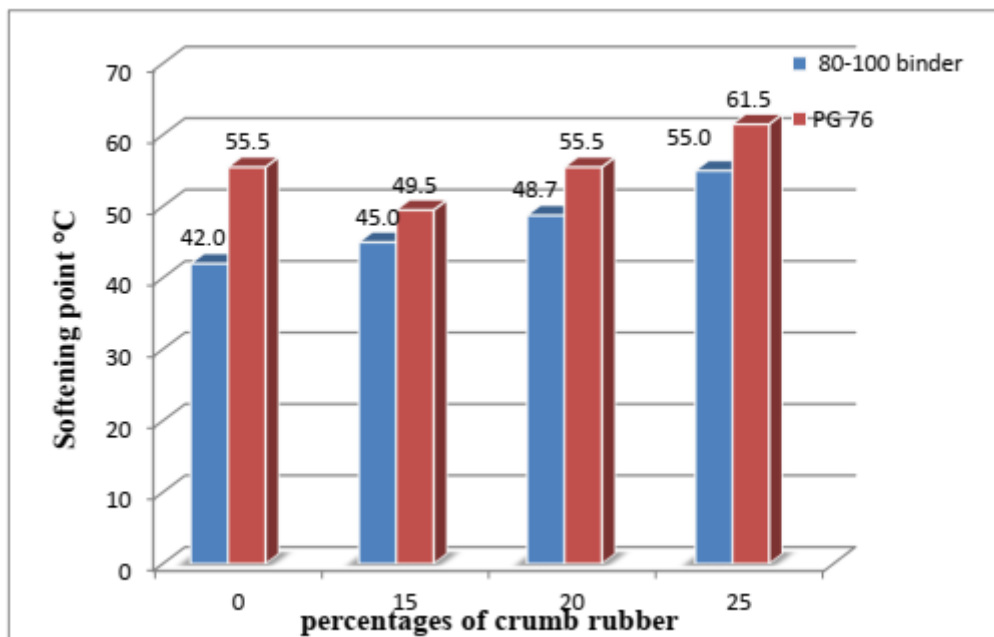


Figure 4.5 Softening point vs. percentages of crumb rubber of penetration grade 80-100 and PG76 unaged modified asphalt binder

5. DISCUSSION AND CONCLUSIONS

5.1 Introduction

The purpose of the study was to determine how different percentages of crumb rubber powder, which were used to partially replace PG76 and 80-100 in the total weight of the asphalt binder mix, would affect the rheological and physical characteristics of the mixture both before and after aging. The Penetration, softening, rolling thin-film oven, viscosity, and pressure-aging vessel tests are the main emphasis of the examination.

5.2 Conclusion

From these tests results, the following conclusions were drawn for the materials used in this study:

- i. The increase in percentages with partial replacement of crumb rubber will reduce the percentage value of penetration value for 80- 100 asphalt binder. However, the PG76 asphalt binder shows the lower result of penetration before and after short term and long term aging compared with 80 - 100 asphalt binder in term of stiffness. The optimum percentage of crumb rubber is the 15% as the partial replacement of total weight of asphalt binder after the long term aging.
- ii . The softening point results shows that the percentage of replacement of asphalt binder with crumb rubber increased the temperature for penetration grade 80-100 and PG76 asphalt binder mix.

iii. The viscosity results shows that the PG76 asphalt binder replaced with crumb rubber has higher viscosity compared with penetration grade 80-100 asphalt binder replacement with crumb rubber before aging.

5.3 Recommendation

The study offers some advice and ideas to enhance the outcome in the future when employing crumb rubber as a partial replacement.

I. When replacing the entire weight of the asphalt binder mix with varying percentages of crumb rubber, research should be done to examine and assess the physical and rheological characteristics of the mixture both before and after the aging process.

ii. Greater research should be done to assess the resistance to rutting and fatigue cracking using the Dynamic Shear Rheometer test (DSR). This will provide greater insight into the characteristics of the crumb rubber modified asphalt binder that can be used as a replacement both before and after the aging process.

Acknowledgements

I appreciate from my supervisor Mr. Azman Mohamad ,Who has checked and helped me about this paper writing.

Ethics Committee Approval / Etik Kurul Onayı

N/A

Peer-review

Externally peer-reviewed.

Author Contributions

All work is done as review paper, I have studied a lot of papers and has written this paper.

Conflict of Interest

The authors have no conflicts of interest to declare.

Funding

The authors declared that this study has received no financial support.

6. REFERENCES

Amirkhanian S. N. (2003). Establishment of an Asphalt-Rubber Technology Service (ARTS), *Proceedings of the Asphalt Rubber 2003 Conference*, Brasilia, Brazil, pp 577-588.

American Society of Testing and Materials. (2001) D 6114 Standard Specification for Asphalt rubber Binder in Vol. 4.03, Road and Paving Materials; Vehicle Pavement Systems, *Annual Book of ASTM Standards 2001*, ASTM, West Conshohocken, PA.

Amirkhanian, S. and Corley, M. (2004). Utilization of Rubberized Asphalt in the United Statesan Overview. *Proceedings of 04 International Symposium Advanced*.

- Avraam I. Isayev. (2005). *Recycling of Rubbers: Science and Technology of Rubber*. Third Edition, Academic Press.
- Bahia, H.U., D. Perdomo, R. Schwartz, and B. Takallou. (1997). Use of Superpave Technology for Design and Construction of Rubberized Asphalt Mixtures', Presented at the *76th Meeting of the Transportation Research Board*, January.
- Bahia, Hussain and Robert Davies (1994). Effect of Crumb Rubber Modifiers (CRM) on Performance-Related Properties of Asphalt Binders. *Journal, AAPT*, 1994, pp. 414-441.
- Brûlé, B. (2007). Polymer-Modified Asphalt Cements Used in the Road Construction Industry: Basic Principles, *Transportation Research Record*, Volume 1535, Is.1, pp. 48-53.
- Benazzouk A., Douzane O, Langlet T., Mezreb K., Roucoult J.M. and Quéneudec M., (2007), "Physico-mechanical properties and water absorption of cement composite containing shredded rubber wastes", *Cement and Concrete Composites*, **29**, 732–740.
- Denning, J. H., Carswell, J. (1981). Improvements in Rolled Asphalt Surfacing by the Addition of Organic Polymers. *Laboratory Report 989, Transport and Road Research Laboratory*, Crowthorne. Edil T.B. (2004), "A review of mechanical and chemical properties of shredded tires and soil mixtures", in *Geotechnical Special Publication No. 127*, Eds A.H.
- Aydilek and J.Wartman, *Recycled Materials in Geotechnics*, pp. 1–21, ASCE, Reston, VA, USA. Federal Highway Administration. (1998). *User Guidelines for Waste and By-Product Materials in Pavement Construction*. US Department of Transportation.
- Glover, C. J., and Bullin. J. A. (1997). Physical Properties of Asphalt-Rubber Binder. *Petroleum Science and Technology*, Vol, Issue 3-4.
- Harvey, J., Bejarano, M., Popescu, L. (2000). Accelerated Pavement Testing of Rutting and Cracking Performance of Asphalt –Rubber and Conventional Asphalt Concrete Overlay Strategies. *Conference on Asphalt Rubber*, Vilamoura, Portugal.
- Huang B., Mohammed, L.N. Graves,P.S., and Abadie, C. (2002). Louisiana Experience with Crumb Rubber-Modified Hot-Mix Asphalt Pavement. *Transportation Research Record*, No: 1789, Washington, D.C.
- Hunt, E.A. (2002). Crumb Rubber Modified Asphalt Concrete in Oregon. *Final Report SPR 355*, Oregon Department of Transportation.
- Heitzman, M. (1991). Design and Construction of Asphalt Paving Materials with Crumb Rubber Modifier. *Transportation Research Record 1339*, TRB, Washington, D.C., pp. 1-8.
- Heitzman, M.A. (1992). State of the Practice for the Design and Construction of Asphalt Paving Materials with Crumb Rubber Additive. *Report No. FHWA-92-022*, Office of Engineering, Pavement Division, Federal Highways Administration.
- Huang, Yue, Roger N. Bird, and Oliver Heidrich. (2007). A Review of the Use of Recycled Solid Waste Materials in Asphalt Pavements. *Resources, Conservation and Recycling* (Elsevier) Vol. 52, no. Issue 1 pp58-73.
- Liu S, Cao W, Fang J, Shang S (2009). Variance Analysis and Performance Evaluation of Different Crumb Rubber Modified (CRM). Asphalt. *Constr. Build. Mater.* 23: 2701-2708.
- Maupin, B.D. (1992). Virginia's Experimentation with Asphalt Rubber Concrete. *Transportation Research Record, No: 1339*, Transportation Research Board, Washington, D.C.
- Maupin, B.D. (1996). Hot Mix Asphalt Rubber Application in Virginia. *Transportation Research Record, No: 1530*, Transportation Research Board, Washington, D.C
- Mark, J. E., Erman, B, and Eirich, F. R. (2005). *The Science and Technology of Rubber* 3rd Edition. Elsevier Academic Press, Burlington, MA.

- Mohamed, A. A. (2007). *A Study on the Physical and Mechanical Properties Of Asphaltic Concrete Incorporating Crumb Rubber Produced Through Dry Process* [TA443. A7 A136 2007 f rb], Universiti Sains Malaysia.
- Magar, N. R. (2014). A Study on the Performance of Crumb Rubber Modified Bitumen by Varying the Sizes of Crumb Rubber.
- Nuha S. Mashaan (2011) Effect of Crumb Rubber Concentration on the Physical and Rheological Properties of Rubberised Bitumen Binder's. Vol. 6(4), pp. 684- 690
- Read, J., Whiteoak, D., & Shell Bitumen. (2003). *The Shell Bitumen Handbook* (5th ed.). London: Thomas Telford.
- Ruth, B.E., and Roque, R. Crumb Rubber Modifier (CRM) in Asphalt Pavements, Proceedings of the Transportation Congress, 768-785. 1995.
- Snyder, R.H. (1998). *Scrap Tires: Disposal and Reuse*. Society of Automotive Engineers, Inc., Warrendale, PA.
- Souza and Weissman (1994). Using a Binder with 15% Rubber Content (size of 0.2, 0.4 and 0.6mm) in Dense- graded Bitumen.
- Shatanawi, Khaldoun M, Szabolcs Biro, Andras Geiger, and Serji N Amirkhanian. (2012). Effects of Furfural Activated Crumb Rubber on the Properties of Rubberized Asphalt. *Construction and Building Materials*. Vol. 28, no. Issue 1 p96-103.
- Takallou H.B., Takallou M.B. (1991). Recycling Tires in Rubber Asphalt Paving Yields Cost, Disposal Benefits, *Elastomerics*, Vol 123, P: 19-24.
- Takallou, H.B. (1988). Development of Improved Mix and Construction Guidelines for Rubber Modified Asphalt Pavements. *Transport Research Record 1171*, Transportation Research Board, Washington, D.C. Whiteoak, D. (1991). *The Shell Bitumen Handbook*. Shell Bitumen, UK 80/11Surrey.

Simulation of a Series Active Filter Using Hysteresis Control from an Electromagnetic Compatibility Perspective: Solution against Unwanted Harmonics

MANA Hassan¹, BOUDJELAL Dounia²

Abstract: Passive filters have several drawbacks that make them less desirable, including resonance with system impedance, large size, heavy weight, sensitivity to variations in system parameters, and fixed harmonic compensation. Series active filters address these shortcomings and are therefore generally preferred over passive filters. This paper discusses the benefits and the applications of series active filters in improving the quality of electrical energy.

Keywords: Harmonics, EMC, Series active filter, hysteresis.

¹**Address:** Ferhat Abbas University, Faculty of technology, Setif/Algeria

²**Address:** Ferhat Abbas University, Faculty of technology, Setif/Algeria

***Corresponding author:** hassan_mana@yahoo.fr

1. INTRODUCTION

Have you ever wondered why sometimes your electronic devices act up or experience sudden malfunctions? It's often due to power quality issues and electromagnetic interference (EMI), which can mess with the smooth flow of electricity and disrupt how our gadgets work. Thankfully, researchers and engineers have been working hard to tackle these problems, and one of the solutions they've explored is using something called series active filters. [2] [4] [6].

Series active filters have emerged as effective solutions for improving power quality and mitigating EMC-related problems. Unlike passive filters, which have limited capabilities, series active filters can actively monitor and adjust electrical signals in real-time, by injecting compensating currents and dynamically responding to changing conditions, these filters can suppress harmonics, regulate voltage levels, and reduce electromagnetic emissions, thereby enhancing overall system performance.

In this article, we'll take a look at what past research has discovered about these active filters, we'll explore how they're designed, how effective they've been in improving electricity quality and reducing interference.

2. ACTIVE POWER FILTERS

Active Power filters have wide range application in modern electrical distribution system for eliminating the harmonics associated with it. The Shunt active power filter (SAPF) is one of power filters which have needs an accurate control algorithm that provides robust performance and it better dynamic performance. The control methods are responsible for generating the reference currents which used to trigger the Voltage Source Inverters (VSI). Harmonic injection in power system due to various nonlinear loads such as uninterruptible power suppliers (UPS), adjustable speed drives (ASD), furnaces and single-phase computer power supply etc. has resulted serious power quality problems and hence we need of Active Power filter [1]

APF system can be divided into two sections as given in Figure 1: The control unit and the power circuit. The control unit consists of reference signal generation, gate signal generation, capacitor voltage balance control and voltage/current measurement. Power circuit of APF is generally comprised of energy storage unit, DC/AC converter, harmonic filter and system protection.

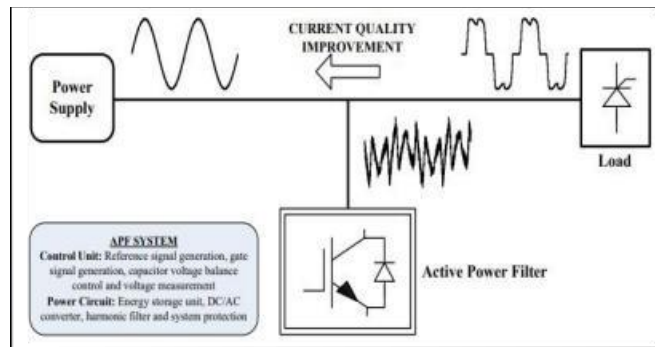


Figure 1. Basic representation of APF.

2.1. Series active filter

This type of filter forms a series connection with the supply mains just before the load; this is achieved through a matching transformer. They are generally used for voltage harmonics mitigation, and for balancing or regulating the load's or line's terminal voltage. Other applications include reduction of negative sequence voltage, voltage regulation on three-phase systems (Singh et al., 1999). Series active filters are not used as much as its shunt counterpart, this is because of some drawbacks such as having to handle high currents, this consequently leads to rising in current rating, and as a result, larger in physical size. An advantage they possess though is that they are best for mitigation of voltage harmonics and three-phase voltage balancing. A series of active filter configuration is shown in Figure 2 [2]

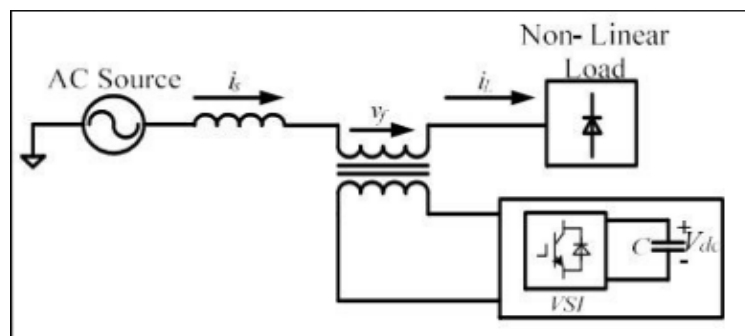


Figure 2. Series active filter configuration.

2.1. Hysteresis current control

Hysteresis current control is used for generating the switching pulses. Among the various current control techniques, The technique of current control through hysteresis controllers is one of the most used due to its simple implementation, good stability, accurate current tracking, rapid response in the transient regime, and robustness to the variation of the load parameters . According to the hysteresis control technique, the error is centered in a predetermined hysteresis band, and when the error exceeds the hysteresis limits, the appropriate switching decision is made to control the error within the hysteresis band so that the reference current is followed faithfully.

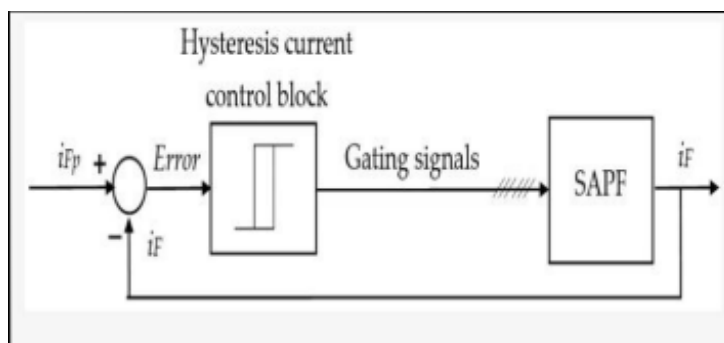


Figure 3. Fixed band current hysteresis control loop structure.

3. MATLAB SIMULATION

A simulation was conducted using Matlab/Simulink. The system parameters used in this simulation are summarized in the following table:

Table 1. (Times New Roman, 10pt, iki yana yasli/two sided)

Paramètre		Valeur numérique
Réseaux Electrique	Tension de source V_s	380 V
	La fréquence f	50 Hz
	La résistance R	1 ohm
	L'inductance L	1.5 mH
Charge perturbatrice	La résistance R	30 ohms
	L'inductance L	10 mH
Le filtre Série	La tension Constante DC	70 V
	Filtre passif	
	La résistance R	5 Ohms
	La capacité C	20 μ F

2.1. before filtering

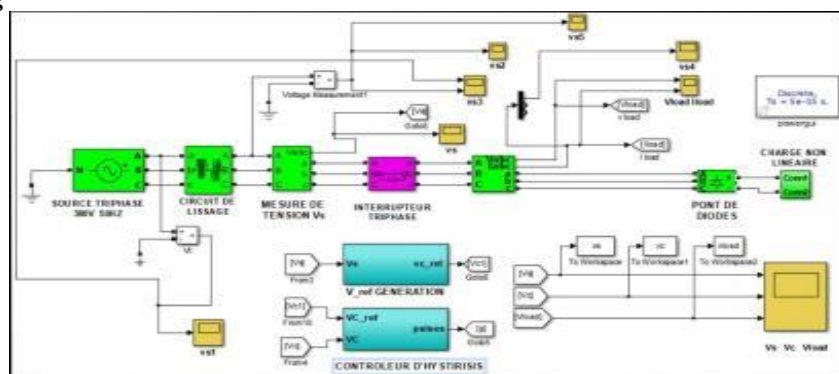


Figure 4. Modeling of a distribution network without filtering.

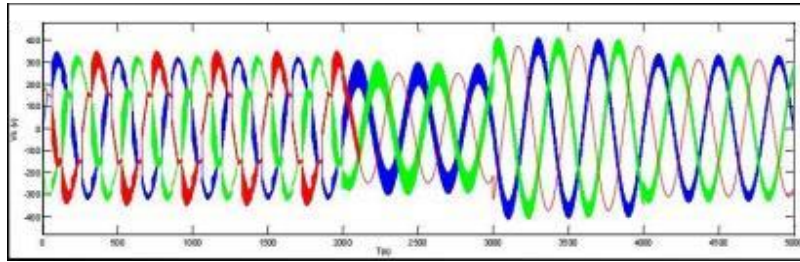


Figure 5. Voltage of the electric network .

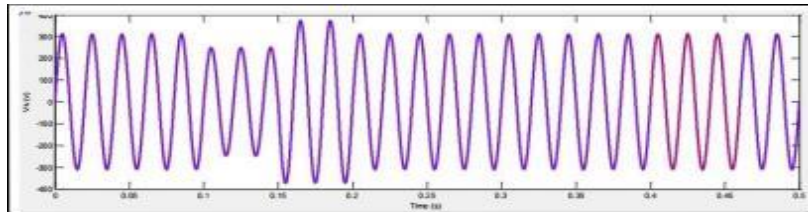


Figure 6. Network voltage before the smoothing circuit.

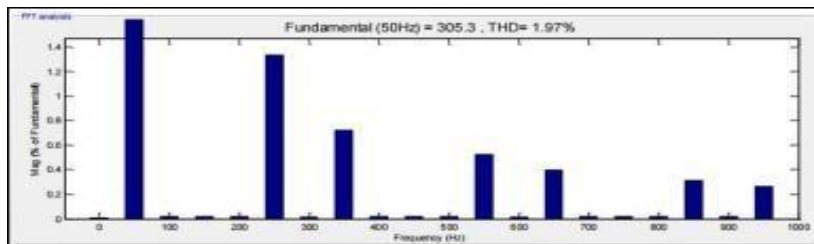
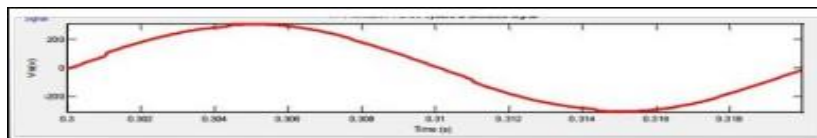


Figure 7. Harmonic spectra (THD=18.55%).

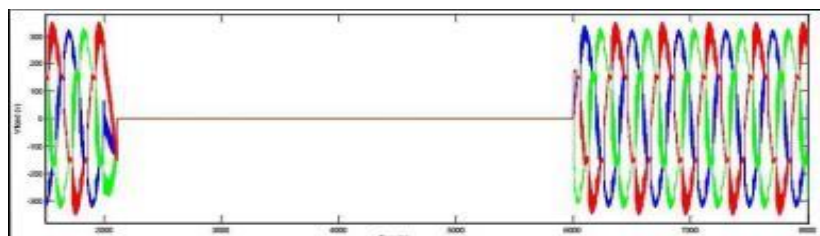


Figure 8. Load voltage

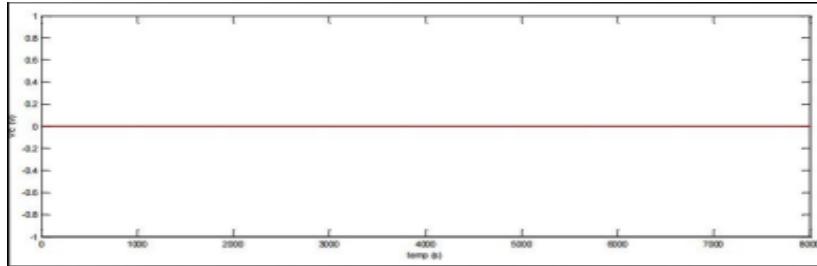


Figure 9. Reference voltage.

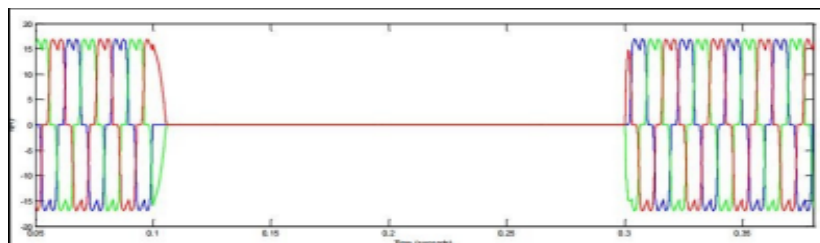


Figure 10. Current drawn by the load.

2.1. After filtering

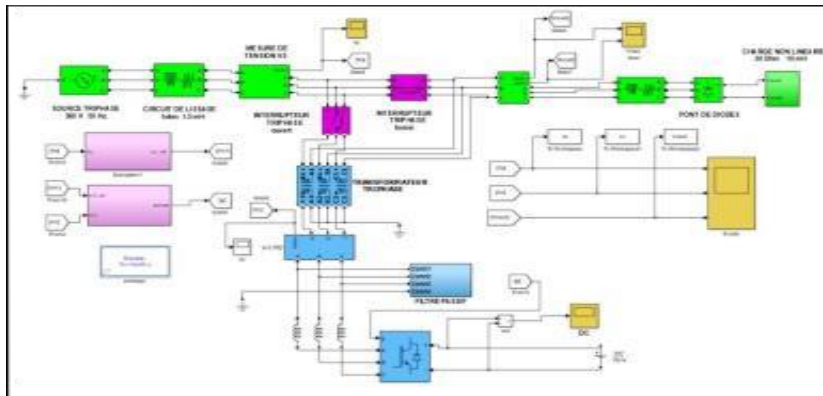


Figure 11. Modeling of a distribution network with a series active filter.

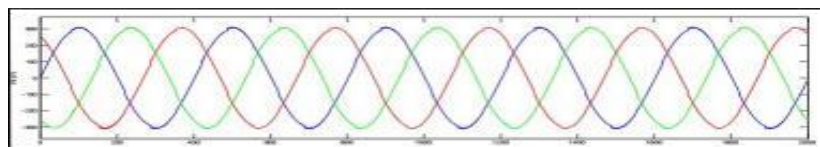


Figure 12. Network voltage.

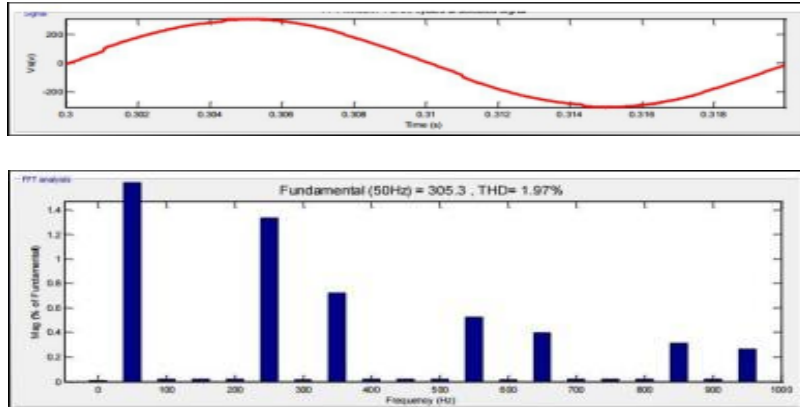


Figure 13. Harmonic spectra (THD=1.97).

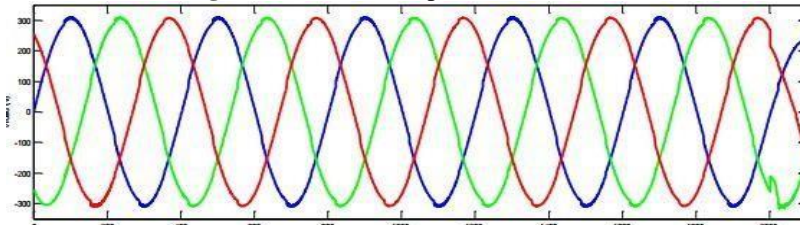


Figure 14. Load voltage.

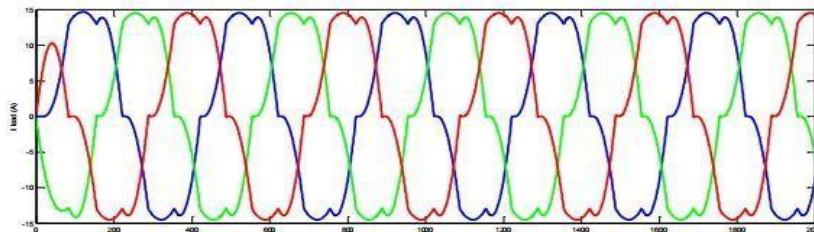


Figure 15. Current drawn by the load.

4. INTERPRETATION OF THE RESULTS

➤ *Before filtering*

- Figure 7 shows the waveform of the source voltages. It can be seen that it is not perfectly sinusoidal, indicating the presence of harmonics, It also shows the voltage harmonic spectra before filtering, the presence of harmonics such as 5th, 7th, and 11th can be observed. Therefore, the load absorbs a non-sinusoidal voltage, and the THD equals 18.55%.
- In figure 9 it can be seen that the reference voltage is zero. This is simply because the filter is not yet connected, so no voltage is injected into the network.
- Figure 10 shows the shape of the current absorbed by the load, and as can be seen, it is not perfectly sinusoidal.

➤ *After filtering*

- Figure 13 shows the waveform of the supply voltages after filtering the 5th, 7th, and 11th harmonics. It can be observed that the voltage distortions are more attenuated than in the case of the voltages presented in the previous figure. It also shows the voltage harmonic spectra after filtering, where the presence of harmonics is noted, and the THD is 1.97%.
- Figure 15 shows the current absorbed by the load, and as can be seen, it is still not sinusoidal, indicating that the series active filter has no effect on the current.

4. DISCUSSION AND CONCLUSIONS

In this article, we explored an alternative method for improving the quality of electrical energy: the active filter. Our study focused on the various possible connections for this filtering method, detailing the advantages of each configuration. Additionally, we modeled a segment of the distribution network both with and without filtering to compare the impact of polluting loads on the network and to assess the effectiveness of a series active filter.

REFERENCES

- [1] R.Chaurasiya, G.P.Rhathor, "Simulation of adaptive hybrid shunt active power filter under non-linear load to improve power quality," international journal of electronics communication and computer engineering, Vol.12, Issue 5, ISSN (Online):2249-071X, 2021.
- [2] I.Kabir, A.F. Shehu, S. Musa, & F.Alhassan, (2020). Active Filters: A Review. *ATBU Journal of Science, Technology and Education*, 8(4), 224-230.
- [3] M. Popescu, A.Bitoleanu, C.V. Suru, M. Linca & L. Alboteanu, (2024). Shunt Active Power Filters in Three-Phase, Three-Wire Systems: A Topical Review. *Energies*, 17(12), 2867.
- [4] F. Danis Wara, A.N. Afandi & Gumilar, L. (2024, February). Design of series active filter simulation model as harmonic distortion reduction using SPWM modulation with ACO algorithm. In *AIP Conference Proceedings* (Vol. 2838, No. 1). AIP Publishing.
- [5] Kuczyński, K., & Szymański, J. R. (2020). Kompensacja harmoniczných–wprowadzenie do filtrów aktywných. *Elektro Info*.
- [6] Kovalenko, M. A, Kovalenko, I. Y., Golovko, V. M., Chumack, V. V., & Svyatnenko, V. A. (2022). Експериментальна оцінка корекції потужності генератора автономної вітроелектроустановки. *Electrical Engineering and Power Engineering*, (1), 8-18
- [7] H.Vahedi, A.Sheikholeslami, M.Tavakoli.Bina and M. Vahedi (2011). Review and simulation of fixed and adaptive hysteresis current control considering switching losses and high-frequency harmonics. *Advances in power electronics Vol 2011*.